AMINODIBORANATES: SYNTHESES, STRUCTURES, AND APPLICATIONS FOR CHEMICAL VAPOR DEPOSITION

BY

SCOTT R. DALY

DISSERTATION

Submitted in partial fulfillment of the requirements
for the degree of Doctor of Philosophy in Chemistry
in the Graduate College of the
University of Illinois at Urbana-Champaign, 2010

Urbana, Illinois

Doctoral Committee:

Professor Gregory S. Girolami, Chair
Professor Thomas B. Rauchfuss
Professor John F. Hartwig
Professor John R. Abelson

ABSTRACT

The reaction $ThCl_4$ with 4 equivalents of sodium *N*,*N*-dimethylaminodiboranate, $Na(H_3BNMe_2BH_3)$, in tetrahydrofuran produces the new complex $Th(H_3BNMe_2BH_3)_4$. The thorium center forms bonds with fifteen hydrogen atoms; accordingly, *this is the first example of a fifteen-coordinate atom of any kind*. As determined by both single crystal X-ray and single crystal neutron diffraction studies, the eight boron atoms describe an approximate D_{2d} dodecahedral structure in which seven of the Th···B distances lie between 2.88 and 2.95 Å, but the eighth is significantly longer at 3.19 Å. Two hydrogen atoms on each boron atom bridge each of the short Th···B contacts, but only one bridges the long Th···B contact. Quantum chemical calculations suggest that $Th(H_3BNMe_2BH_3)_4$ is 16-coordinate in the gas phase and that the 15-coordinate solid-state structure can be attributed to packing effects. Compound **1** reacts at elevated temperatures (80 – 110 °C) to produce $(NMe_2BH_2)_2$ and the mixed aminodiboranate/tetrahydroborate complex $Th(H_3BNMe_2BH_3)_2(BH_4)_2$; the reaction proceeds through the $Th(H_3BNMe_2BH_3)_3(BH_4)$ intermediate. The structure of the fifteen-coordinate $Th(H_3BNMe_2BH_3)_2(BH_4)_2(thf)$ is also described.

The reaction of UCl_4 with $Na(H_3BNMe_2BH_3)$ in diethyl ether affords the uranium(III) product $U(H_3BNMe_2BH_3)_3$, which has been crystallized as two different structural isomers from pentane and toluene, respectively. The isomer crystallized from pentane is a 13-coordinate polymer in which each uranium center is bonded to three chelating $H_3BNMe_2BH_3^-$ (DMADB) ligands and to one hydrogen atom from a neighboring molecule so as to form an intermolecular B-H-U bridge. The isomer crystallized from toluene is also polymeric but the uranium atoms are coordinated by two chelating DMADB ligands and two bridging DMADB ligands bound in a U(κ^3*H*-$H_3BNMe_2BH_3$-κ^3*H*)U fashion, so that each uranium atom is 14-

coordinate. When the reaction of UCl_4 with $Na(H_3BNMe_2BH_3)$ is conducted in tetrahydrofuran (thf) or 1,2-dimethoxyethane (dme), the adducts $U(H_3BNMe_2BH_3)_3$(thf) and $U(H_3BNMe_2BH_3)_3$(dme) are obtained. The rate of reduction from U^{IV} to U^{III} is solvent dependent and is correlated with the donor ability of the solvent, the relative rates being Et_2O > thf > dme. The addition of trimethylphosphine to $U(H_3BNMe_2BH_3)_3$(thf) generates $U(H_3BNMe_2BH_3)_3(PMe_3)_2$. This compound slowly decomposes at room temperature over several months to yield the new borane $PMe_3BH_2NMe_2BH_3$, μ-(*N*,*N*-dimethylamido)pentahydro(trimethylphosphine)diboron. The complex $U_2(\mu\text{-}O)(BH_4)_6(dme)_2$ has also been prepared and the structure suggests that the putative hydride $U_2(\mu\text{-}H)_2(BH_4)_6(dme)_2$ should be reformulated as this oxo species.

New lanthanide complexes of stoichiometry $Ln(H_3BNMe_2BH_3)_3$ and $Ln(H_3BNMe_2BH_3)_3$(thf) have been prepared, where Ln = Y, La, Ce, Pr, Nd, Sm, Eu, Gd, Tb, Dy, Ho, Er, Tm, Yb, and Lu. The tetrahydrofuran complexes are all monomeric, and most of them adopt 13-coordinate structures in which each DMADB group chelates to the metal center by means of four B-H···Ln bridges (each BH_3 group is κ^2H; i.e., forms two B-H···Ln interactions). For the smallest three lanthanides, Tm, Yb, and Lu, the metal center is 12 coordinate because one of the DMADB groups chelates to the metal center by means of only three B-H···Ln bridges. The structures of the base-free $Ln(H_3BNMe_2BH_3)_3$ complexes are highly dependent on the size of the lanthanide ions: as the ionic radius decreases, the coordination number decreases from 14 (Pr) to 13 (Sm) to 12 (Dy, Y, Er). The 14-coordinate $Pr(H_3BNMe_2BH_3)_3$ and the 13-coordinate $Sm(H_3BNMe_2BH_3)_3$ are isostructural with the isomers of $U(H_3BNMe_2BH_3)_3$. The 12-coordinate complexes adopt a dinuclear structure in which each metal center is bound to two chelating DMADB ligands and to two ends of two ligands that bridge in a $Ln(\kappa^2H\text{-}H_3BNMe_2BH_3\text{-}\kappa^2H)Ln$ fashion. The complexes react with

water, and the structure of the partial hydrolysis product $[La(H_3BNMe_2BH_3)_2(OH)]_4$ is described. Field ionization MS data, melting and decomposition points, thermogravimetric data, and NMR data, including an analysis of the paramagnetic lanthanide induced shifts (LIS), are reported for all of the complexes. The $Ln(H_3BNMe_2BH_3)_3$ compounds, which are highly volatile and sublime at temperatures as low as 65 °C in vacuum, are suitable for use as chemical vapor deposition (CVD) and atomic layer deposition (ALD) precursors to thin films.

Under certain circumstances, treatment of the trichlorides $EuCl_3$ or $YbCl_3$ with $Na(H_3BNMe_2BH_3)$ in thf results in reduction to the corresponding divalent europium and ytterbium DMADB complexes $Eu(H_3BNMe_2BH_3)_2(thf)_2$ and $Yb(H_3BNMe_2BH_3)_2(thf)_2$, which can be separated from trivalent $Ln(H_3BNMe_2BH_3)_3(thf)$ byproducts by extraction and crystallization from pentane. These divalent DMADB species can also be prepared directly from the divalent lanthanide iodides EuI_2 and YbI_2 in higher yield and without the need to separate them from trivalent species. Treatment of the thf adducts with an excess of 1,2-dimethoxyethane (dme) in pentane affords the new species $Eu(H_3BNMe_2BH_3)_2(dme)_2$ and $Yb(H_3BNMe_2BH_3)_2(dme)$.

Reaction of $BaBr_2$ with $Na(H_3BNMe_2BH_3)$ in thf, followed by extraction and crystallization from Et_2O, yields $Ba(H_3BNMe_2BH_3)_2(Et_2O)_2$; the coordinated Et_2O molecules can be removed under vacuum. Treatment of $Ba(H_3BNMe_2BH_3)_2$ with 1,2-dimethoxyethane (dme), *N*,*N*,*N*′,*N*′-tetramethylethylenediamine (tmeda), or 1,4,7,10-tetraoxacyclododecane (12-crown-4) in diethyl ether results in formation of the new complexes $Ba(H_3BNMe_2BH_3)_2(dme)$, $Ba(H_3BNMe_2BH_3)_2(tmeda)$, and $Ba(H_3BNMe_2BH_3)_2$(12-crown-4), in high yields (78 – 85%). The reaction of $BaBr_2$ with 2 equiv of $Na(H_3BNMe_2BH_3)$ in di(2-methoxyethyl)ether (diglyme) yields $Ba(H_3BNMe_2BH_3)_2(diglyme)_2$. Single-crystal XRD

studies show that the Et_2O, dme, and tmeda adducts are isostructural linear coordination polymers whereas the 12-crown-4 and diglyme species are monomeric. The DMADB ligands in all of the structures are chelating aside for one unusual in $Ba(H_3BNMe_2BH_3)_2(diglyme)_2$, which binds to the metal by means of only one BH_3 group in a κ^3*H* fashion. The bonding of DMADB with highly electropositive metals such as barium will discussed.

Reduction of ammonia borane, $NH_3{\cdot}BH_3$, with Na in refluxing tetrahydrofuran initially yields the known salt $Na(NH_2BH_3)$, but continued heating affords the new compound, the unsubstituted aminodiboranate $Na(H_3BNH_2BH_3)$. An alternative preparation of this salt is the reaction of 2 equiv of $NH_3{\cdot}BH_3$ with $NaNH_2$ in refluxing thf, which produces $Na(H_3BNH_2BH_3)$ in better yield. Reduction of other amine boranes with Na, where amine = NH_2Me, NH_2Et, $HN(C_4H_8)$, affords the new aminodiboranate salts $Na(H_3BNHMeBH_3)$, $Na(H_3BNHEtBH_3)$, and $Na[H_3BN(C_4H_8)BH_3]$. Addition of dioxane to these salts affords the adducts $Na(H_3BNHMeBH_3)(dioxane)_{0.5}$, $Na(H_3BNHEtBH_3)(dioxane)$, and $Na[H_3BN(C_4H_8)BH_3](dioxane)$, which have been crystallographically characterized. A method to prepare $Na(B_3H_8)$ without the use of Na amalgam or diborane is also described.

The new aminodiboranate salt $Na[H_3BN(C_4H_8)BH_3]$ has been used to prepare new metal complexes with Mg, Mo, and Er, and these exhibit structures and properties similar to their known DMADB analogs. Grinding $MgBr_2$ with two equivalents of $Na(H_3BNHEtBH_3)$ yields the highly volatile $Mg(H_3BNHEtBH_3)_2$, which condenses as a viscous oil during sublimation attempts. The collected oil slowly crystallizes to yield long needles suitable for single-crystal XRD. In contrast to $Mg(H_3BNMe_2BH_3)_2$, which is monomeric and has two chelating DMADB, the structure of $Mg(H_3BNHEtBH_3)_2$ is a highly ordered polymer. The slow crystallization behavior combined with the polymeric structure suggests that $Mg(H_3BNHEtBH_3)_2$ is “crystallographically frustrated”; the asymmetry of the

$H_3BNHEtBH_3$ ligand is disrupting efficient packing in the solid-state. Treatment of $ErCl_3$ with three equivalents of $Na(H_3BNH_2BH_3)$ in tetrahydrofuran affords the new erbium complex $Er(H_3BNH_2BH_3)Cl_2(thf)_3$, where only one chlorine atom has been replaced. The structure obtained by XRD reveals strong N-H···Cl contacts, which may account for the incomplete metathesis.

$Pr(H_3BNMe_2BH_3)_3$ and $Pr(thd)_3$, where thd = 2,2,6,6-tetramethylheptane-3,5-dionate, can serve as volatile carriers for ^{225}Ac. The actinium coordination complexes $Ac(H_3BNMe_2BH_3)_3$ and $Ac(thd)_3$ are the likely species subliming with the carrier material. The ^{225}Ac-doped $Pr(H_3BNMe_2BH_3)_3$ has been used to deposit amorphous ^{225}Ac-doped PrB_x films on glass and Si(100) at 300 °C. The alpha emission spectra of the films are well resolved, suggesting that they could be used as implant devices for diffusing alpha-emitter radiation therapy (DART).

To Carin

“Karissima, noli tardare studeamus nos nunc amare,
sine te non potero vivere iam decet amorem perficere”

ACKNOWLEDGMENTS

There are many people who have supported my endeavors over the last four years by contributing to a productive and enjoyable graduate school experience.

Thanks to my advisor Professor Gregory Girolami for his guidance, our many conversations, and for allowing me to pursue chemistry that I found interesting. I look forward to our continued friendship and correspondence. I also thank my committee members Professors Tom Rauchfuss, John Hartwig, and John Abelson for their helpful discussions, especially those regarding my future career objectives. Thanks to my undergraduate advisor Dr. Phil Horwitz at PG Research Foundation. Much of my research was funded by his generous donations and I am eternally grateful for his mentoring and friendship.

Thanks to present and past Girolami group members: Brian, Wontae, and Richard for teaching me how to do air-sensitive chemistry, Andrew for providing some great one-liners, Chuck for training me how to properly use a shotgun in Halo, and Charity for performing calculations on my behalf. I also thank Jenny and Luke for inspiring some great conversations. A special thanks goes to Brian Bellott for being a rock star and a great friend. I could always count on him to serve as a sounding board for new ideas, to dish out random sports facts, and to be there whenever I needed a helping hand. I would also like to thank Mark, my undergraduate researcher; he is going to be an outstanding chemist.

Thanks to all of my collaborators: Navneet Kumar, Angel Yanguas-Gil, and Shaista Babar (Abelson Research Group), Art Schultz and Paula Piccoli (Intense Pulsed Neutron Source at ANL), Jeff Elam (Argonne National Lab), Dan McCalister (PG Research Foundation), Scott Schmucker (Lyding Research Group), Heinz Nakotte (Lujan Neutron

Scattering Center at LANL), Laura Gagliardi and Tanya Todorova (University of Geneva), and Maria Fortunato (Suslick Research Group).

Thanks to the facilities people that helped collect the data contained in this thesis. Scott Wilson and Teresa Wieckowska-Prussak acquired much of the X-ray data and always provided coffee and great conversation whenever I stopped by. After they retired, Danielle Gray collected the remaining data and solved many of my twinning issues. Thanks to Donnie in the glass shop for repairing broken glassware and making my crackpot ideas come to life. Thanks to Marie Keel for being so pleasant and allowing my samples to occasionally slide when my CHN weights were slightly over 3 mg. Thanks to Steve Mullen for collecting my mass spectrometry data and Feng Lin and Paul Molitor for their assistance on the NMR spectrometers. A special thanks goes to Vera Mainz for her kindness, patience, and dedication. I wish her all the best in her upcoming retirement.

I would like to thank my friends at Illinois, and beyond, for the great memories. Included among those are the secretaries Connie Knight, Beth Myler, Theresa Struss, and Sandy Pijanowski. Their warm smiles and amusing conversations were always welcoming and I would not have survived without their ability to wrangle in the paperwork necessary to complete a PhD. I would like to thank the members of my softball team, Six-Fold Screw Axis, including those who suffered through the utter destruction that we now refer to as “our first season”. Softball was a great outlet, and the beers and conversation that followed were even better.

I thank my father and mother, Jim and Angela Daly, for a lifetime of love and inspiration. I also thank them for always supporting my ambitions, being brave enough to sign the papers that allowed me to go explore the world., and for teaching me that dedication, perseverance, and hard-work are the principal components of success. I thank my brothers,

Robert and Richard, my grandma, and all my aunts, uncles, and cousins for supporting my efforts over the years. I also thank my future in-laws, Larry and Jane Vahle, and Stephanie for embracing me as a member of their family.

Finally, I would like to thank Carin, my future wife, for the love, support, and sacrifices that made this all possible. I thank her for supporting and encouraging my decision to quit a great paying job at Mack's parts distribution warehouse to pursue a chemistry degree, when others clearly thought that I had lost my mind. I thank her for supporting my decision to pursue a PhD degree at the University of Illinois, even though we would be living over two hours apart. I thank her for saying "yes" when I proposed to her with a diamond made out of "chemistry Legos" – her fitting description of molecular modeling kits. I thank her for all of the weekends spent traveling, all of the hours spent sitting on the couch by my side as I worked, and for the years on unyielding dedication, love, and devotion. Carin, my love, this is for you.

TABLE OF CONTENTS

CHAPTER 1. Volatility as it Applies to Chemical Vapor Deposition: A Review of Chemical Factors and Mechanisms that Influence the Volatility of Molecules

Introduction

Thin film deposition is an important process used in the manufacturing of microelectronics[1-6] and hard coatings.[7-12] The most widely used processes to deposit thin films are physical vapor deposition (PVD) methods such as evaporation or sputtering. One of the major limitations of PVD, however, is its line of site nature, which makes it difficult or impossible to grow conformal (i.e., uniformly thick) films on substrates bearing relief features with aspect ratios greater than ~7:1.[6, 13] The line-of-sight character can be attributed to the high reactivity of the atomic species generated by the PVD process, which adhere with near-unity probability upon contact with a substrate. As a result, atomic species are unable to reach the deeper parts of recessed features, because they will be consumed by encounters with parts of the feature that are less deep; similarly, features that project above the surface will generate "shadows" will film growth will be sparse or absent. Another way to state this result is PVD generates growth species with high surface reaction probabilities, β, whereas conformal growth requires small values of β, so that the growth species can repeatedly adsorb and desorb before depositing on the substrate. In other words, growth species with small surface reaction probabilities can reach even the deeper parts of recessed features, so that the rate of film growth will be constant or near-constant everywhere on the surface.[14]

In contrast to PVD, chemical vapor deposition (CVD)[15-17] and atomic layer deposition (ALD)[17-20] utilize molecular precursors that undergo chemical reactions on the surface to effect thin film growth (Figure 1.1). In these processes, passage of the molecular precursor over a heated substrate induces chemical decomposition of the precursor, and under

favorable conditions a useful thin film results. Co-reactants can also be used in these processes to help induce nucleation,[21] tune the film's composition, or control the film conformality.[22, 23] For molecular precursors, the surface reaction probability β, which is a function of temperature and the chemical nature of the surface and the precursor, can vary from 1 down to values of 0.001 and even lower. As a result, CVD and ALD are not line of sight techniques, and they give films that are much more highly conformal than PVD methods.

The ALD process relies on "self-limiting" growth and consists of the following steps: 1) Addition into the sample chamber of a precursor that reacts with the surface. 2) Purging the excess precursor gas from the chamber, leaving the surface covered with approximately a monolayer of reacted precursor. 3) Addition to the chamber of a second precursor, a co-reactant, which reacts with the first adsorbed species, producing the desired film. 4) Purging of the excess co-reactant from the chamber. The cycle is repeated until the desired film thickness is achieved (Figure 1.2).[24]

Even for molecular precursors, however, conformal growth is not always possible. If the vapor pressure of the precursor is low, the precursor will be consumed quickly as it diffuses into a recessed feature, and below a certain depth, little or no precursor will be present to grow a film. Many precursors currently used for CVD do not meet these volatility requirements for conformal growth.[25]

Therefore, key to the development of successful CVD and ALD processes is the identification of highly volatile precursors. Volatility is defined as how readily a substance can undergo a physical transformation from a solid to a gas (sublimation) or a liquid to a gas (vaporization).

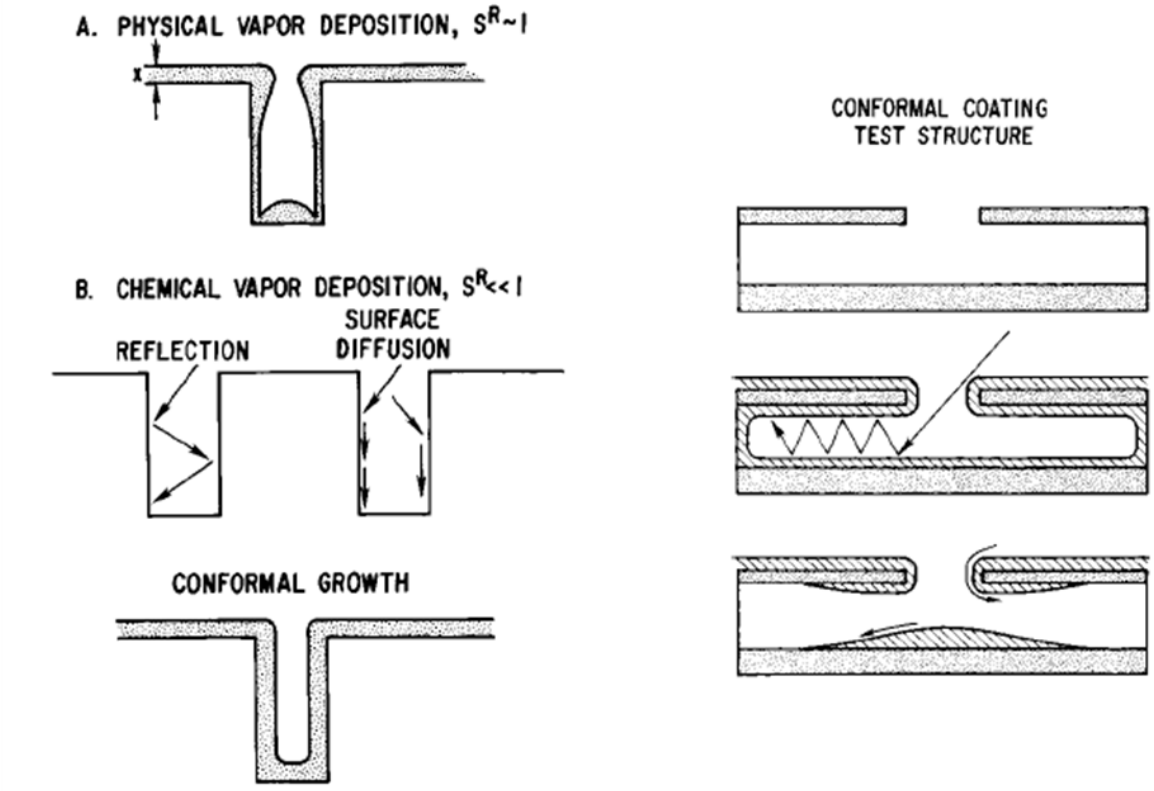

Figure 1.1. Schematic comparison of the PVD and CVD processes. The reactive species used in PVD processes have high reaction probabilities resulting in non-conformal growth for substrates with high aspect ratios (Top left (A) and bottom right). CVD is better suited for conformal growth because precursors are less reactive and have lower reaction probabilities (Bottom left (B) and middle right).[14]

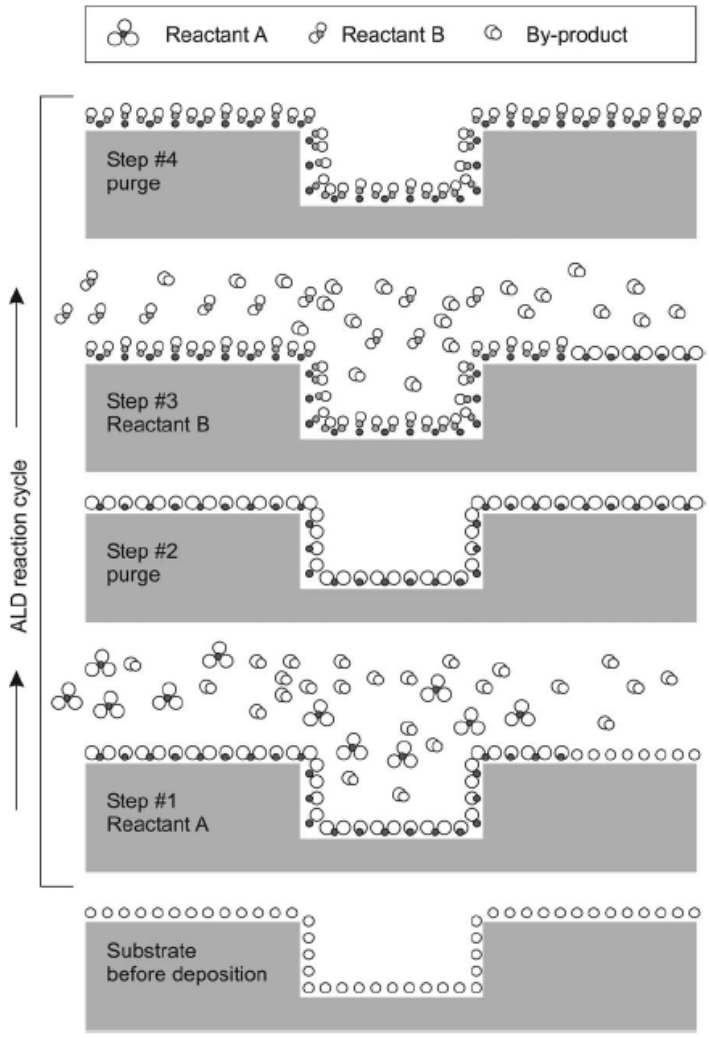

Figure 1.2. Schematic representation of the ALD process.[24]

A review of chemical factors that impact molecular volatility would be useful to direct the design of new CVD precursors with increased vapor pressures. This review is written with applications to neutral, metal-organic complexes in mind, because molecules with these characteristics are the precursors that show the greatest utility for modern CVD and ALD applications. The influence of metal-ligand bonding on volatility will not be discussed here, because correlations and generalities are more difficult to identify for a diverse range of metal and ligand types; other papers have, however, explored this topic.[26] Much of what we know about volatility is derived from studies of organic complexes and binary metal systems, but as will be shown here, many of the relationships and correlations can be usefully applied to metal-organic complexes.

It is important to point out the distinction between vapor pressure (which is a thermodynamic property) and volatilization rate (which is a kinetic property). For molecular species, there generally is a correlation between the lattice binding energy and the activation energy for volatilization: if the vapor pressure is high, generally the vaporization rate will be high too. But for condensed phases that must depolymerize to form the gas, the depolymerization process may be very slow. An example would be the volatilization of Teflon; although the monomer C_2F_4 is highly volatile, temperatures of 300 °C or higher are required to depolymerize the polymer.[27, 28] The majority of this review is dedicated to thermodynamic aspects that control volatility, but the impact of intermolecular bonding (as observed in Teflon) is typically kinetic in nature and will be discussed in terms of rate.

Intermolecular Interactions

Volatilization necessarily converts a solid or liquid material into molecular species, because only the latter are able to enter the gas phase. This is true even if the gas phase

species is not present as such in the condensed (solid or liquid) state; for example, the condensed state may consist of oligomers or polymers of the species present in the gas. Indeed, in some cases, even more complex chemical rearrangements may attend the conversion of a solid or liquid to a gas, a phenomenon that we will consider in more detail below. Fortunately, we can reduce these complexities to a simple question: given the gas phase species formed, what are the energies involved in binding it to others in the condensed phase? We will refer to these energies as the "intermolecular interactions." Although many factors affect the volatility of a given substance, the most important are the strengths of these interactions.

We point out for the sake of completeness that, in some cases, the volatilization of a substance forms two or more different gas phase species. We will not treat this possibility explicitly, but the factors delineated below will apply with equal force.

The volatility of a given molecule depends on the ability of the molecule to free itself from intermolecular interactions in the condensed state. Therefore, minimizing these interactions is the most direct way to increase the volatility. It is convenient to classify intermolecular interactions into two broad categories: intermolecular forces, which include weak or non-bonding interactions, and intermolecular bonding, which includes covalent and ionic bonding in oligomeric and polymeric structures. Generally, intermolecular interactions occur at distances equal to or larger than the sum of the van der Waals radii of the atoms or chemical groups involved, whereas intermolecular bonding occurs at distances less than this sum. Specific contributions to these classes of interactions will be discussed in the following sections.

Intermolecular Forces. Intermolecular forces are the attractive forces that arise from electronic dipoles that interact over distances larger than those characteristic of ionic or covalent bonds.[29] The dipoles can be permanent due to polarized chemical bonds, such as those observed for hydrogen bonds and Keesom interactions (also known as dipole-dipole interactions), or induced dipoles, such as those observed for London dispersion forces. The weakest intermolecular forces are London dispersion forces because of the fleeting lifetime of the induced dipole. The relative strength of the attractive intermolecular forces increases as the strength of the dipole increases. The attractive forces are offset by the repulsive force, which arises from the Coulombic and Pauli repulsions generated by the electrons as two atoms approach one another.[30]

In the condensed phase structure the attractive and repulsive forces are balanced. But because the repulsive forces weaken much more quickly than the attractive forces as the interatomic or intermolecular distances are increased, it takes energy to pull the molecules apart. This dependence of intermolecular interation on distance is often explained using the Lennard-Jones potential.[31, 32] The interaction energy comprises the short-range repulsive force, which has an r^{-12} dependence on interatomic distance, and the attractive force, which has a dependence of r^{-6}. The minima on the potential energy surface lies where the two forces offset.

The strength of intermolecular interactions between two molecules depends on the number and nature of each interaction, which can be rationalized by considering the overall size of the molecule and the types of functional groups present. For instance, straight-chain alkanes have intermolecular interactions that are dominated by London-dispersion forces, and their standard vaporization enthalpies $\Delta H°$(vap) show a linear dependence on the number

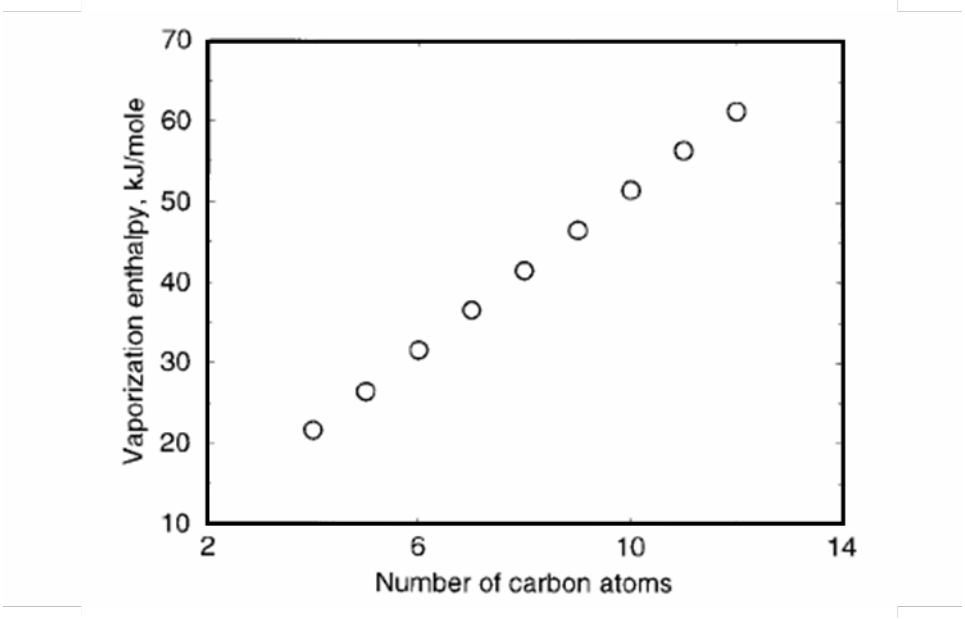

Figure 1.3. Standard vaporization enthalpies, $\Delta H°(\text{vap})$, of normal alkanes C_nH_{2n+2}.[33]

of carbon atoms in the alkane, with $\Delta H°$(vap) increasing ~4.9 kJ mol^{-1} for each additional methylene group (Figure 1.3).[33] Molecules with highly polarized bonds can affect volatility much more dramatically. The classic example is H_2O, which exhibits strong hydrogen bonding between the hydrogen (δ^+) and oxygen atoms (δ^-). Consequently, H_2O exhibits a boiling point of 100 °C. For comparison, H_2S and NH_3, which engage only weakly in hydrogen bonding, have much lower boiling points of -60.3 and -33.3 °C, respectively.

Overall, the local intermolecular interactions for parts of molecules can often be added together to give an estimate of the lattice binding energy for the entire molecule. This additive approach has led to methods that assign energy values to various interactions based on statistical analyses of empirical data.[34, 35] The data can then be used to predict the thermodynamic parameters of other organic molecules. Large molecules generally have larger lattice binding energies than small molecules because of the increased number of intermolecular interactions.[33] This fact is often misrepresented by suggestions that volatility is a direct consequence of molecular weight, as if a "heavier" molecule will perforce be less volatile than a lighter molecule.[36] Actually, there are many counterexamples to this misconception. For example, the lanthanides increase in mass across the series from La (138.91 amu) to Lu (174.97 amu), yet isostructural Cp_3Ln complexes (where Cp = cyclopentadienyl) *increase* in volatility across the series.[37] The same volatility trend is observed for almost all volatile lanthanide complexes, including those that will be presented here (Chapter 4).[38] In another example, the volatility of homologous d^0 metal diketonates (Al, Sc, and Ga) increase with increasing molecular weight whereas the analogues d^n complexes (Cr, Fe, Co), do not conform to this trend (Figure 1.4).[39] Structural investigations reveal that

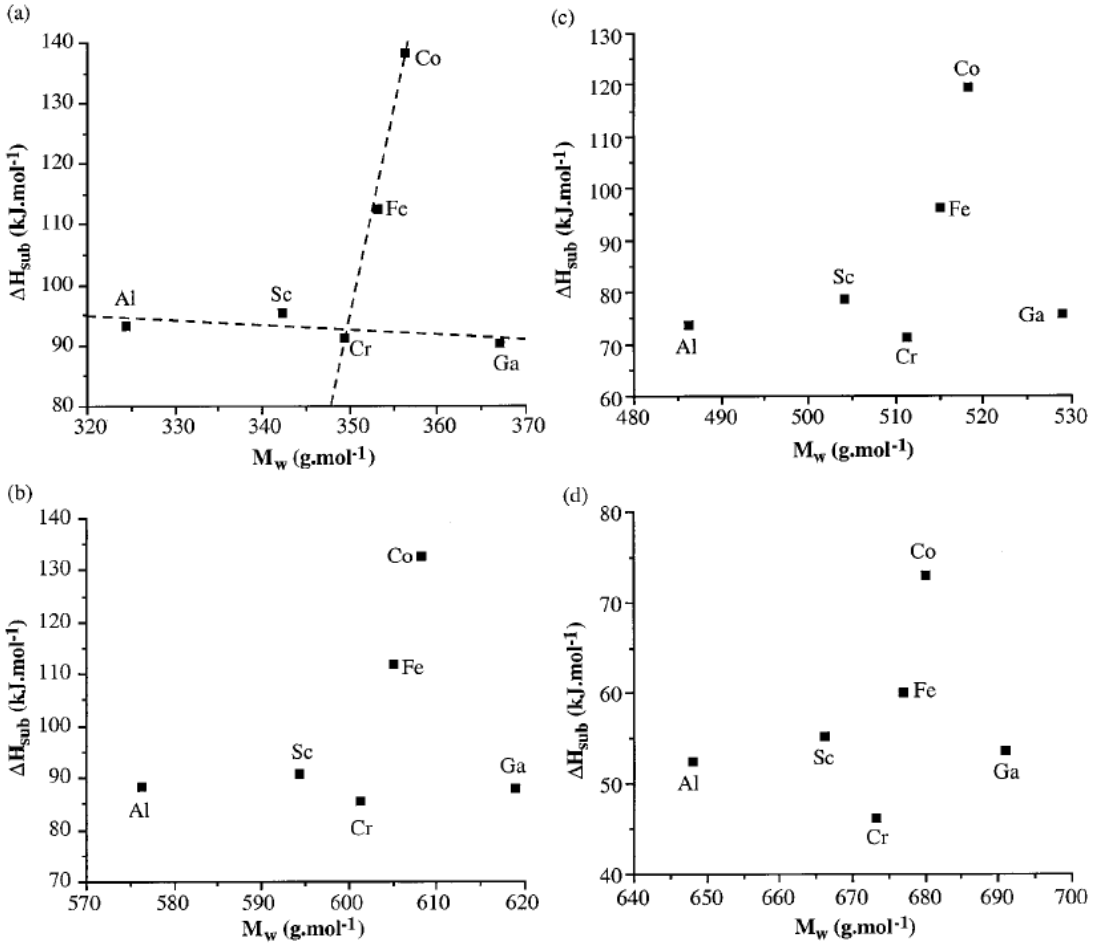

Figure 1.4. Plot of ΔH(sub) versus molecular weight for (a) $M(acac)_3$, (b) $M(tmhd)_3$, (c) $M(tfac)_3$ and (d) $M(hfac)_3$ complexes.[39]

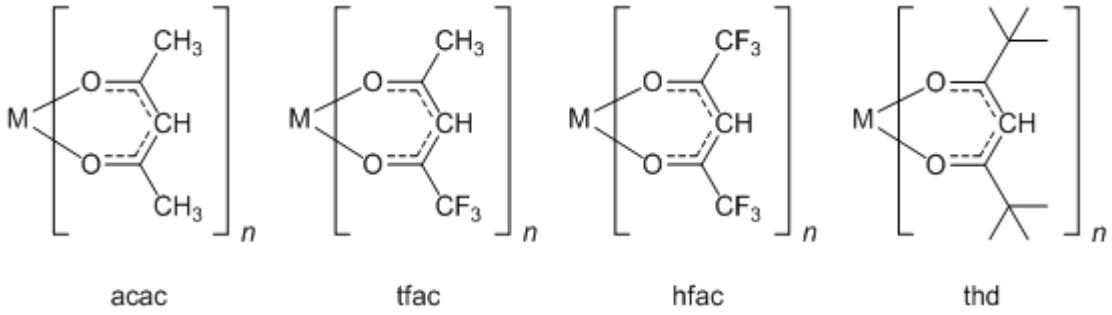

Scheme 1.1. Comparison of various β-diketonates discussed in this review.

the Fe and Co complexes, which have the highest ΔH(sub) values, have stronger intermolecular interactions than Al, Sc, Ga, and Cr, accounting for the decreased volatility.[39]

Crystal packing and lattice energies. The crystal packing of solids can increase the net strength of intermolecular interactions. The attractive forces that an atom experiences arise from *all* interactions, and extend beyond the closest neighboring atoms.[33] Therefore, efficient crystal packing can lead to a higher lattice energy because of the increased density of atoms (i.e., increased attractive forces) within a given volume. As the number of atoms (and attractive intermolecular forces) increase, the molecules pack closer together because a stronger repulsive force is necessary to offset the stronger attractive forces. For example, the H···H contacts in crystals of aromatic hydrocarbons decrease as the number of carbon atoms in the hydrocarbon increases, from 2.6 Å for benzene, C_6H_6, to 2.1 Å for the "superbenzene" kekulene, $C_{46}H_{24}$, which consists of a flat toroid of 12 fused benzene rings. For comparison, the van der Waals diameter for hydrogen is 2.4 Å.[33] The packing coefficient, which is the volume ratio of atoms to available space in the lattice, correspondingly increases as the H···H contact distances decrease, from 0.65 for benzene to 0.76 for kekulene.[33]

Atom-atom pair potentials. A powerful method that gives insight into atom-dependent intermolecular interactions is the calculation of atom-atom pair potentials.[40] The method uses empirical[41] or theoretical data[42] for intermolecular atom-atom interactions to generate a potential energy plot for each atom-atom interaction as a function of internuclear distance. The method has been used to determine the stabilization energy of different atomic interactions in crystals, specifically as the internuclear distances change. However, the plots also provide a qualitative estimation of which atom-atom interactions are the least stabilizing

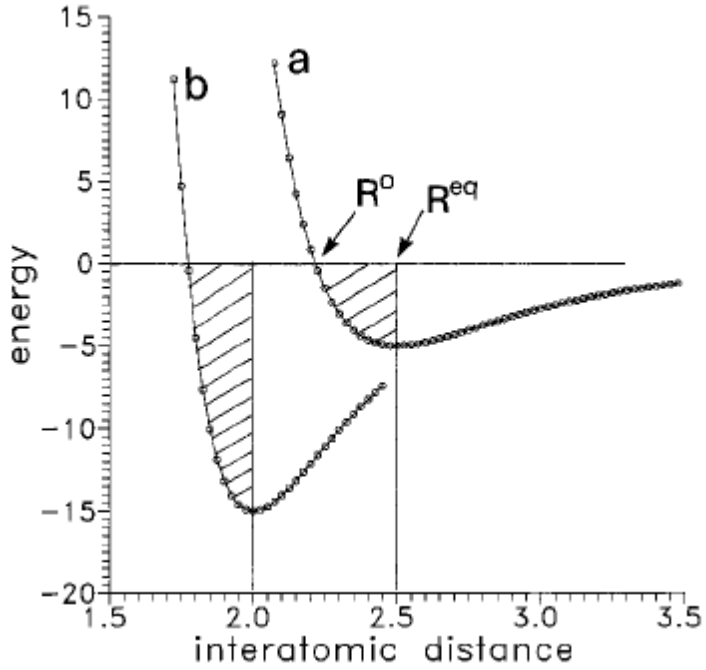

type	depth (J mol^{-1})	R^{eq}	R^{o}	R^{vdW}
H···H	42	3.36	2.98	2.4
H···C	205	3.29	2.92	2.9
H···O	506	2.80	2.48	2.6
C···C	389	3.89	3.45	3.4
N···N	628	3.70	3.28	3.0
O···O	335	3.61	3.20	2.8
F···F	293	3.20	2.84	2.7
S···S	1862	3.83	3.39	3.7
Cl···Cl	1004	3.83	3.39	3.6

Figure 1.5. Top: Typical non-bonded atom-atom curves (distances and energies in arbitrary units): (a) shallow minimum; (b) deep minimum. Bottom: Associated table of atom-atom potentials and interatomic distances.[33]

energetically, which is useful for determining interactions that are favorable for enhancing volatility.

Figure 1.5 shows some of the calculated atom-atom potential well depths for various intermolecular interactions. The H···H interactions have the shallowest energy wells at 42 J mol^{-1}, which is attributed to the lack of polarizability of the small hydrogen atoms. The H···C and F···F interactions are the next lowest in energy at 205 and 293 J mol^{-1}, respectively. The minima for H···H interactions in atom-atom potential curves lie in shallow energy wells, which become deeper as the strength of the interaction increases upon changing the atoms involved (Figure 1.5). The atom-atom potential method has until recently been used exclusively for organic molecules; it is now being used to calculate lattice energies for metal-organic species such as palladium chelates.[43-46]

Intermolecular Bonding. Intermolecular bonds are chemical bonds between molecular or atomic units that yield oligomeric or polymeric structures. These types of interactions can have deleterious effects on volatility, often inhibiting the sublimation altogether because of the high strength of chemical bonds relative to intermolecular forces. Despite the strong chemical bonds, it is possible to volatilize many substances with polymeric structures. These systems rely on one of two mechanisms that precede vaporization: (1) structural rearrangement to yield smaller monomeric or oligomeric units that are more easily volatilized or (2) chemical dissociation.[47, 48] In many cases, the energy required to induce these preceding mechanisms dictates the energy necessary for sublimation. Sublimation in these systems is controlled by the kinetics of the associated transformation.

Sublimation studies performed on crystalline arsenic provide an excellent example of the structural rearrangement necessary to sublime polymeric structures.[49, 50] Grey arsenic, which has a layered structure reminiscent of graphite, rearranges to yellow arsenic, As_4,

which is the volatile species responsible for sublimation. Carefully controlled experiments show that sublimation rates from the (111) crystal face was five to six orders of magnitude slower than from polycrystalline arsenic. These findings suggest that structural rearrangement was controlling the activation energy necessary for vaporization. Structural defects in polycrystalline arsenic helps to promote the structural rearrangement, which was eventually observed for the (111) crystal sample: the rate of evaporation increased over time as the dislocation density in the crystal increased. Interestingly, the evaporation rate can be increased dramatically if thallium is placed in contact with the surface of the crystal face; the increased rate is attributed to thallium catalyzing the structural rearrangement of the As polymer to As_4.[49]

An archetypal example of dissociation during vaporization is ammonium chloride, which dissociates into the gaseous species NH_3 and HCl.[47] The two molecules then recombine upon cooling to reform NH_4Cl. Similarly, it has been shown that the volatile species for CdS are Cd and S_2. The general reaction can be written as:[47]

$$AB(solid) \rightarrow A(vap) + {}^{1}/_{x}\, B_x(vap)$$

Because the process is dissociative, the stochiometry of the material can change during the process due to uneven evaporation of the two components. NH_4Cl and CdS sublime congruently (maintaining stochiometry) whereas materials such as GaAs are non-congruent, as evidenced by the formation of drops of Ga on the surface of sublimed GaAs crystals.[51] Rates of dissociative sublimation, as in cases of rearrangement-dependent sublimation, depend on the energy required to accomplish the preceding transformation event.

Volatility Studies of Metal-Organic Complexes

There have been few studies of the volatilities of metal-organic complexes compared to the large number of studies conducted for organic molecules.[45] The relative lack of such studies can be attributed to several factors. The functional groups found in organic molecules are limited to a handful of atoms (C, H, N, O, etc…) that have relatively consistent properties, whereas physical properties arising from metal-ligand relationships are more difficult to predict because of the wider variety of atomic interactions present. Computational efforts to probe volatility-structure relationships are also more taxing for metal-containing species due to the larger basis sets required, although the advent of faster computers is beginning to alleviate this problem.[45]

Using the small number of studies available, and empirical correlations, we will now point out methods that have been effective for increasing the volatility of metal-organic complexes.

Ligand substituents: the fluorine effect. The incorporation of fluorine into ligands is a common way to increase the volatility of metal complexes. This approach has been used with great success for metal β-diketonates.[38, 52] For instance, a comparison of $M(acac)_n$, $M(tfac)_n$, and $M(hfac)_n$ complexes (Scheme 1.1) shows a clear and sequential increase in volatility as the methyl groups (acac = acetylacetonato) are replaced with CF_3 groups, regardless of the oxidation states of the metal (Figure 1.6).[39] Similar results are observed for lanthanide hfac complexes.[38] The increased volatility of complexes with fluorinated ligands is attributed to two effects: increased intermolecular repulsive forces that arise from the increased negative charge on fluorine owing to its high electronegativity, and fluorine's low polarizability.[53] It should be pointed out that the substitution of fluorine for hydrogen greatly

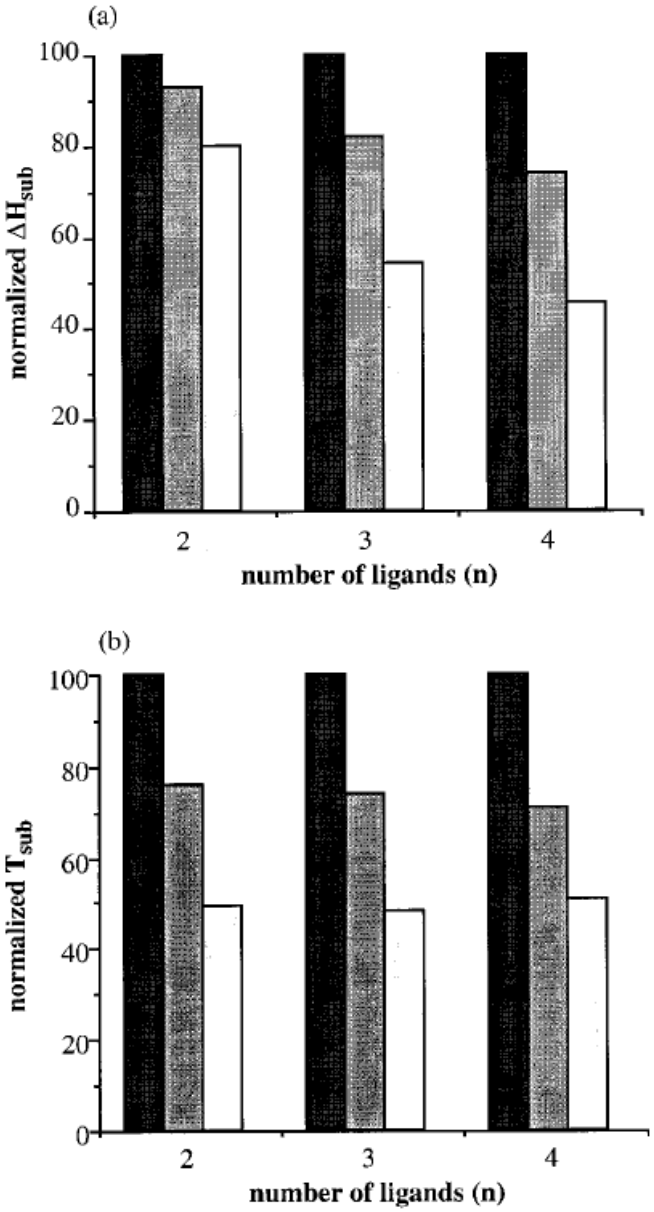

Figure 1.6. Plot of relative (a) ΔH(sub) and (b) T(sub), normalized to M(acac)$_n$, versus the number of β-diketonate ligands (n); acac (■), tfac (■), and hfac (□).[39]

increases the molecular weight of the resulting complex but often increases the volatility, thus providing another counterexample to the common misconception that molecular weight and volatility are directly correlated.

Some substituents other than fluorine also seem to enhance the repulsive interactions that lead to increased volatility. It has been suggested that the enhanced volatility observed for alkaline earth β-diketiminates with NMe_2 substituted for *i*-Pr groups can be attributed to increased intermolecular repulsions due to a fluorine-type effect (Scheme 1.2).[54, 55] Borohydride ligands also exhibit similar effects (see below).

Ligand substituents: disruption of efficient crystal packing. Breaking the symmetry of metal complexes can be used to enhance volatility. Symmetric molecules often pack in crystal lattices more efficiently than asymmetric molecules, leading to increased interactions that decrease volatility. Aside from decreasing the intermolecular interactions, lowering the symmetry slightly destabilizes the molecule in the condensed state due to the entropic penalty paid when the additional degrees of freedom are lost by ordering the molecule in a lattice. To be effective, the total energy gained by lowering the symmetry must be greater than the extra intermolecular interactions that attend an increased number of atoms.

Ligand modification is the easiest way to disrupt the symmetry of a metal complex. Alkyl groups are often used for this purpose because they possess the weakest intermolecular interactions,[36, 56] although other substituents have been used with similar success.[57] A good illustration of the concept is provided by the volatility of a series of modified $(C_5H_4R)_3Nd$ complexes (Figure 1.7).[58] Changing the Cp ring from C_5H_5 to C_5H_4Me decreases the sublimation temperature at 10^{-3} Torr from 220 °C to 200 °C. The temperature

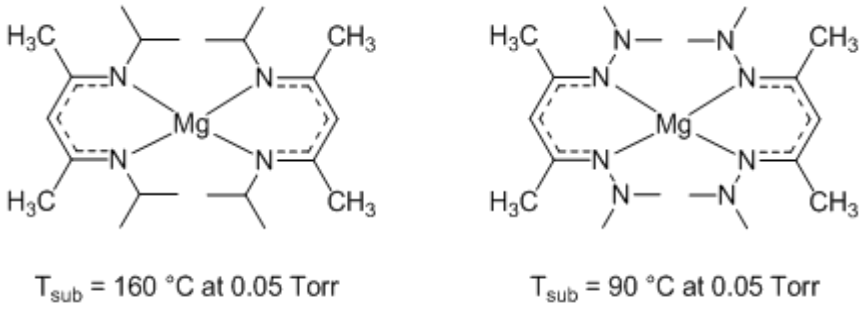

Scheme 1.2. Comparison of magnesium β-diketiminates. Substituting NMe_2 groups in place of the *i*Pr groups at the nitrogen positions increases volatility.[54]

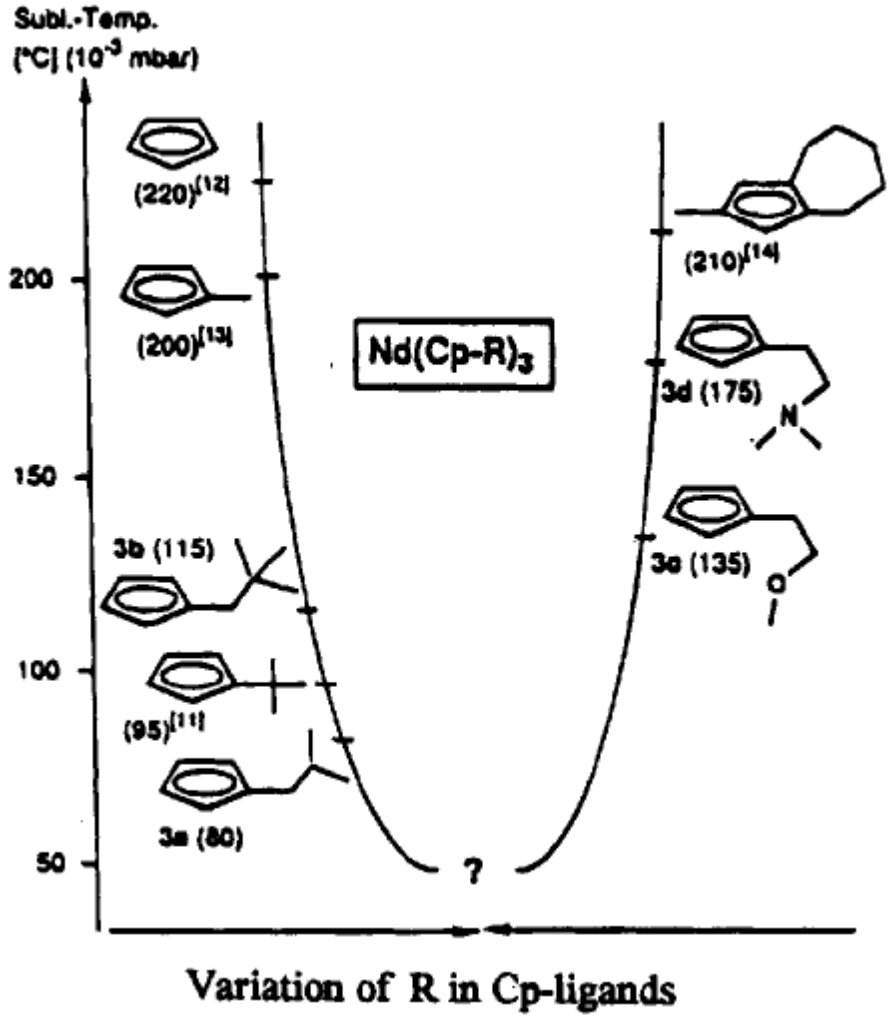

Figure 1.7. Sublimation temperatures for $Nd(C_5H_4\text{-}R)_3$ complexes as the R-group on the cyclopentadienyl rings is varied.[58]

drops more dramatically upon replacement of the methyl substituent with more flexible alkyl groups, such as *t*-Bu (95 °C) and *i*-Bu (80 °C).

Metal encapsulation: impedance of intermolecular bonding. Producing volatile complexes of large metals is problematic because open coordination sites often lead to polymeric and oligomeric structures. For metals with large radii, such as alkaline earth metals and lanthanides, polymerism can best be prevented by employing sterically bulky anionic groups, electrically neutral (often multidentate) ligands, or combinations of the two.[59] For example, $Ln(acac)_3$ complexes have polymeric structures and are not volatile, but $Ln(thd)_3$ complexes, which adopt monomeric and dimeric structures, sublime at relatively low temperatures.[60] The large *t*-Bu groups in thd, compared to the small methyl groups in acac, shield the metal and inhibit polymerization. The dimeric $Ln(thd)_3$ complexes (La-Gd) have sublimation enthalpies that are ~25 kJ mol^{-1} higher than the monomeric species (Tb-Lu), clearly demonstrating how increased intermolecular interactions can depress volatility.[61]

In other cases, the use of neutral, often multidentate, Lewis bases is highly effective for inhibiting polymerization. For example, chelating ethers can be used to fill gaps left by anionic ligands in the coordination spheres of large metals such as barium (Ba^{2+}).[62-65] Chelating ethers such as glymes are most effective for this purpose, but smaller, unidentate donors are typically lost under sublimation conditions.

As an example of combining the two approaches, β-ketoiminates ligands functionalized with ether linkages at the nitrogen position have been used to prepare monomeric alkaline earth and lanthanide complexes with volatilities high enough for chemical vapor deposition.[66-72] Similar modifications have been made to alkoxide,[73, 74] amidiniate,[75] guanidinate,[75] and cyclopentadienyl ligands.[58]

Borohydrides: the hydride effect. The high volatilities of borohydride complexes, particularly those of the tetrahydroborate ligand, BH_4^-, were first reported during the 1940s and 1950s by Schlesinger and Brown.[76, 77] Since that time, numerous reviews of metal tetrahydroborate complexes have been published;[78-80] but the factors responsible for their high volatility have not been thoroughly investigated. Analogies can be drawn, however, to effects observed for fluorine substituents. For instance, hydrogen, like fluorine, is not easily polarized because of its small size. Compared to C-H groups, the B-H groups in BH_4^- should have more electron density on the hydrogen atoms because of the greater electronegativity of hydrogen ($\chi_P = 2.20$) compared to boron ($\chi_P = 2.04$). For comparison, the electronegativity of carbon is 2.55. Calculations comparing the atomic charges in methane and BH_4^- vary greatly depending on the level of theory and the basis set used, but two trends are clearly observed: the hydrogen atoms in methane typically have a net positive charge, whereas the hydrogen atoms in BH_4^- typically carry a net negative charge.[81-84] For comparison, ab intio calculations directly comparing methane to fluorinated analogs, such as CF_4, also suggest that hydrogen atoms carry a positive charge whereas the fluorine atoms carry a negative charge.[85] As seen for fluorine, the increased electron density on the hydrides should result in greater repulsive interactions and may explain the high volatility observed for these complexes. The high repulsive energy of H···H interactions in $M(BH_4)_4$ complexes has been previously noted.[86] Calculated atom-atom pair potentials also suggest that the high volatility of homoleptic borohydride complexes can be attributed to the weakness of the H···H attractive forces.

Contents of Thesis

This thesis reports detailed investigation of the chemistry of aminodiboranates, a kind of chelating borohydride ligand that we have found is able to form a wide variety of new and interesting metal complexes. Many of the topics included in the present chapter will be addressed throughout the thesis, because one of our objectives was the discovery of highly volatile metal complexes useful as CVD and ALD precursors. Chapters 2 through 6 discuss efforts to use the *N*,*N*-dimethylaminodiboranate (DMADB) ligand to prepare volatile complexes of the largest metals: actinides, lanthanides, and barium. Chapter 7 focuses on the synthesis of new aminodiboranate ligands and chapter 8 details the use of the new ligands for the synthesis of metal complexes, some with improved volatility relative to those previously reported. Chapters 3 and 5 focus on the redox chemistry of DMADB with uranium, europium, and ytterbium. Finally, chapter 9 details the use of the volatile praseodymium complexes $Pr(H_3BNMe_2BH_3)_3$ and $Pr(thd)_3$ as carriers for ^{225}Ac. The deposition of ^{225}Ac-doped films by CVD is also described.

References

1. Cote, D. R.; Nguyen, S. V.; Cote, W. J.; Pennington, S. L.; Stamper, A. K.; Podlesnik, D. V. *IBM J. Res. Dev.* **1995,** *39*, 837-864.

2. Smith, R. C.; Ma, T.; Hoilien, N.; Tsung, L. Y.; Bevan, M. J.; Colombo, L.; Roberts, J.; Campbell, S. A.; Gladfelter, W. L. *Adv. Mater. Opt. Electron.* **2000,** *10*, 105-114.

3. Sung, J.; Goedde, D. M.; Girolami, G. S.; Abelson, J. R. *J. Appl. Phys.* **2002,** *91*, 3904-3911.

4. Leskelä, M.; Kukli, K.; Ritala, M. *J. Alloys Compd.* **2006,** *418*, 27-34.

5. Vasilev, V. Y.; Repinsky, S. M. *Russ. Chem. Rev.* **2005,** *74*, 413-441.

6. Rossnagel, S. M. *IBM J. Res. Dev.* **1999,** *43*, 163-179.

7. Sproul, W. D. *J. Vac. Sci. Technol., A* **1994,** *12*, 1595-1601.

8. Hauert, R.; Patscheider, J. *Adv. Eng. Mater.* **2000,** *2*, 247-259.

9. Jayaraman, S.; Gerbi, J. E.; Yang, Y.; Kim, D. Y.; Chatterjee, A.; Bellon, P.; Girolami, G. S.; Chevalier, J. P.; Abelson, J. R. *Surf. Coat. Technol.* **2006,** *200*, 6629-6633.

10. Chatterjee, A.; Jayaraman, S.; Gerbi, J. E.; Kumar, N.; Abelson, J. R.; Bellon, P.; Polycarpou, A. A.; Chevalier, J. P. *Surf. Coat. Technol.* **2006,** *201*, 4317-4322.

11. Chatterjee, A.; Kumar, N.; Abelson, J. R.; Bellon, P.; Polycarpou, A. A. *Wear* **2008,** *265*, 921-929.

12. Doll, G. L.; Mensah, B. A.; Mohseni, H.; Scharf, T. W. *J. Therm. Spray Technol.* **2010,** *19*, 510-516.

13. Rossnagel, S. M. *J. Vac. Sci. Technol., B* **1998,** *16*, 2585-2608.

14. Gates, S. M. *Chem. Rev.* **1996,** *96*, 1519-1532.

15. Hampden-Smith, M. J.; Kodas, T. T. *Chem. Vap. Deposition* **1995,** *1*, 8-23.

16. Jones, A. C.; Hitchman, M. L. *Chem. Vap. Deposition* **2009**, 1-36.

17. Crowell, J. E. *J. Vac. Sci. Technol., A* **2003,** *21*, S88-S95.

18. Leskela, M.; Ritala, M. *Angew. Chem., Int. Ed.* **2003,** *42*, 5548-5554.

19. George, S. M. *Chem. Rev.* **2010,** *110*, 111-131.

20. Choy, K. L. *ECS Trans.* **2009,** *25*, 59-65.

21. Kumar, N.; Yanguas-Gil, A.; Daly, S. R.; Girolami, G. S.; Abelson, J. R. *Appl. Phys. Lett.* **2009**, *95*, 144107/1-144107/3.

22. Kumar, N.; Yanguas-Gil, A.; Daly, S. R.; Girolami, G. S.; Abelson, J. R. *J. Am. Chem. Soc.* **2008,** *130*, 17660-17661.

23. Yanguas-Gil, A.; Kumar, N.; Yang, Y.; Abelson, J. R. *J. Vac. Sci. Technol., A* **2009,** *27*, 1244-1248.

24. Puurunen, R. L. *J. Appl. Phys.* **2005**, *97*, 121301/1-121301/52.

25. Yanguas-Gil, A.; Yang, Y.; Kumar, N.; Abelson, J. R. *J. Vac. Sci. Technol., A* **2009,** *27*, 1235-1243.

26. Ribeiro da Silva, M. D. M. C.; Goncalves, J. M.; Silva, A. L. R.; Oliveira, P. C. F. C.; Schroeder, B.; Ribeiro da Silva, M. A. V. *J. Mol. Catal. A: Chem.* **2004,** *224*, 207-212.

27. Seidel, W. C.; Scherer, K. V., Jr.; Cline, D., Jr.; Olson, A. H.; Bonesteel, J. K.; Church, D. F.; Nuggehalli, S.; Pryor, W. A. *Chem. Res. Toxicol.* **1991,** *4*, 229-236.

28. Ignatieva, L. N.; Tsvetnikov, A. K.; Gorbenko, O. N.; Kaidalova, T. A.; Buznik, V. M. *J. Struct. Chem.* **2004,** *45*, 786-792.

29. Karle, J.; Huang, L. *J. Mol. Struct.* **2003,** *647*, 9-16.

30. Gavezzotti, A. *Synlett* **2002**, 201-214.

31. Jones, J. R. *Proc. R. Soc. London, Ser. A* **1924,** *106*, 463-477.

32. Hirschfelder, J. O.; Curtis, C. F.; Bird, R. B. *Molecular Theory of Gases and Liquids*. Wiley: New York, 1964.

33. Dunitz, J. D.; Gavezzotti, A. *Acc. Chem. Res.* **1999,** *32*, 677-684.

34. Ouvrard, C.; Mitchell, J. B. O. *Acta Crystallogr., Sect. B: Struct. Sci.* **2003,** *B59*, 676-685.

35. Charlton, M. H.; Docherty, R.; Hutchings, M. G. *J. Chem. Soc., Perkin Trans. 2* **1995**, 2023-2030.

36. Gillan, E. G.; Bott, S. G.; Barron, A. R. *Chem. Mater.* **1997,** *9*, 796-806.

37. Birmingham, J. M.; Wilkinson, G. *J. Am. Chem. Soc.* **1956,** *78*, 42-44.

38. Richardson, M. F.; Sievers, R. E. *Inorg. Chem.* **1971,** *10*, 498-504.

39. Fahlman, B. D.; Barron, A. R. *Adv. Mater. Opt. Electron.* **2000,** *10*, 223-232.

40. Pertsin, A. J.; Kitaigorodsky, A. I. *The Atom-Atom Potential Method. Applications to Organic Molecular Solids*. Springer-Verlag: Berlin, 1987.

41. Filippini, G.; Gavezzotti, A. *Acta Crystallogr., Sect. B: Struct. Sci.* **1993,** *B49*, 868-880.

42. Dunitz, J. D.; Gavezzotti, A. *Chem. Soc. Rev.* **2009,** *38*, 2622-2633.

43. Zharkova, G. I.; Stabnikov, P. A.; Sysoev, S. A.; Igumenov, I. K. *J. Struct. Chem.* **2005,** *46*, 320-327.

44. Zharkova, G. I.; Baidina, I. A.; Stabnikov, P. A.; Igumenov, I. K. *J. Struct. Chem.* **2006,** *47*, 716-725.

45. Lousada, C. M.; Pinto, S. S.; Canongia Lopes, J. N.; Minas da Piedade, M. F.; Diogo, H. P.; Minas da Piedade, M. E. *J. Phys. Chem. A* **2008,** *112*, 2977-2987.

46. Prokuda, O. V.; Belosludov, V. R.; Igumenov, I. K.; Stabnikov, P. A. *J. Struct. Chem.* **2006,** *47*, 1032-1041.

47. Somorjai, G. A.; Lester, J. E. *Progr. Solid State Chem.* **1967,** *4*, 1-52.

48. Somorjai, G. A. *Science* **1968,** *162*, 755-760.

49. Brewer, L.; Kane, J. S. *J. Phys. Chem.* **1955,** *59*, 105-109.

50. Rosenblatt, G. M.; Lee, P.-K.; Dowell, M. B. *J. Chem. Phys.* **1966,** *45*, 3454-3455.

51. Lou, C. Y.; Somorjai, G. A. *J. Chem. Phys.* **1971,** *55*, 4554-4565.

52. Dilli, S.; Robards, K. *Aust. J. Chem.* **1979,** *32*, 277-284.

53. Samuels, J. A.; Folting, K.; Huffman, J. C.; Caulton, K. G. *Chem. Mater.* **1995,** *7*, 929-935.

54. Sedai, B.; Heeg, M. J.; Winter, C. H. *J. Organomet. Chem.* **2008,** *693*, 3495-3503.

55. Sedai, B.; Heeg, M. J.; Winter, C. H. *Organometallics* **2009,** *28*, 1032-1038.

56. Chen, T.; Xu, C.; Baum, T. H.; Stauf, G. T.; Roeder, J. F.; DiPasquale, A. G.; Rheingold, A. L. *Chem. Mater.* **2010,** *22*, 27-35.

57. Banger, K. K.; Ngo, S. C.; Higashiya, S.; Claessen, R. U.; Bousman, K. S.; Lim, P. N.; Toscano, P. J.; Welch, J. T. *J. Organomet. Chem.* **2003,** *678*, 15-32.

58. Gun'ko, Y. K.; Edelmann, F. T. *Comments Inorg. Chem.* **1997,** *19*, 153-184.

59. Aspinall, H. C. *Top. Appl. Phys.* **2007,** *106*, 53-72.

60. Eisentraut, K. J.; Sievers, R. E. *J. Am. Chem. Soc.* **1965,** *87*, 5254-5256.

61. Amano, R.; Sato, A.; Suzuki, S. *Bull. Chem. Soc. Jpn.* **1981,** *54*, 1368-1374.

62. Neumayer, D. A.; Studebaker, D. B.; Hinds, B. J.; Stern, C. L.; Marks, T. J. *Chem. Mater*. **1994,** *6*, 878-880.

63. Malandrino, G.; Fragala, I. L.; Neumayer, D. A.; Stern, C. L.; Hinds, B. J.; Marks, T. J. *J. Mater. Chem.* **1994,** *4*, 1061-1066.

64. Tiitta, M.; Niinisto, L. *Chem. Vap. Deposition* **1997,** *3*, 167-182.

65. Belot, J. A.; Neumayer, D. A.; Reedy, C. J.; Studebaker, D. B.; Hinds, B. J.; Stern, C. L.; Marks, T. J. *Chem. Mater*. **1997,** *9*, 1638-1648.

66. Schulz, D. L.; Hinds, B. J.; Stern, C. L.; Marks, T. J. *Inorg. Chem.* **1993,** *32*, 249-250.

67. Schulz, D. L.; Hinds, B. J.; Neumayer, D. A.; Stern, C. L.; Marks, T. J. *Chem. Mater.* **1993,** *5*, 1605-1617.

68. Neumayer, D. A.; Belot, J. A.; Feezel, R. L.; Reedy, C.; Stern, C. L.; Marks, T. J.; Liable-Sands, L. M.; Rheingold, A. L. *Inorg. Chem.* **1998,** *37*, 5625-5633.

69. Belot, J. A.; Wang, A.; McNeely, R. J.; Liable-Sands, L.; Rheingold, A. L.; Marks, T. J. *Chem. Vap. Deposition* **1999,** *5*, 65-69.

70. Matthews, J. S.; Just, O.; Obi-Johnson, B.; Rees, W. S., Jr. *Chem. Vap. Deposition* **2000,** *6*, 129-132.

71. Studebaker, D. B.; Neumayer, D. A.; Hinds, B. J.; Stern, C. L.; Marks, T. J. *Inorg. Chem.* **2000,** *39*, 3148-3157.

72. Edleman, N. L.; Wang, A.; Belot, J. A.; Metz, A. W.; Babcock, J. R.; Kawaoka, A. M.; Ni, J.; Metz, M. V.; Flaschenriem, C. J.; Stern, C. L.; Liable-Sands, L. M.; Rheingold, A. L.; Markworth, P. R.; Chang, R. P. H.; Chudzik, M. P.; Kannewurf, C. R.; Marks, T. J. *Inorg. Chem.* **2002,** *41*, 5005-5023.

73. Jones, A. C.; Aspinall, H. C.; Chalker, P. R.; Potter, R. J.; Manning, T. D.; Loo, Y. F.; O'Kane, R.; Gaskell, J. M.; Smith, L. M. *Chem. Vap. Deposition* **2006,** *12*, 83-98.

74. Chi, Y.; Ranjan, S.; Chou, T.-Y.; Liu, C.-S.; Peng, S.-M.; Lee, G.-H. *J. Chem. Soc., Dalton Trans.* **2001**, 2462-2466.

75. Edelmann, F. T. *Chem. Soc. Rev.* **2009,** *38*, 2253-2268.

76. Hoekstra, H. R.; Katz, J. J. *J. Am. Chem. Soc.* **1949,** *71*, 2488-2492.

77. Schlesinger, H. I.; Brown, H. C. *J. Am. Chem. Soc.* **1953,** *75*, 219-221.

78. Marks, T. J.; Kolb, J. R. *Chem. Rev.* **1977,** *77*, 263-293.

79. Makhaev, V. D. *Russ. Chem. Rev.* **2000,** *69*, 727-746.

80. Ephritikhine, M. *Chem. Rev.* **1997,** *97*, 2193-2242.

81. Hegstrom, R. A.; Palke, W. E.; Lipscomb, W. N. *J. Chem. Phys.* **1967,** *46*, 920-922.

82. Galvez-Ruiz, J. C.; Sanchez, M. *Theochem* **2009,** *908*, 114-116.

83. De Proft, F.; Martin, J. M. L.; Geerlings, P. *Chem. Phys. Lett.* **1996,** *250*, 393-401.

84. Arliguie, T.; Belkhiri, L.; Bouaoud, S.-E.; Thuery, P.; Villiers, C.; Boucekkine, A.; Ephritikhine, M. *Inorg. Chem.* **2009,** *48*, 221-230.

85. Cooper, D. L.; Wright, S. C.; Allan, N. L.; Winterton, N. *J. Fluorine Chem.* **1990,** *47*, 489-507.

86. Haaland, A.; Shorokhov, D. J.; Tutukin, A. V.; Volden, H. V.; Swang, O.; McGrady, G. S.; Kaltsoyannis, N.; Downs, A. J.; Tang, C. Y.; Turner, J. F. C. *Inorg. Chem.* **2002,** *41*, 6646-6655.

CHAPTER 2. Synthesis and Properties of the First Fifteen Coordinate Complex. X-ray Diffraction, Neutron Diffraction, and Decomposition Studies of the Thorium Aminodiboranate $Th(H_3BNMe_2BH_3)_4$

Introduction[1]

The concept of coordination number is extremely useful and widely employed to describe the local chemical environments of atoms in matter. Originally defined by Alfred Werner in 1893,[2] the coordination number is closely tied to many other important properties such as atomic radius,[3-5] molecular and electronic structure,[6-8] and chemical reactivity.[9-11] An important modification of Werner's concept was the recognition that, for certain ligands such as ethylene, two linked atoms jointly occupy a single coordination site.[12] This modified definition is widely used to describe both transition metal (d-block) and inner transition metal (f-block) complexes.[13] In essence, this modified definition considers the coordination number to be equal to the number of two electron bonds that the central atom forms with its ligands.

The modified Werner definition of coordination number serves extremely well for molecular species, but it is often less applicable to metallic and purely ionic materials, which typically lack readily identifiable coordinating groups. In such cases, other definitions have been proposed, one being the number of nearby atoms that define the Voronoi-Dirichlet polyhedron, the domain of space in which all points are closer to the atom of interest than to any other.[14-16] This Frank-Kasper definition affords coordination numbers that sometimes are larger than seems warranted, and various alternative schemes have been devised, including some that result in coordination numbers that are non-integral.[17-24]

An interesting question is: what are the largest and smallest possible coordination numbers? Here we will focus on the transition metals (d-block) and the inner transition metals (f-block). For these elements, a coordination number of zero is possible in the gas phase (e.g., mercury vapor). In the condensed state, the smallest coordination number seen to date is two, for which many examples are known.[25] Less well established is how large a coordination number is possible.[26] This question has recently been considered theoretically, and the 15-coordinate ion $PbHe_{15}^{2+}$ has been predicted to be a bound species.[27] From a first principles perspective, we might expect that the highest possible coordination number is 16, because this is the largest number of valence orbitals that an atom can have: one s-orbital, three p-oribitals, five d-orbitals, and seven f-orbitals. This analysis suggests that the highest coordination numbers should be seen for lanthanide and actinide elements, and indeed this is the case. The formation of complexes with high-coordination number complexes should be facilitated by the fact that these elements have some of the largest radii in the entire periodic table.

We can also address the question of the highest coordination number from an experimental perspective and, as suggested in the previous paragraph, complexes of the f-elements feature prominently. But first we need to distinguish between the number of metal-ligand contacts, and the number of two-electron metal-ligand bonds. Thus, the metal atoms in the complexes tetrakis(cyclopentadienyl)uranium, UCp_4, and its thorium analog $ThCp_4$ each are connected to 20 atoms,[28, 29] but the Werner coordination number of 12 (counting π bonds as occupying one site) is widely acknowledged to be more appropriate to describe the metal-ligand bonding in these compounds.[30]

Very high Werner coordination numbers are seen for metal complexes of the borohydride anion BH_4^-,[31, 32] which can coordinate to a single metal by as many as three

hydrogen atoms. From an electronic perspective, each B-H-M interaction involves a separate electron pair,[9, 33] and each B-H-M interaction can therefore be considered as a separate bond. Accordingly, $Zr(BH_4)_4$,[34-36] $Hf(BH_4)_4$,[34, 35, 37] $Np(BH_4)_4$,[38] and $Pu(BH_4)_4$,[38] all have coordination numbers of twelve, and $Th(BH_4)_4$,[34, 35] $Pa(BH_4)_4$,[38] and $U(BH_4)_4$,[39, 40] all of which are polymers in the solid state, have coordination numbers of 14. Some derivatives of these compounds also have high coordination numbers, such as the 14-coordinate tetrahydrofuran complex $U(BH_4)_4(thf)_2$.[41-43] No complex of any kind, however, has been definitively shown to adopt a Werner coordination number of 15.[35, 44]

We now report the synthesis, single-crystal X-ray and neutron diffraction studies, and DFT investigations of the first 15-coordinate complex. DFT calculations suggest that it may adopt a 16-coordinate structure in the gas phase. This compound extends our recent studies of a new class of chelating borohydride ligands, the aminodiboranates.[45, 46]

Results and Discussion

Synthesis and structure of $Th(H_3BNMe_2BH_3)_4$. The reaction $ThCl_4$ with 4 equiv of sodium *N*,*N*-dimethylaminodiboranate, $Na(H_3BNMe_2BH_3)$, in tetrahydrofuran produces $Th(H_3BNMe_2BH_3)_4$ (**1**), which can be isolated as colorless prisms by crystallization from diethyl ether. The IR spectrum of **1** contains strong bands at 2420 cm^{-1} due to terminal B-H stretches, and at 2264 and 2208 cm^{-1} due to bridging B-H···Th stretches. For comparison, $Th(BH_4)_4$ contains a strong terminal B-H band at 2530 cm^{-1} and bridging B-H-M bands at 2270, 2200, and 2100 cm^{-1}. The ^1H NMR spectrum of **1** in C_6D_6 at 20 °C contains peaks at δ 2.11 (s, NMe_2) and δ 4.23 (br 1:1:1:1 q, J_{BH} = 90 Hz, BH_3); the terminal and bridging B-H units are thus exchanging rapidly on the NMR time scale. The ^{11}B NMR spectrum consists of a binomial quartet at δ -2.75 due to coupling of the ^{11}B nuclei with the three rapidly

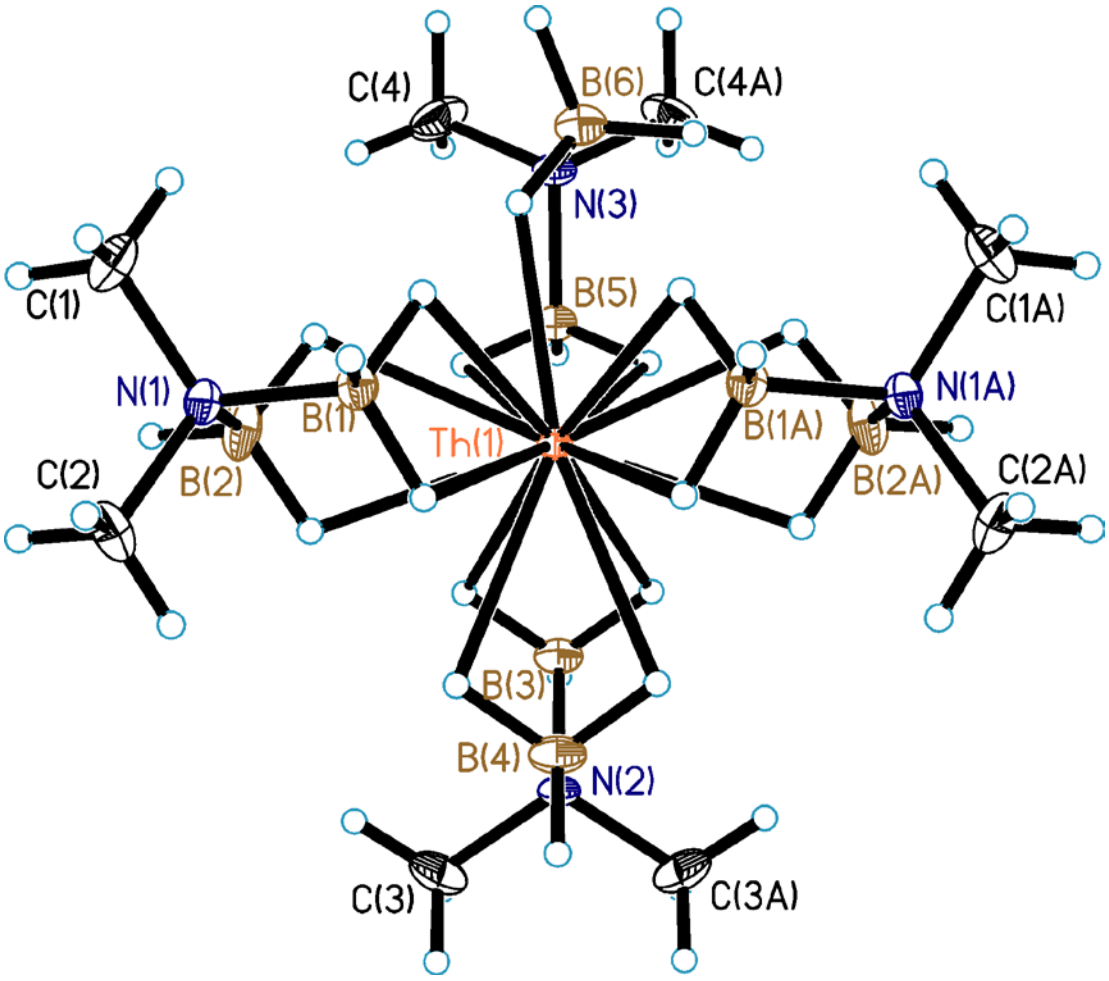

Figure 2.1. Molecular structure of $Th(H_3BNMe_2BH_3)_4$, **1** from X-ray data. Ellipsoids are drawn at the 35% probability level, except for hydrogen atoms, which are represented as arbitrarily-sized spheres.

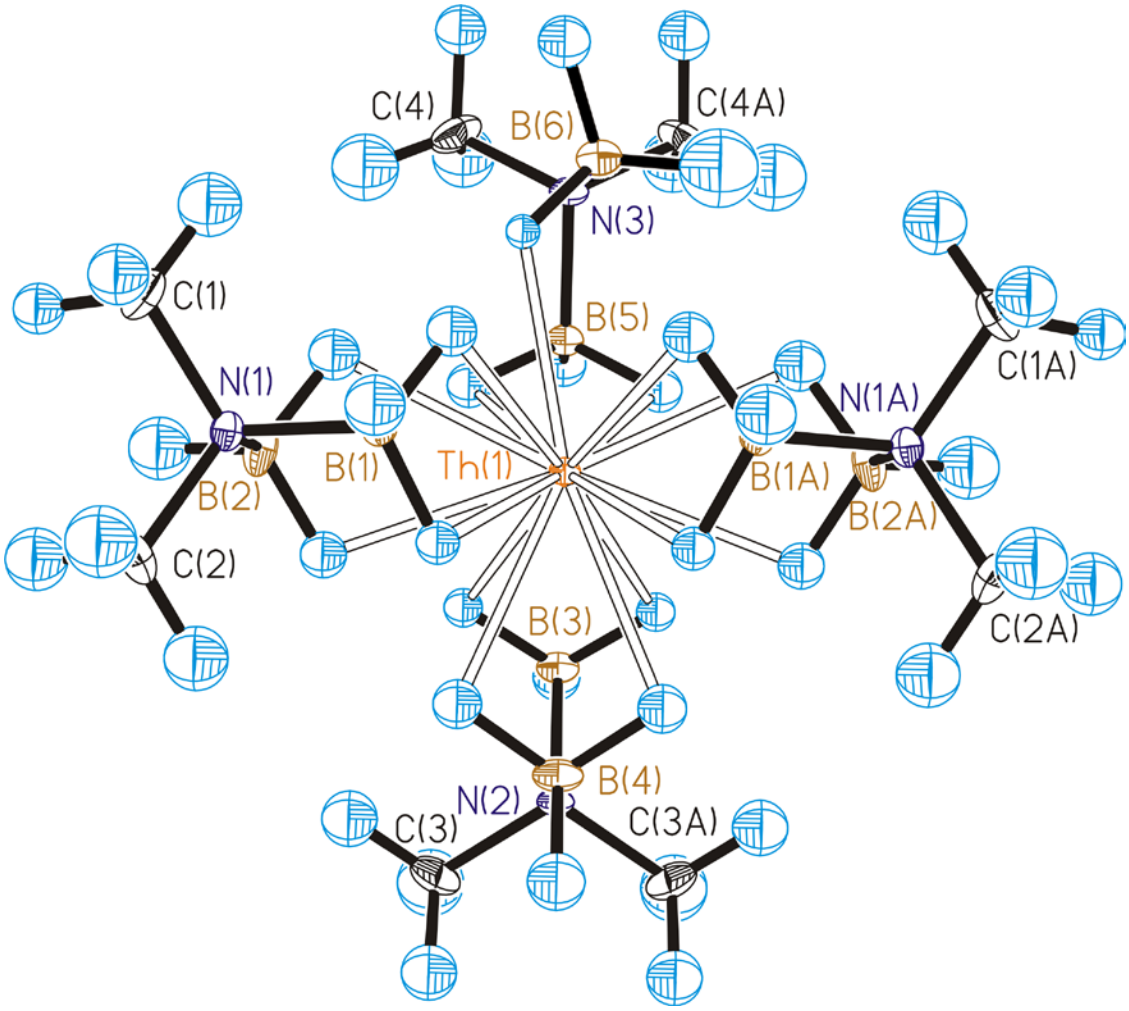

Figure 2.2. Molecular structure of $Th(H_3BNMe_2BH_3)_4$, **1**, from the combined neutron and X-ray data. Ellipsoids are drawn at the 20% probability level.

exchanging ^{1}H nuclei (J_{HB} = 90 Hz). For comparison, the ^{11}B spectrum of $Th(BH_4)_4$ consists of a quintet at δ -8.0 (J_{HB} = 86.5 Hz).[35]

Single crystal X-ray and neutron diffraction studies of **1** reveal that it is monomeric with four chelating aminodiboranate ligands (Figures 2.1 and 2.2). The eight boron atoms describe a distorted D_{2d} dodecahedral structure, in which boron atoms B1, B2, B2A, and B1A describe one planar trapezoidal array, and atoms B3, B4, B5, and B6 describe the other. The B2–Th1–B2A and B4–Th1–B6 angles between wingtip boron atoms are almost linear at 172.61(12)° and 171.85(13)°, respectively (Table 2.3). Interestingly, seven of the eight Th···B distances (those for boron atoms B1 through B5) range from 2.882(3) to 2.949(3) Å, but the eighth distance (Th1···B6) is significantly longer at 3.193(5) Å.

Both the X-ray and neutron diffraction results clearly show that two hydrogen atoms on each boron atom bridge each of the seven short Th···B contacts, but only one bridges the long Th···B contact. The thorium center therefore forms bonds with fifteen hydrogen atoms; accordingly, *this is the first crystallographically characterized complex with a Werner coordination number of 15*. The long Th···B contact is disordered across an internal mirror plane. Generation of the symmetry related fragment without the proper disorder model yields a structure that appears to be 16-coordinate (Figure 2.3).

The Th-H distances from the neutron diffraction study range from 2.37(2) to 2.539(18) Å, which are longer than the bridging thorium hydride from the neutron diffraction study of $(Cp^*_2ThH)_2(\mu\text{-}H)$ (Th-H = 2.29(3) Å),[47] and those observed from the single-crystal XRD study of Cp^*_3ThH and the μ_2-bridging hydrides in $Th_3(\mu_3\text{-}H)_2(\mu_2\text{-}H)_4$(O-2,6-*t*-$Bu_2C_6H_3)_6$ at 2.33(13) and 2.0(1) – 2.3(1) Å, respectively.[48, 49] Structurally characterized complexes containing bridging Th-H-B units, such as $[Th(H_3BCH_3)_4]_2(Et_2O)$ and

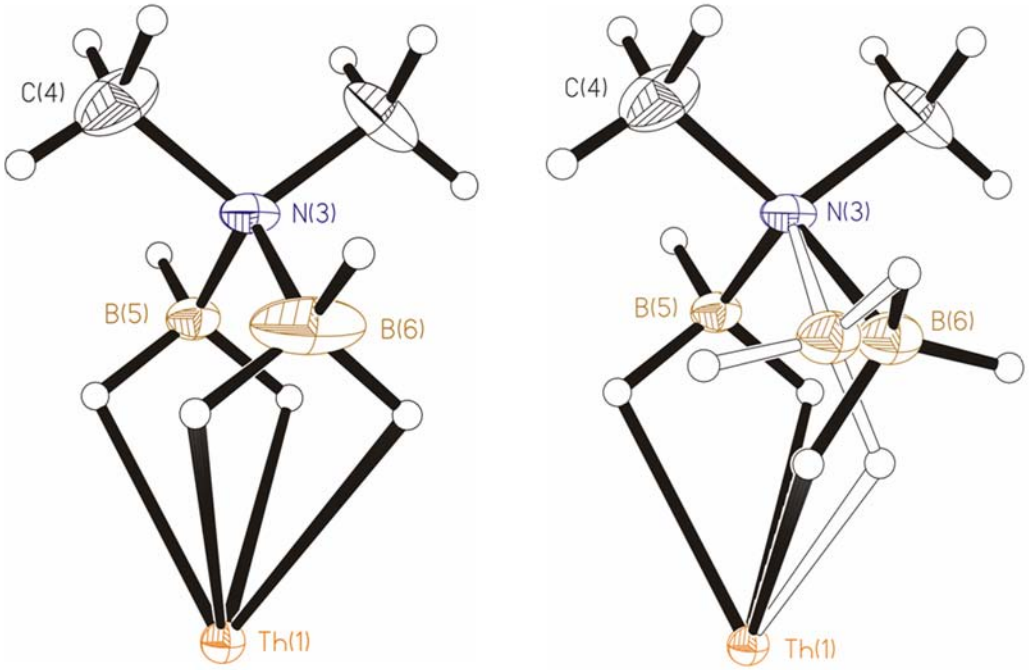

Figure 2.3. Right: X-ray and neutron disorder model for B6 in **1**. Left: Refinement without the disorder model. Ellipsoids are drawn at the 35% probability level, except for hydrogen atoms, which are represented as arbitrarily-sized spheres.

Table 2.1. X-ray Crystallographic Data for $Th(H_3BNMe_2BH_3)_4$ (**1**), $Th(H_3BNMe_2BH_3)_2(BH_4)_2(thf)$ (**2·thf**), and $Th(H_3BNMe_2BH_3)_2(BH_4)_2$ (**2**).

	1	**2·thf**	**2**
formula	$ThB_8N_4C_8H_{48}$	$ThB_6N_2C_8H_{40}$	$ThB_6N_2C_4H_{32}$
formula weight	519.02	477.32	405.22
T, K	193(2)	193(2)	193(2)
λ, Å	0.71073	0.71073	0.71073
space group	*Pnma*	$P2_1$	$P2_1/c$
a, Å	18.8309(5)	8.4910(2)	9.1975(18)
b, Å	13.4269(4)	13.3321(3)	19.625(4)
c, Å	9.6636(3)	9.4659(2)	9.2848(19)
β, deg	90	102.5600(10)	94.923(4)
V, $Å^3$	2443.35(12)	1045.92(4)	1669.7(6)
Z	4	2	4
ρ_{calcd}, g cm^{-3}	1.411	1.452	1.612
μ_{calcd}, mm^{-1}	6.099	7.116	8.898
transm coeff	0.130 – 0.735	0.315 – 0.689	0.330 – 0.690
R_F[a]	0.0156	0.0306	0.0343
wR_2[b]	0.0344	0.0731	0.0648

[a] $R1 = \Sigma| |F_o| - |F_c| | / \Sigma|F_o|$ for reflections with $F_o^2 > 2\,\sigma(F_o^2)$.

[b] $wR2 = [\Sigma w(F_o^2 - F_c^2)^2 / \Sigma\, w(F_o^2)^2]^{1/2}$ for all reflections.

Table 2.2. Neutron Crystallographic Data for $Th(H_3BNMe_2BH_3)_4$, (**1**).

Formula	$ThB_8N_4C_8H_{48}$
formula weight	519.02
T, °C	-80
space group	*Pnma*
a, Å[a]	18.8309(5)
b, Å	13.4269(4)
c, Å	9.6636(3)
V, Å^3	2443.35(12)
Z	4
d_{calc}, g cm^{-3}	1.411
size, mm	2 × 2 × 1
radiation	neutrons
data collection technique	time-of-flight Laue
μ(λ), cm^{-1}	1.850 + 7.075 λ
max, min transmission	0.4621, 0.0259
extinction parameter	9.3(1.2) × 10^{-6}
d_{min}, Å	1.0
no. of reflns[b]	937
no. of unique reflns	620
*R*1[c]	0.1079
*wR*2[d]	0.2473

[a]Unit cell parameters from the X-ray structure.

[b]Outliers with $\left| F_o^2/F_c^2 \right| > 3$ and $\left| F_c^2/F_o^2 \right| > 3$ were rejected.

[c]$R1 = \Sigma| |F_o| - |F_c| | / \Sigma|F_o|$ for reflections with $F_o^2 > 2\,\sigma(F_o^2)$.

[d]$wR2 = [\Sigma w(F_o^2 - F_c^2)^2 / \Sigma\, w(F_o^2)^2]^{1/2}$ for all reflections.

Table 2.3. Selected Bond Lengths and Angles from the X-ray crystallographic data for $Th(H_3BNMe_2BH_3)_4$ (**1**).

Bond Lengths (Å)			
Th(1)-B(1)	2.894(3)	B(1)-H(12)	1.160(10)
Th(1)-B(2)	2.949(3)	B(2)-H(21)	1.155(10)
Th(1)-B(3)	2.898(4)	B(2)-H(22)	1.162(10)
Th(1)-B(4)	2.933(4)	B(3)-H(31)	1.165(9)
Th(1)-B(5)	2.882(3)	B(4)-H(41)	1.149(9)
Th(1)-B(6)	3.193(5)	B(5)-H(51)	1.157(9)
Th(1)-H(11)	2.390(16)	B(6)-H(61)	1.166(10)
Th(1)-H(12)	2.450(16)	B(1)-H(13)	1.097(11)
Th(1)-H(21)	2.516(17)	B(2)-H(23)	1.101(11)
Th(1)-H(22)	2.458(17)	B(3)-H(32)	1.091(11)
Th(1)-H(31)	2.438(11)	B(4)-H(42)	1.098(11)
Th(1)-H(41)	2.486(12)	B(5)-H(52)	1.095(11)
Th(1)-H(51)	2.399(11)	B(6)-H(62)	1.100(11)
Th(1)-H(61)	2.31(2)	B(6)-H(63)	1.101(11)
B(1)-H(11)	1.159(9)		

Bond Angles (deg)			
B(1)-Th(1)-B(2)	51.15(7)	C(1)-N(1)-B(2)	110.25(19)
B(3)-Th(1)-B(4)	51.51(10)	C(2)-N(1)-B(1)	109.97(18)
B(5)-Th(1)-B(6)	49.73(11)	C(2)-N(1)-B(2)	110.8(2)
B(1)-N(1)-B(2)	107.31(18)	C(3)-N(2)-B(3)	109.63(17)
B(3)-N(2)-B(4)	108.4(2)	C(3)-N(2)-B(4)	110.39(17)
B(5)-N(3)-B(6)	109.1(3)	C(4)-N(3)-B(5)	109.3(2)
C(1)-N(1)-B(1)	110.27(19)	C(4)-N(3)-B(6)	118.8(3)

Symmetry transformations used to generate equivalent atoms: ‘ = *x*, -*y*+½, *z*.

Table 2.4. Selected Bond Lengths and Angles (involving hydrogen atoms) from the neutron crystallographic data for $Th(H_3BNMe_2BH_3)_4$ (**1**).

Bond Lengths (Å)			
Th(1)-H(11)	2.440(17)	B(5)-H(51)*	1.211(9)
Th(1)-H(12)	2.429(17)	B(5)-H(52)^	1.187(13)
Th(1)-H(21)	2.539(18)	B(6)-H(61)*	1.212(10)
Th(1)-H(22)	2.484(17)	B(6)-H(62)^	1.190(13)
Th(1)-H(31)	2.443(10)	B(6)-H(63)^	1.188(13)
Th(1)-H(41)	2.494(12)	C(1)-H(1A)‡	1.080(10)
Th(1)-H(51)	2.417(11)	C(1)-H(1B)#	1.075(11)
Th(1)-H(61)	2.37(2)	C(1)-H(1C)#	1.078(11)
B(1)-H(11)*	1.215(9)	C(2)-H(2A)#	1.074(11)
B(1)-H(12)*	1.212(9)	C(2)-H(2B)#	1.076(11)
B(1)-H(13)†	1.188(12)	C(2)-H(2C)#	1.073(11)
B(2)-H(21)*	1.211(10)	C(3)-H(3A)#	1.078(11)
B(2)-H(22)*	1.211(9)	C(3)-H(3B)#	1.080(11)
B(2)-H(23)†	1.187(13)	C(3)-H(3C)#	1.080(11)
B(3)-H(31)*	1.205(9)	C(4)-H(4A)#	1.080(10)
B(3)-H(32)†	1.184(13)	C(4)-H(4B)#	1.075(11)
B(4)-H(41)*	1.209(9)	C(4)-H(4C)#	1.075(11)
B(4)-H(42)†	1.189(13)		

Bond Angles (deg)			
N(1)-B(1)-H(11)	106.1(9)	H(31)-B(3)-H(32)	110.6(8)
N(1)-B(1)-H(12)	108.9(10)	N(2)-B(4)-H(41)	107.8(9)
H(11)-B(1)-H(12)	107.7(8)	N(2)-B(4)-H(42)	113.5(16)

Table 2.4 (cont.)

N(1)-B(1)-H(13)	114.9(11)	H(41)-B(4)-H(42)	109.6(8)
H(11)-B(1)-H(13)	109.3(8)	N(3)-B(5)-H(51)	109.1(9)
H(12)-B(1)-H(13)	109.6(8)	N(3)-B(5)-H(52)	111.6(15)
N(1)-B(2)-H(21)	107.9(11)	Th(1)-B(5)-H(52)	141.4(15)
N(1)-B(2)-H(22)	109.5(11)	H(51)-B(5)-H(52)	109.5(8)
H(21)-B(2)-H(22)	107.8(9)	N(3)-B(6)-H(61)	105.0(16)
N(1)-B(2)-H(23)	112.5(13)	N(3)-B(6)-H(62)	105(2)
Th(1)-B(2)-H(23)	148.0(13)	H(61)-B(6)-H(62)	109.3(10)
H(21)-B(2)-H(23)	109.6(9)	N(3)-B(6)-H(63)	105(5)
H(22)-B(2)-H(23)	109.5(8)	H(61)-B(6)-H(63)	121(5)
N(2)-B(3)-H(31)	105.4(9)	H(62)-B(6)-H(63)	110.9(15)
N(2)-B(3)-H(32)	115.3(15)		

* Soft restraint included in refinement to make all B-H bond lengths in bridging B-H-Th interactions equal.
^ Soft restraint included in refinement to make all terminal B-H bond lengths equal.
# Soft restraint included in refinement to make all C-H bond lengths equal.

$[Th(H_3BCH_3)_4(thf)]_2$, have Th-H distances of 2.27(6) to 2.72(1) Å that are similar to those observed in **1**.[50]

Although the aminodiboronate ligands in **1** are chelating, this coordination mode is not the only one possible for this anion. For example, the analogous reaction of UCl_4 with $Na(H_3BNMe_2BH_3)$ results in reduction to the U^{III} compound $U(H_3BNMe_2BH_3)_3$, which crystallizes in two different forms (Chapter 3).[51] In one of the two forms, some of the aminodiboronate ligands bridge between metal centers in a $U(\kappa^3\text{-}H_3BNMe_2BH_3\text{-}\kappa^3)U$ fashion. We have also seen bridging modes in aminodiboronate compounds of the lanthanides (Chapters 4 and 5).[52]

Theoretical calculations on $Th(BH_3NMe_2BH_3)_4$; origin of the 15 coordinate structure. Quantum chemical calculations using density functional theory (DFT) show that isolated molecules of **1** adopt fully symmetric structures of D_{2d} symmetry; interestingly, the lengthening of one Th···B distance as seen in the crystal structure is not reproduced. In the calculated structure, the 16 hydrogen atoms define the coordination sphere of the thorium atom are arranged at the vertices of a distorted square orthobicupola. This polyhedron, which is one of the Johnson solids (J_{28}),[53] has D_{4h} symmetry and consists of 10 square faces and eight triangular faces. In **1**, the square faces are distorted to rectangles and the symmetry is lowered to D_{2d} (ignoring the lengthening of the one Th···B interaction). Within each aminodiboranate ligand, the four Th-bonded hydrogen atoms describe one of the rectangular faces of the orthobicupola. Although no other 16 coordinate metal centers are known, the 16 carbonyl groups in the cluster $Re_4H_4(CO)_{16}$ are arranged about the Re_4 core at the vertices of a square orthobicupola,[54] and this polyhedron is also formed by a subset of the metal centers in certain nickel carbonyl clusters.[55]

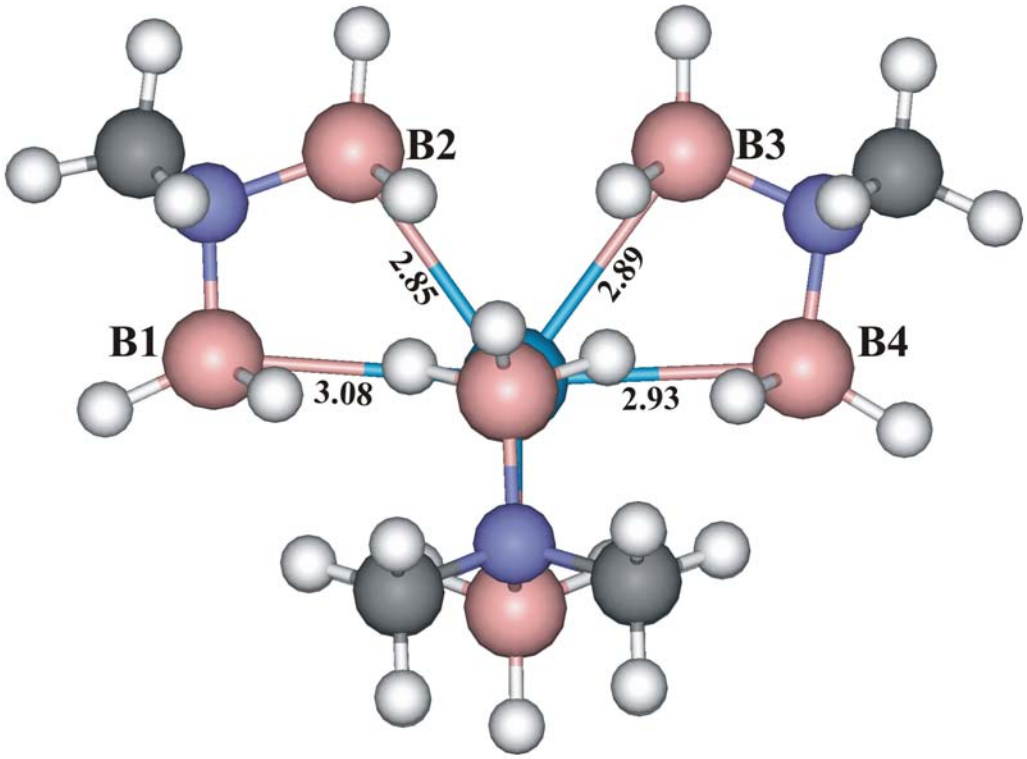

Figure 2.4. Structure of **1** in a crystal constrained by periodic boundary conditions, computed at the DFT/PBE level of theory. Thorium is depicted in light blue, B in pink, N in violet, C in dark gray, and H in white; the Th atom and one aminodiboranate ligand are partly hidden behind other atoms. The unique elongated interaction involves B1 (which corresponds to B6 in the crystal structure). Selected distances (experimental values in parentheses): Th–B1 = 3.08 (3.19), Th–B2 = 2.85 (2.88), Th–B3 = 2.89 (2.90), Th–B4 = 2.93 (2.93), Th–B5 = 2.93 (2.95), Th–B6 = 2.89 (2.89), Th–B7 = 2.89 (2.89), Th–B8 = 2.93 (2.95) Å. For comparison, the Th-B distances calculated in the unconstrained structure range from 2.89 to 2.96 Å. Calculations preformed by Tanya L. Todorova and Laura Gagliardi at the University of Geneva.

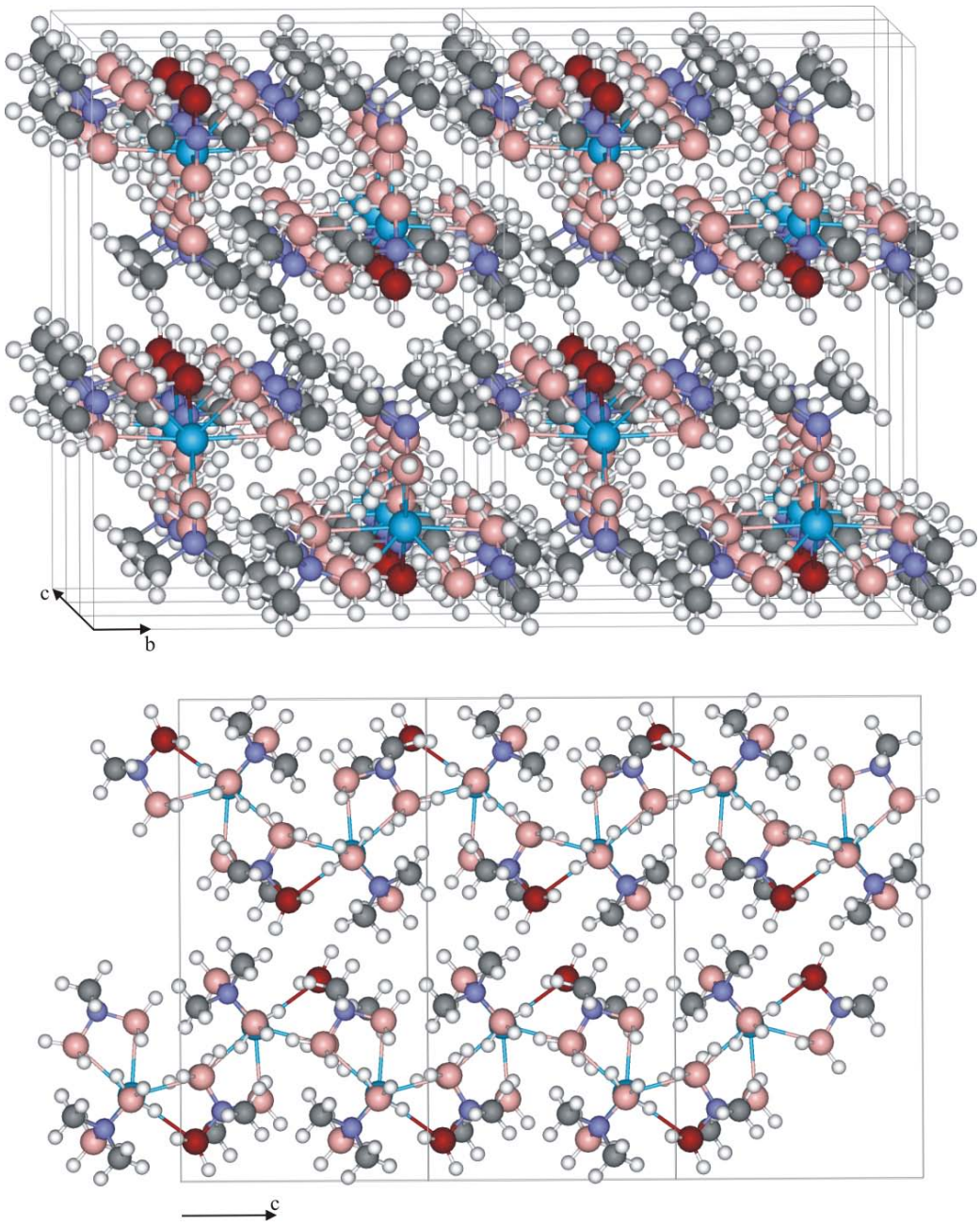

Figure 2.5. Top: (1×2×3) block of unit cells of **1**, as optimized by DFT. The B atoms from the long Th···B distances are depicted in red. Bottom: three unit cells along the c-direction. Calculations preformed by Tanya L. Todorova and Laura Gagliardi at the University of Geneva.

Table 2.5. Bond distances (Å) and bond angles (deg) obtained at the DFT/PBE level of theory for a crystal of **1** constrained by periodic boundary conditions. The experimental values are given in parentheses.

Th – B_1	3.08 (3.19)
Th – B_2	2.85 (2.88)
Th – B_3	2.89 (2.90)
Th – B_4	2.94 (2.93)
Th – B_6/Th – B_7	2.88 (2.89)
Th – B_5/Th – B_8	2.93 (2.95)
B_1 – N – B_2	107.9 (109.1)
B_3 – N – B_4	107.3 (108.4)
B_5 – N – B_6	106.5 (107.3)
B_7 – N – B_8	106.5 (107.3)

Table 2.6. Range of bond distances (Å) obtained at the DFT/PBE level of theory for **1** unconstrained by periodic boundary conditions.

Th – B	2.89 – 2.96
Th – H	2.44 – 2.53

In order to determine whether intermolecular forces are responsible for this structural feature, optimizations were carried out on finite cluster ensembles containing one, two, three, four, and six $Th(BH_3NMe_2BH_3)_4$ units cut out of the experimental crystal structure of **1**. In all cases, the complex maintains the nearly ideal D_{2d} structure seen for the isolated molecule, in which the Th···B distances (for the inner and outer sites of the dodecahedron)[56] are 2.88 and 2.95 Å, respectively. Remarkably, however, imposing periodic boundary conditions on the arrays gives a geometry for **1** that is in a very good agreement with that determined from the X-ray and neutron diffraction experiments (Figure 2.4). Specifically, exactly one Th···B interaction is long (3.08 Å) whereas the others lie between 2.85 and 2.93 Å; the elongated Th···B vector in every molecule in the array lies in the crystallographic ac plane (Figure 2.5). We attribute the distortion to steric crowding between the bulky aminodiboranate ligands attached to the "overcoordinated" Th center, which is relieved by lengthening one bond owing to the nonsymmetric environment surrounding each molecule in the crystal.

Synthesis of other thorium aminodiboranate complexes. We have evidence that the steric crowding in **1** leads to reactivity that lowers the coordination number. When the crude reaction mixture obtained from the reaction of $ThCl_4$ with 4 $Na(H_3BNMe_2BH_3)$ in thf is taken to dryness and the residue is heated in vacuum at 85 °C, a sublimate is obtained. The sublimate was analyzed by ^1H and ^{11}B NMR, which revealed the presence of a boron-containing species that was not **1**. A quintet at δ -2.53 (J_{BH} = 89 Hz) in the ^{11}B NMR spectrum is suggestive of a Th-bound BH_4 group; a new borohydride peak was also observed in the $^1H\{^{11}B\}$ NMR spectra at δ 4.16, along with two broad singlets at δ 1.21 and 3.68 due to thf.

A diffraction study of a crystal obtained from the sublimate confirmed the formation of the new borohydride species $Th(H_3BNMe_2BH_3)_2(BH_4)_2(thf)$, **2·thf** (Figure 2.6). The boron

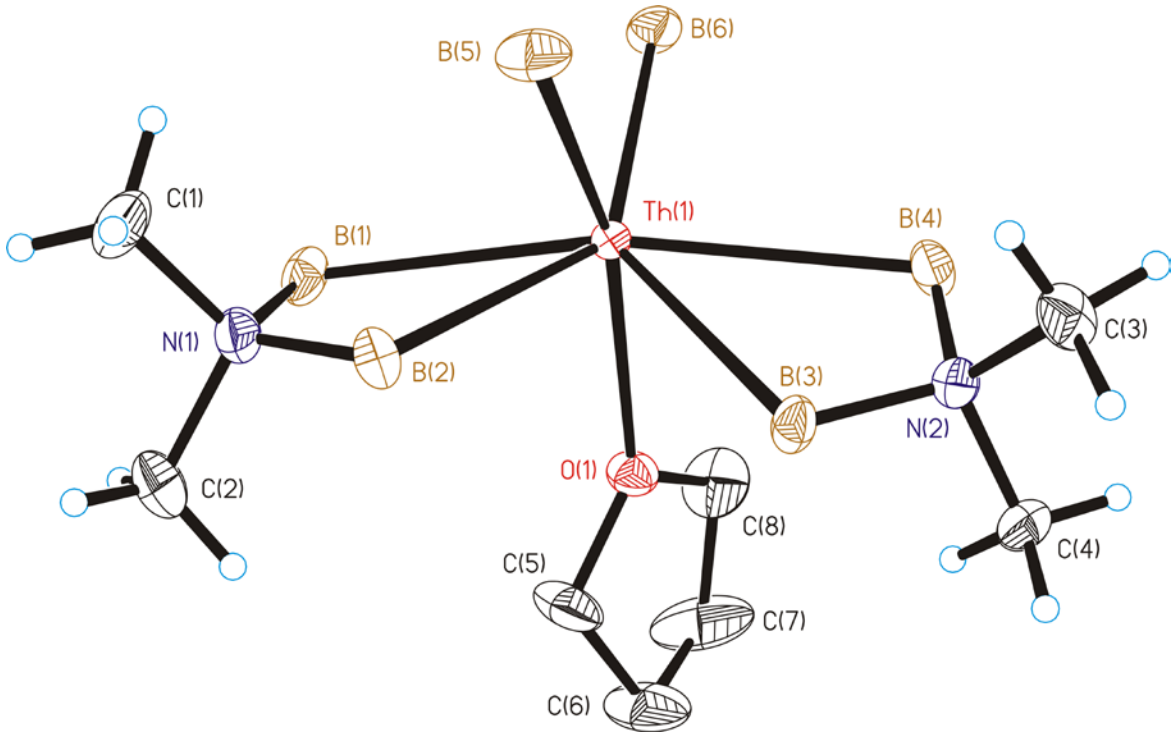

Figure 2.6. Molecular structure of $Th(H_3BNMe_2BH_3)_2(BH_4)_2(thf)$, **2·thf**, from X-ray data. Ellipsoids are drawn at the 35% probability level, except for hydrogen atoms, which are represented as arbitrarily-sized spheres. Hydrogen atoms attached to boron and carbon could not be located in the difference maps. The hydrogen atoms attached to carbon have been placed idealized positions. The hydrogen atoms attached to the thf molecule have been deleted for clarity.

Table 2.7. Selected Bond Lengths and Angles from the X-ray crystallographic data for $Th(H_3BNMe_2BH_3)_2(BH_4)_2(thf)$ (**2·thf**).

Bond Lengths (Å)			
Th(1)-B(1)	2.915(6)	Th(1)-O(1)	2.598(3)
Th(1)-B(2)	2.887(7)	Th(1)-B(5)	2.658(8)
Th(1)-B(3)	2.923(6)	Th(1)-B(6)	2.604(6)
Th(1)-B(4)	2.941(7)		
Bond Angles (deg)			
O(1)-Th(1)-B(1)	84.1(3)	B(2)-Th(1)-B(4)	128.21(19)
O(1)-Th(1)-B(2)	94.58(16)	B(5)-Th(1)-B(2)	63.2(2)
O(1)-Th(1)-B(3)	79.92(17)	B(6)-Th(1)-B(2)	140.1(2)
O(1)-Th(1)-B(4)	82.63(16)	B(3)-Th(1)-B(4)	51.73(18)
O(1)-Th(1)-B(5)	156.3(2)	B(5)-Th(1)-B(3)	86.7(2)
O(1)-Th(1)-B(6)	109.9(2)	B(6)-Th(1)-B(3)	136.9(2)
B(2)-Th(1)-B(1)	52.4(4)	B(5)-Th(1)-B(4)	104.3(2)
B(1)-Th(1)-B(3)	124.9(3)	B(6)-Th(1)-B(4)	87.0(2)
B(1)-Th(1)-B(4)	166.8(3)	B(6)-Th(1)-B(5)	93.2(3)
B(5)-Th(1)-B(1)	87.7(5)	B(2)-N(1)-B(1)	107.6(5)
B(6)-Th(1)-B(1)	98.1(3)	B(4)-N(2)-B(3)	110.1(4)
B(2)-Th(1)-B(3)	76.76(18)		

and oxygen atoms in **2·thf** form a distorted pentagonal bipyramidal geometry around the thorium atom. The two chelating DMADB ligands and one BH_4 group (B6) occupy the equatorial positions, and the thf molecule and the other BH_4 group (B5), occupy the axial positions. The O1-Th1-B5 angle is 156.3(2)°. The Th···B distances to the chelating DMADB ligand are similar to those observed for **1**, and range from 2.887(7) to 2.941(7) Å. The Th···B distances of 2.604(6) and 2.658(8) Å to the BH_4 groups are significantly shorter, and match those typically observed for κ^3 borohydride ligands bound to thorium.[50] The hydrogen positions could not be located in the difference maps, but the Th···B distances suggest that 14 hydrogens are coordinated to thorium (8 from DMADB and 6 from BH_4). Inclusion of the coordinated thf makes **2·thf** the second example of a structurally characterized 15-coordinate complex.

Compound **2·thf** constitutes only a portion of the sublimate obtained from the crude reaction mixture. Microanalyses suggested that the composition of the sublimate closely matched $Th(H_3BNMe_2BH_3)_2(BH_4)_2(thf)_{0.3}$. The thf resonances observed in the ^1H NMR spectrum were also significantly broadened, suggesting that the thf was exchanging rapidly with another species in solution (presumably $Th(H_3BNMe_2BH_3)_2(BH_4)_2$; see below). For comparison, sharp multiplets are assigned to thf in the ^1H NMR spectrum of diamagnetic $La(H_3BNMe_2BH_3)_3(thf)$ (Chapter 4).

To avoid the complications that arise from subliming **1** in the presence of thf, we sublimed crystals of pure **1** in vacuum at 100 °C, and were able to isolate the thf-free complex $Th(H_3BNMe_2BH_3)_2(BH_4)_2$ (**2**) in good yield. The ^1H and ^{11}B NMR resonances for **2** are similar to those observed for **2·thf**, except for the absence of the broadened thf resonances in the ^1H NMR spectrum. The X-ray crystal structure of **2** shows that the six boron atoms are arranged around the metal center in a distorted cis octahedron, as indicated

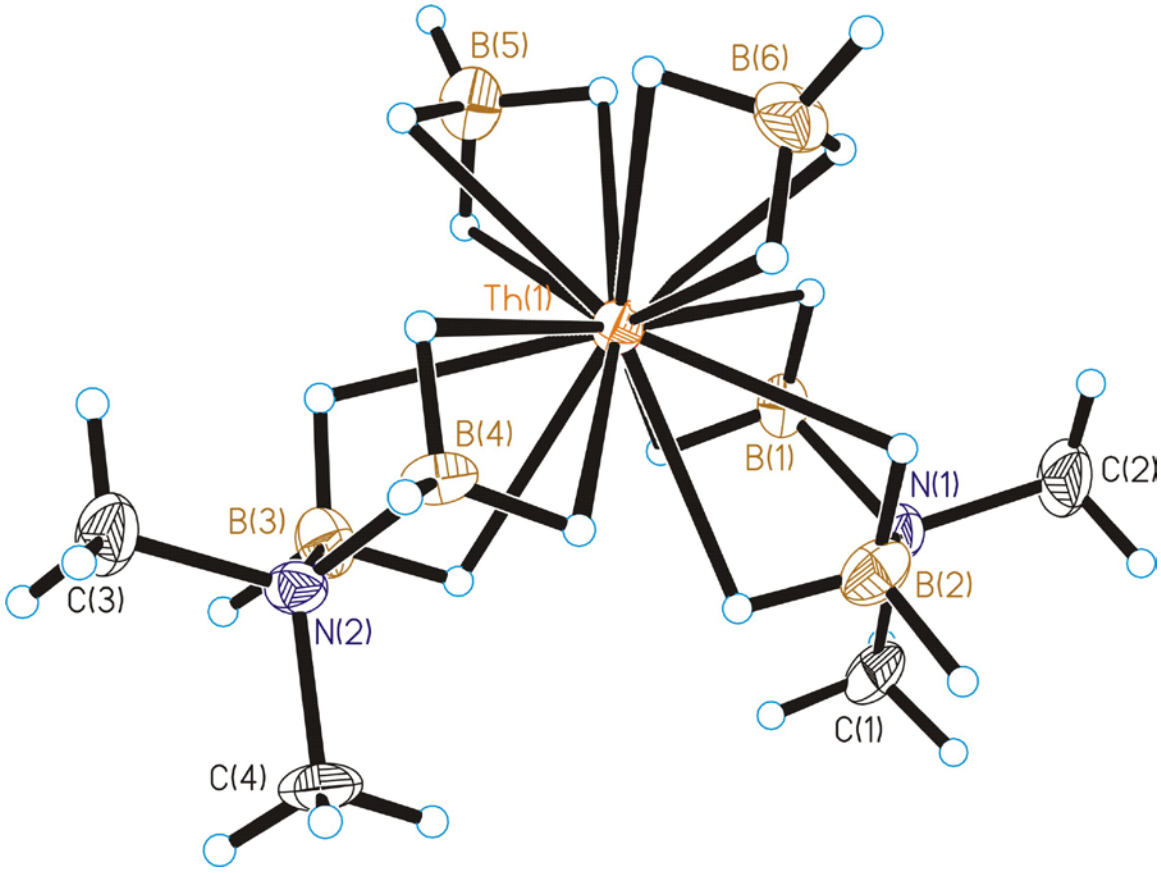

Figure 2.7. Molecular structure of $Th(H_3BNMe_2BH_3)_2(BH_4)_2$, **2** from X-ray data. Ellipsoids are drawn at the 35% probability level, except for hydrogen atoms, which are represented as arbitrarily-sized spheres.

Table 2.8. Selected Bond Lengths and Angles from the X-ray crystallographic data for $Th(H_3BNMe_2BH_3)_2(BH_4)_2$ (**2**).

Bond Lengths (Å)			
Th(1)-B(1)	2.862(10)	B(2)-N(1)	1.575(10)
Th(1)-B(2)	2.862(10)	B(3)-N(2)	1.597(10)
Th(1)-B(3)	2.882(9)	B(4)-N(2)	1.569(10)
Th(1)-B(4)	2.848(9)	N(1)-C(1)	1.489(8)
Th(1)-B(5)	2.608(9)	N(1)-C(2)	1.494(9)
Th(1)-B(6)	2.583(10)	N(2)-C(3)	1.483(9)
B(1)-N(1)	1.546(10)	N(2)-C(4)	1.500(7)
Bond Angles (deg)			
B(1)-Th(1)-B(2)	53.0(3)	B(4)-Th(1)-B(5)	118.6(3)
B(3)-Th(1)-B(4)	53.6(2)	B(4)-Th(1)-B(6)	88.3(3)
B(5)-Th(1)-B(6)	96.6(3)	B(1)-N(1)-B(2)	109.7(6)
B(2)-Th(1)-B(3)	100.1(3)	B(3)-N(2)-B(4)	109.5(6)
B(1)-Th(1)-B(3)	104.8(3)	C(1)-N(1)-B(1)	109.1(6)
B(1)-Th(1)-B(4)	143.5(2)	C(1)-N(1)-B(2)	110.7(6)
B(1)-Th(1)-B(5)	88.2(3)	C(2)-N(1)-B(1)	110.0(6)
B(1)-Th(1)-B(6)	114.2(3)	C(2)-N(1)-B(2)	109.9(6)
B(2)-Th(1)-B(4)	98.2(3)	C(3)-N(2)-B(3)	109.6(6)
B(2)-Th(1)-B(5)	141.0(3)	C(3)-N(2)-B(4)	108.9(5)
B(2)-Th(1)-B(6)	96.8(3)	C(1)-N(1)-C(2)	107.4(6)
B(3)-Th(1)-B(5)	92.6(3)	C(3)-N(2)-C(4)	109.6(5)
B(3)-Th(1)-B(6)	140.1(3)		

by the presence of exactly three large B-Th-B angles: B1-Th1-B4, B2-Th1-B5, and B3-Th1-B6 are 143.5(2)°, 141.0(3)°, and 140.1(3)°, respectively. The Th···B distances to the BH_4^- groups are 2.583(10) and 2.608(9) Å and those to the aminodiboranate ligands range from 2.848(9) to 2.882(9) Å. The decrease in coordination number from 15 in **1** and **2·thf** to 14 in **2** is reflected by the shorter Th···B distances in the latter. The Th-H distances, which were constrained to be equal within an esd of 0.01 Å, are 2.43(2) and 2.35(3)-2.36(3) Å for the aminodiboranate and borohydride ligands, respectively.

The mechanism of conversion of **1** to **2** was investigated by heating **1** to 100 °C in a sealed J. Young tube for 6 h, after which time solvent was condensed into the tube. The resulting NMR spectra revealed near quantitative conversion: only **2** and one equiv of the organic byproduct $[NMe_2BH_2]_2$, which is produced by the dimerization of the two lost NMe_2BH_2 fragments, were observed (Figure 2.8).

Although the NMR data and the X-ray diffraction study confirmed the formation of **2**, subsequent studies showed that heating **1** in vacuum gives a sublimate whose DMADB to BH_4 ratio depends on the heating rate. If **1** is slowly ramped to the sublimation temperature of 100 °C over 5 h in vacuum, the product has a stoichiometry of $Th(H_3BNMe_2BH_3)_{2.2}(BH_4)_{1.8}$, whereas if **1** is rapidly brought (i.e, over a few minutes to 100 °C in vacuum, the product has a stoichiometry of $Th(H_3BNMe_2BH_3)_{2.9}(BH_4)_{1.1}$. In the latter case, new peaks are observed in the ^{11}B NMR spectra that are not due to either **1** or **2** (Figure 2.9). In fact, this new species has a stoichiometry intermediate between that of **1** and **2**: $Th(H_3BNMe_2BH_3)_3(BH_4)$, **3.**

The temperature/composition correlation suggested that, when **1** is heated, the conversion of $H_3BNMe_2BH_3$ groups to BH_4 groups occurs sequentially to form first **3** and then **2**. Time-dependent NMR studies of samples of **1** in toluene at 80 °C revealed that the

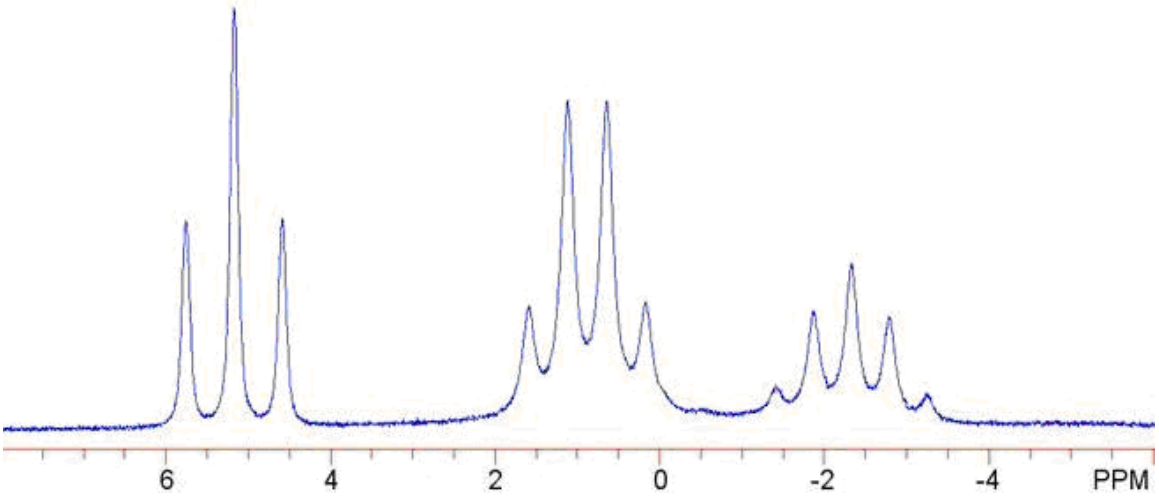

Figure 2.8. ^{11}B NMR spectrum of the products obtained by heating $Th(BH_3NMe_2BH_3)_4$, **1**, in the solid state at 100 °C for 6 h. The organic product $[NMe_2BH_2]_2$ appears at δ 5.17, and the DMDBA and BH_4^- resonances of $Th(BH_3NMe_2BH_3)_2(BH_4)_2$, **2**, appear at δ 0.88 and -2.34, respectively.

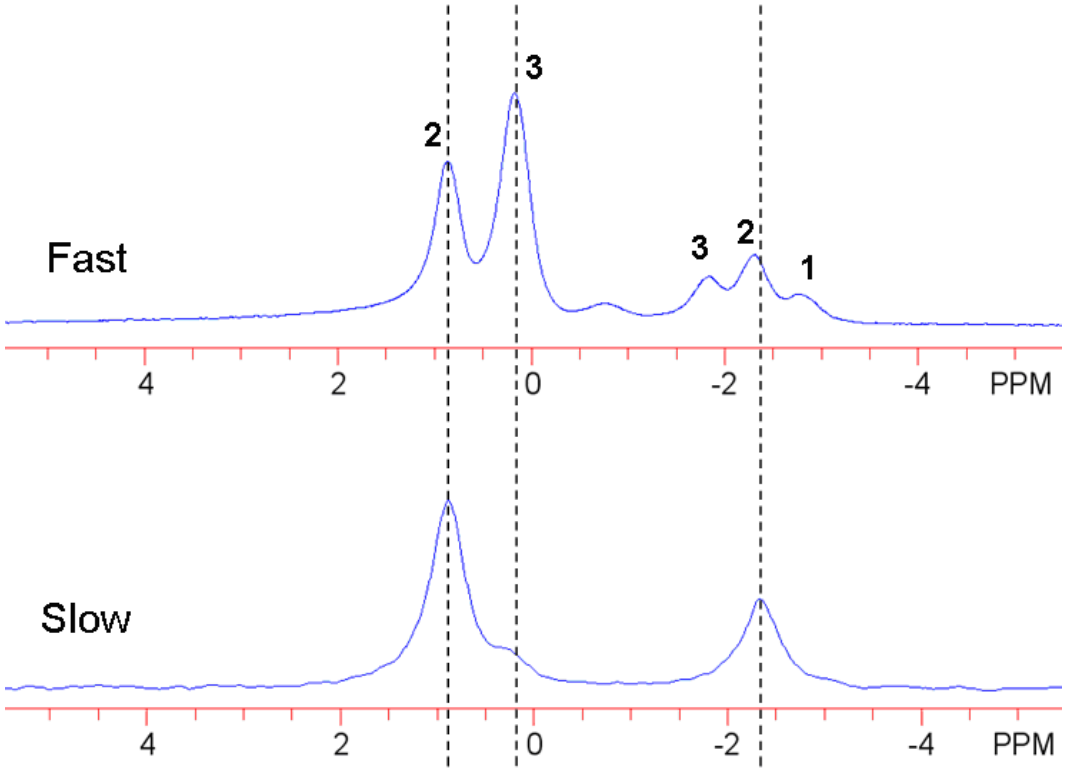

Figure 2.9. ^{11}B NMR spectra (C_6D_6, 25 °C) of the sublimates obtained from $Th(BH_3NMe_2BH_3)_4$, **1** under different sublimation conditions. Top: Rapid heating to 100 – 110 °C at 10^{-2} Torr. Bottom: Slow heating to 100 – 110 °C at 10^{-2} Torr. The resonance at δ -2.75 is due to **1**. The DMDBA and BH_4^- resonances of $Th(BH_3NMe_2BH_3)_2(BH_4)_2$, **2**, appear at δ 0.88 and -2.34, respectively. The DMDBA and BH_4^- resonances of $Th(BH_3NMe_2BH_3)_3(BH_4)$, **3**, appear at δ 0.17 and -1.84. An unidentified species is also present in the top spectrum at δ 0.76. The dashed lines have been included as guide.

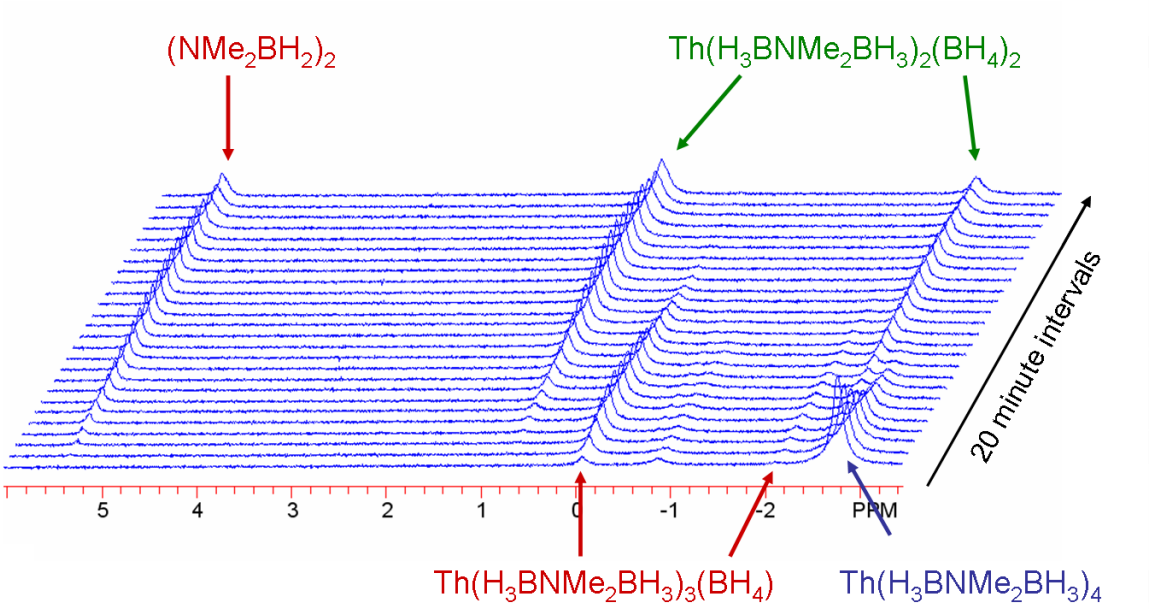

Figure 2.10. Stacked $^{11}B\{^{1}H\}$ NMR spectra of the thermally-induced decomposition of $Th(BH_3NMe_2BH_3)_4$, **1,** at 80 °C in C_7D_8.

transformation of **1** to **2** does indeed proceed through the intermediate $Th(H_3BNMe_2BH_3)_3(BH_4)$, **3**. The identity of **3** was established from the ^{11}B NMR spectrum, which showed two peaks – one a quartet due to the BH_3 groups of aminodiboranate ligands and the other a quintet due to the BH_4 groups – in a 6:1 integration ratio (Figure 2.10). These $^{11}B\{^1H\}$ NMR resonances match those of the third species observed in the sublimate obtained when **1** is heated rapidly. A small peak at ca. -17 is also present in the ^{11}B NMR spectrum, which is due to $(NMe_2)B_2H_5$; we do not believe that the formation of this species is due to hydrolysis. Small peaks due to other boron-containing are also observed in the ^{11}B NMR spectra, but their identities have not been determined due to their low concentrations. These latter species disappear after prolonged reaction times, leaving only **2** and $[NMe_2BH_2]_2$. Evidently, the decomposition mechanism is more complicated than simple intramolecular hydride transfer between the two BH_3 groups in $H_3BNMe_2BH_3^-$ to yield BH_4^- and NMe_2BH_2.

Synthesis of ^{11}B-enriched $Th(H_3BNMe_2BH_3)_4$. The ^{10}B isotope has a large absorption cross-section for neutrons (^{10}B = 3600 barns versus ^{11}B = 0.005 barns), which makes it useful for boron neutron capture therapies,[57-59] but detrimental for neutron diffraction studies. The large absorption cross-section of natural abundance ^{10}B limited the size of the crystal that we could use for neutron diffraction (increased size equals higher absorption probability) and the large amount of absorption limited the number of observed reflections.

In order to obtain better neutron diffraction data, the ^{11}B-enriched $Na(H_3BNMe_2BH_3)$ was prepared according to Scheme 2.1.

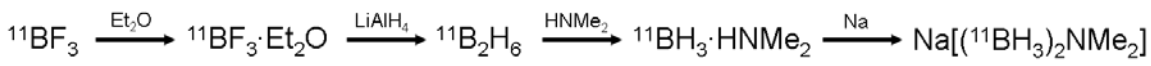

Scheme 2.1

The method uses a modified version of Brown's method to generate diborane from commercially available $^{11}BF_3$ and $LiAlH_4$.[60] Passage of the diborane into a solution of $HNMe_2$ yields $HNMe_2{\cdot}^{11}BH_3$ (Figure 2.11). Sodium reduction of this adduct affords $Na[(^{11}BH_3)_2NMe_2]$, which can then be used to prepare $Th[(^{11}BH_3)_2NMe_2]_4$, by following known syntheses.

Concluding Remarks

The present results set a new record – fifteen – for the highest Werner coordination number seen to date in any form of matter. The high coordination numbers observed are made possible by combining a very large metal atom with very small ligands. DFT calculations suggest that isolated **1** has full D_{2d} symmetry with a coordination number of 16, but that the crowded nature of the inner coordination sphere is sufficiently destabilizing that molecule distorts and becomes 15 coordinate in the solid state. This finding suggests that the discovery of metal complexes with Werner coordination numbers equal to 16 should be possible with the right combination of metal and ligands.

Experimental

All operations were carried out in vacuum or under argon using standard Schlenk techniques. Diethyl ether, tetrahydrofuran, and toluene were distilled under nitrogen from sodium/benzophenone immediately before use. Anhydrous $ThCl_4$ (Cerac), $LiAlH_4$ (Aldrich), and $HNMe_2$ (Aldrich) were used as received. Tetraglyme (Aldrich) was distilled from Na under vacuum. $^{11}BF_3$ (99.9 % ^{11}B-enriched) was purchased from Voltaix. $Na(H_3BNMe_2BH_3)$ and $Na[(^{11}BH_3)NMe_2]$ were prepared as previously reported.[46]

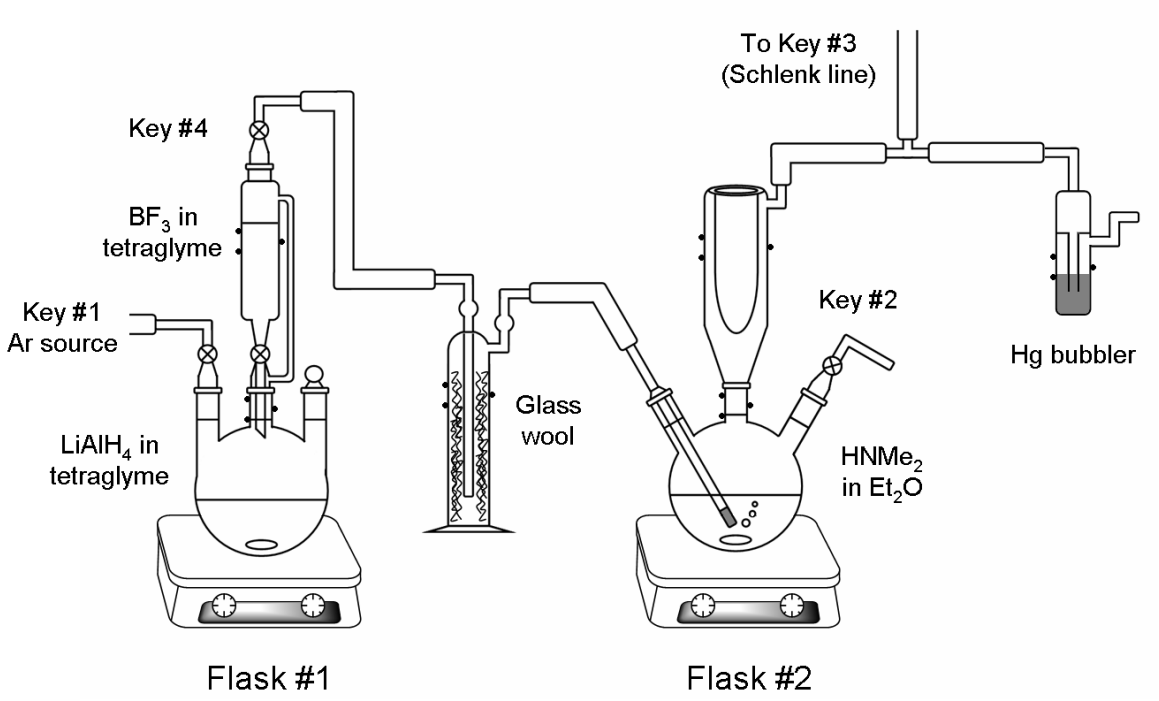

Figure 2.11. Schematic diagram of apparatus used to generate diborane on demand to prepare $HNMe_2 \cdot {}^{11}BH_3$. Cooling bath on Flask #2 is not shown for clarity.

Elemental analyses were carried out by the University of Illinois Microanalytical Laboratory. The IR spectra were recorded on a Nicolet Impact 410 infrared spectrometer as Nujol mulls between KBr plates. The ^{1}H data were obtained on a Varian Unity 400 instrument at 399.951 MHz or on a Varian Unity Inova 600 at 599.765 MHz. The ^{11}B NMR data were collected on a General Electric GN300WB instrument at 96.289 MHz or on a Varian Unity Inova 600 instrument at 192.425 MHz. Chemical shifts are reported in δ units (positive shifts to high frequency) relative to tetramethylsilane (^{1}H) or $BF_3 \bullet Et_2O$ (^{11}B). Field ionization (FI) mass spectra were recorded on a Micromass 70-VSE mass spectrometer. Melting points were determined in closed capillaries under argon on a Thomas-Hoover Unimelt apparatus.

Tetrakis(*N*,*N*-dimethylaminodiboranato)thorium(IV), $Th(H_3BNMe_2BH_3)_4$, (1). To a suspension of $ThCl_4$ (0.47 g, 1.3 mmol) in tetrahydrofuran (15 mL) at -78 °C was added a solution of sodium *N*,*N*-dimethylaminodiboranate (0.47 g, 5.0 mmol) in tetrahydrofuran (15 mL). The reaction mixture was allowed to warm to room temperature and stirred for 36 h. After several hours the mixture consisted of a gray-white precipitate and a colorless solution. The solution was filtered, and the clear filtrate was evaporated to dryness under vacuum. The residue was extracted with toluene (3 x 15 mL), and the extract was filtered and evaporated to dryness under vacuum to afford a white powder. The white powder was extracted with diethyl ether (60 mL + 30 mL), and the resulting solutions were filtered. The first extract was concentrated to ca. 40 mL, and cooled to -20 ˚C to yield 0.20 g of colorless prisms. The mother liquors were combined with the second extract, and this fraction was concentrated to ca. 30 mL and cooled to -20 °C to yield an additional 0.08 g of crystals. Yield: 0.28 g (42 %). Mp: 152 °C. Anal. Calcd for $C_8H_{48}B_8N_4Th$: C, 18.5; H, 9.32; N, 10.8. Found: C, 18.5; H, 9.42; N, 10.5. MS(FI): *m*/*z* 391 [$Th(H_3BNMe_2BH_3)_2(BH_4)^+$, 25], 405

$[Th(H_3BNMe_2BH_3)_2(BH_4)(BH_3)^+$, 85], 448 $[Th(H_3BNMe_2BH_3)_3^+$, 100], 462 $[Th(H_3BNMe_2BH_3)_3(BH_3)^+$, 75], 796 $Th_2(H_3BNMe_2BH_3)_4(BH_4)_3$, 25], 853 $[Th_2(H_3BNMe_2BH_3)_5(BH_4)_2^+$, 40], 910 $[Th_2(H_3BNMe_2BH_3)_6(BH_4)^+$, 30], 967 $[Th_2(H_3BNMe_2BH_3)_7^+$, 20]. ^{1}H NMR (C_6D_6, 20 °C): δ 4.23 (br q, J_{BH} = 90 Hz, BH_3, 24 H), 2.11 (s, fwhm = 4 Hz, NMe_2, 24 H). ^{11}B NMR (C_6D_6, 20 °C): δ -2.75 (q, J_{BH} = 90 Hz, BH_3). IR (cm^{-1}): 2420 s, 2330 m, 2264 s, 2208 vs, 2069 sh, 1400 w, 1275 s, 1240 s, 1186 m, 1161 s, 1132 s, 1036 m, 1011 s, 926 m, 903 w, 827 w, 806 w, 455 m.

The enriched compound $Th[(^{11}BH_3)_2NMe_2]_4$ was prepared similarly; its spectroscopic data matched those of **1**.

Bis(*N*,*N*-dimethylaminodiboranato)bis(tetrahydroborato)(tetrahydrofuran)-thorium(IV), $Th(H_3BNMe_2BH_3)_2(BH_4)_2(thf)$, (2·thf). To a suspension of $ThCl_4$ (0.32 g, 1.0 mmol) in tetrahydrofuran (15 mL) at -78 °C was added a solution of sodium *N*,*N*-dimethylaminodiboranate (0.31 g, 3.8 mmol) in tetrahydrofuran (15 mL). The reaction mixture was warmed to room temperature and stirred overnight. The solution was filtered, and the clear filtrate was evaporated to dryness under vacuum. Sublimation at 85 °C and 10^{-2} Torr onto a water-cooled cold finger afforded long white needles. Yield: 0.11 g (27 %). Microanalytical data suggest that the product is a mixture of **2·thf** and **2**, with the bulk composition being close to $Th(H_3BNMe_2BH_3)_2(BH_4)_2(thf)_{0.3}$. Anal. Calcd for $C_{5.2}H_{34.4}B_6N_2O_{0.3}Th$: C, 14.6; H, 8.12; N, 6.56. Found: C, 14.7; H, 7.60; N, 6.45. ^{1}H NMR (C_6D_6, 20 °C): δ 1.21 (br s, fwhm = 30 Hz, β-CH_2), 1.85 (s, NMe_2, 12 H), 3.68 (br s, fwhm = 20 Hz, α-thf), 4.31 (br q, J_{BH} = 87 Hz, BH_3, 12 H). The BH_4 resonances were masked by the BH_3 resonances. ^{1}H{^{11}B} NMR (C_7D_8, 20 °C): δ 1.22 (br s, fwhm = 30 Hz, β-CH_2), 1.91 (s, NMe_2, 12 H), 3.77 (br s, fwhm = 20 Hz, α-thf), 4.16 (s, BH_4, 8 H), 4.27 (s, BH_3, 12 H). ^{11}B

NMR (C_7D_8, 20 °C): δ -2.53 (quintet, J_{BH} = 89 Hz, BH_4, 2 B), 0.70 (q, J_{BH} = 91 Hz, BH_3, 4 B). The crystal selected for the XRD studies was **2·thf**.

Bis(*N*,*N*-dimethylaminodiboranato)bis(tetrahydroborato)thorium(IV), Th(H_3B-NMe_2BH_3)$_2$(BH_4)$_2$, (2). Method A. A solution of Th($H_3BNMe_2BH_3$)$_4$ (12 mg, 0.023 mmol) in C_7D_8 (1.9 mL) was heated at 80C in a quartz J. Young NMR tube. The reaction was monitored by ^{11}B NMR spectroscopy. The reaction proceeds through the Th($H_3BNMe_2BH_3$)$_3$(BH_4) intermediate [^{11}B{^{1}H} NMR (C_7D_8, 80 °C): δ -2.13 (br s, BH_4, 1 B), -0.07 (br s, BH_3, 6 B)]. Quantitative conversion to **2** was complete after 7 h. ^{11}B{^{1}H} NMR (C_7D_8, 80 °C): δ -2.55 (br s, BH_4, 2 B), 0.77 (br s, BH_3, 4 B).

Method B. A quartz J. Young NMR tube was charged with Th($H_3BNMe_2BH_3$)$_4$ (32 mg, 0.061 mmol) and the solid was heated at 100 °C for 6 h. At the end of this period, the tube was cooled and C_6D_6 (1.5 mL) was condensed into it. Quantitative conversion to **2** was confirmed from the ^{1}H and ^{11}B NMR spectra, which match those given below.

Method C. A flask charged with Th($H_3BNMe_2BH_3$)$_4$ (0.15 g, 0.33 mmol) and a water-cooled cold finger was slowly heated to ca. 90 ˚C at 10^{-2} Torr over the course of 5 h. The temperature, which is just below the T_{sub} for **1**, was maintained for 12 h. The temperature was then increased to 100-110 °C, which afforded white microcrystals. A small amount of Th($H_3BNMe_2BH_3$)$_3$(BH_4), an intermediate in the formation of Th($H_3BNMe_2BH_3$)$_2$(BH_4)$_2$, can be detected in the ^{11}B NMR spectrum and by microanalyses. Yield: 0.11 g. Anal. Calcd for Th($H_3BNMe_2BH_3$)$_{2.2}$(BH_4)$_{1.8}$: C, 12.7; H, 8.13; N, 7.40. Found: C, 12.6; H, 7.86; N, 7.34. ^{1}H{^{11}B} NMR (C_6D_6, 20 °C): δ 1.85 (s, NMe_2, 12 H), 4.29 (s, BH_4, 8 H), 4.35 (s, BH_3, 12 H). ^{11}B NMR (C_6D_6, 20 °C): δ -2.34 (quintet, J_{BH} = 89 Hz, BH_4, 2 B), 0.88 (q, J_{BH} = 92 Hz, BH_3, 4 B). IR (cm^{-1}): 2522 m, 2497 sh, 2453 s, 2428 sh, 2328 m, 2258 m, 2204 vs, 2168

s, 1277 s, 1238 s, 1217 vs, 1196 s, 1184 s, 1163 s, 1126 m, 1101 w, 1014 vs, 928 m, 899 w, 847 w, 438 m.

Tris(*N*,*N*-dimethylaminodiboranato)(tetrahydroborato)thorium(IV), Th(H_3B-NMe_2BH_3)$_3$(BH_4), (3). The regimen used to heat **1** during sublimation strongly influences the composition of the products obtained. For instance, bringing **1** rapidly to the sublimation temperature 100-110 °C yields sublimates with DMADB/BH_4 ratios that approach that of Th($H_3BNMe_2BH_3$)$_3$(BH_4). In one experiment, the ratio was Th($H_3BNMe_2BH_3$)$_{2.7}$(BH_4)$_{1.3}$. Anal. Calcd for $C_{5.4}H_{37.6}B_{6.7}N_{2.7}Th$: C, 14.6; H, 8.52; N, 8.50. Found: C, 14.5; H, 8.58; N, 8.79. In a second experiment, the ratio was Th($H_3BNMe_2BH_3$)$_{2.9}$(BH_4)$_{1.1}$. Anal. Calcd for $C_{5.8}H_{39.2}B_{6.9}N_{2.9}Th$: C, 15.3; H, 8.66; N, 8.90. Found: C, 15.6; H, 8.00; N, 8.97. The ^{11}B NMR spectra (C_6D_6, 20 °C) of the sublimation products obtained in this way contain the following peaks due to Th($H_3BNMe_2BH_3$)$_3$(BH_4): δ -1.84 (quintet, BH_4, 1 B), 0.17 (q, BH_3, J_{BH} = 89 Hz, 6 B).

^{11}B-Boron Trifluoride Etherate, $^{11}BF_3{\cdot}Et_2O$.[61] ***Caution!*** *Boron trifluoride and its diethyl etherate are toxic and flammable. Diethyl ether is flammable. This procedure should be carried out in an efficient hood with explosion shields in place.* Gaseous $^{11}BF_3$ (53 g, 0.78 mol) was passed into diethyl ether (100 mL) with stirring at -10 °C. The exhaust from this flask was passed through a second flask containing diethyl ether (100 mL) that was in turn connected to an oil bubbler vented to air, so that any BF_3 escaping from the first flask was captured. The flow from the BF_3 lecture bottle was controlled using a CGA-330 reverse threaded control valve. The addition was complete in ca. 2 h. The two solutions were combined and the diethyl ether was distilled from the product and discarded. The crude $^{11}BF_3{\cdot}Et_2O$ was distilled under reduced pressure (130 Torr) at a head temperature of 76 – 78 °C to yield a colorless liquid. Yield: 99 g (88 %). ^{11}B NMR: δ (0.0).

^{11}B-Borane Dimethylamine, $HNMe_2 \cdot {}^{11}BH_3$.[60, 62, 63] ***Caution!*** *Boron trifluoride diethyl etherate is toxic and flammable. Diborane is a toxic gas that ignites spontaneously in contact with air. Diethyl ether is flammable. This procedure should be carried out in an efficient hood with explosion shields in place.* In a glove box, a 500 mL three-neck round bottom flask (Flask #1) was charged with a stir bar and $LiAlH_4$ (5.62 g, 148 mmol). The center neck of the flask was equipped with a 100 mL dropping funnel, and the other two necks were equipped with a keyed gas inlet (Key #1) and a stopcock. The dropping funnel was stoppered with a rubber septum and the sealed apparatus was removed from the glove box.

A separate 300 mL three-neck round bottom flask (Flask #2) was equipped with a jacketed dropping funnel topped with a dry ice condenser in the center neck, and a keyed gas inlet (Key #2) in one of the side necks. A stir bar was introduced, and the third neck was stoppered with a rubber septum. The flask was connected to a Schlenk line though Key #2. The glassware was assembled hot and allowed to cool under a strong purge of argon out the top of the dry ice condenser through a 1.3 m long piece of Tygon tubing. After the apparatus had cooled, the tubing was attached to a cylinder of dimethylamine.

Flask #1 was connected to the same Schlenk line through Key #1, and charged under argon with tetraglyme (150 mL), which was added to the flask through the dropping funnel. The dropping funnel was then charged with additional tetraglyme (50 mL), and then Flask #1 was isolated from the argon manifold by closing Key #1.

To Flask #2 was added 125 mL of Et_2O. Flask #2 was immersed in a bath of dry ice and hexanes, and its dry ice condenser, and its jacketed dropping funnel were cooled to -78 °C with dry ice and hexanes (the hexanes will be necessary later in the synthesis). Dimethylamine (70 mL) was condensed into the jacketed dropping funnel and then the

dimethylamine cylinder was closed. The condensed dimethyl amine was added slowly to the Et_2O in Flask #2. At this point, the dry ice condenser and Flask #2 were cooled to -95 °C by replacing the dry ice with judicious amounts of liquid N_2. The Tygon tubing leading from the condenser to the $HNMe_2$ cylinder was removed and replaced with gum rubber tubing fitted with glass T-joint on the end. One end of the T-joint was connected to the Schlenk line (Key #3) and the other to a small Hg bubbler with a piece of gum rubber tubing. The jacketed dropping funnel was removed from the apparatus and replaced with the dry ice condenser at the center neck of Flask #2.

Key #1 on Flask #1 was then reopened to the argon manifold. To the dropping funnel of Flask #1 was added $BF_3{\cdot}Et_2O$ (25 mL, 200 mmol). The septum at the top of the dropping funnel was replaced with a keyed gas inlet (Key #4), which was then connected with a piece of gum rubber tubing to a Dreschel bottle packed with glass wool. A piece of gum rubber tubing was used to connect the Dreschel bottle outlet to a gas dispersion tube mounted though 24/40 ground glass joint. The assembly was purged with argon for 10 min and then, under strong a strong argon purge, the septum in the side neck of Flask #2 was replaced with the modified gas dispersion tube, which was long enough so that the sintered glass end would be submersed in the $HNMe_2$ solution. (***Important!*** Key #2 must be closed before fully seating the gas dispersion tube in the left neck of Flask #2, so as not to drive solution up the tube.) After ensuring that Key #2 and Key #3 were closed, the entire assembly was slowly purged with argon through Key #1 on Flask #1, which vented out of the Hg bubbler connected to the dry ice condenser on Flask #2. The exhaust from the Hg bubbler was vented into a flask containing acetone to destroy any escaping diborane. The apparatus should now look like Figure 2.11.

Key #1 was closed and the $BF_3 \cdot Et_2O$ solution was slowly added dropwise to the $LiAlH_4$ slurry in Flask #1. The rate of addition was closely monitored to maintain a steady rate of addition of the generated diborane to Flask #2. The addition was complete in 3 h. Flask #1 was then heated to 60 °C to drive out any diborane still remaining in the $LiAlH_4$ slurry. When the diborane no longer evolved, Key #1 was partially opened to allow a steady purge of argon through the apparatus. Key #4 was closed and Flask #2 was slowly warmed to RT overnight.

Key #2 was opened and the condenser and the gas dispersion tube were removed from Flask #2. The Et_2O was distilled from the flask and discarded (a ^{11}B NMR spectrum of the distillate revealed no $HNMe_2 \cdot {}^{11}BH_3$) to afford a colorless oil. Pentane (50 mL) was added to the oil, which caused the precipitation of a white solid. Cooling the mixture to -20 °C overnight caused additional solid to form. The solid was collected by filtration and the pentane filtrate was discarded. The solid $HNMe_2 \cdot {}^{11}BH_3$ was dried under vacuum at 0 °C. Yield: 2.67 g (23 % based on $^{11}BF_3 \cdot Et_2O$). Spectroscopic data matched those obtained from unlabeled $HNMe_2 \cdot BH_3$.

X-ray Crystallographic Studies.[64] Single crystals obtained from diethyl ether (**1**) or by sublimation (**2**, **2·thf**) were mounted on glass fibers with Paratone-N oil (Exxon) (**1** and **2·thf)** or Krytox oil (Dupont) (**2**) and immediately cooled to -80 °C in a cold nitrogen gas stream on the diffractometer. Standard peak search and indexing procedures, followed by least-square refinement yielded the cell dimensions given in Table 2.1. The measured intensities were reduced to structure factor amplitudes and their estimated standard deviations by correction for background and Lorentz and polarization effects. No corrections for crystal decay were necessary but a face-indexed absorption correction was applied. Systematically absent reflections were deleted and symmetry equivalent reflections were

averaged to yield the set of unique data. Except where noted, all unique data were used in the least-squares refinements. The analytical approximations to the scattering factors were used, and all structure factors were corrected for both real and imaginary components of anomalous dispersion. Correct atomic position(s) were deduced from an E-map (SHELXTL); least-squares refinement and difference Fourier calculations were used to locate atoms not found in the initial solution. Except where noted below, hydrogen atoms attached to boron were located in the difference maps and hydrogen atoms attached to carbon were placed in idealized positions with C-H (methyl) = 0.98Å and C -H (methylene) = 0.99 Å; the idealized methyl groups were allowed to rotate about their respective axes to find the best least-squares positions. In the final cycle of least squares, independent anisotropic displacement factors were refined for the non-hydrogen atoms. The displacement parameters for methylene hydrogens were set equal to 1.2 times U_{eq} for the attached carbon; those for methyl hydrogens were set to 1.5 times U_{eq}. No correction for isotropic extinction was necessary. Successful convergence was indicated by the maximum shift/error of 0.000 for the last cycle. A final analysis of variance between observed and calculated structure factors showed no apparent errors. Aspects of the refinements unique to each structure are reported below.

$Th(H_3BNMe_2BH_3)_4$, 1. The orthorhombic lattice and systematic absences for $0kl$ ($k + l \neq 2n$) and $h0l$ ($h \neq 2n$) were consistent with space groups $Pna2_1$ and *Pnma*; the centrosymmetric group *Pnma* was shown to be the correct choice by successful refinement of the proposed model. The B6 atom was disordered over two positions that were related by the internal mirror plane; this disordered atom was modeled by treating each partial atom as having a site occupancy factor of 0.5. The quantity minimized by the least-squares program was $\Sigma w(F_o^2 - F_c^2)^2$, where $w = \{[\sigma(F_o^2)]^2 + (0.0167P)^2\}^{-1}$ and $P = (F_o^2 + 2F_c^2)/3$. The

chemically equivalent B–H and H···H distances within the BH_3 units were constrained to be equal within an esd of 0.01Å. An isotropic extinction parameter was refined to a fi nal value of $x = 1.74(8) \times 10^{-6}$ where F_c is multiplied by the factor $k[1 + F_c^2 x\lambda^3/\sin 2\theta]^{-1/4}$ with k being the overall scale factor. The largest peak in the final Fourier difference map (1.50 e $Å^{-3}$) was located 1.36 Å from H61.

$Th(H_3BNMe_2BH_3)_2(BH_4)_2(thf)$, 2·thf. The monoclinic lattice and the systematic absence $0k0$ ($k \neq 2n$) were consistent with the space groups $P2_1$ and $P2_1/m$. The non-centrosymmetric space group $P2_1$ was chosen, and this choice was confirmed by successful refinement of the proposed model. The reflections 021, 0-21, 121, 1-21, -343, 123, 1-23, -1-33, and -133 were found to be statistical outliers and were deleted; the remaining 7762 data were used in the least squares refinement. Some care had to be taken to find the correct model. The non-centrosymmetric space group and the pseudosymmetry created by the location of the Th atom near $y = 0.25$ led to false solutions with low R values but unrealistic arrangements of the ligands about the metal center.[65] The quantity minimized by the least-squares program was $\Sigma w(F_o^2 - F_c^2)^2$, where $w = \{[\sigma(F_o^2)]^2 + (0.0307P)^2\}^{-1}$ and $P = (F_o^2 + 2F_c^2)/3$. The C-O and C-C bond distances in the tetrahydrofuran molecule were fixed at 1.48 ± 0.001 and 1.52 ± 0.001 Å, respectively. Hydrogen atoms attached to carbon were placed in idealized positions i.e., staggered with respect to the atoms on the geminal substituent(s). Hydrogen atoms attached to boron were not included in the model. Analysis of the diffraction intensities suggested the presence of inversion twinning; therefore, the intensities were calculated from the equation $I = xI_a + (1-x)I_b$, where x is a scale factor that relates the volumes of the inversion-related twin components. The scale factor refined to a value of 0.49(1). The largest peak in the final Fourier difference map (1.98 e$Å^{-3}$) was located 0.75 Å from Th1.

$Th(H_3BNMe_2BH_3)_2(BH_4)_2$, 2. The monoclinic lattice and systematic absences $0k0$ ($k \neq 2n$) and $h0l$ ($l \neq 2n$) were uniquely consistent with the space group $P2_1/c$, which was confirmed by the success of the subsequent refinement. The quantity minimized by the least-squares program was $\Sigma w(F_o^2 - F_c^2)^2$, where $w = [\sigma^2(F_o^2)]^{-1}$. The B–H and Th–H distances within the BH_3 units of the diboranamide ligands and the BH_4 units were constrained to be equal within an esd of 0.01Å. The displacement parameters for the boron bound hydrogens were set equal to 1.2 times U_{eq} for the attached boron. The largest peak in the final Fourier difference map (1.93 e $Å^{-3}$) was located 0.46 Å from Th1.

Neutron Crystallographic Study of 1. Neutron diffraction data were obtained at the Intense Pulsed Neutron Source (IPNS) at Argonne National Laboratory using the time-of-flight Laue single-crystal diffractometer (SCD).[66] Details of the data collection and analysis procedures have been published previously.[67]

A crystal of $C_8H_{48}B_8N_4Th$, with approximate dimensions of 2 × 2 × 1 mm^3 and a weight of 3.1 mg, was coated in fluorocarbon grease, wrapped in aluminum foil and glued to an aluminum pin that was mounted on the cold stage of a closed-cycle helium refrigerator. The crystal was then cooled under vacuum to 193 ± 1 K. For each setting of the diffractometer angles, data were stored in three-dimensional histogram form with coordinates x,y,t corresponding to horizontal and vertical detector positions and the time-of-flight, respectively. Data were analyzed using the ISAW software package in addition to other local IPNS SCD programs.[67] An auto-indexing algorithm was used to obtain an initial orientation matrix from the peaks in three preliminary histograms measured for 60 minutes each. This unit cell approximately matched the previously reported X-ray unit cell indicating that the neutron sample was the correct material. For intensity data collection, runs of 12 hours per histogram were initiated for the data set. Settings were arranged at χ and φ values suitable to

cover at least one unique octant of reciprocal space (Laue symmetry *mmm*). With the above counting times, 10 histograms were completed in the 5 days available for the experiment. Bragg peaks in the recorded histograms were indexed and integrated using individual orientation matrices for each histogram, to allow for any misalignment of the sample. Intensities were integrated about their predicted locations and were corrected for the Lorentz factor, the incident spectrum, and the detector efficiency. A wavelength-dependent spherical absorption correction was applied using cross sections from Sears[68] for the nonhydrogen atoms and from Howard *et al.*[69] for the hydrogen atoms ($\mu(cm^{-1}) = 1.850 + 7.075\,\lambda$). Symmetry-related reflections were not averaged because different extinction factors are applicable to reflections measured at different wavelengths.

The GSAS software package was used for the initial structural analysis.[70] Due to the high absorption of neutrons from natural abundance boron in the sample, transmissions ranged from 0.462 to 0.026, resulting in a limited number of observed data with large corrections for absorption. Therefore, structure was refined jointly with the neutron data and with the single crystal X-ray diffraction data collected at 193 K. The atomic positions of the X-ray diffraction structure were used as a starting point in the refinement. Hydrogen atom locations were first approximated from the X-ray structure and subsequently also located in the neutron Fourier maps; any differences were corrected according to the neutron determined data.

The final refinement was performed using SHELX97[71] in the WinGX program suite.[72] The neutron data used in the SHELX97 refinements were scaled and corrected for secondary extinction in the GSAS refinements. In the final refinements with SHELX97, the disordered model from the X-ray structure analysis was used. The non-hydrogen atomic parameters were taken from the X-ray structure and were fixed. Only the hydrogen atoms

were refined with the neutron data. Soft restraints were included to restrain all terminal B-H bond distances to be equal and all bond distances for B-H units bridging to Th to be equal. After the final refinement, the largest peak and hole in the neutron difference Fourier map was 0.925 and -1.037 fm $Å^{-3}$, respectively. Data collection and other parameters for the refinement of the combined X-ray and neutron diffraction data are summarized in Table 2.2.

Computational Studies. Density functional theory (DFT) geometry optimizations, performed by Tanya K. Todorova and Laura Gagliardi at the University of Geneva, show that isolated molecules of **1** adopt fully symmetric structures of D_{2d} symmetry; interestingly, the lengthening of one Th···B distance as seen in the crystal structure is not reproduced. In order to determine whether crystal packing effects were responsible for this structural feature, finite cluster models cut out of the experimental crystal structure **1** containing one, two, three, four, and six $Th(BH_3NMe_2BH_3)_4$ units were considered. The gradient-corrected Perdew-Burke-Ernzerhof (PBE) exchange-correlation functional[73] was used along with a triple-ζ valence basis sets developed by Ahlrichs and coworkers[74] augmented by polarization functions (TZVPP). Scalar relativistic effects were incorporated by employing the (14s13p10d8f3g)/[10s9p5d4f3g] effective core potential basis set on the thorium atom with 60 core electrons. The (5s2p1d)/[3s2p1d] basis set was used for the hydrogen atoms and the (11s6p2d1f)/[5s3p2d1f] basis set for the nitrogen, carbon, and boron atoms. The calculations were carried out using the TURBOMOLE 5.9.1 package.[75] The periodic DFT calculations were carried out using the Vienna ab initio Simulation Package (VASP).[76, 77] A plane-wave basis set with a kinetic energy cutoff of 400 eV was used along with the Perdew-Burke-Ernzerhof (PBE) exchange-correlation functional. The interaction between the ionic cores and the valence electrons was described by the projector augmented wave (PAW) method.[78, 79] The integrations in the Brillouin zone employed a (2×3×4) Monkhorst-Pack grid.[80] All

atoms were allowed to relax while keeping the lattice parameters fixed at the experimentally determined values (a = 18.8309 Å, b = 13.4269 Å and c = 9.6636 Å, $\alpha = \beta = \gamma = 90°$). The ground state of this system is a closed-shell singlet.

References

1. Information contained in this chapter has been published previously and is reprinted with permission. See Daly, S. R.; Piccoli, P. M. B.; Schultz, A. J.; Todorova, T. K.; Gagliardi, L.; Girolami, G. S. *Angew. Chem. Int. Ed.* **2010**, DOI: 10.1002/anie.200905797.

2. Werner, A. *Z. Anorg. Chem.* **1893,** *3*, 267-330.

3. Shannon, R. D. *Acta Crystallogr., Sect. A* **1976,** *A32*, 751-767.

4. Orpen, A. G.; Brammer, L.; Allen, F. H.; Kennard, O.; Watson, D. G.; Taylor, R. *J. Chem. Soc., Dalton Trans.* **1989**, S1-S83.

5. Cordero, B.; Gomez, V.; Platero-Prats, A. E.; Reves, M.; Echeverria, J.; Cremades, E.; Barragan, F.; Alvarez, S. *Dalton Trans.* **2008**, 2832-2838.

6. Kepert, D. L. *Inorganic Stereochemistry*. *Inorganic Chemistry Concepts, Vol. 6*, Springer Verlag: Heidelberg, 1982.

7. Kepert, D. L. Coordination Numbers and Geometries. In *Comprehensive Coordination Chemistry*, Wilkinson, G. W.; Stone, F. G. A.; Abel, E. W., Eds. Pergamon: Oxford, 1987; Vol. 1, pp 31-101.

8. Landis, C. R.; Firman, T. K.; Root, D. M.; Cleveland, T. *J. Am. Chem. Soc.* **1998,** *120*, 1842-1854.

9. Green, M. L. H. *J. Organomet. Chem.* **1995,** *500*, 127-148.

10. Kano, N.; Yamamura, M.; Kawashima, T. *J. Am. Chem. Soc.* **2004,** *126*, 6250-6251.

11. Eckert, N. A.; Vaddadi, S.; Stoian, S.; Lachicotte, R. J.; Cundari, T. R.; Holland, P. L. *Angew. Chem., Int. Ed.* **2006,** *45*, 6868-6871.

12. Pfeiffer, P. *Organische Molekülverbindungen*. 2nd. Verlag F. Enke: Stuttgart, 1927.

13. For example, see: G. B. Deacon, B. M. Gatehouse, S. N. Platts, D. L. Wilkinson, *Aust. J. Chem.* **1987**, *40*, 907; Q. Shen, W. Chen, Y. Jin, C. Shan, *Pure Appl. Chem.* **1988**, *60*, 1251; J. Rebizant, M. R. Spirlet, C. Apostolidis, B. Kanellakopulos, *Acta Crystallogr., Sect. C: Cryst. Struct. Commun.* **1990**, *C46*, 2076; S. D. Stults, R. A. Andersen, A. Zalkin, *Organometallics* **1990**, *9*, 115; G. B. Deacon, G. D. Fallon, B.

M. Gatehouse, A. Rabinovich, B. W. Skelton, A. H. White, *J. Organomet. Chem.* **1995**, *501*, 23; S. Anfang, T. Grob, K. Harms, G. Seybert, W. Massa, A. Greiner, K. Dehnicke, *Z. Anorg. Allg. Chem.* **1999**, *625*, 1853; D. Stellfeldt, G. Meyer, G. B. Deacon, *Z. Anorg. Allg. Chem.* **1999**, *625*, 1252; G. M. Ferrence, R. McDonald, M. Morissette, J. Takats, *J. Organomet. Chem.* **2000**, *596*, 95; W. J. Evans, S. A. Kozimor, J. W. Ziller, *Inorg. Chem.* **2005**, *44*, 7960; U. Baisch, S. Pagano, M. Zeuner, J. Schmedt auf der Guenne, O. Oeckler, W. Schnick, *Organometallics* **2006**, *25*, 3027; W. J. Evans, T. M. Champagne, J. W. Ziller, *Organometallics* **2007**, *26*, 1204; D. M. Roitershtein, M. E. Minyaev, A. A. Mikhailyuk, K. A. Lyssenko, P. A. Belyakov, M. Y. Antipin, *Russ. Chem. Bull.* **2007**, *56*, 1978; T. Cantat, C. R. Graves, K. C. Jantunen, C. J. Burns, B. L. Scott, E. J. Schelter, D. E. Morris, P. J. Hay, J. L. Kiplinger, *J. Am. Chem. Soc.* **2008**, *130*, 17537.

14. Voronoi, G. J. *Reine Angew. Math* **1907,** *133*, 97-178.

15. Frank, F. C.; Kasper, J. S. *Acta Crystallogr.* **1958,** *11*, 184-190.

16. Frank, F. C.; Kasper, J. S. *Acta Crystallogr.* **1959,** *12*, 483-499.

17. Bruzzone, G.; Fornasini, M. L.; Merlo, F. *J. Less-Common Metals* **1970,** *22*, 253-264.

18. Hoppe, R. *Angew. Chem., Int. Ed. Engl.* **1970,** *9*, 25-34.

19. Brunner, G. O.; Schwarzenbach, D. *Z. Kristallogr., Kristallgeometrie, Kristallphys., Kristallchem.* **1971,** *133*, 127-133.

20. Fischer, W.; Koch, E.; Hellner, E. *Neues Jahrb. Mineral., Monatsh.* **1971**, 227-237.

21. Batsanov, S. S. *Zh. Neorg. Khim.* **1977,** *22*, 1155-1159.

22. Carter, F. L. *Acta Crystallogr., Sect. B* **1978,** *B34*, 2962-2966.

23. O'Keeffe, M. *Acta Crystallogr., Sect. A* **1979,** *A35*, 772-775.

24. Hoppe, R. *Z. Kristallogr.* **1979,** *150*, 23-52.

25. For some recent references to two-coordinate complexes, see: R. Wolf, M. Brynda, C. B. Ni, G. J. Long, P. P. Power, *J. Am. Chem. Soc.* **2007**, *129*, 6076; J. Li, H. Song, C. Cui, J.-P. Cheng, *Inorg. Chem.* **2008**, *47*, 3468. Examples of one-coordination are still not known, see: A. Haaland, K. Rypdal, H. P. Verne, W. Scherer, W. R. Thiel, *Angew. Chem., Int. Ed.* **1994**, *33*, 2443.

26. Drew, M. G. B. *Coord. Chem. Rev.* **1977,** *24*, 179-275.

27. Hermann, A.; Lein, M.; Schwerdtfeger, P. *Angew. Chem. Int. Ed.* **2007,** *46*, 2444-2447.

28. Burns, J. H. *J. Organometal. Chem.* **1974,** *69*, 225-233.

29. Maier, R.; Kanellakopulos, B.; Apostolidis, C.; Meyer, D.; Rebizant, J. *J. Alloys Compd.* **1993,** *190*, 269-271.

30. Raymond, K. N.; Eigenbrot, C. W., Jr. *Acc. Chem. Res.* **1980,** *13*, 276-283.

31. Marks, T. J.; Kolb, J. R. *Chem. Rev.* **1977,** *77*, 263-293.

32. Burns, C. J.; Neu, M. P.; Boukhalfa, H.; Gutowski, K. E.; Bridges, N. J.; Rogers, R. D. The Actinides. In *Comprehensive Coordination Chemistry II*, Abel, E. W.; Stone, F. G. A.; Wilkinson, G., Eds. Pergamon: Oxford, 2004; Vol. 3, pp 189-345.

33. Xu, Z.; Lin, Z. *Coord. Chem. Rev.* **1996,** *156*, 139-162.

34. Hoekstra, H. R.; Katz, J. J. *J. Am. Chem. Soc.* **1949,** *71*, 2488-2492.

35. Ehemann, M.; Nöth, H. *Z. Anorg. Allg. Chem.* **1971,** *386*, 87-101.

36. Hedberg, K.; Plato, V. *Inorg. Chem.* **1971,** *10*, 590-594.

37. Broach, R. W.; Chuang, I. S.; Marks, T. J.; Williams, J. M. *Inorg. Chem.* **1983,** *22*, 1081-1084.

38. Banks, R. H.; Edelstein, N. M.; Rietz, R. R.; Templeton, D. H.; Zalkin, A. *J. Am. Chem. Soc.* **1978,** *100*, 1957-1958.

39. Schlesinger, H. I.; Brown, H. C. *J. Am. Chem. Soc.* **1953,** *75*, 219-221.

40. Bernstein, E. R.; Hamilton, W. C.; Keiderling, T. A.; La Placa, S. J.; Lippard, S. J.; Mayerle, J. J. *Inorg. Chem.* **1972,** *11*, 3009-3016.

41. Rietz, R. R.; Zalkin, A.; Templeton, D. H.; Edelstein, N. M.; Templeton, L. K. *Inorg. Chem.* **1978,** *17*, 653-658.

42. Rietz, R. R.; Edelstein, N. M.; Ruben, H. W.; Templeton, D. H.; Zalkin, A. *Inorg. Chem.* **1978,** *17*, 658-660.

43. Zalkin, A.; Rietz, R. R.; Templeton, D. H.; Edelstein, N. M. *Inorg. Chem.* **1978,** *17*, 661-663.

44. The anion $[Th(BH_4)_5^-]$ is claimed to be a 15 coordinate complex on the basis of IR data. [16].

45. Keller, P. C. *Inorg. Chem.* **1971,** *10*, 2256-2259.

46. Nöth, H.; Thomas, S. *Eur. J. Inorg. Chem.* **1999**, 1373-1379.

47. Broach, R. W.; Schultz, A. J.; Williams, J. M.; Brown, G. M.; Manriquez, J. M.; Fagan, P. J.; Marks, T. J. *Science* **1979,** *203*, 172-174.

48. Clark, D. L.; Grumbine, S. K.; Scott, B. L.; Watkin, J. G. *Organometallics* **1996,** *15*, 949-957.

49. Evans, W. J.; Nyce, G. W.; Ziller, J. W. *Organometallics* **2001,** *20*, 5489-5491.

50. Shinomoto, R.; Brennan, J. G.; Edelstein, N. M.; Zalkin, A. *Inorg. Chem.* **1985,** *24*, 2896-2900.

51. Daly, S. R.; Girolami, G. S. *Chem. Commun.* **2010,** *46*, 407-408.

52. Daly, S. R.; Kim, D. Y.; Yang, Y.; Abelson, J. R.; Girolami, G. S. *J. Am. Chem. Soc.* **2010,** *132*, 2106-2107.

53. Johnson, N. W. *Canad. J. Math.* **1966,** *18*, 169-200.

54. Masciocchi, N.; Sironi, A.; D'Alfonso, G. *J. Am. Chem. Soc.* **1990,** *112*, 9395-9397.

55. Femoni, C.; Iapalucci, M. C.; Longoni, G.; Zacchini, S. *Chem. Commun.* **2008**, 3157-3159.

56. Hoard, J. L.; Silverton, J. V. *Inorg. Chem.* **1963,** *2*, 235-243.

57. Barth, R. F.; Soloway, A. H.; Fairchild, R. G.; Brugger, R. M. *Cancer* **1992,** *70*, 2995-3007.

58. Hawthorne, M. F. *Angew. Chem. Int. Ed.* **1993,** *32*, 950-984.

59. Soloway, A. H.; Tjarks, W.; Barnum, B. A.; Rong, F.-G.; Barth, R. F.; Codogni, I. M.; Wilson, J. G. *Chem. Rev.* **1998,** *98*, 1515-1562.

60. Kanth, J. V. B.; Brown, H. C. *Inorg. Chem.* **2000,** *39*, 1795-1802.

61. Becher, H. J. Boron. In *Handbook of Preparative Inorganic Chemistry*, 2nd ed.; Brauer, G., Ed. Academic Press: New York, 1963; Vol. 1.

62. Herber, R. H., *Inorganic Isotopic Syntheses*. Benjamin: New York, 1962; p 24.

63. Goedde, D. M.; Windler, G. K.; Girolami, G. S. *Inorg. Chem.* **2007,** *46*, 2814-2823.

64. Brumaghim, J. L.; Priepot, J. G.; Girolami, G. S. *Organometallics* **1999,** *18*, 2139-2144.

65. See Kuchta, M. C.; Parkin, G. *New J. Chem.* **1998**, *22*, 523-530 for a discussion of this effect.

66. Schultz, A. J.; De Lurgio, P. M.; Hammonds, J. P.; Mikkelson, D. J.; Mikkelson, R. L.; Miller, M. E.; Naday, I.; Peterson, P. F.; Porter, R. R.; Worlton, T. G. *Phys. B* **2006,** *385-386*, 1059-1061.

67. Schultz, A. J.; Carlin, R. L. *Acta Crystallogr., Sect. B: Struct. Sci.* **1995,** *B51*, 43-47.

68. Sears, V. F. *Methods Exp. Phys.* **1986,** *23*, 521-550.

69. Howard, J. A. K.; Johnson, O.; Schultz, A. J.; Stringer, A. M. *J. Appl. Crystallogr.* **1987,** *20*, 120-122.

70. Larson, A. C.; Von Dreele, R. B. *Los Alamos Nat. Lab. Rep. LAUR* **2000,** *86-748*,

71. G. M. Sheldrick. SHELX97. Programs for Crystal Structure Analysis (Release 97-2). University of Göttingen, Germany, 1998.

72. Farrugia, L. J. *J. Appl. Cryst.* **1999,** *32*, 837-838.

73. Perdew, J. P.; Burke, K.; Ernzerhof, M. *Phys. Rev. Lett.* **1996,** *77*, 3865-3868.

74. Schaefer, A.; Huber, C.; Ahlrichs, R. *J. Chem. Phys.* **1994,** *100*, 5829-5835.

75. Ahlrichs, R.; Baer, M.; Haeser, M.; Horn, H.; Koelmel, C. *Chem. Phys. Lett.* **1989,** *162*, 165-169.

76. Kresse, G.; Furthmüller, J. *Comput. Mater. Sci.* **1996,** *6*, 15.

77. Kresse, G.; Furthmueller, J. *Phys. Rev. B* **1996,** *54*, 11169-11186.

78. Blöchl, P. E. *Phys. Rev. B* **1994,** *50*, 17953-17979.

79. Kresse, G.; Joubert, D. *Phys. Rev. B* **1999,** *59*, 1758-1775.

80. Monkhorst, H. J.; Pack, J. D. *Phys. Rev. B* **1976,** *13*, 5188-5192.

CHAPTER 3. Synthesis, Characterization, and Structures of $U(H_3BNMe_2BH_3)_3$ and Related Compounds, and Reformulation of the Putative Hydride $U_2(\mu\text{-}H)_2(BH_4)_6(dme)_2$

Introduction[1]

Actinide borohydride complexes are an intriguing class of metal complexes with fascinating structures and unusual properties.[2, 3] Their inner coordination spheres consist largely or entirely of hydrogen atoms, their coordination numbers are high (often 12 or greater), and many are highly volatile; for example, $U(BH_4)_4$ sublimes readily at room temperature and has a vapor pressure of 4 Torr at 60 °C.[4] The high volatility of this latter complex (and its methylborohydride analog) made it a candidate for enriching uranium in the ^{235}U isotope by gaseous diffusion during the Manhattan project. Ultimately, UF_6 became the material of choice for this purpose: although it is highly corrosive, this problem could be (and was) solved. Using $U(BH_4)_4$ in the gaseous diffusion process would have been less practical because it decomposes rapidly above 100 °C (thus limiting the amount of material that can be put into the vapor phase) and because the ^{10}B and ^{11}B isotopes would have to be separated in a previous step.

Complexes of stoichiometry $M(BH_4)_4$ are known for all of the first five actinides (Th-Pu).[5-7] Crystallographic studies show that $M(BH_4)_4$ complexes of actinides with larger radii – thorium, protactinium, and uranium – adopt three-dimensional polymeric structures in the solid state in which the metal centers are 14 coordinate. Each metal center is bound to two κ^3-BH_4^- ligands and four κ^2-BH_4^- ligands;[8] the latter bridge between metal centers in a κ^2,κ^2 fashion.[9, 10] These compounds are volatile because the polymers readily depolymerize to form $M(BH_4)_4$ monomers in which all four BH_4^- ligands are η^3.[11] In contrast, actinides with smaller radii – neptunium and plutonium – form $M(BH_4)_4$ complexes that adopt 12-

coordinate monomeric structures with four κ^3-BH_4^- ligands even in the condensed state.[7, 12] These monomers are liquids at room temperature, and are more volatile than their polymeric Th, Pa, and U cousins.

The volatility of Th, Np, and U borohydride complexes can be increased by preventing polymerization in the solid-state. One way to accomplish this desideratum is to employ the monomethylborohydride ligand, BH_3Me^-, whose methyl substituent is a poor bridging group.[13, 14] These resulting monomeric $M(\kappa^3\text{-}BH_3Me)_4$ complexes of Th and U are much more volatile than their polymeric BH_4^- analogs. For example, $Th(BH_3Me)_4$ sublimes in vacuum at 50 °C, compared to at 120 °C for $Th(BH_4)_4$. Another strategy to prevent polymerization in the solid state is to employ mixed ligand sets, which combine borohydride with other ligands.[15, 16]

We have recently been exploring a new class of metal borohydride complexes based on the *N*,*N*-dimethylaminodiboranate anion, $H_3BNMe_2BH_3^-$ (DMADB).[17, 18] The DMADB anion, which consists of two BH_3 groups joined by an amido linker, is able to chelate to metals by means of up to four B-H-M bridges. Relative to BH_4^-, it occupies more space in the coordination sphere of a metal center and therefore is better able to inhibit polymerization that can reduce volatility. As a result, some DMADB complexes have proven to be highly volatile. For example, $Mg(H_3BNMe_2BH_3)_2$ is more volatile than any other magnesium compound reported to date: it sublimes at 50 °C at 10^{-2} Torr (P_{vap} = 800 mTorr at 25 °C),[19] vs. a sublimation temperature of 230 °C at 10^{-2} Torr for $Mg(BH_4)_2$.[20] Similarly, DMADB complexes of the lanthanides are some of the most volatile compounds of these metals ever prepared.[21]

Here we describe an extension of our efforts to the chemistry of the actinide element, uranium.

Results and Discussion

Synthesis and Characterization of $U(H_3BNMe_2BH_3)_3$. The reaction of UCl_4 with four equiv of sodium *N*,*N*-dimethylaminodiboranate, $Na(H_3BNMe_2BH_3)$ in Et_2O initially gives a green solution that turns brown within a few hours with evolution of gas. As we will show below, the color change is probably associated with reduction of U^{IV} to U^{III}, with concomitant formation of H_2. Evaporation of the reaction mixture, followed by extraction of the residue into pentane, affords a light brown solution from which crystals of the uranium(III) complex $U(H_3BNMe_2BH_3)_3$, **1a**, may be obtained. The yield of product is low owing to the low solubility of **1a** in pentane (however, see below).

The X-ray crystal structure of **1a** reveals that each uranium center is coordinated to three chelating $H_3BNMe_2BH_3$ ligands arranged in a propeller-like conformation (Figure 3.1; Table 3.2). Two hydrogen atoms on each of the six BH_3 groups bridge to the uranium center; the average of these twelve U-H distances is 2.49 Å. The U···B distances are 2.842(6) - 2.935(6) Å, and the B-N-B angles within the ligands are 108.8(4) - 109.8(4)°. Interestingly, the uranium atom is displaced 0.30 Å out of the plane defined by the three nitrogen atoms, along the axis of the pseudo three-fold rotational symmetry element. Although the U^{III} complexes $U[N(SiMe_3)_2]_3$ and $U[CH(SiMe_3)_2]_3$ also lie 0.46 Å and 0.90 Å out of the plane of the three nitrogen or carbon atoms, respectively,[22, 23] in **1a** the displacement is due to formation on an intermolecular U-H interaction with a hydrogen atom from an adjacent molecule. The extra intermolecular U-H bond, which is coincident with the pseudo three-fold rotation axis, makes the total coordination number of each uranium center 13, and links the uranium atoms into a chain so that the structure is in fact a linear polymer. The intermolecular U-H distance of 2.50 Å falls into the middle of the 2.37 – 2.60 Å range

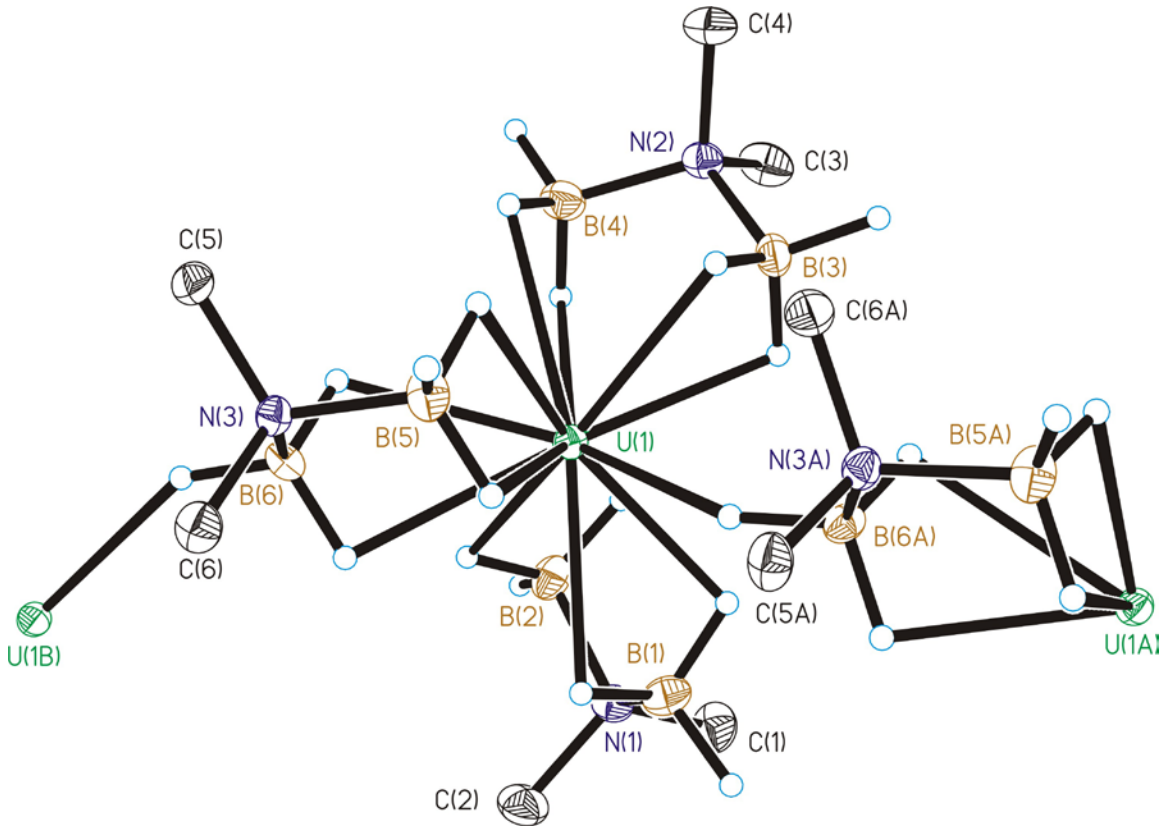

Figure 3.1. Molecular structure of $U(H_3BNMe_2BH_3)_3$, **1a**, obtained from pentane. Ellipsoids are drawn at the 35% probability level, except for hydrogen atoms, which are represented as arbitrarily sized spheres. The hydrogen atoms on the methyl groups have been removed for clarity.

Table 3.1. Crystallographic data for $U(H_3BNMe_2BH_3)_3$ structural isomers **1a** and **1b**, $U(H_3BNMe_2BH_3)_3(thf)$, **2**, $U(H_3BNMe_2BH_3)_3(PMe_3)_2$, **4**, and $PMe_3BH_2NMe_2BH_3$, **5**, and $U_2(\mu\text{-}O)(BH_4)_6(dme)_2$, **6**.

	1a	**1b**	**2**	**4**	**5**	**6**
formula	$C_6H_{36}B_6N_3U$	$C_6H_{36}B_6N_3U$	$C_{10}H_{44}B_6N_3OU$	$C_{12}H_{54}B_6N_3P_2U$	$C_5H_{20}B_2NP$	$C_{15}H_{52}B_6O_5U_2$
FW (g mol^{-1})	453.27	453.27	525.37	605.41	146.81	853.49
λ (Å)	0.71073	0.71073	0.71073	0.71073	0.71073	0.71073
crystal system	Monoclinic	Monoclinic	Cubic	Orthorhombic	Orthorhombic	triclinic
space group	$P2_1/c$	$P2_1/c$	$I23$	$Pbca$	$Pca2_1$	P-1
a (Å)	15.9392(4)	12.3571(6)	16.6987(2)	16.7492(12)	15.3721(13)	9.595(3)
b (Å)	10.2456(3)	10.8128(6)	16.6987(2)	10.4449(7)	6.6323(5)	11.500(4)
c (Å)	11.4154(3)	14.6145(7)	16.6987(2)	33.515(3)	10.1018(9)	14.135(4)
α (deg)	90	90	90	90	90	85.383(4)
β (deg)	97.192(1)	96.116(3)	90	90	90	83.555(4)
γ (deg)	90	90	90	90	90	85.021(4)
V ($Å^3$)	1849.54(9)	1941.6(2)	4656.4(1)	5863.2(7)	1029.90(19)	1540.0(8)
Z	4	4	8	8	4	2
ρ_{calc} (g cm^{-3})	1.628	1.551	1.499	1.372	0.947	1.841
μ (mm^{-1})	8.757	8.342	6.971	5.647	0.199	10.52
R(int)	0.1043	0.091	0.06	0.0726	0.0523	0.089
abs corr method	Face-indexed	Face-indexed	Face-indexed	Face-indexed	Face-indexed	Face-indexed
max., min. transm. factors	0.843, 0.190	0.754, 0.456	0.306, 0.162	0.799, 0.272	0.992, 0.941	0.610, 0.251
data/restraints/params	4251/0/151	5035/49/223	1799/5/90	6684/0/229	1980/5/108	5603/475/395
GOF on F^2	0.925	0.904	1.024	1.01	0.95	0.845
R_1 [$I > 2\sigma(I)$][a]	0.0318	0.0345	0.0144	0.0234	0.0346	0.0236
wR_2 (all data)[b]	0.0701	0.0776	0.0332	0.0512	0.0771	0.0505
max, min $\Delta\rho_{electron}$ (e·$Å^{-3}$)	2.905/-2.556	4.175/-1.927	0.580/-0.351	0.754/-0.756	0.195/-0.152	1.632, -1.219

[a] $R_1 = \sum |F_o| - |F_c| \,| / | \sum |F_o|$ for reflections with $F_o^2 > 2\,\sigma(F_o^2)$. [b] $wR_2 = [\sum w(F_o^2 - F_c^2)^2 / \sum (F_o^2)^2]^{1/2}$ for all reflections.

Table 3.2. Selected Bond Lengths and Angles for $U(H_3BNMe_2BH_3)_3$, **1a**.

	Bond Lengths (Å)		
U(1)-B(1)	2.857(6)	U(1)-H(3D)	2.46
U(1)-B(2)	2.863(6)	U(1)-H(3E)	2.44
U(1)-B(3)	2.842(6)	U(1)-H(4D)	2.50
U(1)-B(4)	2.915(7)	U(1)-H(4E)	2.56
U(1)-B(5)	2.897(6)	U(1)-H(5D)	2.52
U(1)-B(6)	2.935(6)	U(1)-H(5E)	2.48
U(1)-H(1D)	2.57	U(1)-H(6D)	2.48
U(1)-H(1E)	2.37	U(1)-H(6E)	2.60
U(1)-H(2D)	2.42	U(1)-H(6F)′	2.50
U(1)-H(2E)	2.53	U(1)-U(1)’	5.991(6)
	Bond Angles (deg)		
B(1)-U(1)-B(2)	53.45(19)	B(1)-U(1)-B(6)	108.31(19)
B(3)-U(1)-B(4)	53.05(18)	B(2)-U(1)-B(3)	111.2(2)
B(5)-U(1)-B(6)	51.86(17)	B(2)-U(1)-B(4)	93.5(2)
B(1)-N(1)-B(2)	109.4(4)	B(2)-U(1)-B(5)	141.91(19)
B(3)-N(2)-B(4)	109.8(4)	B(2)-U(1)-B(6)	93.56(17)
B(5)-N(3)-B(6)	108.8(4)	B(3)-U(1)-B(5)	106.51(19)
B(1)-U(1)-B(3)	110.90(19)	B(3)-U(1)-B(6)	140.74(18)
B(1)-U(1)-B(4)	138.2(2)	B(4)-U(1)-B(5)	105.1(2)
B(1)-U(1)-B(5)	116.7(2)	B(4)-U(1)-B(6)	97.15(18)

Symmetry transformations used to generate equivalent atoms: ′ = x, -y+½, z-½

observed for the twelve U-H distances of the chelating DMADB ligands. The U···U distance between adjacent uranium centers in the chain is 5.991(6) Å.

The poor solubility of **1a** in pentane and other alkanes led us to investigate toluene as a solvent to extract the crude residue from the reaction of UCl_4 and $Na(H_3BNMe_2BH_3)$ in Et_2O. Cooling the resulting red toluene extracts afforded crystals of analytically pure $U(H_3BNMe_2BH_3)_3$ in much higher yield than when pentane was the extractant. The crystals do not contain toluene or diethyl ether and thus have the same composition as **1a**. Surprisingly, however, the crystals are red rather than brown. A crystallographic study revealed that the red crystals consist of a structural isomer of $U(H_3BNMe_2BH_3)_3$, which we will refer to as **1b** (Scheme 3.1).

Of the three aminodiboranate ligands per uranium center in **1b**, two are chelating and the third is bridging (Figure 3.2; Table 3.3). The local connectivity of each bridging ligand is $U(\kappa^3\text{-}H_3BNMe_2BH_3\text{-}\kappa^3)U$; i.e., the BH_3 groups are bound to different uranium centers, each in a κ^3 fashion. Thus, the uranium centers are again linked into a chain, but the chemical interactions responsible for the polymeric structure are different in **1a** and **1b**. Each uranium center in **1b** is bound to two chelating ligands (forming eight U-H bonds) and to two ends of two bridging ligands (forming six U-H bonds); the total coordination number is therefore 14 (vs. 13 in **1a**). The chelating U···B distances in **1b** range from 2.861(7) – 2.902(6) Å, whereas the bridging U···B distances of 2.665(6) and 2.670(6) Å are much shorter, because these contacts involve κ^3-BH_3 rather than κ^2-BH_3 interactions. The B-N-B angles in the chelating ligands of 108.4(4) and 109.2(4)° are similar to those observed in **1a**, but the B-N-B angles of 112.7(4)° in the bridging ligands are some 3° larger. The U···U distance between adjacent uranium centers in **1b** is 7.339(6) Å.

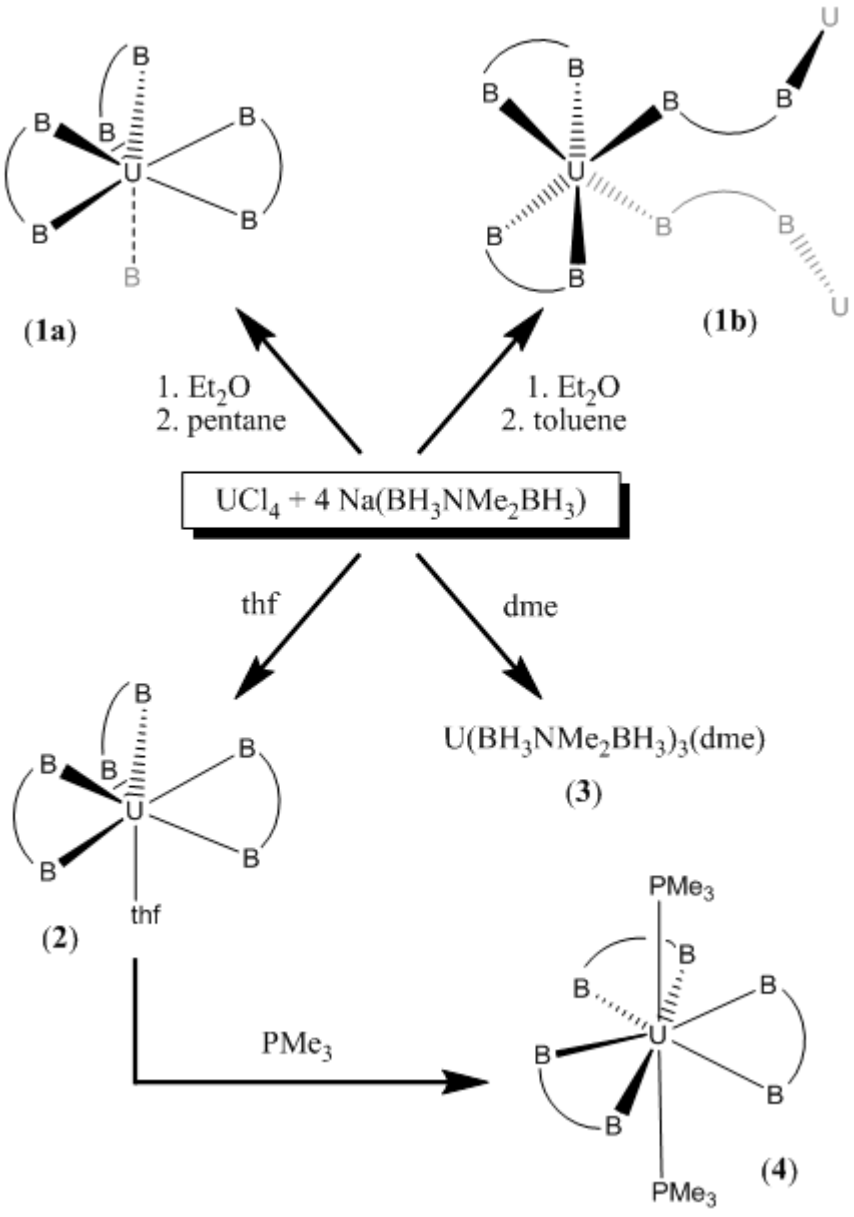

Scheme 3.1. Reaction scheme and reported structures for the uranium aminodiboranates.

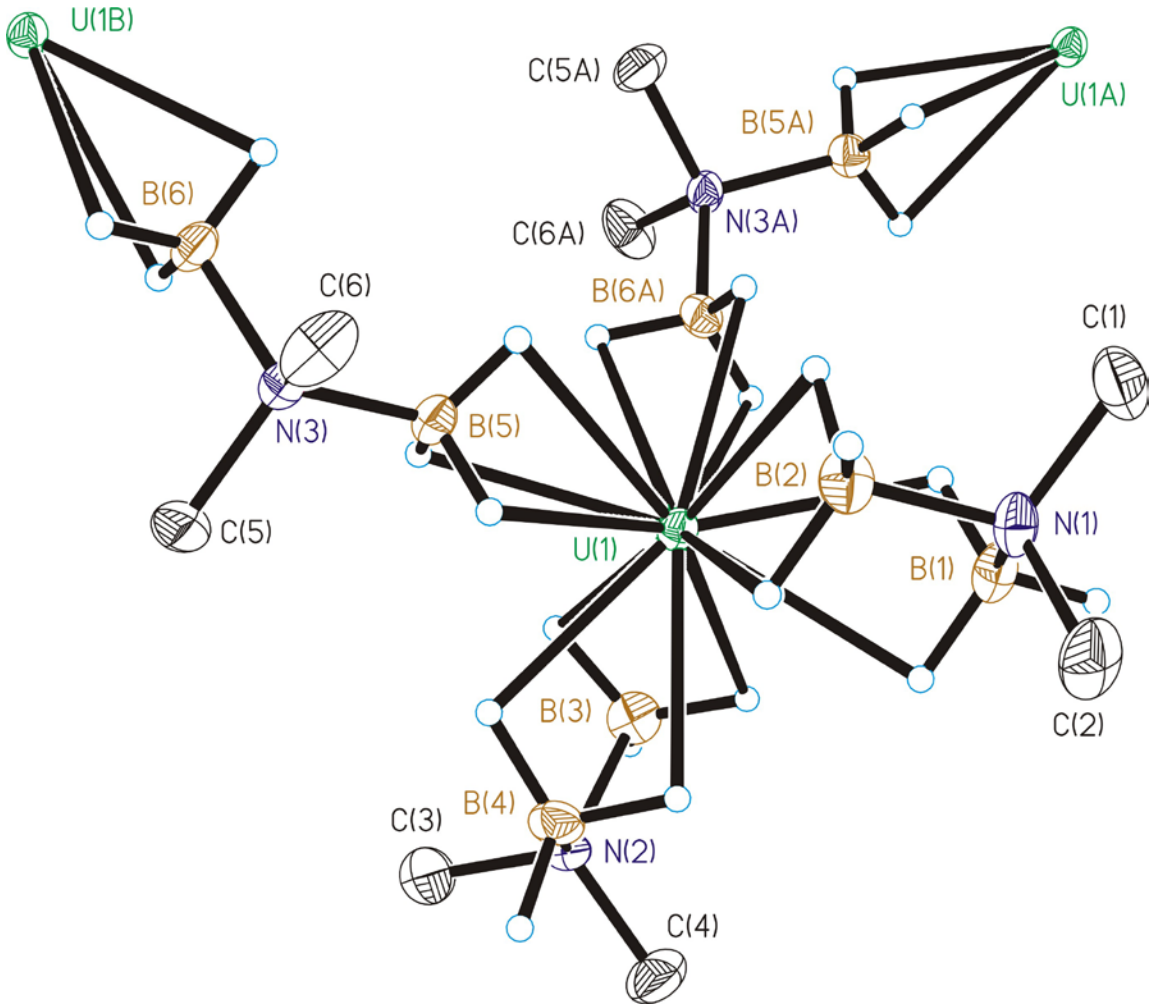

Figure 3.2. Molecular structure of $U(H_3BNMe_2BH_3)_3$, **1b**, obtained from toluene. Ellipsoids are drawn at the 35% probability level, except for hydrogen atoms, which are represented as arbitrarily sized spheres. The hydrogen atoms on the methyl groups have been removed for clarity.

Table 3.3. Selected Bond Lengths and Angles for $U(H_3BNMe_2BH_3)_3$, **1b**.

	Bond Lengths (Å)		
U(1)-B(1)	2.902(6)	U(1)-H(22)	2.48(6)
U(1)-B(2)	2.862(7)	U(1)-H(31)	2.46(5)
U(1)-B(3)	2.861(7)	U(1)-H(32)	2.47(5)
U(1)-B(4)	2.889(6)	U(1)-H(41)	2.47(6)
U(1)-B(5)	2.670(6)	U(1)-H(42)	2.40(5)
U(1)-B(6)′	2.665(6)	U(1)-H(51)	2.31(5)
U(1)-H(11)	2.59(5)	U(1)-H(52)	2.51(5)
U(1)-H(12)	2.46(7)	U(1)-H(53)	2.46(5)
U(1)-H(21)	2.57(6)	U(1)-U(1)′	7.339(6)
	Bond Angles (deg)		
B(1)-N(1)-B(2)	109.2(4)	B(2)-U(1)-B(4)	105.5(2)
B(3)-N(2)-B(4)	108.4(4)	B(2)-U(1)-B(5)	86.2(19)
B(5)-N(3)-B(6)	112.7(4)	B(2)-U(1)-B(6)′	113.2(2)
B(1)-U(1)-B(2)	53.16(18)	B(3)-U(1)-B(4)	53.0(2)
B(1)-U(1)-B(3)	100.2(2)	B(3)-U(1)-B(5)	118.3(2)
B(1)-U(1)-B(4)	104.0(2)	B(3)-U(1)-B(6) ′	91.6(2)
B(1)-U(1)-B(5)	139.07(19)	B(4)-U(1)-B(5)	89.83(19)
B(1)-U(1)-B(6)′	96.70(19)	B(4)-U(1)-B(6)′	141.25(19)
B(2)-U(1)-B(3)	144.0(2)	B(5)-U(1)-B(6)′	95.59(19)

Symmetry transformations used to generate equivalent atoms:′ = -x, y+½, -z+½

The different structural isomers seen for crystals grown from pentane and from toluene prompted us to examine whether the crystal structures were representative of the respective bulk samples. The dry solid obtained by evaporating a toluene solution of **1** gives a powder X-ray diffraction pattern that matches that calculated from the single-crystal X-ray data collected for toluene-grown **1b**, even when the dried powder from toluene was thoroughly washed with pentane (Figure 3.3). In contrast, the XRD pattern of the powder obtained from the pentane extract suggests that a mixture is present, of which **1a** (but not **1b**) is a component.

Structures analogous to those of **1a** and **1b** are also adopted by DMADB complexes of the larger (i.e., earlier) lanthanide ions.[21, 24] Specifically, the 14-coordinate structure seen for **1b** is also adopted by the corresponding Pr^{3+} complex (r_{ionic} = 0.99 Å), whereas the 13-coordinate structure seen for **1a** is adopted by the DMADB complex of the smaller Sm^{3+} complex (r_{ionic} = 0.958 Å). The structural coexistence of both **1a** and **1b** implies that U^{3+} ought to be intermediate in size between Pr^{3+} and Sm^{3+}, but in fact it is significantly larger than both (r_{ionic} = 1.025 Å).[25] The larger size of U^{3+} is also reflected in the average M···B distances to the chelating DMBDA ligands in the U, Pr, and Sm complexes, which are 2.920, 2.877, and 2.823 Å, respectively. Therefore, from steric considerations alone, U^{3+} is too large to adopt a 13 coordinate structure but nevertheless, in structure **1a**, it does. The discrepancy may be ascribed to the usual cause of unexpected features of the chemistry of uranium vs. the lanthanides: the increased covalency of the uranium-ligand interactions.[26]

The IR spectra of solid samples of **1a** and **1b** are essentially identical, and feature a strong terminal B-H stretch at 2399 cm^{-1} and strong bridging B-H stretches at 2202 and 2168 cm^{-1}. Weaker B-H stretches are also observed at 2331 and 2270 cm^{-1}. When **1a** and **1b** are dissolved in toluene, they give identical ^1H NMR spectra: the NMe_2 groups appear as a

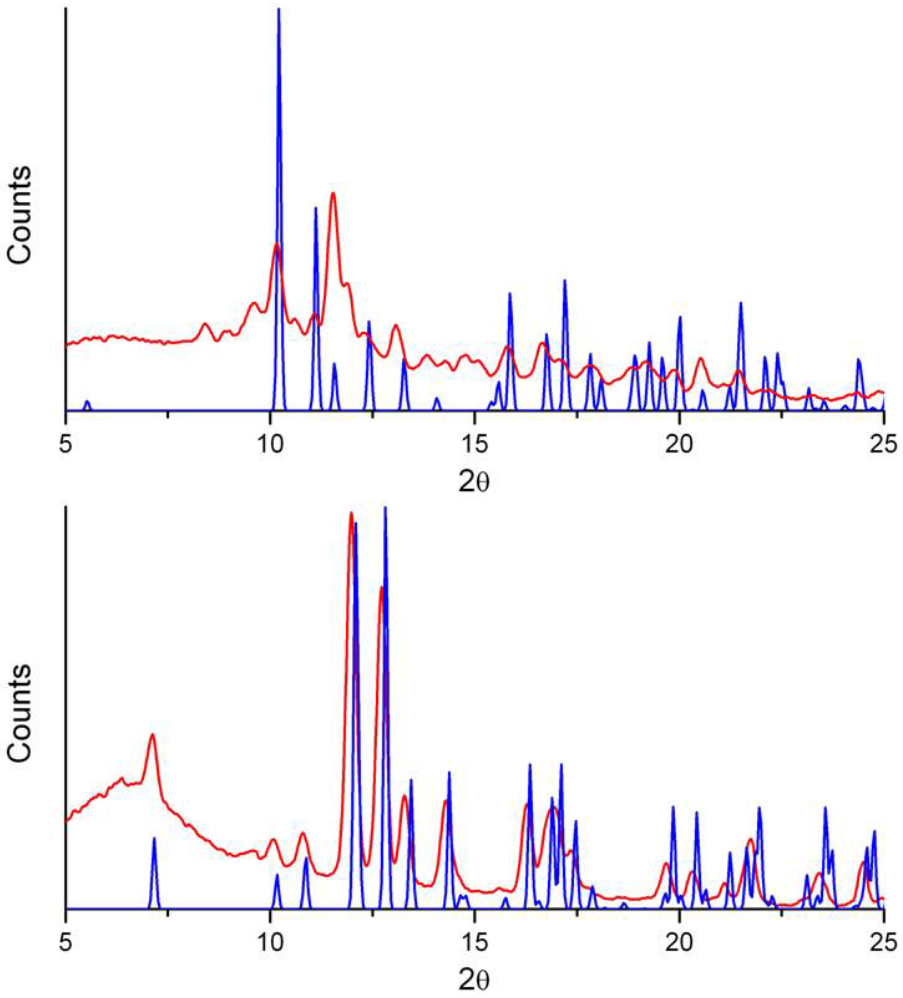

Figure 3.3. Analysis of extracts obtained from reactions to make $U(H_3BNMe_2BH_3)_3$ (see experimental section for details). Top: Experimental powder XRD pattern of solid obtained from pentane extract (red), and calculated powder XRD pattern from the single crystal diffraction data for **1a**. Bottom: Experimental powder XRD pattern of solid obtained from toluene extract (red), and calculated powder XRD pattern from the single crystal diffraction data for **1b** (blue).

paramagnetically shifted and broadened singlet at δ 3.76 (fwhm = 60 Hz) and the BH_3 groups appear as an even broader singlet at δ 91.3 (fwhm = 1100 Hz). The paramagnetism is due to the f^3 uranium(III) center, and the net effect on the NMR spectrum is very similar to that produced by the isoelectronic f^3 ion neodymium(III).[27] Thus, the ^1H NMR chemical shifts for **1a** and **1b** in toluene resemble those seen for $Nd(H_3BNMe_2BH_3)_3$ in benzene, which exhibits a NMe_2 signal at δ 4.66 (fwhm = 230 Hz) and a BH_3 signal at δ 86.8 (fwhm = 1400 Hz).[27] The ^{11}B NMR chemical shift of **1b** in toluene is δ 162.6, vs δ 125.3 for $Nd(H_3BNMe_2BH_3)_3$ in benzene.

Uranium(III) tris(tetrahydroborate) forms adducts of the form $(\eta^6\text{-arene})U(BH_4)_3$,[28, 29] but there is no evidence that **1** forms an analogous adduct with toluene in solution. Almost certainly, the increased steric bulk of DMADB vs BH_4^- leaves insufficient room for coordination of an η^6-arene ring to the uranium center.

Syntheses and Characterization of $U(H_3BNMe_2BH_3)_3(thf)$ and $U(H_3BNMe_2BH_3)_3(dme)$. The reaction of UCl_4 with four equiv of $Na(H_3BNMe_2BH_3)$ in tetrahydrofuran (thf) produces a green solution and some gas (probably H_2). Interestingly, the solution color does not change from green to brown, as seen in the analogous reaction in Et_2O. When the thf solvent is removed, however, the mixture slowly becomes dark brown, indicating reduction to U^{III}, if we assume that the green color attests to the presence of U^{IV}, as it does for $UCl_4(thf)_3$ and known U^{IV} borohydride complexes.[4, 13, 30-35] Extracting the dark residue with pentane and cooling the resulting extracts affords brown crystals of the new uranium(III) complex $U(H_3BNMe_2BH_3)_3(thf)$, **2**, which retains a coordinated tetrahydrofuran molecule.

Similarly, the reaction of UCl_4 with four equiv of $Na(H_3BNMe_2BH_3)$ in 1,2-dimethoxyethane (dme) also gives a solution that retains its original green color even after

the mixture is stirred for several days. After evaporation of the solvent, the green residue slowly darkens under dynamic vacuum, and turns brown over the course of several hours. Extraction of the residue with benzene, followed by removal of the solvent, yields the new uranium(III) compound $U(H_3BNMe_2BH_3)_3(dme)$, **3**, but these samples proved to be somewhat impure. Fortunately, analytically pure samples can be prepared in good yield by adding dme to a solution of the thf adduct **2** in pentane, from which **3** precipitates as a dark mustard colored powder.

Crystals of the thf adduct **2** are isomorphous with those of the corresponding lanthanum compound $La(H_3BNMe_2BH_3)_3(thf)$,[27] both crystallizing in the cubic space group *I*23. The six boron atoms of the anions and the oxygen atom of the thf molecule describe a coordination polyhedron that is intermediate between a capped trigonal prism and a capped octahedron (Figure 3.4; Table 3.4). The U-O bond distance is 2.549(4), and the U···B bond distances of 2.895(3) to 2.901(3) Å are comparable to those seen in **1a** and **1b**. The U-H distances range from 2.45 to 2.56 Å and the average B-N-B angle of the aminodiboranate ligands is 108.9(2)°, which is also very similar to the average angle seen in **1a**.

The IR spectrum of **2** in the B-H stretching region is similar to those observed for **1a** and **1b**. In addition, two IR peaks at 856 and 837 cm^{-1}, which are not present in the IR spectra of **1a** and **1b**, correspond to the symmetric C-O-C stretches of the coordinated thf molecule.[36, 37] The asymmetric C-O-C stretches are masked by other peaks in the spectra. The field ionization mass spectrum of **2** shows peaks at *m*/*e* = 72 and 453 due to thf and the ion $U(H_3BNMe_2BH_3)_3^+$, respectively.

The ^1H NMR chemical shifts of **2** are very similar to those observed for the analogous lanthanide complex $Nd(H_3BNMe_2BH_3)_3(thf)$, which also has an f^3 electronic configuration.[27] The chemical shifts of the NMe_2 and BH_3 protons are δ 3.36 and 104.4, respectively (vs. δ

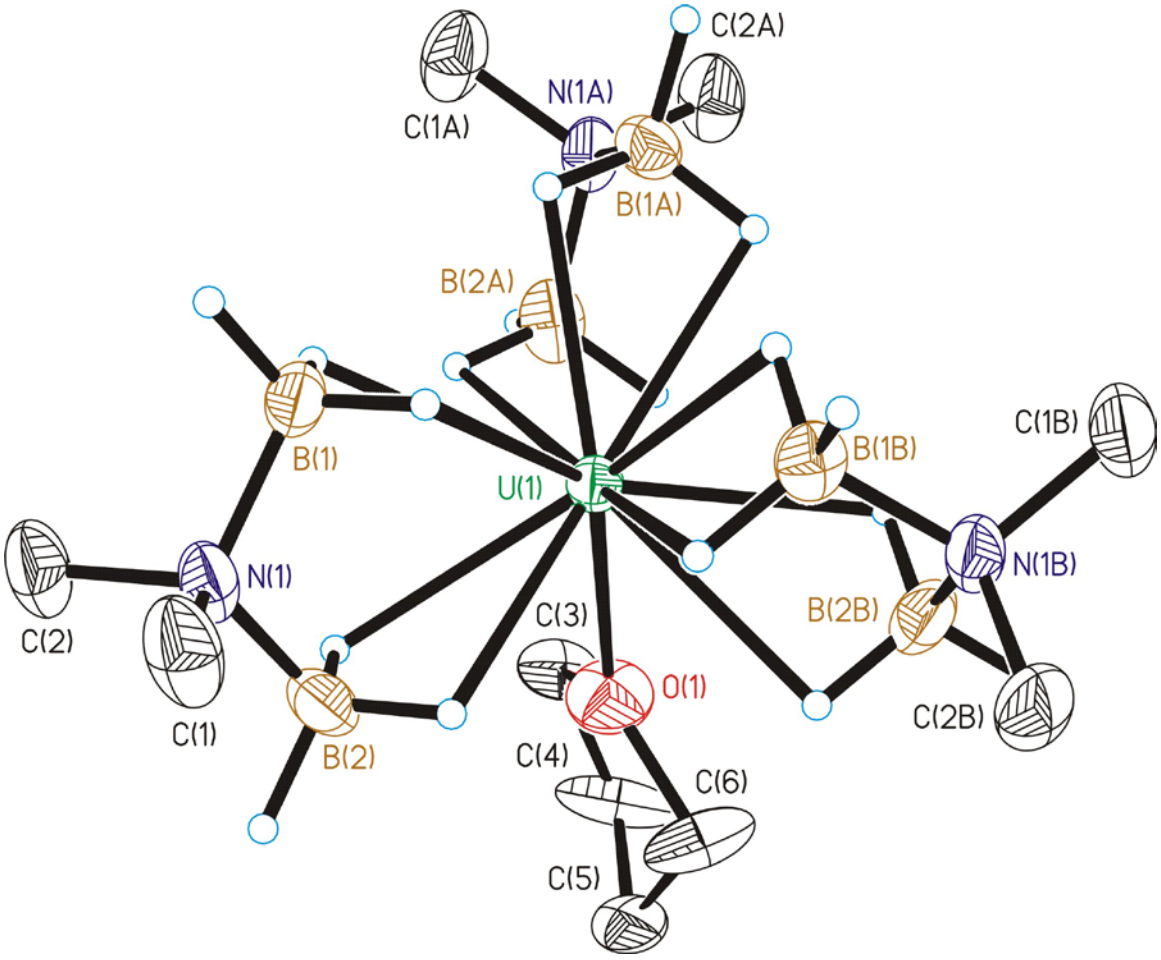

Figure 3.4. Molecular structure of $U(H_3BNMe_2BH_3)_3(thf)$, **2**. Ellipsoids are drawn at the 35% probability level, except for the hydrogen atoms, which are represented as arbitrarily sized spheres. Methyl and methylene hydrogen atoms have been deleted for clarity.

Table 3.4. Selected Bond Lengths and Angles for $U(H_3BNMe_2BH_3)_3$(thf), **2**.

	Bond Lengths (Å)		
U(1)-O(1)	2.549(4)	U(1)-H(1B)	2.4465
U(1)-B(1)	2.895(3)	U(1)-H(2A)	2.4621
U(1)-B(2)	2.901(3)	U(1)-H(2B)	2.5474
U(1)-H(1A)	2.5557		
	Bond Angles (deg)		
H(1A)-U(1)-H(1B)	44.0(1)	B(2)-U(1)-B(1)′	104.2(1)
H(2A)-U(1)-H(2B)	44.0(1)	B(2)-U(1)-B(2)″	115.41(6)
B(1)-U(1)-B(2)	52.3(1)	B(1)-U(1)-O(1)	125.63(8)
B(1)-U(1)-B(1)′	89.49(11)	B(2)-U(1)-O(1)	77.44(9)
B(1)-U(1)-B(2)′	138.31(10)	B(1)-N(1)-B(2)	108.9(2)

Symmetry transformations used to generate equivalent atoms: ′ = -*y*+1, *z*, -*x*+1 ″ = -*z*+1, -*x*+1, *y*

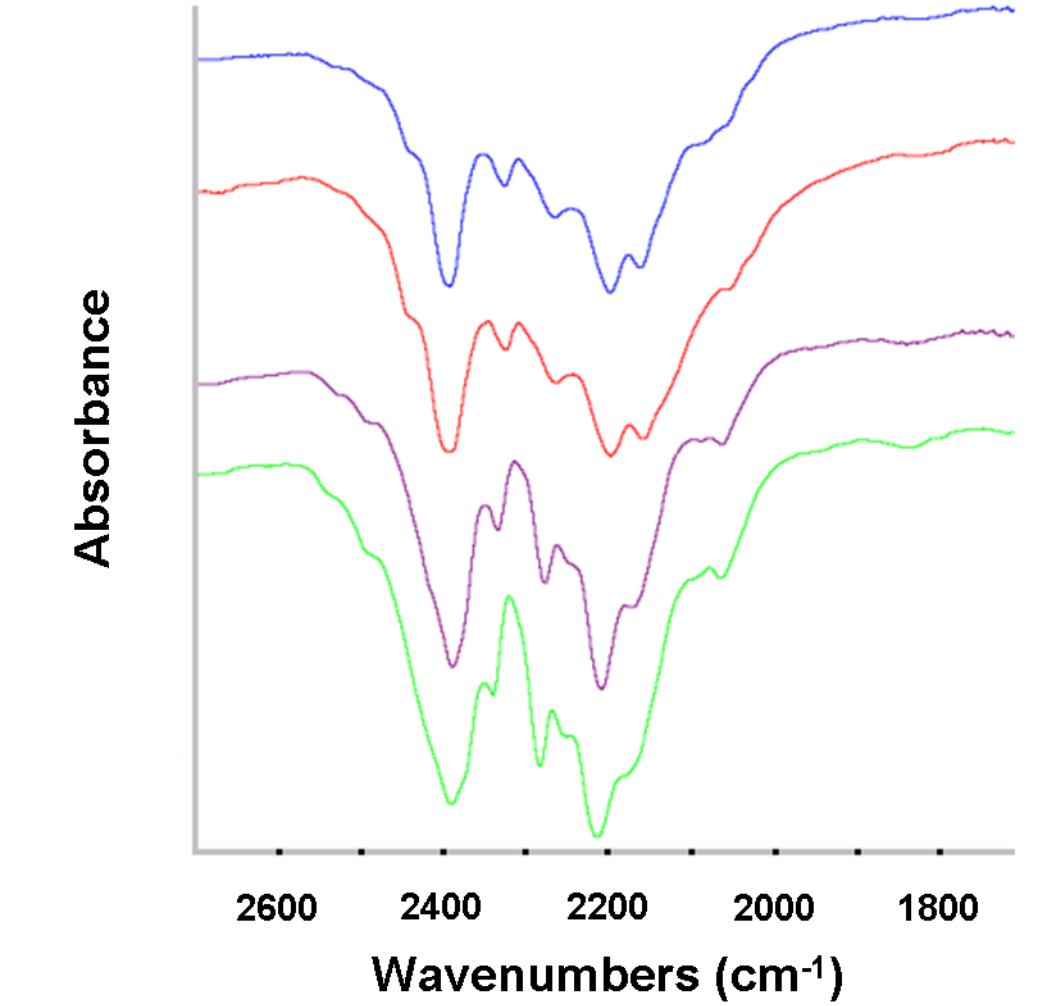

Figure 3.5. The B-H stretching region in the IR spectrum (Nujol) of $U(H_3BNMe_2BH_3)_3$, **1a** (top, blue) and **1b** (red), $U(H_3BNMe_2BH_3)_3(thf)$, **2** (purple), and $Nd(H_3BNMe_2BH_3)_3(thf)$ (bottom, green) for comparison.

3.06 and 82.9 for the Nd analog), and the α and β methylene protons of the thf ligand appear at δ -5.56 and -1.89 (vs. δ 0.66 and 0.95 for the Nd analog). The ^{11}B NMR chemical shift of **1** is δ 152.8, vs. δ 104.8 for $Nd(H_3BNMe_2BH_3)_3(thf)$.

The ^{1}H and ^{11}B NMR spectra of the dme complex **3** are similar to those of **2** except for the resonances due to the coordinated dme. The IR spectrum of **3** exhibits a strong terminal B-H stretch at 2385 cm^{-1} and two strong bridging B-H stretches at 2290 and 2227 cm^{-1}; weaker B-H stretches are also observed at 2341 and 2173 cm^{-1}. Three peaks at 1089, 975, and 858 cm^{-1}, which are not present in the IR spectra of **1a** and **1b**, correspond to stretching vibrations of the coordinated dme molecule.[37]

Synthesis and Characterization of $U(H_3BNMe_2BH_3)_3(PMe_3)_2$. Addition of trimethylphosphine, PMe_3, to the thf adduct **2** in pentane affords a dark red solution, from which dark-red needles of the bis(trimethylphosphine) adduct $U(H_3BNMe_2BH_3)_3(PMe_3)_2$ (**4**) can be isolated. The crystal structure of **4** confirms that the uranium centers are bound to three chelating aminodiboranate ligands and to two PMe_3 ligands. The six boron atoms and two phosphorus atoms describe an approximate trigonal dodecahedron (Figure 3.6; Table 3.5), with atoms P1, P2, B1, and B2 forming one of the two interpenetrating trapezoids, and atoms B3, B4, B5, and B6 forming the second. The two PMe_3 ligands occupy the wingtip positions of one of the two trapezoids, so that the P-U-P angle is 168.92(2)°. The U···B distances range from 2.939(4) to 2.957(3) Å, and are slightly longer than those observed in **1a**, **1b**, and **2**. The U-P bond lengths of 3.1093(9) and 3.1145(8) Å are in good agreement with those in other U^{III} borohydride complexes.[38-40]

The field ionization mass spectrum of **4** shows peaks corresponding to $U(H_3BNMe_2BH_3)_3^{+}$, $U(H_3BNMe_2BH_3)_3(PMe_3)^{+}$, and $U(H_3BNMe_2BH_3)_3(H_3BNMe_2BH_2\text{-}PMe_3)^{+}$ at m/z = 454, 530, and 601, respectively. The ^{1}H NMR spectrum of **4** features a

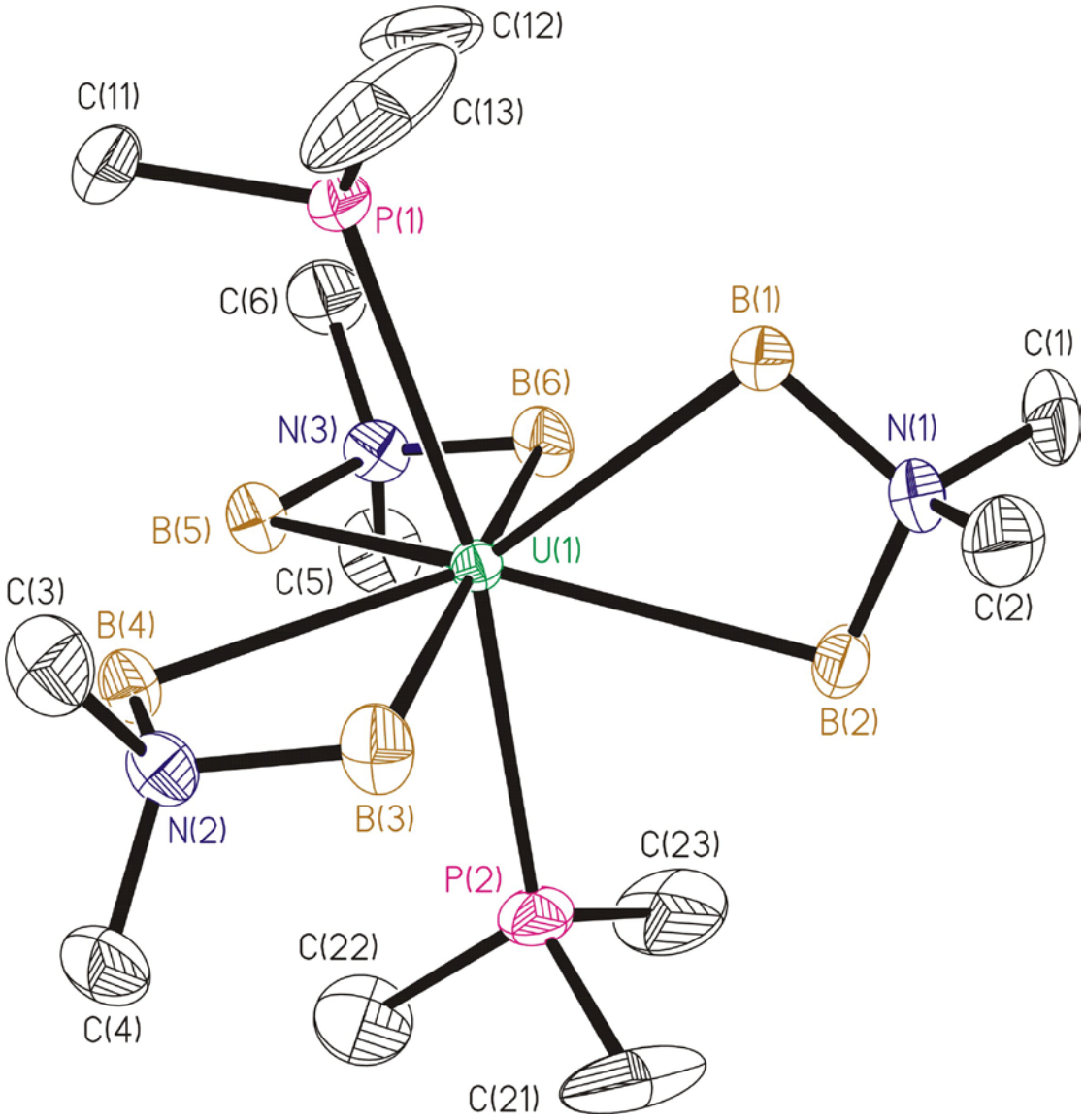

Figure 3.6. Molecular structure of $U(H_3BNMe_2BH_3)_3(PMe_3)_2$, **4**. Ellipsoids are drawn at the 35% probability level. Hydrogen atoms have been deleted for clarity.

Table 3.5. Selected Bond Lengths and Angles for $U(H_3BNMe_2BH_3)_3(PMe_3)_2$, **4**.

	Bond Lengths (Å)		
U(1)-B(1)	2.953(4)	U(1)-B(5)	2.944(3)
U(1)-B(2)	2.957(3)	U(1)-B(6)	2.949(4)
U(1)-B(3)	2.939(4)	U(1)-P(1)	3.114(1)
U(1)-B(4)	2.943(3)	U(1)-P(2)	3.109(1)
	Bond Angles (deg)		
B(1)-U(1)-B(2)	51.21(9)	B(3)-U(1)-B(6)	173.10(11)
B(3)-U(1)-B(4)	50.88(9)	B(3)-U(1)-P(1)	93.75(9)
B(5)-U(1)-B(6)	50.90(9)	B(3)-U(1)-P(2)	86.45(9)
B(1)-U(1)-B(3)	93.07(11)	B(4)-U(1)-B(5)	74.05(9)
B(1)-U(1)-B(4)	133.41(11)	B(4)-U(1)-B(6)	124.94(9)
B(1)-U(1)-B(5)	135.46(10)	B(4)-U(1)-P(1)	83.31(8)
B(1)-U(1)-B(6)	93.31(11)	B(4)-U(1)-P(2)	88.27(8)
B(1)-U(1)-P(1)	69.12(7)	B(5)-U(1)-B(6)	50.90(9)
B(1)-U(1)-P(2)	121.95(7)	P(1)-U(1)-B(5)	84.16(7)
B(2)-U(1)-B(3)	90.08(11)	P(2)-U(1)-B(5)	86.61(7)
B(2)-U(1)-B(4)	137.39(10)	P(1)-U(1)-B(6)	90.97(8)
B(2)-U(1)-B(5)	137.68(10)	P(2)-U(1)-B(6)	87.95(8)
B(2)-U(1)-B(6)	91.87(10)	P(1)-U(1)-P(2)	168.92(2)
P(1)-U(1)-B(2)	120.33(7)	B(1)-N(1)-B(2)	108.4(2)
P(2)-U(1)-B(2)	70.74(7)	B(3)-N(2)-B(4)	107.1(2)
B(3)-U(1)-B(4)	50.88(9)	B(5)-N(3)-B(6)	107.9(2)
B(3)-U(1)-B(5)	124.62(10)		

broadened singlet at δ -1.56 due to the PMe_3 groups and resonances at δ 4.03 and 98.3 due to the NMe_2 and BH_3 groups, respectively. The ^{11}B NMR chemical shift is δ 152.4. No signals were observed in the $^{31}P\{^1H\}$ NMR spectrum owing to the paramagnetism of the U^{III} center.

Magnetic Moments. The magnetic moments of **1**, **2**, and **4** at 293 K are 2.8, 2.9, and 2.7 μ_B, respectively. These values are similar to those of 2.59 – 2.92 μ_B at 300 K reported for certain U^{III} aryl-oxide complexes bearing functionalized triazacyclononane groups,[41-45] but are lower than the calculated μ_{eff} of 3.69 μ_B for a free U^{3+} ion.[46] Interestingly, some other U^{III} species such as $U_3(BH_4)_9$, $U(BH_4)_3$(2,2,2-cryptand), and $U[N(SiMe_3)_2]_3$ have magnetic moments of 3.1 -3.4 μ_B that fall much closer to the free ion value.[23, 47] It has been suggested that reduced magnetic moments can be attributed to a strong ligand field and, to a lesser effect, orbital reduction effects due to covalency in the metal ligand bonding.[44]

Reduction of U^{IV} to U^{III} by $Na(H_3BNMe_2BH_3)$. There are three notable aspects of the isolation of U^{III} products from the reaction of UCl_4 with $Na(H_3BNMe_2BH_3)$. First, the reductions are accompanied by the formation of a gas (H_2) and the organic byproduct (μ-dimethylamino)diborane, $(NMe_2)B_2H_5$; the latter was identified in the ^{11}B NMR spectra of the reaction solutions (see Experimental Section). Over the first several hours in thf, for every equivalent of $Na(H_3BNMe_2BH_3)$ consumed, one equivalent of $(NMe_2)B_2H_5$ is generated, as shown by integrations relative to an internal ^{11}B NMR standard. We believe the experimental conditions were such that adventitious hydrolysis can be ruled out; instead, the data suggest that the reaction of UCl_4 with $Na(H_3BNMe_2BH_3)$ initially generates $(NMe_2)B_2H_5$ and $UCl_3H(solvent)_x$, and that the latter subsequently reductively eliminates H_2 and reduces to $UCl_3(solvent)_x$. Evidently, substitution of the remaining uranium-bound chloride ligands with aminodiboranate anions is slow relative to the reduction step. Similar mechanisms have been invoked in certain reductions of U^{IV} to U^{III} in the presence of BH_4,[38,

[40, 47, 48] and it is known that tetrahydroborate complexes of redox stable metal ions such as Zr^{4+} or Hf^{4+} can produce B_2H_6 and metal hydrides.[49-51]

Second, the reduction of UCl_4 to uranium(III) products is solvent dependent, being slower in strongly coordinating ethers and faster in weakly coordinating ethers, as shown by time-dependent ^{11}B NMR studies of the UCl_4 + 4 $Na(H_3BNMe_2BH_3)$ reaction mixtures in Et_2O and thf. Although resonances for the paramagnetic uranium complexes could not be detected, information about the progress of the reaction was obtained from the increase in the concentration of $(NMe_2)B_2H_5$ and decrease in the concentration of $Na(H_3BNMe_2BH_3)$. In Et_2O the resonance for $Na(H_3BNMe_2BH_3)$ disappears after 4 h of reaction time,[52] whereas in thf significant amounts of this starting material are still present after 22 h. A likely candidate for solvent-dependent step that determines the rate of reduction of U^{IV} to U^{III} is dissociation of solvent from the uranium center to create the open coordination site necessary for the bimolecular reductive elimination of H_2. This dissociation (and subsequent reduction) will be slower for more strongly coordinating solvents.

Third, whereas the aminodiboranate ligand readily reduces U^{IV} to U^{III}, the analogous reactions of UCl_4 with $NaBH_4$ afford U^{IV} products at room temperature, with U^{III} products being generated only upon heating or by adding strong Lewis bases such as trialkylphosphines.[4, 40, 48, 53] The different reducing power is consistent with the previous finding that organic substrates and transition metals are more readily reduced by $Na(H_3BNMe_2BH_3)$ than by $NaBH_4$.[18, 54] We have carried out density functional theory (DFT) calculations to explore whether $Na(H_3BNMe_2BH_3)$ is in fact a stronger reductant than $NaBH_4$. We find that the ionization energy of the BH_4^- anion (calculated from the energy difference between the BH_4^- anion and the BH_4 radical) is 90.6 kcal/mol, whereas the

ionization energy of the $H_3BNMe_2BH_3^-$ anion is 86.1 kcal/mol. In other words, $H_3BNMe_2BH_3^-$ is a stronger reductant than BH_4^- by 4.5 kcal/mol, or 0.2 V.

It is important to consider, however, that the reduction of U^{IV} to U^{III} in this system is not a simple electron transfer but instead involves breaking B-H (and possibly U-H) bonds, and that these chemical steps are very likely irreversible and could drive an otherwise electrochemically unfavorable redox reaction. The fact that the reduction of UCl_4 by $Na(H_3BNMe_2BH_3)$ is faster in some solvents than in others strongly suggests that kinetic factors control the reduction process. All in all, however, the evidence at present does not allow us to distinguish between the following two explanations of why $H_3BNMe_2BH_3^-$ but not BH_4^- reduces U^{IV} to U^{III} at room temperature: $H_3BNMe_2BH_3^-$ is a stronger reductant than BH_4^- (a thermodynamic effect), or the barriers for the chemical processes associated with cleavage of B-H (and possibly U-H) bonds are larger for $H_3BNMe_2BH_3^-$ than for BH_4^- (a kinetic effect).

Chemical and Physical Properties of $U(H_3BNMe_2BH_3)_3$ Complexes and Characterization of $PMe_3BH_2NMe_2BH_3$. Complexes **1a**, **1b**, **2**, and **4** are air-sensitive (**1a** and **1b** especially so) and react vigorously with protic solvents such as alcohols and with halogenated solvents such as chloroform and dichloromethane. Addition of these solvents results in the evolution of gas and an immediate color change from brown to yellow. Similar reactivity has been observed for other U^{III} borohydride complexes.[55]

Compounds **1a**, **1b**, and **2** are thermally stable at room temperature for months when stored in sealed glassware under argon. In contrast, the PMe_3 adduct **4** slowly decomposes with loss of the phosphine-borane $PMe_3BH_2NMe_2BH_3$, **5**. This previously unreported compound has been characterized by its ^1H, ^{11}B, and $^{31}P\{^1H\}$ NMR spectra. The structure of

5 was also confirmed by single crystal X-ray diffraction of crystals grown from pentane (Figure 3.7; Table 3.6).

Our original interest in these uranium aminodiboranate complexes was to determine whether we could discover new volatile uranium complexes. The uranium complexes $U(H_3BNMe_2BH_3)_3$, **1**, and $U(H_3BNMe_2BH_3)_3(thf)$, **2**, are direct analogs of lanthanide complexes that we have already investigated as CVD precursors.[21] Heating the thf adducts $Ln(H_3BNMe_2BH_3)_3(thf)$ in vacuum causes loss of thf and formation of the base-free species $Ln(H_3BNMe_2BH_3)_3$. The latter are highly volatile, and sublime in vacuum at temperatures as low as 65 °C without decomposition.[21] The uranium complexes have structures that are essentially identical to those seen for the early lanthanides, and so we expected their volatilities to be similar.

To our surprise, attempts to sublime $U(H_3BNMe_2BH_3)_3(thf)$, **2**, at 10^{-2} Torr resulted instead in thermal decomposition, which afforded a metallic-appearing film on the surface of the glassware; similar behavior has been noted for $U(BH_4)_3(thf)_x$.[56] These results suggest that the uranium complexes decompose more rapidly than they sublime. The higher covalency of the U-H bond may mean that the B-H bonds in the uranium complexes are more readily cleaved than they are in the analogous lanthanide species.

The Uranium Oxo Borohydride Complex $U_2(\mu\text{-}O)(BH_4)_6(dme)_2$ and Reformulation of $U_2(\mu\text{-}H)_2(BH_4)_6(dme)_2$. The isolation of the uranium(IV) hydride $U_2(\mu\text{-}H)_2(BH_4)_6(dme)_2$, where dme = 1,2-dimethoxyethane, in 1987 provided crystallographic evidence that uranium(IV) hydrides are intermediates in the reduction of U^{IV} borohydrides to U^{III}.[48] This complex is also notable as one of the few crystallographically characterized

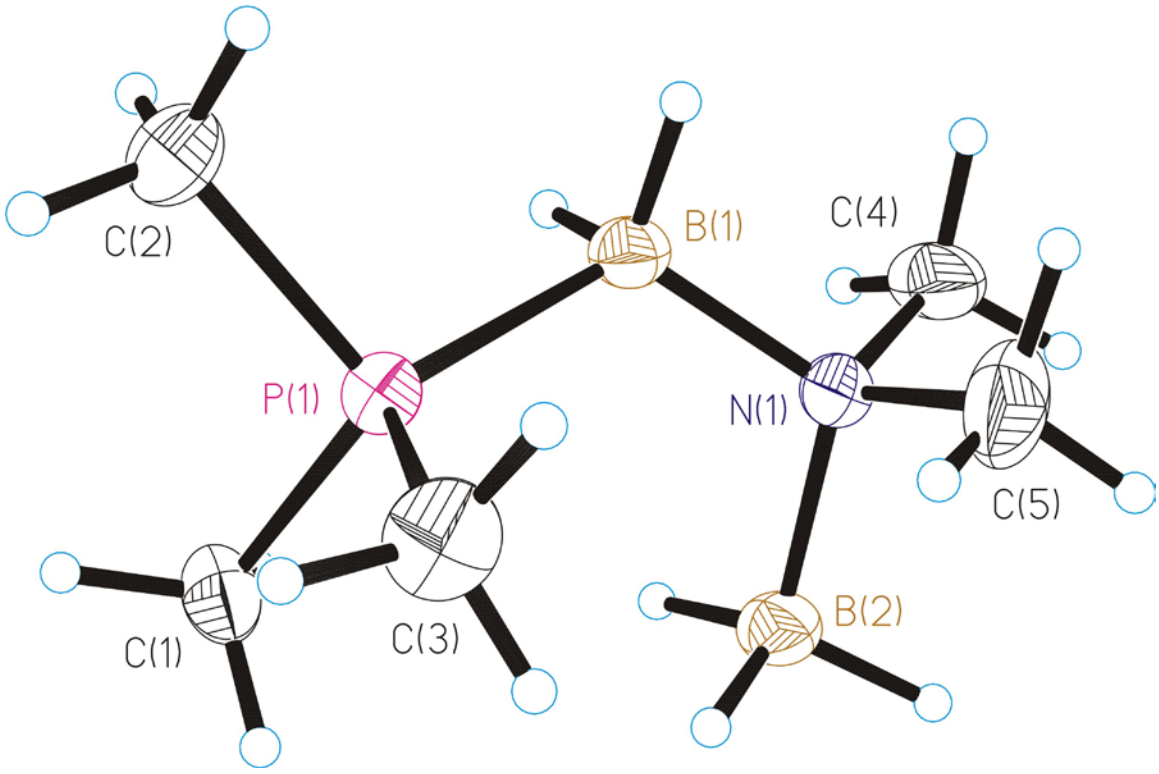

Figure 3.7. Molecular structure of $PMe_3BH_2NMe_2BH_3$, **5**. Ellipsoids are drawn at the 35% probability level, except for the hydrogen atoms, which are represented as arbitrarily sized spheres.

Table 3.6. Selected Bond Lengths and Angles for PMe_3-BH_2-NMe_2-BH_3, **5**.

	Bond Lengths (Å)		
P(1)-B(1)	1.948(3)	B(1)-H(12)	1.074(16)
N(1)-B(1)	1.551(3)	B(2)-H(21)	1.126(13)
N(1)-B(2)	1.604(3)	B(2)-H(22)	1.136(14)
B(1)-H(11)	1.077(16)	B(2)-H(23)	1.123(13)
	Bond Angles (deg)		
C(1)-P(1)-B(1)	117.02(12)	C(5)-N(1)-B(1)	111.09(18)
C(2)-P(1)-B(1)	105.22(13)	C(4)-N(1)-B(2)	108.12(18)
C(3)-P(1)-B(1)	118.24(13)	C(5)-N(1)-B(2)	108.5(2)
N(1)-B(1)-P(1)	118.48(17)	B(1)-N(1)-B(2)	113.38(17)
C(4)-N(1)-C(5)	108.3(2)	H(21)-B(2)-H(22)	110.9(16)
C(4)-N(1)-B(1)	107.3(2)		

actinide hydrides.[2, 3] Evidence is now presented that this $U_2(\mu\text{-}H)_2(BH_4)_6(dme)_2$ complex is actually the bridged oxo species $U_2(\mu\text{-}O)(BH_4)_6(dme)_2$.

In further studying the synthesis of uranium DMADB complexes, we carried out the reaction of UCl_4 and 4 equiv of $Na(H_3BNMe_2BH_3)$ in refluxing dme. This reaction yields small amounts of a new complex, which we formulate as $U_2(\mu\text{-}O)(BH_4)_6(dme)_2 \cdot C_7H_8$, **6**, as emerald green prisms by crystallization from a 1:1 toluene/pentane mixture.

The formation of BH_4^- groups from $H_3BNMe_2BH_3^-$ at elevated temperatures has precedent: we have shown elsewhere that an identical conversion takes place in the coordination sphere of thorium at elevated temperatures, and that this reaction occurs with elimination of 1 equiv of the aminoborane $[Me_2NBH_2]_2$ (Chapter 2). The presence of the bridging oxo ligand in **6** is almost certainly the result of adventitious water.[57, 58]

Single-crystal X-ray diffraction studies of **6** support the assigned stochiometry (Figure 3.8). Each uranium center adopts a *fac* octahedral geometry (counting the BH_4^- groups as occupying one coordination site); the bridging oxygen atom and the two coordinated oxygen atoms of the dme ligand occupy positions *trans* to the three BH_4^- groups. The hydride positions were located in the difference maps and reveal that all three BH_4^- groups are bound in a κ^3*H* (tridentate) fashion. The U··B distance to the BH_4^- group that is *trans* to the bridging oxygen, 2.635(7) Å, is about 0.06 Å longer that the U·B distances to the two groups that are *cis* to the bridging oxygen atom, 2.574(6) and 2.584(6) Å. Thus, the bridging oxygen atom exerts a noticeable *trans* influence, as is usually seen for oxo groups. In general, the U··B distances are similar to those observed in other U^{IV} complexes with κ^3-BH_4^- groups.[3, 11]

The U-O bond distances to the dme molecule are 2.498(3) - 2.544(4) Å. The distances are slightly longer than those observed for adducts of $U(BH_4)_4$ with dimethyl ether (2.44

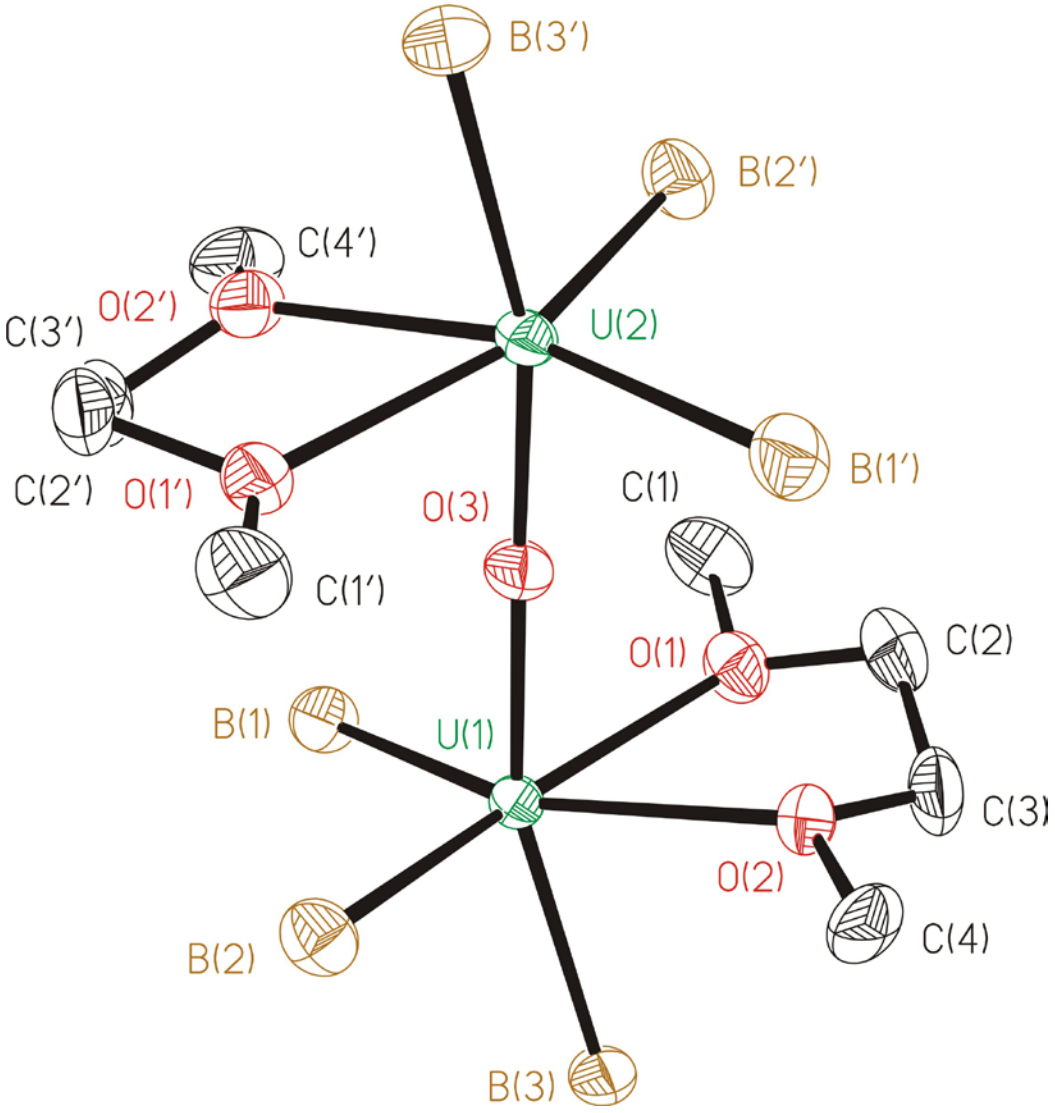

Figure 3.8. Molecular structure of $U_2(\mu\text{-}O)(BH_4)_6(dme)_2$, **6**. Ellipsoids are drawn at the 35% probability level. Hydrogen atoms and the disordered toluene solvate molecule have been omitted. The primed and unprimed atoms are not related by symmetry, but are related by the inversion center in the smaller cell chosen for "$U_2(\mu\text{-}H)_2(BH_4)_6(dme)_2$."

Å),[32] diethyl ether (2.49 Å),[32] di-*n*-propyl ether (2.48 Å),[33] and tetrahydrofuran (2.47 Å).[31] The bridging oxygen atom in **6** rests between the uranium atoms, and the U-O-U angle is nearly linear at 172.9(2)°. The U-O distances of 2.074(3) and 2.080(3) Å are comparable to those observed in other U^{IV} μ-oxo compounds, such as $U_2(\mu\text{-}O)_2[C_5H_3(SiMe_3)_2]_4$ (2.10 and 2.13 Å),[59] $U_2(\mu\text{-}O)(C_5H_4SiMe_3)_6$ (2.11 Å),[60] and $U_3(\mu\text{-}O)_3(C_5H_4SiMe_3)_6$ (2.05 – 2.12 Å).[61] Only one other uranium oxo/borohydride complex has been isolated and crystallographically characterized, the uranyl complex $UO_2(\kappa^2\text{-}BH_4)_2(hmpa)_2$, where hmpa = hexamethylphosphoramide.[62]

Aside from the identity of the bridging ligands, the structure of $U_2(\mu\text{-}O)(BH_4)_6(dme)_2$ is remarkably similar to that of a previously reported complex, the hydride $U_2(\mu\text{-}H)_2(BH_4)_6(dme)_2$ (Table 3.7). Both compounds crystallize from 1:1 pentane:toluene in the triclinic space group $P\bar{1}$, with one molecule of toluene per dinuclear unit. The U···U distance is 4.146(3) Å in **6** vs. 4.12 Å in the hydride, and all the ligands are disposed in exactly the same fashion. Significantly, the structure report for $U_2(\mu\text{-}H)_2(BH_4)_6(dme)_2$ noted that there was a spurious peak of electron density midway between the two uranium atoms that could not be explained. We believe that this peak was due to an oxygen atom. Evidence in support of the presence of two bridging hydrides was unavailable: no hydride resonance could be located in the ^1H NMR spectrum, and no electron density corresponding to a pair of bridging hydrogen atoms could be found in the electron density difference map. Direct evidence of bridging hydrogen atoms in uranium complexes is well known to be difficult to obtain owing to the low X-ray scattering power of hydrogen atoms relative to uranium, but a re-evaluation of the evidence suggests that the bridging atom is oxygen and not hydrogen.

Interestingly, the unit cell for **6** is different from that reported for the putative hydride, the current cell having approximately twice the volume and different cell parameters. But we believe that both crystal structures are of the same crystalline substance. If the cell parameters

Table 3.7. Selected bond lengths and angles for $U_2(\mu\text{-}O)(BH_4)_6(dme)_2 \cdot C_7H_8$, **6**, with those reported for "$U_2(\mu\text{-}H)_2(BH_4)_6(dme)_2 \cdot C_7H_8$" in square brackets and in bold.

Bond Lengths (Å)				
U(1)-O(1)	2.544(4)	[**2.53**]	U(2)-O(1')	2.503(4)
U(1)-O(2)	2.498(3)	[**2.47**]	U(2)-O(2')	2.518(4)
U(1)-B(1)	2.574(6)	[**2.64**]	U(2)-B(1')	2.595(7)
U(1)-B(2)	2.584(8)	[**2.64**]	U(2)-B(2')	2.577(7)
U(1)-B(3)	2.635(7)	[**2.53**]	U(2)-B(3')	2.631(7)
U(1)-U(2)	4.146(3)	[**4.12**]	U(2)-O(3)	2.074(3)
U(1)-O(3)	2.080(3)			
Bond Angles (deg)				
O(1)-U(1)-O(2)	65.12(12)	[**65.1**]	O(1')-U(2)-O(2')	65.39(13)
B(1)-U(1)-B(2)	104.2(2)	[**105**]	B(1')-U(2)-B(2')	104.8(2)
B(1)-U(1)-B(3)	96.8(2)	[**103**]	B(1')-U(2)-B(3')	95.6(2)
B(2)-U(1)-B(3)	96.0(2)	[**97**]	B(2')-U(2)-B(3')	95.6(2)
O(1)-U(1)-B(1)	88.68(19)	[**93.4**]	O(1')-U(2)-B(1')	98.8(2)
O(1)-U(1)-B(3)	88.82(18)	[**84**]	O(1')-U(2)-B(3')	84.63(18)
O(2)-U(1)-B(2)	101.83(18)	[**96**]	O(2')-U(2)-B(2')	90.79(19)
O(2)-U(1)-B(3)	83.00(17)	[**78**]	O(2')-U(2)-B(3')	89.14(18)
U(1)-O(3)-U(2)	172.94(18)			

for the hydride crystal structure are designated with primes, the two unit cells are related by the following transformation: $\vec{a}' = ½ (-\vec{a} + \vec{c})$, $\vec{b}' = ½ (\vec{a} + \vec{c})$, and $\vec{c}' = \vec{b}$. If we apply this transformation to the cell parameters measured for **6**, the result is as follows (with the cell parameters reported for the hydride given in parentheses): $a' = 8.084$ (8.126), $b' = 8.976$ (8.950), $c' = 11.500$ (11.638) Å, $\alpha' = 83.70$ (83.50), $\beta' = 88.92$ (89.44), and $\gamma' = 68.21$ (69.76)°. The exact values are slightly different, probably because the crystal temperature was different for the two data sets.

In the larger (correct) unit cell, the bridging oxygen atom lies at a general position, but its coordinates are very near to (¼, 0, ¾). As a result, this atom lies almost exactly halfway between inversion centers in the *ac* plane of the larger $P\bar{1}$ unit cell. Because the individual molecules of **1** have very nearly ideal (but noncrystallographic) inversion symmetry, there is a large degree of pseudosymmetry: the crystal coordinates almost (but not exactly) correspond to a smaller unit cell, also of $P\bar{1}$ symmetry, in which an additional inversion center is present on the bridging oxygen atom. Several lines of evidence speak in support of the larger unit cell being the correct one: (1) additional (albeit weak) reflections appear in the diffraction record that correspond only to this larger cell, (2) the two molecules in the larger unit cell are not related by symmetry (as assessed by Platon),[63] (3) there are no large correlation coefficients between any of the parameters for the non-hydrogen atoms in the least squares matrix, and (4) hydrogen atoms could be located and refined (which was not possible for the crystal of the putative hydride, although this result could also been a consequence of larger errors in the intensity measurements). In the previous refinement, in contrast, the incorrect choice of unit cell and consequent averaging of the atomic coordinates related by the pseudosymmetry caused some significant errors. For example, the boron atom *trans* to the bridging oxo group had unusually large displacement parameters,

Table 3.8. ^{1}H NMR shifts for $U_2(\mu\text{-}O)(BH_4)_6(dme)_2$, **1**, at -60 °C in toluene (600 MHz) and comparison to those reported for "$U_2(\mu\text{-}H)_2(BH_4)_6(dme)_2$" (60 MHz).[48]

	$U_2(\mu\text{-}O)(BH_4)_6(dme)_2$	"$U_2(\mu\text{-}H)_2(BH_4)_6(dme)_2$"
BH_4	727 (br s, fwhm = 2700 Hz)	752.6 (br s, fwhm = 530 Hz, 4H)
BH_4	-115 (s, fwhm = 290 Hz, 4H)	-121.3 (br s, fwhm = 140 Hz, 8H)
OCH_2	-32.4 (s, fwhm = 80 Hz, 2H)	-31.6 (s, 2H)
OCH_2	-52.9 (s, fwhm = 110 Hz, 2H)	-52.3 (s, 2H)
OMe	-62.0 (s, fwhm = 110 Hz, 3H)	-62.8 (s, 3H)

and its U···B distance was 0.09 Å shorter (instead of 0.06 Å longer) than the two U··B distances to the other two BH_4^- ligands.

The ^{1}H NMR spectrum of $U_2(\mu\text{-}O)(BH_4)_6(dme)_2$ at -60 °C in C_7D_8 closely matches that reported for "$U_2(\mu\text{-}H)_2(BH_4)_6(dme)_2$" under similar conditions (Table 3.8). The most striking resemblance is the chemical shift of one of the BH_4 resonances, which is shifted dramatically to lower field: δ 727, compared to the reported value of δ 753 for $U_2(\mu\text{-}H)_2(BH_4)_6(dme)_2$. We do suggest a reversal of the assignments of the two BH_4 resonances, however: the resonance at δ -115 integrates to four protons in our spectrum (vs. eight reported previously), and thus this resonance is best assigned to the BH_4^- group that is *trans* to the bridging oxo ligand. We could not obtain an accurate integral for the resonance at δ 727 owing to its large shift and line width. Integrations for the dme resonances match those previously reported.

The crystallographic and ^{1}H NMR data presented here strongly suggest that the uranium hydride complex $U_2(\mu\text{-}H)_2(BH_4)_6(dme)_2$ should be reformulated as the oxo complex $U_2(\mu\text{-}O)(BH_4)_6(dme)_2$.

Experimental

All operations were carried out in vacuum or under argon using standard Schlenk techniques. All glassware was dried in an oven at 150 °C, assembled hot, and allowed to cool under vacuum before use. Tetrahydrofuran, diethyl ether, 1,2-dimethoxyethane, and pentane were distilled under nitrogen from sodium/benzophenone and degassed with argon immediately before use. Toluene was dried similarly over molten sodium. The compounds UCl_4,[64] PMe_3,[65] and $Na(H_3BNMe_2BH_3)$[18] were prepared by literature routes.

Elemental analyses were carried out by the University of Illinois Microanalytical Laboratory. The IR spectra were recorded on a Nicolet Impact 410 infrared spectrometer as

Nujol mulls between KBr plates. The ^{1}H data were obtained on a Varian Unity 400 instrument at 400 MHz or on a Varian Unity U500 instrument at 500 MHz. The ^{11}B NMR data were collected on a General Electric GN300WB instrument at 96 MHz or on a Varian Unity Inova 600 instrument at 192 MHz. Chemical shifts are reported in δ units (positive shifts to high frequency) relative to TMS (^{1}H) or BF_3•Et_2O (^{11}B). Field ionization (FI) mass spectra were recorded on a Micromass 70-VSE mass spectrometer. The shapes of all peak envelopes correspond with those calculated from the natural abundance isotopic distributions. Magnetic moments were determined in C_6D_6 by the Evans NMR method[66] on a Varian Gemini 500 instrument at 499.716 MHz. Melting points and decomposition temperatures were determined in closed capillaries under argon on a Thomas-Hoover Unimelt apparatus. Powder X-ray diffraction measurements were carried out on a Bruker P4RA/GADDS wide angle diffractometer using a Cu Kα radiation source.

■ CAUTION: Uranium salts are alpha emitters and are known nephrotoxins. Inhalation should be avoided by conducting all operations of dry materials in an approved fume hood and with proper safety equipment. Complexes **1a** and **1b** enflame upon exposure to air.

Tris(*N*,*N*-dimethylaminodiboranato)uranium(III), $U(H_3BNMe_2BH_3)_3$, structural isomer 1a. To a suspension of UCl_4 (0.27 g, 0.71 mmol) in diethyl ether (20 mL) at 0 °C was added a solution of sodium *N*,*N*-dimethylaminodiboranate (0.27 g, 2.9 mmol) in diethyl ether (20 mL). The mixture was warmed to room temperature and stirred for 17 h. Gas slowly evolved and the bright green solution gradually turned dark brown over several hours. The brown mixture was evaporated to dryness under vacuum and the brown residue was extracted with pentane (6 × 50 mL). The light brown extracts were combined, concentrated to 45 mL, and cooled to -20 °C to yield light brown crystals. Yield: ca. 30 mg (9 %). NMR and IR data were identical to those for isomer **1b**.

Structural isomer 1b. To a suspension of UCl_4 (0.50 g, 1.3 mmol) in diethyl ether (15 mL) at 0 °C was added a solution of sodium *N*,*N*-dimethylaminodiboranate (0.51 g, 5.4 mmol) in diethyl ether (15 mL). The mixture was warmed to room temperature and stirred for 13 h. Gas slowly evolved and the bright green solution gradually turned dark brown over several hours. The brown mixture was evaporated to dryness under vacuum and the brown residue was extracted with toluene (2 × 25 mL). The red extracts were combined and evaporated to dryness under vacuum to yield a dark reddish-brown residue. The residue was washed with pentane (10 mL) and evaporated to dryness under vacuum to yield a dark orange powder. Yield: 0.32 g (53 %). In another reaction, the residue was extracted with toluene (2 × 25 mL), concentrated to ca. 20 mL, and cooled to -20 ˚C to yield red microcrystals. Yield: 0.14 g, (26 %). M.p. 156 ˚C (dec). Anal. Calcd for $C_6H_{36}B_6N_3U$: C, 15.9; H, 8.01; N, 9.27. Found: C, 15.7; H, 7.50; N, 9.06. ^{1}H NMR (C_7D_8, 20 °C): δ 3.76 (br s, fwhm = 60 Hz, NMe_2, 36 H), 91.3 (br s, fwhm = 1100 Hz, BH_3). ^{11}B NMR (C_7D_8, 20 °C): δ 163.4 (br s, fwhm = 510 Hz). Magnetic moment (C_6D_6, 20 °C): 2.8 μ_B. IR (cm^{-1}): 2399 vs, 2331 m, 2270 s, 2202 vs, 2168 s, 2094 sh, 1402 w, 1327 sh, 1265 s, 1238 s, 1215 s, 1182 m, 1166 s, 1161 s, 1132 m, 1032 m, 928 m, 902 w, 808 w, 760 w, 451 m.

Tris(*N*,*N*-dimethylaminodiboranato)(tetrahydrofuran)uranium(III), $U(H_3BNMe_2BH_3)_3$-(thf), 2. To a suspension of UCl_4 (0.52 g, 1.4 mmol) in tetrahydrofuran (20 mL) at 0 °C was added a solution of sodium *N*,*N*-dimethylaminodiboranate (0.52 g, 5.5 mmol) in tetrahydrofuran (20 mL). The reaction mixture was warmed to room temperature and a small amount of gas initially evolved. The mixture stirred for 14 h to generate a green solution and a small amount of white precipitate. The mixture was evaporated to dryness under vacuum to afford a sticky dark brown solid, which was extracted with pentane (3 × 20 mL). The filtered extracts were combined, concentrated to ca. 28 mL, and cooled to -20 ˚C to yield 0.24 g of brown cubes. The

mother liquor was concentrated to ca. 11 mL and cooled to -20 ˚C to yield an additional 0.14 g of product. Yield: 0.38 g (53 %). M.p. 135-136 ˚C. Anal. Calcd for $C_{10}H_{44}B_6N_3OU$: C, 22.9; H, 8.44; N, 7.99. Found: C, 22.8; H, 8.25; N, 7.66. ^{1}H NMR (C_6D_6, 20 °C): δ -5.56 (br s, fwhm = 125 Hz, α-thf, 4 H), -1.89 (br s, fwhm = 38 Hz, β-thf, 4 H), 3.36 (s, fwhm = 4 Hz, NMe_2, 18 H), 104.4 (br d, fwhm = 320 Hz, BH_3, 18 H). ^{11}B NMR (C_6D_6, 20 °C): δ 152.8 (br s, fwhm = 180 Hz). Magnetic moment (C_6D_6, 20 °C): 2.9 μ_B. MS(FI) [fragment ion, relative abundance]: *m*/*z* 453 [$U(H_3BNMe_2BH_3)_3$, 15], 72 [thf, 100]. IR (cm^{-1}): 2390 vs, 2335 m, 2278 s, 2210 vs, 2173 sh, 2064 sh, 1400 w, 1236 s, 1217 s, 1186 s, 1169 s, 1136 s, 930 m, 903 w, 856 m, 837 m, 812 w, 451 m.

Tris(*N*,*N*-dimethylaminodiboranato)(1,2-dimethoxyethane)uranium(III), $U(H_3BNMe_2BH_3)_3$(dme), 3. Method A: To a suspension of UCl_4 (0.34 g, 0.90 mmol) in 1,2-dimethoxyethane (20 mL) at 0 °C was added a solution of sodium *N*,*N*-dimethylaminodiboranate (0.34 g, 3.6 mmol) in dme (20 mL). The reaction mixture was warmed to room temperature and stirred for 15 h to generate a green solution and a small amount of white precipitate. The mixture was evaporated to dryness under vacuum to afford a sticky dark green solid, which slowly turned brown under dynamic vacuum over several hours. The residue was extracted with benzene (2 × 25 mL), and the extracts were filtered, combined, and evaporated to dryness under vacuum. The evaporated residue was washed with pentane (2 × 10 mL) to yield a free-flowing, dark mustard colored powder. Yield: 0.20 g. The NMR spectra of this powder were identical to those seen for the material made by method B below, but the microanalytical data suggested that the powder contained an NMR-silent impurity. Anal. Calcd for $C_{10}H_{46}B_6N_3O_2U$: C, 22.1; H, 8.53; N, 7.73. Ranges found (four samples): C, 16.65 – 18.15; H, 6.44 – 7.27; N, 6.01 – 7.25.

Method B: To $U(H_3BNMe_2BH_3)_3$(thf) (0.16 g, 0.30 mmol) in pentane (20 mL) was added 1,2-dimethoxyethane (0.5 mL). A small amount of precipitate immediately formed. The

brown mixture was stirred for several hours and the filtered. The filtrate was taken to dryness under vacuum to afford a crystalline brown powder. Yield: 0.10 g (58 %). M.p. 138 ˚C (dec.). Anal. Calcd for $C_{10}H_{46}B_6N_3O_2U$: C, 22.1; H, 8.53; N, 7.73. Found: C, 22.2; H, 8.39; N, 7.40. ^{1}H NMR (C_6D_6, 600 MHz, 20 °C): δ -2.23 (br s, fwhm = 100 Hz, OCH_2, 4 H), 2.64 (s, fwhm = 25 Hz, NMe_2, 18 H), 3.25 (s, fwhm = 45 Hz, OMe, 6 H), 94.8 (br s, fwhm = 410 Hz, BH_3, 18 H). ^{11}B NMR (C_6D_6, 192 MHz, 20 °C): 152.6 (br s, fwhm = 230 Hz, BH_3). IR (cm^{-1}): 2385 vs, 2341 m, 2290 s, 2227 vs, 2173 sh, 2056 sh, 1260 s, 1236 s, 1215 m, 1185 m, 1166 s, 1137 s, 1129 sh, 1089 m, 1034 s, 1013 vs, 975 w, 926 w, 904 w, 858 s, 815 w, 724 s, 447 m.

Tris(*N*,*N*-dimethylaminodiboranato)bis(trimethylphosphine)uranium(III), $U(H_3BNMe_2BH_3)_3(PMe_3)_2$, 4. To $U(H_3BNMe_2BH_3)_3$(thf) (0.18 g, 0.34 mmol) in pentane (20 mL) was added trimethylphosphine (0.14 mL, 1.4 mmol). The brown solution immediately turned dark red. The solution was stirred for 20 min, concentrated to 10 mL, and cooled to -20 °C to yield dark red crystals. Yield: 0.13 g (64 %). M.p. 173 ˚C (dec). Anal. Calcd for $C_{12}H_{54}B_6N_3P_2U$: C, 23.8; H, 8.99; N, 6.94. Found: C, 23.7; H, 9.30; N, 6.80. ^{1}H NMR (C_6D_6, 20 °C): δ -1.56 (br s, fwhm = 110 Hz, PMe_3, 18 H), 4.03 (s, fwhm = 4 Hz, NMe_2, 36 H), 98.3 (br s, fwhm = 330 Hz, BH_3, 36 H). ^{11}B NMR (C_6D_6, 20 °C): δ 152.4 (br s, fwhm = 190 Hz). MS(FI) [fragment ion, relative abundance]: *m*/*z* 601 [$U(H_3BNMe_2BH_3)_3(H_3BNMe_2BH_2PMe_3)^+$, 75], 530 [$U(H_3BNMe_2BH_3)_3(PMe_3)^+$, 100], 454 [$U(H_3BNMe_2BH_3)_3^+$, 83]. Magnetic moment ($C_6D_6$, 20 °C): 2.7 μ_B. IR (cm^{-1}): 2379 vs, 2355 vs, 2329 m, 2269 m, 2207 vs, 2164 sh, 2061 w, 1303 w, 1284 w, 1228 s, 1213 m, 1182 sh, 1163 vs, 1136 s, 947 m, 923 sh, 904 sh, 812 w, 459 m.

μ-(*N*,*N*-Dimethylamido)pentahydro(trimethylphosphine)diboron, $PMe_3BH_2NMe_2$-BH_3, 5. Method A. At room temperature under an inert atmosphere, crystals of **4** change color from dark red to grayish-black over several months (in contrast, crystals of **1a**, **1b**, and **2** are

unchanged over these periods). Extraction of these aged crystals with C_6D_6 afforded a red solution and large amounts of an insoluble brown solid. The NMR spectra of the soluble fraction revealed the presence of **4** and the phosphinoborane $PMe_3BH_2NMe_2BH_3$, **5**, which had the following NMR parameters. ^{1}H NMR (C_6D_6, 20 °C): δ 0.78 (d, J_{HP} = 10 Hz, PMe_3, 9 H), 2.24 (q, J_{BH} = 102 Hz, BH_2, 2 H), 2.41 (q, J_{BH} = 93 Hz, BH_3, 3 H), 2.50 (s, NMe_2, 6 H). ^{11}B NMR (C_6D_6, 20 °C): δ -9.7 (td, J_{PB} = 81 Hz, J_{HB} = 102 Hz), -9.1 (q, J_{HB} = 95 Hz). ^{31}P{^{1}H} NMR (C_6D_6, 20 °C): -13.4 (q, J_{BP} = 76 Hz).

Method B. To a suspension of UCl_4 (0.25 g, 0.66 mmol) in thf (10 mL) was added sodium *N*,*N*-dimethylaminodiboranate (0.25 g, 2.6 mmol) in Et_2O (10 mL). The reaction mixture was warmed to room temperature and a small amount of gas initially evolved. The mixture stirred for 14 h to generate a green solution and a small amount of white precipitate. The mixture was evaporated to dryness under vacuum to afford a sticky dark brown solid, which was extracted with pentane (3 × 5 mL) and filtered. To the filtered extract was added PMe_3 (0.21 mL, 2.0 mmol) via syringe. The brown solution immediately turned dark red. The red solution was filtered, concentrated to ca. 8 mL, and cooled to -20 °C. Colorless plates co-crystallized with red crystals of **4**. The NMR spectra showed that the colorless plates were the phosphinoborane **5**.

NMR Studies of the Reaction of UCl_4 with $Na(H_3BNMe_2BH_3)$. Aliquots of the UCl_4 + 4 $Na(H_3BNMe_2BH_3)$ reaction mixtures used to synthesize **1a**, **1b**, and **2** were taken periodically, and the aliquots were examined by ^{11}B NMR spectroscopy. Sealed capillaries containing a 0.7 M solution of $NaBPh_4$ in diglyme were used as an internal ^{11}B NMR standard. Aliquots of the UCl_4 + 4 $Na(H_3BNMe_2BH_3)$ reaction mixtures used to synthesize **1a**, **1b**, and **2** were taken periodically, and the aliquots were examined by ^{11}B NMR spectroscopy. Sealed capillaries containing a 0.7 M solution of $NaBPh_4$ in diglyme were used as an internal ^{11}B NMR standard.

In both Et_2O and thf solvents, a ^{11}B NMR resonance due to the reduction byproduct $B_2H_5(NMe_2)$ grew in over time at ca. δ -17, which was triplet of doublets in Et_2O and a sextet in thf.[67-69]

For the reactions conducted in Et_2O, the aliquots initially consisted of a clear solution and a green solid (UCl_4) that settled out in the NMR tube; later the aliquots were brown with a white precipitate. In this solvent, the $^{11}B\{^1H\}$ NMR resonance due to unreacted $Na(H_3BNMe_2BH_3)$ was significantly broadened (fwhm = 280 Hz vs. 50 Hz for the salt alone in Et_2O), probably owing to ligand association/exchange with paramagnetic uranium species in solution. After 4 h, the $Na(H_3BNMe_2BH_3)$ had been completely consumed, and the only detectable ^{11}B NMR resonances were those due to $(NMe_2)B_2H_5$ and a new, unidentified species at δ -168.8 (fwhm = 250 Hz) in a 1:1 intensity ratio. The new species does not correspond to **1**, which is characterized by a broad ^{11}B NMR resonance at δ 155.7 (fwhm = 600 Hz).

For the reaction conducted in thf, the aliquots initially consisted of a clear green solution. Unlike the reaction in Et_2O, the line width of the $^{11}B\{^1H\}$ NMR peak due to $Na(H_3BNMe_2BH_3)$ was also broadened (fwhm = 80 Hz vs 20 Hz for the salt alone in thf). The concentration of $Na(H_3BNMe_2BH_3)$ decreased slowly with time, although 87% remained after 22 h. The concentration of $(NMe_2)B_2H_5$ increased over this same period, and integrations suggested that 1 equiv of this product was formed for every equiv of $Na(H_3BNMe_2BH_3)$ consumed. At this point, the thf was removed under vacuum, which caused the color of the reaction mixture to change from green to brown. The sticky brown residue was left under dynamic vacuum for ~1 h and then redissolved in the same volume of thf (40 mL). A ^{11}B NMR spectrum revealed that ca. 50% of the $Na(H_3BNMe_2BH_3)$ remained unreacted relative to the initial concentration of $Na(H_3BNMe_2BH_3)$ used. Removal of the solvent, and stirring of the residue with pentane (40 mL) for 18 h afforded a brown solution (containing the product **1**) and a solid that dissolved in thf to afford a green solution suggestive of $UCl_4(thf)_x$.[30] A ^{11}B NMR spectrum of the green

solution showed the same amount of unreacted $Na(H_3BNMe_2BH_3)$ as before the pentane extraction of **1**.

(μ-Oxo)Hexakis(tetrahydroborato)bis(1,2-dimethoxyethane)diuranium(IV), Toluene Solvate, $U_2(\mu\text{-}O)(BH_4)_6(dme)_2\cdot C_7H_8$, 6. To a suspension of UCl_4 (0.27 g, 0.71 mmol) in 1,2-dimethoxyethane (15 mL) was added a solution of sodium *N*,*N*-dimethylaminodiboranate (0.27 g, 2.8 mmol) in 1,2-dimethoxyethane (15 mL). The reaction mixture was heated to reflux for 12 h, over which time the solution color changed from green to light brown, and a dark precipitate formed. The solvent was removed under vacuum to afford a sticky, dark brown solid. The residue was extracted with toluene (20 mL), and the filtered extract was concentrated to ca. 10 mL and layered with pentane (10 mL). The mixture was kept at room temperature for several hours, and small green prisms formed. The crystals were collected, and the mother liquor was decanted and cooled to -20 °C overnight to yield a second crop of green prisms. Yield: 20 mg (7 %). ^{1}H NMR (C_7D_8, -60 °C): δ -115 (s, fwhm = 290 Hz, BH_4, 4H), -62.0 (s, fwhm = 110 Hz, OMe, 3 H), -52.9 (s, fwhm = 110 Hz, OCH_2, 2 H), -32.4 (s, OCH_2, fwhm = 80 Hz, 2H), 727 (br s, fwhm = 2700 Hz, BH_4).

DFT calculations. Calculations were performed with Gaussian03 Rev. C.02 by Charity Flener-Lovitt.[70] All structures were optimized with the B3LYP functional and the valence double-zeta polarized 6-31G* Pople basis set, which includes six d-type Cartesian-Gaussian polarization functions for the non-hydrogen atoms.

Crystallographic Studies.[71] Single crystals obtained from pentane (**1a**, **2**, **4**, and **5**), toluene (**1b**), or a 1:1 mixture of toluene and pentane (**6**) were mounted on glass fibers with Paratone-N oil (Exxon) and immediately cooled to -80 °C (-75 °C for **6**) in a cold nitrogen gas stream on the diffractometer. Standard peak search and indexing procedures, followed by least-square refinement yielded the cell dimensions given in Table 3.1. The measured intensities were

reduced to structure factor amplitudes and their estimated standard deviations by correction for background and Lorentz and polarization effects. No corrections for crystal decay were necessary but a face-indexed absorption correction was applied. Systematically absent reflections were deleted and symmetry equivalent reflections were averaged to yield the set of unique data. Except where noted, all unique data were used in the least-squares refinements. The analytical approximations to the scattering factors were used, and all structure factors were corrected for both real and imaginary components of anomalous dispersion. Correct atomic position(s) were deduced from an E-map (SHELX); least-squares refinement and difference Fourier calculations were used to locate atoms not found in the initial solution. Except where noted below, hydrogen atoms on the anionic ligands were placed in idealized positions with C-H (methyl) = 0.98 Å, C-H (methylene) = 0.99 Å, and B-H = 1.15 Å; idealized methyl and boranyl groups were allowed to rotate about their respective axes to find the best least-squares positions. In the final cycle of least squares, independent anisotropic displacement factors were refined for the non-hydrogen atoms. The displacement parameters for methylene and boranyl hydrogens were set equal to 1.2 times U_{eq} for the attached carbon and boron, respectively; those for methyl hydrogens were set to 1.5 times U_{eq} for the attached carbon. No correction for isotropic extinction was necessary. Successful convergence was indicated by the maximum shift/error of 0.000 for the last cycle. A final analysis of variance between observed and calculated structure factors showed no apparent errors. Aspects of the refinements unique to each structure are reported below.

U(H$_3$BNMe$_2$BH$_3$)$_3$, 1a. The monoclinic lattice and systematic absences $0k0$ ($k \neq 2n$) and $h0l$ ($l \neq 2n$) were uniquely consistent with the space group $P2_1/c$, which was confirmed by the success of the subsequent refinement. The quantity minimized by the least-squares program was $\Sigma w(F_o^2 - F_c^2)^2$, where $w = \{[\sigma(F_o^2)]^2 + (0.0318P)^2\}^{-1}$ and $P = (F_o^2 + 2F_c^2)/3$. The largest peak in

the final Fourier difference map (2.90 eÅ^{-3}) was located 0.96 Å from U1.

U(H$_3$BNMe$_2$BH$_3$)$_3$, 1b. The monoclinic lattice and systematic absences 0*k*0 ($k \neq 2n$) and *h*0*l* ($l \neq 2n$) were uniquely consistent with the space group $P2_1/c$, which was confirmed by the success of the subsequent refinement. The quantity minimized by the least-squares program was $\Sigma w(F_o^2 - F_c^2)^2$, where $w = \{[\sigma(F_o^2)]^2 + (0.374P)^2\}^{-1}$ and $P = (F_o^2 + 2F_c^2)/3$. The boranyl hydrogen atoms were located in the difference maps, and their positions were refined with independent isotropic displacement parameters. Chemically equivalent B–H distances within the BH_3 units were constrained to be equal within a standard deviation of 0.01 Å. The remaining hydrogen atoms were placed in idealized positions. The largest peak in the final Fourier difference map (4.18 eÅ^{-3}) was located 0.96 Å from U1.

U(H$_3$BNMe$_2$BH$_3$)$_3$(thf), 2. The cubic lattice and systematic absences *hkl* ($h + k + l \neq 2n$) were consistent with space groups $Im\bar{3}$, *I*23, $I2_13$, $Im\bar{3}m$, $I\bar{4}3m$, and *I*432; the non-centrosymmetric group *I*23 was shown to be the correct choice by successful refinement of the proposed model. The reflections 011 and 103 were statistical outliers and were deleted. The quantity minimized by the least-squares program was $\Sigma w(F_o^2 - F_c^2)^2$, where $w = \{[\sigma(F_o^2)]^2 + (0.0201P)^2\}^{-1}$ and $P = (F_o^2 + 2F_c^2)/3$. The tetrahydrofuran molecule was disordered about a three-fold axis and its C-O and C-C bond distances were fixed at 1.48 ± 0.01 and 1.52 ± 0.01Å, respectively. The largest peak in the final Fourier difference map (0.58 eÅ^{-3}) was located 0.72 Å from U1.

U(H$_3$BNMe$_2$BH$_3$)$_3$(PMe$_3$)$_2$, 4. The orthorhombic lattice and the systematic absences 0*kl* ($k \neq 2n$), *h*0*l* ($l \neq 2n$), and *hk*0 ($h \neq 2n$) were uniquely consistent with the space group *Pbca*, which was confirmed by the success of the subsequent refinement. The reflections 104, 202, 002, 106, and 102 were statistical outliers and were deleted. The quantity minimized by the least-squares program was $\Sigma w(F_o^2 - F_c^2)^2$, where $w = \{[\sigma(F_o^2)]^2 + (0.0238P)^2\}^{-1}$ and $P = (F_o^2 +$

$2F_c^2)/3$. The largest peak in the final Fourier difference map (0.75 eÅ^{-3}) was located 1.01 Å from U1.

$PMe_3BH_2NMe_2BH_3$, 5. The orthorhombic lattice and the systematic absences $0kl$ ($l \neq 2n$) and $h0l$ ($h \neq 2n$) were consistent with the space groups $Pca2_1$ and $Pbcm$; the non-centrosymmetric space group $Pca2_1$ was shown to be the correct choice by successful refinement of the proposed model. The hydrogen atoms attached to boron were located in the difference maps, and their positions were refined with independent isotropic displacement parameters. Chemically equivalent B–H distances were constrained to be equal within a standard deviation of 0.01 Å. The remaining hydrogen atoms were placed in idealized positions. The quantity minimized by the least-squares program was $\Sigma w(F_o^2 - F_c^2)^2$, where $w = \{[\sigma(F_o^2)]^2 + (0.0398P)^2\}^{-1}$ and $P = (F_o^2 + 2F_c^2)/3$. The largest peak in the final Fourier difference map (0.20 eÅ^{-3}) was located 0.92 Å from C2.

$U_2(\mu\text{-}O)(BH_4)_6(dme)_2 \cdot C_7H_8$, 6. The triclinic lattice and the average values of the normalized structure factors suggested the space group $P\bar{1}$, which was confirmed by the success of the subsequent refinement. The reflections 001 and $0\bar{1}1$ were obscured by the beam stop and were deleted; the remaining 5603 unique data were used in the least squares refinement. A toluene molecule co-crystallized with the compound and was disordered over two positions. The quantity minimized by the least-squares program was $\Sigma w(F_o^2 - F_c^2)^2$, where $w = \{[\sigma(F_o)]^2 + (0.0106P)^2\}^{-1}$ and $P = (F_o^2 + 2F_c^2)/3$. The C-Me distances in the disordered toluene molecule were constrained to be equal within an esd of 0.01 Å, and the aromatic cores were constrained to hexagonal geometries. The boranyl hydrogen atoms were located in the difference maps, and their positions were refined with independent isotropic displacement parameters. The chemically equivalent B-H and H···H distances were constrained to be equal within an esd of 0.01 Å. The largest peak in the final Fourier difference map (1.63 e Å^{-3}) was located 1.07 Å from U2.

References

1. Information contained in this chapter has been published previously and is reprinted with permission. See Daly, S. R.; Girolami, G. S. *Chem. Commun.* **2010**, *46*, 407-408.

2. Ephritikhine, M. *Chem. Rev.* **1997,** *97*, 2193-2242.

3. Makhaev, V. D. *Russ. Chem. Rev.* **2000,** *69*, 727-746.

4. Schlesinger, H. I.; Brown, H. C. *J. Am. Chem. Soc.* **1953,** *75*, 219-221.

5. Hoekstra, H. R.; Katz, J. J. *J. Am. Chem. Soc.* **1949,** *71*, 2488-2492.

6. Ehemann, M.; Nöth, H. *Z. Anorg. Allg. Chem.* **1971,** *386*, 87-101.

7. Banks, R. H.; Edelstein, N. M.; Rietz, R. R.; Templeton, D. H.; Zalkin, A. *J. Am. Chem. Soc.* **1978,** *100*, 1957-1958.

8. We employ here a sensible but non-standard version of the kappa nomenclature, using it as a prefix and omitting as unnecessary the descriptor that indicates which kind of atom bridges to the metal center. See *Nomenclature of Inorganic Chemistry, IUPAC Recommendations* 2005, Connelly, N. G.; Damhus, T.; Hartshorn, R. M.; Hutton, A. T., eds., RSC Publishing, Cambridge: 2005; Section IR-9.2.4.2.

9. Bernstein, E. R.; Hamilton, W. C.; Keiderling, T. A.; La Placa, S. J.; Lippard, S. J.; Mayerle, J. J. *Inorg. Chem.* **1972,** *11*, 3009-3016.

10. Charpin, P.; Nierlich, M.; Vigner, D.; Lance, M.; Baudry, D. *Acta Crystallogr., Sect. C: Cryst. Struct. Commun.* **1987,** *C43*, 1465-1467.

11. Haaland, A.; Shorokhov, D. J.; Tutukin, A. V.; Volden, H. V.; Swang, O.; McGrady, G. S.; Kaltsoyannis, N.; Downs, A. J.; Tang, C. Y.; Turner, J. F. C. *Inorg. Chem.* **2002,** *41*, 6646-6655.

12. Banks, R. H.; Edelstein, N. M.; Spencer, B.; Templeton, D. H.; Zalkin, A. *J. Am. Chem. Soc.* **1980,** *102*, 620-623.

13. Schlesinger, H. I.; Brown, H. C.; Horvitz, L.; Bond, A. C.; Tuck, L. D.; Walker, A. O. *J. Am. Chem. Soc.* **1953,** *75*, 222-224.

14. Shinomoto, R.; Gamp, E.; Edelstein, N. M.; Templeton, D. H.; Zalkin, A. *Inorg. Chem.* **1983,** *22*, 2351-2355.

15. Baudry, D.; Charpin, P.; Ephritikhine, M.; Folcher, G.; Lambard, J.; Lance, M.; Nierlich, M.; Vigner, J. *J. Chem. Soc., Chem. Commun.* **1985**, 1553-1554.

16. Scott, P.; Hitchcock, P. B. *J. Chem. Soc., Dalton Trans.* **1995**, 603-609.

17. Keller, P. C. *Inorg. Chem.* **1971,** *10*, 2256-2259.

18. Nöth, H.; Thomas, S. *Eur. J. Inorg. Chem.* **1999**, 1373-1379.

19. Kim, D. Y.; Girolami, G. S. *Inorg. Chem.* **2010**, in press.

20. Plesek, J.; Hermanek, S. *Collect. Czech. Chem. Commun.* **1966,** *31*, 3845-3858.

21. Daly, S. R.; Kim, D. Y.; Yang, Y.; Abelson, J. R.; Girolami, G. S. *J. Am. Chem. Soc.* **2010,** *132*, 2106-2107.

22. Van der Sluys, W. G.; Burns, C. J.; Sattelberger, A. P. *Organometallics* **1989,** *8*, 855-857.

23. Stewart, J. L.; Andersen, R. A. *Polyhedron* **1998,** *17*, 953-958.

24. Daly, S. R.; Girolami, G. S. *Chem. Commun.* **2010,** *46*, 407-408.

25. Shannon, R. D. *Acta Crystallogr., Sect. A* **1976,** *A32*, 751-767.

26. For some recent examples, including experimental and computational comparisons of metal-ligand covalency in trivalent lanthanide and actinide borohydride complexes, see Arliguie, T.; Belkhiri, L.; Bouaoud, S.-E.; Thuery, P.; Villiers, C.; Boucekkine, A.; Ephritikhine, M. *Inorg. Chem.* **2009**, *48*, 221-230.; Roger, M.; Belkhiri, L.; Arliguie, T.; Thuery, P.; Boucekkine, A.; Ephritikhine, M. *Organometallics* **2008**, *27*, 33-42.; Ingram, K. I. M.; Tassell, M. J.; Gaunt, A. J.; Kaltsoyannis, N. *Inorg. Chem.* **2008**, *47*, 7824-7833.; Gaunt, A. J.; Reilly, S. D.; Enriquez, A. E.; Scott, B. L.; Ibers, J. A.; Sekar, P.;

Ingram, K. I. M.; Kaltsoyannis, N.; Neu, M. P. *Inorg. Chem.* **2008**, *47*, 29-41.; Guillaumont, D. *Theochem* **2006**, *771*, 105-110.; Gaunt, A. J.; Scott, B. L.; Neu, M. P. *Angew. Chem., Int. Ed.* **2006**, *45*, 1638-1641.

27. Daly, S. R.; Kim, D. Y.; Girolami, G. S., manuscript in preparation.

28. Baudry, D.; Bulot, E.; Ephritikhine, M. *J. Chem. Soc., Chem. Commun.* **1988**, 1369-1370.

29. Baudry, D.; Bulot, E.; Charpin, P.; Ephritikhine, M.; Lance, M.; Nierlich, M.; Vigner, J. *J. Organomet. Chem.* **1989,** *371*, 155-162.

30. Van Der Sluys, W. G.; Berg, J. M.; Barnhardt, D.; Sauer, N. N. *Inorg. Chim. Acta* **1993,** *204*, 251-256.

31. Rietz, R. R.; Edelstein, N. M.; Ruben, H. W.; Templeton, D. H.; Zalkin, A. *Inorg. Chem.* **1978,** *17*, 658-660.

32. Rietz, R. R.; Zalkin, A.; Templeton, D. H.; Edelstein, N. M.; Templeton, L. K. *Inorg. Chem.* **1978,** *17*, 653-658.

33. Zalkin, A.; Rietz, R. R.; Templeton, D. H.; Edelstein, N. M. *Inorg. Chem.* **1978,** *17*, 661-663.

34. Shinomoto, R.; Zalkin, A.; Edelstein, N. M. *Inorg. Chim. Acta* **1987,** *139*, 91-95.

35. Shinomoto, R.; Zalkin, A.; Edelstein, N. M.; Zhang, D. *Inorg. Chem.* **1987,** *26*, 2868-2872.

36. Clark, R. J. H.; Lewis, J.; Machin, D. J.; Nyholm, R. S. *J. Chem. Soc.* **1963**, 379-387.

37. Avens, L. R.; Bott, S. G.; Clark, D. L.; Sattelberger, A. P.; Watkin, J. G.; Zwick, B. D. *Inorg. Chem.* **1994,** *33*, 2248-2256.

38. Brennan, J.; Shinomoto, R.; Zalkin, A.; Edelstein, N. *Inorg. Chem.* **1984,** *23*, 4143-4146.

39. Wasserman, H. J.; Moody, D. C.; Ryan, R. R. *J. Chem. Soc., Chem. Commun.* **1984**, 532-533.

40. Ban, B.; Folcher, G.; Marquet-Ellis, H.; Rigny, P. *Nouv. J. Chim.* **1985,** *9*, 51-53.

41. Castro-Rodriguez, I.; Olsen, K.; Gantzel, P.; Meyer, K. *Chem. Commun.* **2002**, 2764-2765.

42. Castro-Rodriguez, I.; Nakai, H.; Zakharov Lev, N.; Rheingold Arnold, L.; Meyer, K. *Science* **2004,** *305*, 1757-1759.

43. Nakai, H.; Hu, X.; Zakharov Lev, N.; Rheingold Arnold, L.; Meyer, K. *Inorg. Chem.* **2004,** *43*, 855-857.

44. Castro-Rodriguez, I.; Meyer, K. *Chem. Commun.* **2006**, 1353-1368.

45. Lam Oanh, P.; Feng Patrick, L.; Heinemann Frank, W.; O'Connor Joseph, M.; Meyer, K. *J. Am. Chem. Soc.* **2008,** *130*, 2806-2816.

46. Jones, E. R., Jr.; Hendricks, M. E.; Stone, J. A.; Karraker, D. G. *J. Chem. Phys.* **1974,** *60*, 2088-2094.

47. Dejean-Meyer, A.; Folcher, G.; Marquet-Ellis, H. *J. Chim. Phys. Phys.-Chim. Biol.* **1983,** *80*, 579-581.

48. Baudry, D.; Charpin, P.; Ephritikhine, M.; Lance, M.; Nierlich, M.; Vigner, J. *J. Chem. Soc., Chem. Commun.* **1987**, 739-740.

49. Marks, T. J.; Kolb, J. R. *Chem. Rev.* **1977,** *77*, 263-293.

50. Gozum, J. E.; Girolami, G. S. *J. Am. Chem. Soc.* **1991,** *113*, 3829-3837.

51. Gozum, J. E.; Wilson, S. R.; Girolami, G. S. *J. Am. Chem. Soc.* **1992,** *114*, 9483-9492.

52. The decrease in the $Na(H_3BNMe_2BH_3)$ concentration is not attributed to precipitation because of its high solubility in diethyl ether.

53. Ghiassee, N.; Clay, P. G.; Walton, G. N. *J. Inorg. Nucl. Chem.* **1981,** *43*, 2909-2913.

54. Girolami, G. S.; Kim, D. Y.; Abelson, J. R.; Kumar, N.; Yang, Y.; Daly, S. U.S. Pat. Appl. 59728, April 9, 2008.

55. Dejean, A.; Charpin, P.; Folcher, G.; Rigny, P.; Navaza, A.; Tsoucaris, G. *Polyhedron* **1987,** *6*, 189-195.

56. Moody, D. C.; Odom, J. D. *J. Inorg. Nucl. Chem.* **1979,** *41*, 533-535.

57. Hunter, W. E.; Hrncir, D. C.; Bynum, R. V.; Penttila, R. A.; Atwood, J. L. *Organometallics* **1983,** *2*, 750-755.

58. Yakelis, N. A.; Bergman, R. G. *Organometallics* **2005,** *24*, 3579-3581.

59. Zalkin, A.; Beshouri, S. M. *Acta Crystallogr., Sect. C: Cryst. Struct. Commun.* **1988,** *C44*, 1826-1827.

60. Berthet, J. C.; Le Marechal, J. F.; Nierlich, M.; Lance, M.; Vigner, J.; Ephritikhine, M. *J. Organomet. Chem.* **1991,** *408*, 335-341.

61. Berthet, J.-C.; Ephritikhine, M.; Lance, M.; Nierlich, M.; Vigner, J. *J. Organomet. Chem.* **1993,** *460*, 47-53.

62. Villiers, C.; Thuery, P.; Ephritikhine, M. *Inorg. Chem. Commun.* **2007,** *10*, 891-893.

63. Spek, A. L. *J.Appl.Cryst.* **2003,** *36*, 7-13.

64. Hermann, J. A.; Suttle, J. F. *Inorg. Synth.* **1957,** *5*, 143-145.

65. Luetkens, M. L., Jr.; Sattelberger, A. P.; Murray, H. H.; Basil, J. D.; Fackler, J. P., Jr. *Inorg. Synth.* **1990,** *28*, 305-310.

66. Sur, S. K. *J. Magn. Reson.* **1989,** *82*, 169-173.

67. Eaton, G. R.; Lipscomb, W. N. *N.M.R. Studies of Boron Hydrides and Related Compounds*. 1969; pp 617.

68. Gaines, D. F.; Schaeffer, R. *J. Am. Chem. Soc.* **1964,** *86*, 1505-1507.

69. Jaska, C. A.; Manners, I. *J. Am. Chem. Soc.* **2004,** *126*, 9776-9785.

70. Frisch, M. J.; et al. *Gaussian03, Rev. C.02*; Gaussian, Inc.: Wallingford, CT, 2004.

71. Brumaghim, J. L.; Priepot, J. G.; Girolami, G. S. *Organometallics* **1999,** *18*, 2139-2144.

CHAPTER 4. Trivalent Lanthanide *N,N*-Dimethylaminodiboranates

Introduction[1]

Lanthanide materials exhibit a wide variety of fascinating electrical, optical, and magnetic properties that make them ideally suited for a diverse range of applications. Lanthanide oxides are excellent high-κ dielectrics and are also constituents in superconducting materials such as $LnBa_2Cu_3O_{7-x}$.[2] Lanthanide borides exhibit unusual electronic characteristics and remarkable magnetic properties.[3] The lanthanide hexaborides (LnB_6) have high electron emissivities and are currently used as thermionic emitters in electron microscopes,[4-6] and some of the lanthanide tetraborides, LnB_4, exhibit magnetically-induced phase transitions.[3] Ternary boride phases with the transition metals, such as $Ln_2Fe_{14}B$, are strong permanent magnets.[3, 7, 8] Lanthanides are also commonly used as dopants to impart or enhance the properties of photonic devices[9] such as lasers,[10] electroluminescent displays,[11-15] fiber-optics,[16] light-emitting diodes,[17, 18] and light-emitting organic-inorganic hybrids.[19, 20] Another application of lanthanides is the doping of $SrTiO_3$ films, which greatly increases their thermoelectric power output.[21]

For some advanced applications, particularly in thin film deposition and nanoscale manufacturing, a significant technological challenge is to develop appropriate fabrication methods. A prominent example is the potential use of lanthanide oxides as replacements for the SiO_2 gate dielectric in metal-oxide-semiconductor field-effect transistors (MOSFETS). The exponential scaling of transistors, in accordance with the semiconductor roadmap,[22] has required materials with higher dielectric constants, κ, relative to SiO_2 (κ = 3.9) in order to avoid significant gate leakage current as the thickness of the dielectric layer decreases. The lanthanide oxides have been suggested as next-generation dielectric barriers because they

have high dielectric constants (La_2O_3 κ = 27, Pr_2O_3 κ = 26-30, and Gd_2O_3 κ = 16), relatively large bandgaps, and high thermodynamically stablilty on silicon.[23-28] A significant challenge, however, is the oxides must be deposited, unlike SiO_2, which is thermally grown. Of all the methods to deposit lanthanide oxides, chemical vapor deposition (CVD) and atomic layer deposition (ALD) are highly attractive because they can achieve uniform step coverage even in recessed features with high aspect ratios (AR > 5:1).[29, 30] Physical vapor deposition (PVD), which is a line-of-site method, will eventually be unable to coat uniformly the high AR trenches and vias that will constitute future microelectronic architectures.

Ideal CVD and ALD precursors for microelectronic applications must be volatile enough to enable conformal coverage and must react under mild conditions to afford the desired film composition. The generation of lanthanide-containing precursors with high volatility is difficult for several reasons.[31] Because lanthanides have large radii, they often form complexes that have polymeric (and thus nonvolatile) structures. Polymerization can be prevented by incorporating additional Lewis bases into the metal coordination spheres, but heating often results in dissociation of the Lewis bases (and a return to a polymeric structure) rather than sublimation. Lanthanide precursors that do have sufficient volatility for CVD and ALD applications typically employ anionic ligands that either are sterically bulky, such as silylamides,[32-36] or are multidentate (or polyhapto), such as β-diketonates,[37-42] cyclopentadienyls,[43-48] amidinates,[49-51] and guanidinates.[52] Neutral chelating donors (such as glymes) are often employed to fill remaining vacancies in the coordination sphere, sometimes by grafting them onto the anionic ligands. Examples of these ligand types include ether-functionalized β-ketoiminates[53, 54] and alkoxides.[55-62] Several reviews of lanthanide precursors and their use in CVD and ALD have been published.[13, 27, 28, 31, 63-70]

In previous studies, we have found that monomeric borohydride complexes of group 4 and group 6 transition metals are outstanding CVD precursors because they are highly volatile and have low decomposition temperatures. For instance, $Ti(BH_4)_3(dme)$,[71-73] $Zr(BH_4)_4$,[74] $Hf(BH_4)_4$,[75-79] and $Cr(B_3H_8)_2$[80-82] have all been used for the deposition of highly conformal metal diboride thin films. Unfortunately, few lanthanide(III) borohydride complexes are volatile below their respective decomposition temperatures. The 1,2-dimethoxyethane complexes of stoichometry $Ln(BH_4)_3(dme)$ are volatile only if Ln is relatively small; thus the complexes of yttrium and the later lanthanides (Gd – Lu) sublime in the relatively-high temperature range of 150 – 190 °C at 10^{-2} Torr.[83] Of the known tetrahydrofuran complexes of stoichiometry $Ln(BH_4)_3(thf)_3$,[84-86] only $Y(BH_4)_3(thf)_3$ is reported to be volatile, subliming at 90 °C in vacuum, but it tends to lose two thf molecules upon heating to form the salt $[Y(BH_4)_2(thf)_4][Y(BH_4)_4]$.[87] The most volatile lanthanide borohydride complexes reported to date employ the monomethylborohydride ligand, $BH_3CH_3^-$.[88] The complexes $Ln(BH_3CH_3)_3(Et_2O)$ and $Ln(BH_3CH_3)_3(thf)$, where Ln = Yb, Lu, and Ho, sublime under vacuum at 50 and 100 °C, respectively. The authors report, however, that similar complexes of the larger lanthanides, such as samarium, are not volatile. Lanthanide borohydride and monomethylborohydride complexes also form adducts with nitrogenous donors such as acetonitrile and pyridine, but the volatilities of these complexes are likely to be poor.[88-90]

Recently, we reported a new class of metal complexes known as the aminodiboranates.[91] In particular, we have used the *N*,*N*-dimethylaminodiboranate ligand, $H_3BNMe_2BH_3^-$, (DMADB),[92, 93] to prepare complexes of transition metals, alkaline earths, and the actinides, many of which are highly volatile (Chapters 2, 3, and 6).[91, 94-96] The DMADB ligand typically chelates to metal centers through four B-H-M bridges, so that it

occupies more of the coordination sphere than do the smaller borohydrides BH_4^- and $BH_3CH_3^-$. As we will show below, in some cases the DMADB ligand can bridge between metals, a feature also characteristic of the BH_4^- ligand.[97-99] Several metal DMADB complexes have already been shown to serve as excellent CVD precursors. For example, $Ti(H_3BNMe_2BH_3)_2$ affords high-quality TiB_2 films, and $Mg(H_3BNMe_2BH_3)_2$ reacts with water under CVD conditions to form MgO.[94, 100]

These results prompted us to explore the chemistry of lanthanide DMADB complexes; such species could serve as excellent precursors for the deposition of lanthanide borides or lanthanide oxides by CVD or ALD. We now report the synthesis, characterization, and volatilities of lanthanide DMADB complexes (Table 4.1).

Results and Discussion

Synthesis and Characterization of $Ln(H_3BNMe_2BH_3)_3(thf)$ Complexes. For almost all of the lanthanides (Y, Pr-Nd, Sm-Lu), treatment of the anhydrous lanthanide(III) chloride, $LnCl_3$, with three equiv of $Na(H_3BNMe_2BH_3)$ in tetrahydrofuran readily affords the new complexes $Ln(H_3BNMe_2BH_3)_3(thf)$.

$$LnCl_3 + 3\,Na(H_3BNMe_2BH_3) \xrightarrow{thf} Ln(H_3BNMe_2BH_3)_3(thf) + 3\,NaCl$$

Ln = Y, Pr-Nd, Sm-Lu

These compounds can be isolated by extraction and crystallization from pentane in good yields (51–71%). By means of this method, however, we have been unable to prepare the corresponding lanthanum complex, $La(H_3BNMe_2BH_3)_3(thf)$ (**2a**), and we obtain the cerium analog $Ce(H_3BNMe_2BH_3)_3(thf)$ (**3a**) only in low yield (13%). The reactions of $LaCl_3$ and $CeCl_3$ with Na(DMDAB) in thf give little or no pentane-extractable product, and only

Table 4.1. Numbering scheme for Ln DMADB complexes.

Lanthanide	$Ln(H_3BNMe_2BH_3)_3(thf)$	$Ln(H_3BNMe_2BH_3)_3$
Y	**1a**	**1b**
La	**2a**	**2b**
Ce	**3a**	**3b**
Pr	**4a**	**4b**
Nd	**5a**	**5b**
Sm	**6a**	**6b**
Eu	**7a**	**7b**
Gd	**8a**	**8b**
Tb	**9a**	**9b**
Dy	**10a**	**10b**
Ho	**11a**	**11b**
Er	**12a**	**12b**
Tm	**13a**	**13b**
Yb	**14a**	**14b**
Lu	**15a**	**15b**

$LaCl_3(thf)_x$ has been recovered from the lanthanum reaction. Fortunately, **2a** and **3a** can be prepared from the corresponding lanthanide iodide starting material in place of the chloride.

$$LnI_3 + 3\,Na(H_3BNMe_2BH_3) \xrightarrow{thf} Ln(H_3BNMe_2BH_3)_3(thf) + 3\,NaI$$

Ln = La, Ce

The La and Ce complexes can also be prepared by adding thf to the base-free compounds $La(H_3BNMe_2BH_3)_3$ (**2b**) and $Ce(H_3BNMe_2BH_3)_3$ (**3b**), which we will describe below.

X-ray diffraction studies of the crystals obtained from pentane reveal that the $Ln(H_3BNMe_2BH_3)_3(thf)$ complexes for Y (**1a**), Nd (**5a**) , Sm (**6a**), Eu (**7a**), Gd (**8a**), Dy (**10a**), and Er (**12a**) are isomorphous and crystallize in the orthorhombic space group $Pca2_1$. The La complex **2a** crystallizes in the cubic space group $I23$ (Table 4.2) but, despite this difference, its structure is similar to those of the others; an ORTEP view of a representative example is given in Figure 4.1. Of all the lanthanides, La has the largest radius in the +3 oxidation state, and thus it is not entirely surprising that it crystallizes somewhat differently. In most cases, the hydrogen atoms attached to boron surfaced in the difference maps and their locations could be refined, although sometimes with light constraints on the B-H distances. Each $H_3BNMe_2BH_3$ group chelates to the metal center by means of four B-H···Ln bridges in which each BH_3 group is κ^2H (i.e., forms two B-H···Ln interactions).

The $Ln(H_3BNMe_2BH_3)_3(thf)$ complexes of Y and La-Er are formally 13-coordinate (12 hydrogen atoms and one oxygen atom), but their structures are more conveniently described by the arrangement of the six boron atoms and the thf oxygen, which define a polyhedron that is best described as a capped octahedron with the thf ligand in the capping site.[101] The three DMADB ligands are related by a three-fold rotational axis coincident with

Table 4.2. Crystallographic data for $Ln(H_3BNMe_2BH_3)_3(thf)$ compounds collected at 193 K.

	La (2a)	**Nd (5a)**	**Sm (6a)**	**Eu (7a)**	**Gd (8a)**	**Er (12a)**	**Tm (13a)**	**Lu (15a)**
formula	$C_{10}H_{44}B_6N_3OLa$	$C_{10}H_{44}B_6N_3ONd$	$C_{10}H_{44}B_6N_3OSm$	$C_{10}H_{44}B_6N_3OEu$	$C_{10}H_{44}B_6N_3OGd$	$C_{10}H_{44}B_6N_3OEr$	$C_{10}H_{44}B_6N_3OTm$	$C_{10}H_{44}B_6N_3OLu$
FW (g mol^{-1})	426.25	431.58	437.69	439.30	444.59	454.60	456.27	462.31
λ (Å)	0.71073	0.71073	0.71073	0.71073	0.71073	0.71073	0.71073	0.71073
crystal system	cubic	orthorhombic	orthorhombic	orthorhombic	orthorhombic	orthorhombic	monoclinic	monoclinic
space group	*I*23	$Pca2_1$	$Pca2_1$	$Pca2_1$	$Pca2_1$	$Pca2_1$	$P2_1/c$	$P2_1/c$
a (Å)	16.772(5)	22.0316(7)	21.936(3)	21.989(5)	21.946(5)	21.858(5)	10.5926(5)	10.5517(4)
b (Å)	16.772(5)	10.4494(3)	10.3975(15)	10.426(3)	10.398(2)	10.378(3)	10.8626(5)	10.8434(4)
c (Å)	16.772(5)	20.6503(6)	20.590(3)	20.651(5)	20.609(4)	20.625(5)	19.3830(9)	19.4142(7)
β (deg)	90	90	90	90	90	90	95.399(2)	95.423(2)
V ($Å^3$)	4718(1)	4754.1(2)	4696(1)	4734(2)	4703(2)	4679(2)	2220.38(18)	2211.36(14)
Z	8	8	8	8	8	8	4	4
ρ_{calc} (g cm^{-3})	1.200	1.206	1.238	1.233	1.256	1.291	1.365	1.389
μ (mm^{-1})	1.810	2.183	2.500	2.648	2.819	3.586	3.995	4.463
abs. corr.	face-indexed	face-indexed	face-indexed	face-indexed	face-indexed	face-indexed	face-indexed	face-indexed
transm. coeff.	0.869, 0.755	0.477, 0.663	0.633, 0.530	0.705, 0.485	0.717, 0.429	0.480, 0.251	0.269, 0.061	0.272, 0.673
data/restr./param	1514/35/80	19703/13/402	15617/11/391	8672/1/400	8646/1/401	8542/1/401	4912/55/268	4075/55/262
GOF on F^2	0.856	0.920	0.900	0.742	0.777	0.954	1.067	1.030
*R*1 [$I > 2\sigma(I)$]	0.0522	0.0272	0.0285	0.0258	0.0280	0.0228	0.0221	0.0229
w*R*2 (all data)	0.1053	0.0525	0.0529	0.0443	0.0555	0.0483	0.0583	0.0542
larg. peak/ hole	1.171/-0.729	1.030/-0.760	0.934/-0.743	0.682/-0.478	0.887/-0.524	0.0867/-0.848	1.383/-0.913	0.828/-0.417

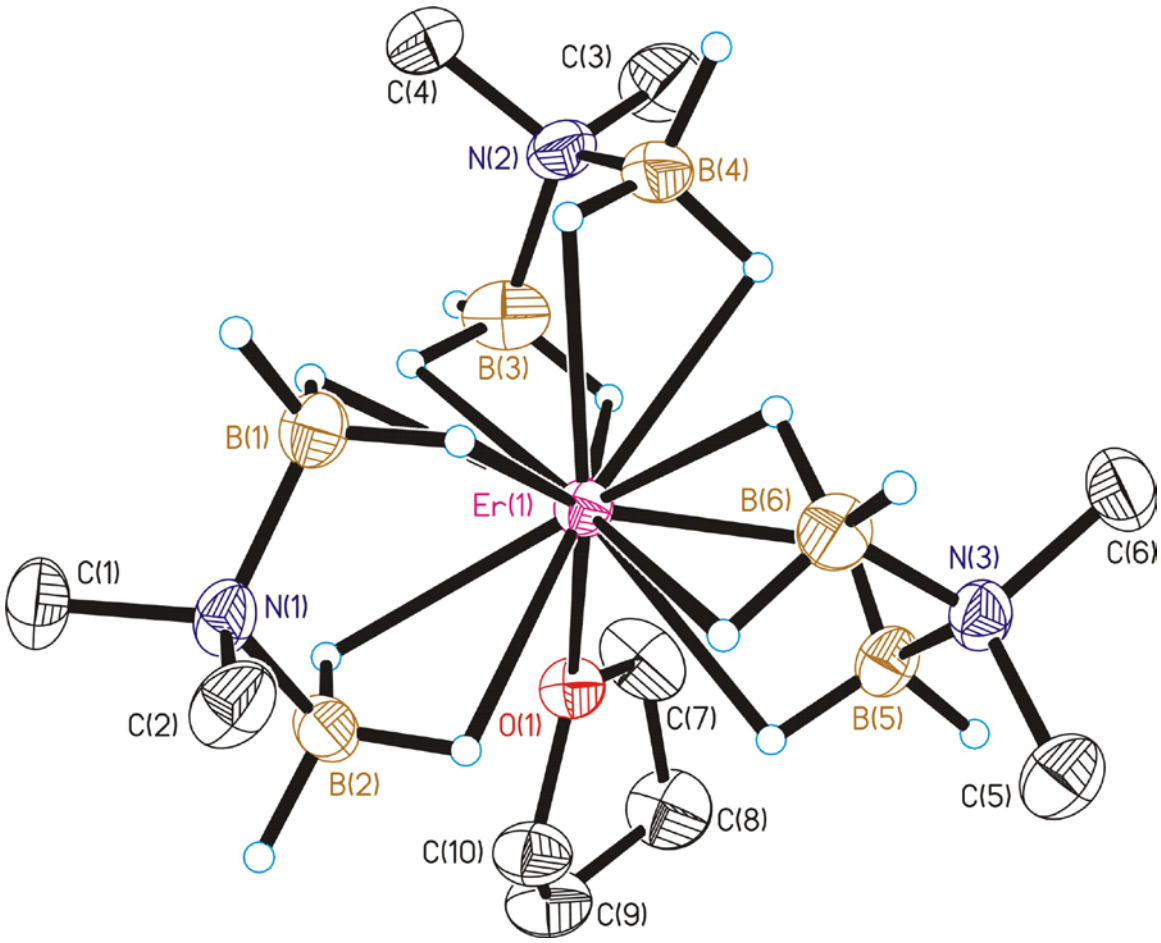

Figure 4.1. Molecular structure of $Er(H_3BNMe_2BH_3)_3(thf)$, **12a**. Ellipsoids are drawn at the 35% probability level, except for the hydrogen atoms, which are represented as arbitrarily-sized spheres. Methyl and methylene hydrogen atoms have been deleted for clarity.

the M-O bond of the coordinated thf molecule. The mean lanthanide-boron and lanthanide-oxygen distances decrease across the period, as expected from the corresponding decrease in ionic radii (Table 4.3). As the ionic radius of the lanthanide decreases, so does the B-N-B angle of the DMADB ligand. For example, the B-N-B angle is 109.9° for the La complex **2a** but 107.0° for the Er complex **12a**. Thus, the aminodiboranate ligands can adjust slightly depending on the size of the metal to which they are ligated: the B-N-B angle opens up slightly if the metal is large, and closes down slightly if the metal is small.

Initially, we assumed that the $Ln(H_3BNMe_2BH_3)_3(thf)$ complexes of the late lanthanides Tm, Yb, and Lu would have the same 13-coordinate structures. However, analysis of the paramagnetic lanthanide induced shifts (see below) suggested that the structures of the Tm and Yb complexes were different. Single-crystal XRD studies of $Tm(H_3BNMe_2BH_3)_3(thf)$ (**13a**) and $Lu(H_3BNMe_2BH_3)_3(thf)$ (**15a**) revealed that the structures indeed differ from the other $Ln(H_3BNMe_2BH_3)_3(thf)$ complexes: one Ln···B distance is ~ 0.3–0.4 Å longer than the other five (Table 4.4). Refinement of the hydride positions shows that this BH_3 unit is in fact bound to the metal atom by means of one hydrogen bridge instead of two (Figure 4.2). As a result, these complexes have coordination numbers of 12 (11 hydrogen atoms and one oxygen atom) rather than 13.

The IR spectra of all of the $Ln(H_3BNMe_2BH_3)_3(thf)$ complexes are essentially identical. A representative complex, $Nd(H_3BNMe_2BH_3)_3(thf)$ (**5a**), exhibits two stretching bands for the terminal B-H bonds at 2392 and 2342 cm^{-1} and five distinct stretching bands for the bridging B-H bonds at 2285, 2252, 2216, 2173, and 2066 cm^{-1} (Figure 4.3). Of the bands due to the briding B-H bonds, the most intense are at 2392, 2216, and 2173 cm^{-1}; over the entire lanthanide period, the frequencies of these three strong B-H bands vary slightly: from 2390 – 2420, from 2213 – 2230, and from 2168 – 2191 cm^{-1}, respectively. The frequencies

Table 4.3. Average atomic distances and angles for $Ln(H_3BNMe_2BH_3)_3(thf)$ complexes.

	Y (1a)[94]	**La (2a)**	**Nd (5a)**	**Sm (6a)**	**Eu (7a)**	**Gd (8a)**	**Dy (10a)**[94]	**Er (12a)**
				Mean atomic distances (Å)				
Ln - B	2.82(5)	2.94(2)	2.88(2)	2.85(2)	2.85(3)	2.84(3)	2.82(4)	2.80(5)
Ln - O	2.436(8)	2.513(12)	2.504(7)	2.48(1)	2.48(1)	2.468(6)	2.447(3)	2.423(8)
				Mean bond angles (deg)				
B-N-B	107.9(7)	109.9(7)	108.7(5)	108.3(4)	108(1)	107.9(6)	107.6(6)	107.0(8)
B-Ln-B	53.4(3)	51.3(3)	52.7(3)	52.97(8)	53.2(3)	53.1(1)	53.6(3)	53.7(1)

Table 4.4. Selected atomic distances and angles for $Tm(H_3BNMe_2BH_3)_3(thf)$ and $Lu(H_3BNMe_2BH_3)_3(thf)$.

	Tm (13a)	**Lu (15a)**
	Atomic distances (Å)	
Ln – O1	2.343(2)	2.328(3)
Ln – B1	2.727(3)	2.770(5)
Ln – B2	2.827(3)	2.729(5)
Ln – B3	2.746(3)	2.699(5)
Ln – B4	2.786(3)	2.826(5)
Ln – B5	2.733(3)	2.728(5)
Ln – B6	3.136(3)	3.139(5)
	Bond angles (deg)	
B1 - N1 - B2	106.8(2)	107.7(3)
B3 - N2 - B4	108.2(2)	106.7(3)
B5 - N3 - B6	108.3(2)	108.1(3)

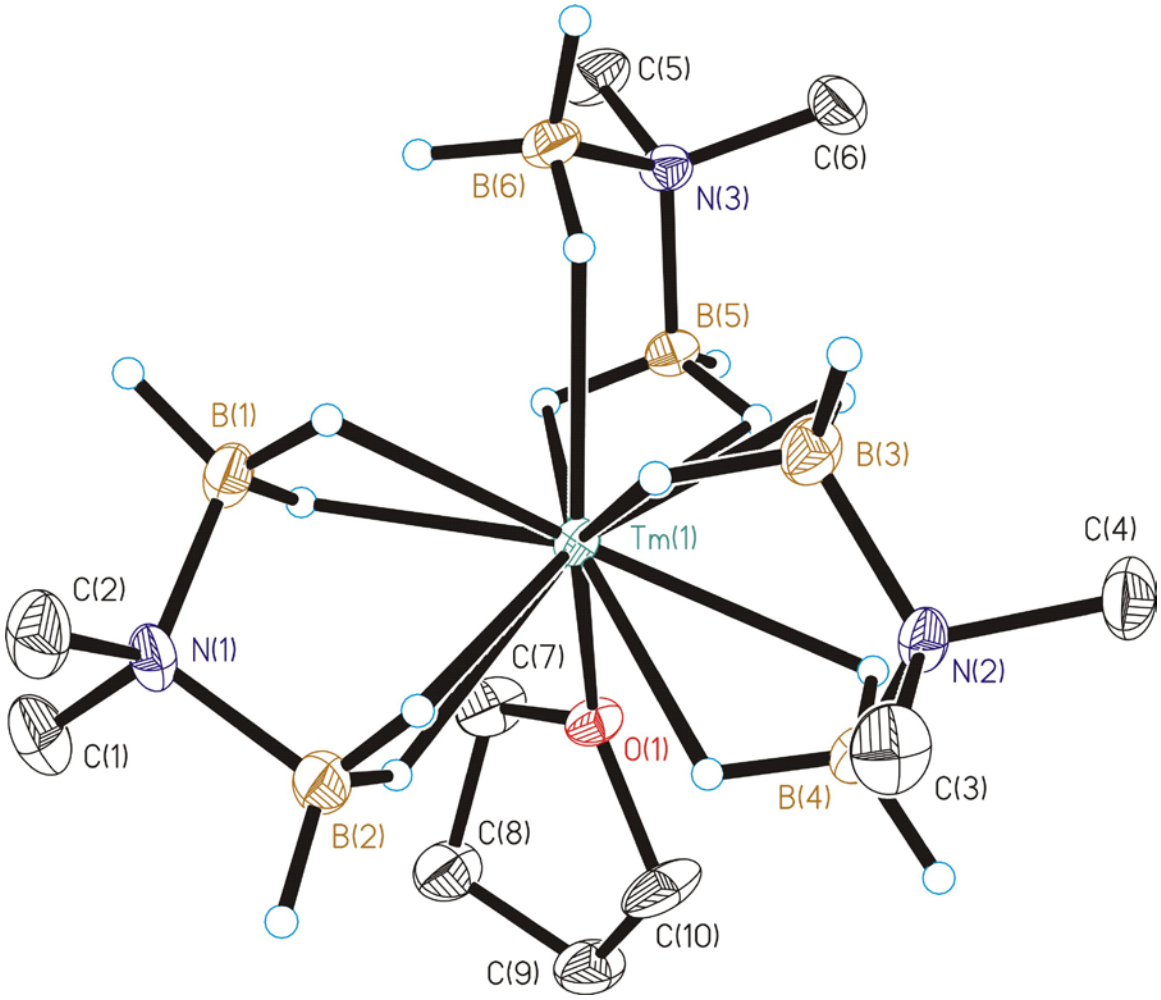

Figure 4.2. Molecular structure of $Tm(H_3BNMe_2BH_3)_3(thf)$, **13a**. Ellipsoids are drawn at the 35% probability level, except for the hydrogen atoms, which are represented as arbitrarily-sized spheres. Methyl and methylene hydrogen atoms have been deleted for clarity.

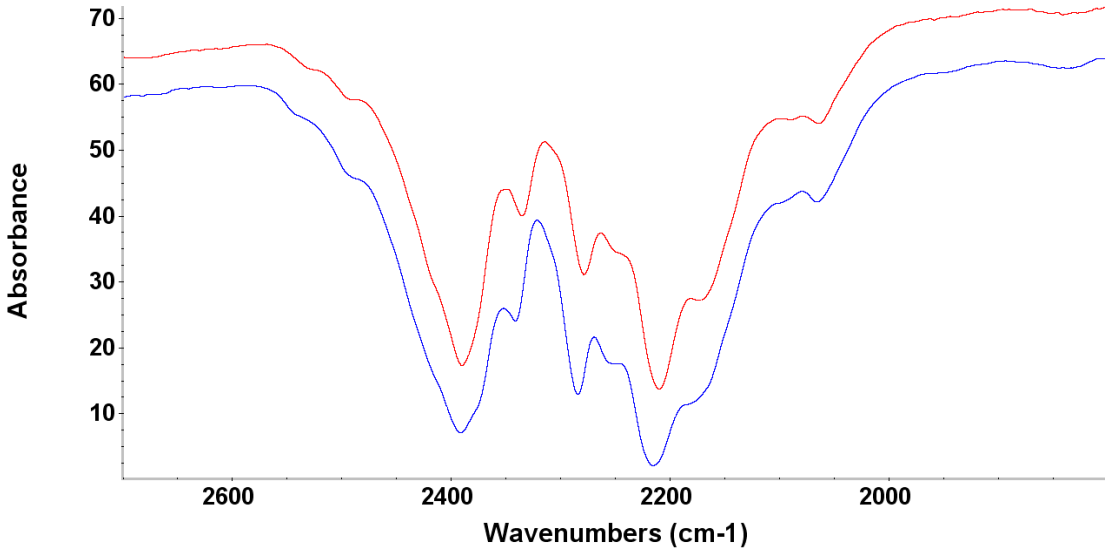

Figure 4.3. The B-H stretching region of the IR spectrum of $Nd(H_3BNMe_2BH_3)_3(thf)$, **5a**, (bottom, blue) and $U(H_3BNMe_2BH_3)_3(thf)$ (top, red).

of these intense bands are similar to those observed for the uranium analog $U(H_3BNMe_2BH_3)_3(thf)$, as shown in Figure 4.3.[102] Two diagnostic peaks corresponding to the symmetric C-O-C stretching frequency of the coordinated thf molecule are clearly observed in most of the IR spectra between 856 and 837 cm^{-1}.[103, 104]

The ^1H NMR spectra in C_6D_6 of the diamagnetic species $Y(H_3BNMe_2BH_3)_3(thf)$ (**1a**), $La(H_3BNMe_2BH_3)_3(thf)$ (**2a**), and $Lu(H_3BNMe_2BH_3)_3(thf)$ (**14a**) are very similar. The NMe_2 group is a singlet (δ 2.24 – 2.30) and the bound thf molecule exhibits multiplets for the α (δ 3.78 – 3.83) and β (δ 1.13 – 1.21) protons. A very broad 1:1:1:1 quartet is also observed at δ 2.51 – 3.05 in each spectrum; this resonance is due to the BH_3 protons, which are coupled to the quadripolar ^{11}B nuclei (I = 3/2) (Table 4.5). The ^{11}B NMR spectra of these species feature binomial quartets due to coupling to the three equivalent BH_3 hydrogen atoms. Thus, exchange of the terminal and bridging hydrogens is rapid on the NMR time scale at room temperature, as is typical of most borohydride complexes.[97] The ^{11}B NMR chemical shifts become slightly more shielded as the size of the metal center decreases: δ -2.9 for the La^{3+} compound **2a** (r_{ionic} = 1.032 Å), δ -5.7 for the Y^{3+} compound **1a** (r_{ionic} = 0.900 Å), and δ -6.4 for the Lu^{3+} compound **14a** (r_{ionic} = 0.861 Å).[105] A similar trend is observed for the ^1H NMR shifts. NMR data for the paramagnetic lanthanide species will be discussed below.

The dominant ions in the positive-ion field ionization (FI) mass spectra of the $Ln(H_3BNMe_2BH_3)_3(thf)$ complexes (Table 4.6) are missing thf, and many have also lost one DMADB anion. Predominant among these species is $Ln(H_3BNMe_2BH_3)_3^+$, and most of the spectra also contain peaks due to $Ln(H_3BNMe_2BH_3)_2^+$ and $Ln_2(H_3BNMe_2BH_3)_5^+$ fragments, the latter presumably arising by loss of thf and subsequent dimerization. In some of the spectra, small peaks due to the thf-containing species $Ln(H_3BNMe_2BH_3)_3(thf)^+$ and $Ln_2(H_3BNMe_2BH_3)_5(thf)^+$ can also be seen; the low relative abundances suggest that the thf

Table 4.5. ^{1}H and ^{11}B NMR resonances of $Ln(H_3BNMe_2BH_3)_3(thf)$ complexes.

Ln	NMe_2	α-thf	β-thf	BH_3	^{11}B
Y	2.28	3.83	1.18	2.51	-5.7
La	2.30	3.78	1.13	2.87	-2.9
Ce	0.79	7.11	3.84	20.39	23.1
Pr	0.02	9.93	6.48	58.06	75.1
Nd	3.06	0.66	0.95	82.86	104.8
Sm	2.25	3.80	1.29	-1.86	-9.8
Eu	-	-	-	-	-176.8
Gd	-	-	-	-	-
Tb	-27.47	95.57	54.49	-	-556.3
Dy	-22.72	94.84	59.71	-	-428.4
Ho	11.46	-1.80	2.05	-	-269.4
Er	14.79	-43.14	-28.57	-	-171.5
Tm[a]	-6.60	-17.86	-17.86	-92.87	-133.0
Yb	-0.26	1.15	3.48	-18.72	-47.4
Lu	2.24	3.80	1.21	3.05	-6.4

[a] The thf resonances for Tm overlap at δ -17.84, which was verified by VT ^{1}H NMR studies.

* Blank entries indicate resonances that could not be located in the spectra.

Table 4.6. Major fragments, and those containing thf, observed in the FI mass spectra of $Ln(H_3BNMe_2BH_3)_3(thf)$ complexes.

	ML_2^+		[b]ML_3^+		$ML_3(thf)^+$		$M_2L_5^+$		$M_2L_5(thf)^+$	
M	mass (*m*/*z*)	rel. int. (%)	mass (*m*/*z*)	rel. int. (%)	mass (*m*/*z*)	rel. int. (%)	mass (*m*/*z*)	rel. int. (%)	mass (*m*/*z*)	rel. int. (%)
La (**2a**)	283	25	353	100	-	-	636	30	-	-
Ce (**3a**)	-	-	355	15	414	2	640	5	710	2
Pr (**4a**)	-	-	355	40	-	-	642	15	-	-
Nd (**5a**)	286	15	358	100	-	-	645	60	718	15
Sm (**6a**)	296	60	362	100	-	-	606	80	732	5
Eu (**7a**)	295	40	367	75	-	-	663	15	-	-
Gd (**8a**)	301	3	379	25	-	-	674	5	-	-
Tb (**9a**)	303	5	373	15	-	-	676	5	-	-
Dy (**10a**)	-	-	377	95	-	-	684	100	-	-
Ho (**11a**)	308	30	380	70	-	-	688	100	760	10
Y[a] (**1a**)	233	40	303	100	376	6	538	40	608	15
Er (**12a**)	-	-	381	5	-	-	-	-	-	-
Tm (**13a**)	312	100	383	80	-	-	697	65	-	-
Yb (**14a**)	316	45	388	100	-	-	704	65	-	-
Lu (**15a**)	319	20	389	30	-	-	709	100	-	-

[a] Yttrium placed in the series according to its ionic radii; $L = H_3BNMe_2BH_3^-$.

[b] ML_3^+ fragments are mixtures of $Ln(H_3BNMe_2BH_3)_3^+$ and $M(H_3BNMe_2BH_3)_2(thf)$.

molecule is easily dissociated upon ionization. Assignment of stoichiometries to the masses seen requires some care because thf and $H_3BNMe_2BH_3^-$ both have masses near 72. The isotropic distributions of many of the observed fragments are slightly altered compared to their calculated peak envelopes, suggesting that small amounts of thf-containing fragments are also present. This problem seems to be especially prevalent for the assigned $Ln(H_3BNMe_2BH_3)_3^+$ fragment, which likely contains some proportion of $Ln(H_3BNMe_2BH_3)_2(thf)^+$. The peak distributions do not match those calculated for the suspected thf-contaning fragments alone and, given the low relative abundance of verified thf-containing fragments, these species seem to be a small component of the overlapping peaks. Comparison of these fragments to analgous fragments in the FI mass spectra of the $Ln(H_3BNMe_2BH_3)_3$ complexes (see below) confirms that thf-containing species are present in these peak distributions. The ionized fragments for the $Ln(H_3BNMe_2BH_3)_3$ complexes, which have no thf present, have peak envelopes identical to those calculated for the associated thf-free fragments.

The melting points of the $Ln(H_3BNMe_2BH_3)_3(thf)$ complexes are essentially identical for La through Sm (132 - 137 °C) but then steadily decrease from Gd (128 – 129 °C) to Lu (99 – 101 °C). The complexes $Eu(H_3BNMe_2BH_3)_3(thf)$ and $Yb(H_3BNMe_2BH_3)_3(thf)$ decompose rather than melt, and evolve gas as the solid liquefies. This behavior is likely a consequence of thermally induced reduction of Eu^{III} and Yb^{III} to their corresponding divalent oxidation states, as has been observed for trivalent europium and ytterbium tetrahydroborate complexes.[106] The Eu^{II} and Yb^{II} complexes $M(H_3BNMe_2BH_3)_2(thf)_2$ can in fact be isolated; the synthesis and characterization of these divalent lanthanide aminodiboranate complexes will be described separately (Chapter 5).[107]

Synthesis and Characterization of $Ln(H_3BNMe_2BH_3)_3$ Complexes. Grinding anhydrous $LnCl_3$ with three equiv. of Na(DMADB) in the absence of solvent produces the corresponding base-free $Ln(H_3BNMe_2BH_3)_3$ complexes, which can be isolated by sublimation under vacuum. The volatility of these complexes at 10^{-2} Torr increases across the period: $La(H_3BNMe_2BH_3)_3$ (**2b**) sublimes at 125 °C, whereas $Lu(H_3BNMe_2BH_3)_3$ (**15b**) sublimes at the remarkably low temperature of 65 °C. The yields are typically low (< 33%) and are somewhat variable by this preparative method.

$$LnCl_3 + 3\,Na(H_3BNMe_2BH_3) \xrightarrow{\text{grinding}} Ln(H_3BNMe_2BH_3)_3 + 3\,NaCl$$

Fortunately, sublimation of the thf adducts $Ln(H_3BNMe_2BH_3)_3(thf)$ under dynamic vacuum results in the loss of thf to produce the corresponding $Ln(H_3BNMe_2BH_3)_3$ species in high yields. Thus, whereas the ^1H NMR spectrum of $Er(H_3BNMe_2BH_3)_3(thf)$ (**12a**) exhibits resonances due coordinated thf ligand at δ -43.14 (OCH_2) and δ -28.57 (β-CH_2) and a singlet for the NMe_2 protons at δ 14.79, sublimation of this material under a dynamic vacuum affords a product that shows no thf resonances and only a single peak at δ -32.50 for the NMe_2 protons of $Er(H_3BNMe_2BH_3)_3$ (**12b**) (Figure 4.4). Desolvation also causes the ^{11}B NMR resonance to move from δ -171.5 in **12a** to δ -324.4 for **12b**.

Neither the solid state method nor the thf desolvation method works particularly well to afford the $Ln(H_3BNMe_2BH_3)_3$ complexes of Eu and Yb. The DMADB complexes of both of these lanthanides reduce readily to their corresponding divalent analogs when heated, although sublimation of $Eu(H_3BNMe_2BH_3)_3(thf)$ under very mild conditions affords a solid of which the base free compound appears to be a component.

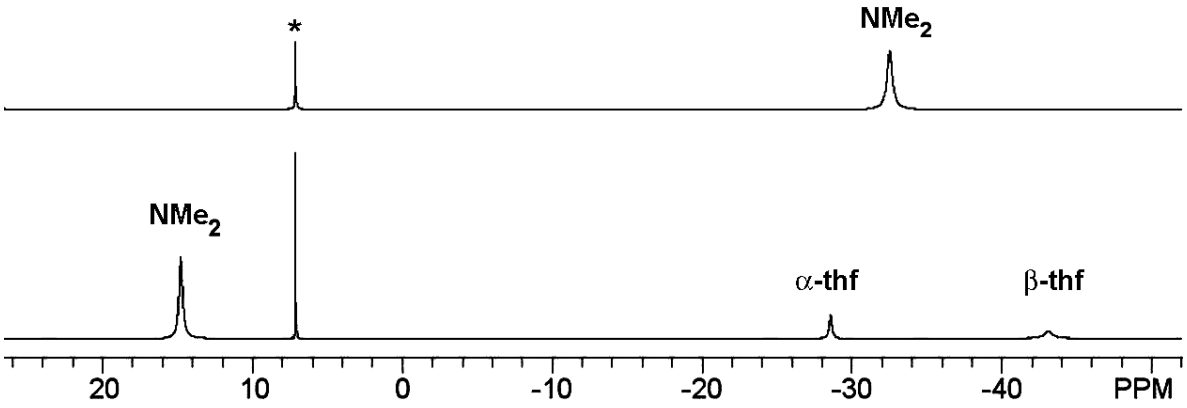

Figure 4.4. ^{1}H NMR spectra (C_6D_6, 20 °C) of $Er(H_3BNMe_2BH_3)_3(thf)$ (**12a**, bottom) and $Er(H_3BNMe_2BH_3)_3$ (**12b**, top) obtained by sublimation of **12a**. The asterisk denotes the deuterobenzene solvent resonance.

Single crystal X-ray diffraction studies of the base-free $Ln(H_3BNMe_2BH_3)_3$ complexes reveal that their structures depend sensitively on the ionic radius of the lanthanide ion, with the coordination number decreasing as the radius decreases across the period. As for the thf adducts, hydrogen atoms attached to boron surfaced in most of the difference maps, and their positions could be refined.

$Pr(H_3BNMe_2BH_3)_3$ (**4b**) adopts a polymeric structure in which each metal center is surrounded by two chelating DMADB ligands and two ligands that bridge between metal centers in a $Pr(\kappa^3\text{-}H_3BNMe_2BH_3\text{-}\kappa^3)Pr$ fashion. The total coordination number is 14 for each metal center (Figure 4.5). For the chelating DMADB ligands, in which each BH_3 unit is bound κ^2, the Pr···B distances range from 2.855(4) - 2.891(4) Å (Table 4.8). In contrast, for the bridging DMADB ligands, in which the BH_3 groups coordinate to the metal in a κ^3 fashion, the Pr···B distances are much shorter: 2.656(4) and 2.671(4) Å. For comparison, the Pr···B distances to the κ^3-BH_4 groups in the methoxyethyl-substituted cyclopentadienyl complex $(MeOCH_2CH_2C_5H_4)_2Pr(BH_4)$ and sevearal heteroleptic β-diketoiminato-borohydride complexes range from 2.644(8) to 2.757(18) Å.[108, 109] A complex with a Pr···B distance of 2.824(5) Å is claimed to involve a κ^3-BH_4 group, but the present results strongly suggest that this distance is to a κ^2 group instead.[109] The structure of **4b** is the same as that of the $U(H_3BNMe_2BH_3)_3$ isomer grown from toluene;[91] the isomorphous nature of the Pr and U compounds is not surprising in view of the similar ionic radii: 0.99 Å for Pr^{3+} and 1.025 for U^{3+}.[105] The Pr···B distances in **4b** are very similar to the U···B distances in $U(H_3BNMe_2BH_3)_3$ of 2.861(7) – 2.902(6) for the κ^2 interactions, and 2.665(6) and 2.670(6) Å for the κ^3 interactions.

$Sm(H_3BNMe_2BH_3)_3$ (**6b**), which contains the smaller Sm^{3+} ion (r_{ionic} = 0.96 Å),[105] adopts a structure in which the three DMADB ligands all chelate to the metal center in the

Table 4.7. Crystallographic data for $Ln(H_3BNMe_2BH_3)_3$ complexes at 193 K.

	Pr (4b)	**Sm (6b)**	**Er (12b)**
formula	$C_6H_{36}B_6N_3Pr$	$C_6H_{36}B_6N_3Sm$	$C_{12}H_{72}B_{12}N_6Er_2$
FW (g mol^{-1})	365.59	365.59	765.00
λ (Å)	0.71073	0.71073	0.71073
crystal system	monoclinic	monoclinic	orthorhombic
space group	$P2_1/c$	$P2_1/c$	$Pna2_1$
a (Å)	12.3657(5)	15.8615(6)	28.464(3)
b (Å)	10.8176(5)	10.1549(4)	14.042(1)
c (Å)	14.6115(6)	11.3788(4)	9.3917(9)
β	96.022(2)	96.7440(10)	90
V (Å^3)	1943.75(14)	1820.12(12)	3753.7(6)
Z	4	4	4
ρ_{calc} (g cm^{-3})	1.217	1.334	1.354
μ (mm^{-1})	2.488	3.206	4.452
absorption correction	face-indexed	face-indexed	face-indexed
max. min. transm. factors	0.717, 0.237	0.356, 0.214	0.916, 0.729
data/restraints/parameters	4272/49/224	3331/0/152	6720/79/298
goodness-of-fit on F^2	1.015	1.143	0.711
$R1$ [$I > 2\sigma(I)$]	0.0469	0.0429	0.0475
w$R2$ (all data)	0.0964	0.1103	0.076
largest diff. peak and hole (e·Å^{-3})	2.485/-3.110	1.746/-2.386	1.083/-0.762

Table 4.8. Selected atomic distances and angles for $Ln(H_3BNMe_2BH_3)_3$ complexes.

	Y (1b)[94]	**Pr (4b)**	**Sm (6b)**	**Dy (10a)**[94]	**Er (12b)**
			Atomic distances (Å)		
Ln – B1	2.701(7)	2.867(2)	2.849(4)	2.725(10)	2.733(19)
Ln – B2	2.739(7)	2.893(2)	2.782(3)	2.734(14)	2.745(18)
Ln – B3	2.718(7)	2.890(3)	2.785(4)	2.758(13)	2.744(16)
Ln – B4	2.756(7)	2.859(3)	2.812(4)	2.699(11)	2.71(2)
Ln – B5	2.719(8)	2.671(2)	2.869(3)	2.723(10)	2.735(18)
Ln – B6	2.763(7)	2.661(2)	2.839(3)	2.747(12)	2.730(19)
Ln – B7	2.732(7)			2.738(14)	2.733(17)
Ln – B8	2.717(7)			2.723(10)	2.68(2)
Ln – B11	2.837(7)			2.687(10)	2.849(19)
Ln – B12	2.672(7)			2.837(11)	2.590(17)
Ln – B21	2.734(7)			2.838(12)	2.719(18)
Ln – B22	2.853(7)			2.725(10)	2.849(17)
			Bond angles (deg)		
B1 - N1 - B2	107.3(10)	109.69(16)	109.5(2)	107.9(11)	109.6(13)
B3 - N2 - B4	110.8(9)	109.74(17)	108.5(2)	110.8(9)	110.4(13)
B5 - N3 - B6	108.4(9)	112.63(17)	108.2(2)	108.4(9)	109.0(13)
B7 - N4 - B8	110.2(9)			110.2(9)	107.5(13)
B11 - N11 - B12	113.2(10)			113.2(10)	111.5(13)
B21 - N21 - B22	109.4(8)			109.4(8)	115.5(12)

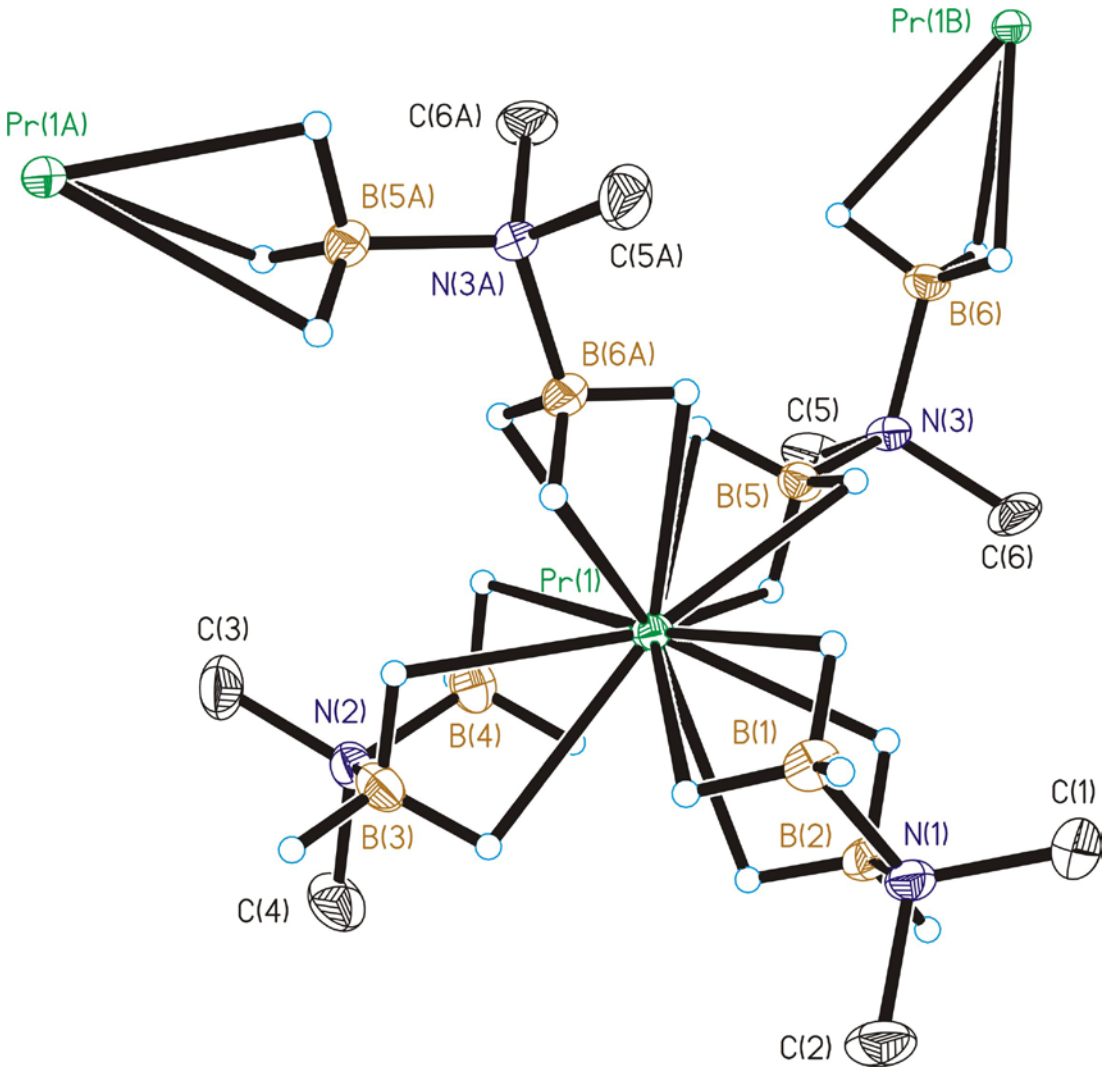

Figure 4.5. Molecular structure of $Pr(H_3BNMe_2BH_3)_3$, **4b**. Ellipsoids are drawn at the 35% probability level, except for the hydrogen atoms, which are represented as arbitrarily-sized spheres. Methyl hydrogen atoms have been deleted for clarity.

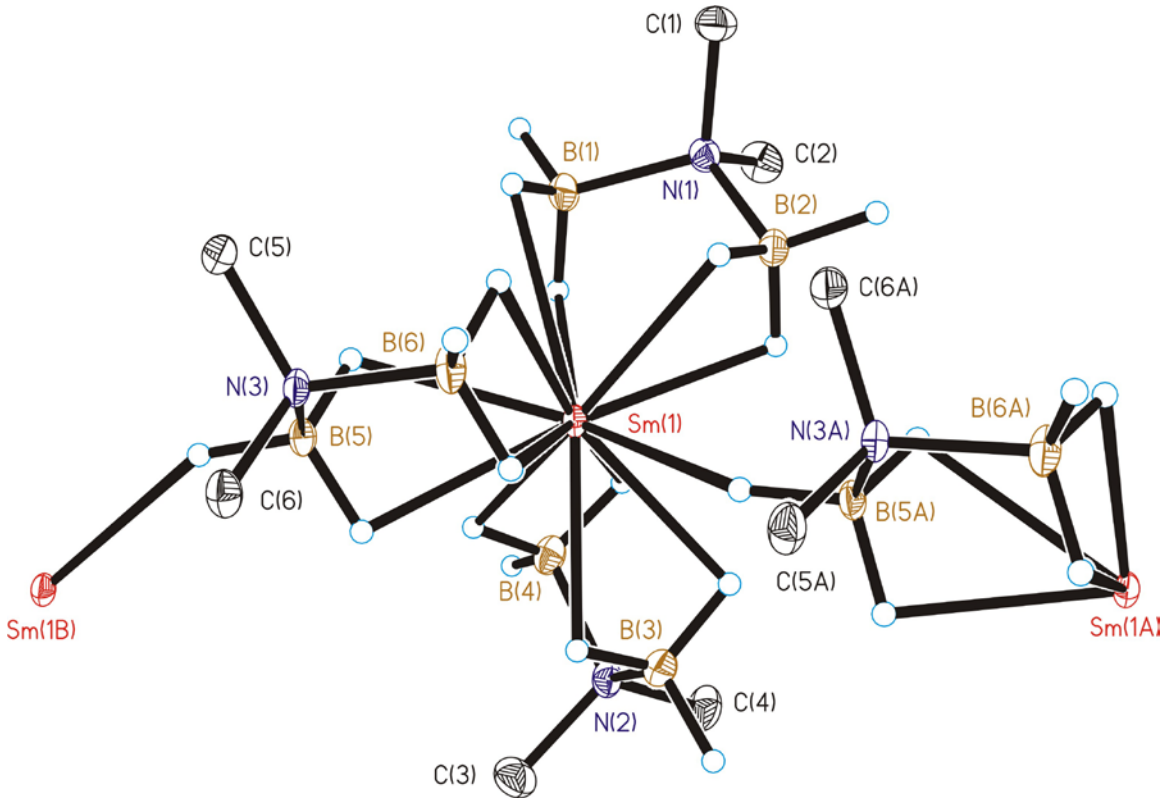

Figure 4.6. Molecular structure of $Sm(H_3BNMe_2BH_3)_3$, **6b**. Ellipsoids are drawn at the 35% probability level, except for the hydrogen atoms, which are represented as arbitrarily-sized spheres. Methyl hydrogen atoms have been deleted for clarity.

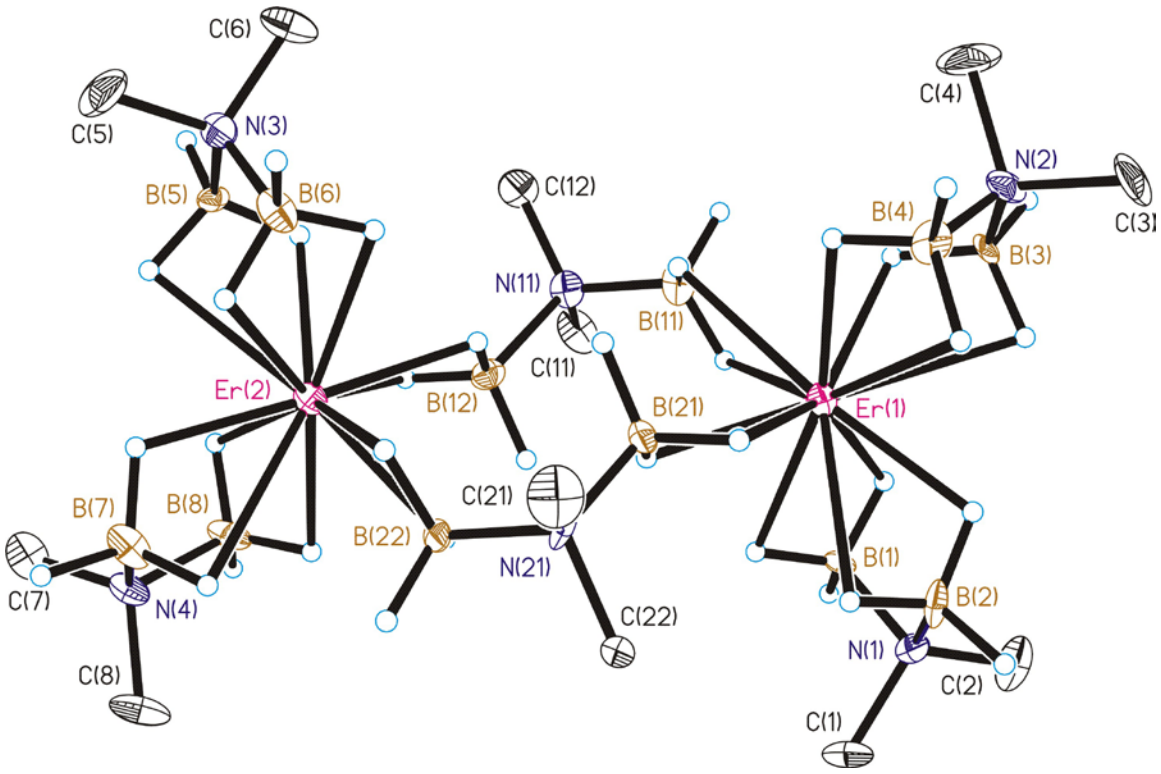

Figure 4.7. Molecular structure of $Er(H_3BNMe_2BH_3)_3$, **12b**. Ellipsoids are drawn at the 35% probability level, except for the hydrogen atoms, which are represented as arbitrarily-sized spheres. Methyl hydrogen atoms have been deleted for clarity.

usual fashion. The Sm···B distances of 2.783(4) – 2.870(4) Å for theseκ^2-BH_3 interactions are, as expected, significantly longer than the κ^3 interactions of 2.579(3) to 2.680(5) Å seen for certain samarium borohydride complexes.[110-114] The samarium ion in **6b** is located 0.32 Å out of the plane of the three nitrogen atoms, which opens up a thirteenth coordination site that is occupied by an intermolecular Sm···H-B bridge from an adjacent molecule (Figure 4.6). The intermolecular Sm-H distance of 2.50 Å is similar to the average intramolecular Sm-H distance of 2.44 Å. The 13-coordinate structure of **6b** matches the structural isomer of $U(H_3BNMe_2BH_3)_3$ grown from pentane, in which the uranium atom is also displaced, by 0.30 Å, out of the plane of the nitrogen atoms and forms one intermolecular U-H contact.[91]

The DMADB complexes of Dy^{3+} (**10b**), Y^{3+} (**1b**), and Er^{3+} (**12b**), which have even smaller ionic radii of 0.912, 0.900, and 0.890 Å, respectively,[105] adopt dinuclear structures (Figure 4.7). Each metal center bears two chelating DMADB ligands and two DMADB ligands that bridge between the two metals. The connectivity of each bridging ligand is $Ln(\kappa^2\text{-}H_3BNMe_2BH_3\text{-}\kappa^2)Ln$, making these complexes formally 12-coordinate. The average B-N-B bond angles of 109.0–109.3° for the chelating DMADB ligands are smaller than the 112.9, 111.3, and 113.4° angles seen for the bridging ligands in **1b**, **10b**, and **12b**, respectively.

Despite the fact that all the Ln···B interactions in **10b**, **1b**, and **12b** are κ^2, the Ln···B distances in these compounds vary significantly: 2.687(10) – 2.838(12) Å for **10b**, 2.672(7) – 2.853(7) Å for **1b**, and 2.590(17) – 2.849(19) Å for **12b** (Table 4.8). Most likely, the variations reflect differences in the local interligand repulsions, and comparisons with other complexes show that even the shortest of these distances is longer than expected for a κ^3 interaction. For example, Y···B distances reported for κ^2-BH_4^- groups of 2.693(8) to 2.836(1) Å[108, 115-118] are similar to those observed in **1b**, whereas Y···B distances for κ^3-BH_4^- groups

are significantly shorter at 2.485(3) – 2.584(3) Å.[116, 119, 120] Few structurally characterized dysprosium and erbium borohydride complexes are known, but the data again are consistent with our findings: the Ln···B distances for the κ^2-borohydride in $(Cp^{ttt})_2Dy(BH_4)$ is 2.660(4) Å whereas those for the κ^3-borohydrides in (2,4,6-*t*-Bu-C_6H_2O)$Er(BH_4)_2(thf)_2$ and $[(Me_3Si)_2NC(NCy)_2]Ln(BH_4)_2(thf)_2$ are 2.483(8) and 2.559(4) Å, respectively.[121, 122]

As seen for the diamagnetic $Ln(H_3BNMe_2BH_3)_3(thf)$ complexes, the ^1H and ^{11}B NMR spectra of the diamagnetic $Ln(H_3BNMe_2BH_3)_3$ species **1b**, **2b**, and **15b** are readily interpretable (Table 4.9). Only one ^1H NMR signal is observed for the NMe_2 and BH_3 groups for these complexes in deuterobenzene solution, and no decoalescence is observed upon cooling the samples to -70 °C. Because **1b** (and presumably also **15b**) adopts a diuclear structure in the solid state with multiple NMe_2 and BH_3 environments, either the complexes are monomeric in solution or they remain dinuclear but undergo dynamic processes that exchange the different sites.

Despite the differences in DMADB coordination modes, the solid state IR spectra of the $Ln(H_3BNMe_2BH_3)_3$ complexes in the B-H stretch region are similar to those of their $Ln(H_3BNMe_2BH_3)_3(thf)$ counterparts. The two thf bands at 856 and 837 cm^{-1} seen for the $Ln(H_3BNMe_2BH_3)_3(thf)$ complexes are not present in the IR spectra of the base-free compounds, as expected.

The field ionization mass spectra of the $Ln(H_3BNMe_2BH_3)_3$ complexes are also similar to those observed for their $Ln(H_3BNMe_2BH_3)_3(thf)$ analogs, except for the absence of thf-containing species (Table 4.10). Peaks corresponding to the ion $Ln(H_3BNMe_2BH_3)_3^+$ and the dinuclear species $Ln_2(H_3BNMe_2BH_3)_5^+$ can be observed in all of the spectra., and the fragment $Ln(H_3BNMe_2BH_3)_2^+$ is evident for all but **10b** (Dy) and **12b** (Er). For the early lanthanides (La – Tb), a peak for the trinuclear species $Ln_3(H_3BNMe_2BH_3)_8^+$ is also present;

Table 4.9. ^{1}H and ^{11}B NMR resonances of $Ln(H_3BNMe_2BH_3)_3$ complexes.

	NMe_2	**BH_3**	**^{11}B**
Y	2.12	2.49	-5.1
La	2.22	2.78	-2.8
Ce	4.23	26.39	39.8
Pr	5.13	68.41	103.9
Nd	4.66	86.84	125.3
Sm	3.89	-4.85	-10.8
Eu	-	-	-221.6
Gd	-	-	-
Tb	118.77	-	-343.8
Dy	94.43	-	-269.1
Ho	63.61	-	-216.5
Er	-32.50	-	-324.4
Tm	-116.02	-	-416.8
Lu	2.10	3.19	-6.3

* Blank entries indicate resonances that could not be located in the spectra.

Table 4.10. Major fragments observed in the FI mass spectra of $Ln(H_3BNMe_2BH_3)_3$ complexes.

	ML_2^+		ML_3^+		$M_2L_5^+$		$M_3L_8^+$	
M	mass (*m*/*z*)	rel. int. (%)	mass (*m*/*z*)	rel. int. (%)	mass (*m*/*z*)	rel. int. (%)	mass (*m*/*z*)	rel. int. (%)
La (**2b**)	282	50	353	80	637	100	991	80
Ce (**3b**)	285	5	356	100	639	35	995	5
Pr (**4b**)	285	35	356	65	642	35	999	10
Nd (**5b**)	288	55	358	100	648	95	1007	10
Sm (**6b**)	296	95	367	80	660	100	1029	10
Gd (**8b**)	300	100	370	90	674	95	1042	10
Tb (**9b**)	303	40	373	65	677	100	1051	4
Dy (**10b**)	-	-	377	100	684	40	-	-
Ho (**11b**)	309	90	379	80	688	100	-	-
Y[a] (**1b**)	233	65	303	100	537	90	-	-
Er (**12b**)	-	-	381	100	693	15	-	-
Tm (**13b**)	312	45	383	100	700	85	-	-
Lu (**15b**)	318	70	390	100	709	80	-	-

[a] Yttrium placed in the series according to its ionic radii; L = $H_3BNMe_2BH_3^-$.

the largest relative abundance (80%) is seen for **2b** (La), suggesting that these larger clusters are favored for metals with the largest radii.

All of the $Ln(H_3BNMe_2BH_3)_3$ complexes decompose rather than melt: the solids change color irreversibly when strongly heated, and colorless (presumably organic) crystals deposit in the cooler parts of the sealed capillaries. For example, at 185 °C $Pr(H_3BNMe_2BH_3)_3$ (**4b**) changes color from light green to orange. The decomposition temperatures are similar for La through Pr (183 - 185 °C) but then steadily decrease across the period from Nd ($T_{dec.}$ = 176 °C) to Lu ($T_{dec.}$ = 147 °C), similar to the melting point trend observed for the $Ln(H_3BNMe_2BH_3)_3(thf)$ complexes.

NMR Spectra of the Paramagnetic Lanthanide DMADB Complexes. The large NMR frequency shifts induced by paramagnetic lanthanide ions has been well documented and remains of great interest.[123] This behavior is known as the lanthanide induced shift (LIS) and is defined as the difference in the chemical shift of a nucleus in the presence of a paramagnetic lanthanide ion (Ce^{3+}, Pr^{3+}, etc…) relative to the shift observed in the presence of a diamagnetic analog (Y^{3+}, La^{3+}, or Lu^{3+}). The direction and magnitude of the LIS depends on the paramagnetism of the lanthanide and the spatial location of the nucleus with respect to the metal center and the magnetic susceptibility tensor.

The LIS is embodied in the parameter $\Delta_{a,i}$, in which the index *a* refers to the nucleus whose NMR shift is being measured and the index *i* refers to the identity of the lanthanide ion. The magnitude of $\Delta_{a,i}$ is the result of two contributions: the Fermi contact shift (δ_c), which arises from through-bond interactions, and the pseudo-contact shift (δ_{pc}), which arises from through-space dipolar interactions.[124] The contact shift contribution is the product of a contact shift factor F_a, which is proportional to the electron-nuclear hyperfine coupling constant, and the electron-spin expectation value of the lanthanide ion ($<S_z>_i$). The pseudo-

contact shift contribution in the general case is given by a relatively complicated expression, which is greatly simplified for systems with axial symmetry (i.e., at least a three-fold principal rotation axis). Under these circumstances, the pseudo-contact shift contribution is given by the product of the magnetic constant of the lanthanide (D_i), a crystal field parameter (B_0^2), and a geometric factor (G_a) equal to $(3\cos^2\theta - 1)/r^3$, where r is the distance of the nucleus from the metal center and θ is the angle between the vector **r** and the principal axis of symmetry. These relationships are summarized in equation 1:

$$\Delta_{a,i} = \delta_c + \delta_{pc} = F_a\langle S_z\rangle_i + G_a B_0^2 D_i \quad (1)$$

Because the values of $\langle S_z\rangle_i$ and D_i are constants that have been calculated for each Ln^{3+} ion,[125-128] equation 1 can be rearranged into the following two forms shown in equations 2 and 3.[129, 130]

$$\Delta_{a,i}/D_i = F_a\langle S_z\rangle_i/D_i + G_a B_0^2 \quad (2)$$

$$\Delta_{a,i}/\langle S_z\rangle_i = F_a + G_a B_0^2 D_i/\langle S_z\rangle_i \quad (3)$$

Typically, these equations are used to analyze LIS values for a certain reporter nucleus in a series of complexes with the same chemical formula but with different lanthanide ions. In such cases, if plots of $\Delta_{a,i}/\langle S_z\rangle_i$ vs. $D_i/\langle S_z\rangle_i$, or of $\Delta_{a,i}/D_i$ vs. $\langle S_z\rangle_i/D_i$, for different lanthanide ions give points that fall on a straight line, then this implies that the geometric factor G_a (as well as the crystal field parameter B_0^2 and the contact shift factor F_a) is the same for all the complexes, and thus the complexes are very likely isostructural.[131]

The ^1H and ^{11}B NMR spectra of the paramagnetic lanthanide DMADB complexes exhibit resonances that are broadened and shifted to varying degrees depending on the identity of the lanthanide ion. For the base free complexes, we measured three different sets of LIS data in deuterobenzene at room temperature: the ^{11}B NMR shifts of the BH_3 groups, and the ^1H NMR shifts of the BH_3 and NMe_2 groups. For the thf complexes, we also

measured the ^{1}H NMR shifts of the α and β thf resonances. The ^{11}B NMR resonances could be observed as broadened singlets for all the complexes except that of Gd, for which no resonances could be seen owing to rapid relaxation of the ^{11}B nuclei by this highly paramagnetic ion. For similar reasons, ^{1}H NMR resonances assigned to BH_3 groups could be observed for all complexes except Eu, Gd, Tb, Dy, Ho, and Er, and resonances assigned to thf and NMe_2 could be observed for all except Eu and Gd. Note that, for the base-free compounds, pure samples of the Eu and Yb complexes could not be prepared, but we were able to measure the ^{11}B NMR shift of $Eu(H_3BNMe_2BH_3)_3$ from a mixture that contained this species.

In all cases, only a single BH_3 resonance and a single NMe_2 resonance are present in the NMR spectra (the same is true for the α and β thf protons); thus, these complexes must be dynamic in solution. The effective (i.e., time averaged) symmetry of these complexes is at least axial, and very likely to be cubic, and thus the LIS shifts should be amenable to analysis by equations 1-3. Structural differences across the series, if present, should be detectable, because the dynamic processes will average different ensembles of structures.

Table 4.11 shows an analysis of the ^{1}H and ^{11}B LIS data for the $Ln(H_3BNMe_2BH_3)_3$ and $Ln(H_3BNMe_2BH_3)_3(thf)$ complexes.[132] It has been previously pointed out that equation 2 is better suited when the contact term makes a larger contribution to the LIS than the pseudocontact term.[131] Owing to their close proximity to the lanthanide ions, the BH_3 groups experience large contact contributions (denoted by the values of F_a in Table 4.11), and fits of the ^{1}H and ^{11}B LIS data for the BH_3 groups to equation 2 are linear with high correlation coefficients (Figure 4.8). The contact contributions for the NMe_2 and thf resonances are much smaller owing to their larger distances from the metal center, with the contact contribution for the α resonances of thf being larger than for the β resonances, as expected.

Table 4.11. ^{1}H and ^{11}B LIS data for lanthanide DMADB complexes using equations 2 and 3.

$Ln(H_3BNMe_2BH_3)_3(thf)$

Nucleus	**eqn used**	**# metals**	F_a	B_0^2	R^2
BH_3 (^{11}B)	2	10	-21.9	-0.48	0.971
BH_3 (^{1}H)	2	5	-18.5	0.60	0.995
NMe_2 (^{1}H)	3	7 [a]	0.050	0.23	0.806
α-thf (^{1}H)	3	7 [a]	0.215	-0.66	0.798
β-thf (^{1}H)	3	7 [a]	-0.0205	-0.48	0.900

$Ln(H_3BNMe_2BH_3)_3$

Nucleus	**eqn used**	**# metals**	F_a	B_0^2	R^2
BH_3 (^{11}B)	2	8 [b]	-21.4	-4.2	0.925
BH_3 (^{1}H)	2	3	-17.7	-1.08	0.999
NMe_2 (^{1}H)	3	7 [a]	1.03	-0.64	0.825

[a]Excludes Tm and Yb data, which were omitted from the least squares fit.

[b]Excludes Eu data because the formation of $Eu(H_3BNMe_2BH_3)_3$ could not be verified by other analytical techniques.

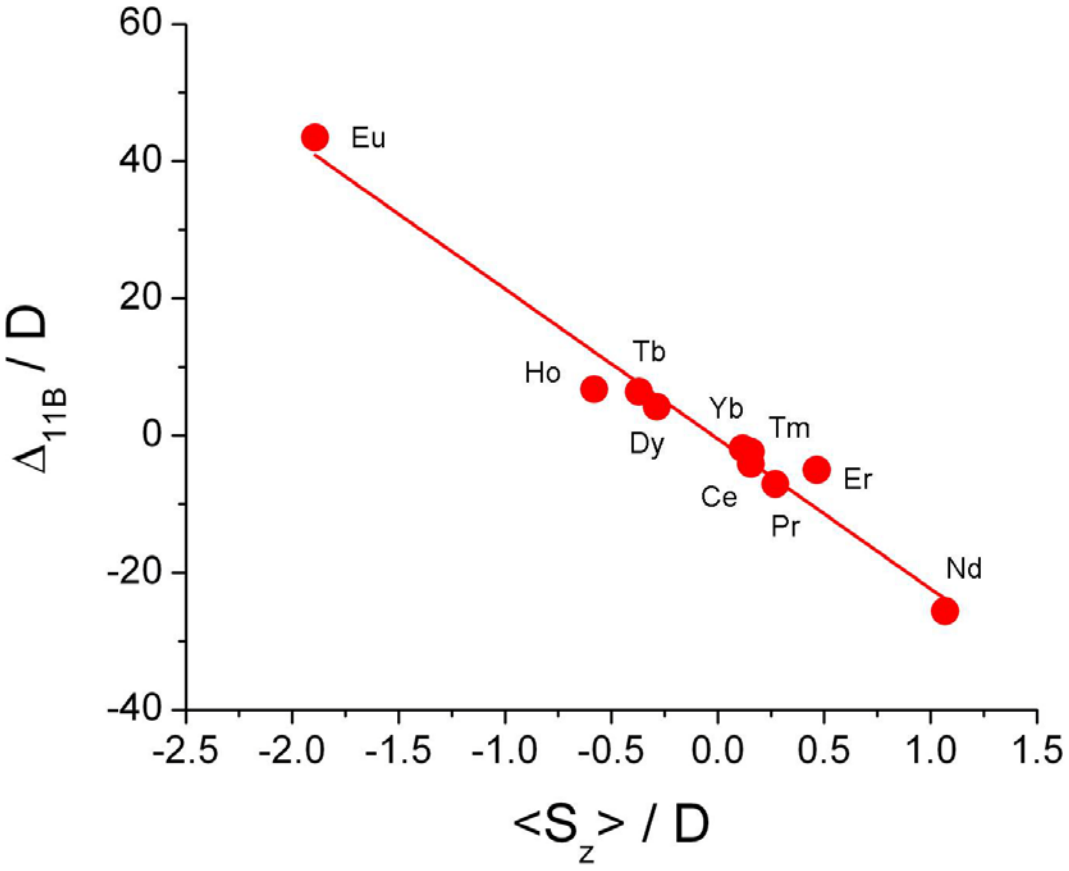

Figure 4.8. Plot of $\Delta_{a,i}/D$ vs $\langle S_z \rangle_i/D$ (equation 2) for the lanthanide induced shifts of the ^{11}B NMR resonances in the paramagnetic $Ln(H_3BNMe_2BH_3)_3(thf)$ complexes.

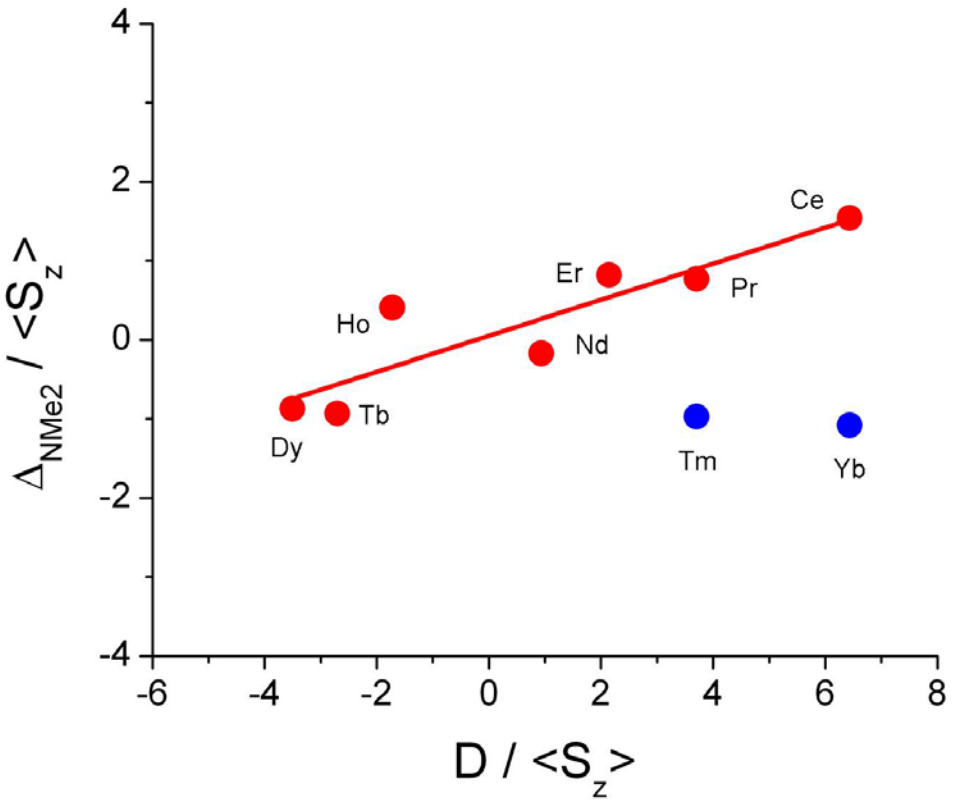

Figure 4.9. Plot of $\Delta_{a,i}/\langle S_z\rangle_i$ vs $D/\langle S_z\rangle_i$ (equation 3) for the lanthanide induced shifts of the ^{1}H NMR resonances of the NMe_2 groups in the paramagnetic $Ln(H_3BNMe_2BH_3)_3(thf)$ complexes. The least squares fit excluded the points for Tm and Yb.

Fits of these data to equation 3 are linear (Figure 4.9), but the points for Tm and Yb fall distinctly off the line generated by the other elements.

Although there is some scatter in all of the plots, the data are most consistent with the conclusion that, in benzene solution, all of the $Ln(H_3BNMe_2BH_3)_3$ complexes are isostructural, as are the $Ln(H_3BNMe_2BH_3)_3(thf)$ complexes, except for those with Ln = Tm or Yb (and also, by inference, Lu). For the base-free complexes, this finding is interesting because these compounds adopt a variety of solid state structures. If we assume that the complexes of Y, Dy, and Er, which are dinuclear in the solid state and dissolve with retention of the dinuclear structure, then the LIS data suggest that the polymeric $Ln(H_3BNMe_2BH_3)_3$ complexes readily break up in solution to their respective dimeric forms. This respeciation would also account for why the polymeric $Ln(H_3BNMe_2BH_3)_3$ complexes are soluble in hydrocarbon solvents.

In order to address residual doubts about whether the scatter in the plots was too large to conclude that the complexes are isostructural, and also to obtain additional evidence that the Tm and Yb complexes adopt different structures, we carried out an alternative analysis of the LIS data. It has been pointed out that low correlation coefficients for the least squares fits to equations 2 and 3 can result from a failure of any of the underlying assumptions. In this context, Reuben has noted that the crystal field parameter B_0^2 is not strictly invariant across the series of lanthanides.[133] In particular, it is quite common for the late lanthanides Yb and especially Tm to deviate from the least squares lines obtained by fits to equations 2 and 3,[134-138] and the deviations for Tm have been attributed in at least one case to the larger than expected value for B_0^2 relative to the other lanthanide ions.[139]

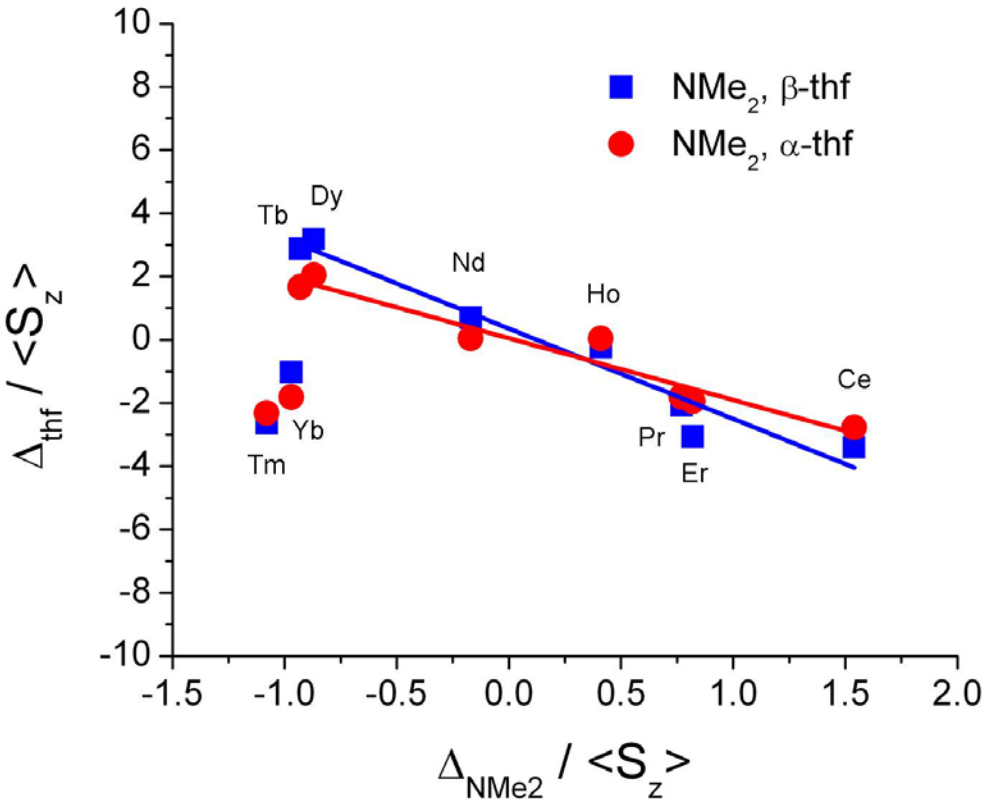

Figure 4.10. Plot of $\Delta_{a,i}/\langle S_z\rangle_i$ for the ^{1}H α (red) and β (blue) thf resonances vs $\Delta_{b,i}/\langle S_z\rangle_i$ for the NMe_2 resonances in the paramagnetic $Ln(H_3BNMe_2BH_3)_3(thf)$ complexes. The least squares fits excluded the points for Tm and Yb.

To factor out this effect, we employed a method to analyze the LIS data that is independent of B_0^2.[133] This method combines equation 1 for two different nuclei (designated by the indices *a* and *b*) within the same complex, eliminating the B_0^2 term, to give equation 4:

$$\Delta_{a,i}/\langle S_z\rangle_i = (F_a - R_{ab}F_b) + R_{ab}\Delta_{b,i}/\langle S_z\rangle_i \qquad (4)$$

If a series of lanthanide complexes is isostructural across the period, a plot of $\Delta_{a,i}/\langle S_z\rangle_i$ vs $\Delta_{b,i}/\langle S_z\rangle_i$ using equation 4 should be linear with a slope of R_{ab} ($R_{ab} = G_a/G_b$), and an intercept of $(F_a - R_{ab}F_b)$. Deviations from linearity in such a plot can be attributed to changes in the value of R_{ab} (i.e., a change in structure), provided that all other assumptions are valid (especially the assumption of axial symmetry).

For the $Ln(H_3BNMe_2BH_3)_3(thf)$ complexes, plots of $\Delta_{a,i}/\langle S_z\rangle_i$ for the α and β thf resonances vs $\Delta_{b,i}/\langle S_z\rangle_i$ for the NMe_2 resonances result in highly linear trends for all the lanthanide ions except for Tm and Yb (Figure 4.10). This finding suggests that the complexes of the latter two ions do indeed adopt a different structure. To corroborate the analysis, crystallographic studies of both the Tm and Lu complexes were conducted, which confirmed that these two complexes adopt structures that are different from those of the earlier lanthanides. In particular, these two complexes are 12 coordinate instead of 13 coordinate because one Ln···B distance is longer than the rest (see above). The LIS analysis suggests that all of the $Ln(H_3BNMe_2BH_3)_3(thf)$ complexes retain their solid state structures in hydrocarbon solutions.

Thermogravimetric Analysis of $Ln(H_3BNMe_2BH_3)_3(thf)$ and $Ln(H_3BNMe_2BH_3)_3$ Complexes. We have carried out thermogravimetric analyses (TGA) of the lanthanide aminodiboranate complexes in order to obtain quantitative assessments of their volatilities. The measurements were conducted under 0.3 Torr of N_2; under these conditions, sublimation

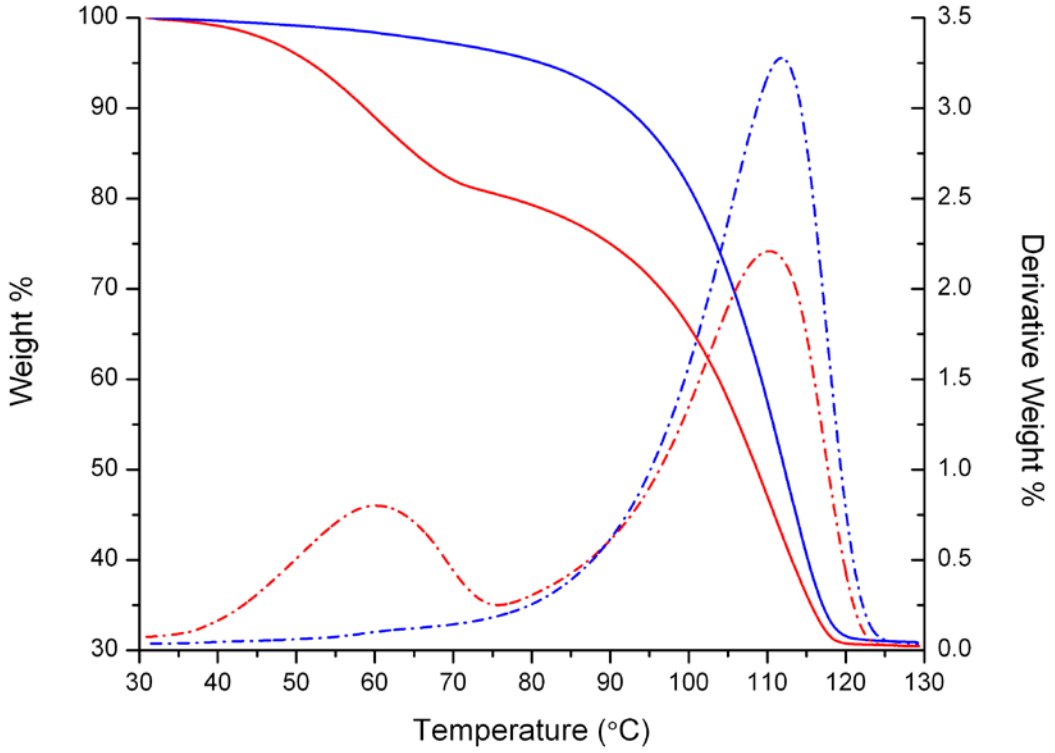

Figure 4.11. TGA traces (solid) with the corresponding first derivative plots (dashed) for $Tb(H_3BNMe_2BH_3)_3(thf)$ (**9a**, red) and $Tb(H_3BNMe_2BH_3)_3$ (**9b**, blue), obtained at 1 °C/min at 0.3 Torr.

occurs without significant decomposition and, for samarium through lutetium, at rates high enough to give good quantitative results. For the thf adducts of stoichiometry $Ln(H_3BNMe_2BH_3)_3(thf)$, the TGA traces show two features: a lower temperature feature due to loss of thf, and a higher temperature feature due to sublimation of the resulting base-free $Ln(H_3BNMe_2BH_3)_3$ material (Figure 4.11). The assignment of the higher temperature feature was confirmed from studies of isolated samples of the base-free materials, which give a single TGA peak at exactly the same temperature as the higher temperature peak seen for the thf adducts.

In most of the TGA studies, approximately 15 – 30 % of non-volatile residue remains after sublimation. As has been proposed in other systems,[52, 54] it is likely that most of the non-volatile material is generated by hydrolysis during the ~1 min exposure to ambient humidity that occurs during loading of the sample in the instrument. During sample loading, crystals of the lanthanide complexes that are colored (i.e. Nd = purple, Er = pink, etc.) become noticeably lighter in color along the crystal edges. In separate larger scale studies, samples of the $Ln(H_3BNMe_2BH_3)_3(thf)$ complexes that had not been exposed to air sublimed to afford the corresponding $Ln(H_3BNMe_2BH_3)_3$ complexes in isolated yields of 82 – 96 %, which are essentially quantitative if mechanical losses are taken into account.

The derivatives of the TGA traces reveal the temperatures at which the rate of weight change for each of these processes is at a maximum (Table 4.12). Comparison of these maxima reveals that the thf desolvation temperature decreases across the period from 78 °C (Sm) to 45 °C (Lu). Similarly, the sublimation temperature of the desolvated complex also decreases across the series. A representative set of TGA traces and first derivative plots is shown in Figure 4.11. For example, the rate of thf loss from $Tb(H_3BNMe_2BH_3)_3(thf)$, **9a**, peaks at 60.3 °C whereas the rate of sublimation peaks at ca. 111.7 °C. The latter

Table 4.12. TGA trace data for selected $Ln(H_3BNMe_2BH_3)_3(thf)$ complexes at 0.31 Torr and 1°C/min and comparison to sublimation yields obtained without atmospheric exposure.

Ln	Temp of max rate (°C)		Total wt loss (%)	Subl yield (%) under inert conditions
	thf loss	Sublimation		
Sm (**6a**)	78.1	121.3	> 71	84
Gd (**8a**)	71.6	117.6	84	92
Tb (**9a**)	60.3	110.4	70	-
Dy (**10a**)	61.9	112.4	82	-
Ho (**11a**)	60.1	111.8	74	-
Y (**1a**)[a]	61.1	106.7	80	-
Er (**12a**)	53.6	104.8	72	96
Tm (**13a**)	48.8	105.1	68	91
Lu (**15a**)	48.5	103.8	76	96

[a]Yttrium has been placed in the series according to its ionic radius.

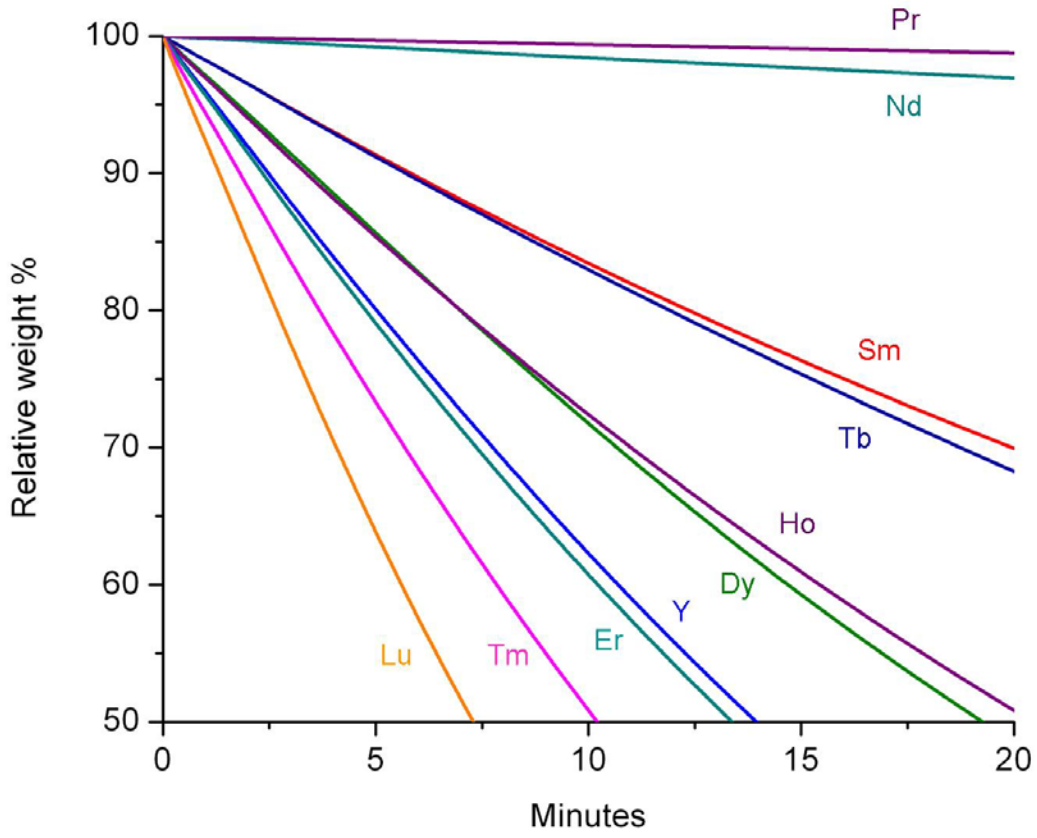

Figure 4.12. Isothermal TGA traces of selected $Ln(H_3BNMe_2BH_3)_3$ complexes obtained at 100 °C at 0.3 Torr.

temperature matches the 110.4 °C temperature for the maximum sublimation rate of isolated samples of the base free material $Tb(H_3BNMe_2BH_3)_3$, **9b**.

Isothermal TGA data collected from samples of the base-free complexes at 100 °C and 0.29 Torr of N_2 corroborate the observed trends in volatility (Figure 4.12). The mass decrease is initially linear with time, but slows at longer times due to depletion and surface area effects, as has been reported in other TGA sublimation studies.[52, 54] Taking the initial rates of weight loss as a measure of volatility, a comparison of the isothermal data shows that there is a steady increase in sublimation rate across the lanthanide period from $Sm(H_3BNMe_2BH_3)_3$ at 0.21 mg/min to $Lu(H_3BNMe_2BH_3)_3$ at 0.93 mg/min (Table 4.13), for sample charges of 15 – 20 mg. The rates of sublimation for the earlier lanthanides $Pr(H_3BNMe_2BH_3)_3$ and $Nd(H_3BNMe_2BH_3)_3$ are slow under these conditions, 0.01 and 0.02 mg/min, respectively, and these TGA studes were stopped before sublimation was complete. Overall, the TGA data closely track the sublimation temperatures, which range from 65 to 125 °C at 10^{-2} Torr (Table 4.14).

The $Ln(H_3BNMe_2BH_3)_3$ complexes are some of the most volatile lanthanide compounds ever reported. The silylamide complexes $Ln[N(SiMe_3)_2]_3$ and certain functionalized β-ketoiminates are also appreciably volatile, but these complexes require pressures two orders of magnitude lower than the aminodiboranates to sublime at comparable temperatures. Among lanthanide β-diketonates, complexes of stoichiometry $Ln(thd)_3$ (thd = 2,2,6,6-tetramethyl-3,5-heptanedionate) are among the most volatile and are commonly used in CVD processes.[13] The thd derivatives have been used previously as a benchmark for volatility comparisons of lanthanide CVD precursors.[54] In Figure 4.13, we make a direct comparison of the TGA traces of $Er(thd)_3$, thd = 2,2,6,6-tetramethylheptanedionate, and our

Table 4.13. TGA data for selected $Ln(H_3BNMe_2BH_3)_3$ complexes collected at 0.29 Torr.

	TGA trace at 1 °C/min		Isothermal trace at 100 °C	
Ln	**Temp of max subl rate (°C)**	**Subl yield (%)**	**Rate of subl (mg/min)**	**Subl yield (%)**
Pr (**4b**)	-	-	0.01	-
Nd (**5b**)	-	-	0.02	-
Sm (**6b**)	115.9	73	0.21	70
Tb (**9b**)	111.7	69	0.28	73
Dy (**10b**)	109.6	81	0.44	80
Ho (**11b**)	109.7	72	0.42	78
Y[a] (**1b**)	107.8	91	0.56	90
Er (**12b**)	106.3	77	0.59	87
Tm (**13b**)	104.3	78	0.78	87
Lu (**15b**)	97.0	63	0.93	79

[a]Yttrium has been placed in the series according to its ionic radii.

Table 4.14. Comparison of sublimation temperatures of $Ln(H_3BNMe_2BH_3)_3$ complexes with those of other lanthanide complexes.

Complex type	Lanthanides surveyed	Subl range (°C)	pressure (Torr)	Reference
Aminodiboranates, $Ln(H_3BNMe_2BH_3)_3$	Y, La-Sm, Gd-Tm, Lu	65 – 125	10^{-2}	this work
Silylamides, $Ln[N(SiMe_3)_2]_3$	Y, La-Gd, Ho, Yb, Lu	75 – 102	10^{-4}	[32]
Ether-functionalized β-ketoiminates	Ce, Nd, Gd, Er	80 – 110	10^{-4}	[54]
Guanidinates, $Ln[(N^iPr)_2CNR_2]_3$	Y, Gd, Dy	120 – 165	0.05	[52]
Amididinates, $Ln(^tBuNC(CH_3)N^tBu)_3$	Y, La, Ce, Nd, Eu, Er, Lu	180 – 220	0.05	[50]
Cyclopentadienyls, $LnCp_3$	Sc, Y, La-Sm, Gd, Dy, Er, Yb	150 – 260	10^{-4}	[44]
β-diketonates, $Ln(thd)_3$	Y,Ce,Pr,Sm-Tb,Tm, Yb	215 – 290	760	[37]

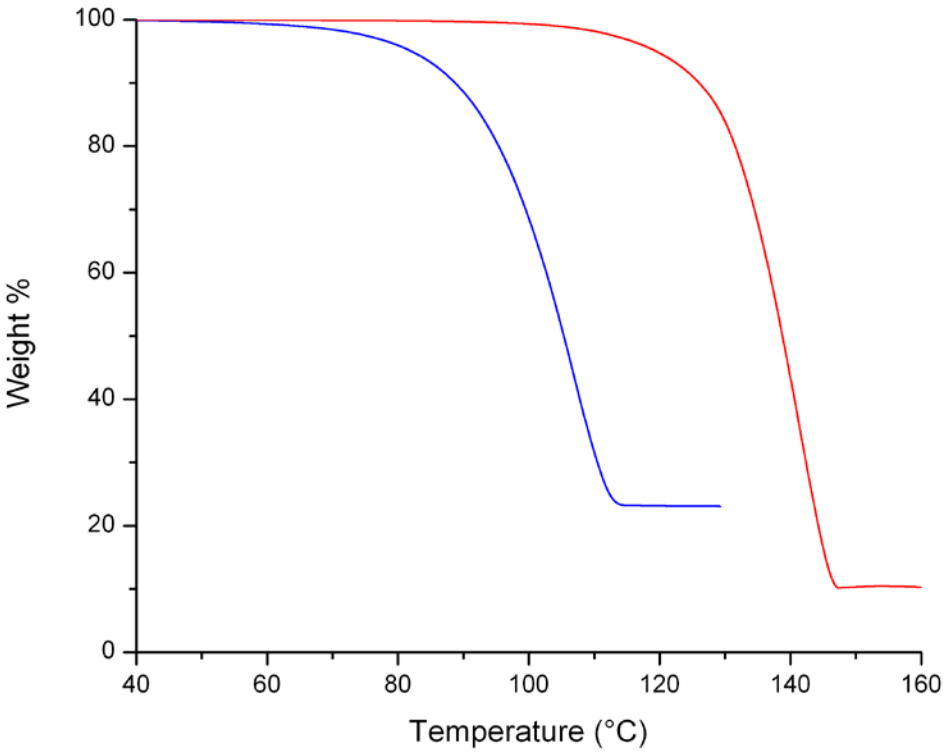

Figure 4.13. TGA traces of $Er(H_3BNMe_2BH_3)_3$, **12b** (blue) and commercially available $Er(thd)_3$ (red), obtained at 1 °C/min at 0.3 Torr.

erbium compound $Er(H_3BNMe_2BH_3)_3$, **12b**, under identical conditions. The traces clearly show that the latter sublimes at a significantly lower temperature.

Interestingly, the $Ln(H_3BNMe_2BH_3)_3$ complexes are highly volatile, even for those that are polymeric in the solid state. Polymerization typically leads to lowered volatility owing to the increased energy required to free molecules from covalent bonding interactions (as opposed to weaker van der Waals interactions) with their neighbors, and to compensate for the reorganization energy required to induce the conformational change that attends the depolymerization process. It has been shown, however, that homoleptic tetrahydroborate complexes such as $U(BH_4)_4$, which also has a polymeric 14-coordinate solid-state structure but is highly volatile, has a low barrier to ligand-rearrangement to the volatile, 12-coordinate monomeric form.[140, 141]

Consistent with the above considerations, the lowest sublimation rates are seen for the DMADB complexes of the earlier $Pr(H_3BNMe_2BH_3)_3$ (**4b**) and $Nd(H_3BNMe_2BH_3)_3$ (**5b**). The Pr compound (and probably Nd as well) adopts a polymeric structure with $Ln(\kappa^3\text{-}H_3BNMe_2BH_3\text{-}\kappa^3)Ln$ bridging ligands. Evidently, the volatilities of these 14-coordinate compounds are reduced owing to the reorganization energy required to convert them to a volatile (probably monomeric or dimeric) form. Intermediate volatilities are seen for the DMADB complexes of the mid-lanthanides $Sm(H_3BNMe_2BH_3)_3$ (**6b**) and $Tb(H_3BNMe_2BH_3)_3$ (**9b**). The Sm complex (and probably those of Eu, Gd, and Tb) adopts weakly polymerized structure, in which tris(chelate) monomers are associated into chains by means of one intermolecular Ln-H-B interaction. Only this bond needs to be broken to convert the polymer into monomers. The highest volatilities are seen for the late lanthanides Dy through Lu (and including Y). All of these DMADB complexes adopt dinuclear structures with no strong interactions between the dimers in the solid state. These 12

coordinate complexes may sublime as dimers, or they may be able to rearrange into the corresponding $Ln(H_3BNMe_2BH_3)_3$ monomer.

The field ionization MS data for the $Ln(H_3BNMe_2BH_3)_3$ complexes lend support to these conclusions. The ion $Ln(H_3BNMe_2BH_3)_3^+$ and the dinuclear fragment $Ln_2(H_3BNMe_2BH_3)_5^+$ can be observed in the spectra of all of the complexes, and the trinuclear fragment $Ln_3(H_3BNMe_2BH_3)_8^+$ can be observed in the spectra of the larger lanthanides (Table 4.10). Care must be taken when drawing inferences from mass spectra because the ionization process can affect the chemistry, but the data support the hypothesis that the gas phase species responsible for sublimation of the $Ln(H_3BNMe_2BH_3)_3$ complexes are monomers and/or dimers for the late lanthanides, and possibly also trimers for the early lanthanides.

Solubility and Reactivity. The $Ln(H_3BNMe_2BH_3)_3(thf)$ complexes are soluble in non-polar solvents such as pentane, benzene, toluene, and diethyl ether. They are also soluble in and unreactive towards dichloromethane, which is not the case for redox active DMADB complexes, such as $U(H_3BNMe_2BH_3)_3(thf)$. The lanthanide complexes are slow to react with O_2 but react readily with water, the major hydrolysis products being lanthanide hydroxides, H_2, and (μ-dimethylamino)diborane, $(NMe_2)B_2H_5$.

The identity of the hydrolysis product $(NMe_2)B_2H_5$ has been established from the ^{11}B NMR spectrum of hydrolysed lanthanide DMADB samples, which yields of a triplet of doublets at ca. δ -17 in benzene.[142] The moisture-sensitivity is not surprising in view of the hydridic nature of the DMADB ligand and, as expected, these complexes are reactive towards most other protic reagents. The base-free complexes seem to be more susceptible to hydrolysis and are slightly less soluble in non-polar solvents than their $Ln(H_3BNMe_2BH_3)_3(thf)$ counterparts.

Table 4.15. Crystallographic data for $[La(H_3BNMe_2BH_3)_2(OH)]_4$ (**16**).

formula	$C_{16}H_{100}B_{16}La_4N_8O_4$
FW (g mol^{-1})	1197.61
T (K)	193(2)
λ (Å)	0.71073
crystal system	tetragonal
space group	*P*-4*n*2
a (Å)	15.213(2)
b (Å)	15.213(2)
c (Å)	14.092(3)
β (deg)	90
volume (Å^3)	3261.4(10)
Z	2
ρ_{calc} (g cm^{-3})	1.366
μ (mm^{-1})	2.598
absorption correction	psi-scan
max. min. transm. factors	0.806, 0.666
data/restraints/parameters	2999/2/144
goodness-of-fit on F^2	0.625
*R*1 [$I > 2\sigma(I)$]	0.0213
w*R*2 (all data)	0.0232
largest diff. peak and hole (e·Å^{-3})	0.525/-0.288

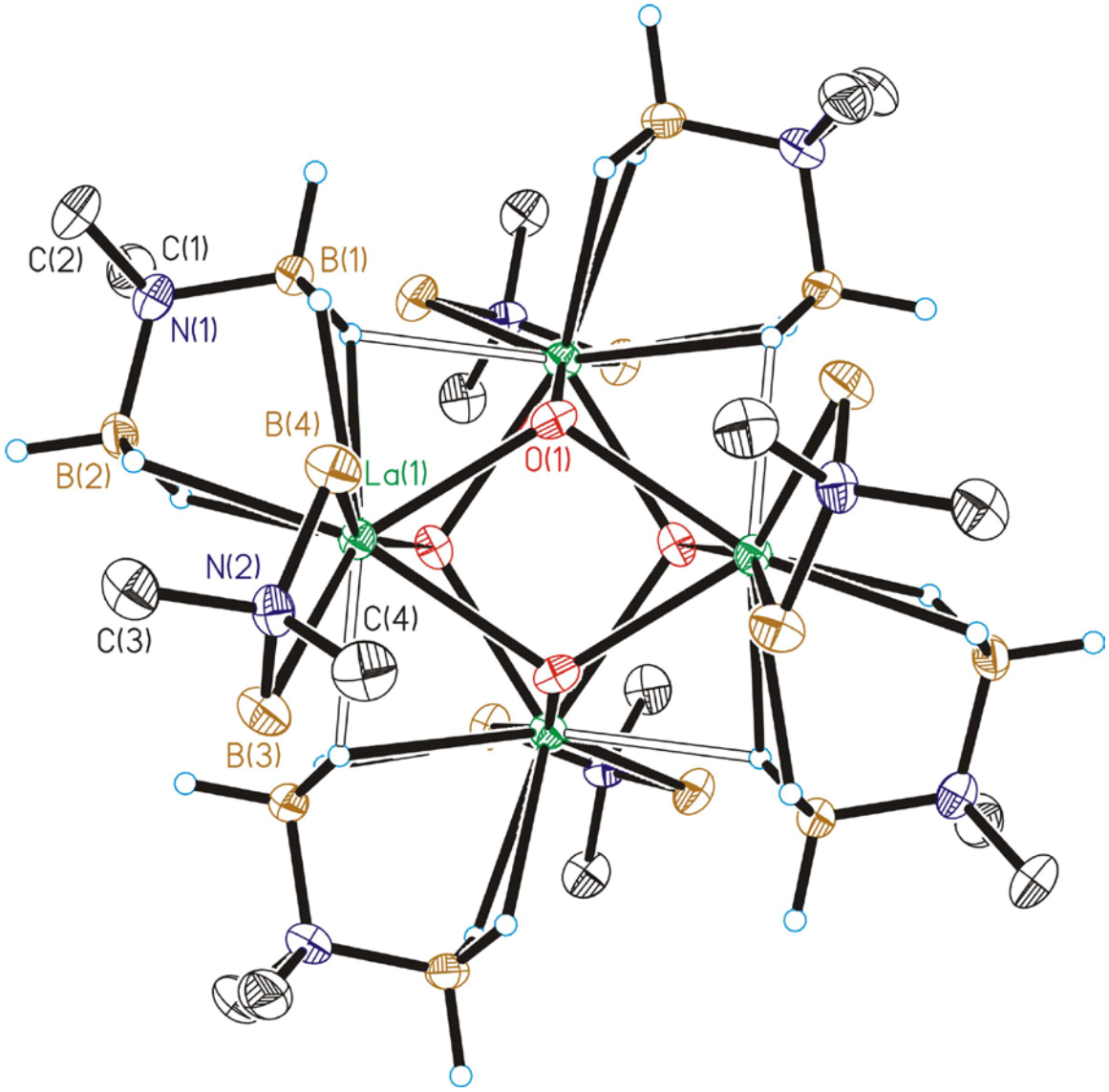

Figure 4.14. Molecular structure of $[La(H_3BNMe_2BH_3)_2(OH)]_4$, **16**. Ellipsoids are drawn at the 35% probability level, except for the hydrogen atoms, which are represented as arbitrarily-sized spheres. Hydrogen atoms attached to all atoms except for B1 and B2 have been deleted for clarity. The interaction between the bridging B-H hydrogen atom on B1 and the adjacent La atom is depicted as an open bond for emphasis.

We adventitiously obtained crystals of the partial hydrolysis product $[La(H_3BNMe_2BH_3)_2(OH)]_4$ (**16**), which presumably was generated by means of the following reaction:

$$Ln(H_3BNMe_2BH_3)_3(thf) + H_2O \longrightarrow Ln(H_3BNMe_2BH_3)_2(OH) + H_2 + (NMe_2)B_2H_5$$

X-ray diffraction studies of this material of confirm that hydrolysis affords products bearing hydroxide ligands (Figure 4.14). The lanthanum and oxygen atoms in **16** form the core of a distorted cube; each lanthanum atom is connected to three bridging hydroxyl groups and to two chelating DMADB ligands. One B-H bond of each chelating DMADB ligand forms a bridge to an adjacent metal center; the La···B distances to the borane group that shares the hydride is considerably longer at 3.107(4) Å compared to 2.917(4) – 2.982(4) Å distances for the other La···B contacts. The latter are similar to the average La···B distance of 2.94(2) Å observed in the thf adduct **2a**. The La-O bond distances of 2.443(2), 2.516(2), and 2.554(2) Å are similar to the Ln-O distance of 2.513(12) Å to the thf ligand in **2a**. These also compare well with other La-O bond distances reported for complexes containing a $La_3(\mu_3\text{-OH})$ core, which range from 2.417(2) to 2.583(12) Å.[62, 143-145]

The hydrolysis of the $Ln(H_3BNMe_2BH_3)_3$ complexes, as detailed above, has important implications for the deposition of lanthanide oxides thin films. Carrying out depositions in the presence of water should readily convert the DMADB ligands into $(NMe_2)B_2H_5$, thereby providing a mechanism to form pure oxide films free of carbon, nitrogen, or boron heteratoms. The deposition of pure lanthanide oxide films by CVD and ALD from these DMADB complexes in the presence of water as a co-reactant has already been demonstrated, as we have shown elsewhere.[146]

Synthesis and Characterization of $Pr(H_3BNMe_2BH_3)_3(dme)$. The $Ln(H_3BNMe_2BH_3)_3(thf)$ complexes can be used to prepare other Lewis bases adducts of lanthanide aminodiboranates. In a representative example, $Pr(H_3BNMe_2BH_3)_3(dme)$ was prepared by adding dme to a solution of **4a** in pentane, which yielded a large amount of light green precipitate. Filtering the mother liquor and washing the precipitate with cold pentane yields analytically pure $Pr(H_3BNMe_2BH_3)_3(dme)$ in high yield (76%). Aside from two new peaks in the ^1H NMR spectrum, corresponding to the methyl and methylene resonances at δ 6.50 and -2.62, the NMR spectra obtained of $Pr(H_3BNMe_2BH_3)_3(dme)$ closely match those of **4a**. A new peak in the FI mass spectrum at *m*/*z* 374, corresponding to $Pr(H_3BNMe_2BH_3)_2(dme)^+$, confirmed the presence of coordinated dme.

Experimental

All operations were carried out in vacuum or under argon using standard Schlenk techniques. All glassware was dried in an oven at 150 °C, assembled hot, and allowed to cool under vacuum before use. Tetrahydrofuran and pentane were distilled under nitrogen from sodium/benzophenone and degassed with argon immediately before use. Anhydrous $LnCl_3$ and LnI_3 were purchased from commercial vendors (Aldrich and Strem) and were used as received. $Na(H_3BNMe_2BH_3)$ was prepared by a literature route.[93]

Elemental analyses were carried out by the University of Illinois Microanalytical Laboratory. The IR spectra were recorded on a Nicolet Impact 410 infrared spectrometer as Nujol mulls between KBr plates. The ^1H data were obtained on a Varian Unity 400 instrument at 400 MHz or on a Varian Unity U500 instrument at 500 MHz. The ^{11}B NMR data were collected on a General Electric GN300WB instrument at 96 MHz or on a Varian Unity Inova 600 instrument at 192 MHz. Chemical shifts are reported in δ units (positive

shifts to high frequency) relative to TMS (^{1}H) or BF_3•Et_2O (^{11}B). Field ionization (FI) mass spectra were recorded on a Micromass 70-VSE mass spectrometer. The shapes of all peak envelopes correspond with those calculated from the natural abundance isotopic distributions in the observed spectra, except for the $Ln(H_3BNMe_2BH_3)_3^+$ and $Ln(H_3BNMe_2BH_3)_2(thf)^+$ fragments for the $Ln(H_3BNMe_2BH_3)_3(thf)$ complexes, which overlapped. Melting points and decomposition temperatures were determined in closed capillaries under argon on a Thomas-Hoover Unimelt apparatus. Thermogravimetric analysis (TGA) data were collected with a TA Instruments Q600 SDT simultaneous DSC-TGA instrument.

Tris(*N*,*N*-dimethylaminodiboranato)(tetrahydrofuran)yttrium(III), $Y(H_3BNMe_2BH_3)_3(thf)$, (1a). To a suspension of YCl_3 (0.30 g, 1.5 mmol) in tetrahydrofuran (20 mL) at 0 °C was added a solution of sodium *N*,*N*-dimethylaminodiboranate (0.44 g, 4.6 mmol) in tetrahydrofuran (20 mL). The white reaction mixture was stirred at 0 °C for 15 min before being allowed to warm to room temperature. The resulting mixture was stirred for 15 h and then evaporated to dryness under vacuum to afford a sticky, white solid. The residue was extracted with pentane (2 × 25 mL). The filtered extracts were combined, concentrated to ca. 16 mL, and cooled to -20 ˚C to afford 0.24 g of large, white crystals. The mother liquor was concentrated to 8 mL and cooled to -20 ˚C to yield an additional 0.10 g of white crystals. Yield: 0.34 g (59 %). M.p.: 116 - 120 ˚C. Anal. Calcd for $C_{10}H_{44}B_6N_3OY$: C, 31.9; H, 11.8; N, 11.2. Found: C, 31.8; H, 12.2; N, 10.9. ^{1}H NMR (C_6D_6, 20 °C): δ 1.18 (m, β-CH_2, 4H), 2.28 (s, NMe_2, 18H), 2.51 (br 1:1:1:1 q, J_{BH} = 85 Hz, BH_3, 18H), 3.83 (m, OCH_2, 4H). ^{11}B NMR (C_6D_6, 20 °C): δ -5.7 (q, J_{BH} = 89 Hz, BH_3). MS(FI) [fragment ion, relative abundance]: *m*/*z* 176 [$Y(H_3BNMe_2BH_3)(BH_4)^+$, 8], 233 [$Y(H_3BNMe_2BH_3)_2^+$, 40], 303 [$Y(H_3BNMe_2BH_3)_3^+$ / $Y(H_3BNMe_2BH_3)_2(thf)^+$, 100], 376 [$Y(H_3BNMe_2BH_3)_3(thf)^+$, 6], 538 [$Y_2(H_3BNMe_2BH_3)_5^+$, 40], 608 [$Y_2(H_3BNMe_2BH_3)_5(thf)^+$, 15]. IR ($cm^{-1}$): 2399 vs, 2294 m,

2227 s, 2177 w, 2060 sh, 1283 s, 1241 s, 1217 s, 1189 w, 1171 s, 1137 s, 1020 s, 924 m, 856 m, 837 w, 819 w, 666 w. Single crystals for the X-ray diffraction study were grown by sublimation at 90 °C at 10^{-2} Torr under static vacuum.

Tris(*N*,*N*-dimethylaminodiboranato)(tetrahydrofuran)lanthanum(III), $La(H_3BNMe_2BH_3)_3(thf)$, (2a). Method A. This complex was prepared analogously to compound **1a** from LaI_3 (1.20 g, 2.3 mmol) and sodium *N*,*N*-dimethylaminodiboranate (0.65 g, 6.9 mmol). The white residue was extracted with pentane (55 mL), the extract was filtered, and the clear filtrate was concentrated to ca. 20 mL and cooled to -20 ˚C to yield 0.29 g of large, colorless blocks. The mother liquor was concentrated to 10 mL and cooled to -20 ˚C to yield an additional 0.21 g of crystals. Yield: 0.50 g (51 %). Microanalyses, ^{1}H and ^{11}B NMR spectra match those obtained for product prepared by Method B.

Method B. To $La(H_3BNMe_2BH_3)_3$ (0.10 g, 0.28 mmol) was added 15 mL of tetrahydrofuran. The resulting clear solution was stirred for 15 min and evaporated to dryness under vacuum. The white residue was extracted with pentane (40 mL), the extract was filtered, and the clear filtrate was concentrated to 10 mL and stored at -20 ˚C to yield large, cubic crystals. Yield: 0.06 g (50 %). M.p.: 136 – 137 °C. Anal. Calcd for $C_{10}H_{44}B_6N_3OLa$: C, 28.2; H, 10.4; N, 9.86. Found: C, 27.9; H, 11.0; N, 9.65. ^{1}H NMR (C_6D_6, 20 ˚C): δ 1.13 (m, β-CH_2, 4H), 2.30 (s, NMe_2, 18H), 2.87 (br 1:1:1:1 q, J_{BH} = 82 Hz, BH_3, 18H), 3.78 (m, OCH_2, 4H). ^{11}B NMR (C_6D_6, 20 °C): δ -2.87 (br q, J_{BH} = 91 Hz, BH_3). MS(FI) [fragment ion, relative abundance]: *m*/*z* 114 [$(H_2BNMe_2)_2$, 100], 226 [$La(H_3BNMe_2BH_3)(BH_4)^+$, 10], 283 [$La(H_3BNMe_2BH_3)_2^+$, 25], 353 [$La(H_3BNMe_2BH_3)_3^+$ / $La(H_3BNMe_2BH_3)_2(thf)^+$, 100], 636 [$La_2(H_3BNMe_2BH_3)_5^+$, 30]. IR ($cm^{-1}$): 2487 sh, 2421 sh, 2390 s, 2339 m, 2288 m, 2259 sh, 2220 vs, 2181 sh, 2064 w, 1399 w, 1259 s, 1236 s, 1218 s, 1188 m, 1170 vs, 1141 s, 1034 sh, 1017 s, 930 m, 901 w, 855 w, 836 w, 808 w, 723 w, 667 w, 445 m.

Tris(*N*,*N*-dimethylaminodiboranato)(tetrahydrofuran)cerium(III), $Ce(H_3BNMe_2BH_3)_3(thf)$, (3a). Method A. This complex was prepared analogously to compound **1a** from $CeCl_3$ (0.27 g, 1.1 mmol) and sodium *N*,*N*-dimethylaminodiboranate (0.30 g, 3.2 mmol). The white residue was extracted with pentane (2 × 25 mL), the extracts were filtered and combined, and the clear filtrate was concentrated to ca. 5 mL and cooled to -20 ˚C to yield 0.041 g of large, white crystals. The mother liquor was concentrated to 3 mL and cooled to -20 ˚C to yield an additional 0.02 g of white crystals. Yield: 0.061 g (13 %). Microanalyses, ^{1}H and ^{11}B NMR spectra match those obtained for product prepared by Method C.

Method B. Prepared analogously to compound **1a** from CeI_3 (0.95 g, 1.8 mmol) and sodium *N*,*N*-dimethylaminodiboranate (0.52 g, 5.5 mmol). The white residue was extracted with pentane (65 mL), the extract was filtered, and the clear filtrate was concentrated to ca. 18 mL and cooled to -20 °C to yield 0.49 g of large, colorless blocks. The mother liquor was concentrated to 6 mL and cooled to -20 °C to yield an additional 0.085 g of crystals. Yield: 0.58 g (74 %). Microanalyses, ^{1}H and ^{11}B NMR spectra match those obtained for product prepared by Method C.

Method C. Prepared using the same procedure as **2a** from 0.13 g of **3b**. Yield: 0.09 g (58 %). M.p.: 132 - 134 ˚C. Anal. Calcd for $C_{10}H_{44}B_6N_3OCe$: C, 28.1; H, 10.4; N, 9.83. Found: C, 27.9; H, 10.8; N, 9.65. ^{1}H NMR (C_6D_6, 20 °C): δ 0.79 (s, fwhm = 6 Hz, NMe_2, 18H), 3.84 (s, fwhm = 12 Hz, β-CH_2, 4H), 7.11 (s, fwhm = 22 Hz, OCH_2, 4H), 20.39 (br q, J_{BH} = 92 Hz, BH_3, 18H). ^{11}B NMR (C_6D_6, 20 °C): δ 23.1 (br s, fwhm = 49 Hz, BH_3). MS(FI) [fragment ion, relative abundance]: *m*/*z* 72 [thf, 100], 355 [$Ce(H_3BNMe_2BH_3)_3^+$ / $Ce(H_3BNMe_2BH_3)_2(thf)^+$, 15], 414 [$Ce(H_3BNMe_2BH_3)_3(thf)^+$, 2], 640 [$Ce_2(H_3BNMe_2BH_3)_5^+$, 5], 710 [$Ce_2(H_3BNMe_2BH_3)_5(thf)^+$, 2]. IR ($cm^{-1}$): 2492 sh, 2390 s, 2340 w, 2285 m, 2255 sh,

2216 vs, 2168 sh, 2064 w, 1261 s, 1235 s, 1216 s, 1186 s, 1169 vs, 1138 s, 1032 sh, 1017 s, 929 w, 901 w, 855 m, 836 w , 809 w, 722 w, 666 w, 449 m.

Tris(*N*,*N*-dimethylaminodiboranato)(tetrahydrofuran)praseodymium(III), $Pr(H_3BNMe_2BH_3)_3(thf)$, (4a). This complex was prepared analogously to compound **1a** from $PrCl_3$ (0.53 g, 2.1 mmol) and sodium *N*,*N*-dimethylaminodiboranate (0.61 g, 6.4 mmol). The pale-green residue was extracted with pentane (45 mL), the extract was filtered, and the pale-green filtrate was concentrated to ca. 10 mL and cooled to -20 ˚C to yield large, pale green crystals. Yield: 0.51 g (56 %). M.p.: 134 - 136 ˚C. Anal. Calcd for $C_{10}H_{44}B_6N_3OPr$: C, 28.1; H, 10.4; N, 9.81. Found: C, 28.2; H, 10.9; N, 9.89. ^{1}H NMR (C_6D_6, 20 °C): δ 0.02 (s, fwhm = 7 Hz, NMe_2, 18H), 6.48 (s, fwhm = 13 Hz, β-CH_2, 4H), 9.93 (s, fwhm = 22 Hz, OCH_2, 4H), 58.06 (br d, J_{BH} = 98 Hz, BH_3, 18H). ^{11}B NMR (C_6D_6, 20 °C): δ 75.1 (br s, fwhm = 200 Hz, BH_3). MS(FI) [fragment ion, relative abundance]: *m*/*z* 58 [H_2BNMe_2H, 100], 355 [$Pr(H_3BNMe_2BH_3)_3^+$ / $Pr(H_3BNMe_2BH_3)_2(thf)^+$, 40], 642 [$Pr_2(H_3BNMe_2BH_3)_5^+$, 15]. IR ($cm^{-1}$): 2491 sh, 2390 vs, 2340 m, 2284 s, 2250 sh, 2213 vs, 2169 sh, 2066 w, 1262 s, 1237 s, 1216 s, 1185 m, 1170 s, 1137 s, 1031 sh, 1017 s, 960 w, 929 m, 901 w, 856 m, 838 w, 812 w, 722 w, 666 w.

Tris(*N*,*N*-dimethylaminodiboranato)(tetrahydrofuran)neodymium(III), $Nd(H_3BNMe_2BH_3)_3(thf)$, (5a). This complex was prepared analogously to compound **1a** from $NdCl_3$ (0.42 g, 1.7 mmol) and sodium *N*,*N*-dimethylaminodiboranate (0.48 g, 5.1 mmol). The lavender colored residue was extracted with pentane (2 × 10 mL), the extracts were filtered and combined, and the pale purple filtrate was concentrated to ca. 8 mL and cooled to -20 ˚C to yield 0.26 g of large, lavender colored crystals. The mother liquor was concentrated to 3 mL and cooled to -20 ˚C to yield an additional 0.11 g of lavender-colored crystals. Yield: 0.37 g (51 %). M.p.: 133 - 134 ˚C. Anal. Calcd for $C_{10}H_{44}B_6N_3ONd$: C,

27.8; H, 10.3; N, 9.74. Found: C, 28.4; H, 10.6; N, 9.72. ^{1}H NMR (C_6D_6, 20 °C): δ 0.66 (s, fwhm = 21 Hz, OCH_2, 4H), 0.95 (s, fwhm = 9 Hz, β-CH_2, 4H), 3.06 (s, fwhm = 7 Hz, NMe_2, 18H), 82.86 (br s, fwhm = 330 Hz, BH_3, 18H). ^{11}B NMR (C_6D_6, 20 °C): δ 104.8 (br s, fwhm = 170 Hz, BH_3). MS(FI) [fragment ion, relative abundance]: *m*/*z* 115 [H_2B-NMe_2-BH_2-NMe_2H, 20], 286 [$Nd(H_3BNMe_2BH_3)_2^+$, 15], 358 [$Nd(H_3BNMe_2BH_3)_3^+$ / $Nd(H_3BNMe_2BH_3)_2(thf)^+$, 100], 645 [$Nd_2(H_3BNMe_2BH_3)_5^+$, 60], 718 [$Nd_2(H_3BNMe_2BH_3)_5(thf)^+$, 15], 1003 [$Nd_3(H_3BNMe_2BH_3)_8^+$, 10]. IR (cm^{-1}): 2493 sh, 2392 s, 2342 m, 2285 s, 2252 sh, 2216 vs, 2173 sh, 2066 w, 1264 s, 1238 s, 1216 s, 1186 s, 1170 s, 1137 s, 1031 sh, 1018 s, 926 m, 902 w, 857 m, 837 w, 813 w, 722 w, 667 w.

Tris(*N*,*N*-dimethylaminodiboranato)(tetrahydrofuran)samarium(III), $Sm(H_3BNMe_2BH_3)_3(thf)$, (6a). This complex was prepared analogously to compound **1a** from $SmCl_3$ (0.30 g, 1.2 mmol) and sodium *N*,*N*-dimethylaminodiboranate (0.33 g, 3.5 mmol). The ivory colored residue was extracted with pentane (2 × 15 mL), and the extracts were combined, filtered, concentrated to ca. 15 mL, and cooled to -20 ˚C to yield 0.18 g of large, ivory-colored crystals. The mother liquor was concentrated to 7 mL and cooled to -20 ˚C to yield an additional 0.11 g of ivory-colored crystals. Yield: 0.29 g (57 %). M.p.: 134 - 135 ˚C. Anal. Calcd for $C_{10}H_{44}B_6N_3OSm$: C, 27.4; H, 10.1; N, 9.60. Found: C, 27.6; H, 10.5; N, 9.73. ^{1}H NMR (C_6D_6, 20 °C): δ -1.86 (br q, J_{BH} = 104 Hz, BH_3, 18H), 1.29 (s, fwhm = 10 Hz, β-CH_2, 4H), 3.80 (s, fwhm = 14 Hz, OCH_2, 4H), 2.25 (s, fwhm = 4 Hz, NMe_2, 18H). ^{11}B NMR (C_6D_6, 20 °C): δ -9.8 (br q, J_{BH} = 87 Hz, BH_3). MS(FI) [fragment ion, relative abundance]: *m*/*z* 239 [$Sm(H_3BNMe_2BH_3)(BH_4)^+$, 20], 296 [$Sm(H_3BNMe_2BH_3)_2^+$, 60], 362 [$Sm(H_3BNMe_2BH_3)_3^+$ / $Sm(H_3BNMe_2BH_3)_2(thf)^+$, 100], 660 [$Sm_2(H_3BNMe_2BH_3)_5^+$, 80], 732 [$Sm_2(H_3BNMe_2BH_3)_5(thf)^+$, 5]. IR (cm^{-1}): 2496 sh, 2392 vs, 2344 m, 2286 s, 2255 m, 2218 vs, 2173 s, 2067 w, 1268 s, 1238 s, 1216 s, 1187 m, 1170

s, 1137 s, 1114 sh, 1034 sh, 1019 s, 962 w, 924 m, 902 w, 856 m, 838 w, 814 w, 723 w, 667 w, 457 m.

Tris(*N*,*N*-dimethylaminodiboranato)(tetrahydrofuran)europium(III), Eu($H_3BNMe_2BH_3$)$_3$(thf), (7a). To a suspension of $EuCl_3$ (0.32 g, 1.2 mmol) in tetrahydrofuran (20 mL) at -78 °C was added a solution of sodium *N*,*N*-dimethylaminodiboranate (0.34 g, 3.6 mmol) in tetrahydrofuran (20 mL). The grey reaction mixture was stirred at -78 °C for 20 min before being allowed to warm to room temperature. The grey suspension slowly gained a yellow hue after several hours at room temperature. The mixture was stirred for 20 h at room temperature and then was evaporated to dryness under vacuum to afford a light yellow residue. The residue was extracted with pentane (10 mL). The yellow extract was filtered and cooled to -20 ˚C to yield 0.14 g of large, bright yellow crystals mixed with 0.05 g of straw colored crystals of [$Eu_2(H_3BNMe_2BH_3)_4(thf)_4$] that could be removed by hand. The mother liquor was concentrated to 5 mL and cooled to -20 ˚C to yield an additional 0.09 g of yellow crystals and 0.01 g of straw colored crystals. Yield: 0.23 g (44 %). M.p.: 107˚C (dec.). Anal. Calcd for $C_{10}H_{44}B_6N_3OEu$: C, 27.3; H, 10.1; N, 9.57. Found: C, 27.2; H, 10.3; N, 9.30. ^{11}B NMR (C_6D_6, 20 °C): δ -176.8 (br s, fwhm = 2140 Hz, BH_3). MS(FI) [fragment ion, relative abundance]: *m*/*z* 114 [$(H_2BNMe_2)_2$, 100], 295 [$Eu(H_3BNMe_2BH_3)_2^+$, 40], 355 [$Eu(H_3BNMe_2BH_3)_3 - BH_2$, 25], 367 [$Eu(H_3BNMe_2BH_3)_3^+$ / $Eu(H_3BNMe_2BH_3)_2(thf)^+$, 75], 663 [$Eu_2(H_3BNMe_2BH_3)_5^+$, 15]. IR ($cm^{-1}$): 2392 vs, 2351 m, 2294 s, 2248 sh, 2227 vs, 2191 sh, 2112 sh, 2079 w, 1273 s, 1240 s, 1219 s, 1173 vs, 1144 s, 1034 sh, 1020 vs, 970 w, 928 m, 914 w, 877 w, 872 w, 820 w, 777 w, 723 m, 669 w, 461 w.

Tris(*N*,*N*-dimethylaminodiboranato)(tetrahydrofuran)gadolinium(III), Gd($H_3BNMe_2BH_3$)$_3$(thf), (8a). This complex was prepared analogously to compound **1a** from $GdCl_3$ (0.28 g, 1.1 mmol) and sodium *N*,*N*-dimethylaminodiboranate (0.30 g, 3.2

mmol). The white residue was extracted with pentane (2 × 25 mL), the extracts were filtered and combined, and the clear filtrate was concentrated to ca. 12 mL and cooled to -20 ˚C to yield 0.22 g of large, white crystals. The mother liquor was concentrated to 5 mL and cooled to -20 ˚C to yield an additional 0.10 g of white crystals. Yield: 0.32 g (68 %). M.p.: 128 - 129 ˚C. Anal. Calcd for $C_{10}H_{44}B_6N_3OGd$: C, 27.0; H, 9.98; N, 9.45. Found: C, 27.1; H, 10.4; N, 9.77. MS(FI) [fragment ion, relative abundance]: *m*/*z* 72 [thf, 100], 243 [$Gd(H_3BNMe_2BH_3)(BH_4)^+$, 3], 301 [$Gd(H_3BNMe_2BH_3)_2^+$, 3], 359 [$Gd(H_3BNMe_2BH_3)_3 - BH_2$, 5], 370 [$Gd(H_3BNMe_2BH_3)_3^+$ / $Gd(H_3BNMe_2BH_3)_2(thf)^+$, 25], 674 [$Gd_2(H_3BNMe_2BH_3)_5^+$, 5]. IR ($cm^{-1}$): 2506 sh, 2394 s, 2342 m, 2290 s, 2268 m, 2222 vs, 2176 s, 2071 sh, 1274 s, 1239 s, 1216 s, 1189 s, 1171 vs, 1137 s, 1114 sh, 1034 sh, 1019 vs, 962 w, 923 m, 903 w, 856 m 838 w, 816 w, 723 w, 667 w.

Tris(*N*,*N*-dimethylaminodiboranato)(tetrahydrofuran)terbium(III), $Tb(H_3BNMe_2BH_3)_3(thf)$, (9a). This complex was prepared analogously to compound **1a** from $TbCl_3$ (0.30 g, 1.1 mmol) and sodium *N*,*N*-dimethylaminodiboranate (0.32 g, 3.4 mmol). The white residue was extracted with pentane (3 × 15 mL), the extracts were filtered and combined, and the clear filtrate was concentrated to ca. 10 mL and cooled to -20 ˚C to yield 0.27 g of large, white crystals. The mother liquor was concentrated to 3 mL and cooled to -20 ˚C to yield an additional 0.09 g of white crystals. Yield: 0.34 g (67 %). M.p.: 122 - 123 ˚C. Anal. Calcd for $C_{10}H_{44}B_6N_3OTb$: C, 26.9; H, 9.94; N, 9.42. Found: C, 26.6; H, 9.80; N, 9.31. ^1H NMR (C_6D_6, 20 °C): δ -27.50 (br s, fwhm = 210 Hz, NMe_2, 18H), 54.50 (s, fwhm = 520 Hz, β-CH_2, 4H), 95.55 (s, fwhm = 1600 Hz, OCH_2, 4H). ^{11}B NMR (C_6D_6, 20 °C): δ -556.3 (br s, fwhm = 320 Hz, BH_3). MS(FI) [fragment ion, relative abundance]: *m*/*z* 72 [thf, 100], 303 [$Tb(H_3BNMe_2BH_3)_2^+$, 5], 373 [$Tb(H_3BNMe_2BH_3)_3^+$ / $Tb(H_3BNMe_2BH_3)_2(thf)^+$, 15], 676 [$Tb_2(H_3BNMe_2BH_3)_5^+$, 5]. IR ($cm^{-1}$): 2506 sh, 2394 s,

2342 m, 2290 s, 2268 m, 2222 vs, 2176 s, 2071 sh, 1276 s, 1239 s, 1216 s, 1189 s, 1171 vs, 1137 s, 1114 sh, 1034 sh, 1019 vs, 962 w, 923 m, 903 w, 856 m 838 w, 816 w, 723 w, 667 w.

Tris(*N*,*N*-dimethylaminodiboranato)(tetrahydrofuran)dysprosium(III), Dy($H_3BNMe_2BH_3$)$_3$(thf), (10a). This complex was prepared analogously to compound **1a** from $DyCl_3$ (0.31 g, 1.2 mmol) and sodium *N*,*N*-dimethylaminodiboranate (0.33 g, 3.5 mmol). The white residue was extracted with pentane (40 mL), the extract was filtered, and the clear filtrate was concentrated to ca. 15 mL and cooled to -20 ˚C to yield 0.18g of large, off-white crystals. The mother liquor was concentrated to 8 mL and cooled to -20 ˚C to yield an additional 0.13 g of white crystals. Yield: 0.31 g (60 %). M.p.: 121 - 124 ˚C. Anal. Calcd for $C_{10}H_{44}B_6N_3ODy$: C, 26.7; H, 9.86; N, 9.34. Found: C, 26.7; H, 10.1; N, 9.26. ^{1}H NMR (C_6D_6, 20 °C): δ -22.72 (s, fwhm = 190 Hz, NMe_2, 18H), 59.71 (s, fwhm = 300 Hz, β-CH_2, 4H), 94.84 (br s, fwhm = 900 Hz, OCH_2, 4H). ^{11}B NMR (C_6D_6, 20 °C): δ -428.4 (br s, fwhm = 260 Hz, BH_3). MS(FI) [fragment ion, relative abundance]: *m*/*z* 377 [Dy($H_3BNMe_2BH_3$)$_3^+$ / Dy($H_3BNMe_2BH_3$)$_2$(thf)$^+$, 95], 684 [Dy$_2$($H_3BNMe_2BH_3$)$_5^+$, 100]. IR (cm^{-1}): 2410 vs, 2280 m, 2223 s, 2178 w, 2064 w, 1279 vs, 1238 m, 1217 w, 1168 s, 1139 s, 1017 vs, 927 s, 902 w, 836 s, 817 w, 666 w. Single crystals for the X-ray diffraction study were grown by sublimation at 90 °C at 10^{-2} Torr under static vacuum.

Tris(*N*,*N*-dimethylaminodiboranato)(tetrahydrofuran)holmium(III), Ho($H_3BNMe_2BH_3$)$_3$(thf), (11a). This complex was prepared analogously to compound **1a** from $HoCl_3$ (0.34 g, 1.2 mmol) and sodium *N*,*N*-dimethylaminodiboranate (0.35 g, 3.7 mmol). The salmon-colored residue was extracted with pentane (2 × 20 mL), the extracts were filtered and combined, and the clear filtrate was concentrated to ca. 14 mL and cooled to -20 ˚C to yield 0.15 g of large, pink crystals. The mother liquor was concentrated to 8 mL and cooled to -20 ˚C to yield an additional 0.16 g of pink crystals. Yield: 0.31 g (56 %).

M.p.: 119 - 120 ˚C. Anal. Calcd for $C_{10}H_{44}B_6N_3OHo$: C, 26.6; H, 9.81; N, 9.29. Found: C, 26.2; H, 9.81; N, 9.14. ^{1}H NMR (C_6D_6, 20 °C): δ -1.80 (s, fwhm = 460 Hz, OCH_2, 4H), 2.05 (s, fwhm = 150 Hz, β-CH_2, 4H), 11.46 (br s, fwhm = 170 Hz, NMe_2 18H). ^{11}B NMR (C_6D_6, 20 °C): δ -269.4 (br s, fwhm = 200 Hz, BH_3). MS(FI) [fragment ion, relative abundance]: *m*/*z* 251 [$Ho(H_3BNMe_2BH_3)(BH_4)^+$, 5], 308 [$Ho(H_3BNMe_2BH_3)_2^+$, 30], 367 [$Ho(H_3BNMe_2BH_3)_3 - BH_2$, 25], 380 [$Ho(H_3BNMe_2BH_3)_3^+$ / $Ho(H_3BNMe_2BH_3)_2(thf)^+$, 70], 688 [$Ho_2(H_3BNMe_2BH_3)_5^+$, 100], 760 [$Ho_2(H_3BNMe_2BH_3)_5(thf)^+$, 10]. IR ($cm^{-1}$): 2506 sh, 2394 s, 2342 m, 2290 s, 2268 m, 2222 vs, 2176 s, 2071 sh, 1282 s, 1239 s, 1216 s, 1189 s, 1171 vs, 1137 s, 1114 sh, 1034 sh, 1019 vs, 962 w, 923 m, 903 w, 856 m 838 w, 816 w, 723 w, 667 w.

Tris(*N*,*N*-dimethylaminodiboranato)(tetrahydrofuran)erbium(III), Er($H_3BNMe_2BH_3$)$_3$(thf), (12a). To a suspension of $ErCl_3$ (2.11g, 7.71 mmol) in tetrahydrofuran (125 mL) at 0 °C was added a solution of sodium *N*,*N*-dimethylaminodiboranate (2.27 g, 24.0 mmol) in tetrahydrofuran (50 mL). The pale pink reaction mixture was stirred at 0 °C for 15 min before being allowed to warm to room temperature. The pink suspension slowly turned to a hazy pink solution after several hours at room temperature. The mixture was stirred for 42 h at room temperature and then evaporated to dryness under vacuum to afford a sticky, pink solid. The residue was extracted with pentane (3 × 40 mL). The filtered extracts were combined, concentrated to ca. 50 mL, and cooled to -20 ˚C to yield 1.89 g of large, pale pink crystals. The mother liquor was concentrated to 8 mL and cooled to -20 ˚C to yield an additional 0.61 g of pale pink crystals. Yield: 2.50 g (71 %). M.p.: 114 - 117 ˚C. Anal. Calcd for $C_{10}H_{44}B_6N_3OEr$: C, 26.4; H, 9.76; N, 9.24. Found: C, 26.4; H, 9.96; N, 9.17. ^{1}H NMR (C_6D_6, 20 °C): δ -43.14 (br s, fwhm = 250 Hz, OCH_2, 4H), -28.57 (s, fwhm = 87 Hz, β-CH_2, 4H), 14.79 (s, fwhm = 110

Hz, NMe_2, 18H). ^{11}B NMR (C_6D_6, 20 °C): δ -171.5 (s, fwhm = 180 Hz, BH_3). MS(FI) [fragment ion, relative abundance]: *m*/*z* 72 [thf, 100], 381 [$Er(H_3BNMe_2BH_3)_3^+$ / $Er(H_3BNMe_2BH_3)_2(thf)^+$, 5]. IR ($cm^{-1}$): 2405 s, 2355 sh, 2297 m, 2293 m, 2230 vs, 2185 s, 2087 sh, 1286 s, 1242 s, 1219 m, 1173 vs, 1140 s, 926 w, 856 m, 849 w, 825 sh, 468 m.

Tris(*N*,*N*-dimethylaminodiboranato)(tetrahydrofuran)thulium(III), $Tm(H_3BNMe_2BH_3)_3(thf)$, (13a). This complex was prepared analogously to compound **1a** from $TmCl_3$ (0.28 g, 1.0 mmol) and sodium *N*,*N*-dimethylaminodiboranate (0.31 g, 3.3 mmol). The white residue was extracted with pentane (3 × 15 mL), filtered, and the light green filtrate was concentrated to ca. 5 mL and cooled to -20 ˚C to yield large, light blue-green crystals. Yield: 0.24 g (52 %). M.p.: 100 - 103 ˚C. Anal. Calcd for $C_{10}H_{44}B_6N_3OTm$: C, 26.3; H, 9.72; N, 9.21. Found: C, 26.4; H, 9.93; N, 8.96. ^1H NMR (C_6D_6, 20 °C): δ -92.87 (br s, fwhm = 1900 Hz, BH_3, 18H), -17.86 (s, fwhm = 270 Hz, α and β-CH_2, 8H), -6.60 (br s, fwhm = 170 Hz, NMe_2 18H). ^{11}B NMR (C_6D_6, 20 °C): δ -133.0 (br s, fwhm = 370 Hz, BH_3). MS(FI) [fragment ion, relative abundance]: *m*/*z* 71 [$NMe_2(BH_2)_2^+$, 40], 254 [$Tm(H_3BNMe_2BH_3)(BH_4)^+$, 5], 312 [$Tm(H_3BNMe_2BH_3)_2^+$, 100], 383 [$Tm(H_3BNMe_2BH_3)_3^+$ / $Tm(H_3BNMe_2BH_3)_2(thf)^+$, 80], 697 [$Tm_2(H_3BNMe_2BH_3)_5^+$, 65]. IR ($cm^{-1}$): 2401 vs, 2350 sh, 2274 m, 2230 vs, 2179 vs, 2069 sh, 1400 w, 1312 sh, 1287 s, 1242 s, 1220 s, 1169 vs, 1138 s, 1112 w, 1017 vs, 960 w, 922 m, 907 w, 855 m, 849 w, 821 w, 723 w, 672 w, 469 m.

Tris(*N*,*N*-dimethylaminodiboranato)(tetrahydrofuran)ytterbium(III), $Yb(H_3BNMe_2BH_3)_3(thf)$, (14a). This complex was prepared analogously to compound **1a** from $YbCl_3$ (0.55 g, 2.0 mmol) and sodium *N*,*N*-dimethylaminodiboranate (0.56 g, 5.9 mmol). The dull yellow residue was extracted with pentane (2 × 20 mL), the extracts were filtered and combined, and the dull yellow filtrate was concentrated to ca. 10 mL and cooled to -20 ˚C to yield dull yellow crystals. Yield: 0.43 g (47 %). M.p.: 85˚C (dec). Anal. Calcd

for $C_{10}H_{44}B_6N_3OYb$: C, 26.1; H, 9.63; N, 9.13. Found: C, 26.0; H, 10.10; N, 9.43. ^{1}H NMR (C_6D_6, 20 °C): δ -18.72 (br s, fwhm = 440 Hz, BH_3, 18H), -3.48 (s, fwhm = 140 Hz, β-CH_2, 4H), -0.26 (s, fwhm = 30 Hz, NMe_2, 18H), 1.15 (br s, fwhm = 370 Hz, OCH_2, 4H). ^{11}B NMR (C_6D_6, 20 °C): δ -47.4 (br s, fwhm = 150 Hz, BH_3). MS(FI) [fragment ion, relative abundance]: *m*/*z* 115 [H_2B-NMe_2-BH_2-NMe_2, 24], 316 [$Yb(H_3BNMe_2BH_3)_2^+$, 45], 376 [$Yb(H_3BNMe_2BH_3)_3 - BH_2$, 40], 388 [$Yb(H_3BNMe_2BH_3)_3^+$ / $Yb(H_3BNMe_2BH_3)_2(thf)^+$, 100], 704 [$Yb_2(H_3BNMe_2BH_3)_5^+$, 65]. IR ($cm^{-1}$): 2421 vs, 2397 vs, 2348 sh, 2282 m, 2226 vs, 2179 vs, 2063 sh, 1400 w, 1315 sh, 1289 s, 1240 s, 1217 s, 1187 sh, 1171 s, 1150 sh, 1136 s, 1110 w, 1019 vs, 960 w, 923 m, 905 w, 891 w, 857 m, 819 w, 770 w, 723 w, 674 w, 468 m.

Tris(*N*,*N*-dimethylaminodiboranato)(tetrahydrofuran)lutetium(III), $Lu(H_3BNMe_2BH_3)_3(thf)$, (15a). This complex was prepared analogously to compound **1a** from $LuCl_3$ (0.29 g, 1.0 mmol) and sodium *N*,*N*-dimethylaminodiboranate (0.30 g, 3.2 mmol). The white residue was extracted with pentane (3 × 15 mL), the extracts were filtered and combined, and the clear filtrate was concentrated to ca. 11 mL and cooled to -20 ˚C to yield 0.16 g of large, white crystals. The mother liquor was concentrated to 7 mL and cooled to -20 ˚C to yield an additional 0.07 g of white crystals. Yield: 0.23 g (50 %). M.p.: 99 - 101 ˚C. Anal. Calcd for $C_{10}H_{44}B_6N_3OLu$: C, 26.0; H, 9.59; N, 9.09. Found: C, 25.8; H, 9.59; N, 9.01. ^{1}H NMR (C_6D_6, 20 °C): δ 1.21 (m, β-CH_2, 4H), 2.24 (s, NMe_2, 18H), 3.05 (br 1:1:1:1 q, J_{BH} = 87 Hz, BH_3, 18H), 3.80 (m, OCH_2, 4H). ^{11}B NMR (C_6D_6, 20 °C): δ -6.43 (q, J_{BH} = 90 Hz, BH_3). MS(FI) [fragment ion, relative abundance]: *m*/*z* 319 [$Lu(H_3BNMe_2BH_3)_2^+$, 20], 377 [$Lu(H_3BNMe_2BH_3)_3 - BH_2$, 10], 389 [$Lu(H_3BNMe_2BH_3)_3^+$ / $Lu(H_3BNMe_2BH_3)_2(thf)^+$, 30], 709 [$Lu_2(H_3BNMe_2BH_3)_5^+$, 100]. IR ($cm^{-1}$): 2420 vs, 2395 sh, 2344 w, 2290 m, 2227 vs, 2183 vs, 2065 sh, 1401 w, 1312 sh, 1296 s, 1245 s, 1220 m, 1188

sh, 1173 vs, 1137 s, 1112 w, 1021 vs, 973 w, 926 m, 910 w, 888 w, 856 m, 843 sh, 821 w, 726 w, 675 w, 473 m.

Tris(*N*,*N*-dimethylaminodiboranato)yttrium(III), Y($H_3BNMe_2BH_3$)$_3$, (1b). YCl_3 (0.51 g, 2.6 mmol) and sodium *N*,*N*-dimethylaminodiboranate (0.75 g, 7.9 mmol) were added to a 100 mL Schlenk tube with 30 – 40 stainless steel balls (4.5 mm diameter). The flask was gently agitated by hand for 25 min and the powdery solid slowly became sticky. Sublimation at 85 – 90 ˚C and 10^{-2} Torr afforded white microcrystals. Yield: 0.41 g (52 %). M.p.: 158 ˚C (dec). Anal. Calcd for $C_6H_{36}B_6N_3Y$: C, 23.7; H, 11.9; N, 13.8. Found: C, 23.5; H, 12.4; N, 13.4. ^{1}H NMR (C_6D_6, 20 °C): δ 2.12 (s, NMe_2, 36H), 2.49 (br 1:1:1:1 q, J_{BH} = 89 Hz, BH_3, 36H). ^{11}B NMR (C_6D_6, 20 °C): δ -5.1 (br q, J_{BH} = 90 Hz, BH_3). MS(FI) [fragment ion, relative abundance]: *m*/*z* 233 [Y($H_3BNMe_2BH_3$)$_2^+$, 65], 303 [Y($H_3BNMe_2BH_3$)$_3^+$, 100], 537 [Y_2($H_3BNMe_2BH_3$)$_5^+$, 90]. IR (cm^{-1}): 2424 vs, 2336 m, 2273 m, 2220 s, 2166 s, 2058 sh, 1399 w, 1335 s, 1286 s, 1237 w, 1212 w, 1170 s, 1015 s, 969 m, 927 m, 902 m, 841 m, 814 s, 464 s.

Tris(*N*,*N*-dimethylaminodiboranato)lanthanum(III), La($H_3BNMe_2BH_3$)$_3$, (2b). This complex was prepared analogously to **1b** from $LaCl_3$ (0.51 g, 2.1 mmol) and sodium *N*,*N*-dimethylaminodiboranate (0.58 g, 6.1 mmol). Sublimation at 125 ˚C and 10^{-2} Torr afforded white microcrystals. Yield: 0.11 g (15 %). M.p.: 185 °C (dec). Anal. Calcd for $C_6H_{36}B_6N_3La$: C, 20.4; H, 10.3; N, 11.9. Found: C, 20.6; H, 10.3; N, 11.8. ^{1}H NMR (C_6D_6, 20 °C): δ 2.22 (s, fwhm = 40 Hz, NMe_2, 36H), 2.78 (br 1:1:1:1 q, J_{BH} = 110 Hz, BH_3, 36H). ^{11}B NMR (C_6D_6, 20 °C): δ -2.8 (br q, J_{BH} = 79 Hz, BH_3). MS(FI) [fragment ion, relative abundance]: *m*/*z* 227 [La($H_3BNMe_2BH_3$)(BH_4)$^+$, 5], 282 [La($H_3BNMe_2BH_3$)$_2^+$, 50], 353 [La($H_3BNMe_2BH_3$)$_3^+$, 80], 637 [La_2($H_3BNMe_2BH_3$)$_5^+$, 100], 935 [La_3($H_3BNMe_2BH_3$)$_7$(BH_4)$^+$, 5], 991 [La_3($H_3BNMe_2BH_3$)$_8^+$, 80]. IR (cm^{-1}): 2443 w, 2396 vs,

2333 m, 2279 m, 2205 vs, 2171 s, 2057 w, 1259 s, 1237 s, 1214 m, 1180 m, 1170 m, 1157 m, 1137 s, 1032 w, 1014 s, 929 m, 900 w, 809 w, 758 w, 722 w, 485 w, 444 m.

Tris(*N*,*N*-dimethylaminodiboranato)cerium(III), Ce($H_3BNMe_2BH_3$)$_3$, (3b). This complex was prepared analogously to **1b** from $CeCl_3$ (0.53 g, 2.2 mmol) and sodium *N*,*N*-dimethylaminodiboranate (0.66 g, 7.0 mmol). Sublimation at 110 ˚C and 10^{-2} Torr afforded white microcrystals. Yield: 0.25 g (33 %). M.p.: 183 ˚C (dec). Anal. Calcd for $C_6H_{36}B_6N_3Ce$: C, 20.3; H, 10.2; N, 11.8. Found: C, 20.6; H, 11.1; N, 11.7. ^{1}H NMR (C_6D_6, 20 °C): δ 4.23 (s, fwhm = 40 Hz, NMe_2, 36H), 26.4 (br s, fwhm = 330 Hz, BH_3, 36H). ^{11}B NMR (C_6D_6, 20 °C): δ 39.8 (s, fwhm = 190 Hz, BH_3). MS(FI) [fragment ion, relative abundance]: *m*/*z* 285 [Ce($H_3BNMe_2BH_3$)$_2^+$, 5], 356 [Ce($H_3BNMe_2BH_3$)$_3^+$, 100], 639 [Ce$_2$($H_3BNMe_2BH_3$)$_5^+$, 35], 995 [Ce$_3$($H_3BNMe_2BH_3$)$_8^+$, 5]. IR (cm^{-1}): 2445 w, 2396 vs, 2333 m, 2276 m, 2206 vs, 2173 s, 2059 w, 1261 s, 1236 s, 1214 m, 1180 m, 1168 m, 1156 m, 1136 s, 1032 w, 1014 s, 929 m, 900 w, 809 w, 758 w, 722 w, 487 w, 446 m.

Tris(*N*,*N*-dimethylaminodiboranato)praseodymium(III), Pr($H_3BNMe_2BH_3$)$_3$, (4b). Sublimation of **4a** (0.15 g, 0.35 mmol) at 100 - 105 ˚C and 10^{-2} Torr afforded pale green microcrystals. Yield: 0.11 g (85 %). M.p.: 185 ˚C (dec). Anal. Calcd for $C_6H_{36}B_6N_3Pr$: C, 20.2; H, 10.2; N, 11.8. Found: C, 19.7; H, 9.84; N, 11.7. ^{1}H NMR (C_6D_6, 20 °C): δ 5.13 (s, fwhm = 130 Hz, NMe_2, 36H), 68.41 (br s, fwhm = 500 Hz, BH_3, 36H). ^{11}B NMR (C_6D_6, 20 °C): δ 103.9 (s, fwhm = 350 Hz, BH_3). MS(FI) [fragment ion, relative abundance]: *m*/*z* 114 [(H_2BNMe_2)$_2$, 100], 228 [Pr($H_3BNMe_2BH_3$)(BH_4)$^+$, 25], 288 [Pr($H_3BNMe_2BH_3$)$_2^+$, 35], 343 [Pr($H_3BNMe_2BH_3$)$_3$ – BH_2, 85], 358 [Pr($H_3BNMe_2BH_3$)$_3^+$, 65], 402 [Pr($H_3BNMe_2BH_3$)$_3$(NMe_2H), 60], 642 [Pr$_2$($H_3BNMe_2BH_3$)$_5^+$, 35], 701 [Pr$_2$($H_3BNMe_2BH_3$)$_6$ – BH_2, 50], 999 [Pr$_3$($H_3BNMe_2BH_3$)$_8^+$, 10]. IR (cm^{-1}): 2440 w, 2394

vs, 2334 m, 2279 m, 2209 vs, 2168 s, 2059 w, 1262 s, 1236 s, 1214 m, 1182 m, 1168 m, 1157 m, 1136 s, 1032 w, 1015 s, 928 m, 900 w, 809 w, 758 w, 722 w, 485 w, 444 m.

Tris(*N*,*N*-dimethylaminodiboranato)neodymium(III), Nd($H_3BNMe_2BH_3$)$_3$, (5b). Sublimation of **5a** (0.11 g, 0.25 mmol) at 105 - 110 ˚C and 10^{-2} Torr afforded lavender microcrystals. Yield: 0.072 g (82 %). M.p.: 176˚C (dec). Anal. Calcd for $C_6H_{36}B_6N_3Nd$: C, 20.1; H, 10.1; N, 11.7. Found: C, 20.1; H, 10.3; N, 11.5. ^{1}H NMR (C_6D_6, 20 °C): δ 4.66 (s, fwhm = 230 Hz, NMe_2, 36H), 86.8 (br s, fwhm = 1400 Hz, BH_3, 36H). ^{11}B NMR (C_6D_6, 20 °C): δ 125.3 (s, fwhm = 1200 Hz, BH_3). MS(FI) [fragment ion, relative abundance]: *m*/*z* 232 [$Nd(H_3BNMe_2BH_3)(BH_4)^+$, 25], 285 [$Nd(H_3BNMe_2BH_3)_2^+$, 55], 345 [$Nd(H_3BNMe_2BH_3)_3 - BH_2$, 15], 356 [$Nd(H_3BNMe_2BH_3)_3^+$, 100], 648 [$Nd_2(H_3BNMe_2BH_3)_5^+$, 95], 1007 [$Nd_3(H_3BNMe_2BH_3)_8^+$, 10]. IR ($cm^{-1}$): 2412 vs, 2333 m, 2279 m, 2206 vs, 2165 s, 2140 sh, 2057 w, 1403 m, 1284 sh, 1267 s, 1237 s, 1232 m, 1219 m, 1183 m, 1162 s, 1127 s, 1031 w, 1017 s, 944 m, 932 m, 904 w, 812 m, 722 w, 458 m.

Tris(*N*,*N*-dimethylaminodiboranato)samarium(III), Sm($H_3BNMe_2BH_3$)$_3$, (6b). Sublimation of **6a** (0.12 g, 0.28 mmol) at 75 ˚C and 10^{-2} Torr afforded ivory microcrystals. Yield: 0.086 g (84 %). M.p.: 158˚C (dec). Anal. Calcd for $C_6H_{36}B_6N_3Sm$: C, 19.7; H, 9.93; N, 11.5. Found: C, 19.5; H, 10.2; N, 11.6. ^{1}H NMR (C_6D_6, 20 °C): δ 3.89 (s, fwhm = 16 Hz, NMe_2, 36H), -4.85 (br s, fwhm = 360 Hz, BH_3, 36H). ^{11}B NMR (C_6D_6, 20 °C): δ -10.8 (s, fwhm = 240 Hz, BH_3). MS(FI) [fragment ion, relative abundance]: *m*/*z* 238 [$Sm(H_3BNMe_2BH_3)(BH_4)^+$, 10], 296 [$Sm(H_3BNMe_2BH_3)_2^+$, 95], 367 [$Sm(H_3BNMe_2BH_3)_3^+$, 80], 660 [$Sm_2(H_3BNMe_2BH_3)_5^+$, 100], 1029 [$Sm_3(H_3BNMe_2BH_3)_8^+$, 10]. IR ($cm^{-1}$): 2412 vs, 2333 m, 2265 m, 2207 vs, 2167 s, 2147 sh, 2060 w, 1403 m, 1333 w, 1289 sh, 1270 s, 1237 s, 1232 m, 1217 m, 1186 m, 1162 s, 1127 s, 1032 w, 1017 s, 945 m, 932 m, 906 w, 812 m, 722 w, 705 w, 696 w, 464 m.

Tris(*N*,*N*-dimethylaminodiboranato)gadolinium(III), $Gd(H_3BNMe_2BH_3)_3$, (8b). Sublimation of **8a** (85 mg, 0.19 mmol) at 70 - 75 ˚C and 10^{-2} Torr afforded white microcrystals. Yield: 0.064 g (90 %). M.p.: 151˚C (dec). Anal. Calcd for $C_6H_{36}B_6N_3Gd$: C, 19.4; H, 9.74; N, 11.3. Found: C, 19.4; H, 9.83; N, 10.8. MS(FI) [fragment ion, relative abundance]: *m/z* 241 $[Gd(H_3BNMe_2BH_3)(BH_4)^+$, 10], 300 $[Gd(H_3BNMe_2BH_3)_2^+$, 100], 370 $[Gd(H_3BNMe_2BH_3)_3^+$, 90], 674 $[Gd_2(H_3BNMe_2BH_3)_5^+$, 95], 1042 $[Gd_3(H_3BNMe_2BH_3)_8^+$, 10]. IR (cm^{-1}): 2415 vs, 2334 m, 2285 m, 2269 m, 2217 vs, 2169 s, 2130 sh, 2059 w, 1430 w, 1401 m, 1323 w, 1279 s, 1238 s, 1218 m, 1185 m, 1164 s, 1157 s, 1133 m, 1032 w, 1019 s, 974 w, 945 m, 930 m, 904 w, 846 w, 815 w, 728 w, 699 w, 457 m.

Tris(*N*,*N*-dimethylaminodiboranato)terbium(III), $Tb(H_3BNMe_2BH_3)_3$, (9b). $TbCl_3$ (0.46 g, 1.7 mmol) and sodium *N*,*N*-dimethylaminodiboranate (0.49 g, 5.2 mmol) were added to a 100 mL round-bottom Schlenk flask with 30 – 40 steel balls (4.5-mm diameter). The flask was gently agitated by hand for 25 min. Sublimation at 90 - 100 °C and 10^{-2} Torr afforded white crystals. Yield: 0.23 g (36%). M.p.: 159˚C (dec) . Anal. Calcd for $C_6H_{36}N_3B_6Tb$: C, 19.3; H, 10.1; N, 11.2. Found: C, 19.6; H, 10.1; N, 11.2. ^1H NMR (C_6D_6, 20 (C): δ 118.8 (s, fwhm = 3300 Hz, NMe_2). ^{11}B NMR (C_6D_6, 20 °C): δ -343.8 (s, fwhm = 690 Hz, BH_3). MS (FI): *m/z* 246 $[Tb(H_3BNMe_2BH_3)(BH_4)^+$, 2], 303 $[Tb(H_3BNMe_2BH_3)_2^+$, 40], 373 $[Tb(H_3BNMe_2BH_3)_3^+$, 65], 620 $[Tb_2(H_3BNMe_2BH_3)_4(BH_4)^+$, 5], 677 $[Tb_2(H_3BNMe_2BH_3)_5^+$, 100], 1051 $[Tb_3(H_3BNMe_2BH_3)_8^+$, 4]. IR (cm^{-1}): 2420 vs, 2336 m, 2270 m, 2217 vs, 2169 s, 2129 sh, 2059 w, 1400 w, 1327 w, 1281 s, 1239 m, 1218 m, 1184 m, 1166 m, 1158 s, 1132 m, 1032 w, 1018 s, 975 w, 928 m, 904 w, 844 w, 815 w, 726 w, 459 m.

Tris(*N*,*N*-dimethylaminodiboranato)dysprosium(III), $Dy(H_3BNMe_2BH_3)_3$, (10b). $DyCl_3$ (0.48 g, 1.8 mmol) and sodium *N*,*N*-dimethylaminodiboranate (0.51 g, 5.4 mmol)

were transferred to a 100 mL round-bottom Schlenk flask, and 30 – 40 steel balls (4.5-mm diameter) were added. The flask was gently agitated by hand for 25 min. Sublimation at 90 – 95 °C and 10^{-2} Torr afforded white crystals. Yield: 0.20 g (30%). M.p.: 159 ˚C (dec). Anal. Calcd for $C_6H_{36}N_3B_6Dy$: C, 19.1; H, 9.61; N, 11.1. Found: C, 19.5; H, 10.1; N, 10.7. ^{1}H NMR (C_6D_6, 20 (C): δ 94.43 (s, fwhm = 550 Hz, NMe_2). ^{11}B NMR (C_6D_6, 20 °C): δ -269.1 (s, fwhm = 300 Hz, BH_3). MS(FI) [fragment ion, relative abundance]: *m/z* 377 [$Dy(H_3BNMe_2BH_3)_3^+$, 100], 684 [$Dy_2(H_3BNMe_2BH_3)_5^+$, 40]. IR (cm^{-1}): 2416 vs, 2334 m, 2272 m, 2216 s, 2170 s, 2061 w, 1282 vs, 1237 s, 1218 m, 1183 m, 1162 vs, 1130 m, 1031 w, 1020 s, 973 w, 925 m, 904 m, 844 w, 814 w, 463 s.

Tris(*N*,*N*-dimethylaminodiboranato)holmium(III), $Ho(H_3BNMe_2BH_3)_3$, (11b). $HoCl_3$ (0.49 g, 1.8 mmol) and sodium *N*,*N*-dimethylaminodiboranate (0.49 g, 5.2 mmol) were added to a 100 mL round-bottom Schlenk flask with 30 – 40 steel balls (4.5-mm diameter). The flask was gently agitated by hand for 25 min. Sublimation at 95 - 105 °C and 10^{-2} Torr afforded salmon-colored crystals. Yield: 0.23 g (35%). M.p.: 148˚C (dec). Anal. Calcd for $C_6H_{36}N_3B_6Ho$: C, 19.0; H, 9.54; N, 11.0. Found: C, 19.2; H, 9.68; N, 10.9. ^{1}H NMR (C_6D_6, 20 (C): δ 63.61 (s, fwhm = 390 Hz, NMe_2). ^{11}B NMR (C_6D_6, 20 °C): δ -216.5 (s, fwhm = 260 Hz, BH_3). MS(FI): *m/z* 115 [H_2B-NMe_2-BH_2-NMe_2H, 30], 251 [$Ho(H_3BNMe_2BH_3)(BH_4)^+$, 3], 309 [$Ho(H_3BNMe_2BH_3)_2^+$, 90], 367 [$Ho(H_3BNMe_2BH_3)_3$ – BH_2, 50], 379 [$Ho(H_3BNMe_2BH_3)_3^+$, 80], 423 [$Ho(H_3BNMe_2BH_2)_3(NMe_2)^+$, 20], 688 [$Ho_2(H_3BNMe_2BH_3)_5^+$, 100]. IR ($cm^{-1}$): 2419 vs, 2339 m, 2287 m, 2271 m, 2223 vs, 2169 s, 2132 sh, 2059 w, 1430 w, 1401 m, 1333 w, 1286 s, 1240 s, 1218 m, 1186 m, 1162 br s, 1144 m, 1132 m, 1032 w, 1019 s, 974 w, 945 m, 927 m, 905 w, 843 w, 816 w, 726 w, 697 w, 465 m.

Tris(*N*,*N*-dimethylaminodiboranato)erbium(III), Er($H_3BNMe_2BH_3$)$_3$, (12b). Sublimation of **12a** (2.51 g, 5.52 mmol) at 95 - 100 ˚C and 10^{-2} Torr afforded pink microcrystals. Yield: 2.03 g (96 %). M.p.: 148˚C (dec). Anal. Calcd for $C_6H_{36}B_6N_3Er$: C, 18.8; H, 9.49; N, 11.0. Found: C, 18.8; H, 9.67; N, 10.7. ^{1}H NMR (C_6D_6, 20 °C): δ -32.50 (s, fwhm = 150 Hz, NMe_2). ^{11}B NMR (C_6D_6, 20 °C): δ -324.4 (s, fwhm = 240 Hz, BH_3). MS(FI) [fragment ion, relative abundance]: *m*/*z* 381 [$Er(H_3BNMe_2BH_3)_3^+$, 100], 693 [$Er_2(H_3BNMe_2BH_3)_5^+$, 15]. IR (cm^{-1}): 2418 vs, 2336 m, 2271 m, 2223 vs, 2174 s, 2133 sh, 2058 w, 1429 w, 1400 m, 1334 w, 1288 s, 1240 s, 1218 m, 1186 m, 1159 br s, 1144 m, 1133 m, 1032 w, 1020 s, 974 w, 945 m, 928 m, 905 w, 844 w, 816 w, 727 w, 698 w, 468 m.

Tris(*N*,*N*-dimethylaminodiboranato)thulium(III), Tm($H_3BNMe_2BH_3$)$_3$, (13b). This complex was prepared analogously to **1b** from $TmCl_3$ (0.48 g, 1.7 mmol) and sodium *N*,*N*-dimethylaminodiboranate (0.50 g, 5.3 mmol). Sublimation at 85 – 95 ˚C and 10^{-2} Torr afforded white microcrystals. Yield: 0.35 g (52 %). M.p.: 153˚C (dec). Anal. Calcd for $C_6H_{36}B_6N_3Tm$: C, 18.8; H, 9.45; N, 10.9. Found: C, 18.7; H, 9.61; N, 10.9. ^{1}H NMR (C_6D_6, 20 °C): δ -116.02 (s, fwhm = 70 Hz, NMe_2). ^{11}B NMR (C_6D_6, 20 °C): δ -416.8 (s, fwhm = 180 Hz, BH_3). MS(FI) [fragment ion, relative abundance]: *m*/*z* 256 [$Tm(H_3BNMe_2BH_3)(BH_4)^+$, 4], 312 [$Tm(H_3BNMe_2BH_3)_2^+$, 45], 371 [$Tm(H_3BNMe_2BH_3)_3 - BH_2$, 35], 383 [$Tm(H_3BNMe_2BH_3)_3^+$, 100], 700 [$Tm_2(H_3BNMe_2BH_3)_5^+$, 85]. IR ($cm^{-1}$): 2420 vs, 2337 m, 2274 m, 2224 vs, 2174 s, 2137 sh, 2058 w, 1432 w, 1401 m, 1336 w, 1293 s, 1240 s, 1219 m, 1186 m, 1163 br s, 1144 m, 1132 m, 1089 w, 1032 w, 1019 s, 971 w, 928 m, 906 m, 842 w, 818 w, 726 w, 699 w, 469 m.

Tris(*N*,*N*-dimethylaminodiboranato)lutetium(III), Lu($H_3BNMe_2BH_3$)$_3$, (14b). Sublimation of **14a** (0.32 g, 0.69 mmol) at 65 – 75 ˚C and 10^{-2} Torr afforded white microcrystals. Yield: 0.26 g (96 %). M.p.: 147˚C (dec). Anal. Calcd for $C_6H_{36}B_6N_3Lu$: C,

18.5; H, 9.30; N, 10.8. Found: C, 18.2; H, 9.74; N, 10.4. ^{1}H NMR (C_6D_6, 20 °C): δ 2.10 (s, fwhm = 4 Hz, NMe_2), 3.19 (br 1:1:1:1 q, J_{BH} = 87 Hz, BH_3). ^{11}B NMR (C_6D_6, 20 °C): δ -6.27 (q, J_{BH} = 90 Hz, BH_3). MS(FI) [fragment ion, relative abundance]: *m*/*z* 261 [$Lu(H_3BNMe_2BH_3)(BH_4)^+$, 5], 318 [$Lu(H_3BNMe_2BH_3)_2^+$, 70], 377 [$Lu(H_3BNMe_2BH_3)_3 - BH_2$, 15], 390 [$Lu(H_3BNMe_2BH_3)_3^+$, 100], 709 [$Lu_2(H_3BNMe_2BH_3)_5^+$, 80]. IR ($cm^{-1}$): 2424 vs, 2341 m, 2274 m, 2228 vs, 2173 s, 2142 sh, 2060 w, 1433 w, 1401 w, 1342 w, 1298 s, 1241 m, 1220 m, 1188 m, 1164 s, 1143 m, 1133 m, 1032 sh, 1020 s, 972 w, 928 m, 907 w, 842 w, 820 w, 724 w, 472 m.

Tris(*N*,*N*-dimethylaminodiboranato)(1,2-dimethoxyethane)prasedymium(III), $Pr(H_3BNMe_2BH_3)_3(dme)$. To a solution of **4a** (0.24 g, 0.56 mmol) in pentane (15 mL) was added dme (3 mL, 30 mmol). A light green precipitate slowly formed. The mixture was stirred for 1 h, and then was filtered. The filtrate was discarded, and the solid was washed with cold pentane (3 x 15 mL) and dried under vacuum to yield a light green powder. Yield: 0.19 g (76%). M.p.: 122 °C (dec.). Anal. Calcd for $C_{10}H_{46}B_6N_3O_2Pr$: C, 26.9; H, 10.4; N, 9.42. Found: C, 26.9; H, 10.6; N, 9.09. ^{1}H NMR (C_6D_6, 20 °C): δ -2.62 (s, fwhm = 220 Hz, OCH_2, 4H), 3.45 (s, fwhm = 80 Hz, NMe_2, 18H), 6.50 (s, fwhm = 230 Hz, CH_3, 6H), 59.89 (br s, fwhm = 370 Hz, BH_3, 18H). ^{11}B NMR (C_6D_6, 20 °C): δ 73.2 (br s, fwhm = 200 Hz, BH_3). MS(FI) [fragment ion, relative abundance]: *m*/*z* 115 [H_2B-NMe_2-BH_2-NMe_2H, 100], 343 [$Pr(H_3BNMe_2BH_3)_3 - BH_2$, 40], 355 [$Pr(H_3BNMe_2BH_3)_3^+$, 70], 374 [$Pr(H_3BNMe_2BH_3)_2(dme)^+$, 50], 401 [$Pr(H_3BNMe_2BH_2)_3(NMe_2)^+$, 30]. IR ($cm^{-1}$): 2385 vs, 2346 m, 2333 sh, 2288 vs, 2227 vs, 1299 w, 1255 m, 1235 s, 1213 m, 1185 sh, 1167 s, 1140 s, 1129 sh, 1089 m, 1036 s, 1013 vs, 975 m, 926 m, 903 w, 857 s, 815 w, 448 w.

Crystallographic Studies. Single crystals of **2a**, **4b**, **6b**, and **12b**, grown by sublimation, were mounted on glass fibers with Paratone-N oil (Exxon) or Krytox oil

(Dupont) and immediately cooled to -80 °C in a cold nitrogen gas stream on the diffractometer. Single crystals of **5a**-**8a**, **12a**, and **16** were crystallized from pentane and treated similarly. Crystallographic studies of **1a**, **1b**, **10a**, and **10b** have been reported elsewhere.[94] Standard peak search and indexing procedures, followed by least-square refinement, yielded the cell dimensions given in Tables 4.2, 4.7, and 4.15. Data were collected with an area detector by using the measurement parameters listed in Tables 4.2, 4.7, and 4.15. For all crystals, the measured intensities were reduced to structure factor amplitudes, and their estimated standard deviations by correction for background and Lorentz and polarization effects. Although corrections for crystal decay were unnecessary, face-indexed absorption corrections were applied. Systematically absent reflections were deleted, and symmetry equivalent reflections were averaged to yield the set of unique data. Unless specified otherwise, all unique data were used in the least-squares refinement.

The structures were solved using direct methods (SHELXTL). The correct position of all the non-hydrogen atoms were deduced from *E*-maps and subsequent difference Fourier calculations. The analytical approximations to the scattering factors were used, and all structure factors were corrected for both real and imaginary components of anomalous dispersion. Unless otherwise stated, the refinement models had the following features: (1) Independent anisotropic displacement factors were refined for the non-hydrogen atoms. (2) Hydrogen atoms were placed in idealized positions with C-H = 0.99 and 0.98 Å for methylene and methyl hydrogen atoms, respectively, and with B-H = 1.15 Å for the boranyl hydrogen atoms. (3) The methyl and boranyl groups were allowed to rotate about the C-N and B-N bonds to find the best least-squares positions. (4) Methyl hydrogen atoms were given displacement parameters equal to 1.5 times U_{eq} for the attached carbon atom, whereas for the boranyl hydrogen atoms and methylene hydrogen atoms the multiplier was 1.2. For all

data sets, successful convergence was indicated by the maximum shift/error of <0.002 for the last cycle. Unless otherwise stated, a final analysis of variance between observed and calculated structure factors showed no apparent errors. Final refinement parameters are given in Tables 4.2, 4.7, and 4.15. Characteristics specific to the individual refinements are given in the following paragraphs.

2a: The reflections 011 and 013 were found to be statistical outliers and were not used in the least-squares refinement. The tetrahydrofuran molecule is disordered about a three-fold axis and its C-O and C-C bond distances were fixed at 1.48 ± 0.01 and 1.52 ± 0.01 Å, respectively. The hydrogen atoms on the disordered tetrahydrofuran molecule were not included in the model. An isotropic extinction parameter was refined to a final value of x = 1.36(3) × 10^{-6} where F_c is multiplied by the factor $k[1 + F_c^2 x\lambda^3/\sin 2\theta]^{-1/4}$ with k being the overall scale factor. Analysis of the diffraction intensities suggested slight inversion twinning; therefore, the intensities were calculated from the equation $I = vI_a + (1\text{-}v)I_b$, where v is a scale factor that relates the volumes of the inversion-related twin components. The scale factor refined to a value of 0.67(7). The largest peak in the final Fourier difference map (1.17 eÅ^{-3}) was located 1.12 Å from H2A.

5a: The reflection 200 was found to be a statistical outlier and was not used in the least-squares refinement. The C29 atom in the tetrahydrofuran ring of molecule 2 was disordered; to produce satisfactory ellipsoids, the atom was partitioned over two positions and the site occupancy factors of these positions were refined independently so that the sum of these SOF's was equal to one. The C-O and C-C bond distances of the tetrahydrofuran molecule were fixed at 1.48 ± 0.001 and 1.52 ± 0.001 Å, respectively. The largest peak in the final Fourier difference map (1.03 eÅ^{-3}) was located 0.79 Å from Nd1.

6a: The C29 atom in the tetrahydrofuran ring of molecule 2 was disordered, and it

was treated as described for compound **5a**. The largest peak in the final Fourier difference map (0.84 eÅ^{-3}) was located 0.85 Å from Sm1.

7a: The reflections 014, 413, and 403 were found to be statistical outliers and were not used in the least-squares refinement. The C28 atom in the tetrahydrofuran ring of molecule 2 was disordered; to produce satisfactory ellipsoids, the atom was partitioned over two positions and the site occupancy factors of these positions were refined independently so that the sum of these SOF's was equal to one. The largest peak in the final Fourier difference map (0.68 eÅ^{-3}) was located 1.02 Å from Eu2.

8a: The reflection 00-2 was found to be a statistical outlier and was not used in the least squares refinement. The C29 atom in the tetrahydrofuran ring of molecule 2 was disordered, and it was treated as described for compound **7a**. The largest peak in the final Fourier difference map (0.89 eÅ^{-3}) was located 1.10 Å from Gd2.

12a: The reflections 010, 110, and 11-2 were found to be statistical outliers and were not used in the least-squares refinement. The C29 atom in the tetrahydrofuran ring of molecule 2 was disordered, and it was treated as described for compound **7a**. The largest peak in the final Fourier difference map (0.87 eÅ^{-3}) was located 0.83 Å from Er2.

13a: The reflection 100 was found to be a statistical outlier and was not used in the least squares refinement. Hydrogen atoms attached to boron were located in the difference maps, and their positions were refined with independent isotropic displacement parameters. The chemically equivalent B-H distances were constrained to be equal within 0.01 Å. The largest peak in the final Fourier difference map (1.38 eÅ^{-3}) was located 0.83 Å from Tm1.

15a: The reflection 100 was found to be a statistical outlier and was not used in the least squares refinement. Hydrogen atoms attached to boron were located in the difference maps, and their positions were refined with independent isotropic displacement parameters.

The chemically equivalent B-H distances were constrained to be equal within 0.01 Å. The largest peak in the final Fourier difference map (0.83 eÅ^{-3}) was located 0.94 Å from Lu1.

4b: The boranyl hydrogen atoms were located in the difference maps, and their positions were refined with independent isotropic displacement parameters. The chemically equivalent B – H distances within the BH_3 groups were constrained to be equal within an esd of 0.01 Å. The largest peak in the final Fourier difference map (0.62 eÅ^{-3}) was located 0.90 Å from Pr1.

6b: An isotropic extinction parameter was refined to a final value of x = 7.3(5) × 10^{-6} where F_c is multiplied by the factor $k[1 + F_c^2 x\lambda^3/\sin 2\theta]^{-1/4}$ with k being the overall scale factor. The largest peak in the final Fourier difference map (1.77 eÅ^{-3}) was located 0.99 Å from Sm1.

12b: The orthorhombic lattice and systematic lattices 0kl ($k + l \neq 2n$) and h0l ($h \neq 2n$) were consistent with the space groups $Pna2_1$ and $Pnma$; the non-centrosymmetric space group $Pna2_1$ was shown to be the correct choice by successful refinement of the proposed model. The reflection 020 was obscured by the beamstop and was not used in the least-squares refinement.

After initial refinements, the weighted R-factor remained unacceptably high, two unusually large peaks remained in the difference map that appeared to be “ghosts” related to the two erbium atoms by the transformation (x + 0.33333, 0.5 – y, z). We concluded that the crystal was probably characterized by a kind of stacking fault. The molecules are lined up in columns along the x-axis, with their Er-Er vectors aligned this direction also, so that, part of the time, the molecules in one column could be displaced by a fractional cell distance along the x-axis and still pack well. A stacking fault model was constructed in which a second molecule was added that was related by the first by the transformation (x + 0.33333, 0.5 – y,

z). This second molecule was treated as a rigid group in which all the non-hydrogen atoms were assigned a common isotropic displacement parameter and a common partial site occupancy factor. The site occupancy factors for the major and minor locations were constrained to sum 1; the SOF for the major site refined to 0.931(1). Atoms B1, B12, and C7 were constrained to be near isotropic, and the displacement parameters of atoms bonded to one another were subjected to rigid bond constraints. The quantity minimized by the least-squares program was $\Sigma w(F_O^2 - F_C^2)^2$, where $w = \{[\sigma(F_O)]^2\}^{-1}$ and $P = (F_O^2 + 2F_C^2)/3$. Analysis of the diffraction intensities suggested slight inversion twinning; therefore, the intensities were calculated from the equation $I = xI_a + (1-x)I_b$, where x is a scale factor that relates the volumes of the inversion-related twin components. The scale factor refined to a value of 0.17(4). The largest peak in the final Fourier difference map (1.08 eÅ^{-3}) was located 1.18 Å from H21V.

References

1. Information contained in this chapter has been published previously and is reprinted with permission. See Daly, S. R.; Kim, D. Y.; Yang, Y.; Abelson, J. R.; Girolami, G. S. *J. Am. Chem. Soc.* **2010**, *132*, 2106-2107.

2. MacManus-Driscoll, J. L. *Adv. Mater.* **1997,** *9*, 457-473.

3. Etourneau, J. *J. Less-Common Met.* **1985,** *110*, 267-281.

4. Broers, A. N. *Rev Sci Instrum* **1969,** *40*, 1040-1045.

5. Mumaw, V. R.; Munger, B. L. *Proc. - Annu. Meet., Electron Microsc. Soc. Am.* **1977,** *35*, 64-65.

6. Joy, D. C.; Schmidt, P. H. Low work function hexaboride electron source. U.S. Patent 4,200,555, April 29, 1980.

7. Gasgnier, M. *J. Mater. Sci.* **1991,** *26*, 1989-1999.

8. Collocott, S. J.; Dunlop, J. B.; Lovatt, H. C.; Ramsden, V. S. *Mater. Sci. Forum* **1999,** *315-317*, 77-83.

9. Buenzli, J.-C. G.; Piguet, C. *Chem. Soc. Rev.* **2005,** *34*, 1048-1077.

10. Monocorgé, R. *Springer Ser. Mater. Sci.* **2005,** *83*, 320-378.

11. Srivastava, A. M. *Uses of phosphors in display technologies*. *Handbook of Luminescence, Display Materials, and Devices*, Nalwa, H. S.; Rohwer, L. S., American Scientific Publishers: Los Angeles, 2003; Vol. 3, pp 79-100.

12. Haerkoenen, G.; Leppaenen, M.; Soininen, E.; Toernqvist, R.; Viljanen, J. *J. Alloys Compd.* **1995,** *225*, 552-554.

13. Tiitta, M.; Niinistö, L. *Chem. Vap. Deposition* **1997,** *3*, 167-182.

14. Leskelä, M. *J. Alloys Compd.* **1998,** *275-277*, 702-708.

15. Bénalloul, P.; Barthou, C.; Benoit, J. *J. Alloys Compd.* **1998,** *275-277*, 709-714.

16. Tanabe, S. *Compt. Rend. Chim.* **2002,** *5*, 815-824.

17. Kido, J.; Okamoto, Y. *Chem. Rev.* **2002,** *102*, 2357-2368.

18. de Bettencourt-Dias, A. *Dalton Trans.* **2007**, 2229-2241.

19. Escribano, P.; Julian-Lopez, B.; Planelles-Arago, J.; Cordoncillo, E.; Viana, B.; Sanchez, C. *J. Mater. Chem.* **2008,** *18*, 23-40.

20. Carlos, L. D.; Ferreira, R. A. S.; de Zea Bermudez, V.; Ribeiro, S. J. L. *Adv. Mater.* **2009,** *21*, 509-534.

21. Scullin, M. L.; Yu, C.; Huijben, M.; Mukerjee, S.; Seidel, J.; Zhan, Q.; Moore, J.; Majumdar, A.; Ramesh, R. *Appl. Phys. Lett.* **2008,** *92*, 202113/1-202113/3.

22. The International Technology Roadmap for Semiconductors. http://public.itrs.net/ 2009.

23. Wilk, G. D.; Wallace, R. M.; Anthony, J. M. *J. Appl. Phys.* **2001,** *89*, 5243-5275.

24. Wallace, R. M.; Wilk, G. *Mat. Res. Soc. Bull.* **2002,** *27*, 192-197.

25. Robertson, J. *Eur. Phys. J.: Appl. Phys.* **2004,** *28*, 265-291.

26. Locquet, J.-P.; Marchiori, C.; Sousa, M.; Fompeyrine, J.; Seo, J. W. *J. Appl. Phys.* **2006,** *100*, 051610/1-051610/14.

27. Leskelae, M.; Kukli, K.; Ritala, M. *J. Alloys Compd.* **2006,** *418*, 27-34.

28. Jones, A. C.; Aspinall, H. C.; Chalker, P. R.; Potter, R. J.; Kukli, K.; Rahtu, A.; Ritala, M.; Leskelä, M. *Mater. Sci. Eng., B* **2005,** *B118*, 97-104.

29. Yanguas-Gil, A.; Yang, Y.; Kumar, N.; Abelson, J. R. *J. Vac. Sci. Technol., A* **2009,** *27*, 1235-1243.

30. George, S. M. *Chem. Rev.* **2010,** *110*, 111-131.

31. Aspinall, H. C. *Top. Appl. Phys.* **2007,** *106*, 53-72.

32. Bradley, D. C.; Ghotra, J. S.; Hart, F. A. *J. Chem. Soc., Dalton Trans.* **1973**, 1021-1023.

33. Kukli, K.; Ritala, M.; Pilvi, T.; Sajavaara, T.; Leskelä, M.; Jones, A. C.; Aspinall, H. C.; Gilmer, D. C.; Tobin, P. J. *Chem. Mater.* **2004,** *16*, 5162-5168.

34. Triyoso, D. H.; Hegde, R. I.; Grant, J. M.; Schaeffer, J. K.; Roan, D.; White, B. E., Jr.; Tobin, P. J. *J. Vac. Sci. Technol., B* **2005,** *23*, 288-297.

35. Kukli, K.; Ritala, M.; Pore, V.; Leskela, M.; Sajavaara, T.; Hegde, R. I.; Gilmer, D. C.; Tobin, P. J.; Jones, A. C.; Aspinall, H. C. *Chem. Vap. Deposition* **2006,** *12*, 158-164.

36. Scarel, G.; Wiemer, C.; Tallarida, G.; Spiga, S.; Seguini, G.; Bonera, E.; Fanciulli, M.; Lebedinskii, Y.; Zenkevich, A.; Pavia, G.; Fedushkin, I. L.; Fukin, G. K.; Domrachev, G. A. *J. Electrochem. Soc.* **2006,** *153*, F271-F276.

37. Leskela, M.; Niinisto, L.; Nykanen, E.; Soininen, P.; Tiitta, M. *Thermochim. Acta* **1991,** *175*, 91-98.

38. Putkonen, M.; Sajavaara, T.; Johansson, L.-S.; Nunistö, L. *Chem. Vap. Deposition* **2001,** *7*, 44-50.

39. Päiväsaari, J.; Putkonen, M.; Sajavaara, T.; Niinistö, L. *J. Alloys Compd.* **2004,** *374*, 124-128.

40. Niinistoe, J.; Petrova, N.; Putkonen, M.; Niinistoe, L.; Arstila, K.; Sajavaara, T. *J. Cryst. Growth* **2005,** *285*, 191-200.

41. Paeivaesaari, J.; Putkonen, M.; Niinistoe, L. *Thin Solid Films* **2005,** *472*, 275-281.

42. Frohlich, K.; Luptak, R.; Dobrocka, E.; Husekova, K.; Cico, K.; Rosova, A.; Lukosius, M.; Abrutis, A.; Pisecny, P.; Espinos, J. P. *Mater. Sci. Semicond. Process.* **2007,** *9*, 1065-1072.

43. Wilkinson, G.; Birmingham, J. M. *J. Am. Chem. Soc.* **1954,** *76*, 6210.

44. Birmingham, J. M.; Wilkinson, G. *J. Am. Chem. Soc.* **1956,** *78*, 42-44.

45. Niinistoe, J.; Putkonen, M.; Niinistoe, L. *Chem. Mater.* **2004,** *16*, 2953-2958.

46. Scarel, G.; Bonera, E.; Wiemer, C.; Tallarida, G.; Spiga, S.; Fanciulli, M.; Fedushkin, I. L.; Schumann, H.; Lebedinskii, Y.; Zenkevich, A. *Appl. Phys. Lett.* **2004,** *85*, 630-632.

47. Malvestuto, M.; Scarel, G.; Wiemer, C.; Fanciulli, M.; D'Acapito, F.; Boscherini, F. *Nucl. Instrum. Methods Phys. Res., Sect. B* **2006,** *246*, 90-95.

48. Losurdo, M.; Giangregorio, M. M.; Bruno, G.; Yang, D.; Irene, E. A.; Suvorova, A. A.; Saunders, M. *Appl. Phys. Lett.* **2007,** *91*, 091914/1-091914/3.

49. Lim, B. S.; Rahtu, A.; de Rouffignac, P.; Gordon, R. G. *Appl. Phys. Lett.* **2004,** *84*, 3957-3959.

50. Päiväsaari, J.; Dezelah, C. L. I. V.; Back, D.; El-Kaderi, H. M.; Heeg, M. J.; Putkonen, M.; Niinistö, L.; Winter, C. H. *J. Mater. Chem.* **2005,** *15*, 4224-4233.

51. Kwon, J.; Dai, M.; Halls, M. D.; Langereis, E.; Chabal, Y. J.; Gordon, R. G. *J. Phys. Chem. C* **2008,** *113*, 654-660.

52. Milanov, A. P.; Fischer, R. A.; Devi, A. *Inorg. Chem.* **2008,** *47*, 11405-11416.

53. Belot, J. A.; Wang, A.; McNeely, R. J.; Liable-Sands, L.; Rheingold, A. L.; Marks, T. J. *Chem. Vap. Deposition* **1999,** *5*, 65-69.

54. Edleman, N. L.; Wang, A.; Belot, J. A.; Metz, A. W.; Babcock, J. R.; Kawaoka, A. M.; Ni, J.; Metz, M. V.; Flaschenriem, C. J.; Stern, C. L.; Liable-Sands, L. M.; Rheingold, A. L.; Markworth, P. R.; Chang, R. P. H.; Chudzik, M. P.; Kannewurf, C. R.; Marks, T. J. *Inorg. Chem.* **2002,** *41*, 5005-5023.

55. Herrmann, W. A.; Anwander, R.; Denk, M. *Chem. Ber.* **1992,** *125*, 2399-2405.

56. Aspinall, H. C.; Gaskell, J.; Williams, P. A.; Jones, A. C.; Chalker, P. R.; Marshall, P. A.; Bickley, J. F.; Smith, L. M.; Critchlow, G. W. *Chem. Vap. Deposition* **2003,** *9*, 235-238.

57. Aspinall, H. C.; Gaskell, J.; Williams, P. A.; Jones, A. C.; Chalker, P. R.; Marshall, P. A.; Smith, L. M.; Critchlow, G. W. *Chem. Vap. Deposition* **2004,** *10*, 13-17.

58. Aspinall, H. C.; Gaskell, J.; Williams, P. A.; Jones, A. C.; Chalker, P. R.; Marshall, P. A.; Smith, L. M.; Critchlow, G. W. *Chem. Vap. Deposition* **2004,** *10*, 83-89.

59. Aspinall, H. C.; Gaskell, J. M.; Loo, Y. F.; Jones, A. C.; Chalker, P. R.; Potter, R. J.; Smith, L. M.; Critchlow, G. W. *Chem. Vap. Deposition* **2004,** *10*, 301-305.

60. Loo, Y. F.; Potter, R. J.; Jones, A. C.; Aspinall, H. C.; Gaskell, J. M.; Chalker, P. R.; Smith, L. M.; Critchlow, G. W. *Chem. Vap. Deposition* **2004,** *10*, 306-310.

61. Potter, R. J.; Chalker, P. R.; Manning, T. D.; Aspinall, H. C.; Loo, Y. F.; Jones, A. C.; Smith, L. M.; Critchlow, G. W.; Schumacher, M. *Chem. Vap. Deposition* **2005,** *11*, 159-169.

62. Aspinall, H. C.; Bickley, J. F.; Gaskell, J. M.; Jones, A. C.; Labat, G.; Chalker, P. R.; Williams, P. A. *Inorg. Chem.* **2007,** *46*, 5852-5860.

63. Deacon, G. B.; MacKinnon, P.; Dickson, R. S.; Pain, G. N.; West, B. O. *Appl. Organomet. Chem.* **1990,** *4*, 439-449.

64. Gun'ko, Y. K.; Edelmann, F. T. *Comments Inorg. Chem.* **1997,** *19*, 153-184.

65. Jones, A. C.; Aspinall, H. C.; Chalker, P. R.; Potter, R. J.; Kukli, K.; Rahtu, A.; Ritala, M.; Leskelä, M. *J. Mater. Chem.* **2004,** *14*, 3101-3112.

66. Niinistoe, L.; Paeivaesaari, J.; Niinistoe, J.; Putkonen, M.; Nieminen, M. *Phys. Status Solidi A* **2004,** *201*, 1443-1452.

67. Jones, A. C.; Aspinall, H. C.; Chalker, P. R.; Potter, R. J.; Manning, T. D.; Loo, Y. F.; O'Kane, R.; Gaskell, J. M.; Smith, L. M. *Chem. Vap. Deposition* **2006,** *12*, 83-98.

68. Lo Nigro, R.; Malandrino, G.; Toro, R. G.; Fragalà, I. L. *Chem. Vap. Deposition* **2006,** *12*, 109-124.

69. Malandrino, G.; Fragalà, I. L. *Coord. Chem. Rev.* **2006,** *250*, 1605-1620.

70. Päiväsaari, J.; Niinistö, J.; Myllymäki, P.; Dezelah, C. I. V.; Winter, C. H.; Putkonen, M.; Nieminen, M.; Niinistö, L. *Top. Appl. Phys.* **2007,** *106*, 15-32.

71. Jensen, J. A.; Gozum, J. E.; Pollina, D. M.; Girolami, G. S. *J. Am. Chem. Soc.* **1988,** *110*, 1643-1644.

72. Kumar, N.; Yang, Y.; Noh, W.; Girolami, G. S.; Abelson, J. R. *Chem. Mater.* **2007,** *19*, 3802-3807.

73. Kumar, N.; Yanguas-Gil, A.; Daly, S. R.; Girolami, G. S.; Abelson, J. R. *J. Am. Chem. Soc.* **2008,** *130*, 17660-17661.

74. Sung, J.; Goedde, D. M.; Girolami, G. S.; Abelson, J. R. *J. Appl. Phys.* **2002,** *91*, 3904-3911.

75. Jayaraman, S.; Yang, Y.; Kim, D. Y.; Girolami, G. S.; Abelson, J. R. *J. Vac. Sci. Technol., A* **2005,** *23*, 1619-1625.

76. Jayaraman, S.; Gerbi, J. E.; Yang, Y.; Kim, D. Y.; Chatterjee, A.; Bellon, P.; Girolami, G. S.; Chevalier, J. P.; Abelson, J. R. *Surf. Coat. Technol.* **2006,** *200*, 6629-6633.

77. Yang, Y.; Jayaraman, S.; Kim, D. Y.; Girolami, G. S.; Abelson, J. R. *Chem. Mater.* **2006,** *18*, 5088-5096.

78. Yang, Y.; Jayaraman, S.; Kim, D. Y.; Girolami, G. S.; Abelson, J. R. *J. Cryst. Growth* **2006,** *294*, 389-395.

79. Yang, Y.; Jayaraman, S.; Sperling, B.; Kim, D. Y.; Girolami, G. S.; Abelson, J. R. *J. Vac. Sci. Technol., A* **2007,** *25*, 200-206.

80. Goedde, D. M.; Girolami, G. S. *J. Am. Chem. Soc.* **2004,** *126*, 12230-12231.

81. Jayaraman, S.; Klein, E. J.; Yang, Y.; Kim, D. Y.; Girolami, G. S.; Abelson, J. R. *J. Vac. Sci. Technol., A* **2005,** *23*, 631-633.

82. Goedde, D. M.; Windler, G. K.; Girolami, G. S. *Inorg. Chem.* **2007,** *46*, 2814-2823.

83. Makhaev, V. D.; Borisov, A. P.; Semenenko, K. N. *Russ. J. Inorg. Chem.* **1986,** *31*, 908-910.

84. Zange, E. *Chem. Ber.* **1960,** *93*, 652-657.

85. Mirsaidov, U.; Shaimuradov, I. B.; Khikmatov, M. *Russ. J. Inorg. Chem.* **1986,** *31*, 753-754.

86. Shaimuradov, I. B.; Badalov, A. B.; Marufi, V. I.; Mirsaidov, U. *Russ. J. Inorg. Chem.* **1991,** *36*, 773.

87. Lobkovskii, É. B.; Kravchenko, S. E.; Kravchenko, O. V. *J. Struct. Chem. USSR* **1983,** *23*, 582-586.

88. Shinomoto, R.; Zalkin, A.; Edelstein, N. M. *Inorg. Chim. Acta* **1987,** *139*, 97-101.

89. Mirsaidov, U.; Rotenberg, T. G.; Dymova, T. N. *Dokl. Akad. Nauk Tadzh. SSR* **1976,** *19*, 30-33.Chem. Abstr. 85:136374.

90. White, J. P., III; Deng, H.; Shore, S. G. *Inorg. Chem.* **1991,** *30*, 2337-2342.

91. Daly, S. R.; Girolami, G. S. *Chem. Commun.* **2010,** *46*, 407-408.

92. Keller, P. C. *Inorg. Chem.* **1971,** *10*, 2256-2259.

93. Nöth, H.; Thomas, S. *Eur. J. Inorg. Chem.* **1999**, 1373-1379.

94. Kim, D. Y. Part 1. Synthesis of metal hydroborates as potential chemical vapor deposition. Part 2. Chemical vapor deposition of titanium-doped magnesium diboraide thin films. Ph.D. Thesis, University of Illinois at Urbana-Champaign, 2007.

95. Kim, D. Y.; Girolami, G. S. *Inorg. Chem.* **2010**, manuscript in press.

96. Daly, S. R.; Piccoli, P. M. B.; Schultz, A. J.; Todorova, T. K.; Gagliardi, L.; Girolami, G. *Angew. Chem. Int. Ed.* **2010**, DOI: 10.1002/anie.200905797.

97. Marks, T. J.; Kolb, J. R. *Chem. Rev.* **1977,** *77*, 263-293.

98. Ephritikhine, M. *Chem. Rev.* **1997,** *97*, 2193-2242.

99. Makhaev, V. D. *Russ. Chem. Rev.* **2000,** *69*, 727-746.

100. Kumar, N.; Yanguas-Gil, A.; Daly, S. R.; Girolami, G. S.; Abelson, J. R. *Appl. Phys. Lett.* **2009,** *95*, 144107/1-144107/3.

101. See Kepert, D. L. *Inorganic Stereochemistry* (Inorganic Chemistry Concepts, Vol. 6), Springer-Verlag, Berlin, 1982, section 11 C.

102. Daly, S. R.; Girolami, G. S. *Inorg. Chem.* **2010**, manuscript in press.

103. Clark, R. J. H.; Lewis, J.; Machin, D. J.; Nyholm, R. S. *J. Chem. Soc.* **1963**, 379-387.

104. Deacon, G. B.; Evans, D. J.; Junk, P. C. *Z. Anorg. Allg. Chem.* **2002,** *628*, 2033-2036.

105. Shannon, R. D. *Acta Crystallogr., Sect. A* **1976,** *A32*, 751-767.

106. Makhaev, V. D.; Borisov, A. P. *Russ. J. Inorg. Chem.* **1999,** *44*, 1411-1413.

107. Daly, S. R.; Girolami, G. S. *Inorg. Chem.* **2010**, manuscript in press.

108. Deng, D.; Zheng, X.; Qian, C.; Sun, J.; Zhang, L. *J. Organomet. Chem.* **1994,** *466*, 95-100.

109. Neculai, D.; Roesky, H. W.; Neculai, A. M.; Magull, J.; Schmidt, H.-G.; Noltemeyer, M. *J. Organomet. Chem.* **2002,** *643-644*, 47-52.

110. Schumann, H.; Keitsch, M. R.; Muhle, S. H. *Acta Crystallogr., Sect. C: Cryst. Struct. Commun.* **2000,** *C56*, 48-49.

111. Barbier-Baudry, D.; Blacque, O.; Hafid, A.; Nyassi, A.; Sitzmann, H.; Visseaux, M. *Eur. J. Inorg. Chem.* **2000**, 2333-2336.

112. Trifonov, A. A.; Skvortsov, G. G.; Lyubov, D. M.; Fukin, G. K.; Fedorova, E. A.; Bochkarev, M. N. *Russ. Chem. Bull.* **2005,** *54*, 2511-2518.

113. Skvortsov, G. G.; Yakovenko, M. V.; Fukin, G. K.; Cherkasov, A. V.; Trifonov, A. A. *Russ. Chem. Bull.* **2007,** *56*, 1742-1748.

114. Bonnet, F.; Visseaux, M.; Hafid, A.; Baudry-Barbier, D.; Kubicki, M. M.; Vigier, E. *Inorg. Chem. Commun.* **2007,** *10*, 690-694.

115. Lobkovskii, É. B. *J. Struct. Chem. USSR* **1983,** *24*, 224-230.

116. Segal, B. G.; Lippard, S. J. *Inorg. Chem.* **1978,** *17*, 844-850.

117. Schumann, H.; Keitsch, M. R.; Demtschuk, J.; Muehle, S. *Z. Anorg. Allg. Chem.* **1998,** *624*, 1811-1818.

118. Qian, C.-T.; Zou, G.; Nie, W.-L.; Sun, J.; Lemenovskii, D. A.; Borzov, M. V. *Polyhedron* **2000,** *19*, 1955-1959.

119. Wang, H.; Wang, H.; Li, H.-W.; Xie, Z. *Organometallics* **2004,** *23*, 875-885.

120. Robert, D.; Kondracka, M.; Okuda, J. *Dalton Trans.* **2008**, 2667-2669.

121. Yuan, F.; Yang, J.; Xiong, L. *J. Organomet. Chem.* **2006,** *691*, 2534-2539.

122. Yuan, F.; Zhu, Y.; Xiong, L. *J. Organomet. Chem.* **2006,** *691*, 3377-3382.

123. Peters, J. A.; Huskens, J.; Raber, D. J. *Prog. Nucl. Magn. Reson. Spectrosc.* **1996,** *28*, 283-350.

124. Bertini, I.; Turano, P.; Vila, A. J. *Chem. Rev.* **1993,** *93*, 2833-2932.

125. Bleaney, B. *J. Magn. Resonance* **1972,** *8*, 91-100.

126. Golding, R. M.; Halton, M. P. *Aust. J. Chem.* **1972,** *25*, 2577-2581.

127. Golding, R. M.; Pyykko, P. *Mol. Phys.* **1973,** *26*, 1389-1396.

128. Pinkerton, A. A.; Rossier, M.; Spiliadis, S. *J. Magn. Reson.* **1985,** *64*, 420-425.

129. Reilley, C. N.; Good, B. W.; Allendoerfer, R. D. *Anal. Chem.* **1976,** *48*, 1446-1458.

130. Elgavish, G. A.; Reuben, J. *J. Am. Chem. Soc.* **1977,** *99*, 5590-5591.

131. Reuben, J.; Elgavish, G. A. *J. Magn. Reson.* **1980,** *39*, 421-430.

132. Lanthanum was used to determine LIS values for the larger paramagnetic lanthanides Ce - Sm and lutetium was used to determine the LIS values for the smaller lanthanides Tb - Yb. The data for the samarium complex was excluded from the LIS plots using eq (3) and (4) because it yielded poor linear regressions. Poor fits in LIS plots have been previously attributed to samarium complexes due to its very small <Sz> value (0.06). See Ren, J.; Zhang, S.; Sherry, A. D.; Geraldes, C. F. G. C. *Inorg. Chim. Acta* **2002**, *339*, 273-282. .

133. Reuben, J. *J. Magn. Reson.* **1982,** *50*, 233-236.

134. Geraldes, C. F. G. C.; Sherry, A. D.; Kiefer, G. E. *J. Magn. Reson.* **1992,** *97*, 290-304.

135. Marques, M. P. M.; Geraldes, C. F. G. C.; Sherry, A. D.; Merbach, A. E.; Powell, H.; Pubanz, D.; Aime, S.; Botta, M. *J. Alloys Compd.* **1995,** *225*, 303-307.

136. Forsberg, J. H.; Delaney, R. M.; Zhao, Q.; Harakas, G.; Chandran, R. *Inorg. Chem.* **1995,** *34*, 3705-3715.

137. Ren, J.; Zhang, S.; Sherry, A. D.; Geraldes, C. F. G. C. *Inorg. Chim. Acta* **2002,** *339*, 273-282.

138. Bag, P.; Floerke, U.; Nag, K. *Dalton Trans.* **2006**, 3236-3248.

139. Ren, J.; Sherry, A. D. *J. Magn. Reson., Ser. B* **1996,** *111*, 178-182.

140. Bernstein, E. R.; Hamilton, W. C.; Keiderling, T. A.; La Placa, S. J.; Lippard, S. J.; Mayerle, J. J. *Inorg. Chem.* **1972,** *11*, 3009-3016.

141. Haaland, A.; Shorokhov, D. J.; Tutukin, A. V.; Volden, H. V.; Swang, O.; McGrady, G. S.; Kaltsoyannis, N.; Downs, A. J.; Tang, C. Y.; Turner, J. F. C. *Inorg. Chem.* **2002,** *41*, 6646-6655.

142. Phillips, W. D.; Miller, H. C.; Muetterties, E. L. *J. Am. Chem. Soc.* **1959,** *81*, 4496-4500.

143. Aspinall, H. C.; Black, J.; Dodd, I.; Harding, M. M.; Winkley, S. J. *J. Chem. Soc., Dalton Trans.* **1993**, 709-714.

144. Thompson, M. K.; Lough, A. J.; White, A. J. P.; Williams, D. J.; Kahwa, I. A. *Inorg. Chem.* **2003,** *42*, 4828-4841.

145. Lama, M.; Mamula, O.; Kottas, G. S.; Rizzo, F.; De Cola, L.; Nakamura, A.; Kuroda, R.; Stoeckli-Evans, H. *Chem.--Eur. J.* **2007,** *13*, 7358-7373.

146. Daly, S. R.; Kim, D. Y.; Yang, Y.; Abelson, J. R.; Girolami, G. S. *J. Am. Chem. Soc.* **2010,** *132*, 2106-2107.

CHAPTER 5. Synthesis and Characterization of Divalent Europium and Ytterbium *N*,*N*-Dimethylaminodiboranates

Introduction

Although the +3 oxidation state dominates the solution chemistry of the lanthanide elements, it has been known since 1906 that some of the lanthanides also have accessible divalent oxidation states.[1] In recent years, there has been a remarkable expansion in the availability of lanthanide dihalide starting materials;[2-6] as a result, divalent complexes are now known for many of the lanthanides.[7-11] In addition, divalent species such as SmI_2 find use in organic syntheses as powerful one-electron reductants; for example, they are widely used to promote the coupling of alkyl halides with ketones to form tertiary alcohols.[12-18]

The +2 oxidation state of lanthanides can be accessed either by oxidation of the bulk metal or by reduction of trivalent lanthanide species. The reduction of Ln^{3+} to Ln^{2+} can be accomplished by comproprotionation reactions involving Ln^0 metal; alternatively, such reductions can be achieved by addition of an alkali metal.[19, 20] There are also a few examples in which the reduction of Ln^{3+} to Ln^{2+} is effected by a reagent that serves both as a reductant and as a ligand for the metal center; this approach invariably involves the most easily reduced lanthanides Eu, Yb, and Sm.[21] For example, reactions of Eu^{III} halides with bulky cyclopentadienide anions or of Eu^{III} metallocene halides with alkyllithium reagents can afford organometallic compounds of Eu^{II}.[22-25] The Yb^{III} complex $[(C_5H_4Me)_2YbMe]_2$ slowly reduces to the corresponding $(C_5H_4Me)_2Yb$ complex upon being heated to 80 °C or photolyzed in toluene.[26] The reactions of $Ln[N(SiMe_3)_2]_3(\mu\text{-}Cl)Li(thf)_3$, where Ln = Eu or Yb, with indenes or fluorenes bearing pendant amine or ether functional groups yield the corresponding Ln^{II} metallocenes.[27-37] Similarly, treatment of the substituted benzyl complex

$Sm(CH_2C_6H_4\text{-}2\text{-}NMe_2)_3$ with the bulky cyclopentadiene $C_5(C_6H_4\text{-}4\text{-}n\text{-}Bu)_5H$ ($Cp^{BIG}H$) at 60 °C yields the Sm^{II} product $Sm(Cp^{BIG})_2$.[38]

A closely related phenomenon is sterically-induced reduction,[9-11, 39, 40] which is characteristic of tris(pentamethylcyclopentadienyl) complexes $Ln(C_5Me_5)_3$. The C_5Me_5 ligand is not usually redox active, but the $Ln(C_5Me_5)_3$ complexes are sufficiently crowded that there is a strong driving force to eliminate one of the rings. As a result, these complexes react with various substrates to give products that appear to have been generated via the divalent intermediate $Ln(C_5Me_5)_2$.[41-45]

All of the above reactions involve organic ligands, but there are other chemical groups that can also serve as both a reductant and as a ligand. Prominent among these is tetrahydroborate, BH_4^-, a ligand known for its reducing power.[46, 47] For example, treatment of most lanthanide trichlorides with BH_4^- in tetrahydrofuran at room temperature affords trivalent borohydride complexes, but $EuCl_3$ is reduced to Eu^{II}.[48] The Ln^{II} complexes $Ln(BH_4)_2(thf)_2$, where Ln = Eu, Yb, and Sm, have been prepared by decomposing $NaLn(BH_4)_4(dme)_4$ at 150 – 200 °C under dynamic vacuum.[49]

Most divalent lanthanide borohydride complexes, however, are synthesized from divalent starting materials. For example, the pyridine and acetonitrile complexes $Ln(BH_4)_2(py)_4$ and $Ln(BH_4)_2(MeCN)_4$ have been prepared by treating $EuCl_2$ and $YbCl_2$ with $NaBH_4$.[50] Similar reactions afford Eu^{II} and Yb^{II} complexes of the organohydroborate $H_2BC_8H_{14}^-$ (9-BBN)[51, 52] In addition, the heteroleptic ytterbium pyrazolylborate ($Tp^{tBu,Me}$)Yb(BH_4) has been prepared by metathesis from ($Tp^{tBu,Me}$)YbI(thf), and also by addition of $BH_3{\cdot}NMe_3$ to the ytterbium hydride $[(Tb^{tBu,Me})YbH]_2$.[53] Finally, one divalent lanthanide tetrahydroborate has been prepared by oxidation of the metal: the reaction of ytterbium amalgam with $BH_3{\cdot}$thf affords a mixture of $Yb(BH_4)_2$ and $Yb(B_3H_8)_2$.[54]

We have previously shown that *N*,*N*-dimethylaminodiboranate (DMADB)[55-57] can be used to prepare trivalent lanthanide complexes that are highly volatile and are useful as CVD and ALD precursors to lanthanide-containing thin films.[58] We now describe the synthesis, characterization, and molecular structures of divalent lanthanide *N*,*N*-dimethylaminodiboranates. In several of these reactions, the DMADB ligand serves simultaneously as a ligand and as a reductant.

Results and Discussion

Synthesis of $Ln(H_3BNMe_2BH_3)_2(thf)_2$ and $Ln(H_3BNMe_2BH_3)_2(dme)_x$, where Ln = Eu and Yb. Treatment of the trichlorides $EuCl_3$ or $YbCl_3$ with $Na(H_3BNMe_2BH_3)$ in thf results in reduction to the corresponding divalent europium and ytterbium *N*,*N*-dimethylaminodiboranate complexes $Eu(H_3BNMe_2BH_3)_2(thf)_2$ (**1**) and $Yb(H_3BNMe_2BH_3)_2(thf)_2$ (**2**). The products can be isolated from the reaction residues by extraction and crystallization from pentane:

$$LnCl_3 + 3\ Na(H_3BNMe_2BH_3) \xrightarrow{thf} Ln(H_3BNMe_2BH_3)_2(thf)_2 + {}^1/_2\ H_2 + (NMe_2)B_2H_5 + 3\ NaCl$$

Ln = Eu (**1**), Yb (**2**)

The reactions of $EuCl_3$ and $YbCl_3$ with $Na(H_3BNMe_2BH_3)$ are not quantitative, but instead both produce a mixture of these divalent products and the corresponding trivalent species $Ln(H_3BNMe_2BH_3)_3(thf)$, which we have described in Chapter 4. The relative amounts of divalent and trivalent products generated depend on the temperature during the reaction. Specifically, addition of $Na(H_3BNMe_2BH_3)$ to $EuCl_3$ at -78 °C yields the Eu^{III} complex as the major product, whereas the same addition carried out at 0 °C largely yields the Eu^{II} complex. A similar trend is seen for Yb, except that the reaction temperatures are

higher: 0 °C generates more of the Yb^{III} product whereas 25 °C generates more of the Yb^{II} complex. The trivalent and divalent complexes can be easily distinguished by their colors. The Eu^{2+} complex **1** is off-white whereas its Eu^{3+} analog is yellow; for ytterbium, the colors are reversed: the Yb^{2+} complex **2** is intensely yellow whereas the Yb^{3+} analog is pale yellow (Figure 5.1). Both the trivalent and divalent lanthanide species co-crystallize out of pentane, but such mixtures are predominately observed in the second and third crops. The mixtures of crystals can be manually separated based on the difference in color, and these separated crystals were determined to be analytically pure by microanalysis.

The formation of a mixture of products can be avoided by employing the divalent lanthanide iodides EuI_2 and YbI_2 as starting materials. Treatment of these salts with $Na(H_3BNMe_2BH_3)$ affords **1** and **2** in 53 – 74 % yields; analogous reactions using the divalent chlorides $LnCl_2$ are unsuccessful.

$$LnI_2 + 2\ Na(H_3BNMe_2BH_3) \xrightarrow{thf} Ln(H_3BNMe_2BH_3)_2(thf)_2 + 2\ NaI$$
$$Ln = Eu\ (\mathbf{1}),\ Yb\ (\mathbf{2})$$

The tetrahydrofuran molecules in **1** and **2** can be readily displaced by treatment with an excess of 1,2-dimethoxyethane (dme) in pentane to afford the new species $Eu(H_3BNMe_2BH_3)_2(dme)_2$, (**3**) and $Yb(H_3BNMe_2BH_3)_2(dme)$, (**4**). The different numbers of coordinated dme molecules in the two compounds are consistent with the larger size of Eu^{II} vs. Yb^{II} (see below).

$$Ln(H_3BNMe_2BH_3)_2(thf)_2 + xs\ DME \xrightarrow{pentane} Ln(H_3BNMe_2BH_3)_2(dme)_x + 2\ thf$$
$$Ln = Eu\ (\mathbf{3};\ x = 2),\ Yb\ (\mathbf{4},\ x = 1)$$

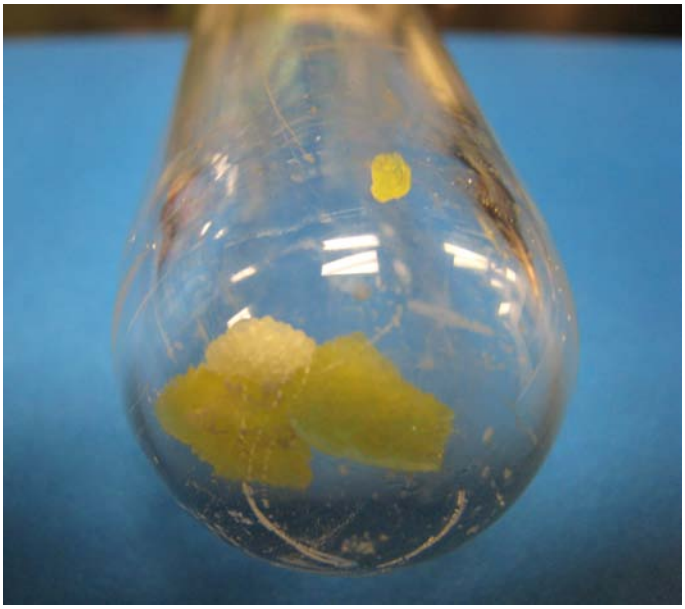

Figure 5.1. Second crystallization crop from the reaction of $EuCl_3$ and $Na(H_3BNMe_2BH_3)$ at -78 °C. Both off-white $Eu(H_3BNMe_2BH_3)_2(thf)_2$ (**1**) and yellow $Eu(H_3BNMe_2BH_3)_3(thf)$ are present

Unlike the trivalent $Ln(H_3BNMe_2BH_3)_3(thf)$ complexes, which lose thf under vacuum to form highly volatile, base-free $Ln(H_3BNMe_2BH_3)_3$ complexes,[58] the divalent lanthanide DMADB complexes do not show any appreciable volatility except for **4**, which sublimes at 65 – 75 °C at 10^{-2} Torr in low yield (10 %). The low sublimation yields for **1**-**4** suggest that these complexes readily desolvate when heated under vacuum, as is seen for the trivalent analogs. For the present molecules, however, the two remaining DMADB ligands are too small to saturate the coordination spheres of Eu^{II} or Yb^{II} to yield a volatile base-free species.

Crystal Structures. Although the thf adducts **1** and **2** have the same stoichiometry, their solid state structures differ. The Eu compound **1** is dinuclear: each metal center is bound to two chelating DMADB ligands, one of which also bridges to the other metal (Figure 5.2). Overall, the coordination geometry about each each Eu atom can be described as a distorted pentagonal bipyramid, in which five boron atoms from the DMADB ligands occupy the equatorial sites and two thf molecules occupy the axial sites. The B-Eu-O angles are all close to 90°, ranging from 82.5(1)° to 96.2(1)°, and the O1-Eu1-O2 angle deviates slightly from linearity at 167.91(6)° (Table 5.2).

The Eu···B distances to the non-bridging boron atoms B1, B2, and B3 are 2.885(4), 3.127(4), and 2.991(4) Å, respectively. These distances are slightly longer than those of 2.794(6) to 2.920(7) Å observed for the κ^2H borohydride groups in $Eu(H_2BC_8H_{14})_2(thf)_4$ and similar complexes.[51, 52] The refined least-squares positions for the calculated hydrogen atom locations in **1** show that two hydrogen atoms bridge the Eu···B1 and Eu···B3 contacts, with Eu-H hydrogen distances of 2.44 to 2.68 Å. The longer Eu···B2 contact is also best thought of as involving a κ^2H interaction, although one of the Eu-H distances is rather long at 2.83 Å. Boron atom B4 both chelates to Eu(1) and bridges to Eu(1)′ but does so unsymmetrically: the Eu(1)···B(4) distance is 3.215(6) Å whereas the Eu(1)′···B(4) distance is 2.975(4) Å. The

Table 5.1. Crystallographic data for **1**, **2**, and **3** at 193 K.

	1	**2**	**3**
formula	$C_{24}H_{80}B_8N_4O_4Eu_2$	$C_{12}H_{40}B_4N_2O_2Yb$	$C_{12}H_{44}B_4N_2O_4Eu$
FW (g mol^{-1})	879.32	460.74	475.69
λ (Å)	0.71073	0.71073	0.71073
crystal system	monoclinic	monoclinic	monoclinic
space group	$P2_1/c$	$P2_1/n$	$P2_1/n$
a (Å)	10.2155(2)	9.3382(10)	10.4304(11)
b (Å)	20.5596(5)	21.0643(3)	14.3523(15)
c (Å)	10.4732(3)	11.3500(13)	16.6107(18)
β (deg)	90.5740(10)	94.452(2)	103.552(6)
V (Å^3)	2199.54(9)	2225.8(4)	2417.4(4)
Z	2	4	4
ρ_{calc} (g cm^{-3})	1.328	1.375	1.307
μ (mm^{-1})	2.854	4.204	2.608
R(int)	0.0723	0.1040	0.0869
absorption correction	face-indexed	face-indexed	face-indexed
max. min. transm. factors	0.734, 0.594	0.166, 0.028	0.792, 0.544
data/restraints/parameters	4865 / 34 / 306	5780 / 68 / 242	5347 / 34 / 264
goodness-of-fit on F^2	0.999	1.005	0.961
*R*1 [$I > 2\sigma(I)$][a]	0.0285	0.0377	0.0227
*wR*2 (all data)[b]	0.0766	0.1036	0.0548

[a] $R_1 = \sum |F_o| - |F_c| \, | \, / \, | \sum |F_o|$ for reflections with $F_o^2 > 2\,\sigma(F_o^2)$.

[b] $wR_2 = [\sum w(F_o^2 - F_c^2)^2 \, / \, \sum (F_o^2)^2]^{1/2}$ for all reflections.

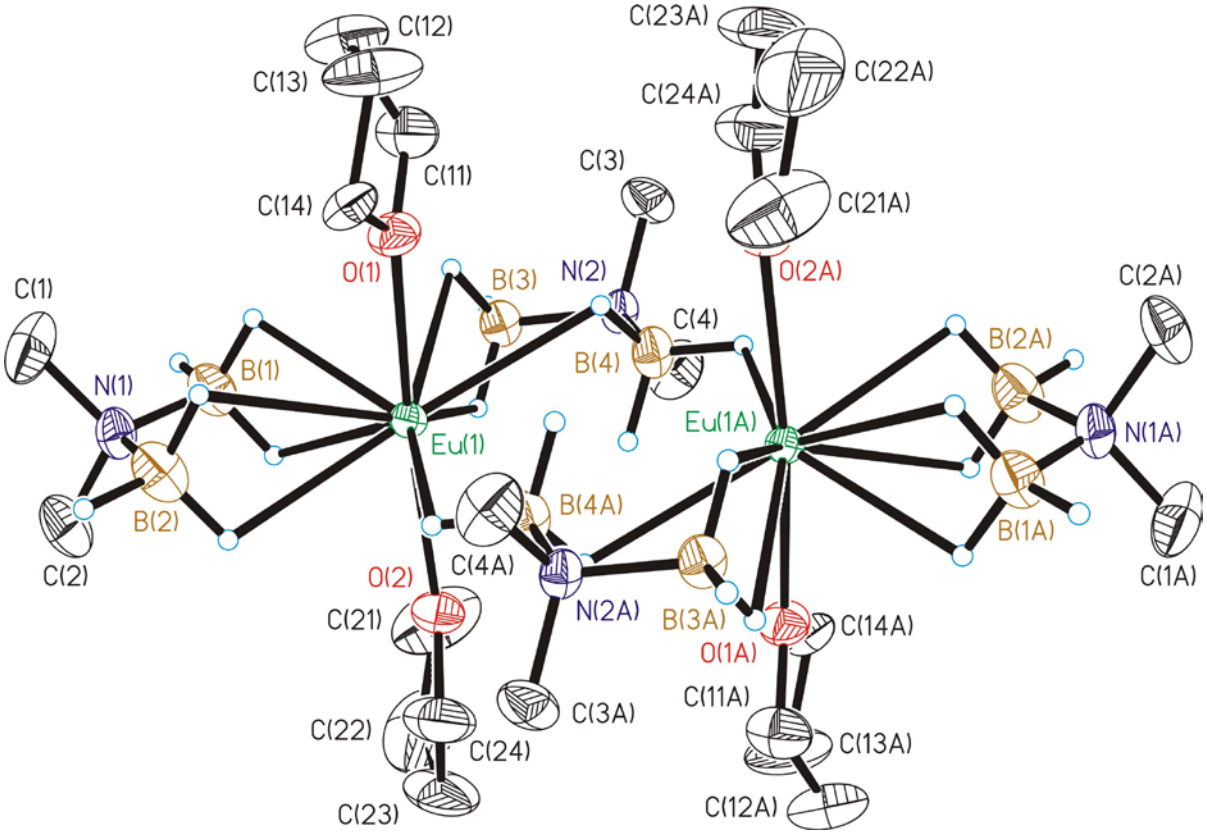

Figure 5.2. Molecular structure of $Eu(H_3BNMe_2BH_3)_2(thf)_2$, **1**. Ellipsoids are drawn at the 35% probability level. Hydrogen atoms attached to carbon and disordered components have been deleted for clarity.

Table 5.2. Selected Bond Lengths and Angles for $Eu(H_3BNMe_2BH_3)_2(thf)_2$, (**1**).

Bond Lengths (Å)			
Eu(1)-O(1)	2.5820(19)	Eu(1)-B(3)	2.991(4)
Eu(1)-O(2)	2.605(2)	Eu(1)-B(4)	3.215(6)
Eu(1)-B(1)	2.885(4)	Eu(1)-B(4)'	2.975(4)
Eu(1)-B(2)	3.127(4)	Eu(1)–Eu(1)′	4.741(4) Å
Bond Angles (deg)			
O(1)-Eu(1)-O(2)	167.91(6)	B(1)-Eu(1)-B(3)	82.86(10)
O(1)-Eu(1)-B(1)	96.13(10)	B(1)-Eu(1)-B(4)	132.05(10)
O(1)-Eu(1)-B(2)	87.36(9)	B(1)-Eu(1)-B(4)'	147.84(13)
O(1)-Eu(1)-B(3)	96.23(11)	B(3)-Eu(1)-B(2)	133.91(10)
O(1)-Eu(1)-B(4)	86.95(12)	B(2)-Eu(1)-B(4)	173.81(13)
O(1)-Eu(1)-B(4)'	85.42(13)	B(2)-Eu(1)-B(4)'	97.04(13)
O(2)-Eu(1)-B(1)	93.53(10)	B(3)-Eu(1)-B(4)	49.33(11)
O(2)-Eu(1)-B(2)	93.09(10)	B(3)-Eu(1)-B(4)'	129.03(14)
O(2)-Eu(1)-B(3)	92.16(11)	B(4)-Eu(1)-B(4)'	80.09(13)
O(2)-Eu(1)-B(4)	91.97(12)	B(2)-N(1)-B(1)	110.9(2)
O(2)-Eu(1)-B(4)'	82.53(13)	B(3)-N(2)-B(4)	111.6(4)
B(1)-Eu(1)-B(2)	51.13(9)		

Symmetry transformation used to generate equiv atoms: -*x*+1, -*y*+1, -*z*.

refined least-squares positions for the hydrogens attached to B(4) suggest that only one hydrogen atom bridges to each of the metals, as shown in Figure 5.2. The Eu–O distances to the coordinated thf atoms are 2.582(2) and 2.605(2) Å, which closely match the Eu–O distances reported for $Eu(H_2BC_8H_{14})_2(thf)_4$, which range from of 2.591(4) to 2.635(5) Å. The Eu(1)–Eu(1)′ distance of 4.741(4) Å is far too long to suggest any metal-metal bonding.

We note in passing that the Eu atoms and the bridging DMADB ligands in **1** are each disordered over two sites in the solid state. The two sites are related by a pseudo two-fold axis that runs the length of the molecule and passes approximately through the nitrogen atoms of the two terminal aminodiboranate ligands (Figure 5.3). The occupancy factor for the major site refined to 69 %. The disorder adds to the uncertainty in the hydrogen atom locations, which are already uncertain owing to their small scattering factors.

Unlike **1**, the ytterbium thf complex **2** is monomeric (Figure 5.4); this structural difference is certainly attributable to the larger ionic radius of Eu^{II} (r_{ionic} = 1.17 Å) vs. Yb^{II} (1.02 Å).[59] The arrangement of the boron and oxygen atoms in **2** is best described as a distorted *cis* octahedron, because there are exactly three large interligand angles: B1-Yb1-B3 = 163.4(2)°, O2-Yb1-B4 = 140.5(2)°, and O1-Yb1-B2 = 134.2(1) (Table 5.3). The Yb···B distances range from 2.809(5) to 2.856(5) Å and the Yb-O distances to the coordinated thf molecules are 2.397(3) and 2.416(3) Å. These distances are slightly shorter than those observed for $Yb(H_2BC_8H_{14})_2(thf)_4$, which are 2.876(7) Å (Yb-B) and 2.424(11) and 2.462(6) Å (Yb-O).[51] All of the BH_3 groups are bound to the Yb center by means of two hydrogen bridges; as expected, the κ^2*H* Yb-B distances in **2** are much longer than those observed for κ^3*H* tetrahydroborate groups bound to Yb^{II}, which range from 2.596(5) to 2.692(4) Å.[53, 54] The Yb-H distances range from 2.35(3) to 2.54(3) Å and are consistent with those previously observed.[52-54]

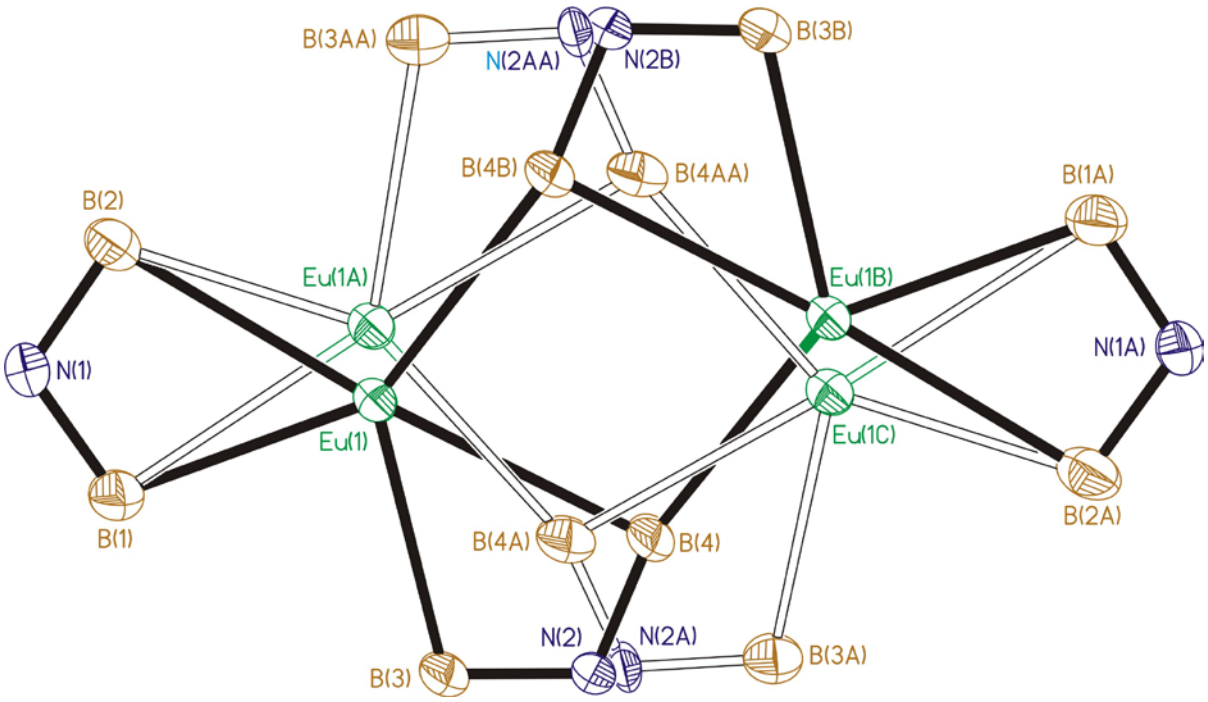

Figure 5.3. Single-crystal XRD disorder model for $Eu(H_3BNMe_2BH_3)_2(thf)_2$, **1**. Ellipsoids are drawn at the 35% probability level. Methyl groups, thf molecules, and hydrogen atoms have been removed for clarity.

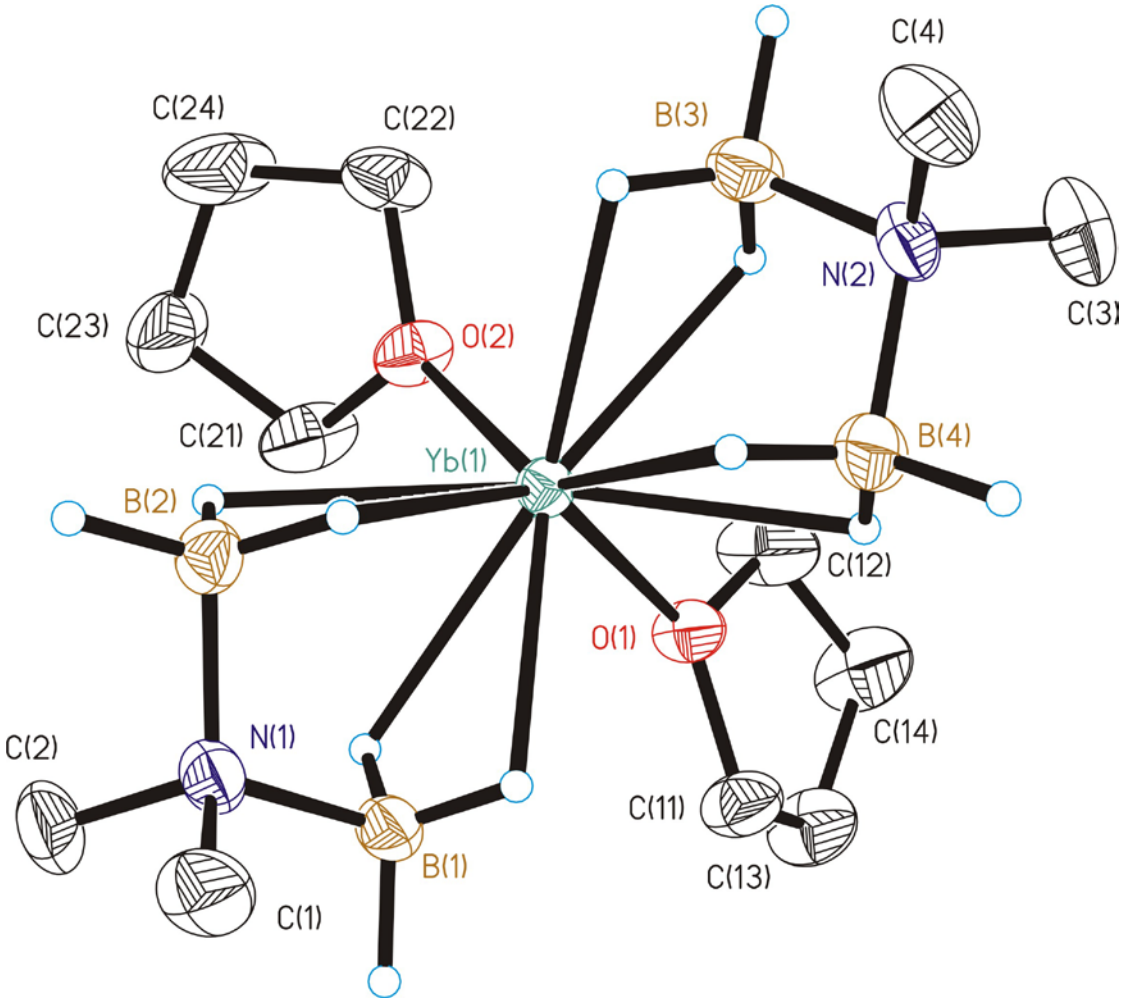

Figure 5.4. Molecular structure of $Yb(H_3BNMe_2BH_3)_2(thf)_2$, **2**. Ellipsoids are drawn at the 35% probability level. Hydrogen atoms attached to carbon have been deleted for clarity.

Table 5.3. Selected Bond Lengths and Angles for $Yb(H_3BNMe_2BH_3)_2(thf)_2$, (**2**).

Bond Lengths (Å)			
Yb(1)-O(2)	2.397(3)	Yb(1)-H(12)	2.35(3)
Yb(1)-O(1)	2.416(3)	Yb(1)-H(21)	2.43(3)
Yb(1)-B(1)	2.809(5)	Yb(1)-H(22)	2.53(3)
Yb(1)-B(3)	2.809(5)	Yb(1)-H(31)	2.44(4)
Yb(1)-B(2)	2.849(5)	Yb(1)-H(32)	2.43(4)
Yb(1)-B(4)	2.856(5)	Yb(1)-H(41)	2.54(3)
Yb(1)-H(11)	2.53(3)	Yb(1)-H(42)	2.45(4)
Bond Angles (deg)			
O(1)-Yb(1)-B(1)	81.98(13)	B(1)-Yb(1)-B(2)	55.34(15)
O(1)-Yb(1)-B(2)	134.17(13)	B(1)-Yb(1)-B(3)	163.39(16)
O(1)-Yb(1)-B(3)	104.25(14)	B(1)-Yb(1)-B(4)	109.65(17)
O(1)-Yb(1)-B(4)	95.20(16)	B(2)-Yb(1)-B(3)	121.43(16)
O(2)-Yb(1)-O(1)	81.40(12)	B(2)-Yb(1)-B(4)	113.03(18)
O(2)-Yb(1)-B(1)	108.78(14)	B(3)-Yb(1)-B(4)	54.96(17)
O(2)-Yb(1)-B(2)	96.09(14)	B(1)-N(1)-B(2)	111.1(4)
O(2)-Yb(1)-B(3)	87.52(14)	B(4)-N(2)-B(3)	111.1(3)
O(2)-Yb(1)-B(4)	140.50(15)		

The europium dme complex **3** is monomeric; both DMADB ligands and both dme molecules chelate to the metal center (Figure 5.5). The four boron atoms and the four oxygen atoms describe a distorted square antiprism, in which the oxygen atoms occupy one square face and the boron atoms occupy the other. The Eu···B distances of 3.040(4) to 3.115(4) Å are similar to those observed in the thf complex **1** (Table 5.4). In contrast, the four Eu-O distances of 2.579(2) to 2.701(2) Å are longer than those observed in **1**, which suggests that **3** is sterically crowded. The BH_3 hydrogen atoms were located in the difference maps and could be refined with light constraints; all the BH_3 groups are bound to metal in a κ^2*H* fashion, with Eu-H distances that range from 2.55(3) to 2.77(3) Å. The Eu···B, Eu-O, and Eu-H distances are all significantly longer than those in $Eu(H_2BC_8H_{14})_2(thf)_4$,[51] which is consistent with the conclusion that **3** is somewhat sterically crowded.

Crystals of the Yb dme complex **4** suitable for diffraction studies could not be obtained.

NMR, IR, and Field Ionization Mass Spectra. Complexes **1** and **3** contain the highly paramagnetic f^7 Eu^{II} ion and are NMR-silent; this finding is consistent with the observation that the Gd^{III} DMADB complex $Gd(H_3BNMe_2BH_3)_3(thf)$, which also contains an f^7 ion, is NMR silent as well.[60] In contrast, complexes **2** and **4** contain the diamagnetic f^{14} Yb^{II} ion and their ^1H and ^{11}B NMR resonances are readily observable. The ^1H NMR spectrum of **2** contains singlets at δ 2.45 for the NMe_2 protons and at δ 3.61 and 1.30 for the α and β thf protons, respectively. These chemical shifts closely match those of δ 2.24, 3.80, and 1.21 observed for the corresponding f^{14} $Lu(H_3BNMe_2BH_3)_3(thf)$ complex.[60] A broad 1:1:1:1 quartet at δ 2.63 is assignable to the BH_3 group; the coupling constant to the ^{11}B nucleus (I = 3/2) is 86 Hz. A similar quartet is present at δ 3.05 in the ^1H NMR spectrum of $Lu(H_3BNMe_2BH_3)_3(thf)$. Evidently, exchange of the terminal and briding B-H groups within

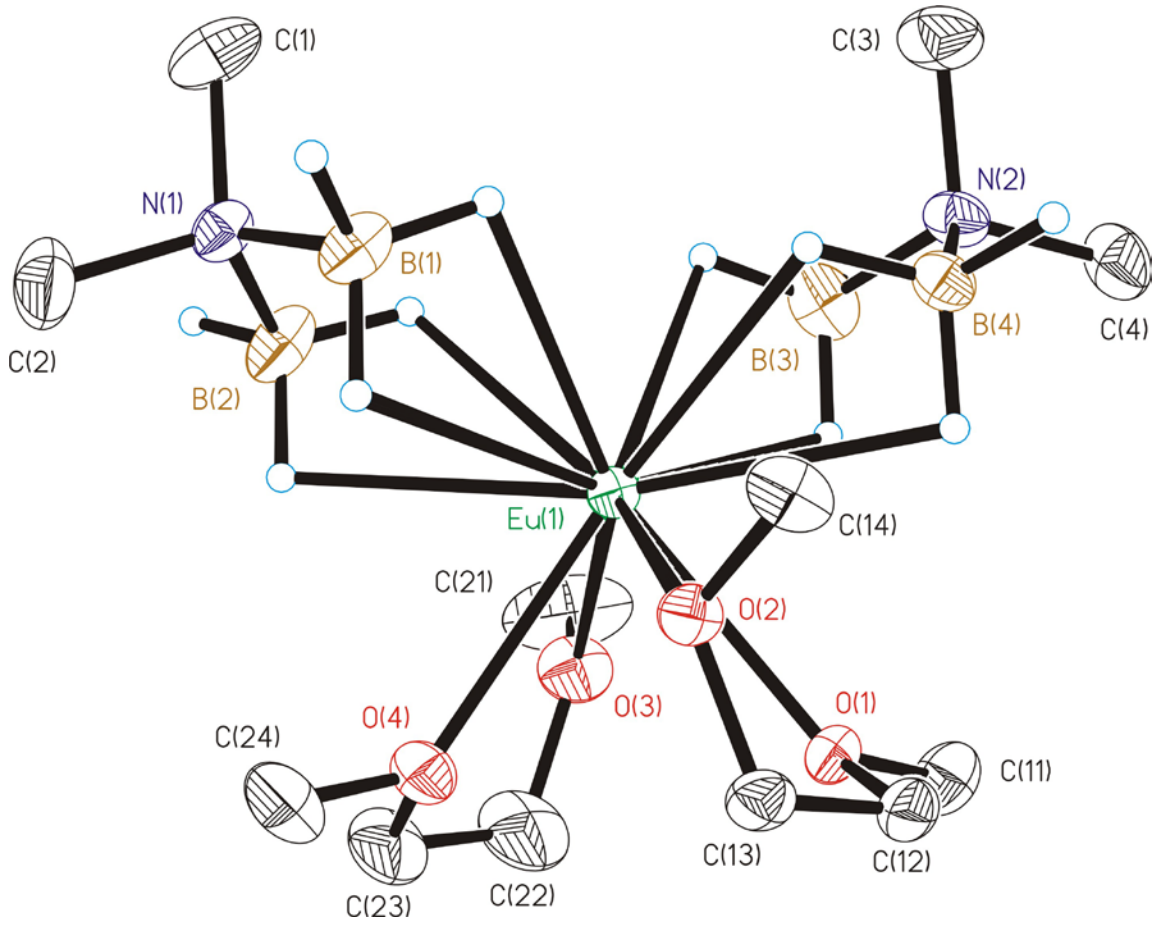

Figure 5.5. Molecular structure of $Eu(H_3BNMe_2BH_3)_2(dme)_2$, **3**. Ellipsoids are drawn at the 35% probability level. Hydrogen atoms attached to carbon have been deleted for clarity.

Table 5.4. Selected Bond Lengths and Angles for $Eu(H_3BNMe_2BH_3)_2(dme)_2$, (**3**).

Bond Lengths (Å)			
Eu(1)-O(3)	2.5786(19)	Eu(1)-H(11)	2.70(3)
Eu(1)-O(2)	2.6089(16)	Eu(1)-H(12)	2.65(3)
Eu(1)-O(4)	2.6705(18)	Eu(1)-H(21)	2.58(3)
Eu(1)-O(1)	2.7008(16)	Eu(1)-H(22)	2.75(3)
Eu(1)-B(3)	3.040(4)	Eu(1)-H(31)	2.55(3)
Eu(1)-B(1)	3.070(3)	Eu(1)-H(32)	2.60(3)
Eu(1)-B(4)	3.109(3)	Eu(1)-H(41)	2.57(2)
Eu(1)-B(2)	3.115(3)	Eu(1)-H(42)	2.77(3)
Bond Angles (deg)			
O(2)-Eu(1)-O(1)	63.70(5)	O(3)-Eu(1)-B(2)	83.74(8)
O(3)-Eu(1)-O(1)	71.07(6)	O(3)-Eu(1)-B(3)	84.03(9)
O(4)-Eu(1)-O(1)	73.92(6)	O(3)-Eu(1)-B(4)	125.06(8)
O(3)-Eu(1)-O(2)	124.34(6)	O(4)-Eu(1)-B(1)	94.49(8)
O(2)-Eu(1)-O(4)	74.17(5)	O(4)-Eu(1)-B(2)	82.42(9)
O(3)-Eu(1)-O(4)	63.23(7)	O(4)-Eu(1)-B(3)	147.12(8)
O(1)-Eu(1)-B(1)	146.78(7)	O(4)-Eu(1)-B(4)	150.19(7)
O(1)-Eu(1)-B(2)	151.15(8)	B(1)-Eu(1)-B(2)	49.77(8)
O(1)-Eu(1)-B(3)	93.54(9)	B(3)-Eu(1)-B(1)	110.72(11)
O(1)-Eu(1)-B(4)	82.15(7)	B(1)-Eu(1)-B(4)	96.00(9)
O(2)-Eu(1)-B(1)	83.29(7)	B(3)-Eu(1)-B(2)	97.68(12)
O(2)-Eu(1)-B(2)	125.34(8)	B(4)-Eu(1)-B(2)	125.02(10)
O(2)-Eu(1)-B(3)	127.87(8)	B(3)-Eu(1)-B(4)	50.08(9)
O(2)-Eu(1)-B(4)	79.45(7)	B(1)-N(1)-B(2)	110.6(2)
O(3)-Eu(1)-B(1)	131.81(8)	B(4)-N(2)-B(3)	110.5(2)

each BH_3 unit is rapid on the NMR time scale, as is observed for most metal-bound borohydride species.[61] The ^{11}B NMR spectrum of **2** consists of a 1:3:3:1 quartet at δ -7.7 due to coupling of the ^{11}B spin to the three hydrogen atoms; these values again are similar to those observed for $Lu(H_3BNMe_2BH_3)_3(thf)$.[60]

The ^{1}H and ^{11}B NMR spectra of $Yb(H_3BNMe_2BH_3)_2(dme)$, **4**, are also readily observable. The ^{1}H NMR spectrum contains a singlet for the NMe_2 group at δ 2.50 and broad quartet for the BH_3 groups at δ 2.76, and dme resonances at δ 2.88 (CH_2) and 2.98 (OMe). Integration of the ^{1}H NMR resonances confirms the stochiometry determined from the microanalytical data. The ^{11}B NMR spectrum consists of a 1:3:3:1 quartet at δ -7.6.

The IR spectra of the thf complexes **1** and **2** both exhibit characteristic peaks between 2500 and 2000 cm^{-1} due to B-H stretches, but the two spectra are very different. The spectrum of **1** has two strong, broad peaks at 2299 and 2249 cm^{-1} whereas that of **2** has four strong, well-defined peaks at 2357, 2303, 2271, and 2227 cm^{-1}. The high energy peak at 2357 cm^{-1} seen for **2** is assigned to a terminal B-H stretch, whereas the lower energy peaks correspond to bridging B-H-M stretches, as observed in other DMADB complexes.[58, 62] The B-H peaks are broader in the spectrum of **1**, probably as a result of the greater variety of bonding modes compared with **2**, as seen in the solid state structure. The frequencies of the symmetric and asymmetric O-C-O stretches of the coordinated thf molecule, 880 and 1016 cm^{-1} for **1** and 879 and 1019 cm^{-1} for **2**, are similar to those previously reported.[63]

For the dme complexes, the IR spectrum of the Eu compound **3** reveals strong, well resolved terminal and bridging B-H stretches at 2302 and 2255 cm^{-1}, respectively, whereas the IR spectrum of the Yb compound **4** has three strong peaks at 2331, 2296 and 2233 cm^{-1}. Two peaks at 852 and 1006 cm^{-1} in **3** and at 861 and 1105 cm^{-1} in **4** correspond to the C-O-C stretches of the coordinated dme molecules.

The IR spectra of **1**-**4** suggest that the metal-DMADB bonding is more covalent in the Yb complexes than in the Eu complexes. Specifically, the energy difference between the principal terminal and bridging B-H stretches is 50 and 47 cm^{-1} in **1** and **3**, vs. 130 and 98 cm^{-1} for **2** and **4**.

The Eu compound **1** gives no metal-containing species in its field ionization mass spectrum, but the spectrum of **2** contains envelopes of metal-containing ions centered at *m*/*z* values of 317, 388, and 704. Assignment of formulas to these ions is somewhat complicated by the similar molecular weights of thf (72.11 g/mol) and the DMADB ligand (71.75 g/mol). Analysis of the isotropic distributions suggest that the peaks in the mass spectrum are best assigned as follows: the 317 envelope is a mixture of $Yb(H_3BNMe_2BH_3)(thf)^+$ and $Yb(H_3BNMe_2BH_3)_2^+$, the 388 envelope is a mixture of $Yb(H_3BNMe_2BH_3)(thf)_2^+$ and $Yb(H_3BNMe_2BH_3)_2(thf)^+$, and the envelope at 704 is a mixture of $Yb_2(H_3BNMe_2BH_3)_3(thf)_2^+$ and $Yb_2(H_3BNMe_2BH_3)_4(thf)^+$. Similar behavior has been observed in the FI mass spectra of $Ln(H_3BNMe_2BH_3)_3(thf)$ complexes.[60]

Like **1**, compound **3** does not give metal-containing ions in its FI mass spectrum, but **4** gives a strong parent peak at *m*/*z* = 406 corresponding to $Yb(H_3BNMe_2BH_3)_2(dme)^+$.

Concluding Remarks.

Like BH_4^-, the aminodiboranate anion $H_3BNMe_2BH_3^-$ is able to serve both as a ligand and as a reductant for lanthanides. Only the two most easily reduced lanthanides, Eu and Yb, are converted to their +2 oxidation states; in the analogous reaction of $SmCl_3$ with $Na(H_3BNMe_2BH_3)$, the only isolable product is $Sm(H_3BNMe_2BH_3)_3(thf)$, and there is no evidence of reduction to Sm^{II}. For both Eu and Yb, a mixture of the Ln^{II} and Ln^{III} aminodiboranate products is generated, with the ratio being temperature dependent: the Ln^{II}

products are favored if the metal trichloride is mixed with $Na(H_3BNMe_2BH_3)$ at higher temperatures. Relevant in the current context is our finding that $Na(H_3BNMe_2BH_3)$ is able to reduce U^{IV} to U^{III}.[62]

The aqueous Ln^{3+}/Ln^{2+} reduction potentials of these metals are Eu (-0.36 V), Yb (-1.05 V), and Sm (-1.55 V), and the redox potential of the U^{4+}/U^{3+} couple is –0.61 V.[64] These values suggest that $Na(H_3BNMe_2BH_3)$ has an effective reduction potential of between -1.05 and -1.55 V. For comparison, recent DFT calculations have suggested that $H_3BNMe_2BH_3^-$ is 0.2 V more reducing than BH_4^-.[65]

Experimental

All operations were carried out in vacuum or under argon using standard Schlenk techniques. All glassware was dried in an oven at 150 °C, assembled hot, and allowed to cool under vacuum before use. Tetrahydrofuran, 1,2-dimethoxyethane, diethyl ether, and pentane were distilled under nitrogen from sodium/benzophenone and degassed with argon immediately before use. Anhydrous $LnCl_3$ (Strem) and LnI_2 (Aldrich) were used as received. $Na(H_3BNMe_2BH_3)$ was prepared by a literature route.[57]

Elemental analyses were carried out by the University of Illinois Microanalytical Laboratory. The IR spectra were recorded on a Nicolet Impact 410 infrared spectrometer as Nujol mulls between KBr plates. The ^1H data were obtained on a Varian Unity 400 instrument at 400 MHz or on a Varian Unity U500 instrument at 500 MHz. The ^{11}B NMR data were collected on a General Electric GN300WB instrument at 96 MHz or on a Varian Unity Inova 600 instrument at 192 MHz. Chemical shifts are reported in δ units (positive shifts to high frequency) relative to TMS (^1H) or $BF_3•Et_2O$ (^{11}B). Field ionization (FI) mass spectra were recorded on a Micromass 70-VSE mass spectrometer. The shapes of all peak

envelopes correspond with those calculated from the natural abundance isotopic distributions in the observed spectra. Melting points and decomposition temperatures were determined in closed capillaries under argon on a Thomas-Hoover Unimelt apparatus.

▪ CAUTION: Complexes **2** and **4** enflame upon exposure to air.

Bis(*N*,*N*-dimethylaminodiboranato)bis(tetrahydrofuran)europium(II), Eu(H_3B-NMe_2BH_3)$_2$(thf)$_2$, (1). Method A. To a suspension of $EuCl_3$ (0.50 g, 1.9 mmol) in tetrahydrofuran (20 mL) at 0 °C was added a solution of sodium *N*,*N*-dimethylaminodiboranate (0.56 g, 5.9 mmol) in tetrahydrofuran (20 mL). The grey reaction mixture was stirred at 0 °C for 15 min and then was warmed to room temperature. The solution over the grey suspension slowly became yellow. The mixture was stirred for 40 h at room temperature and then was evaporated to dryness under vacuum to afford a sticky, yellow solid. The residue was extracted with pentane (2 × 20 mL). The pale yellow extracts were filtered, combined, concentrated to ca. 15 mL, and cooled to -20 ˚C to yield pale yellow crystals. Yield: 0.39 g (47 %). Calcd for $C_{12}H_{40}B_4N_2O_2Eu$: C, 32.8; H, 9.17; N, 6.37. Found: C, 31.5; H, 9.04; N, 6.41.

Method B. To a suspension of EuI_2 (0.52 g, 1.3 mmol) in tetrahydrofuran (20 mL) was added a solution of sodium *N*,*N*-dimethylaminodiboranate (0.25 g, 2.6 mmol) in tetrahydrofuran (20 mL). Most of the EuI_2 suspension immediately dissolved, and the yellow mixture was stirred for 20 h and then evaporated to dryness under vacuum to afford a sticky, light yellow solid. The residue was extracted with pentane (55 mL), and the pale yellow extract was filtered, concentrated to 20 mL, and cooled to -20 °C to yield 0.26 g of pale yellow crystals. Concentrating the mother liquor to 5 mL and cooling to -20 °C yielded an additional 0.04 g of crystals. Yield: 0.30 g (53 %). M.p.: 74 – 76 °C. Anal. Calcd for $C_{12}H_{40}B_4N_2O_2Eu$: C, 32.8; H, 9.17; N, 6.37. Found: C, 32.2; H, 9.31; N, 6.50. IR (cm^{-1}):

2397 w, 2321 sh, 2299 vs, 2249 vs, 2068 w, 1339 w, 1247 m, 1227 m, 1208 m, 1177 s, 1153 s, 1143 s, 1038 s, 1016 s, 967 w, 927 m, 902 m, 880 s, 797 w.

Bis(*N*,*N*-dimethylaminodiboranato)bis(tetrahydrofuran)ytterbium(II), Yb(H_3B-NMe_2BH_3)$_2$(thf)$_2$, (2). Method A. To a suspension of $YbCl_3$ (0.55 g, 2.0 mmol) in tetrahydrofuran (15 mL) was added a solution of sodium *N*,*N*-dimethylaminodiboranate (0.56 g, 5.9 mmol) in tetrahydrofuran (15 mL). The off-white reaction mixture was stirred for 15 h at room temperature and then evaporated to dryness under vacuum to afford a sticky, yellow residue. The residue was extracted with pentane (50 mL), and the intense yellow extract was filtered, concentrated to ca. 15 mL, and cooled to -20 ˚C to yield intense yellow crystals. Yield: 0.35 g (39 %). Anal. Calcd for $C_{12}H_{40}B_4N_2O_2Yb$: C, 31.3; H, 8.75; N, 6.08. Found: C, 30.7; H, 9.04; N, 6.41. NMR data match those of **2** obtained by Method B. $Yb(H_3BNMe_2BH_3)_3(thf)$, which sometimes co-crystallizes with **2**, can be readily differentiated by comparison of the NMR spectra: ^{1}H NMR (C_6D_6, 20 °C): δ -18.72 (br s, fwhm = 440 Hz, BH_3, 18H), -3.48 (s, fwhm = 140 Hz, β-CH_2, 4H), -0.26 (s, fwhm = 30 Hz, NMe_2, 18H), 1.15 (br s, fwhm = 370 Hz, OCH_2, 4H). ^{11}B NMR (C_6D_6, 20 °C): δ -47.4 (br s, fwhm = 150 Hz, BH_3).[60]

Method B. To a suspension of YbI_2 (0.50 g, 1.2 mmol) in tetrahydrofuran (20 mL) was added a solution of sodium *N*,*N*-dimethylaminodiboranate (0.22 g, 2.3 mmol) in tetrahydrofuran (20 mL). Most of the YbI_2 suspension slowly dissolved, and the yellow mixture was stirred for 24 h and then evaporated to dryness under vacuum to afford a sticky, intense yellow solid. The residue was extracted with pentane (40 mL), and the intense yellow extract was filtered, concentrated to 22 mL, and cooled to -20 °C to yield 0.37 g of pale yellow crystals. Concentrating the mother liquor to 8 mL and cooling to -20 °C yielded an additional 0.03 g of crystals. Yield: 0.40 g (74 %). M.p.: 110 – 113 °C. Anal. Calcd for

$C_{12}H_{40}B_4N_2O_2Yb$: C, 31.3; H, 8.75; N, 6.08. Found: C, 30.5; H, 8.81; N, 6.08. ^{1}H NMR (C_7D_8, 20 °C): δ 1.30 (s, fwhm = 20 Hz, β-CH_2, 8H), 2.45 (s, fwhm = 12 Hz, NMe_2, 12 H), 2.63 (br q, J_{BH} = 86 Hz, BH_3, 12 H), 3.61 (s, fwhm = 20 Hz, α-CH_2, 8 H). ^{11}B NMR (C_7D_8, 20 °C): δ -7.7 (q, J_{BH} = 91 Hz, BH_3). MS(FI) [fragment ion, relative abundance]: *m*/*z* 115 [H_2B-NMe_2-BH_2-NMe_2, 60], 316 [$Yb(H_3BNMe_2BH_3)_2$, 60], 376 [$Yb(H_3BNMe_2BH_3)_3 - BH_2$, 45], 388 [$Yb(H_3BNMe_2BH_3)_2(thf)$ / $Yb(H_3BNMe_2BH_3)(thf)_2$, 100], 704 [$Yb_2(H_3BNMe_2BH_3)_4(thf)$ / $Yb_2(H_3BNMe_2BH_3)_3(thf)_2$, 55]. IR ($cm^{-1}$): 2385 sh, 2357 vs, 2303 m, 2271 s, 2227 vs, 2075 w, 1342 w, 1261 m, 1232 m, 1211 m, 1177 s, 1147 s, 1031 s, 1019 s, 931 m, 918 w, 905 m, 879 m, 801 m.

Bis(*N*,*N*-dimethylaminodiboranato)bis(1,2-dimethoxyethane)europium(II), $Eu(H_3BNMe_2BH_3)_2(dme)_2$, (3). To a suspension of **1** (0.22 g, 0.50 mmol) in pentane (16 mL) was added dme (0.5 mL, 5 mmol). A thick, grey precipitate formed immediately. The mixture was stirred for 2 h, and then was filtered. The filtrate was discarded, and the solid was washed with pentane (10 mL) and dried under vacuum to yield a light grey powder. Yield: 0.17 g (71%). Concentration and cooling solutions of **3** in diethyl ether produced large, cubic crystals suitable for diffraction studies. M.p.: 107 – 115 °C (dec.). Anal. Calcd for $C_{12}H_{44}B_4N_2O_4Eu$: C, 30.3; H, 9.32; N, 5.89. Found: C, 29.8; H, 9.32; N, 5.87. IR (cm^{-1}): 2391 w, 2366 w, 2347 sh, 2302 vs, 2255 s, 2226 sh, 2071 w, 1303 w, 1254 w, 1223 m, 1210 m, 1178 s, 1152 s, 1106 m, 1060 s, 1016 s, 979 w, 926 m, 904 w, 852 s, 802 w.

Bis(*N*,*N*-dimethylaminodiboranato)(1,2-dimethoxyethane)ytterbium(II), $Yb(H_3BNMe_2BH_3)_2(dme)$, (4). To a bright yellow suspension of **2** (0.22 g, 0.48 mmol) in pentane (16 mL) was added dme (0.5 mL, 5 mmol). Most of the solid dissolved immediately. The mixture was stirred for 2 h, and the intense yellow mixture was filtered, concentrated to 3 mL, and cooled to -20 °C to yield an intense yellow, semi-crystalline solid. Yield: 0.16 g

(82 %). M.p.: 107 – 115 °C (dec). Anal. Calcd for $C_8H_{34}B_4N_2O_2Yb$: C, 23.6; H, 8.43; N, 6.89. Found: C, 23.9; H, 8.69; N, 6.73. ^{1}H NMR (C_6D_6, 20 °C): δ 2.50 (s, fwhm = 15 Hz, NMe_2, 12 H), 2.76 (br q, J_{BH} = 90 Hz, BH_3, 12 H), 2.88 (s, fwhm = 16 Hz, CH_2, 4 H), 2.98 (s, fwhm = 20 Hz, CH_3, 6 H). ^{11}B NMR (C_7D_8, 20 °C): δ -7.6 (q, J_{BH} = 91 Hz, BH_3). MS(FI) [fragment ion, relative abundance]: *m*/*z* 115 [H_2B-NMe_2-BH_2-NMe_2, 100], 406 [$Yb(H_3BNMe_2BH_3)_2$(dme), 25]. IR (cm^{-1}): 2391 w, 2331 vs, 2296 vs, 2233 vs, 2071 w, 1303 w, 1286 w, 1265 w, 1233 m, 1214 m, 1178 s, 1149 s, 1105 m, 1069 sh, 1060 s, 1020 s, 944 w, 929 m, 906 w, 861 m, 834 w, 805 w.

Crystallographic studies.[66] Single crystals of **1** and **2**, grown from pentane, and **3**, grown from diethyl ether, were mounted on glass fibers with Paratone-N oil (Exxon) and immediately cooled to -80 °C in a cold nitrogen gas stream on the diffractometer. Standard peak search and indexing procedures, followed by least-square refinement, yielded the cell dimensions given in Table 5.1. Data were collected with an area detector by using the measurement parameters listed in Table 5.1. For all crystals, the measured intensities were reduced to structure factor amplitudes, and their estimated standard deviations by correction for background and Lorentz and polarization effects. Although corrections for crystal decay were unnecessary, face-indexed absorption corrections were applied. Systematically absent reflections were deleted, and symmetry equivalent reflections were averaged to yield the set of unique data. All unique data were used in the least-squares refinements.

The structures were solved using direct methods (SHELXTL). The correct position of all the non-hydrogen atoms were deduced from *E*-maps and subsequent difference Fourier calculations. The analytical approximations to the scattering factors were used, and all structure factors were corrected for both real and imaginary components of anomalous dispersion. Unless otherwise stated, the refinement models had the following features: (1)

Independent anisotropic displacement factors were refined for the non-hydrogen atoms. (2) Methylene and methyl hydrogen atoms were placed in idealized positions with C-H = 0.99 and 0.98 Å, respectively. (3) The methyl groups were allowed to rotate about the C-N bonds to find the best least-squares positions. (4) Methylene and methyl hydrogen atoms were given displacement parameters equal to 1.2 and 1.5 times U_{eq} for the attached carbon atom, respectively. In **1**, the boranyl hydrogen atoms were placed in idealized positions with B-H = 1.15 Å and were given displacement parameters equal to 1.2 times U_{eq} for the attached boron atom, and the boranyl groups were allowed to rotate about the B-N bonds to find the best least-squares positions. The hydrogen atoms attached to boron in **2** and **3** were located in the difference maps, and their positions were refined with independent isotropic displacement parameters. No corrections for isotropic extinction were necessary. For all data sets, successful convergence was indicated by the maximum shift/error of 0.000 for the last cycle. Unless otherwise stated, a final analysis of variance between observed and calculated structure factors showed no apparent errors. Final refinement parameters are given in Table 5.1. Aspects specific to the individual refinements are detailed in the following paragraphs.

$Eu(H_3BNMe_2BH_3)_2(thf)_2$, 1: The monoclinic lattice and systematic absences $0k0$ ($k \neq 2n$) and $h0l$ ($l \neq 2n$) were uniquely consistent with the space group $P2_1/c$, which was confirmed by the success of the subsequent refinement. The europium centers and the bridging aminodiboranate ligands are disordered over two positions related by a pseudo two-fold axis running along the length of the molecule and passing approximately through the nitrogen atoms of the two terminal aminodiboranate ligands. The terminal aminodiboranate ligands and the tetrahydrofuran molecules of the two disordered components are essentially superimposed and could be refined as full occupancy groups. The site occupancy factors (SOFs) for these two disordered components were constrained to sum to one; the SOF. for

the major occupancy component refined to 0.690. The tetrahydrofuran molecules show further disorder; only the α-carbons are disordered in one molecule whereas all the carbon atoms are disordered in the other. The site occupancy factors for the disordered components were also constrained to sum to one; the SOF for the major occupancy components refined to 0.512 and 0.563, respectively. The quantity minimized by the least-squares program was $\Sigma w(F_o^2 - F_c^2)^2$, where $w = \{[\sigma(F_o)]^2 + (0.421P)^2\}^{-1}$ and $P = (F_o^2 + 2F_c^2)/3$. The chemically equivalent C-N, B-N, B···C, and C···C distances within the aminodiboranate ligands were constrained to be equal within an esd of 0.005 Å. The C-O and C-C distances in the tetrahydrofuran molecules were constrained to be 1.48 ± 0.005 and 1.52 ± 0.005 Å, respectively. The largest peak in the final Fourier difference map (0.65 e $Å^{-3}$) was located 0.95 Å from Eu1.

$Yb(H_3BNMe_2BH_3)_2(thf)_2$, 2: The monoclinic lattice and systematic absences $0k0$ ($k \neq 2n$) and $h0l$ ($h + l \neq 2n$) were uniquely consistent with the space group $P2_1/n$, which was confirmed by the success of the subsequent refinement. The quantity minimized by the least-squares program was $\Sigma w(F_o^2 - F_c^2)^2$, where $w = \{[\sigma(F_o)]^2 + (0.0578P)^2\}^{-1}$ and $P = (F_o^2 + 2F_c^2)/3$. The chemically equivalent B-H and H···H distances were constrained to be equal within 0.01 Å. The largest peak in the final Fourier difference map (2.65 e $Å^{-3}$) was located 0.82 Å from Yb1.

$Eu(H_3BNMe_2BH_3)_2(dme)_2$, 3: The monoclinic lattice and systematic absences $0k0$ ($k \neq 2n$) and $h0l$ ($h + l \neq 2n$) were uniquely consistent with the space group $P2_1/n$, and this choice was confirmed by successful refinement of the proposed model. The quantity minimized by the least-squares program was $\Sigma w(F_o^2 - F_c^2)^2$, where $w = \{[\sigma(F_o)]^2 + (0.0210P)^2\}^{-1}$ and $P = (F_o^2 + 2F_c^2)/3$. The chemically equivalent B-H distances were constrained to be equal within an esd of 0.01 Å. The largest peak in the final Fourier

difference map (0.83 e $Å^{-3}$) was located 1.03 Å from C22.

References

1. Matignon, C.; Cazes, E. *Compt. rend.* **1906,** *142*, 83-85.

2. Girard, P.; Namy, J. L.; Kagan, H. B. *J. Am. Chem. Soc.* **1980,** *102*, 2693-2698.

3. Bochkarev, M. N.; Fedushkin, I. L.; Fagin, A. A.; Petrovskaya, T. V.; Ziller, J. W.; Broomhall-Dillard, R. N. R.; Evans, W. J. *Angew. Chem., Int. Ed.* **1997,** *36*, 133-135.

4. Evans, W. J.; Allen, N. T.; Ziller, J. W. *J. Am. Chem. Soc.* **2000,** *122*, 11749-11750.

5. Bochkarev, M. N.; Fedushkin, I. L.; Dechert, S.; Fagin, A. A.; Schumann, H. *Angew. Chem., Int. Ed.* **2001,** *40*, 3176-3178.

6. Evans, W. J.; Allen, N. T.; Workman, P. S.; Meyer, J. C. *Inorg. Chem.* **2003,** *42*, 3097-3099.

7. Bochkarev, M. N. *Coord. Chem. Rev.* **2004,** *248*, 835-851.

8. Hitchcock, P. B.; Lappert, M. F.; Maron, L.; Protchenko, A. V. *Angew. Chem., Int. Ed.* **2008,** *47*, 1488-1491.

9. Evans, W. J. *J. Organomet. Chem.* **2002,** *647*, 2-11.

10. Evans, W. J. *Inorg. Chem.* **2007,** *46*, 3435-3449.

11. Evans, W. J. *J. Alloys Compd.* **2009,** *488*, 493-510.

12. Kagan, H. B.; Namy, J.-L. *Top. Organomet. Chem.* **1999,** *2*, 155-198.

13. Krief, A.; Laval, A.-M. *Chem. Rev.* **1999,** *99*, 745-777.

14. Mikami, K.; Terada, M.; Matsuzawa, H. *Angew. Chem., Int. Ed.* **2002,** *41*, 3554-3571.

15. Kagan, H. B. *Tetrahedron* **2003,** *59*, 10351-10372.

16. Berndt, M.; Gross, S.; Hoelemann, A.; Reissig, H.-U. *Synlett* **2004**, 422-438.

17. Dahlen, A.; Hilmersson, G. *Eur. J. Inorg. Chem.* **2004**, 3393-3403.

18. Edmonds, D. J.; Johnston, D.; Procter, D. J. *Chem. Rev.* **2004,** *104*, 3371-3403.

19. Corbett, J. D. Conproportionation routes to reduced lanthanide halides. In *Topics in f-Element Chemistry*, Meyer, G.; Morss, L. R., Eds. Kluwer Academic: Dordrecht, 1991; Vol. 2, pp 159-173.

20. Meyer, G.; Schleid, T. Action of alkali metals on lanthanide(III) halides: an alternative to the conproportionation route to reduced lanthanide halides. In *Topics in f-Element Chemistry*, Meyer, G.; Morss, L. R., Eds. Kluwer Academic: Dordrecht, 1991; Vol. 2, pp 175-185.

21. Morss, L. R. *Chem. Rev.* **1976,** *76*, 827-842.

22. Tilley, T. D.; Andersen, R. A.; Spencer, B.; Ruben, H.; Zalkin, A.; Templeton, D. H. *Inorg. Chem.* **1980,** *19*, 2999-3003.

23. Arnaudet, L.; Ban, B. *New J. Chem.* **1988,** *12*, 201-203.

24. Sitzmann, H.; Dezember, T.; Schmitt, O.; Weber, F.; Wolmershauser, G.; Ruck, M. *Z. Anorg. Allg. Chem.* **2000,** *626*, 2241-2244.

25. Gudilenkov, I. D.; Fukin, G. K.; Baranov, E. V.; Trifonov, A. A. *Russ. Chem. Bull.* **2008,** *57*, 40-46.

26. Zinnen, H. A.; Pluth, J. J.; Evans, W. J. *J. Chem. Soc., Chem. Commun.* **1980**, 810-812.

27. Sheng, E.; Wang, S.; Yang, G.; Zhou, S.; Cheng, L.; Zhang, K.; Huang, Z. *Organometallics* **2003,** *22*, 684-692.

28. Zhang, K.; Zhang, W.; Wang, S.; Sheng, E.; Yang, G.; Xie, M.; Zhou, S.; Feng, Y.; Mao, L.; Huang, Z. *Dalton Trans.* **2004**, 1029-1037.

29. Sheng, E.; Zhou, S.; Wang, S.; Yang, G.; Wu, Y.; Feng, Y.; Mao, L.; Huang, Z. *Eur. J. Inorg. Chem.* **2004**, 2923-2932.

30. Wu, Y.; Wang, S.; Qian, C.; Sheng, E.; Xie, M.; Yang, G.; Feng, Q.; Zhang, L.; Tang, X. *J. Organomet. Chem.* **2005,** *690*, 4139-4149.

31. Wang, S.; Feng, Y.; Mao, L.; Sheng, E.; Yang, G.; Xie, M.; Wang, S.; Wei, Y.; Huang, Z. *J. Organomet. Chem.* **2006,** *691*, 1265-1274.

32. Wang, S.; Tang, X.; Vega, A.; Saillard, J.-Y.; Sheng, E.; Yang, G.; Zhou, S.; Huang, Z. *Organometallics* **2006,** *25*, 2399-2401.

33. Wang, S.; Wang, S.; Zhou, S.; Yang, G.; Luo, W.; Hu, N.; Zhou, Z.; Song, H.-B. *J. Organomet. Chem.* **2007,** *692*, 2099-2106.

34. Zhou, S.; Wang, S.; Sheng, E.; Zhang, L.; Yu, Z.; Xi, X.; Chen, G.; Luo, W.; Li, Y. *Eur. J. Inorg. Chem.* **2007**, 1519-1528.

35. Cheng, L.; Feng, Y.; Wang, S.; Luo, W.; Yao, W.; Yu, Z.; Xi, X.; Huang, Z. *Eur. J. Inorg. Chem.* **2007**, 1770-1777.

36. Wang, S.; Tang, X.; Vega, A.; Saillard, J.-Y.; Zhou, S.; Yang, G.; Yao, W.; Wei, Y. *Organometallics* **2007,** *26*, 1512-1522.

37. Wei, Y.; Yu, Z.; Wang, S.; Zhou, S.; Yang, G.; Zhang, L.; Chen, G.; Qian, H.; Fan, J. *J. Organomet. Chem.* **2008,** *693*, 2263-2270.

38. Ruspic, C.; Moss, J. R.; Schuermann, M.; Harder, S. *Angew. Chem., Int. Ed.* **2008,** *47*, 2121-2126.

39. Evans, W. J.; Davis, B. L. *Chem. Rev.* **2002,** *102*, 2119-2136.

40. Evans, W. J. *Coord. Chem. Rev.* **2000,** *206-207*, 263-283.

41. Evans, W. J.; Forrestal, K. J.; Ziller, J. W. *J. Am. Chem. Soc.* **1995,** *117*, 12635-12636.

42. Evans, W. J.; Forrestal, K. J.; Ziller, J. W. *J. Am. Chem. Soc.* **1998,** *120*, 9273-9282.

43. Evans, W. J.; Nyce, G. W.; Clark, R. D.; Doedens, R. J.; Ziller, J. W. *Angew. Chem., Int. Ed.* **1999,** *38*, 1801-1803.

44. Evans, W. J.; Perotti, J. M.; Kozimor, S. A.; Champagne, T. M.; Davis, B. L.; Nyce, G. W.; Fujimoto, C. H.; Clark, R. D.; Johnston, M. A.; Ziller, J. W. *Organometallics* **2005,** *24*, 3916-3931.

45. Evans William, J.; Davis Benjamin, L.; Champagne Timothy, M.; Ziller Joseph, W. *Proc. Natl. Acad. Sci. U.S.A.* **2006,** *103*, 12678-12683.

46. Marks, T. J.; Kolb, J. R. *Chem. Rev.* **1977,** *77*, 263-293.

47. Pelter, A.; Smith, K.; Brown, H. C. *Borane Reagents*. Academic Press: San Diego, 1988; pp 503.

48. Rossmanith, K.; Muckenhuber, E. *Monatsh. Chem.* **1961,** *92*, 600-604.

49. Makhaev, V. D.; Borisov, A. P. *Russ. J. Inorg. Chem.* **1999,** *44*, 1411-1413.

50. White, J. P., III; Deng, H.; Shore, S. G. *Inorg. Chem.* **1991,** *30*, 2337-2342.

51. Chen, X.; Lim, S.; Plecnik, C. E.; Liu, S.; Du, B.; Meyers, E. A.; Shore, S. G. *Inorg. Chem.* **2004,** *43*, 692-698.

52. Chen, X.; Lim, S.; Plecnik, C. E.; Liu, S.; Du, B.; Meyers, E. A.; Shore, S. G. *Inorg. Chem.* **2005,** *44*, 6052-6061.

53. Saliu, K. O.; Maunder, G. H.; Ferguson, M. J.; Sella, A.; Takats, J. *Inorg. Chim. Acta* **2009,** *362*, 4616-4622.

54. Hill, T. G.; Godfroid, R. A.; White, J. P., III; Shore, S. G. *Inorg. Chem.* **1991,** *30*, 2952-2954.

55. Keller, P. C. *J. Chem. Soc. D* **1969**, 1465.

56. Keller, P. C. *Inorg. Chem.* **1971,** *10*, 2256-2259.

57. Nöth, H.; Thomas, S. *Eur. J. Inorg. Chem.* **1999**, 1373-1379.

58. Daly, S. R.; Kim, D. Y.; Yang, Y.; Abelson, J. R.; Girolami, G. S. *J. Am. Chem. Soc.* **2010**, ACS ASAP.

59. Shannon, R. D. *Acta Crystallogr., Sect. A* **1976,** *A32*, 751-767.

60. Daly, S. R.; Kim, D. Y.; Girolami, G. S., manuscript in preparation.

61. Eaton, G. R.; Lipscomb, W. N. *N.M.R. Studies of Boron Hydrides and Related Compounds*. Benjamin: New York, 1969; pp 617.

62. Daly, S. R.; Girolami, G. S. *Chem. Commun.* **2010,** *46*, 407-408.

63. Clark, R. J. H.; Lewis, J.; Machin, D. J.; Nyholm, R. S. *J. Chem. Soc.* **1963**, 379-387.

64. Lide, D. R. *CRC Handbook of Chemistry and Physics*, 77th ed. CRC Press: Boca Raton, 1996; pp 2512.

65. Daly, S. R.; Girolami, G. S. *Inorg. Chem.*, accepted.

66. Brumaghim, J. L.; Priepot, J. G.; Girolami, G. S. *Organometallics* **1999,** *18*, 2139-2144.

CHAPTER 6. Barium *N*,*N*-Dimethylaminodiboranates

Introduction

Barium is a constituent in a wide variety of materials that can be exploited for electronic applications. For instance, the versatile and ubiquitous $BaTiO_3$, a ferroelectric ceramic, has been extensively used in electronic devices because it has a high dielectric constant and piezoelectric and thermoresistive properties.[1-4] The renowned $YBa_2Cu_3O_{7-x}$ (YBCO) and similar derivatives are high-T_c superconductors and were the first materials to be superconducting above the boiling point of nitrogen.[5-10] In another example, it has been shown that crystalline β-BaB_2O_4 has optoelectronic properties that are especially useful for non-linear optical devices and for solid-state UV lasers.[11, 12]

Although barium-containing materials have properties that make them potentially useful for electronic applications, many of the methods used to prepare them (e.g., sintering, co-precipitation, mechanochemical synthesis) are not conducive to device fabrication on the micro- and nano-scale. In contrast, chemical vapor deposition (CVD) and atomic layer deposition (ALD) are useful methods for depositing thin films on substrates with advanced architectures and high aspect ratios within this size regime.[13, 14] CVD and ALD also allow discreet control over film stochiometry and provide a convenient way to introduce dopants, which dramatically influence the properties of the materials but can be difficult to control using other preparative methods.

The main limitation to preparing barium-containing materials by CVD and ALD is the lack of barium precursors with adequate volatility.[15, 16] Although volatile barium complexes are known, few precursors have vapor pressures high enough to access the conformal growth regime necessary to grow conformal films by CVD.[14, 17] Many molecular

barium complexes suffer from low volatility because of the high radius to charge ratio for Ba^{2+} and the ionic nature of barium-ligands bonds. Volatile Ba complexes require ligands that can encapsulate the metal so that it is protected from bridging interactions that can inhibit volatility. The ligands employed must be large enough to shield the metal; multidentate ligands are excellent choices in this regard.[16] Neutral ancillary ligands, such as glymes, are also used to help fill the coordination sphere if the anionic ligands themselves are not sufficiently saturating.[18] The majority of barium complexes that have been explored as thin film precursors utilize diketonate or ketoiminate ligands,[19-29] and many of these have been functionalized with flexible donor pendants that can occupy additional coordination sites around the metal.[30-32] Other barium precursors that are suitable for thin film growth include those that utilize alkoxide,[33] cyclopentadienyl,[17, 34-39] and (pyrazolyl)borate ligands.[40-42] Like barium, lanthanide metals also have large radius to charge ratios and ionic metal-ligand bonds. As a result, many of the same ligands and strategies that are used to prepare volatile lanthanide complexes have also been successful in preparing volatile barium complexes.[43]

In previous chapters we have shown that the *N*,*N*-dimethylaminodiboranate ligand, $H_3BNMe_2BH_3^-$,[44-46] (DMADB) can be used to prepare highly volatile complexes of lanthanides and transition metals that are excellent precursors for the deposition of lanthanide-containing thin films by CVD.[47] The DMADB ligand is a multidentate borohydride ligand that consists of two BH_3 groups joined together by a dimethylamido linker, which makes it larger than other borohydride ligands such as BH_4^-, BH_3Me^-, and even $B_3H_8^-$. The larger size of the DMADB ligand renders it better able to saturate the coordination spheres of large metals, and, as a result, many metals that form non-volatile complexes with other borohydride anions form quite volatile complexes with DMADB. For

example, the DMADB ligand has been used successfully to prepare volatile derivatives of other alkaline earths: $Mg(H_3BNMe_2BH_3)_2$ is the most volatile Mg complexes known and is an excellent precursor for the deposition of MgO by CVD.[48, 49]

We now describe the synthesis, characterization, and molecular structures of barium DMADB complexes as possible precursors for CVD applications. This study also provides an opportunity to explore how the metal-DMADB bonding depends on the size and electronegativity of the metal.

Results and Discussion

Synthesis of Barium Aminodiboranate Complexes. The reaction of $BaBr_2$ with 2 equiv of $Na(H_3BNMe_2BH_3)$ in tetrahydrofuran (thf), followed by crystallization from diethyl ether yields $Ba(H_3BNMe_2BH_3)_2(Et_2O)_2$ (**1**) as large white needles in good yield:

$$BaBr_2 + 2\ Na(H_3BNMe_2BH_3) \xrightarrow[-\ 2\ NaBr]{thf} \xrightarrow{Et_2O} Ba(H_3BNMe_2BH_3)_2(Et_2O)_2 \quad (\mathbf{1})$$

Crystals of **1** readily lose the diethyl ether, and exposure to dynamic vacuum for several hours results in partial desolvation and formation of $Ba(H_3BNMe_2BH_3)_2(Et_2O)_x$ (**1′**), where x ~0.4 as shown by microanalytical data and ^{1}H NMR spectroscopy.

Neither **1** nor **1′** is volatile, in part because they have polymeric structures (see below). Accordingly, we investigated the synthesis of analogs of **1** with more strongly coordinating Lewis bases that might form monomeric complexes capable of being sublimed in vacuum. We find that treatment of **1** or **1′** with 1,2-dimethoxyethane (dme), *N*,*N*,*N*′,*N*′-tetramethylethylenediamine (tmeda), or 1,4,7,10-tetraoxacyclododecane (12-crown-4) in diethyl ether results in formation of the new complexes $Ba(H_3BNMe_2BH_3)_2$(dme) (**2**),

$Ba(H_3BNMe_2BH_3)_2$(tmeda) (**3**), and $Ba(H_3BNMe_2BH_3)_2$(12-crown-4) (**4**), in high yields (78 – 85%). Recrystallization of **4** from tetrahydrofuran affords the related compound $Ba(H_3BNMe_2BH_3)_2$(12-crown-4)(thf)·thf (**4′**). Adducts of this type can also be made directly from $BaBr_2$: the reaction of $BaBr_2$ with 2 equiv of $Na(H_3BNMe_2BH_3)$ in di(2-methoxyethyl)ether (diglyme) yields $Ba(H_3BNMe_2BH_3)_2(diglyme)_2$, **5**.

$$Ba(H_3BNMe_2BH_3)_2 + \text{xs L} \xrightarrow{Et_2O} Ba(H_3BNMe_2BH_3)_2(L)$$

L = dme (**2**)
L = tmed (**3**)
L = 12-crown-4 (**4**)

$$BaBr_2 + 2\ Na(H_3BNMe_2BH_3) \xrightarrow[-\ 2\ NaBr]{diglyme} Ba(H_3BNMe_2BH_3)_2(diglyme)_2$$

(**5**)

Complexes **2-5** retain their coordinated bases even when exposed to dynamic vacuum over extended periods.

Molecular Structures. The molecular structures of **1-5** were determined by single-crystal X-ray diffraction. Each barium atom in the Et_2O adduct **1** resides on a 2-fold axis, and is coordinated to two chelating $H_3BNMe_2BH_3^-$ (DMADB) ligands, two diethyl ether molecules, and two BH_3 groups from DMADB ligands that chelate to adjacent Ba centers. Owing to the latter bridging intereactions, the $Ba(H_3BNMe_2BH_3)_2(Et_2O)_2$ units are linked into a polymer chain (Figure 6.1). The boron and oxygen atoms describe a distorted bicapped trigonal prism around each barium center, in which the two bridging boron atoms cap two of the square faces. Boron atoms B(1), B(2), and O(1A) define one of the distorted triangular faces of the inner trigonal prism, and their 2-fold related counterparts B(1A), B(2A), and O(1) define the other.

The Ba···B distances to the chelating DMADB ligands are 3.216(6) and 3.265(6) Å; in contrast, the Ba···B distances to the BH_3 groups from neighboring centers in the chain are

Table 6.1. Crystallographic data for the new barium *N*,*N*-dimethylaminodiboranate complexes at 193(2) K.

	1	**2**	**3**	**4′**	**5**
formula	$C_{12}H_{44}B_4N_2O_2Ba$	$C_8H_{34}B_4N_2O_2Ba$	$C_{10}H_{40}B_4N_4Ba$	$C_{16}H_{52}N_2O_6B_4Ba$	$C_{20}H_{52}B_4N_2O_6Ba$
FW (g mol^{-1})	429.07	370.77	397.04	549.18	597.22
λ (Å)	0.71073	0.71073	0.71073	0.71073	0.71073
crystal system	monoclinic	monoclinic	monoclinic	monoclinic	triclinic
space group	C_2/c	$P2_1/c$	C_2/c	$P2_1/c$	$P\bar{1}$
a (Å)	21.8381(12)	10.384(3)	21.1428(5)	9.147(3)	11.8304(4)
b (Å)	11.0420(6)	17.411(5)	10.3259(2)	17.141(5)	16.8151(6)
c (Å)	10.7710(6)	10.679(3)	10.6711(2)	18.377(5)	16.8646(6)
α (deg)	90	90	90	90	71.134(2)
β (deg)	117.704(3)	104.108(4)	116.4000(10)	90.453(4)	83.495(2)
γ (deg)	90	90	90	90	87.735(2)
V (Å^3)	2299.5(2)	1872.6(9)	2086.74(7)	2881.3(14)	3154.18(19)
Z	4	4	4	4	4
ρ_{calc} (g cm^{-3})	1.239	1.316	1.264	1.266	1.258
μ(mm^{-1})	1.730	2.113	1.897	1.406	1.29
R(int)	0.0683	0.0390	0.0519	0.0559	0.0979
abs correction method	face-indexed	face-indexed	face-indexed	face-indexed	face-indexed
max. min. transm. factors	0.883/0.483	0.817/0.476	0.964/0.654	0.819/0.506	0.946/0.841
data/restraints/params	2112/0/124	3414/0/290	2157/0/167	7049/13/319	11617/298/758
GOF on F^2	1.031	0.891	0.880	0.847	0.789
R_1 [$I > 2\sigma(I)$][a]	0.0325	0.0155	0.0206	0.0228	0.0433
wR_2 (all data)[b]	0.0792	0.0304	0.0307	0.0442	0.0751
max, min $\Delta\rho_{electron}$ (e·Å^{-3})	1.035/-0.531	0.800/-0.330	0.395/-0.338	1.616/-0.766	0.895/-0.496

[a] $R_1 = \sum |F_o| - |F_c| \,| / |\sum |F_o|$ for reflections with $F_o^2 > 2\,\sigma(F_o^2)$. [b] $wR_2 = [\sum w(F_o^2 - F_c^2)^2 / \sum (F_o^2)^2]^{1/2}$ for all reflections.

Table 6.2. Selected Bond Lengths and Angles for $Ba(H_3BNMe_2BH_3)_2(Et_2O)_2$, **1**.

	Bond Lengths (Å)		
Ba(1)-O(1)	2.800(3)	Ba(1)-H(1A)	2.79(4)
Ba(1)-B(1)	3.216(6)	Ba(1)-H(1B)	2.78(5)
Ba(1)-B(2)	3.265(6)	Ba(1)-H(2A)	2.88(5)
Ba(1)-B(2)′	3.477(5)	Ba(1)-H(2B)	2.79(4)
	Bond Angles (deg)		
B(1)-Ba(1)-B(2)	47.31(13)	B(1)-Ba(1)-B(1)′	124.1(3)
O(1)-Ba(1)-B(1)	146.10(13)	B(1)-Ba(1)-B(2)′	97.04(17)
O(1)-Ba(1)-B(2)	154.76(12)	B(1)-Ba(1)-B(2)″	112.77(14)
O(1)-Ba(1)-B(1)′	85.89(15)	B(1)-Ba(1)-B(2)‴	76.61(14)
O(1)-Ba(1)-B(2)′	93.17(12)	B(2)-Ba(1)-B(2)′	107.3(2)
O(1)-Ba(1)-B(2)′	87.41(11)	B(2)-Ba(1)-B(2)″	69.10(14)
O(1)-Ba(1)-B(2)″	77.08(12)	B(2)-Ba(1)-B(2)‴	123.61(15)
O(1)-Ba(1)-O(1)′	71.91(13)	B(2)″-Ba(1)-B(2)‴	160.89(19)

Symmetry transf. used to generate equivalent atoms: ′ = -*x*+2, *y*, -*z*+3/2; ″ = -*x*+2, -*y*, -*z*+1; ‴ = *x*, -*y*, *z*+1/2.

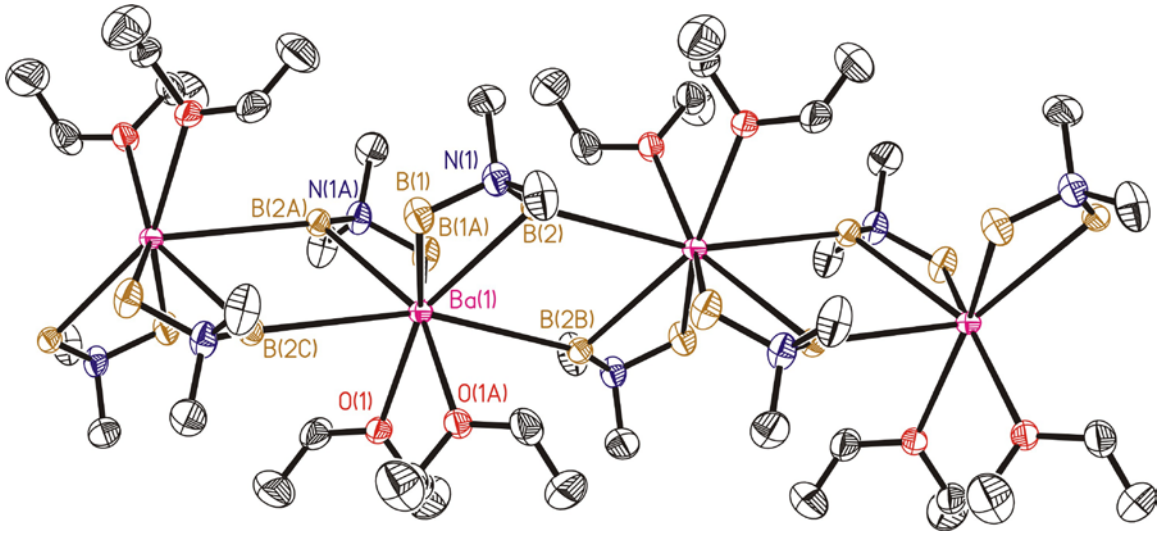

Figure 6.1. Molecular structure of $Ba(H_3BNMe_2BH_3)_2(Et_2O)_2$, **1**. Ellipsoids are drawn at the 35% probability level. The hydrogen atoms have been removed for clarity.

much longer at 3.477(5) Å (Table 6.2). The location of the hydrogen atoms provides an explanation of this difference. The shorter Ba···B contacts (to the BH_3 groups of the chelating DMADB ligands) are each κ^2*H* interactions, whereas the longer Ba···B contacts (to the BH_3 groups of DMADB ligands that chelate to neighboring Ba centers) are κ^1*H* interactions. The two BH_3 groups within each DMADB ligand are different: one of the BH_3 groups interacts with only one Ba center, whereas the other interacts with two. In all, the barium centers in **1** are 12-coordinate and are bound to 10 hydrogen atoms and two oxygen atoms.

The Ba···B distances are consistent with those seen in other barium borohydride complexes. For example, in $Ba(BH_3R)_2(L)_x$ complexes (R = H or $PMe_2[C(SiMe_3)_2]$; L = thf, diglyme, or 18-crown-6), the Ba···B distances to the bound κ^3*H*-BH_3R groups range from 2.975(9) to 3.063(6) Å.[50, 51] These comparisons show that the Ba···B distance decreases by ~0.2 Å as the denticity of the borohydride group increases by one (i.e., from κ^1*H* to κ^2*H* or from κ^2*H* to κ^3*H*). The Ba-O distances in the $Ba(BH_3R)_2(L)_x$ complexes, which range from 2.707(3) – 2.895(4) Å, compare well with those of 2.800(3) Å for the coordinated diethyl ether molecules in **1**.[51]

The structure of the 1,2-dimethoxyethane (dme) adduct **2** is also polymeric and the coordination geometry is very similar to that of **1**. The two oxygen atoms of the coordinated dme molecule occupy the same coordination sites that the two Et_2O molecules occupy in **1** (Figure 6.2). The chelating and bridging Ba···B distances of 3.251(3) – 3.271(3) Å and 3.412(3) – 3.461(3) Å, respectively, are similar to those in **1**, as are the Ba-O distances of 2.815(2) and 2.823(2) Å (Table 6.3).

The structure of the *N*,*N*,*N*′,*N*′-tetramethylethylenediamine (tmeda) adduct **3** is also similar except that the bridging Ba···B distances of 3.512(3) Å are ~0.05 Å longer than those

Table 6.3. Selected Bond Lengths and Angles for $Ba(H_3BNMe_2BH_3)_2(dme)$, **2**.

Bond Lengths (Å)			
Ba(1)-O(2)	2.8150(14)	Ba(1)-H(11)	2.873(16)
Ba(1)-O(1)	2.8233(15)	Ba(1)-H(12)	2.781(17)
Ba(1)-B(4)	3.251(3)	Ba(1)-H(21)	2.920(17)
Ba(1)-B(3)	3.252(3)	Ba(1)-H(22)	2.806(17)
Ba(1)-B(1)	3.260(3)	Ba(1)-H(31)	2.813(18)
Ba(1)-B(2)	3.271(2)	Ba(1)-H(32)	2.848(16)
Ba(1)-B(2)′	3.412(3)	Ba(1)-H(41)	2.850(17)
Ba(1)-B(3)″	3.461(3)	Ba(1)-H(42)	2.772(18)
Bond Angles (deg)			
B(1)-Ba(1)-B(2)	47.20(6)	B(2)′-Ba(1)-B(3)″	157.03(6)
B(1)-Ba(1)-B(3)	101.66(6)	O(1)-Ba(1)-O(2)	60.09(4)
B(1)-Ba(1)-B(4)	133.15(6)	O(1)-Ba(1)-B(1)	86.32(5)
B(1)-Ba(1)-B(2)′	112.93(6)	O(1)-Ba(1)-B(2)	102.10(6)
B(1)-Ba(1)-B(3)″	76.52(6)	O(1)-Ba(1)-B(3)	154.31(5)
B(2)-Ba(1)-B(3)	101.12(7)	O(1)-Ba(1)-B(4)	137.96(5)
B(2)-Ba(1)-B(4)	98.39(7)	O(1)-Ba(1)-B(2)′	72.58(5)
B(2)-Ba(1)-B(3)″	121.13(6)	O(1)-Ba(1)-B(3)″	87.76(5)
B(2)-Ba(1)-B(2)′	75.76(7)	O(2)-Ba(1)-B(1)	134.17(5)
B(3)-Ba(1)-B(4)	47.33(6)	O(2)-Ba(1)-B(2)	158.91(5)
B(3)-Ba(1)-B(2)′	124.24(6)	O(2)-Ba(1)-B(3)	98.80(5)
B(3)-Ba(1)-B(3)″	70.81(7)	O(2)-Ba(1)-B(4)	90.02(6)
B(4)-Ba(1)-B(2)′	77.56(6)	O(2)-Ba(1)-B(2)′	87.35(5)
B(4)-Ba(1)-B(3)″	112.06(6)	O(2)-Ba(1)-B(3)″	72.27(5)

Symmetry transformations used to generate equivalent atoms: ′ = -x+1, -y, -z; ″ = -x, -y, -z.

Table 6.4. Selected Bond Lengths and Angles for $Ba(H_3BNMe_2BH_3)_2(tmeda)$, **3.**

	Bond Lengths (Å)		
Ba(1)-B(1)	3.237(3)	Ba(1)-H(12)	2.794(17)
Ba(1)-B(2)	3.261(3)	Ba(1)-H(21)	2.794(16)
Ba(1) -B(2)′	3.512(3)	Ba(1)-H(22)	2.851(16)
Ba(1)-N(2)	2.9965(15)	Ba(1)-H(23)′	2.832(17)
Ba(1)-H(11)	2.808(17)		
	Bond Angles (deg)		
B(1)-Ba(1)-B(2)	47.29(6)	B(2)-Ba(1)-B(2)′	103.11(10)
B(1)-Ba(1)-B(1)′	132.15(10)	B(2)-Ba(1)-N(2)	99.04(6)
B(1)-Ba(1)-B(2)′	100.02(7)	B(2)-Ba(1)-N(2)′	154.39(6)
B(1)-Ba(1)-N(2)	85.66(6)	N(2)-Ba(1)-B(2)′	154.39(6)
B(1)-Ba(1)-N(2)′	140.03(6)	N(2)′-Ba(1)-B(2)′	99.04(6)
B(2)-Ba(1)-B(1)′	100.02(7)	N(2)-Ba(1)-N(2)′	63.24(6)

Symmetry transformations used to generate equivalent atoms: ′ = -x+2, y, $-z+^{3}/_{2}$

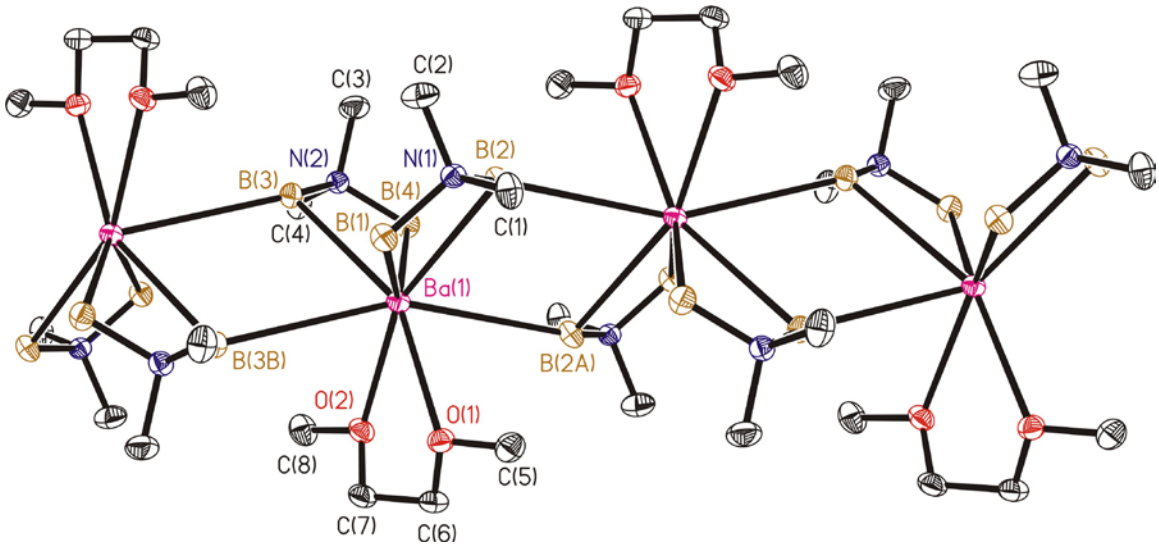

Figure 6.2. Molecular structure of $Ba(H_3BNMe_2BH_3)_2(dme)$, **2**. Ellipsoids are drawn at the 35% probability level. The hydrogen atoms have been removed for clarity.

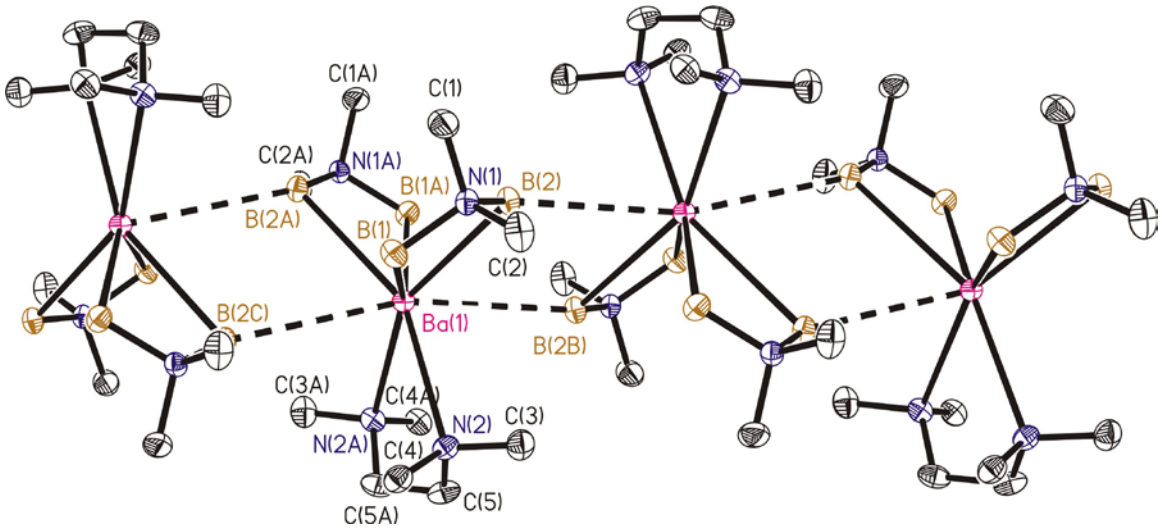

Figure 6.3. Molecular structure of $Ba(H_3BNMe_2BH_3)_2(tmeda)$, **3**. Ellipsoids are drawn at the 35% probability level. The hydrogen atoms have been removed for clarity. The dashed lines reflect the increased bridging Ba···B distances relative to **1** and **2**.

in **1** and **2**, which can be attributed to the increase steric bulk of the tmeda ligand relative to Et_2O and dme (Figure 6.3). As seen in 1 and 2, the κ^2*H* (i.e, doubly hydrogen bridged) Ba···B distances of 3.261(3) Å to the BH_3 groups that are both chelating and bridging to an adjacent metal (boron atom B2) are ~0.02 longer than the κ^2*H* Ba···B distances of 3.237(3) Å to the BH_3 groups that have no bridging interaction (B1) (Table 6.4). The Ba-N distance of at 2.996(2) Å to the coordinated tmeda molecule is ca. 0.2 Å longer than the Ba-O distances observed in **1** and **2**. This difference, which is much larger than the 0.03 Å difference in atomic radii between oxygen and nitrogen, most likely reflects the larger degree of steric crowding in **3**.[52]

X-ray quality crystals of the 12-crown-4 adduct **4** could not be grown, but cooling concentrated solutions of **4** in thf yielded **4′**, which has the stoichiometry $Ba(H_3BNMe_2BH_3)_2$(12-crown-4)(thf)·thf. Unlike the polymeric structures of **1**-**3**, compound **4′** is a monomer. The coordination geometry of the barium center in **4′** is best described as a distorted capped antiprism, in which the thf molecule occupies the capping site and the 12-crown-4 ligand and the boron atoms define the antiprism (Figure 6.4). Boron atoms B2 and B4, which are located closest to the 12-crown-4 molecule, form Ba···B distances of 3.399(7) Å and 3.316(8) Å that are longer than Ba1···B1 and Ba1···B3 distances, which are 3.270(7) and 3.278(7) Å (Table 6.5). All of these entail κ^2*H* interactions, so that the overall coordination number of the barium center is 13 coordinate. The Ba-O distances to the thf and 12-crown-4 ligands range from 2.838(4) - 2.922(4) Å, and are longer than those in **1** and **2**, which may be attributed to the higher coordination number of 13 vs. 12 in the latter species.

For the bis(diglyme) adduct **5**, one of the DMADB ligand chelates to the Ba center in the typical κ^2*H*-$H_3BNMe_2BH_3$-κ^2*H* fashion, but the other DMADB ligand binds to the metal

by means of only one BH_3 group in a κ^3*H* fashion (Figure 6.5). This is first time this bonding mode has ever been observed for the DMADB ligand. Overall, the barium atom forms bonds with seven hydrogen atoms and six oxygen atoms, so that the total coordination number is 13. The two DMADB ligands are arranged *trans* with respect to each other and the two diglyme molecules are approximately coplanar and wrap around the metal atom to form an equatorial belt. The six equatorial oxygen atoms and the three Ba-bound boron atoms describe a nine-coordinate polyhedron that has been given the plebian name of "the hula hoop".[53] The idealized hula hoop polyhedron, which has C_{2v} symmetry, consists of a planar hexagonal girdle capped on one side by a single vertex, and on the other by a pair of vertices. In **5**, the six oxygen atoms of the two diglyme molecules are not exactly coplanar, and deviate more or less from the mean plane in order to accommodate the steric demands of the chelating DMADB ligand. As a result, the B-Ba-O angles to the κ^3*H*-DMADB ligand of 79.58(5) – 88.74(5)° are all less than the ideal 90° angle (Table 6.6). A few other complexes have been described that adopt a hula hoop geometry; the present complex, however, is evidently the first to adopt it without the constraints of a cyclic hexadentate ligand.[53]

The Ba···B distances of 3.266(3) and 3.280(3) Å to the chelating DMADB ligand are similar to those seen in **1**-**4**. In contrast, the Ba···B distance of 3.051(2) Å to the ^{3}*H*-DMADB ligand is much shorter, as expected from the increased denticity. This Ba···B distance is similar to those reported for the $Ba(BH_3R)(L)_x$ complexes mentioned above, which also contain metal-bound κ^3*H*-BH_3R groups. The Ba-O bond distances, which range from 2.827(1) to 2.970(1) Å, are longer than those observed for **1**, **2**, and **4′**, probably owing to the increased crowding around the metal due to the arrangement of the six oxygen atoms within the same plane. Apart from the chelating nature of one of the DMADB ligands, the structure of **5** is similar to those of $Ba(BH_4)_2(diglyme)_2$ and $Ba(BH_4)_2$(18-crown-6). In both

Table 6.5. Selected Bond Lengths and Angles for $Ba(H_3BNMe_2BH_3)_2$(12-crown 4)(thf), **4′**.

Bond Lengths (Å)			
Ba(1)-O(1)	2.854(4)	Ba(1)-H(11)	2.8983
Ba(1)-O(11)	2.864(4)	Ba(1)-H(12)	2.7544
Ba(1)-O(12)	2.904(4)	Ba(1)-H(21)	3.095
Ba(1)-O(13)	2.922(4)	Ba(1)-H(23)	2.847
Ba(1)-O(14)	2.838(4)	Ba(1)-H(31)	2.7848
Ba(1)-B(1)	3.270(7)	Ba(1)-H(32)	2.9063
Ba(1)-B(2)	3.399(7)	Ba(1)-H(41)	2.8249
Ba(1)-B(3)	3.278(7)	Ba(1)-H(43)	2.9513
Ba(1)-B(4)	3.316(8)		
Bond Angles (deg)			
O(1)-Ba(1)-O(11)	140.52(12)	O(12)-Ba(1)-B(1)	170.88(16)
O(1)-Ba(1)-O(12)	118.48(12)	O(13)-Ba(1)-B(1)	129.46(16)
O(1)-Ba(1)-O(13)	66.74(12)	O(14)-Ba(1)-B(1)	92.53(15)
O(1)-Ba(1)-O(14)	82.60(12)	O(1)-Ba(1)-B(2)	114.85(15)
O(11)-Ba(1)-O(12)	57.71(13)	O(11)-Ba(1)-B(2)	74.40(15)
O(11)-Ba(1)-O(13)	86.23(11)	O(12)-Ba(1)-B(2)	125.49(16)
O(11)-Ba(1)-O(14)	58.29(13)	O(13)-Ba(1)-B(2)	149.11(17)
O(12)-Ba(1)-O(13)	55.95(12)	O(14)-Ba(1)-B(2)	91.29(17)
O(12)-Ba(1)-O(14)	85.04(11)	O(1)-Ba(1)-B(3)	76.29(15)
O(13)-Ba(1)-O(14)	57.88(12)	O(11)-Ba(1)-B(3)	136.56(16)
B(1)-Ba(1)-B(2)	45.67(17)	O(12)-Ba(1)-B(3)	87.04(15)
B(1)-Ba(1)-B(3)	99.23(19)	O(13)-Ba(1)-B(3)	94.37(16)
B(1)-Ba(1)-B(4)	105.1(2)	O(14)-Ba(1)-B(3)	150.41(16)
B(2)-Ba(1)-B(3)	116.27(19)	O(1)-Ba(1)-B(4)	122.16(15)
B(2)-Ba(1)-B(4)	87.1(2)	O(11)-Ba(1)-B(4)	95.72(16)
B(3)-Ba(1)-B(4)	46.83(17)	O(12)-Ba(1)-B(4)	74.36(17)
O(1)-Ba(1)-B(1)	69.76(15)	O(13)-Ba(1)-B(4)	119.16(18)
O(11)-Ba(1)-B(1)	113.65(16)	O(14)-Ba(1)-B(4)	153.22(16)

Table 6.6. Selected Bond Lengths and Angles for $Ba(H_3BNMe_2BH_3)_2(diglyme)_2$, **5**.

	Bond Lengths (Å)		
Ba(1)-O(1)	2.9474(13)	Ba(1)-B(3)	3.051(2)
Ba(1)-O(2)	2.8353(14)	Ba(1)-H(11)	2.79(2)
Ba(1)-O(3)	2.9698(14)	Ba(1)-H(12)	2.830(16)
Ba(1)-O(4)	2.8905(13)	Ba(1)-H(21)	2.847(17)
Ba(1)-O(5)	2.9539(13)	Ba(1)-H(22)	2.918(19)
Ba(1)-O(6)	2.8273(13)	Ba(1)-H(31)	2.773(17)
Ba(1)-B(1)	3.266(3)	Ba(1)-H(32)	2.931(15)
Ba(1)-B(2)	3.280(3)	Ba(1)-H(33)	2.952(15)
	Bond Angles (deg)		
O(1)-Ba(1)-O(2)	56.26(4)	O(1)-Ba(1)-B(1)	104.11(6)
O(1)-Ba(1)-O(3)	114.72(4)	O(2)-Ba(1)-B(1)	89.86(6)
O(1)-Ba(1)-O(4)	65.56(4)	O(3)-Ba(1)-B(1)	69.20(5)
O(1)-Ba(1)-O(5)	123.73(4)	O(4)-Ba(1)-B(1)	121.74(5)
O(1)-Ba(1)-O(6)	167.24(4)	O(5)-Ba(1)-B(1)	101.79(6)
O(2)-Ba(1)-O(3)	58.83(4)	O(6)-Ba(1)-B(1)	87.20(6)
O(2)-Ba(1)-O(4)	119.09(4)	O(1)-Ba(1)-B(2)	85.86(6)
O(2)-Ba(1)-O(5)	167.48(4)	O(2)-Ba(1)-B(2)	114.98(6)
O(2)-Ba(1)-O(6)	118.95(4)	O(3)-Ba(1)-B(2)	116.23(6)
O(4)-Ba(1)-O(3)	169.00(4)	O(4)-Ba(1)-B(2)	74.70(5)
O(5)-Ba(1)-O(3)	121.03(4)	O(5)-Ba(1)-B(2)	76.85(6)
O(6)-Ba(1)-O(3)	63.41(4)	O(6)-Ba(1)-B(2)	106.42(6)
O(4)-Ba(1)-O(5)	58.29(4)	O(1)-Ba(1)-B(3)	87.82(5)
O(4)-Ba(1)-O(6)	113.65(4)	O(2)-Ba(1)-B(3)	81.10(6)
O(5)-Ba(1)-O(6)	57.91(4)	O(3)-Ba(1)-B(3)	88.74(5)
B(1)-Ba(1)-B(2)	47.05(6)	O(4)-Ba(1)-B(3)	80.27(5)
B(1)-Ba(1)-B(3)	157.68(6)	O(5)-Ba(1)-B(3)	86.39(6)
B(2)-Ba(1)-B(3)	154.59(6)	O(6)-Ba(1)-B(3)	79.58(5)

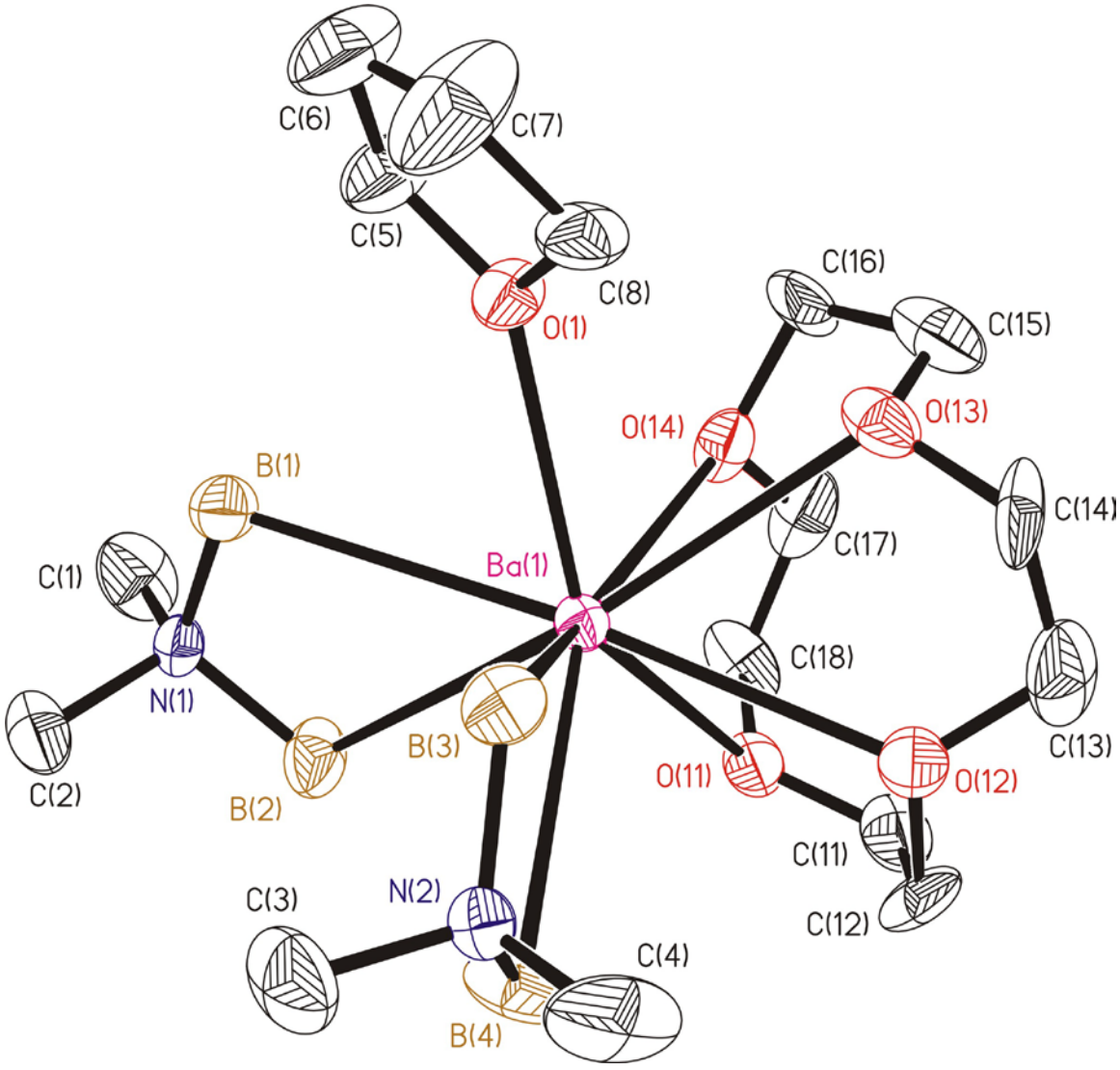

Figure 6.4. Molecular structure of $Ba(H_3BNMe_2BH_3)_2$(12-crown-4)(thf), **4′**. Ellipsoids are drawn at the 35% probability level. The hydrogen atoms have been removed for clarity.

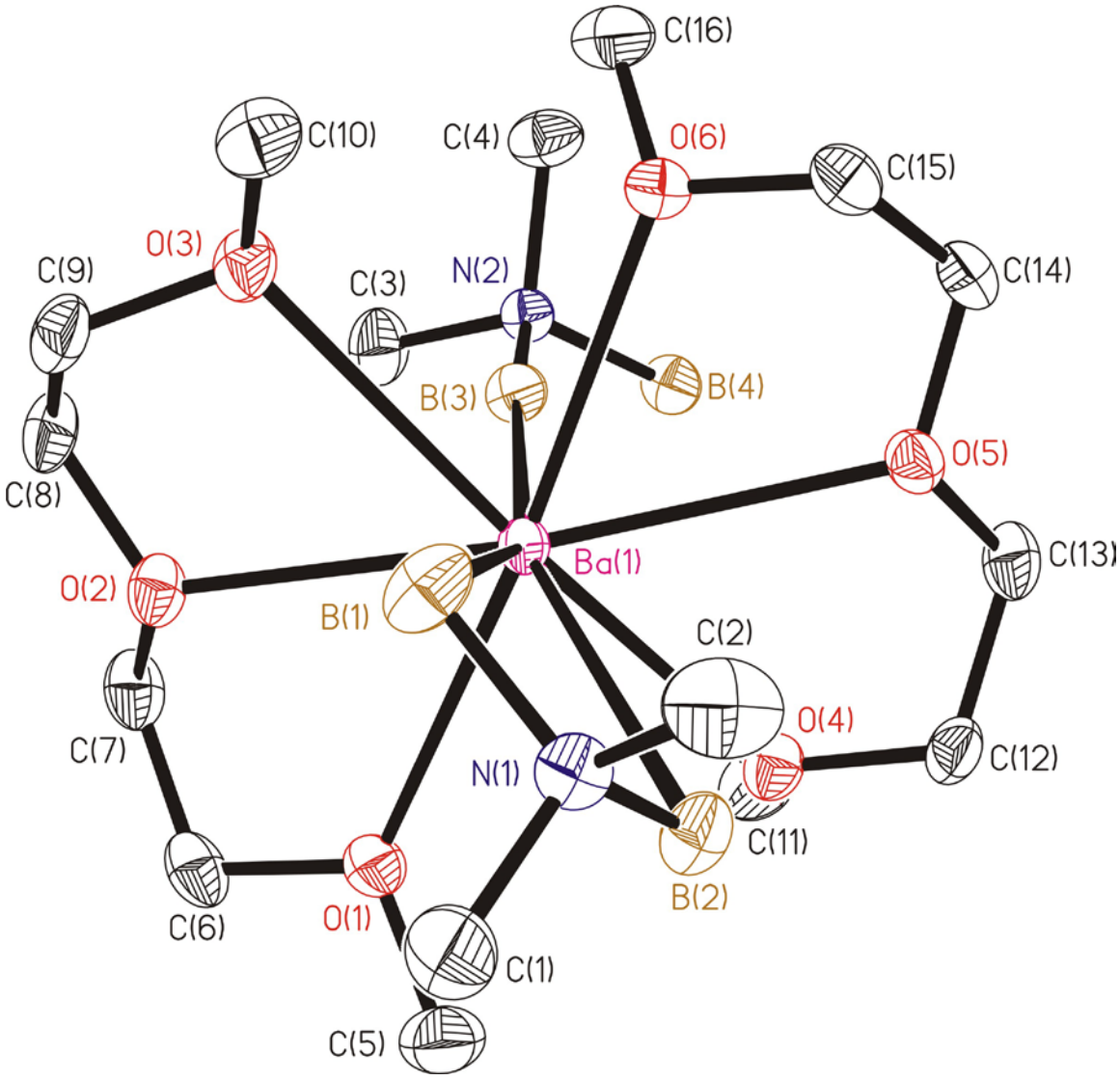

Figure 6.5. Molecular structure of $Ba(H_3BNMe_2BH_3)_2(diglyme)_2$, **5**. Ellipsoids are drawn at the 35% probability level. The hydrogen atoms have been removed for clarity.

of these complexes, the six oxygen atoms from the two diglyme molecules and the 18-crown-6 ligand describe a hexagonal bipyramid, in which the two κ^3*H*-BH_4 groups occupy the axial positions.

NMR Spectra. The barium DMADB complexes are insoluble in non-polar solvents such benzene and toluene. DMADB complexes are also known to react with halogenated solvents such as chloroform and dichloromethane so thf-d_8 and dmso-d_6 were used to obtain the NMR data. The dmso-d_6 solvent so that direct comparisons could be made to NMR data of selected $Ba(BH_4)_2$ complexes, which were collected in this solvent.[50] It is also much cheaper than thf-d_8. The ^{1}H NMR spectra of **1**, **2**, and **5** in thf-d_8 all reveal a singlet at δ 2.23 for the NMe_2 group and a broad 1:1:1:1 quartet (J_{BH} = 87 Hz) at δ 1.81 for the BH_3 groups. The ^{11}B NMR spectra all contain a binomial quartet (J_{BH} ~ 90 Hz) at δ -7.6. The three hydrogen atoms on each BH_3 group are either chemically equivalent or are rapidly exchanging with one another on the NMR time scale, as is typically observed for borohydride complexes.[54] Similarly, the ^{1}H NMR spectra of **3** and **4** in dmso-d_6 all show a singlet at δ 2.09 for the NMe_2 resonance and a quartet at δ 1.39 for the BH_3 groups; the ^{11}B NMR shifts are δ -8.6. The identical position and nature of these NMR resonances can be attributed to the displacement of the ancillary ligands upon dissolution of **1**-**5** in the coordinating deuterated solvents. The proton NMR shifts due to the Lewis bases in **2**-**5** closely match the literature values for free ligand in these solvents, which provides further evidence that these ligands are displaced from the Ba center when the complexes are dissolved in coordinating solvents.[55]

Infrared and Mass Spectra. The IR spectra of **1**-**5** contain features for both terminal and bridging B-H stretches that are separated by 60 – 70 cm^{-1}: the terminal B-H stretching bands range from 2290 – 2309 $cm^{-1}$and the strong bridging bands range from 2236 – 2249

cm^{-1}. The frequencies of the B-H bands closely match those reported for $Na(H_3BNMe_2BH_3)$ (2312 and 2244 cm^{-1}),[46] and the relatively small frequency difference between the frequencies for the terminal and bridging B-H stretching modes indicates that the M-H-B bonding is relatively weak and ionic. Interestingly, the bonding between magnesium and DMADB ligands is substantially stronger: the terminal and bridging B-H stretching frequencies in $Mg(H_3BNMe_2BH_3)_2$, 2449 and 2195 cm^{-1}, respectively, are separated by 250 cm^{-1}.[49]

Field desorption mass spectra of **3** and **5** at high emitter currents showed a peak envelope at *m*/*z* 491 corresponding to $Ba_2(H_3BNMe_2BH_3)_3^+$. A peak at *m*/*z* 210 corresponding to $Ba(H_3BNMe_2BH_3)^+$ was also observed in the spectrum of **5**. No Ba-containing ions were seen in the FDMS spectra of **1**, **2**, or **4**, or in the field ionization mass spectra of any of the complexes.

Melting points and volatility studies. The diglyme adduct **5** melts sharply at 102 °C, whereas compounds **1**-**4** do not melt even at temperatures as high as 215 °C. Instead, heating **1** and **2** results in the deposition of colorless crystals on the cooler parts of the melting point capillaries, suggestive of thermal decomposition of the DMADB ligand. None of the complexes is appreciably volatile in vacuum. For example, attempts to sublime **5** at 10^{-2} Torr did not yield any sublimate up to 135 °C, at which point only liquid (presumably diglyme) began to condense on the coldfinger.

Discussion

Ideal metal-containing precursors useful for the chemical vapor deposition of thin films are highly volatile. One design criterion is that the ligands must be sufficiently large to saturate (or nearly saturate) the coordination sphere of the metal atom, so as to prevent the

formation of non-volatile polymers. In addition, the ligands must be sufficiently strongly bound robust so that the complexes sublime rather than decompose when heated.

The present results show that the *N*,*N*-dimethylaminodiboranate (DMADB) ligand is not large enough to saturate the coordination sphere of the Ba^{2+} ion. Even when the barium DMADB complexes are provided with Et_2O, dme, or tmeda ligands as ancillary Lewis bases, the resulting heteroleptic complexes are still polymeric, as observed in the structures of compounds **1**-**3**. We have, however, been able to obtain monomeric complexes with the assistance of multidentate Lewis bases such as 12-crown-4 and diglyme. Interestingly, in complex **5**, the steric demands of the chelating diglyme molecules force one of the DMADB ligands to bind to Ba through only one of its BH_3 groups, rather than to both. This result demonstrates that care must be taken in the choice of ancillary Lewis base. If the Lewis base is too strongly coordinating or too sterically demanding, it can displace coordinated -BH_3 groups, with possible formation of salts with charge-separated DMDAB anions. We have seen very similar behavior in Lewis base adducts of magnesium B_3H_8 complexes, for example.[56]

The Ba-H-B bonding in **1**-**5** can be best described as ionic, and the barium complexes exhibit properties closer to those of $Na(H_3BNMe_2BH_3)$ than to the group 2 congener $Mg(H_3BNMe_2BH_3)_2$. First, $Mg(H_3BNMe_2BH_3)_2$ is highly soluble in non-polar solvents (benzene and toluene), has a low melting point, and is highly volatile, whereas **1**-**5** and $Na(H_3BNMe_2BH_3)$ possess none of these properties.[46, 49] Second, the frequency separation between the terminal and bridging B-H stretches in the IR spectrum is much smaller than that in the magnesium analogs, but rather similar to that in the sodium salt. Third, the ability of diglyme to displace -BH_3 groups (as seen in the structure of **5**) is also consistent with ionic M-DMADB bonding.

Although to date none of the barium DMADB complexes we have prepared sublimes in vacuum, the results are helping us refine the synthetic strategies that lead to the discovery of new and useful CVD precursors. Barium is a stringent test of these strategies because its large radius, small charge, and ionic bonding. As discussed above, barium complexes often have polymeric structures, weakly bound ligands, and large intermolecular attractive forces that render them completely non-volatile. The development of new classes of volatile barium complexes would be of great interest in the context of the deposition of thin films of perovskite ferrielectrics and high temperature superconductors.

Experimental

All operations were carried out in vacuum or under argon using standard Schlenk techniques. All glassware was dried in an oven at 150 °C, assembled hot, and allowed to cool under vacuum before use. Tetrahydrofuran, 1,2-dimethoxyethane, diethyl ether, and pentane were distilled under nitrogen from sodium/benzophenone and degassed with argon immediately before use. Diglyme and TMEDA (Aldrich) were distilled from sodium under argon. The crown ether 12-crown-4 (Avocado Research) was dried over 4 Å sieves (Aldrich). Anhydrous $BaBr_2$ (Strem) was used as received. The salt $Na(H_3BNMe_2BH_3)$ was prepared by a literature route.[46]

Elemental analyses were carried out by the University of Illinois Microanalytical Laboratory. The IR spectra were recorded on a Nicolet Impact 410 infrared spectrometer as Nujol mulls between KBr plates. The ^{1}H NMR data were obtained on a Varian Unity 400 instrument at 400 MHz or on a Varian Unity Inova 600 instrument at 600 MHz. The ^{11}B NMR data were collected on a General Electric GN300WB instrument at 96 MHz or on a Varian Unity Inova 600 instrument at 192 MHz. Chemical shifts are reported in δ units

(positive shifts to high frequency) relative to TMS (^{1}H) or BF_3•Et_2O (^{11}B). Field ionization (FI) mass spectra were recorded on a Micromass 70-VSE mass spectrometer. The shapes of all peak envelopes correspond with those calculated from the natural abundance isotopic distributions in the observed spectra. Melting points were determined in closed capillaries under argon on a Thomas-Hoover Unimelt apparatus.

Bis(*N*,*N*-dimethylaminodiboranato)bis(diethylether)barium(II), $Ba(H_3BNMe_2BH_3)_2$ $(Et_2O)_2$ (1). To a suspension of $BaBr_2$ (0.50 g, 1.7 mmol) in tetrahydrofuran (20 mL) at 0 °C was added a solution of sodium *N*,*N*-dimethylaminodiboranate (0.32 g, 3.4 mmol) in tetrahydrofuran (20 mL). The reaction mixture was warmed to room temperature and stirred for 41 h. The solvent was removed under vacuum to afford a white residue. The residue was extracted with diethyl ether (35 mL), the extracts were filtered, and the filtrates were combined, concentrated to ca. 30 mL, and cooled to -20 ˚C to yield a crop of large, white needles. The mother liquor was concentrated to ca. 8 mL and cooled to -20 °C to yield an additional crop of white needles. These crystals readily desolvated to the following compound.

Bis(*N*,*N*-dimethylaminodiboranato)barium(II), $Ba(H_3BNMe_2BH_3)_2(Et_2O)_x$ (1′). Crystals of **1** were left under dynamic vacuum at room temperature for 12 h. Yield: 0.33 g (63 %). M.p. >215 °C. Anal. Calcd. for $Ba(H_3BNMe_2BH_3)_2(Et_2O)_{0.45}$: C, 22.2; H, 9.14; N, 8.92. Found: C, 22.1; H, 9.28; N, 8.62. ^{1}H NMR (thf-d_8, 20 °C): δ 1.81 (br q, J_{BH} = 87 Hz, BH_3, 12 H), 2.23 (s, NMe_2, 12 H). ^{11}B NMR (thf-d_8, 20 °C): δ -7.6 (1:3:3:1 q, J_{BH} = 91 Hz, BH_3). IR (cm^{-1}): 2398 sh, 2306 vs, 2246 vs, 2091 w, 1217 s, 1194 sh, 1176 s, 1150 s, 1103 w, 1030 s, 951 m, 910 m, 805 w, 413 w.

In a similar experiment, using an identical work-up, the microanalysis supported $Ba(H_3BNMe_2BH_3)_2(Et_2O)_{0.30}$. Anal. Calcd.: C, 20.6; H, 8.98; N, 9.24. Found: C, 20.8; H,

9.11; N, 9.32. Heating this same batch of material at 100 °C at 10^{-2} Torr for 24 hours yields $Ba(H_3BNMe_2BH_3)_2(Et_2O)_{0.04}$. Anal. Calcd.: C, 17.6; H, 8.67; N, 9.87. Found: C, 17.6; H, 8.41; N, 9.66.

Bis(*N*,*N*-dimethylaminodiboranato)(1,2-dimethoxyethane)barium(II), (2). To a solution of **1′** (73 mg, 0.23 mmol) in diethyl ether (10 mL) was added 1,2-dimethoxyethane (10 mL). The solution was evaporated to dryness under vacuum to yield a white solid. Yield: 75 mg (88 % after transfer losses). Crystals of **2** suitable for diffraction studies can be grown from Et_2O. M.p. >215 °C. Anal. Calcd. for $C_8H_{34}B_4N_2O_2Ba$: C, 25.9; H, 9.24; N, 7.55. Found: C, 26.3; H, 9.59; N, 7.11. ^{1}H NMR (thf-d_8, 20 °C): δ 1.80 (br 1:1:1:1 q, J_{BH} = 87 Hz, BH_3, 12 H), 2.23 (s, NMe_2, 12 H), 3.27 (s, OMe, 6 H), 3.43 (s, OCH_2, 4 H). ^{11}B NMR (thf-d_8, 20 °C): δ -7.6 (q, J_{BH} = 91 Hz, BH_3). IR (cm^{-1}): 2309 vs, 2287 sh, 2242 s, 1192 m, 1176 s, 1150 s, 1119 w, 1100 w, 1071 s, 1027 s, 948 m, 907 m, 859 m, 837 w, 805 m.

Bis(*N*,*N*-dimethylaminodiboranato)(*N*,*N*,*N′*,*N′*-tetramethylethylenediamine)-barium(II), (3). To a solution of **1′** (0.16 g, 0.51 mmol) in diethyl ether (30 mL) was added *N*,*N*,*N′*,*N′*-tetramethylethylenediamine (0.25 mL, 1.7 mmol). A thick, white precipitate formed immediately. The mixture was stirred overnight, and then the solid was collected by filtration, washed with pentane (3 x 20 mL), and dried under vacuum to yield a white powder. Yield: 0.19 g (94 %). Crystals of **3** suitable for diffraction studies can be grown from Et_2O. M.p. >215 °C. Anal. Calcd. for $C_{10}H_{40}B_4N_4Ba$: C, 30.3; H, 10.2; N, 14.1. Found: C, 30.3; H, 10.8; N, 13.6. ^{1}H NMR (DMSO-d_6, 20 °C): δ 1.39 (1:1:1:1 q, J_{BH} = 91 Hz, BH_3, 12 H), 2.09 (br s, NMe_2 of DMADB, 12 H), 2.11 (s, NMe_2 of tmed, 6 H), 2.27 (s, NCH_2, 4 H). ^{11}B NMR (DMSO-d_6, 20 °C): δ -8.6 (q, J_{BH} = 92 Hz, BH_3). MS (FD) [fragment ion, relative abundance]: *m*/*z* 491 [$Ba_2(H_3BNMe_2BH_3)_3^+$, 100]. IR (cm^{-1}): 2794 m, 2778 m, 2379 m, 2309 vs, 2283 vs, 2255 s, 2243 vs, 2090 w, 1293 m, 1245 w, 1213 s, 1192 w, 1176

s, 1154 vs, 1128 m, 1078 w, 1027 s, 954 m, 942 m, 919 w, 908 w, 808 m, 786 m, 697 w, 574 w, 438 w, 413 w.

Bis(*N*,*N*-dimethylaminodiboranato)(12-crown-4)barium(II), (4). To a solution of **1′** (0.10 g, 0.32 mmol) in diethyl ether (25 mL) was added 12-crown-4 (70 μL, 0.43 mmol). A thick, white precipitate formed immediately. The mixture was stirred overnight, and then the solid was collected by filtration, washed with pentane (3 x 20 mL), and dried under vacuum to yield a white powder. Yield: 0.14 g (96 %). M.p. >215 °C. Anal. Calcd. for $C_{12}H_{40}B_4N_2O_4Ba$: C, 31.5; H, 8.82; N, 6.13. Found: C, 31.8; H, 9.16; N, 5.90. ^{1}H NMR (DMSO-d_6, 20 °C): δ 1.39 (1:1:1:1 q, J_{BH} = 91 Hz, BH_3, 12 H), 2.10 (br s, NMe_2, 12 H), 3.56 (s, OCH_2, 16 H). ^{11}B NMR (DMSO-d_6, 20 °C): δ -8.6 (q, J_{BH} = 92 Hz, BH_3). IR (cm^{-1}): 2394 w, 2340 w, 2303 vs, 2249 s, 1305 w, 1290 w, 1248 w, 1216 m, 1205 m, 1177 s, 1149 s, 1133 m, 1086 s, 1018 vs, 933 w, 921 m′ 904 w, 852 s, 800 w, 561 w, 548 w.

Bis(*N*,*N*-dimethylaminodiboranato)(12-crown-4)(tetrahydrofuran)barium(II) Tetrahydrofuran, (4′). Concentrating and cooling solutions of **4** in thf produced crystals of the solvate **4′** suitable for diffraction studies.

Bis(*N*,*N*-dimethylaminodiboranato)bis[di(2-methoxyethyl)ether]barium(II), (5). To $BaBr_2$ (0.50 g, 1.7 mmol) and sodium *N*,*N*-dimethylaminodiboranate (0.32 g, 3.4 mmol) was added di(2-methoxyethyl)ether (50 mL). After the cloudy mixture had been stirred for 20 h, the solvent was removed by distillation under vacuum to afford a white residue. The residue was extracted with diethyl ether (2 x 30 mL), the extracts were filtered, and the filtrates were combined, concentrated to ca. 55 mL, and cooled to -20 ˚C to yield 0.21 g of white crystals. The mother liquor was concentrated to 10 mL and cooled to -20 °C to yield an additional 0.10 g of white needles. Yield: 0.31 g (34 %). M.p. 102 °C. Anal. Calcd. for $C_{16}H_{52}B_4N_2O_6Ba$: C, 35.0; H, 9.54; N, 5.10. Found: C, 34.7; H, 9.89; N, 5.06. ^{1}H NMR

(thf-d_8, 20 °C): δ 1.79 (br q, J_{BH} = 87 Hz, BH_3, 12 H), 2.23 (s, NMe_2, 12 H), 3.29 (s, OMe, 12 H), 3.46 (m, OCH_2, 8 H), 3.55 (m, OCH_2, 8 H). ^{11}B NMR (thf-d_8, 20 °C): δ -7.6 (q, J_{BH} = 91 Hz, BH_3). MS(FD) [fragment ion, relative abundance]: *m*/*z* 210 [$Ba(H_3BNMe_2BH_3)^+$, 100], 491 [$Ba_2(H_3BNMe_2BH_3)_3^+$, 70]. IR (cm^{-1}): 2340 sh, 2290 vs, 2236 s, 2186 sh, 2069 m, 1353 m, 1302 w, 1258 m, 1203 s, 1174 s, 1150 vs, 1135 s, 1102 s, 1083 s, 1071 s, 1061 s, 1015 s, 995 m, 942 sh, 925 m, 904 w, 873 sh, 863 s, 830 w, 799 m, 685 w, 529 w, 457 w, 413 w.

Crystallographic Studies. Single crystals obtained from diethyl ether (**1**, **2**, **3** and **5**) or tetrahydrofuran (**4′**) were mounted on glass fibers with Paratone-N oil (Exxon) and immediately cooled to -80 °C in a cold nitrogen gas stream on the diffractometer. Standard peak search and indexing procedures, followed by least-square refinement yielded the cell dimensions given in Table 6.1. The measured intensities were reduced to structure factor amplitudes and their estimated standard deviations by correction for background and Lorentz and polarization effects. No corrections for crystal decay were necessary but a face-indexed absorption correction was applied. Systematically absent reflections were deleted and symmetry equivalent reflections were averaged to yield the set of unique data. Except where noted, all unique data were used in the least-squares refinements. The analytical approximations to the scattering factors were used, and all structure factors were corrected for both the real and imaginary components of anomalous dispersion. Unless otherwise specified, correct atomic position(s) were deduced from an E-map (SHELX) and from subsequent least-squares refinement and difference Fourier calculations. Except where noted, hydrogen atoms attached to boron were located in the difference maps and hydrogen atoms attached to carbon were placed in idealized positions with C-H (methyl) = 0.98 Å and C-H (methylene) = 0.99Å; the methyl groups were allowed to rotate about their respective

C-N or C-O axes to find the best least-squares positions. In the final cycle of least squares, independent anisotropic displacement factors were refined for the non-hydrogen atoms. The displacement parameters for methylene hydrogens were set equal to 1.2 times U_{eq} for the attached carbon; those for methyl hydrogens were set to 1.5 times U_{eq}. No correction for isotropic extinction was necessary. Successful convergence was indicated by the maximum shift/error of 0.000 for the last cycle. A final analysis of variance between observed and calculated structure factors showed no apparent errors. Aspects of the refinements unique to each structure are reported in the Supporting Information.

$Ba(H_3BNMe_2BH_3)_2(Et_2O)_2$, 1. The systematic absences hkl ($h + k \neq 2n$) or $h0l$ ($l \neq 2n$) were consistent with the space groups Cc and $C2/c$. The centrosymmetric space group $C2/c$ was chosen, and this choice was confirmed by successful refinement of the proposed model. The reflection $\bar{2}23$ was a statistical outlier and was deleted; the remaining 2112 unique data were used in the least squares refinement. The quantity minimized by the least-squares program was $\Sigma w(F_o^2 - F_c^2)^2$, where $w = \{[\sigma(F_o)]^2 + (0.0444P)^2\}^{-1}$ and $P = (F_o^2 + 2F_c^2)/3$. The largest peak in the final Fourier difference map (1.03 eÅ^{-3}) was located 1.02 Å from Ba1.

$Ba(H_3BNMe_2BH_3)_2$(dme), 2. The monoclinic lattice and systematic absences $0k0$ ($k \neq 2n$) and $h0l$ ($l \neq 2n$) were uniquely consistent with the space group $P2_1/c$, which was confirmed by the success of the subsequent refinement. The quantity minimized by the least-squares program was $\Sigma w(F_o^2 - F_c^2)^2$, where $w = \{[\sigma(F_o)]^2 + (0.0135P)^2\}^{-1}$ and $P = (F_o^2 + 2F_c^2)/3$. All hydrogen atoms were located in the difference maps, and their positions were refined with independent isotropic displacement parameters. The largest peak in the final Fourier difference map (0.80 eÅ^{-3}) was located 1.33 Å from Ba1.

$Ba(H_3BNMe_2BH_3)_2$(tmeda), 3. The systematic absences hkl ($h + k \neq 2n$) and $h0l$ ($l \neq$

2*n*) were consistent with the space groups *Cc* and *C*2/*c*. The centrosymmetric space group *C*2/*c* was chosen, and this choice was confirmed by successful refinement of the proposed model. Correct positions for the Ba atoms were deduced from a Patterson map (SHELXTL). The quantity minimized by the least-squares program was $\Sigma w(F_o^2 - F_c^2)^2$, where $w = \{[\sigma(F_o)]^2 + (0.0077P)^2\}^{-1}$ and $P = (F_o^2 + 2F_c^2)/3$. The largest peak in the final Fourier difference map (0.33 eÅ^{-3}) was located 1.13 Å from Ba1.

Ba($H_3BNMe_2BH_3$)$_2$(12-crown-4)(thf), 4′. The triclinic lattice and the average values of the normalized structure factors suggested the space group $P\bar{1}$, which was confirmed by the success of the subsequent refinement. The reflections $\bar{1}01$, 021, 101, and $\bar{1}\bar{1}1$ were statistical outliers and were deleted; the remaining 11617 unique data were used in the least squares refinement. The coordinated 12-crown-4 ligand in molecule 2 and the non-coordinated thf molecule closest to molecule 2 were each disordered over two positions. The site occupancy factors (SOFs) for the two disordered components in each molecule were constrained to sum to one; the SOF for the major occupancy components refined to 0.575 for the 12-crown-4 molecule and 0.588 for the thf molecule. The quantity minimized by the least-squares program was $\Sigma w(F_o^2 - F_c^2)^2$, where $w = \{[\sigma(F_o)]^2 + (0.0130P)^2\}^{-1}$ and $P = (F_o^2 + 2F_c^2)/3$. The C-C and C-O distances in the disordered thf molecule were fixed at 1.52 ± 0.01 and 1.48 ± 0.01 Å, respectively, and the chemically equivalent C-O distances in the disordered 12-crown-4 ligand were constrained to be equal within an esd of 0.01 Å; the same constraint was applied to the C-C distances in this ligand. The displacement parameters for the disordered atoms of the 12-crown-4 molecules were constrained to be near-isotropic to produce satisfactory ellipsoids. Hydrogen atoms attached to boron were placed in idealized positions with B-H distances set to 1.15 Å; the boranyl groups were allowed to rotate about their B-N axes to find the best least-squares positions. The displacement parameters for

boranyl hydrogens were set equal to 1.2 times U_{eq} for the attached boron. The positions of the hydrogen atoms attached to the disordered thf molecule were not located or calculated. The largest peak in the final Fourier difference map (0.90 eÅ^{-3}) was located 1.05 Å from O12.

$Ba(H_3BNMe_2BH_3)_2(diglyme)_2$, 5. The monoclinic lattice and systematic absences $0k0$ ($k \neq 2n$) and $h0l$ ($l \neq 2n$) were uniquely consistent with the space group $P2_1/c$, which was confirmed by the success of the subsequent refinement. The quantity minimized by the least-squares program was $\Sigma w(F_o^2 - F_c^2)^2$, where $w = \{[\sigma(F_o)]^2 + (0.0168P)^2\}^{-1}$ and $P = (F_o^2 + 2F_c^2)/3$. The chemically equivalent B – H distances within the BH_3 units were constrained to be equal within an esd of 0.01Å. An isotropic extinction parameter was refined to a final value of x = 0.38(7) × 10^{-6} where F_c is multiplied by the factor $k[1 + F_c^2 x\lambda^3/\sin 2\theta]^{-1/4}$ with k being the overall scale factor. The largest peak in the final Fourier difference map (1.62 eÅ^{-3}) was located 1.50 Å from H31.

References

1. Phule, P. P.; Risbud, S. H. *J. Mater. Sci.* **1990,** *25*, 1169-1183.

2. Wessels, B. W. *Annu. Rev. Mater. Sci.* **1995,** *25*, 525-546.

3. Hwang, C. S. *Mater. Sci. Eng., B* **1998,** *B56*, 178-190.

4. Vijatovic, M. M.; Bobic, J. D.; Stojanovic, B. D. *Sci. Sintering* **2008,** *40*, 155-165.

5. Wu, M. K.; Ashburn, J. R.; Torng, C. J.; Hor, P. H.; Meng, R. L.; Gao, L.; Huang, Z. J.; Wang, Y. Q.; Chu, C. W. *Phys. Rev. Lett.* **1987,** *58*, 908-910.

6. Otway, D. J.; Obi, B.; Rees, W. S., Jr. *J. Alloys Compd.* **1997,** *251*, 254-263.

7. Fisk, Z.; Sarrao, J. L. *Annu. Rev. Mater. Sci.* **1997,** *27*, 35-67.

8. Dou, S. X.; Nikheenko, P. N.; Wang, X. L.; Liu, H. K. *Annu. Rep. Prog. Chem., Sect. C: Phys. Chem.* **1997,** *93*, 363-399.

9. Tretyakov, Y. D.; Goodilin, E. A. *Russ. Chem. Rev.* **2000,** *69*, 1-34.

10. Kuppusami, P.; Raghunathan, V. S. *Int. Mater. Rev.* **2003,** *48*, 1-43.

11. Lu, J.; Wu, X.; Chen, C.; Liang, J.; Cheng, W. *Chin. Sci. Bull.* **1997,** *42*, 1233-1240.

12. Fedorov, P. P.; Kokh, A. E.; Kononova, N. G. *Russ. Chem. Rev.* **2002,** *71*, 651-671.

13. George, S. M. *Chem. Rev.* **2010,** *110*, 111-131.

14. Yanguas-Gil, A.; Yang, Y.; Kumar, N.; Abelson, J. R. *J. Vac. Sci. Technol., A* **2009,** *27*, 1235-1243.

15. Wojtczak, W. A.; Fleig, P. F.; Hampden-Smith, M. J. *Adv. Organomet. Chem.* **1996,** *40*, 215-340.

16. Matthews, J. S.; Rees, W. S., Jr. *Adv. Inorg. Chem.* **2000,** *50*, 173-192.

17. Vehkamaki, M.; Hatanpaa, T.; Hanninen, T.; Ritala, M.; Leskela, M. *Electrochem. Solid-State Lett.* **1999,** *2*, 504-506.

18. Condorelli, G. G.; Malandrino, G.; Fragala, I. L. *Coord. Chem. Rev.* **2007,** *251*, 1931-1950.

19. Tammenmaa, M.; Antson, H.; Asplund, M.; Hiltunen, L.; Leskela, M.; Niinisto, L.; Ristolainen, E. *J. Cryst. Growth* **1987,** *84*, 151-154.

20. Purdy, A. P.; Berry, A. D.; Holm, R. T.; Fatemi, M.; Gaskill, D. K. *Inorg. Chem.* **1989,** *28*, 2799-2803.

21. Gardiner, R.; Brown, D. W.; Kirlin, P. S.; Rheingold, A. L. *Chem. Mater.* **1991,** *3*, 1053-1059.

22. Wills, L. A.; Wessels, B. W.; Richeson, D. S.; Marks, T. J. *Appl. Phys. Lett.* **1992,** *60*, 41-43.

23. Sievers, R. E.; Turnipseed, S. B.; Huang, L.; Lagalante, A. F. *Coord. Chem. Rev.* **1993,** *128*, 285-291.

24. Belot, J. A.; Neumayer, D. A.; Reedy, C. J.; Studebaker, D. B.; Hinds, B. J.; Stern, C. L.; Marks, T. J. *Chem. Mater.* **1997,** *9*, 1638-1648.

25. Tiitta, M.; Niinisto, L. *Chem. Vap. Deposition* **1997,** *3*, 167-182.

26. Saanila, V.; Ihanus, J.; Ritala, M.; Leskela, M. *Chem. Vap. Deposition* **1998,** *4*, 227-233.

27. Dhote, A. M.; Meier, A. L.; Towner, D. J.; Wessels, B. W.; Ni, J.; Marks, T. J. *J. Vac. Sci. Technol., B: Microelectron. Nanometer Struct.--Process., Meas., Phenom.* **2005,** *23*, 1674-1678.

28. Nilsen, O.; Rauwel, E.; Fjellvag, H.; Kjekshus, A. *J. Mater. Chem.* **2007,** *17*, 1466-1475.

29. Wersand-Quell, S.; Orsal, G.; Thevenin, P.; Bath, A. *Thin Solid Films* **2007,** *515*, 6507-6511.

30. Schulz, D. L.; Hinds, B. J.; Neumayer, D. A.; Stern, C. L.; Marks, T. J. *Chem. Mater.* **1993,** *5*, 1605-1617.

31. Neumayer, D. A.; Belot, J. A.; Feezel, R. L.; Reedy, C.; Stern, C. L.; Marks, T. J.; Liable-Sands, L. M.; Rheingold, A. L. *Inorg. Chem.* **1998,** *37*, 5625-5633.

32. Studebaker, D. B.; Neumayer, D. A.; Hinds, B. J.; Stern, C. L.; Marks, T. J. *Inorg. Chem.* **2000,** *39*, 3148-3157.

33. Chi, Y.; Ranjan, S.; Chou, T.-Y.; Liu, C.-S.; Peng, S.-M.; Lee, G.-H. *J. Chem. Soc., Dalton Trans.* **2001**, 2462-2466.

34. Ihanus, J.; Haenninen, T.; Hatanpaeae, T.; Aaltonen, T.; Mutikainen, I.; Sajavaara, T.; Keinonen, J.; Ritala, M.; Leskelae, M. *Chem. Mater.* **2002,** *14*, 1937-1944.

35. Hatanpaeae, T.; Vehkamaeki, M.; Mutikainen, I.; Kansikas, J.; Ritala, M.; Leskelae, M. *Dalton Trans.* **2004**, 1181-1188.

36. Ihanus, J.; Haenninen, T.; Hatanpaeae, T.; Ritala, M.; Leskelae, M. *J. Electrochem. Soc.* **2004,** *151*, H221-H225.

37. Putkonen, M.; Niinisto, L. *Top. Organomet. Chem.* **2005,** *9*, 125-145.

38. Hatanpaa, T.; Ritala, M.; Leskela, M. *J. Organomet. Chem.* **2007,** *692*, 5256-5262.

39. Vehkamaki, M.; Hatanpaa, T.; Ritala, M.; Leskela, M.; Vayrynen, S.; Rauhala, E. *Chem. Vap. Deposition* **2007,** *13*, 239-246.

40. Malandrino, G.; Lo Nigro, R.; Fragala, I. L. *Chem. Vap. Deposition* **2007,** *13*, 651-655.

41. Saly, M. J.; Heeg, M. J.; Winter, C. H. *Inorg. Chem.* **2009,** *48*, 5303-5312.

42. Saly, M. J.; Munnik, F.; Baird, R. J.; Winter, C. H. *Chem. Mater.* **2009,** *21*, 3742-3744.

43. Aspinall, H. C. *Top. Appl. Phys.* **2007,** *106*, 53-72.

44. Keller, P. C. *J. Chem. Soc. D* **1969**, 1465.

45. Keller, P. C. *Inorg. Chem.* **1971,** *10*, 2256-2259.

46. Nöth, H.; Thomas, S. *Eur. J. Inorg. Chem.* **1999**, 1373-1379.

47. Daly, S. R.; Kim, D. Y.; Yang, Y.; Abelson, J. R.; Girolami, G. S. *J. Am. Chem. Soc.* **2010,** *132*, 2106-2107.

48. Kumar, N.; Yanguas-Gil, A.; Daly, S. R.; Girolami, G. S.; Abelson, J. R. *Appl. Phys. Lett.* **2009,** *95*, 144107/144101-144107/144103.

49. Girolami, G. S.; Kim, D. Y.; Abelson, J. R.; Kumar, N.; Yang, Y.; Daly, S. U.S. Pat. Appl. 59728, April 9, 2008.

50. Bremer, M.; Nöth, H.; Thomann, M.; Schmidt, M. *Chem. Ber.* **1995,** *128*, 455-460.

51. Izod, K.; Wills, C.; Clegg, W.; Harrington, R. W. *Inorg. Chem.* **2007,** *46*, 4320-4325.

52. Bondi, A. *J. Phys. Chem.* **1964,** *68*, 441-451.

53. Ruiz-Martinez, A.; Casanova, D.; Alvarez, S. *Chem.--Eur. J.* **2008,** *14*, 1291-1303.

54. Eaton, G. R.; Lipscomb, W. N. *NMR Studies of Boron Hydrides and Related Compounds*. Benjamin: New York, 1969.

55. Gottlieb, H. E.; Kotlyar, V.; Nudelman, A. *J. Org. Chem.* **1997,** *62*, 7512-7515.

56. Kim, D. Y.; Yang, Y.; Abelson, J. R.; Girolami, G. S. *Inorg. Chem.* **2007,** *46*, 9060-9066.

CHAPTER 7. Synthesis of the Long-Sought Unsubstituted Aminodiboranate Na($H_3BNH_2BH_3$) and its *N*-Alkyl and *N,N*-Dialkyl Analogs

Introduction

One of the main obstructions impeding the development of an operational hydrogen economy is finding a safe and economical way to store H_2, and recover the stored H_2 on demand under ambient conditions.[1-9] Ammonia borane, $NH_3{\cdot}BH_3$, and other borane amines are currently being evaluated as chemical hydrogen storage materials because they have a high gravimetric concentration of hydrogen (19.6 wt.% for $NH_3{\cdot}BH_3$) and can release multiple equivalents of H_2.[10-14] Metal amidoboranes such as $M(NH_2\text{-}BH_3)$ or $M(NH_2\text{-}BH_3)_2$, where M is an alkali or alkaline earth metal, are also being explored as chemical hydrogen storage agents.[15-18]

Here we report the synthesis of a new hydrogen-rich material, the unsubstituted aminodiboranate salt $Na(BH_3\text{-}NH_2\text{-}BH_3)$. The anion in this species has never been prepared previously, but it nevertheless occupies an important place in the history of inorganic chemistry: it was originally suggested by Schlesinger and Berg[19] to be present in the "diammoniate of diborane" first prepared by Alfred Stock.[20] Later work established that this compound does not have Schlesinger and Berg's structure $[NH_4][H_3B\text{-}NH_2\text{-}BH_3]$ but rather is the borohydride salt $[H_2N\text{-}BH_2\text{-}NH_2][BH_4]$.[21]

The aminodiboranate anion is the parent compound of another anion, *N,N*-dimethylaminodiboranate, $H_3B\text{-}NMe_2\text{-}BH_3^-$, salts of which have been known since 1969 when Keller prepared it by treating NaH with $(NMe_2)B_2H_5$ in 1,2-dimethoxyethane (dme).[22] At that time, the dioxane adduct was also reported, which was prepared by treating the crude oil obtained from the reaction mixture with dioxane, followed by evaporation of the solvent

under vacuum. In 1999, Nöth reported the crystal structures of $[Na(H_3BNMe_2BH_3)]_5$(thf) (crystallized from a 2:1 mix of toluene and pentane) and $Na(H_3BNMe_2BH_3)$(Benzo-15-crown-5) (crystallized from thf), which were grown in the presence of the coordinating etherates.[23]

In addition to their potential use as hydrogen storage materials, aminodiboranate ligands are useful as molecular precursors for chemical vapor deposition (CVD) and atomic layer deposition (ALD) processes (see Chapter 8). Our group has carried out extensive investigations of the *N*,*N*-dimethylaminodiboranate anion, $H_3B\text{-}NMe_2\text{-}BH_3^-$ as a ligand to prepare a wide variety of transition metal, alkaline earth, lanthanide, and actinide complexes, many of which are highly volatile and afford useful films under CVD growth conditions.[24-27] If aminodiboranate ligands with a variety of substituents attached to the nitrogen atom were available, they would provide valuable opportunities to synthesize new CVD precursors with tailored volatilities, melting points, and chemical reactivities. We now report the synthesis of several new aminodiborante ligands, including the unsubstituted aminodiboranate salt $Na(H_3B\text{-}NH_2\text{-}BH_3)$.

Results and Discussion

Synthesis and characterization of new aminodiboranate salts. Reduction of dimethylamine-borane, $HNMe_2{\cdot}BH_3$, with Na in refluxing tetrahydrofuran is known to generate the *N*,*N*-dimethylaminodiboranate salt $Na(H_3B\text{-}NMe_2\text{-}BH_3)$.[23] We find that this synthesis can be extended to prepare other aminodiboranates, including the previously unknown parent compound. In particular, reduction of $NH_3{\cdot}BH_3$ with excess Na in tetra-hydrofuran at room temperature yields a solution of the known[17, 18] salt $Na(NH_2BH_3)$, as shown by a strong signal at δ -21.9 in the ^{11}B NMR spectrum (Figure 7.1). When this

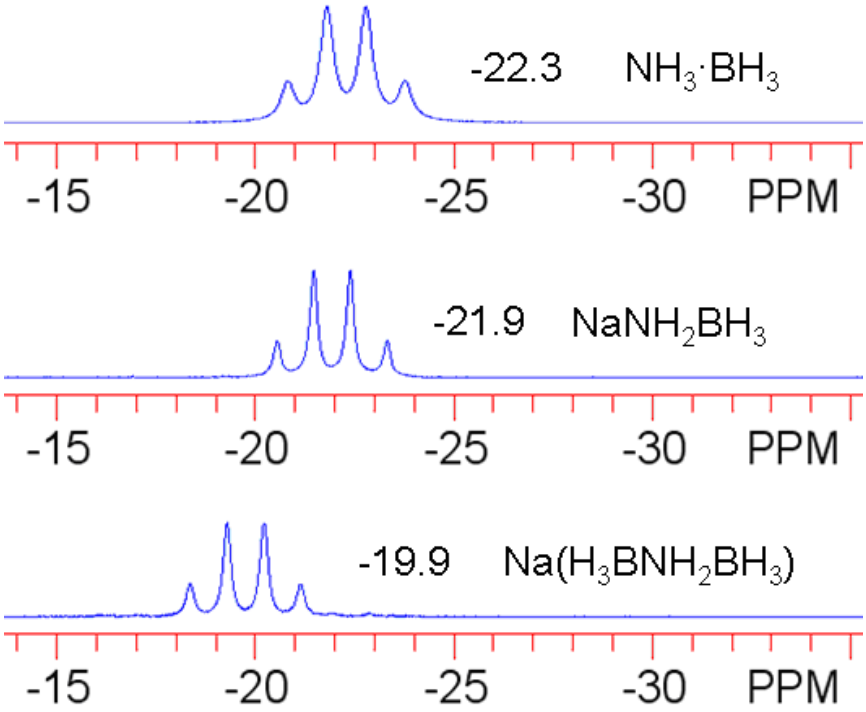

Figure 7.1. ^{11}B NMR spectra of (upper) $NH_3 \cdot BH_3$ before addition to Na, (middle) after stirring $NH_3 \cdot BH_3$ over Na at room temperature, and {lower) after refluxing the solution of $NaNH_2BH_3$ over Na.

mixture is heated to reflux, however, the unsubstituted aminodiboranate Na(H_3B-NH_2-BH_3) is formed, along with a white byproduct that precipitates from the reaction solution. Filtration of the solution, removal of the solvent, and washing successively with benzene and pentane affords Na(H_3B-NH_2-BH_3)$(thf)_x$ (**1a**). Similar reactions with other amine-boranes affords Na(H_3B-NHMe-BH_3) (**1b**), Na(H_3B-NHEt-BH_3) (**1c**), and Na[H_3B-N(C_4H_8)-BH_3] (**1d**). Typically, $NaBH_4$ is a minor byproduct of the synthesis of all aminodiboranates, as reported previously for the *N*,*N*-dimethyl derivative Na(H_3B-NMe_2-BH_3) (**1e**),[23] but the syntheses of the unsubstituted aminodiboranates **1b** and **1c** are accompanied by larger amounts than usual of this material.

$$4\ HNRR'{\cdot}BH_3 + 2\ Na \rightarrow 2\ Na(H_3B\text{-}NRR'\text{-}BH_3) + H_2 + 2\ HNRR'$$

The relatively low yield of Na(H_3B-NH_2-BH_3) from the reaction of $NH_3{\cdot}BH_3$ and Na (32 %) led us to seek new methods to prepare this salt. An alternative preparation of the parent salt (and its substituted analogs) is the reaction of $NaNH_2$ with 2 equiv of $NH_3{\cdot}BH_3$ in refluxing thf, which produces Na(H_3B-NH_2-BH_3) in better yield (50%). This reaction also proceeds through the $NaNH_2BH_3$ intermediate.

The ^{1}H NMR spectra of the new aminodiboranates (Table 7.1.1) all contain broad 1:1:1:1 quartets for the BH_3 hydrogen atoms at δ 1.1-1.5, which are coupled to ^{11}B (I = 3/2) with $^1J_{BH}$ ~ 90 Hz. The groups attached to nitrogen are readily identifiable in the ^{1}H NMR spectra; the N-H protons in the unsubstituted and monosubstituted aminodiboranates appear as broad resonances with chemical shifts (δ 1.5 to 2.1) and line widths that are similar to those observed for amine-borane complexes. The ^{11}B NMR spectra (Table 7.1.1) consist of binomial quartets with the characteristic coupling constant (Figure 7.1). The shifts of δ -19.9

Table 7.1.1. ^{1}H and ^{11}B NMR data for new aminodiboranates and comparison to $Na(H_3BNMe_2BH_3)$ in thf-d_8 at 20 °C.

	^{1}**H NMR**		^{11}**B NMR**
	NRR'	**BH_3**	
$Na(H_3B\text{-}NH_2\text{-}BH_3)$, **1a**	1.63 (br s, NH_2)	1.17 (q, J_{BH} = 90 Hz)	-19.9 (q, J_{BH} = 90 Hz)
$Na(H_3B\text{-}NHMe\text{-}BH_3)$, **1b**	2.09 (d, J_{HH} = 6 Hz, NMe), 2.11 (br s, NH)	1.22 (q, J_{BH} = 89 Hz)	-15.7 (q, J_{BH} = 91 Hz)
$Na(H_3B\text{-}NHEt\text{-}BH_3)$, **1c**	1.07 (t, CH_3), 2.41 (quint, NCH_2), 1.57 (br s, NH)	1.18 (q, J_{BH} = 89 Hz)	-17.2 (q, J_{BH} = 90 Hz)
$Na[H_3B\text{-}N(C_4H_8)\text{-}BH_3]$, **1d**	1.77 (m, $NCH_2C\underline{H}_2$), 2.61 (br s, $NC\underline{H}_2CH_2$)	1.32 (q, J_{BH} = 90 Hz)	-12.7 (q, J_{BH} = 91 Hz)
$Na(H_3B\text{-}NMe_2\text{-}BH_3)$, **1e**	2.21 (s, NMe_2)	1.36 (q, J_{BH} = 90 Hz)	-11.5 (q, J_{BH} = 91 Hz)

Table 7.1.2. ^{1}H and ^{11}B NMR data for sodium aminodiboranate dioxane-adducts at 20 °C.

	^{1}H NMR (dmso-d_6)		**^{11}B NMR (thf)**
	NRR'	**BH_3**	
$Na(H_3B\text{-}NHMe\text{-}BH_3)(1,4\text{-dioxane})_{0.5}$, **2b**	2.00 (m, NMe), 2.06 (br s, NH)	1.26 (q, J_{BH} = 89 Hz)	-13.4 (q, J_{BH} = 90 Hz)
$Na(H_3B\text{-}NHEt\text{-}BH_3)(1,4\text{-dioxane})$, **2c**	0.99 (t, CH_3), 2.29 (quint, NCH_2), 1.56 (br s, NH)	1.23 (q, J_{BH} = 89 Hz)	-14.8 (q, J_{BH} = 91 Hz)
$Na[H_3B\text{-}N(C_4H_8)\text{-}BH_3](1,4\text{-dioxane})$, **2d**	1.68 (m, $NCH_2C\underline{H}_2$), 2.49 (br s, $NC\underline{H}_2CH_2$)	1.36 (q, J_{BH} = 91 Hz)	-10.1 (q, J_{BH} = 92 Hz)
$Na(H_3B\text{-}NMe_2\text{-}BH_3)(1,4\text{-dioxane})$, **2e**	2.15 (s, NMe_2)	1.45 (q, J_{BH} = 91 Hz)	-8.7 (q, J_{BH} = 92 Hz)

Table 7.2. Crystallographic data for Na(H_3B-NMe_2-BH_3), **1e**, Na($H_3BNMeHBH_3$)(dioxane)$_{0.5}$, **2b**, Na(H_3B-NHEt-BH_3)(dioxane), **2c**, Na[H_3B-N(C_4H_8)-BH_3](dioxane), **2d**, and Na(H_3B-NMe_2-BH_3)(dioxane), **2e**.

	1e	**2b**	**2c**	**2d**	**2e**
formula	$C_8H_{48}B_8N_4Na_4$	$C_3H_{14}B_2NONa$	$C_6H_{20}B_2NO_2Na$	$C_8H_{22}B_2NO_2Na$	$C_6H_{20}B_2NO_2Na$
FW (g mol^{-1})	378.94	124.76	182.84	208.88	182.84
temp (K)	193(2)	193(2)	193(2)	193(2)	193(2)
wavelength (Å)	0.71073	0.71073	0.71073	0.71073	0.71073
crystal system	monoclinic	triclinic	triclinic	triclinic	orthorhombic
space group	$P2_1/n$	$P\bar{1}$	$P\bar{1}$	$P\bar{1}$	*Cmcm*
a (Å)	13.915(3)	8.2911(3)	7.9953(12)	7.781(2)	9.1875(6)
b (Å)	13.419(3)	9.9884(4)	8.9580(13)	9.048(3)	8.3590(6)
c (Å)	15.026(3)	10.8264(4)	9.566(2)	10.230(3)	14.1500(10)
α (deg)	90	91.984(2)	106.786(4)	111.583(4)	90
β (deg)	91.941(3)	97.495(2)	98.357(2)	101.318(4)	90
γ (deg)	90	114.189(2)	110.880(2)	101.330(4)	90
volume (Å^3)	2804.1(11)	807.02(5)	588.78(13)	627.5(3)	1086.70(13)
Z	4	4	2	2	4
D_{calc} (g cm^{-3})	0.898	1.027	1.031	1.105	1.118
μ(mm^{-1})	0.102	0.111	0.100	0.102	0.109
abs correction method	face-indexed	face-indexed	multi-scan	face-indexed	face-indexed
max. min. transm. factors	0.328, 0.132	0.989, 0.968	0.745, 0.659	0.980, 0.934	0.984, 0.970
data/restraints/params	5137/0/264	3563/1/203	2245/21/168	2923/0/151	766/0/58
GOF on F^2	0.837	1.007	1.094	0.962	1.093
$R1$ [I > 2$\sigma(I)$][a]	0.0451	0.0319	0.0547	0.0525	0.048
$wR2$ (all data)[b]	0.1148	0.082	0.1751	0.1586	0.1376
max, min $\Delta\rho_{electron}$ (e·Å^{-3})	0.196/-0.246	0.219/-0.164	0.269/-0.242	0.641/-0.351	0.335/-0.404

[a] $R_1 = \sum |F_o| - |F_c| \,| / | \sum |F_o|$ for reflections with $F_o^2 > 2\,\sigma(F_o^2)$. [b] $wR_2 = [\sum w(F_o^2 - F_c^2)^2 / \sum (F_o^2)^2]^{1/2}$ for all reflections.

for $Na(H_3B\text{-}NH_2\text{-}BH_3)$, δ -15.7 for $Na(H_3B\text{-}NHMe\text{-}BH_3)$, and δ -11.5 for $Na(H_3B\text{-}NMe_2\text{-}BH_3)$ show that the ^{11}B NMR resonance is deshielded by 4.2 ppm for each methyl group that is replaced with hydrogen, and suggest that all these salts are in the same chemical class. For comparison, $Na(H_3B\text{-}NHEt\text{-}BH_3)$ and $Na[H_3B\text{-}N(C_4H_8)\text{-}BH_3]$ exhibit ^{11}B NMR resonances at δ -17.2 and -12.7.

Synthesis, characterization, and structures of 1,4-dioxane adduct of sodium aminodiboranates. With one exception (see below), we were unable to obtain crystals of the unsolvated aminodiboranate salts suitable for crystallographic studies. As a result, we investigated the synthesis of adducts of the salts with Lewis bases. In 1969, Keller reported that addition of 1,4-dioxane to $Na(H_3B\text{-}NMe_2\text{-}BH_3)$ affords a crystalline product, which was formulated as $Na(H_3B\text{-}NMe_2\text{-}BH_3)(1,4\text{-dioxane})_{0.5}$.[22] We find that this method is a general one: addition of dioxane to the aminodiboranate salts, **1b-e**, followed by extraction and crystallization from diethyl ether, affords the dioxane adducts $Na(H_3B\text{-}NHMe\text{-}BH_3)(dioxane)_{0.5}$ (**2b**), $Na(H_3B\text{-}NHEt\text{-}BH_3)(dioxane)$ (**2c**), $Na[H_3B\text{-}N(C_4H_8)\text{-}BH_3](dioxane)$ (**2d**), and $Na(H_3B\text{-}NMe_2\text{-}BH_3)(1,4\text{-dioxane})$ (**2e**). Unfortunately, crystals of the $Na(H_3BNH_2BH_3)$ dioxane adduct could not be prepared this way. Interestingly, the 1:1 stoichiometry of **2e** is different from that reported by Keller, who formulated the dioxane adduct as the 2:1 complex $Na(H_3B\text{-}NMe_2\text{-}BH_3)(1,4\text{-dioxane})_{0.5}$.[22] Very likely, the amount of dioxane present in the crystallized material depends on the amount of dioxane present during crystallization.

The NMR shifts of the 1,4-dioxane adducts **2b**-**2e** in dmso-d_6 are similar to those observed for the unsolvated materials **1b**-**1e** in thf (Table 7.1.2). For all these compounds, the ^1H NMR chemical shift of the 1,4-dioxane resonance in dmso-d_6 is close to the δ 3.56 shift characteristic of free 1,4-dioxane,[28] which suggests that solvent molecules the coordinated

dioxane in solution. Similar behavior has been observed for Lewis-base adducts of $Ba(H_3B\text{-}NMe_2\text{-}BH_3)_2$ in dmso (Chapter 6). The ^{11}B NMR chemical shifts of **2b**-**e** in thf exhibit resonances that are deshielded relative to those of their dioxane-free analogs. The IR spectra of **2b**-**2d** are similar to those obtained for **1b**-**1d**, except for the dioxane resonances.

The crystal structures of **2b**, **2c**, **2d**, and **2e** (Table 7.2) show that all four compounds are polymeric. The *N*-methyl derivative **2b** crystallizes in the triclinic space group $P\bar{1}$ with two formula units per asymmetric unit. The Na atoms are each coordinated to one chelating $H_3B\text{-}NHMe\text{-}BH_3^-$ ligand, two BH_3 groups from adjacent $Na(H_3B\text{-}NHMe\text{-}BH_3)$ fragments, and to one dioxane ligand (Figure 7.2) Pairs of sodium cations are bridged by two *N*-methylaminodiboranate anions, which can be viewed as simultaneously chelating to one Na atom and bridging to the second. The dioxane molecules bridge between sodium cations and further crosslink the polymeric network. In all, each Na atom is surrounded by four boron atoms and one oxygen atom to form a distorted trigonal bipyramid in which the oxygen atom occupies an equatorial site. The Na···B distances range from 2.769(1) to 2.934(1) Å, and the Na-O distances are all 2.335(1) Å (Table 7.3). Hydrogen atoms were located (but not shown in the figure); the borane hydrogens all interact with either one or two sodium atoms.

The *N*-ethyl derivative **2c** crystallizes in the triclinic space group $P\bar{1}$ with one equivalents of dioxane, vs 0.5 equivalents for **2b**. The sodium atoms are each coordinated to one chelating $H_3B\text{-}NHEt\text{-}BH_3$ ligand, one BH_3 group from an adjacent unit, and two dioxane ligands, again in a trigonal bipyramidal arrangement, but with the oxygen atoms occupying one axial and one equatorial site (Figure 7.3). As seen in the structure of **2b**, pairs of sodium cations are bridged by two *N*-ethylaminodiboranate anions, which both chelate and bridge. All of the BH_3 groups are bound to the Na atoms in a κ^2H fashion as indicated by the Na···B distances, which range from 2.720(3) to 2.823(3) Å (Table 7.4). The dinuclear units in **2c** are

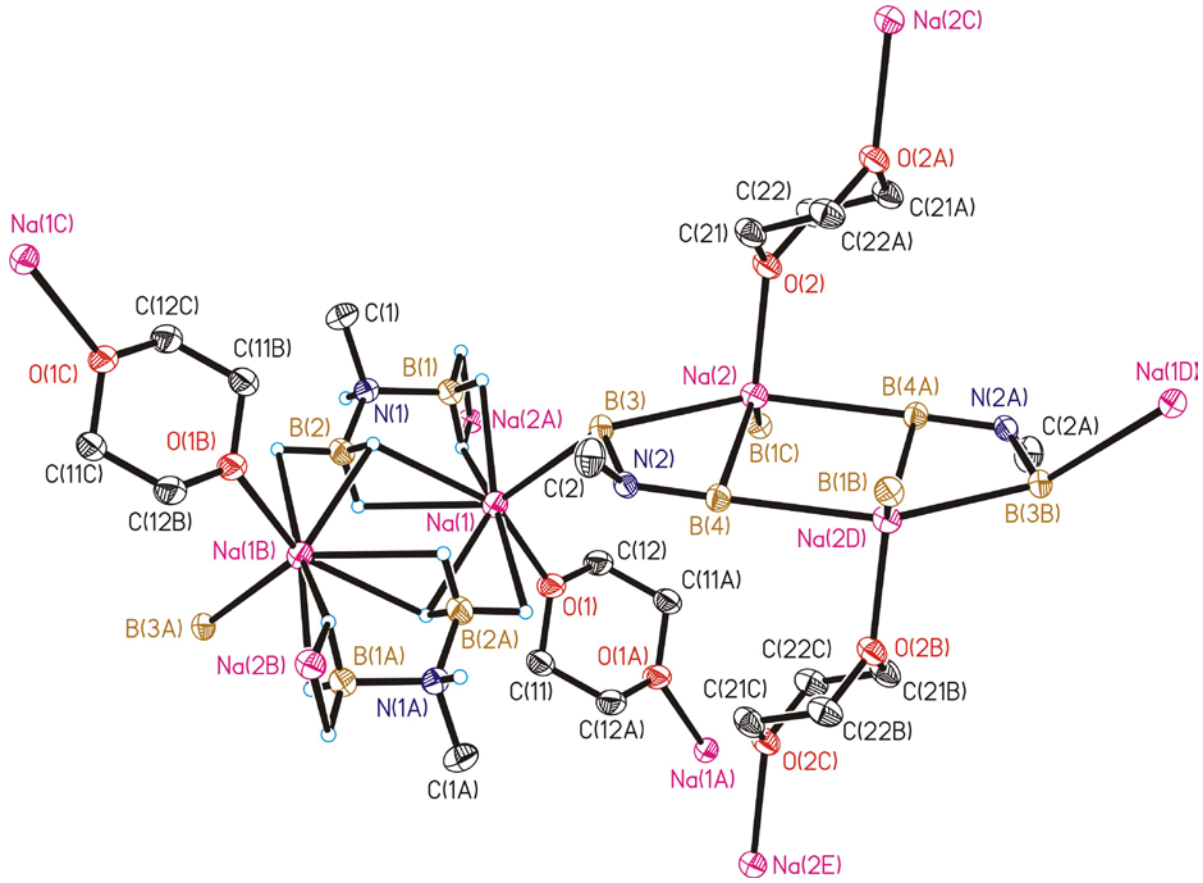

Figure 7.2. Molecular structure of $Na(H_3BNMeHBH_3)(dioxane)_{0.5}$, **1b**. Ellipsoids are drawn at the 35% probability level. Hydrogen atoms have been deleted except for those attached to B1, B2, and N1, which have been included to illustrate the local coordination environment around Na1 and Na2.

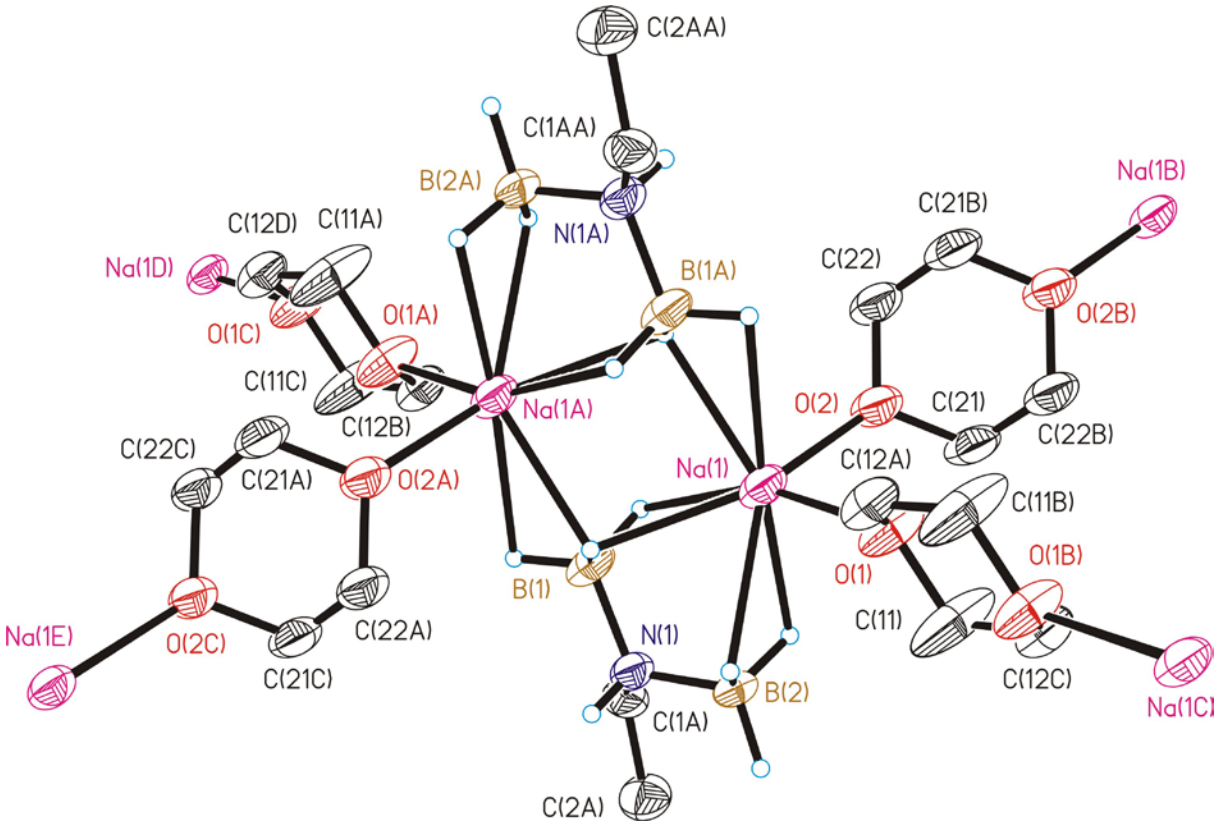

Figure 7.3. Molecular structure of $Na(H_3BNEtHBH_3)(dioxane)_{0.5}$, **1c**. Ellipsoids are drawn at the 35% probability level. Hydrogen atoms attached to carbon have been deleted for clarity.

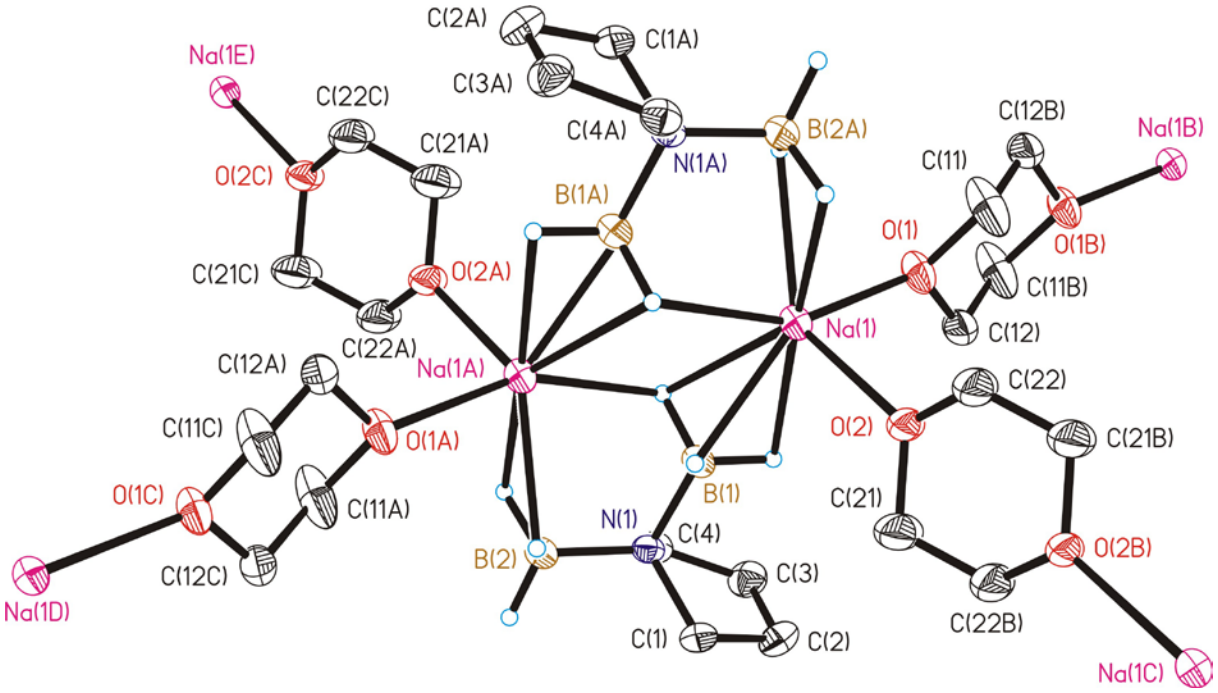

Figure 7.4. Molecular structure of $Na(H_3BN(C_4H_8)BH_3)(dioxane)_{0.5}$, **1d**. Ellipsoids are drawn at the 35% probability level. Hydrogen atoms attached to carbon have been deleted for clarity.

Table 7.3. Selected Bond Lengths and Angles for $Na(H_3B\text{-}NHMe\text{-}BH_3)(dioxane)_{0.5}$, **2b**.

	Bond Lengths (Å)		
Na(1)-O(1)	2.3346(9)	Na(2)-O(2)	2.3354(8)
Na(1)-B(1)	2.8503(13)	Na(2)-B(3)	2.8509(13)
Na(1)-B(2)	2.9341(14)	Na(2)-B(4)	2.8335(14)
Na(1)-B(3)	2.8603(13)	Na(2)-B(1)″	2.7766(14)
Na(1)-B(2)′	2.7694(14)	Na(2)-B(4)‴	2.8449(13)
Na(1)-H(11)	2.505(11)	Na(2)-H(31)	2.354(11)
Na(1)-H(12)	2.413(12)	Na(2)-H(32)	2.595(12)
Na(1)-H(21)	2.603(12)	Na(2)-H(41)	2.410(11)
Na(1)-H(22)	2.472(11)	Na(2)-H(42)	2.524(12)
Na(1)-H(32)	2.502(12)	Na(1)-Na(1)′	3.8365(8)
Na(1)-H(33)	2.338(11)	Na(2)-Na(2)‴	3.8072(8)
	Bond Angles (deg)		
B(1)-Na(1)-B(2)	54.26(4)	O(2)-Na(2)-B(3)	101.82(3)
B(3)-Na(1)-B(2)	122.34(4)	O(2)-Na(2)-B(4)	115.08(4)
B(1)-Na(1)-B(3)	103.76(4)	O(2)-Na(2)-B(1)″	114.96(4)
O(1)-Na(1)-B(1)	102.25(4)	O(2)-Na(2)-B(4)‴	90.83(3)
O(1)-Na(1)-B(2)	123.22(4)	B(4)-Na(2)-B(3)	55.56(4)
O(1)-Na(1)-B(3)	112.86(4)	B(1)″-Na(2)-B(3)	107.94(4)
O(1)-Na(1)-B(2)′	97.06(4)	B(1)″-Na(2)-B(4)	129.59(4)
B(2)′-Na(1)-B(1)	149.64(4)	B(1)″-Na(2)-B(4)‴	89.20(4)
B(2)′-Na(1)-B(2)	95.51(4)	B(4)‴-Na(2)-B(3)	151.34(4)
B(2)′-Na(1)-B(3)	89.76(4)	B(4)-Na(2)-B(4)‴	95.79(4)
B(2)-N(1)-B(1)	113.79(8)	B(4)-N(2)-B(3)	113.82(8)

Symm. transformation used to generate equiv atoms:′ = -x+1, -y+1 ,-z ″ = -x+1, -y, -z ‴ = -x+1, -y, -z+1

Table 7.4. Selected Bond Lengths and Angles for $Na(H_3B\text{-}NHEt\text{-}BH_3)$(dioxane), **2c**.

	Bond Lengths (Å)		
Na(1)-O(1)	2.362(2)	Na(1)-H(11)	2.436(19)
Na(1)-O(2)	2.3333(18)	Na(1)-H(12)	2.46(2)
Na(1)-B(1)	2.822(4)	Na(1)-H(21)	2.53(2)
Na(1)-B(2)	2.823(3)	Na(1)-H(22)	2.40(2)
Na(1)-B(1)′	2.720(3)	Na(1)-Na(1)′	3.7916(18)
	Bond Angles (deg)		
O(2)-Na(1)-O(1)	92.71(8)	O(2)-Na(1)-B(1)′	95.45(8)
O(1)-Na(1)-B(1)	140.48(8)	B(1)-Na(1)-B(2)	55.18(8)
O(1)-Na(1)-B(2)	92.39(9)	B(1)′-Na(1)-B(1)	93.69(10)
O(1)-Na(1)-B(1)′	106.69(9)	B(1)′-Na(1)-B(2)	144.79(9)
O(2)-Na(1)-B(1)	119.18(9)	B(1)-N(1)-B(2)	111.9(2)
O(2)-Na(1)-B(2)	113.28(8)		

Symmetry transformations used to generate equivalent atoms: ′ = -x, -y+1, -z

Table 7.5. Selected Bond Lengths and Angles for Na[H_3B-N(C_4H_8)-BH_3](dioxane), **2d**.

	Bond Lengths (Å)		
Na(1)-O(1)	2.3816(17)	Na(1)-H(11)	2.49(2)
Na(1)-O(2)	2.4179(17)	Na(1)-H(12)	2.623(19)
Na(1)-B(1)	2.666(3)	Na(1)-H(13)	2.401(19)
Na(1)-B(2)′	2.799(3)	Na(1)-Na(1)′	3.8912(18)
Na(1)-B(1)′	2.968(3)		
	Bond Angles (deg)		
O(1)-Na(1)-O(2)	93.58(7)	O(2)-Na(1)-B(2)′	108.86(7)
O(1)-Na(1)-B(1)	110.45(8)	B(1)-Na(1)-B(1)′	92.80(8)
O(1)-Na(1)-B(1)′	135.68(7)	B(1)-Na(1)-B(2)′	144.47(8)
O(1)-Na(1)-B(2)′	91.23(7)	B(2)′-Na(1)-B(1)′	53.57(7)
O(2)-Na(1)-B(1)	97.85(7)	B(1)-N(1)-B(2)	109.92(16)
O(2)-Na(1)-B(1)′	120.85(8)		

Symmetry transformations used to generate equivalent atoms: ′ = -x, -y+2, -z+1

connected into a network by the dioxane molecules, which bridge between Na atoms in different dinuclear units. The Na-O distances and distances in **2c** of 2.333(2) and 2.362(2) Å are similar to those in **2b**.

The pyrrolidinyl compound **2d** crystallizes in the triclinic space group $P\bar{1}$, and its structure is very similar to that of **2c** except the ligands in **2d** bridge the dinuclear fragments in an unusual way: the ligands chelate to the Na atoms so that one BH_3 group is κ^2H and the other BH_3 group is κ^1H and simultaneously bridges to the adjacent Na atom in κ^3H fashion (Figure 7.4). Like **2c**, the dinuclear fragments in **2d** are connected together by the dioxane molecules, which bridge the Na atoms to complete the polymeric array. The Na···B and Na-O distances in **2d** are similar to those in **2b** and **2c,** except for the κ^3H and κ^1H Na···B distances in **3**, which are 2.666(3) and 2.968(3) Å, respectively (Table 7.5).

Structures of solvate-free Na(H_3B-NMe_2-BH_3) and Na(H_3B-NMe_2-BH_3)(1,4-dioxane). The structures of ether-free Na(H_3B-NMe_2-BH_3) (**1e**) and its dioxane adduct Na(H_3B-NMe_2-BH_3)(1,4-dioxane) (**2e**) have not been reported. We were able to obtain crystals of the solvent-free material by cooling a concentrated solution of **1e** in diethyl ether.

The unsolvated material **1e** crystallizes in the space group $P2_1/n$. There are four unique Na environments per asymmetric unit; the structure is polymeric and rather complex. Each Na ion is surrounded by four boron atoms, but there are three different types of coordination environments (Figure 7.5). Sodium ions Na2 and Na4 ions are coordinated to one chelating H_3B-NMe_2-BH_3^- (DMADB) ligand and two bridging DMADB ligands, sodium ion Na1 is coordinated to four bridging DMADB ligands, and sodium ion Na3 ion is chelated by two DMADB ligands and one bridging DMADB ligand. Each DMADB group simultaneously chelates to one Na atom and bridges to two neighboring Na atoms. Most of the Na···B distances range from 2.695(3) to 2.904(2) Å, and the locations of the hydrogen

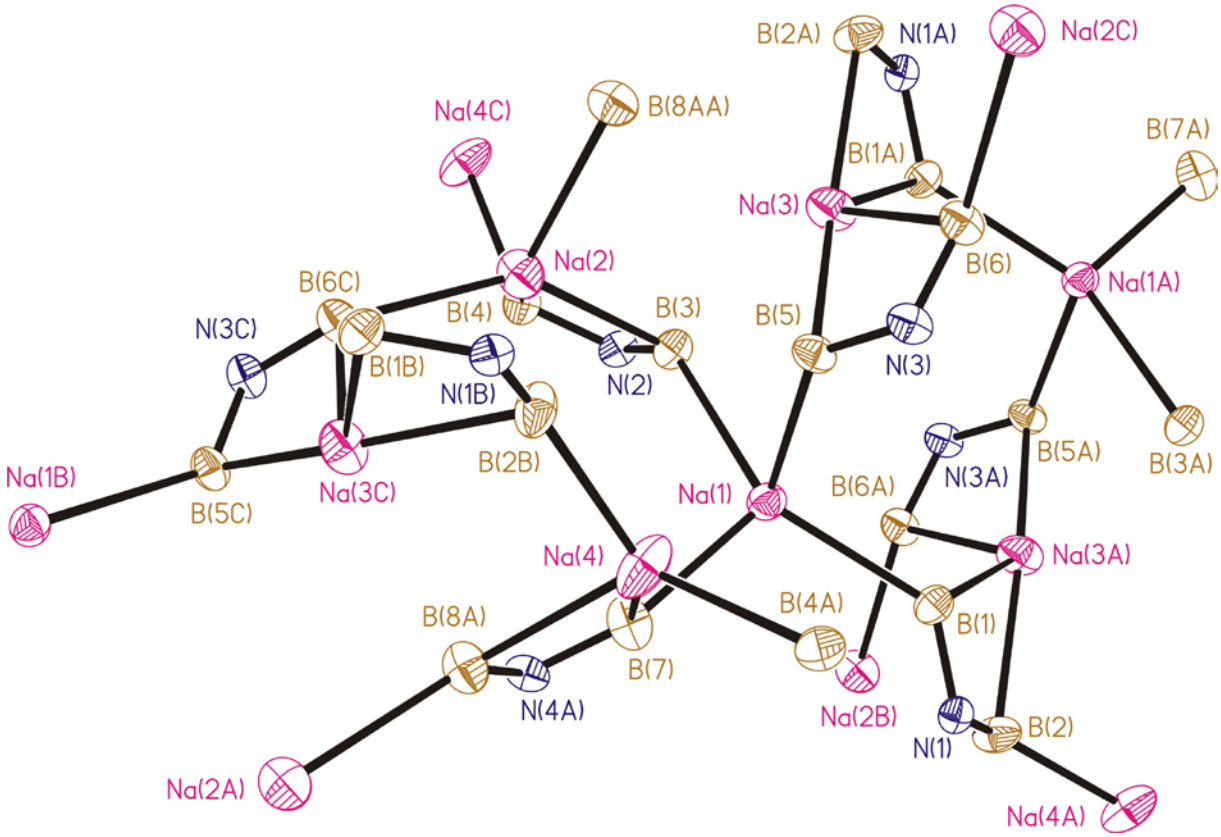

Figure 7.5. Molecular structure of unsolvated $Na(H_3BNMe_2BH_3)$, **1e**. Ellipsoids are drawn at the 35% probability level. Hydrogen and carbon atoms have been deleted for clarity.

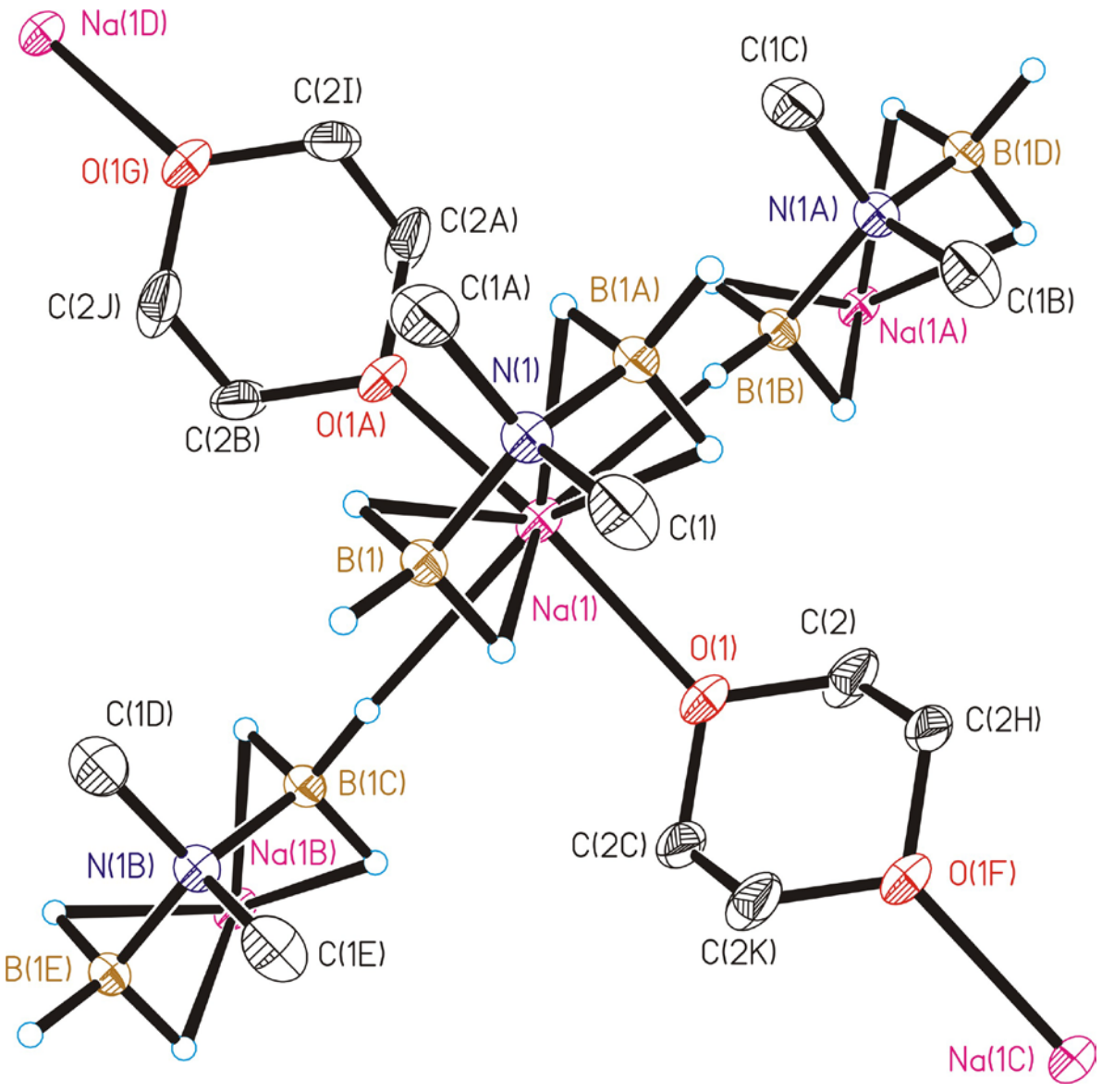

Figure 7.6. Molecular structure of $Na(H_3BNMe_2BH_3)(1,4\text{-dioxane})$, **2e**. Ellipsoids are drawn at the 35% probability level. Hydrogen atoms attached to carbon have been deleted for clarity.

Table 7.6. Selected Bond Lengths and Angles for $Na(H_3B\text{-}NMe_2\text{-}BH_3)$, **1e**.

	Bond Lengths (Å)		
Na(1)-B(1)	2.805(2)	Na(3)-B(1)′	2.933(2)
Na(1)-B(3)	2.904(2)	Na(3)-B(2)′	2.795(3)
Na(1)-B(5)	2.800(2)	Na(3)-B(5)	2.809(2)
Na(1)-B(7)	2.695(3)	Na(3)-B(6)	2.898(2)
Na(1)-Na(3)	4.1653(12)	Na(3)-Na(4)‴	4.1191(14)
Na(1)-Na(4)	4.1412(14)	Na(4)-B(2)†	2.719(3)
Na(2)-B(3)	2.804(2)	Na(4)-B(7)	2.829(3)
Na(2)-B(4)	2.795(2)	Na(4)-B(4)‡	2.886(2)
Na(2)-B(6)″	2.840(2)	Na(4)-B(8A)	3.046(8)
Na(2)-B(8A)‴	2.883(7)	Na(4)-Na(3)″	4.1191(14)
	Bond Angles (deg)		
B(7)-Na(1)-B(5)	108.95(8)	B(2)′-Na(3)-B(1)′	54.25(6)
B(7)-Na(1)-B(1)	109.63(8)	B(5)-Na(3)-B(1)′	140.67(7)
B(5)-Na(1)-B(1)	107.70(7)	B(6)-Na(3)-B(1)′	116.40(7)
B(7)-Na(1)-B(3)	108.77(8)	B(2)†-Na(4)-B(7)	129.54(8)
B(5)-Na(1)-B(3)	83.75(7)	B(2)†-Na(4)-B(4)‡	109.49(7)
B(1)-Na(1)-B(3)	133.15(7)	B(7)-Na(4)-B(4)‡	120.12(8)
B(4)-Na(2)-B(3)	56.00(6)	B(2)†-Na(4)-B(8A)	99.45(16)
B(4)-Na(2)-B(6)″	114.88(7)	B(7)-Na(4)-B(8A)	51.87(13)
B(3)-Na(2)-B(6)″	144.27(8)	B(4)‡-Na(4)-B(8A)	133.59(18)
B(4)-Na(2)-B(8A)‴	122.36(16)	B(1)-N(1)-B(2)	111.44(15)
B(3)-Na(2)-B(8A)‴	100.39(16)	B(4)-N(2)-B(3)	112.24(15)
B(6)″-Na(2)-B(8A)‴	111.07(15)	B(5)-N(3)-B(6)	111.52(14)
B(2)′-Na(3)-B(5)	159.91(7)	B(7)-N(4A)-B(8A)	108.0(7)
B(2)′-Na(3)-B(6)	109.59(8)	Na(1)-B(1)-Na(3)′	116.42(8)
B(5)-Na(3)-B(6)	54.50(6)	Na(2)-B(3)-Na(1)	109.00(7)

Symmetry transformations used to generate equivalent atoms: ′ = -x+1,-y+1,-z

″ = -x+½, y-½,-z+½ ‴ = -x+½, y+½, -z+½ † = x-½, -y+½, z+½ ‡ = x+½, -y+½, z+½

Table 7.7. Selected Bond Lengths and Angles for $Na(H_3B\text{-}NMe_2\text{-}BH_3)$(dioxane), **2e**.

	Bond Lengths (Å)		
Na(1)-O(1)	2.3638(14)	B(1)-N(1)	1.591(2)
Na(1)-B(1)	2.851(2)	B(1)-H(11)	1.137(16)
Na(1)-H(11)	2.484(16)	B(1)-H(12)	1.12(3)
	Bond Angles (deg)		
O(1)′-Na(1)-O(1)	141.90(8)	O(1)′-Na(1)-H(11)	127.3(4)
O(1)-Na(1)-B(1)	106.84(3)	O(1)-Na(1)-H(11)	83.7(4)
B(1)″-Na(1)-B(1)	54.82(8)	B(1)″-Na(1)-H(11)	64.3(4)
B(1)-N(1)-B(1)″	111.21(18)	B(1)-Na(1)-H(11)	23.3(4)

Symmetry transformations used to generate equivalent atoms: ′ = x, y, -z+½ ″ = -x, y, -z+½

atoms suggest that these Na···B interactions are bridged by two hydrogen atoms (Table 7.6). In contrast the Na(3)···B(1) and Na(4)···B(8A) distances are 2.933(2) and 3.046(8) Å, and the location of the hydrogen atoms suggest that these contacts are each bridged by only one hydrogen atom.

The structure of the dioxane adduct **2e** is much easier to describe; there is only one $Na(H_3B\text{-}NMe_2\text{-}BH_3)$(1,4-dioxane) environment. Each Na ion is chelated by one DMADB ligand, and is connected to other fragments by two dioxane molecules and two DMADB groups that simultaneously chelate and bridge to neighboring Na centers via κ^1H linkages (Figure 7.6). The six hydrogen and two oxygen atoms about each Na atom describe a distorted antiprism with one square face and one rectangular face owing to the constraints imposed by the chelating nature of the DMADB ligands. The Na···B distances are 2.851(2) Å, the Na-O distances are 2.364(1) Å, and the Na-H distances are 2.48(2) Å (Table 7.7). These distances are similar to those observed in **2b** and **2c**.

Attempts to prepare $Na(H_3B\text{-}NH_2\text{-}BH_3)$ from $NaNH_2$ and BH_3·thf. A diborane and mercury free synthesis of $Na(B_3H_8)$. In previous work, we reported the synthesis of several metal complexes of the octahydrotriborato anion, $B_3H_8^-$.[29-33] For example, the chromium compound $Cr(B_3H_8)_2$ is volatile and useful for the deposition of highly conformal CrB_2 thin films by plasma-assisted CVD. We also were able to prepare the new magnesium compound $Mg(B_3H_8)_2$, which is also volatile; we are currently investigating whether this compound can serve as a CVD precursor to the remarkable superconductor MgB_2.[30-32] The preparations of both $Cr(B_3H_8)_2$ and $Mg(B_3H_8)_2$ were enabled by our development of a large-scale synthesis of solvent-free sodium octahydrotriborate, NaB_3H_8, which involved reducing diborane with Na amalgam in diethyl ether. Although this procedure works well, diborane is toxic and pyrophoric, and mercury is also toxic and costly to dispose.

There only known synthesis of NaB_3H_8 that does not use diborane or mercury entails treatment of $NaBH_4$ with I_2 or $BF_3{\cdot}Et_2O$ in diglyme, but these solutions yield an oil of composition $NaB_3H_8(diglyme)_x$ upon removal of the solvent. The diglyme can only be removed by treating the $NaB_3H_8(diglyme)_x$ with $[(n\text{-}C_4H_9)_4N]I$ to form $[(n\text{-}C_4H_9)_4N][B_3H_8]$, followed by cation exchange with $Na(BPh_4)$ in isopropanol to yield solvent-free NaB_3H_8. This procedure is tedious, expensive, and atom inefficient.

In the course of seeking alternative preparations of the parent aminodiboranate $Na(H_3B\text{-}NH_2\text{-}BH_3)$, we treated sodium amide, $NaNH_2$, with 2 equiv of $BH_3{\cdot}$thf in tetrahydrofuran. The reaction was monitored by $^{11}B\{^1H\}$ NMR spectroscopy (Figure 7.7). At room temperature, the reaction generates several products: among them are NH_3BH_3, NaB_2H_7, NaB_3H_8, and $NaBH_4$ in a ~2.1 : 1.3 : 0.1 : 1.0 molar ratio. Some unreacted $BH_3{\cdot}$thf is also present and there are two unassignable peaks at -24.0 and -26.4. Heating the mixture to reflux for 188 hours converts all of the NaB_2H_7 and the remaining $BH_3{\cdot}$thf to products, the product distribution then consists of borazine (δ 30.6, J_{BH} = 140 Hz), NaB_3H_8, and $NaBH_4$ in a ~1.2 : 3.6 : 1.0 molar ratio.

The ^{11}B NMR spectrum of NaB_3H_8 at room temperature consists of a nonet at δ 30.9 (J_{BH} is 33 Hz) due to coupling to the eight hydrogen atoms, which are rapidly exchanging on the NMR time scale. The ^1H NMR spectrum of NaB_3H_8 consists of a 1:3:6:10:12:12:10:6:3:1 decet at δ 0.05 due to coupling of the hydrogen atoms to the three ^{11}B nuclei (I = 3/2). These NMR data agree with literature values.[31, 34]

Although this procedure does not afford $Na(H_3B\text{-}NH_2\text{-}BH_3)$, it represents a new method to prepare $Na(B_3H_8)$ that avoids the use of toxic and potentially explosive reagents.[31] A disadvantage is that the product contains small amounts of nitrogen and carbon-containing impurities, as determined by microanalysis, but no boron-containing impurities are observed

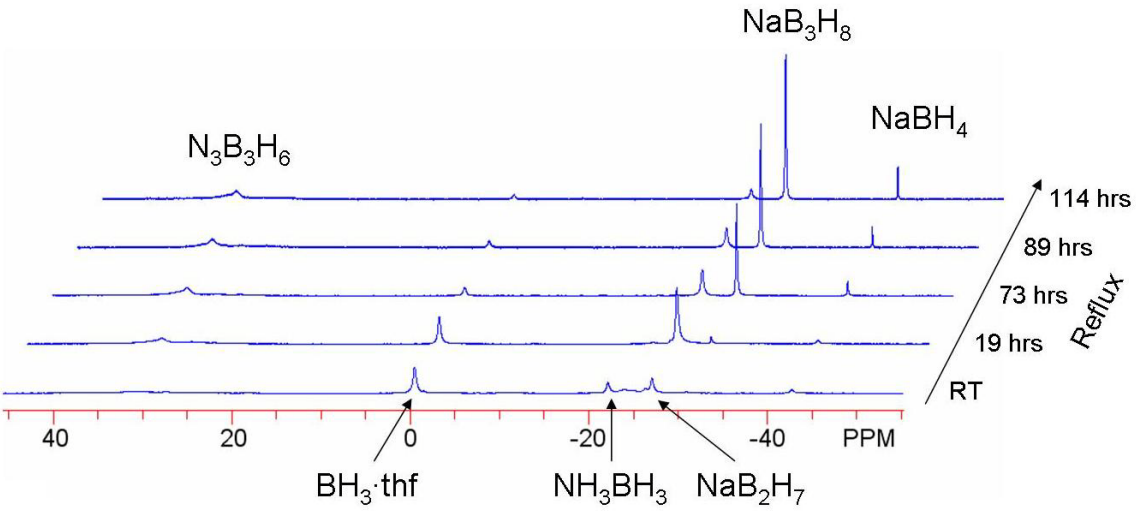

Figure 7.7. Stacked plot of $^{11}B\{^{1}H\}$ NMR spectra of the solutions of the reaction of $NaNH_2$ with BH_3·thf in tetrahydrofuran as a function of reflux time.

in the ^{11}B NMR spectrum after the material has been purified by extraction with diethyl ether. The carbon impurity is likely coordinated thf, as is often observed for Na(B_3H_8). The nitrogen impurity is still under investigation.

Attempts to prepare B-substituted aminodiboranates. The successful syntheses of new aminodiboranates with different substituents on the nitrogen atom prompted us to explore the preparation of B-substituted aminodiboranates. Such anions would have larger steric profiles, and would be better able to saturate the coordination spheres of large metals such as lanthanides, actinides, and alkaline earths. Two different synthetic strategies were considered, both of which first generate the required monoalkylboranes, which then is used to synthesize the desired ligands.

The first method employs thexylborane as an intermediate. Thexylborane was prepared by treating BH_3·thf with 2,3-dimethyl-2-butene, as previously described.[35] Unlike most hydroboration reactions, the resulting thexylborane does not continue to hydroborate further equivalents of 2,3-dimethyl-2-butene because of the steric bulk of the thexyl group.[36] The borane-amine adduct was then prepared by combining thexylborane with a solution of dimethylamine in thf.[37] The resulting solution of the amine-borane adduct was treated with Na at reflux, as for the synthesis of other aminodiborante salts. All steps were monitored by ^{11}B NMR spectroscopy (Figure 7.8). The reaction does not yield the expected aminodiboranate. Instead two new peaks are observed: a doublet at δ -25.7 (J_{BH} = 123 Hz) and a quartet at δ 44.2 (J_{BH} = 76 Hz), respectively, which correspond to the aminoborane BH(CMe_2Pr^i)-NMe_2 and the borohydride salt Na(H_3B-CMe_2Pr^i).[38] The amidoborane BH(CMe_2Pr^i)-NMe_2 is a new compound but its ^{11}B NMR shift closely matches those observed for other BHR-NMe_2 complexes with R = Bu^t, Bu^i, or Me.[39] No peaks corresponding to the thexyl-functionalized aminodiboranate were observed.

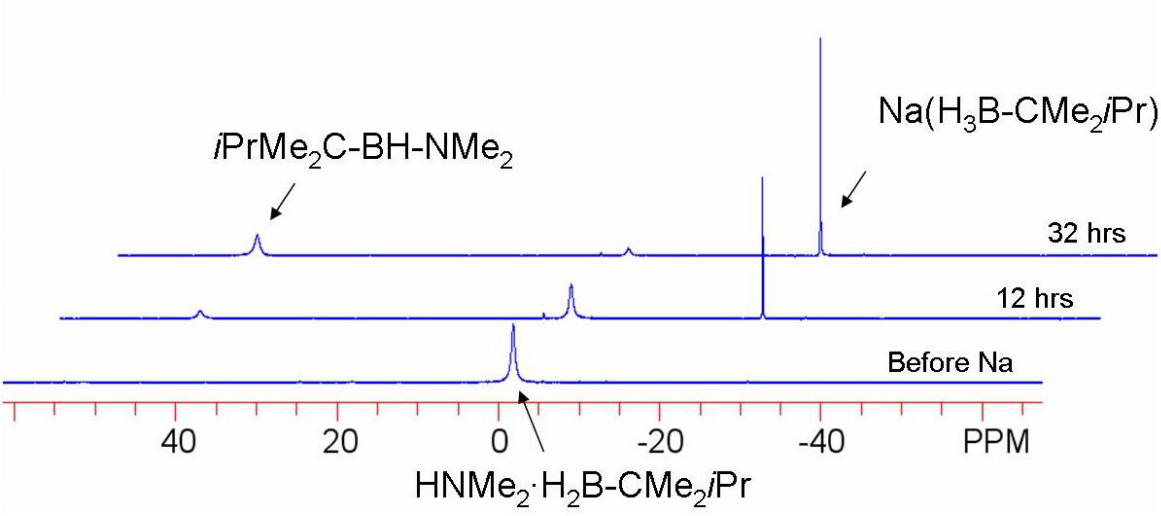

Figure 7.8. Stacked plot of $^{11}B\{^{1}H\}$ NMR spectra of the solutions from the reaction of dimethylamine-thexylborane with Na in refluxing tetrahydrofuran.

The two products $BH(CMe_2Pr^i)$-NMe_2 and $Na(H_3B$-$CMe_2Pr^i)$ can be considered as fragments of the desired thexyl-substituted DMADB anion (Scheme 7.1), generated by transfer of a hydride anion from one BH_2R group to the other. A similar fragmentation reaction is observed in the thermal decomposition of $Th(H_3B$-NMe_2-$BH_3)_4$ to $Th(H_3B$-NMe_2-$BH_3)_2(BH_4)_2$ and $HNMe_2$-BH_2 (Chapter 2). At least two driving forces could account for why the thexyl-substituted DMADB anion is disfavored relative to its fragments: (1) the thexyl group is so sterically demanding that it destabilizes the aminodiboranate anion or (2) the thexyl group is sufficiently electron donating that the Lewis acidity of thexylborane is too low to form the amidodiboranate.

Future investigations will be focused on preparing B-substituted amidodiboranates that bear less sterically demanding substituents than thexyl. A alternative synthetic strategy for preparing such anions, which employs monoalkylborane intermediates, is shown in Scheme 7.2. Monoalkylboranes can be prepared with the assistance protecting groups such as catecholate to limit alkylation to one B-X site (X = halide, H). Treatment of the resulting monoalkylboranes with dimethylamine should yield $HNMe_2 \cdot BH_2R$ adducts, and subsequent reduction with sodium may afford the desired B-substituted aminodiboranates salts.

Concluding remarks

Although to date we have been unable to obtain X-ray quality crystals of the parent sodium salt $Na(H_3B$-NH_2-$BH_3)$ or its ether adducts, we have been successful in using it as a ligand for metal complexes. For example, treatment of $ErCl_3$ with $Na(H_3B$-NH_2-$BH_3)$ in tetrahydrofuran affords the new erbium complex $Er(H_3B$-NH_2-$BH_3)Cl_2(thf)_3$ (Chapter 8). This erbium complex provides crystallographic verification of the H_3B-NH_2-BH_3^- motif.

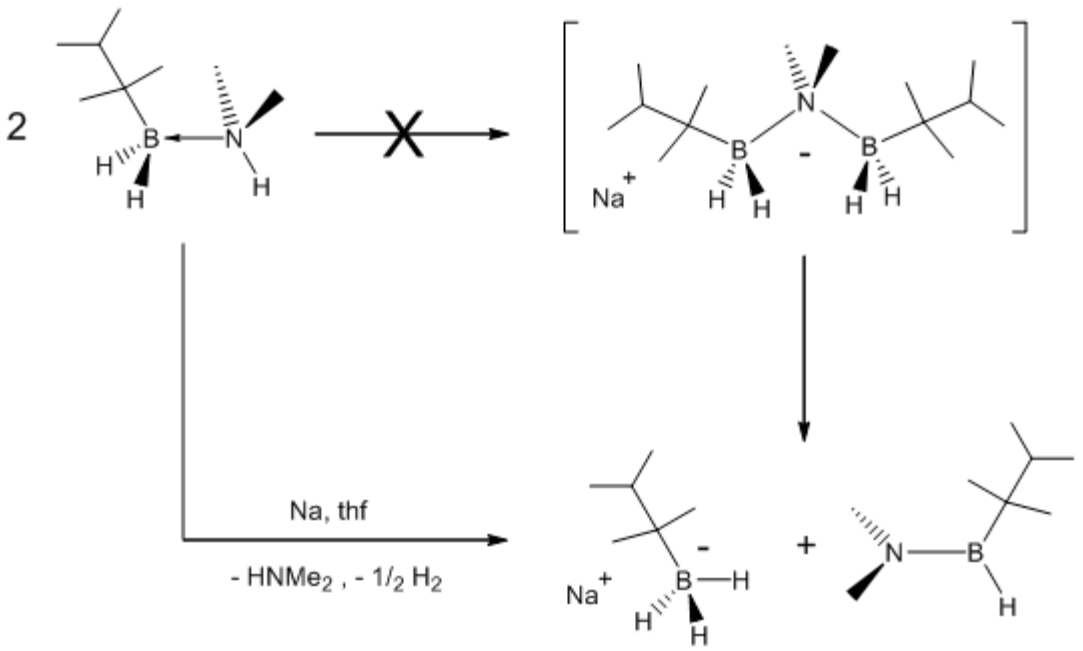

Scheme 7.1

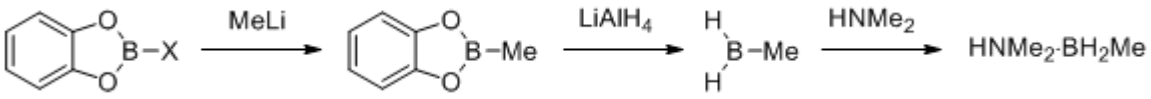

Scheme 7.2

Others have noted that the $-NH_2BH_3^-$ group is isoelectronic with ethyl groups and can bind to metals to form agostic structures;[40] the $H_3B\text{-}NH_2\text{-}BH_3^-$ group is isoelectronic with propane and can similarly serve as a structural model for the binding of this alkane to metal centers.

The successful synthesis of the $H_3B\text{-}NH_2\text{-}BH_3^-$ anion resolves a 90 year old debate about the existence of this species. These aminodiboranates are of interest not only in the context of hydrogen storage materials, but also as ligands for chemical vapor deposition precursors.[25, 27] The absence of carbon in $H_3B\text{-}NH_2\text{-}BH_3^-$ is significant in this regard, because carbon contamination is a problem in many CVD processes.

Experimental

All operations were carried out in vacuum or under argon using standard Schlenk techniques. All glassware was dried in an oven at 150 °C, assembled hot, and allowed to cool under vacuum before use. Tetrahydrofuran, diethyl ether, benzene, and pentane were distilled under nitrogen from sodium/benzophenone and degassed with argon immediately before use. 1,4-Dioxane was distilled from molten sodium and treated similarly. Pyrrolidine, sodium metal, NH_3BH_3, $NaNH_2$, and solutions of BH_3·thf (1.0 M), H_2NMe (2.0 M), and H_2NEt (2.0 M) in tetrahydrofuran were used as received (Aldrich). The salt $Na(H_3B\text{-}NMe_2\text{-}BH_3)$ was prepared by the literature route.[23]

Elemental analyses were carried out by the University of Illinois Microanalytical Laboratory. The IR spectra were recorded on a Nicolet Impact 410 infrared spectrometer as Nujol mulls between KBr plates. The ^1H data were obtained on a Varian Unity 400 instrument at 400 MHz or on a Varian Unity U500 instrument at 500 MHz. The ^{11}B NMR data were collected on a General Electric GN300WB instrument at 96 MHz or on a Varian

Unity Inova 600 instrument at 192 MHz. Chemical shifts are reported in δ units (positive shifts to high frequency) relative to TMS (^{1}H) or BF_3•Et_2O (^{11}B). X-ray crystallographic data were collected by the George L. Clark X-ray Laboratory at the University of Illinois.

Sodium Aminodiboranate, $Na(H_3B\text{-}NH_2\text{-}BH_3)(thf)_x$, 1a. Method A. A solution of $NH_3{\cdot}BH_3$ (3.00 g, 97.1 mmol) in tetrahydrofuran (75 mL) was slowly added to sodium cubes (20 g, 0.9 mol) in thf (75 mL). Gas slowly evolved, and the mixture was stirred at room temperature for 18 h. An aliquot of the reaction mixture was assayed by ^{11}B NMR spectroscopy, which confirmed that the $NH_3{\cdot}BH_3$ (δ -22.3) had been converted to $NaNH_2BH_3$ (δ -21.9). The mixture was then heated to reflux for 21 h, causing a flocculent white solid to precipitate. The solution was filtered and the filtrate was evaporated to dryness under vacuum to yield a white solid. The solid was washed with benzene (2 x 40 mL) and pentane (3 x 30 mL) and then was dried under vacuum to yield a free-flowing white powder. Yield: 1.03 g (28 %). Anal. Calcd for $Na(H_3B\text{-}NH_2\text{-}BH_3)(thf)_{0.08}$, $C_{0.32}H_{8.64}B_2NO_{0.08}Na$: C, 5.30; H, 12.0; N, 19.3. Found: C, 5.28; H, 12.1; N, 19.2. ^{1}H NMR (thf-d_8, 20 °C): δ 1.17 (1:1:1:1 q, J_{BH} = 90 Hz, BH_3, 6 H), 1.63 (br s, NH_2, 2 H). ^{11}B NMR (thf-d_8, 20 °C): δ -19.9 (q, J_{BH} = 90 Hz, BH_3). IR (cm^{-1}): 3306 vs, 3265 vs, 2316 vs, 2289 sh, 2254 sh, 2224 vs, 1572 m, 1556 s, 1237 vs, 1209 m, 1177 s, 1070 sh, 1057 m, 1021 m, 907 w, 871 w, 749 w.

The composition of the white precipitate from the synthesis of **1a** is still under investigation. The principal thermal decomposition product of $NaNH_2BH_3$ has been suggested to be either Na(NBH) or mixtures of NaH and BN.[17, 18] Our microanalytical data are close to the formula $NaNHBH_2(thf)_{0.06}$. Anal. Calcd for $C_{0.24}H_{3.48}BNO_{0.06}Na$: C, 5.23; H, 6.36; N, 25.4. Found: C, 4.62; H, 7.29; N, 25.2.

Method B. A solution of $NH_3{\cdot}BH_3$ (3.14 g, 102 mmol) in tetrahydrofuran (75 mL) was slowly added to a suspension of $NaNH_2$ (1.95 g, 50.0 mmol) in thf (75 mL). Gas slowly

evolved and the solution developed a strong ammonia odor. The mixture was stirred at room temperature for 18 h, over which time most of the $NaNH_2$ was consumed. An aliquot of the reaction mixture was assayed by ^{11}B NMR spectroscopy, which confirmed that the $NH_3{\cdot}BH_3$ had been converted to $NaNH_2BH_3$. The mixture was then heated to reflux for 39 h, causing a flocculent white solid to precipitate. The solution was filtered and the filtrate was evaporated to dryness under vacuum to yield a white solid. The solid was washed benzene (40 mL), diethyl ether (2 x 25 mL), and pentane (2 x 40 mL), and then was dried under vacuum for 12 h to yield a free-flowing white powder. Yield: 1.69 g (50%). The ^{11}B NMR data match that of $Na(H_3B\text{-}NH_2\text{-}BH_3)$ prepared by method A.

Sodium *N*-Methylaminodiboranate, $Na(H_3B\text{-}NHMe\text{-}BH_3)$, 1b. To $BH_3{\cdot}$thf (100 mL of a 1.0 M solution in tetrahydrofuran, 100 mmol) at 0 °C was added dropwise $MeNH_2$ (50 mL of a 2.0 M solution in tetrahydrofuran, 100 mmol). The solution was stirred for 1 h at 0 °C and then slowly transferred to a separate flask containing sodium cubes (20 g, 0.9 mol). Gas slowly evolved. The mixture was refluxed for 70 h, over which time solution slowly turned cloudy and a small amount of precipitate formed. The solution was filtered and the filtrate was evaporated to dryness under vacuum to yield a sticky white solid. The solid was washed with benzene (3 x 50 mL) and pentane (3 x 75 mL), and then was dried under vacuum for 40 h to yield a free-flowing white powder. Yield: 3.32 g (82 %). A small amount of $NaBH_4$ (< 10%) was present as an impurity in the sample, which could be detected by ^1H and ^{11}B NMR spectroscopy. $NaBH_4$-free $Na(H_3B\text{-}NHMe\text{-}BH_3)$ could be obtained by extracting the solid with diethyl ether and then removing the solvent. Anal. Calcd for $Na(H_3B\text{-}NHMe\text{-}BH_3)(thf)_{0.02}$, $C_{1.08}H_{10.16}B_2NO_{0.02}Na$: C, 15.8; H, 12.5; N, 17.0. Found: C, 15.8; H, 12.7; N, 17.0. ^1H NMR (thf-d_8, 20 °C): δ 1.22 (1:1:1:1 q, J_{BH} = 89 Hz, BH_3, 6 H), 2.09 (d, J_{HH} = 6 Hz, NMe, 3 H), 2.11 (br s, NH, 1 H). ^{11}B NMR (thf-d_8, 20 °C): δ -15.7 (q,

J_{BH} = 91 Hz, BH_3). IR (cm^{-1}): 3270 s, 2324 s, 2289 vs, 2262 s, 2226 vs, 1354 m, 1240 s, 1207 m, 1155 vs, 1130 s, 1076 m, 983 m, 956 m, 847 w, 804 w.

Sodium *N*-Ethylaminodiboranate, Na(H_3B-NHEt-BH_3), 1c. To BH_3·thf (100 mL of a 1.0 M solution in tetrahydrofuran, 100 mmol) at 0 °C was added dropwise $EtNH_2$ (50 mL of a 2.0 M solution in tetrahydrofuran, 100 mmol). The solution was stirred for 1 h at 0 °C and then slowly transferred to a separate flask containing sodium cubes (20 g, 0.9 mol). Gas slowly evolved. The mixture was heated to reflux for 65 h, during which time the solution slowly turned cloudy and a small amount of precipitate formed. The solution was filtered and the filtrate was evaporated to dryness under vacuum to yield a sticky grey solid. The solid was washed with benzene (2 x 50 mL) and pentane (3 x 50 mL) and dried under vacuum for 20 h to yield a free-flowing white powder. Yield: 3.21 g (68 %). A small amount of $NaBH_4$ (< 10 %) was present, which could be observed in the ^1H and ^{11}B NMR spectra and by microanalysis. Anal. Calcd for $Na(H_3B\text{-}NHEt\text{-}BH_3)_{0.92}(NaBH_4)_{0.08}$, $C_{1.84}H_{11.36}B_{1.92}N_{0.92}Na$ C, 24.5; H, 12.7; N, 14.3. Found: C, 24.2; H, 12.7; N, 14.5. $NaBH_4$-free Na(H_3B-NHEt-BH_3) could be obtained by extracting the solid with diethyl ether and the absence of $NaBH_4$ was verified by ^{11}B NMR spectroscopy. ^1H NMR (thf-d_8, 20 °C): δ 1.07 (t, J_{HH} = 7 Hz, CH_3, 2 H), 1.18 (1:1:1:1 q, J_{BH} = 89 Hz, BH_3, 6 H), 1.57 (br s, NH, 1 H), 2.41 (quintet, J_{HH} = 7 Hz, NCH_2, 3 H). ^{11}B NMR (thf-d_8, 20 °C): δ -17.2 (q, J_{BH} = 90 Hz, BH_3). IR (cm^{-1}): 3243 vs, 2284 vs, 2240 vs, 1398 s, 1250 m, 1226 m, 1174 s, 1144 vs, 1122 s, 1076 m, 1019 m, 956 s, 852 m, 803 m.

Sodium Pyrrolidinyldiboranate, Na[H_3B-N(C_4H_8)-BH_3], 1d. To BH_3·thf (100 mL of a 1.0 M solution in tetrahydrofuran, 100 mmol) at 0 °C was added dropwise pyrrolidine (8.3 mL, 0.10 mol). The solution was stirred for 2 h at 0 °C and then slowly transferred to a separate flask containing sodium cubes (20 g, 0.9 mol) and thf (50 mL). Gas slowly evolved.

The mixture was heated to reflux for 36 h, over which time the solution slowly turned cloudy. The suspension was filtered and the filtrate was evaporated to dryness under vacuum to yield a sticky grey solid. The solid was washed with benzene (2 x 75 mL) and pentane (2 x 75 mL) and then dried under vacuum to yield a free-flowing white powder. Yield: 4.27 g (71 %). Anal. Calcd for $C_4H_{14}NB_2Na$: C, 39.8; H, 11.7; N, 11.6. Found: C, 39.5; H, 12.0; N, 11.6. ^{1}H NMR (thf-d_8, 20 °C): δ 1.32 (1:1:1:1 q, J_{BH} = 90 Hz, BH_3, 6 H), 1.77 (m, β-CH_2, 4 H), 2.60 (br s, NCH_2, 4 H). ^{11}B NMR (thf-d_8, 20 °C): δ -12.7 (q, J_{BH} = 91 Hz, BH_3). IR (cm^{-1}): 2292 vs, 2235 vs, 1231 s, 1207 s, 1169 s, 1128 m, 1087 s, 1076 m, 1032 w, 1002 m, 943 m, 920 w, 904 w, 866 w.

Sodium *N*,*N*-Dimethylaminodiboranate, Na(H_3B-NMe_2-BH_3), 1e. Crystals of this material were obtained adventitiously from a failed reaction of $YbCl_3$ with three equivalents of **1e** in 1,2-dimethoxyethane. The reaction mixture was evaporated to dryness under vacuum and the yellow residue was extracted with diethyl ether, and the yellow extract was cooled to -20 °C to yield large colorless blocks of **1e**.

Sodium *N*-Methylaminodiboranate Dioxane (1:0.5), Na(H_3B-NHMe-BH_3)(1,4-dioxane)$_{0.5}$, 2b. To Na(H_3B-NHMe-BH_3) (100 mg, 1.24 mmol) was added 1,4-dioxane (2 mL). The solution was stirred for 10 min and evaporated to dryness under vacuum to yield a white solid. The residue was extracted with Et_2O (50 mL), the extract was filtered, and the filtrate was concentrated to 30 mL and stored at -20 °C to yield colorless prisms. Anal. Calcd for $C_3H_{14}B_2NONa$: C, 28.9; H, 11.3; N, 11.2. Found: C, 29.1; H, 11.6; N, 11.3. ^{1}H NMR (dmso-d_6, 20 °C): δ 1.26 (1:1:1:1 q, J_{BH} = 90 Hz, BH_3, 6 H), 2.00 (m, NCH_3, 3 H), 2.06 (br s, NH, 1 H), 3.56 (s, OCH_2, 4 H). ^{11}B NMR (thf-d_8, 20 °C): δ -13.4 (q, J_{BH} = 90 Hz, BH_3). IR (cm^{-1}): 3262 s, 2289 vs, 2246 vs, 1259 m, 1231 m, 1193 m, 1160 s, 1117 m, 1076 s, 1041 w, 978 w, 942 w, 913 m, 874 m, 801 m, 615 m.

Sodium *N*-Ethylaminodiboranate Dioxane (1:1), Na(H_3B-NHEt-BH_3)(1,4-dioxane), 2c. To Na(H_3B-NHEt-BH_3) (100 mg, 1.06 mmol) was added 1,4-dioxane (4 mL). The solution was stirred for 10 min and evaporated to dryness under vacuum to yield a white solid. The residue was extracted with Et_2O (35 mL), the extract was filtered, and the filtrate was stored at -20 °C to yield colorless prisms. Anal. Calcd for Na(H_3B-NHEt-BH_3)(1,4-dioxane)$_{0.85}$: C, 38.2; H, 11.2; N, 8.26. Found: C, 38.2; H, 11.5; N, 8.09. ^{1}H NMR (dmso-d_6, 20 °C): δ 0.99 (t, J_{HH} = 7 Hz, CH_3, 3H), 1.23 (1:1:1:1 q, J_{BH} = 89 Hz, BH_3, 6 H), 1.56 (br s, NH, 1 H), 2.29 (quintet, J_{HH} = 7 Hz, NCH_2, 2 H), 3.56 (s, OCH_2). ^{11}B NMR (thf-d_8, 20 °C): δ -14.8 (q, J_{BH} = 91 Hz, BH_3). IR (cm^{-1}): 3255 s, 2298 vs, 2235 vs, 1291 w, 1256 m, 1221 m, 1193 m, 1150 s, 1117 vs, 1082 s, 1046 w, 956 w, 890 m, 874 vs, 836 w, 801 w, 615 m.

Sodium Pyrrolidinylaminodiboranate Dioxane (1:1), Na[H_3B-N(C_4H_8)-BH_3](1,4-dioxane), 2d. To Na[H_3B-N(C_4H_8)-BH_3] (100 mg, 0.83 mmol) was added 1,4-dioxane (4 mL). The solution was stirred for 10 min and evaporated to dryness under vacuum to yield a white solid. The residue was extracted with Et_2O (35 mL), the extract was filtered, and the filtrate was stored at -20 °C to yield colorless prisms. Anal. Calcd for $C_8H_{22}B_2NO_2Na$: C, 46.0; H, 10.8; N, 6.71. Found: C, 46.1; H, 10.8; N, 6.69. ^{1}H NMR (dmso-d_6, 20 °C): δ 1.36 (1:1:1:1 q, J_{BH} = 91 Hz, BH_3, 6 H), 1.68 (m, βCH_2, 4 H), 2.49 (m, NCH_2, 4 H), 3.56 (s, OCH_2, 8 H). ^{11}B NMR (thf-d_8, 20 °C): δ -10.1 (q, J_{BH} = 92 Hz, BH_3). IR (cm^{-1}): 2311 vs, 2246 vs, 1346 w, 1322 w, 1294 m, 1258 m, 1228 m, 1212 s, 1199 s, 1163 vs, 1130 s, 1114 s, 1079 s, 1049 m, 1032 w, 1003 m, 943 m, 909 w, 891 s, 877 vs, 850 w, 615 s.

Sodium *N,N*-Dimethylaminodiboranate Dioxane (1:1), Na(H_3B-NMe_2-BH_3)(1,4-dioxane), 2e. To Na(H_3B-NMe_2-BH_3) (100 mg, 1.1 mmol) was added 1,4-dioxane (4 mL). The solution was stirred for 10 min and evaporated to dryness under vacuum to yield a white

solid. The residue was extracted with Et_2O (30 mL), the extract was filtered, and the filtrate was stored at -20 °C to yield colorless prisms. Anal. Calcd for $C_6H_{20}B_2NO_2Na$: C, 39.4; H, 11.0; N, 7.66. Found: C, 39.8; H, 11.7; N, 7.58. ^{1}H NMR (dmso-d_6, 20 °C): δ 1.45 (1:1:1:1 q, J_{BH} = 91 Hz, BH_3, 6 H), 2.15 (s, NCH_3, 6 H), 3.56 (s, OCH_2, 8 H). ^{11}B NMR (thf-d_8, 20 °C): δ -8.7 (q, J_{BH} = 92 Hz, BH_3). IR (cm^{-1}): 2390 s, 2297 vs, 2246 s, 1302 s, 1212 s, 1168 vs, 1144 vs, 1114 s, 1087 s, 1046 m, 1029 m, 1016 s, 923 m, 904 m, 888 vs, 877 vs, 790 s, 615 s, 410 s.

Sodium Octahydrotriborate, NaB_3H_8. To a solution of BH_3·thf (200 mL, 1.0 M), cooled to 0 °C in a 500 mL round bottom Schlenk flask, was added $NaNH_2$ (3.62 g, 92.8 mmol) using a solid addition funnel. The mixture was stirred for 1 h at 0 °C and then was warmed to room temperature. The flask was equipped with a reflux condenser and the mixture was refluxed for 5 days. The pale yellow solution was filtered, and the filtrate was evaporated to dryness under vacuum to a sticky, off-white solid. The solid was extracted with Et_2O (100 + 25 mL), the extracts were filtered from some solid ($NaBH_4$), and the filtrates were combined evaporated to dryness under vacuum to yield a sticky, white solid. The solid was washed with benzene (3 x 50 mL) and pentane (3 x 25 mL), and then dried under vacuum to yield a free-flowing white powder. Yield: 2.04 g. Spectroscopic data are consistent with literature values.[31, 34]

Crystallographic Studies.[41] Single crystals of **1e**, **2b**, **2c, 2d,** and **2e**, obtained from diethyl ether, were mounted on glass fibers with Paratone-N oil (Exxon) and immediately cooled to -80 °C in a cold nitrogen gas stream on the diffractometer. Standard peak search and indexing procedures, followed by least-square refinement yielded the cell dimensions given in Table 2. The measured intensities were reduced to structure factor amplitudes and their estimated standard deviations by correction for background and Lorentz and

polarization effects. No corrections for crystal decay were necessary but a face-indexed absorption correction was applied. Systematically absent reflections were deleted and symmetry equivalent reflections were averaged to yield the set of unique data. Except where noted, all unique data were used in the least-squares refinements. The analytical approximations to the scattering factors were used, and all structure factors were corrected for both real and imaginary components of anomalous dispersion. Correct atomic position(s) were deduced from an E-map (SHELXTL); least-squares refinement and difference Fourier calculations were used to locate atoms not found in the initial solution. Except where noted below, hydrogen atoms attached to boron and nitrogen were located in the difference maps and their locations were refined without constraints. Hydrogen atoms attached to carbon were placed in idealized positions with C-H (methyl) = 0.98Å and C -H (methylene) = 0.99 Å; the idealized methyl groups were allowed to rotate about their respective axes to find the best least-squares positions. In the final cycle of least squares, independent anisotropic displacement factors were refined for the non-hydrogen atoms. The displacement parameters for methylene hydrogens were set equal to 1.2 times U_{eq} for the attached carbon; those for methyl hydrogens were set to 1.5 times U_{eq}. No correction for isotropic extinction was necessary. Successful convergence was indicated by the maximum shift/error of 0.000 for the last cycle. A final analysis of variance between observed and calculated structure factors showed no apparent errors. Aspects of the refinements unique to each structure are reported below.

Na(H_3B-NMe_2-BH_3), 1e. The monoclinic lattice and systematic absences $0k0$ ($k \neq 2n$) and $h0l$ ($h + l \neq 2n$) were uniquely consistent with the space group $P2_1/n$, which was confirmed by the success of the subsequent refinement. The DMADB anion bound to Na4 was disordered; to produce satisfactory ellipsoids, the atoms were partitioned over two sites

and the site occupancy factors (SOFs) were constrained to sum to one. The quantity minimized by the least-squares program was $\Sigma w(F_o^2 - F_c^2)^2$, where $w = \{[\sigma(F_o)]^2 + (0.0520 P)^2\}^{-1}$ and $P = (F_o^2 + 2F_c^2)/3$. Hydrogen atoms attached to boron were placed in idealized positions with B-H equal to 1.12 Å; the boranyl groups were allowed to rotate about their B-N axis to find the best least-squares positions. The displacement parameters for the boranyl hydrogens were set to 1.2 times U_{eq} for the attached boron. The largest peak in the final Fourier difference map (0.19 eÅ^{-3}) was located 1.19 Å from H42I.

Na(H_3B-NHMe-BH_3)(1,4-dioxane)$_{0.5}$, 2b. The triclinic lattice and the average values of the normalized structure factors suggested the space group $P\bar{1}$, which was confirmed by the success of the subsequent refinement. The quantity minimized by the least-squares program was $\Sigma w(F_o^2 - F_c^2)^2$, where $w = \{[\sigma(F_o)]^2 + (0.0466P)^2\}^{-1}$ and $P = (F_o^2 + 2F_c^2)/3$. The N-H distances were constrained to be equal with an esd of 0.01 Å. The largest peak in the final Fourier difference map (0.22 eÅ^{-3}) was located 0.74 Å from O2.

Na(H_3B-NHEt-BH_3)(1,4-dioxane), 2c. The crystal selected was twinned and all reflections could be indexed to a triclinic cell with two twin components. Reflections from each component were separated using TWINABS;[42] data from both twin individuals were merged and used in the refinement. The triclinic lattice and the average values of the normalized structure factors suggested the space group $P\bar{1}$, which was confirmed by the success of the subsequent refinement. An absorption correction was applied using TWINABS, the minimum and maximum transmission factors being 0.659 and 0.745. The ethyl group and the C12 atom in the dioxane molecule were disordered; to produce satisfactory ellipsoids, the atoms were partitioned over two sites and the site occupancy factors (SOFs) of these positions were constrained to sum to one. The C-N and C-C bond distances of the ethyl groups were fixed at 1.46 ± 0.01 and 1.52 ± 0.01 Å, respectively. The

disordered O1-C12 distances were constrained to be equal within an esd of 0.01 Å. The C-C bond distances in the dioxane molecules were fixed at 1.47 ± 0.01 Å. The quantity minimized by the least-squares program was $\Sigma w(F_o^2 - F_c^2)^2$, where $w = \{[\sigma(F_o)]^2 + (0.0994P)^2\}^{-1}$ and $P = (F_o^2 + 2F_c^2)/3$. The chemically equivalent B-H and H···H were constrained to be equal within an esd of 0.01 Å. The largest peak in the final Fourier difference map (0.27 eÅ^{-3}) was located 0.73 Å from H11B.

Na[H_3B-N(C_4H_8)-BH_3](1,4-dioxane), 2d. The triclinic lattice and the average values of the normalized structure factors suggested the space group $P\bar{1}$, which was confirmed by the success of the subsequent refinement. The reflection $\bar{3}\bar{1}2$ was a statistical outlier and was deleted; the remaining 2923 unique data were used in the least squares refinement. The quantity minimized by the least-squares program was $\Sigma w(F_o^2 - F_c^2)^2$, where $w = \{[\sigma(F_o)]^2 + (0.0907P)^2\}^{-1}$ and $P = (F_o^2 + 2F_c^2)/3$. The largest peak in the final Fourier difference map (0.64 eÅ^{-3}) was located 1.05 Å from C22.

Na(H_3B-NMe_2-BH_3)(1,4-dioxane), 2e. The systematic absences *hkl* ($h + k \neq 2n$), *h*0*l* ($h,l \neq 2n$), and *h*00 ($h \neq 2n$) were consistent with the space groups $Cmc2_1$, *Cmcm*, and *Ama*2. The centrosymmetric space group *Cmcm* was chosen, and this choice was confirmed by successful refinement of the proposed model. The quantity minimized by the least-squares program was $\Sigma w(F_o^2 - F_c^2)^2$, where $w = \{[\sigma(F_o)]^2 + (0.0724P)^2 + 0.9343P\}^{-1}$ and $P = (F_o^2 + 2F_c^2)/3$. The largest peak in the final Fourier difference map (0.34 eÅ^{-3}) was located 0.74 Å from C2.

References

1. Yang, J.; Sudik, A.; Wolverton, C.; Siegel, D. J. *Chem. Soc. Rev.* **2010,** *39*, 656-675.

2. Lim, K. L.; Kazemian, H.; Yaakob, Z.; Daud, W. R. W. *Chem. Eng. Technol.* **2010,** *33*, 213-226.

3. Murray, L. J.; Dinca, M.; Long, J. R. *Chem. Soc. Rev.* **2009,** *38*, 1294-1314.

4. Graetz, J. *Chem. Soc. Rev.* **2009,** *38*, 73-82.

5. Eberle, U.; Felderhoff, M.; Schueth, F. *Angew. Chem., Int. Ed.* **2009,** *48*, 6608-6630.

6. Wang, P.; Kang, X.-d. *Dalton Trans.* **2008**, 5400-5413.

7. van den Berg, A. W. C.; Arean, C. O. *Chem. Commun.* **2008**, 668-681.

8. Orimo, S.-i.; Nakamori, Y.; Eliseo, J. R.; Zuettel, A.; Jensen, C. M. *Chem. Rev.* **2007,** *107*, 4111-4132.

9. Langmi, H. W.; McGrady, G. S. *Coord. Chem. Rev.* **2007,** *251*, 925-935.

10. Smythe, N. C.; Gordon, J. C. *Eur. J. Inorg. Chem.* **2010**, 509-521.

11. Hamilton, C. W.; Baker, R. T.; Staubitz, A.; Manners, I. *Chem. Soc. Rev.* **2009,** *38*, 279-293.

12. Xu, Q.; Chandra, M. *J. Alloys Compd.* **2007,** *446-447*, 729-732.

13. Stephens, F. H.; Pons, V.; Baker, R. T. *Dalton Trans.* **2007**, 2613-2626.

14. Marder, T. B. *Angew. Chem., Int. Ed.* **2007,** *46*, 8116-8118.

15. Zhang, Q.; Tang, C.; Fang, C.; Fang, F.; Sun, D.; Ouyang, L.; Zhu, M. *J. Phys. Chem. C* **2010,** *114*, 1709-1714.

16. Chua, Y. S.; Wu, G.; Xiong, Z.; He, T.; Chen, P. *Chem. Mater.* **2009,** *21*, 4899-4904.

17. Xiong, Z.; Yong, C. K.; Wu, G.; Chen, P.; Shaw, W.; Karkamkar, A.; Autrey, T.; Jones, M. O.; Johnson, S. R.; Edwards, P. P.; David, W. I. F. *Nat. Mater.* **2008,** *7*, 138-141.

18. Xiong, Z.; Wu, G.; Chua, Y. S.; Hu, J.; He, T.; Xu, W.; Chen, P. *Energy Environ. Sci.* **2008,** *1*, 360-363.

19. Schlesinger, H. I.; Burg, A. B. *J. Am. Chem. Soc.* **1938,** *60*, 290-299.

20. Stock, A.; Kuss, E. *Ber. Dtsch. Chem. Ges. B* **1923,** *56B*, 789-808.

21. Schultz, D. R.; Parry, R. W. *J. Am. Chem. Soc.* **1958,** *80*, 4-8.

22. Keller, P. C. *J. Chem. Soc. D* **1969**, 1465.

23. Nöth, H.; Thomas, S. *Eur. J. Inorg. Chem.* **1999**, 1373-1379.

24. Daly, S. R.; Girolami, G. S. *Chem. Commun.* **2010,** *46*, 407-408.

25. Daly, S. R.; Kim, D. Y.; Yang, Y.; Abelson, J. R.; Girolami, G. S. *J. Am. Chem. Soc.* **2010,** *132*, 2106-2107.

26. Girolami, G. S.; Kim, D. Y.; Abelson, J. R.; Kumar, N.; Yang, Y.; Daly, S. U.S. Pat. Appl. 59728, April 9, 2008.

27. Kumar, N.; Yanguas-Gil, A.; Daly, S. R.; Girolami, G. S.; Abelson, J. R. *Appl. Phys. Lett.* **2009**, *95*, 144107/1-144107/3.

28. Gottlieb, H. E.; Kotlyar, V.; Nudelman, A. *J. Org. Chem.* **1997,** *62*, 7512-7515.

29. Kim, D. Y.; Girolami, G. S. *J. Am. Chem. Soc.* **2006,** *128*, 10969-10977.

30. Goedde, D. M.; Girolami, G. S. *J. Am. Chem. Soc.* **2004,** *126*, 12230-12231.

31. Goedde, D. M.; Windler, G. K.; Girolami, G. S. *Inorg. Chem.* **2007,** *46*, 2814-2823.

32. Kim, D. Y.; Yang, Y.; Abelson, J. R.; Girolami, G. S. *Inorg. Chem.* **2007,** *46*, 9060-9066.

33. Kim, D. Y.; You, Y.; Girolami, G. S. *J. Organomet. Chem.* **2008,** *693*, 981-986.

34. Eaton, G. R.; Lipscomb, W. N. *N.M.R. Studies of Boron Hydrides and Related Compounds*. Benjamin: New York, 1969.

35. Zweifel, G.; Brown, H. C. *J. Am. Chem. Soc.* **1963,** *85*, 2066-2072.

36. Brown, H. C.; Moerikofer, A. W. *J. Am. Chem. Soc.* **1962,** *84*, 1478-1484.

37. Paul, V.; Roberts, B. P. *J. Chem. Soc., Perkin Trans. 2* **1988**, 1183-1193.

38. Brown, H. C.; Singaram, B.; Mathew, C. P. *J. Org. Chem.* **1981,** *46*, 2712-2717.

39. Hawthorne, M. F. *J. Am. Chem. Soc.* **1961,** *83*, 2671-2673.

40. Forster, T. D.; Tuononen, H. M.; Parvez, M.; Roesler, R. *J. Am. Chem. Soc.* **2009,** *131*, 6689-6691.

41. Brumaghim, J. L.; Priepot, J. G.; Girolami, G. S. *Organometallics* **1999,** *18*, 2139-2144.

42. Sheldrick, G. M. *TWINABS*, 2008.

CHAPTER 8. Synthesis, Characterization, and Properties of New *N*,*N*-dialkyl, *N*-alkyl, and Unsubstituted Metal Aminodiboranate Complexes

Introduction

Molecular precursors for chemical vapor deposition (CVD) and atomic layer deposition (ALD) require suitable reactivity to produce desired film compositions, and high volatility to enhance the conformality of deposited films and increase the precursor cycling rates.[1-7] It is well known that the reactivity and volatility within a specific class of metal complexes can be modulated by changing the substituents attached to the ligands.[8-10] For example, the volatility of metal complexes can be enhanced by employing substituents that (1) are large enough to inhibit polymerization or oligomerization of the complexes in the solid state, (2) reduce intermolecular dipolar attractions in the solid state, (3) disrupt efficient packing of the metal complexes in the solid state, and (4) have conformal degrees of freedom that are constrained in the solid state but liberated in the gas phase.[9-14] Changing substituents may also change the mechanistic pathways responsible for the nucleation, growth, and morphologies of the deposited films.[15]

The *N*,*N*-dimethylaminodiboranate anion, $H_3BNMe_2BH_3^-$,[16-18] is a versatile ligand that has been used to prepare volatile complexes of magnesium, transition metals, and the lanthanides that are useful as CVD precursors for the deposition of metal borides and metal oxides.[19] For instance, $Ti(H_3BNMe_2BH_3)_2$ has been used for the deposition of TiB_2, and $Mg(H_3BNMe_2BH_3)_2$ and $Y(H_3BNMe_2BH_3)_3$ have been used for the deposition of MgO and Y_2O_3, respectively, using water as a secondary reactant.[20, 21] We have shown elsewhere that the method used to prepare $H_3BNMe_2BH_3^-$ (DMADB) can be modified to afford other aminodiboranate ligands (Chapter 7). We now show that these new anions can serve as

ligands toward metals. The new *N,N*-dialkylaminodiboranates complexes behave much like their DMADB analogs; in contrast, the chemical and physical properties of the monoalkyl and unsubstituted aminodiboranate complexes are rather different.

Results and Discussion

Synthesis and characterization of new pyrrolidinyldiboranate complexes. By modifying the literature procedure to obtain the chelating borohydride salt $Na(H_3BNMe_2BH_3)$, Na(DMADB),[18] we have recently synthesized a family of related salts with the stoichiometry $Na(H_3BNR_2BH_3)$ where NR_2 = NH_2, NHMe, NHEt, NMeEt, and NC_4H_8 (pyrrolidinyl). We have investigated the synthetic utility of the new aminodiboranate salts by carrying out reactions analogous to those known to afford isolable metal DMADB complexes.[19]

Thus, pyrrolidinyldiboranate complexes of magnesium, molybdenum, and erbium were prepared by treatment of the corresponding metal halide with $H_3BN(C_4H_8)BH_3^-$ (PYDDB):

$$MgBr_2 + 2\ Na[H_3BN(C_4H_8)BH_3] \xrightarrow{\text{grinding}} Mg[H_3BN(C_4H_8)BH_3]_2 + 2\ NaBr \quad (\mathbf{1})$$

$$MoCl_3(thf)_3 + 2\ Na[H_3BN(C_4H_8)BH_3] \xrightarrow{Et_2O} Mo[H_3BN(C_4H_8)BH_3]_2 + {}^1/_2\ H_2 + [N(C_4H_8)]B_2H_5 + 3\ NaCl \quad (\mathbf{2})$$

$$ErCl_3 + 3\ Na[H_3BN(C_4H_8)BH_3] \xrightarrow{thf} Er[H_3BN(C_4H_8)BH_3]_3(thf) + 3\ NaCl \quad (\mathbf{3})$$

These complexes can be isolated from the corresponding reaction mixtures in the same as for the DMADB analogues: $Mg[H_3BN(C_4H_8)BH_3]_2$ (**1**) can be sublimed at 75 °C at 10^{-2} Torr,

Table 8.1. Crystallographic data for $Mg[H_3BN(C_4H_8)BH_3]_2$ (**1**), $Mo[H_3BN(C_4H_8)BH_3]_2$ (**2**), $Er[H_3BN(C_4H_8)BH_3]_3(thf)$ (**3**), $Mg(H_3BNEtHBH_3)_2$ (**4**), and $Er(H_3BNH_2BH_3)Cl_2(thf)_3 \cdot thf$ (**5**).

	1	**2**	**3**	**4**	**5·thf**
formula	$C_8H_{28}B_4N_2Mg$	$C_8H_{28}B_4N_2Mo$	$C_{16}H_{50}B_6N_3OEr$	$C_4H_{24}B_4N_2Mg$	$C_{16}H_{40}B_2Cl_2NO_4Er$
FW (g mol^{-1})	219.87	291.5	532.71	167.80	570.27
temp (K)	193(2)	198(2)	198(2)	193(2)	193(2)
wavelength (Å)	0.71073	0.71073	0.71073	0.71073	0.71073
crystal system	triclinic	monoclinic	monoclinic	triclinic	monoclinic
space group	*P*-1	$P2_1/c$	*Cc*	*P*-1	$P2_1/n$
a (Å)	6.2839(6)	5.8097(15)	17.341(5)	9.644(2)	9.9649(4)
b (Å)	9.8180(10)	10.589(3)	13.395(4)	10.563(2)	21.9294(8)
c (Å)	12.5022(12)	11.985(3)	11.375(3)	12.487(3)	11.2331(4)
α (deg)	73.916(4)	90	90	83.435(14)	90
β (deg)	89.382(4)	102.036(3)	95.397(4)	78.395(14)	90.552(2)
γ (deg)	84.782(4)	90	90	76.727(13)	90
volume (Å^3)	737.98(13)	721.1(3)	2630.6(13)	1209.6(5)	2454.59(16)
Z	2	2	4	4	4
D_{calc} (g cm^{-3})	0.989	1.343	1.345	0.921	1.543
μ (mm^{-1})	0.092	0.881	3.200	0.096	3.655
absorption correction	multi-scan	face-indexed	face-indexed	face-indexed	face-indexed
max. min. transm. factors	0.970, 0.802	0.859, 0.733	0.680, 0.437	0.996, 0.947	0.477/0.204
data/restraints/parameters	15152/0/174	1752/7/127	6278/7/244	4408/88/316	5678/1/267
goodness-of-fit on F^2	0.997	0.959	0.979	0.791	1.073
*R*1 [I > 2σ(I)][a]	0.0562	0.0155	0.0302	0.0711	0.0229
*wR*2 (all data)[b]	0.1558	0.0408	0.0679	0.1903	0.0554
max, min $\Delta\rho_{electron}$ (e·Å^{-3})	0.229/-0.220	0.296/-0.344	1.518/-0.427	0.267/-0.256	0.957/-0.783

[a] $R_1 = \sum |F_o| - |F_c| \,| / |\sum |F_o|$ for reflections with $F_o^2 > 2\,\sigma(F_o^2)$. [b] $wR_2 = [\sum w(F_o^2 - F_c^2)^2 / \sum (F_o^2)^2]^{1/2}$ for all reflections.

green crystals of $Mo[H_3BN(C_4H_8)BH_3]_2$ (**2**) can be grown from diethyl ether, and pink crystals of $Er[H_3BN(C_4H_8)BH_3]_3(thf)$ (**3**) can be grown from pentane.

Single-crystal X-ray diffraction studies of **1** reveal that the two chelating PYDDB ligands each coordinate to the magnesium atom by means of four B-H-M bridges, and that the two ligands backbones form a dihedral angle of 45° with respect to each other (Figure 8.1), exactly as seen in the structure of $Mg(H_3BNMe_2BH_3)_2$. The geometry of the inner coordination sphere, which consists of the eight bridging hydrogen atoms, is rectangular anitprismatic. The idealized point symmetry (i.e., ignoring the carbon atoms in the pyrrolidyl rings) is D_2. The Mg···B distances, which range from 2.377 – 2.386 Å, are similar to those in $Mg(H_3BNMe_2BH_3)_2$ (Table 8.2).[19]

The ^{1}H NMR spectrum of **1** reveals two pyrrolidyl resonances, a multiplet at δ 1.56 and a broad singlet at δ 2.52 that correspond to the β-CH_2 and α-CH_2 groups, respectively. The BH_3 resonance is a 1:1:1:1 quartet at δ 1.95 (J_{BH} = 90 Hz) due to coupling with the quadripolar ^{11}B nuclei (I = 3/2). The terminal and bridging B-H groups are rapidly exchanging on the NMR time scale, as observed for other diamagnetic borohydride complexes.[22] Correspondingly, the ^{11}B NMR spectrum features a binomial quartet at δ -13.7 (J_{BH} = 90 Hz). The IR spectrum of **2** is similar to that of $Mg(H_3BNMe_2BH_3)_2$: there are strong terminal and bridging B-H stretching bands at 2439 and 2198 cm^{-1}, respectively, and weaker bands at 2353, 2290, and 2141 cm^{-1}.[19] The field-ionization mass spectrum (FI-MS) exhibits a peak at m/z 219 corresponding to the parent ion $Mg[H_3BN(C_4H_8)BH_3]_2^+$.

The structure of the molybdenum complex **2** is similar to that of **1** except the B-N-B backbone of the two chelating PYDDB ligands reside in the same plane, yielding local D_{2h} symmetry around the molybdenum atom (Figure 8.2). The Mo···B distances are 2.292(2) and 2.293(2) Å and the Mo-H distances range from 1.83(1) – 1.89(2) Å (Table 8.3). The

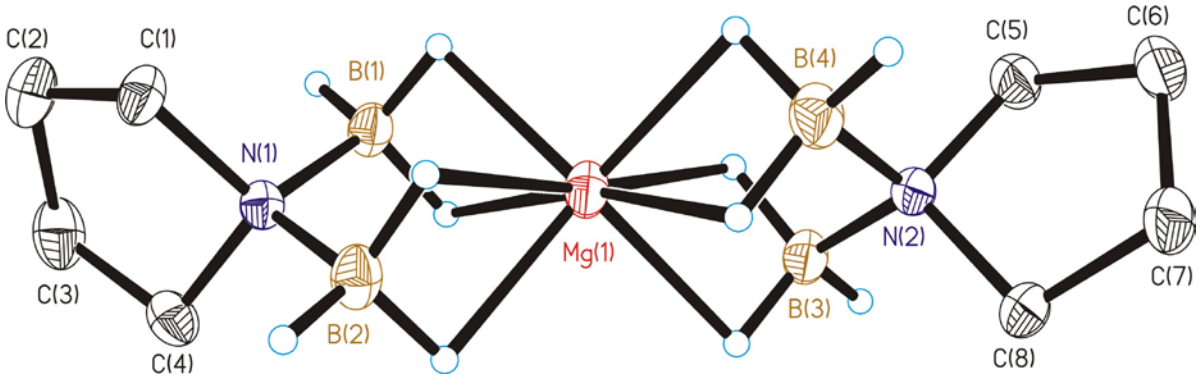

Figure 8.1. Molecular structure of $Mg[H_3BN(C_4H_8)BH_3]_2$. Ellipsoids are drawn at the 35% probability level, except for hydrogen atoms, which are represented as arbitrarily sized spheres. The hydrogen atoms on the methylene groups have been removed for clarity.

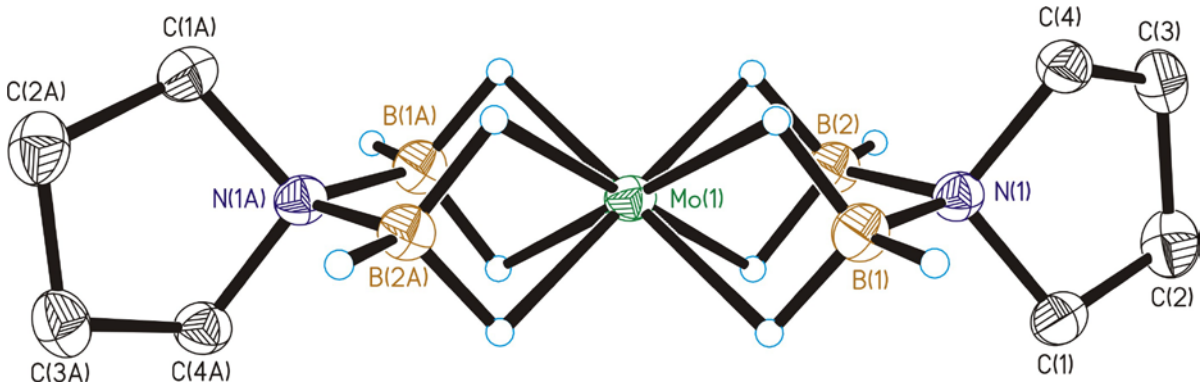

Figure 8.2. Molecular structure of $Mo[H_3BN(C_4H_8)BH_3]_2$. Ellipsoids are drawn at the 35% probability level, except for hydrogen atoms, which are represented as arbitrarily sized spheres. The hydrogen atoms on the methylene groups have been removed for clarity.

Table 8.2. Selected Bond Lengths and Angles for $Mg[H_3BN(C_4H_8)BH_3]_2$, (**2**).

	Bond Lengths (Å)		
Mg(1)-B(1)	2.3878(15)	Mg(1)-H(21)	1.984(11)
Mg(1)-B(2)	2.3773(15)	Mg(1)-H(22)	2.020(10)
Mg(1)-B(3)	2.3827(14)	Mg(1)-H(31)	2.039(11)
Mg(1)-B(4)	2.3818(15)	Mg(1)-H(32)	2.018(10)
Mg(1)-H(11)	2.007(11)	Mg(1)-H(41)	2.010(11)
Mg(1)-H(12)	2.051(11)	Mg(1)-H(42)	2.035(11)
	Bond Angles (deg)		
B(2)-Mg(1)-B(4)	151.09(6)	B(4)-Mg(1)-B(1)	122.00(5)
B(2)-Mg(1)-B(3)	126.07(5)	B(3)-Mg(1)-B(1)	146.44(5)
B(4)-Mg(1)-B(3)	65.40(5)	B(1)-N(1)-B(2)	109.36(9)
B(2)-Mg(1)-B(1)	65.40(5)	B(3)-N(2)-B(4)	109.31(9)

Table 8.3. Selected Bond Lengths and Angles for $Mo[H_3BN(C_4H_8)BH_3]_2$, (**2**).

	Bond Lengths (Å)		
Mo(1)-B(1)	2.2920(17)	Mo(1)-H(11)	1.852(16)
Mo(1)-B(1)'	2.2920(17)	Mo(1)-H(12)	1.891(15)
Mo(1)-B(2)	2.2926(17)	Mo(1)-H(21)	1.883(16)
Mo(1)-B(2)'	2.2926(17)	Mo(1)-H(22)	1.832(13)
	Bond Angles (deg)		
B(1)-Mo(1)-B(2)	64.23(6)	H(11)-Mo(1)-H(12)	60.4(5)
B(1)-Mo(1)-B(1)'	180.00(5)	H(11)-Mo(1)-H(21)	71.2(6)
B(1)-Mo(1)-B(2)'	115.77(6)	H(11)-Mo(1)-H(22)	101.3(5)
B(1)'-Mo(1)-B(2)	115.77(6)	H(12)-Mo(1)-H(21)	101.1(5)
B(1)'-Mo(1)-B(2)'	64.23(6)	H(12)-Mo(1)-H(22)	72.2(6)
B(2)-Mo(1)-B(2)'	180.00(6)	H(21)-Mo(1)-H(22)	60.5(5)
B(1)-N(1)-B(2)	101.17(11)		

Symmetry transformations used to generate equivalent atoms: ' = -x,-y+1,-z

rectangular prismatic geometry described by the eight hydrogen atoms, matches the structure observed for $Mo(H_3BNMe_2BH_3)_2$.[19] The color and chemical properties of **2** also resemble those of its DMADB analog: both complexes are dark green and are surprisingly unreactive toward water, air, and even hydrochloric acid solutions.

The NMR data of **2** are also similar to those of $Mo(H_3BNMe_2BH_3)_2$: both complexes are diamagnetic (low-spin d^4) and exist in solution as two NMR-distinguishable isomers. It has been shown in previous studies (VT NMR spectroscopy and DFT calculations)[23] that the major isomer has the D_{2h} structure and the minor isomer adopts a D_{2d} structure in which the two ligand backbones form a dihedral angle of 90°. The ^1H NMR data of **2** are unusual because the bridging and terminal B-H groups are not exchanging rapidly on the NMR time scale, and can be readily distinguished. The $^1H\{^{11}B\}$ spectrum reveals doublets corresponding to the Mo-H-B groups at δ -6.19 for the major isomer and δ -6.21 for the minor isomer. Similarly, the terminal B-H groups appear as triplets at δ 5.33 and 4.93 for the major and minor isomers, respectively. The ^{11}B NMR spectrum exhibits two quartets at δ 24.0 (J_{BH} = 70 Hz) and 23.2 (J_{BH}= 75 Hz) that also correspond to the major and minor isomers. All proton resonances attributed to the pyrrolidyl rings are readily identifiable.

The IR spectrum of **2** reveals a strong terminal B-H stretch at 2423 cm^{-1} that is characteristic of most transition metal aminodiboranate complexes, but the bridging M-H-B stretch is shifted to much lower energy than is typically observed at 1882 cm^{-1}. For comparison, the M-H-B stretches of the Ti, Cr, and Mn DMADB complexes range from 2156 – 2088 cm^{-1}.[19] Similar frequencies are observed in the IR spectra of $Mo(H_3BNMe_2BH_3)_2$ (1865 cm^{-1}) and $Mo(H_3BNEtMeBH_3)_2$ (1885 cm^{-1}), which suggests that the Mo-H-B bonding in these complexes is highly covalent.[19] The FI-MS data collected for **2** yield the expected $Mo[H_3BN(C_4H_8)BH_3]_2^+$ parent ion at *m*/*z* 291.

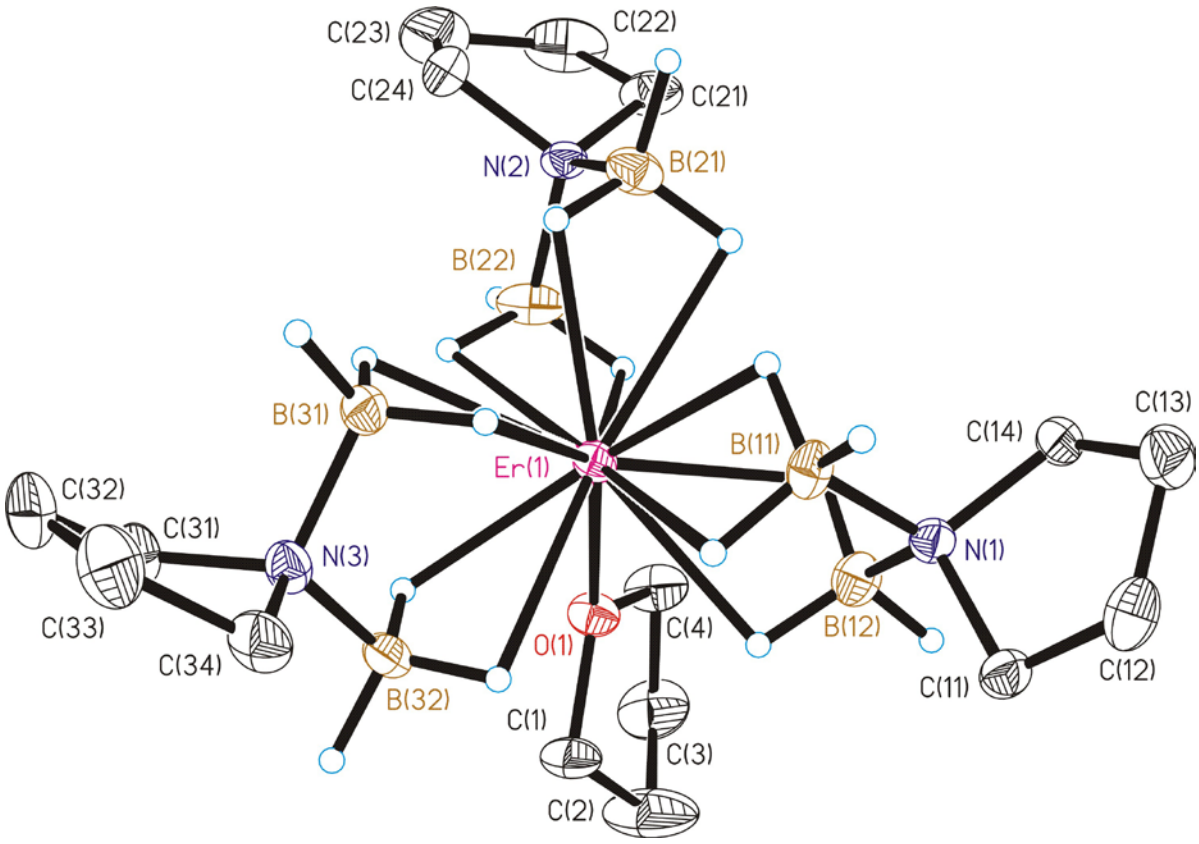

Figure 8.3. Molecular structure of $Er[H_3BN(C_4H_8)BH_3]_3(thf)$. Ellipsoids are drawn at the 35% probability level, except for hydrogen atoms, which are represented as arbitrarily sized spheres. The hydrogen atoms on the methylene groups have been removed for clarity.

Table 8.4. Selected Bond Lengths and Angles for $Er[H_3BN(C_4H_8)BH_3]_3(thf)$, (**3**).

		Bond Lengths (Å)	
Er(1)-O(1)	2.463(3)	Er(1)-B(22)	2.784(6)
Er(1)-B(11)	2.865(6)	Er(1)-B(31)	2.780(6)
Er(1)-B(12)	2.761(6)	Er(1)-B(32)	2.760(6)
Er(1)-B(21)	2.842(6)		
		Bond Angles (deg)	
B(12)-Er(1)-B(11)	53.80(17)	B(31)-Er(1)-B(22)	102.57(19)
B(21)-Er(1)-B(11)	88.85(17)	B(32)-Er(1)-B(22)	114.6(2)
B(22)-Er(1)-B(11)	138.60(19)	B(32)-Er(1)-B(31)	54.28(16)
B(31)-Er(1)-B(11)	92.17(17)	O(1)-Er(1)-B(11)	124.25(14)
B(32)-Er(1)-B(11)	105.51(18)	O(1)-Er(1)-B(12)	73.40(15)
B(12)-Er(1)-B(21)	106.45(19)	O(1)-Er(1)-B(21)	125.47(15)
B(12)-Er(1)-B(22)	115.0(2)	O(1)-Er(1)-B(22)	76.33(14)
B(12)-Er(1)-B(31)	141.41(17)	O(1)-Er(1)-B(31)	126.51(15)
B(32)-Er(1)-B(12)	112.58(19)	O(1)-Er(1)-B(32)	77.16(14)
B(22)-Er(1)-B(21)	53.79(17)	B(12)-N(1)-B(11)	107.4(4)
B(31)-Er(1)-B(21)	88.27(18)	B(21)-N(2)-B(22)	107.2(4)
B(32)-Er(1)-B(21)	139.55(19)	B(32)-N(3)-B(31)	106.3(4)

Like **1** and **2**, the structure of the erbium complex **3** matches that of its DMADB counterpart $Er(H_3BNMe_2BH_3)_3(thf)$ (Figure 8.3). The boron and oxygen atoms of the three chelating PYDDB ligands and a thf molecule form a geometry best described as intermediate between a capped trigonal prism and a capped octahedron. The Er···B and Er-O distances are 2.760(6) – 2.865(6) Å and 2.463(3) Å, respectively (Table 8.4). The ^1H NMR spectrum yields paramagnetically shifted and broadened resonances at δ -38.69 (fwhm = 370 Hz) and -26.86 (fwhm = 120 Hz) for the coordinated thf molecule and δ 5.75 (fwhm = 30 Hz) and 15.97 (fwhm = 130 Hz) for the pyrollidyl fragment. A very broad peak is also observed at 109.2 (fwhm = 2400 Hz) due to the BH_3 hydrides. The large width and paramagnetic shielding is due to the proximity of these hydrogen atoms to the erbium ion. The ^{11}B NMR spectrum shows a similarly broadened and shifted BH_3 resonance at δ -154.0 (fwhm = 200 Hz). For comparison, the ^{11}B NMR spectrum of $Er(H_3BNMe_2BH_3)_3(thf)$ consists of a broad resonance at δ -171.5 (fwhm = 180 Hz) (Chapter 4).[24]

Synthesis and characterization of the mono-alkyl and unsubstituted aminodiboranate complexes $Mg(H_3BNHEtBH_3)_2$ and $Er(H_3BNH_2BH_3)Cl_2(thf)_3$. Treatment of $MgBr_2$ with the monoalkyl diboranate salt $Na(H_3BNHEtBH_3)$ affords the new complex $Mg(H_3BNEtHBH_3)_2$, **4**. Although the stoichiometry of **4** is analogous to that of the pyrrolidinyl complex **1**, the properties of **4** are very different from those of its dialkyl aminodiboranate analogs. For example, when **4** is sublimed, it condenses on the cold-finger as a viscous oil, which slowly crystallizes over several days to produce long needles.

The supercooling behavior observed for **4** suggests that the crystallization process is "frustrated.". A single-crystal X-ray diffraction study of the needles reveals the potential source of the crystallographic frustration. Whereas the DMADB complex $Mg(H_3BNMe_2BH_3)_2$ and its pyrrolidinyl analog **1** are monomeric, the *N*-

ethylaminodiboranate complex **4** is a complex polymer (Figure 8.4). The structure consists of fused 16-membered rings formed from four aminodiboranate ligands and four Mg atoms. Two different Mg environments are present. The first, denoted by Mg1 and Mg1a, is coordinated to one chelating and two bridging $H_3BNEtHBH_3^-$ ligands, and the second, denoted by Mg2 and Mg2a, is coordinated to four bridging $H_3BNEtHBH_3^-$ ligands. The coordination geometry of both magnesium environments, as described by the positions of the boron atoms, is distorted tetrahedral. The Mg···B distances, which range from 2.392(7) – 2.498(7) Å, are slightly longer than those observed for the chelating PYDDB ligands in **1** (Table 8.5). The Mg-H distances range from 2.00(3) – 2.19(4) Å.

The DMADB complex $Mg(H_3BNMe_2BH_3)_2$ sublimes in vacuum at 70 °C and is currently the most volatile magnesium complex known. Despite the polymeric nature of the *N*-ethyl analog **4** in the solid state, it sublimes at ca. 65 °C at 10^{-2} Torr, and therefore appears to supplant the *N*,*N*-dimethylaminodiboranate complex as the new title holder. Compound **4** melts at 61 – 62 °C ,and we believe that melting is accompanied by depolymerization of the polymeric structure, probably to $Mg(H_3BNEtHBH_3)_2$ monomers. For comparison, the melting point of the DMADB complex $Mg(H_3BNMe_2BH_3)_2$ is 70 °C. The asymmetry of the $H_3BNEtHBH_3^-$ ligand evidently helps to disrupt effective packing of $Mg(H_3BNEtHBH_3)_2$ in the solid-state, thereby decreasing its melting point and increasing its volatility.

The ^1H and ^{11}B NMR spectra of the oil and the needles of **4** are identical. The ^1H NMR spectra reveal a triplet at δ 0.72 and a quintet at δ 2.18 that are assignable to the *N*-ethyl group. A broad resonance (fwhm = 50 Hz) attributed to the N-H group is located at δ 0.94 and a 1:1:1:1 quartet corresponding to the BH_3 groups is observed at δ 1.81. The ^{11}B NMR spectra reveal a binomial quartet at δ -17.2 (J_{BH} = 91 Hz). The IR spectrum contains an N-H stretching band due to the N-H bond in $H_3BNEtHBH_3^-$ ligand at 3266 cm^{-1}; this

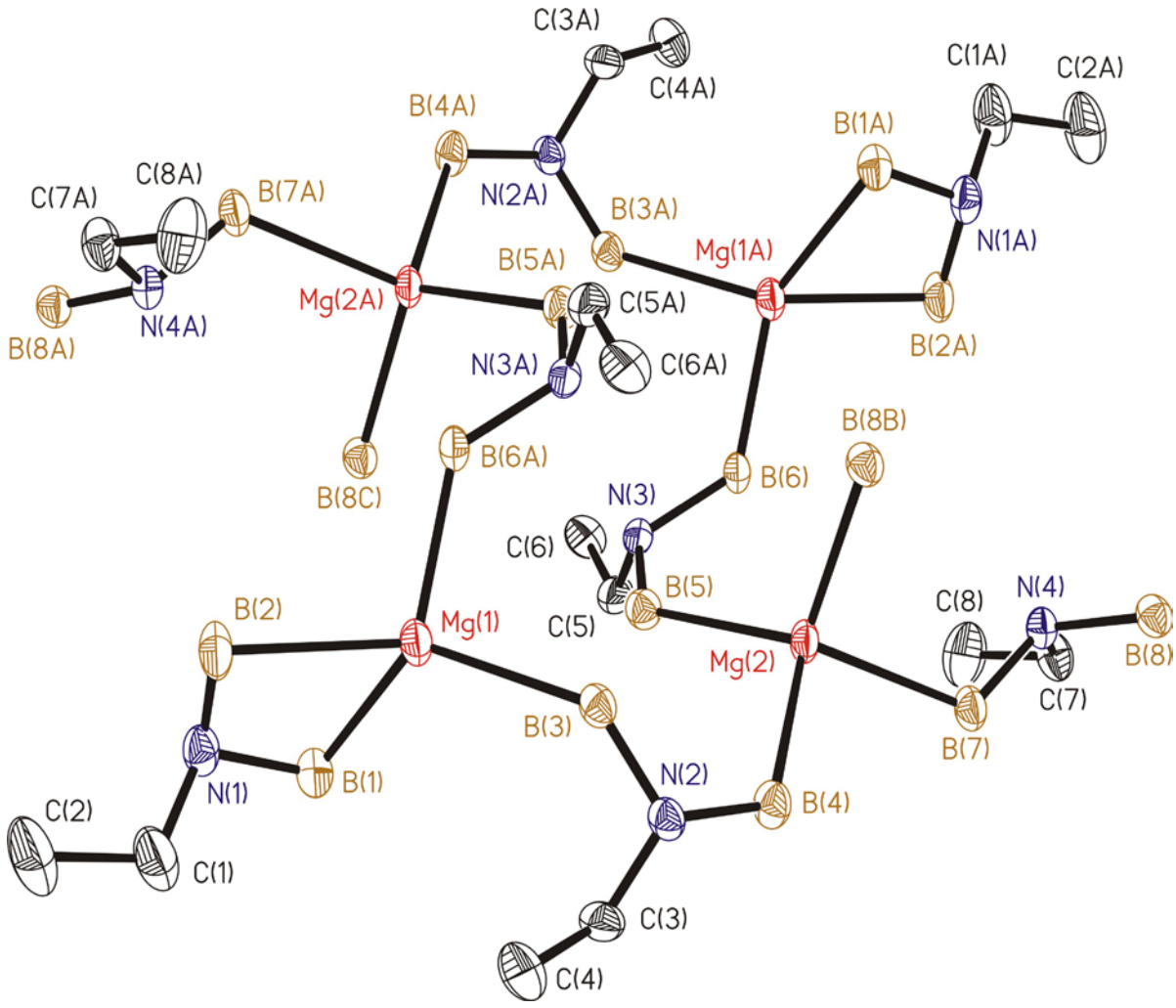

Figure 8.4. Molecular structure of $Mg(H_3BNEtHBH_3)_2$. Ellipsoids are drawn at the 35% probability level. The hydrogen atoms have been removed for clarity.

Table 8.5. Selected Bond Lengths and Angles for $Mg(H_3BNEtHBH_3)_2$, (**4**).

Bond Lengths (Å)			
Mg(1)-B(1)	2.397(8)	Mg(1)-H(21)	2.19(4)
Mg(1)-B(2)	2.428(7)	Mg(1)-H(22)	2.10(4)
Mg(1)-B(3)	2.447(7)	Mg(1)-H(31)	2.02(4)
Mg(1)-B(6)'	2.392(7)	Mg(1)-H(32)	2.02(4)
Mg(2)-B(4)	2.489(8)	Mg(2)-H(41)	2.08(4)
Mg(2)-B(5)	2.498(7)	Mg(2)-H(42)	2.03(4)
Mg(2)-B(7)	2.481(7)	Mg(2)-H(51)	2.14(5)
Mg(2)-B(8)"	2.469(7)	Mg(2)-H(52)	2.08(4)
Mg(1)-H(11)	2.02(4)	Mg(2)-H(71)	2.04(4)
Mg(1)-H(12)	2.00(3)	Mg(2)-H(72)	2.14(4)
Bond Angles (deg)			
B(1)-Mg(1)-B(2)	64.9(3)	B(7)-Mg(2)-B(4)	95.3(2)
B(1)-Mg(1)-B(3)	116.5(3)	B(4)-Mg(2)-B(8)"	122.1(3)
B(2)-Mg(1)-B(3)	139.5(3)	B(5)-Mg(2)-B(8)"	107.1(2)
B(1)-Mg(1)-B(6)'	140.1(3)	B(7)-Mg(2)-B(8)"	100.7(2)
B(2)-Mg(1)-B(6)'	102.9(3)	B(2)-N(1)-B(1)	109.7(5)
B(3)-Mg(1)-B(6)'	97.4(2)	B(3)-N(2)-B(4)	111.1(5)
B(4)-Mg(2)-B(5)	108.1(2)	B(5)-N(3)-B(6)	111.5(5)
B(7)-Mg(2)-B(5)	124.7(3)	B(8)-N(4)-B(7)	111.6(5)

Symmetry transformations used to generate equiv atoms: ' = -x+1,-y+2,-z " = -x+1,-y+1,-z

frequency is similar to that observed of 3243 $cm^{-1}$for the sodium salt. Two strong terminal B-H stretches are observed at 2439 and 2411 cm^{-1}, which compliment two strong bridging B-H stretches at 2207 and 2176 cm^{-1}. The two sets of B-H stretches are probably a result of the presence of two aminodiboranate environments, one that bridges the magnesium atoms and the other that is chelating. One other strong bridging B-H stretch is observed at 2293 cm^{-1}. The FI-MS spectrum corroborates the formula of **4**, yielding the parent fragment $Mg(H_3BNEtHBH_3)_2^+$ at *m*/*z* 167.

Despite the successful preparation of **4**, in general the reactions of metal halides with monosubstituted aminodiboranates such as $Na(H_3BNHEtBH_3)$ and $Na(H_3BNHMeBH_3)$ and with the unsubstituted parent salt $Na(H_3BNH_2BH_3)$ proceed differently than the analogous reactions with dialkylaminodiboranates. For example, the reactions of $ErCl_3$ with the monoalkyl or unsubstituted salts in thf do not yield pentane soluble products analogous to $Er(H_3BNMe_2BH_3)_3(thf)$ and its PYDDB analog **3**. The dried reaction residues, however, can be extracted with Et_2O to initially afford clear pink solutions, but no crystalline material has yet been obtained from these extracts owing to a pink solid that slowly precipitates from these solutions.

If the thf reaction solutions are filtered, concentrated, and cooled, the solutions deposit large pink blocks of stoichiometry $Er(H_3BNMe_2BH_3)Cl_2(thf)_3{\cdot}thf$, **5**. The ^{11}B NMR spectrum of **5** in thf exhibits a peak at δ -176.2 (fwhm = 250 Hz); this shift is similar to those observed for **3** and for $Er(H_3BNMe_2BH_3)_3(thf)$ (see above)

A single-crystal X-ray diffraction study of **5** confirms that only one aminodiboranate ligand is coordinated to the Er center (Figure 8.5). This erbium complex provides the first crystallographic verification of the $H_3B\text{-}NH_2\text{-}BH_3^-$ structural unit. The coordination geometry of **5** is a distorted pentagonal bipyramid, in which the two chloride atoms occupy

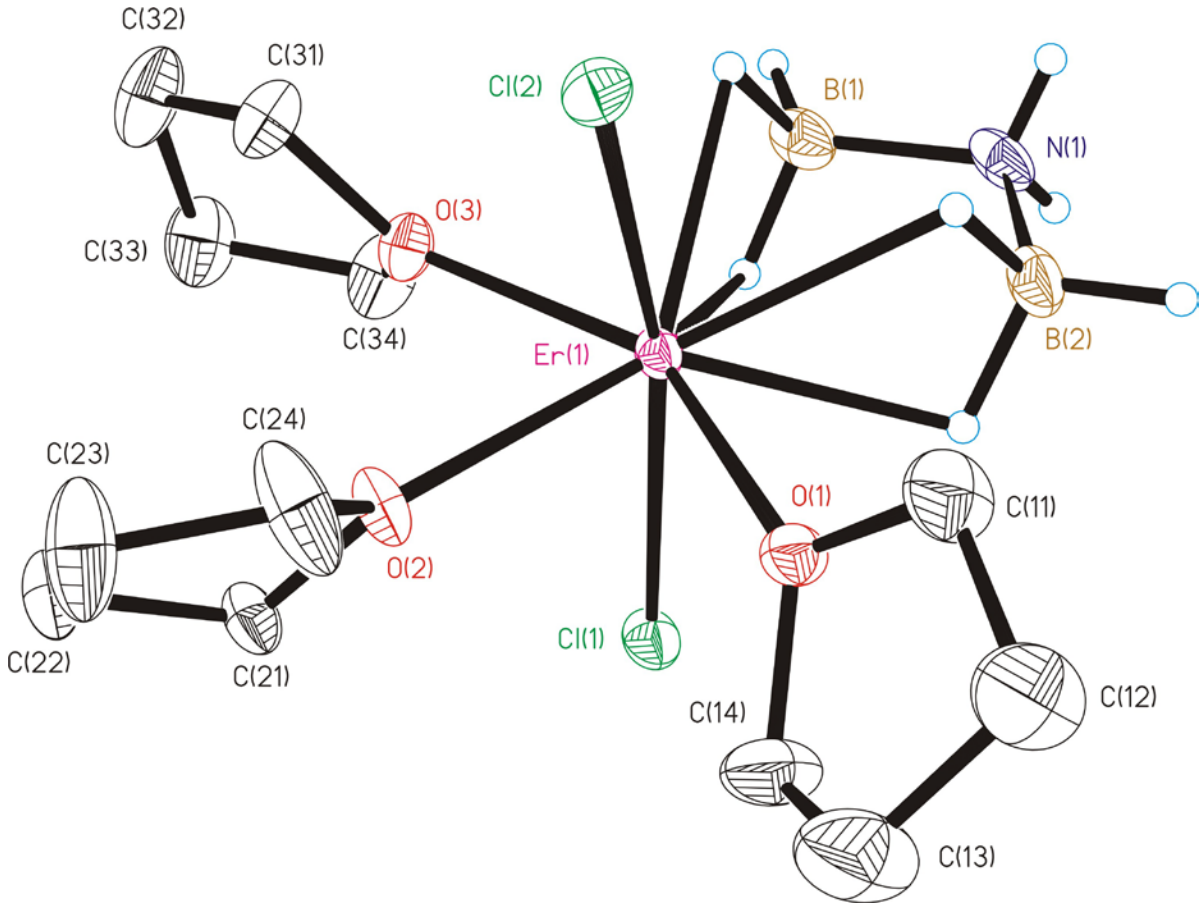

Figure 8.5. Molecular structure of $Er(H_3BNH_2BH_3)Cl_2(thf)_3$. Ellipsoids are drawn at the 35% probability level. The hydrogen atoms attached to carbon have been removed for clarity.

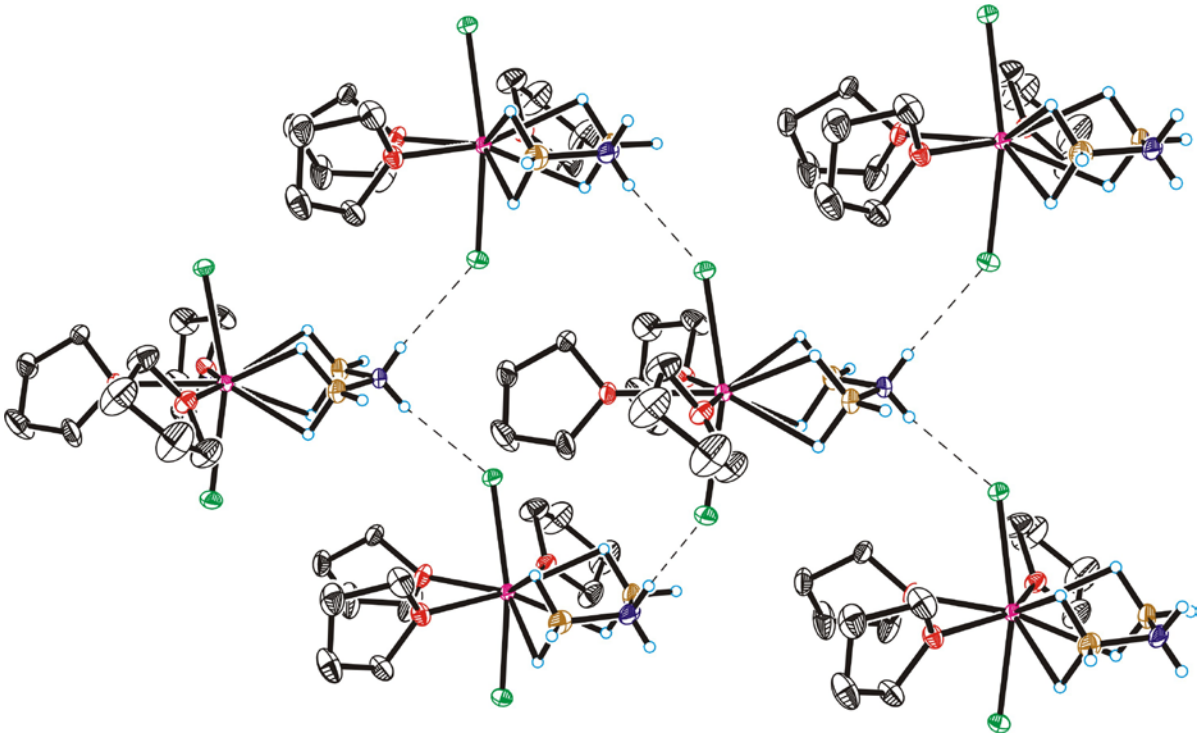

Figure 8.6. Intermolecular N-H···Cl interactions observed for $Er(H_3BNH_2BH_3)Cl_2(thf)_3$. Ellipsoids are drawn at the 35% probability level. The hydrogen atoms attached to carbon have been removed for clarity.

Table 8.6. Selected Bond Lengths and Angles for $Er(H_3BNH_2BH_3)Cl_2(thf)_3 \cdot thf$, (**5**).

Bond Lengths (Å)			
Er(1)-B(1)	2.775(4)	Er(1)-O(1)	2.366(2)
Er(1)-B(2)	2.791(4)	Er(1)-O(2)	2.3954(19)
Er(1)-H(11)	2.35(3)	Er(1)-O(3)	2.364(2)
Er(1)-H(12)	2.39(3)	Er(1)-Cl(1)	2.5956(7)
Er(1)-H(21)	2.36(3)	Er(1)-Cl(2)	2.5922(7)
Er(1)-H(22)	2.37(3)	N(1)-H(1)	0.84(2)
Bond Angles (deg)			
O(1)-Er(1)-O(2)	75.46(7)	O(1)-Er(1)-B(2)	78.98(10)
O(3)-Er(1)-O(1)	148.96(7)	O(2)-Er(1)-B(1)	150.54(10)
O(3)-Er(1)-O(2)	73.50(7)	O(2)-Er(1)-B(2)	154.44(11)
O(1)-Er(1)-Cl(1)	86.30(5)	O(3)-Er(1)-B(1)	77.09(10)
O(2)-Er(1)-Cl(1)	81.03(5)	O(3)-Er(1)-B(2)	132.06(11)
O(3)-Er(1)-Cl(1)	89.60(5)	Cl(1)-Er(1)-B(1)	97.15(8)
O(1)-Er(1)-Cl(2)	84.45(5)	Cl(1)-Er(1)-B(2)	96.94(8)
O(2)-Er(1)-Cl(2)	82.13(5)	Cl(2)-Er(1)-B(1)	100.08(8)
O(3)-Er(1)-Cl(2)	90.63(5)	Cl(2)-Er(1)-B(2)	95.97(8)
Cl(2)-Er(1)-Cl(1)	162.37(3)	B(1)-Er(1)-B(2)	54.99(13)
O(1)-Er(1)-B(1)	133.95(10)		

the axial sites. The Cl-Er···B and Cl-Er-O angles (which should be 90° in an ideal pentagonal bipyramid) range from 81.03(5) to 100.08(8)°, and the Cl-Er-Cl angle (which ideally should be 180°) is 162.37(3)° (Table 8.6). The Er···B distances are 2.775(4) and 2.791(4) Å, and the Er-O distances to the coordinated thf molecules range from 2.364(2) to 2.395(2) Å; these distances are similar to those observed for $Er(H_3BNMe_2BH_3)_3$,[21] $Er(H_3BNMe_2BH_3)_3(thf)$,[24] (Chapter 4) and **3**. An non-coordinated thf molecule is also observed in the crystal, which is corroborated by the observation that isolated blocks of **5** turn from clear to opaque as they are exposed to dynamic vacuum, indicative of desolvation. Microanalysis of these crystals after exposure to dynamic vacuum overnight supports the formulation $Er(H_3BNMe_2BH_3)Cl_2(thf)_{3.3}$.

The diffraction study of **5** also sheds some light about why the reactivity of the monoalkyl aminodiboranates differs from that of dialkyl aminodiboranates such as DMADB and PYDDB. There are significant intermolecular hydrogen bonding interactions between the chloride atoms and the N-H groups in the $H_3BNH_2BH_3^-$ ligand (Figure 8.6). The H···Cl distance of 2.568 Å is significantly shorter than the sum of the van der Waals radii, which is 2.95 Å,[25] and the N-H···Cl distance of 3.387 Å compares well to the hydrogen-bonded distances observed in CsCl-type ammonium chloride at 3.35 Å.[26] The hydrogen bonding may also reflected in the IR frequencies of **5**: relative to $Na(H_3BNH_2BH_3)$, a peak in the N-H stretching region is observed 3148 cm^{-1}, which is shifted by 99 cm^{-1} to lower energy relative to the closest N-H stretching peak (Figure 8.7). All of the N-H groups are involved in hydrogen bonding, which suggests that the extra peak can not be attributed solely to a lower energy N-H···Cl stretch. A more likely explanation is that the peak is a Fermi resonance that arises due to the hydrogen bonding interaction.

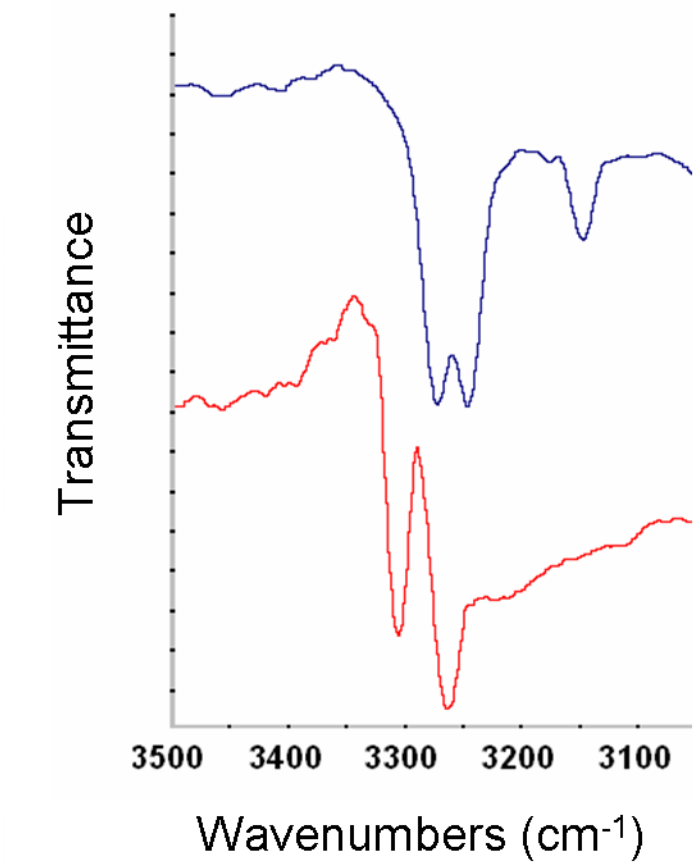

Figure 8.7. N-H stretching region in the IR spectra for **5** (top, blue) and Na($H_3BNH_2BH_3$) (bottom, red).

The strong hydrogen bonding in **5** is the most likely source of the incomplete metathesis of $ErCl_3$ and sodium aminodiboranates with exposed N-H groups and suggests that the N-H···Cl interactions impede the displacement of additional chloride ions. It is possible that $ErBr_3$ or ErI_3 would be better starting materials because the hydrogen-bonding interactions are weaker for these halides; the same effect may also explain why **4** can be prepared from $MgBr_2$.

Further studies will be required to determine how substituents at the nitrogen position impact volatility for a given series of aminodiboranate complexes.

Experimental

All operations were carried out in vacuum or under argon using standard Schlenk techniques. All glassware was dried in an oven at 150 °C, assembled hot, and allowed to cool under vacuum before use. Tetrahydrofuran, diethyl ether, and pentane were distilled under nitrogen from sodium/benzophenone and degassed with argon immediately before use. Anhydrous $MgBr_2$ (Aldrich) and $ErCl_3$ (Strem) were used as received. Sodium aminodiboranates and $MoCl_3(thf)_3$ were prepared by literature routes.[18, 27]

Elemental analyses were carried out by the University of Illinois Microanalytical Laboratory. The IR spectra were recorded on a Nicolet Impact 410 infrared spectrometer as Nujol mulls between KBr plates. The ^1H data were obtained on a Varian Unity 400 instrument at 400 MHz or on a Varian Unity U500 instrument at 500 MHz. The ^{11}B NMR data were collected on a General Electric GN300WB instrument at 96 MHz or on a Varian Unity Inova 600 instrument at 192 MHz. Chemical shifts are reported in δ units (positive shifts to high frequency) relative to TMS (^1H) or $BF_3{\cdot}Et_2O$ (^{11}B). Field ionization (FI) mass spectra were recorded on a Micromass 70-VSE mass spectrometer. The shapes of all peak

envelopes correspond with those calculated from the natural abundance isotopic distributions. Melting points and decomposition temperatures were determined in closed capillaries under argon on a Thomas-Hoover Unimelt apparatus.

Bis(pyrrolidinyldiboranato)magnesium(II), $Mg[H_3BN(C_4H_8)BH_3]_2$, 1. To a mixture of $MgBr_2$ (0.38 g, 2.1 mmol) and sodium pyrrolidinyldiboranate (0.50 g, 4.1 mmol) was added ca. 25 stainless steel balls (4.5 mm diameter). The flask was gently agitated for 30 min and the powdery solid slowly became sticky. Sublimation at 75 ˚C and 10^{-2} Torr afforded white microcrystals. Yield: 0.24 g (53 %). Mp: 87 - 88 ˚C. Anal. Calcd for $C_8H_{28}B_4N_2Mg$: C, 43.7; H, 12.8; N, 12.7. Found: C, 43.8; H, 12.8; N, 12.7. ^{1}H NMR (C_7D_8, 20 °C): δ 1.56 (m, J_{HH} = 4 Hz, β-CH_2, 8 H), 1.95 (br 1:1:1:1 q, J_{BH} = 90 Hz, BH_3, 12 H), 2.52 (br s, NCH_2, 8 H). ^{11}B NMR (C_7D_8, 20 °C): δ -13.7 (br q, J_{BH} = 90 Hz, BH_3). MS(FI) [fragment ion, relative abundance]: *m*/*z* 97 [$B_2H_5[N(C_4H_8)]$, 15], 219 [$Mg[H_3BN(C_4H_8)BH_3]_2^+$, 100], 303 [$Mg_2[H_3BN(C_4H_8)BH_3]_3^+$, 10]. IR ($cm^{-1}$): 2613 w, 2439 vs, 2353 m, 2290 s, 2236 sh, 2198 vs, 2141 s, 2074 w, 1327 s, 1299 s, 1252 m, 1217 m, 1176 vs, 1144 vs, 1128 w, 1078 s, 1030 m, 1002 m, 938 m, 907 m, 852 w.

Bis(*N*-methylaminodiboranato)magnesium(II), $Mg(H_3BNEtHBH_3)_2$, 4. To a mixture of $MgBr_2$ (1.00 g, 5.43 mmol) and sodium *N*-methylaminodiboranate (0.98 g, 10.3 mmol) was added ca. 25 stainless steel balls (4.5 mm diameter). The flask was gently agitated for 25 min and the powdery solid slowly became sticky. The flask was equipped with a cold finger cooled to -78 °C with a slurry of dry ice in ethanol. Sublimation at 65 ˚C and 10^{-2} Torr afforded a viscous oil. The oil slowly crystallized on the cold-finger over a period of several days at room temperature to yield long, white needles. Some of the oil dripped off the cold-finger after it was allowed to warm to room temperature; this material could be recovered with successive sublimations. Yield: 0.57 g (63 %). Mp: 61 - 62 ˚C.

Anal. Calcd for $C_4H_{24}B_4N_2Mg$: C, 28.6; H, 14.4; N, 16.7. Found: C, 28.8; H, 14.9; N, 16.4. ^{1}H NMR (C_6D_6, 20 °C): δ 0.72 (t, J_{HH} = 7 Hz, CH_3, 6 H), 0.94 (br s, fwhm = 50 Hz, NH, 2 H), 1.81 (br 1:1:1:1 q, J_{BH} = 89 Hz, BH_3, 12 H), 2.18 (quintet, J_{HH} = 7 Hz, NCH_2, 4 H). ^{11}B NMR (C_6D_6, 20 °C): δ -17.2 (br q, J_{BH} = 91 Hz, BH_3). MS(FI) [fragment ion, relative abundance]: *m*/*z* 167 [$Mg(H_3BNEtHBH_3)_2^+$, 100], 264 [$Mg_2(H_3BNEtHBH_3)_3^+$, 10], 336 [$Mg_2(H_3BNEtHBH_3)_4^+$, 3]. IR (cm^{-1}): 3266 m, 3255 w, 2439 s, 2411 s, 2293 s, 2207 vs, 2176 vs, 1349 w, 1321 w, 1274 w, 1226 m, 1198 w, 1179 m, 1144 vs, 1131 vs, 1119 sh, 1090 w, 1068 wm, 1043 w, 1017 w, 992 w, 976 w, 957 w, 891 w, 865 w, 849 w, 802 m.

Bis(pyrrolidinyldiboranato)molybdenum(II), $Mo[H_3BN(C_4H_8)BH_3]_2$, 2. To an orange suspension of $MoCl_3(thf)_3$ (0.47 g, 1.1 mmol) in diethyl ether (20 mL) at 0 °C was added a solution of sodium pyrrolidinyldiboranate (0.40 g, 3.3 mmol) in diethyl ether (20 mL). The reaction mixture was stirred at 0 °C for 1 h before being warmed to room temperature. The reaction mixture slowly darkened from orange to green. The mixture was stirred for 5 h at room temperature to afford a green solution and a grey solid. The green solution was filtered, concentrated to ca. 10 mL, and cooled to -20 ˚C to yield 85 mg of large green blocks. The mother liquor was concentrated to 5 mL and cooled to -20 ˚C to yield an additional 33 mg of green crystals. Yield: 0.11 g (36 %). Mp: 97 ˚C (dec). Anal. Calcd for $C_8H_{28}B_4N_2Mo$: C, 33.0; H, 9.68; N, 9.61. Found: C, 32.6; H, 9.65; N, 9.69. Two species are present in the solutions, with NMR peak intensities that are in the ratio of 65 % to 35 %. Major isomer: ^{1}H NMR (C_7D_8, 20 °C): δ -6.20 (br 1:3:3:1 q, J_{BH} = 70 Hz, MoHB, 8 H), 1.62 (q, J_{HH} = 3 Hz, β-CH_2, 8 H), 2.83 (br m, NCH_2, 8 H), 5.33 (br 1:1:1:1 q, J_{BH} = 123 Hz, BH, 4 H). ^{1}H{^{11}B} NMR (C_7D_8, 20 °C): δ -6.19 (d, J_{HH} = 10 Hz, MoHB, 8 H), 5.33 (t, J_{HH} = 9 Hz, MoHB, 4 H).^{11}B NMR (C_7D_8, 20 °C): δ 24.0 (br 1:3:3:1 q, J_{BH} = 76 Hz, BH_3). Minor isomer: ^{1}H NMR (C_7D_8, 20 °C): δ -6.20 (br 1:3:3:1 q, J_{BH} = 70 Hz, MoHB, 8 H), 1.58 (q, J_{HH} = 3

Hz, β-CH_2, 8 H), 2.83 (br m, NCH_2, 8 H), 4.93 (br 1:1:1:1 q, J_{BH} = 123 Hz, BH, 4 H). $^1H\{^{11}B\}$ NMR (C_7D_8, 20 °C): δ -6.20 (d, J_{HH} = 10 Hz, MoHB, 8 H), 4.93 (t, J_{HH} = 10 Hz, MoHB, 4 H). ^{11}B NMR (C_7D_8, 20 °C): δ 23.2 (br 1:3:3:1 q, J_{BH} = 75 Hz, BH_3). MS(FI) [fragment ion, relative abundance]: *m*/*z* 291 [$Mo[H_3BN(C_4H_8)BH_3]_2^+$, 100] . IR ($cm^{-1}$): 2452 w, 2423 vs, 1926 m, 1882 s, 1841 sh, 1353 w, 1334 s, 1312 s, 1236 w, 1214 w, 1103 vs, 1065 m, 1043 w, 1005 m, 992 m, 938 m, 913 m, 859 m, 722 m, 596 w, 466 m, 444 w, 438 w.

Tris(pyrrolidinyldiboranato)(tetrahydrofuran)erbium(III), $Er[H_3BN(C_4H_8)BH_3]_3(thf)$, 3. To a suspension of $ErCl_3$ (0.24 g, 0.88 mmol) in tetrahydrofuran (10 mL) at 0 °C was added a solution of sodium *N*,*N*-pyrrolidinodiboranate (0.31 g, 2.6 mmol) in tetrahydrofuran (10 mL). The pale pink reaction mixture was stirred at 0 °C for 20 min before being warmed to room temperature. The pink suspension slowly turned to a hazy pink solution after several hours at room temperature. The mixture was stirred for 42 h at room temperature and then evaporated to dryness under vacuum to afford a sticky, pink solid. The residue was extracted with pentane (2 × 10 mL). The filtered extracts were combined, concentrated to ca. 6 mL, and cooled to -20 ˚C to yield pink crystals. Yield: 0.22 g (48 %). M.p.: 92 – 94 ˚C. Anal. Calcd for $C_{16}H_{50}B_6N_3OEr$: C, 36.0; H, 9.46; N, 7.89. Found: C, 35.9; H, 9.97; N, 7.82. ^1H NMR (C_6D_6, 20 °C): δ -38.69 (br s, fwhm = 370 Hz, OCH_2, 4H), -26.86 (s, fwhm = 120 Hz, β-CH_2, 4H), 5.75 (s, fwhm = 30 Hz, $NCH_2C\underline{H}_2$, 12 H), 15.97 (s, fwhm = 130 Hz, NCH_2, 12 H), 109.2 (br s, fwhm = 2400 Hz, BH_3, 18 H). ^{11}B NMR (C_6D_6, 20 °C): δ -154.0 (s, fwhm = 200 Hz, BH_3). MS(FI) [fragment ion, relative abundance]: *m*/*z* 72 [thf, 60], 349 $[Er[H_3BN(C_4H_8)BH_3][H_3BN(C_4H_8)]^+$, 100], 421 $[Er[H_3BN(C_4H_8)BH_3][H_3BN(C_4H_8)](thf)^+$, 50], 713 $[Er[H_3BN(C_4H_8)BH_3]_2[H_3BN(C_4H_8)]_2$-$(BH_4)^+$, 10]. IR ($cm^{-1}$): 2398 vs, 2357 sh, 2290 s, 2230 vs, 2185 sh, 2078 w, 1280 s, 1261 s,

1214 m, 1176 vs, 1141 vs, 1075 vs, 1030 m, 1008 m, 941 m, 913 w, 897 w, 862 m, 840 sh, 568 w, 441 w.

(Aminodiboranato)tris(tetrahydrofuran)dichloroerbium(III), $Er(H_3BNH_2BH_3)Cl_2(thf)_3 \cdot thf$, 5. To a mixture of $ErCl_3$ (0.30 g, 1.1 mmol) in tetrahydrofuran (15 mL) cooled to 0 °C was added a solution of $Na(H_3BNH_2BH_3)$ (0.23 g, 3.5 mmol) in tetrahydrofuran (15 mL). The light pink suspension was warmed to room temperature and stirred for 24 h. The mixture was filtered and the clear, pink filtrate was concentrated to 10 mL and cooled to -20 °C to yield 0.14 g of small, light pink blocks. The mother liquor was concentrated to 6 mL and cooled to -20 °C to yield an additional 0.10 g of crystals. The crystals were placed under dynamic vacuum overnight, which resulted in the partial loss of the co-crystallized non-ordinated thf molecule observed in the diffraction studies. During this time the clear pink blocks turned opaque. Yield: 0.24 g (41 %). Anal. Calcd for $Er(H_3BNH_2BH_3)Cl_2(thf)_{3.3}$: C, 30.5; H, 6.67; N, 2.69; Cl, 13.6. Found: C, 30.6; H, 6.87; N, 3.29; Cl, 13.9. ^{1}H NMR (thf-d_8, 20 °C): δ -0.03 (br s, fwhm = 35 Hz, NH_2), 1.70 (br s, fwhm = 110 Hz, β-CH_2), 3.76 (br s, fwhm = 160 Hz, OCH_2). ^{11}B NMR (thf-d_8, 20 °C): δ -176.2 (br s, fwhm = 250 Hz, BH_3). IR (cm^{-1}): 3275 vs, 3247 vs, 3148 m, 2388 vs, 2306 m, 2281 m, 2236 vs, 1587 m, 1347 w, 1290 s, 1230 s, 1188 s, 1150 s, 1081 w, 1017 vs, 957 w, 919 m, 855 vs, 771 w, 673 w, 447 w.

Crystallographic Studies.[28] Single crystals obtained by sublimation (**1**, **4**), or by crystallization from pentane (**3**), diethyl ether (**2**), or thf (**5**) were mounted on glass fibers with Paratone-N oil (Exxon) and immediately cooled to -80 °C (-75 °C for **2** and **3**) in a cold nitrogen gas stream on the diffractometer. Standard peak search and indexing procedures, followed by least-square refinement yielded the cell dimensions given in Table 8.1. The measured intensities were reduced to structure factor amplitudes and their estimated standard

deviations by correction for background and Lorentz and polarization effects. No corrections for crystal decay were necessary but a face-indexed absorption correction was applied. Systematically absent reflections were deleted and symmetry equivalent reflections were averaged to yield the set of unique data. Except where noted, all unique data were used in the least-squares refinements. The analytical approximations to the scattering factors were used, and all structure factors were corrected for both real and imaginary components of anomalous dispersion. Correct atomic position(s) were deduced from an E-map (SHELXTL); least-squares refinement and difference Fourier calculations were used to locate atoms not found in the initial solution. Except where noted below, hydrogen atoms attached to boron and nitrogen were located in the difference maps and hydrogen atoms attached to carbon were placed in idealized positions with C-H (methyl) = 0.98Å and C-H (methylene) = 0.99Å ; the idealized methyl groups were allowed to rotate about their respective axes to find the best least-squares positions. In the final cycle of least squares, independent anisotropic displacement factors were refined for the non-hydrogen atoms. The displacement parameters for methylene hydrogens were set equal to 1.2 times U_{eq} for the attached carbon; those for methyl hydrogens were set to 1.5 times U_{eq}. No correction for isotropic extinction was necessary. Successful convergence was indicated by the maximum shift/error of 0.000 for the last cycle. A final analysis of variance between observed and calculated structure factors showed no apparent errors. Aspects of the refinements unique to each structure are reported below.

$Mg[H_3BN(C_4H_8)BH_3]_2$, 1: The crystal selected was twinned and all reflections could be fitted to a triclinic cell with three twin components. Reflections from each twin component were separated using TWINABS;[29] data from all twin individuals were merged and used in the refinement. The three twin domains refined to 49%, 38%, and 13%. The

triclinic lattice and the average values of the normalized structure factors suggested the space group $P\bar{1}$, which was confirmed by the success of the subsequent refinement. The quantity minimized by the least-squares program was $\Sigma w(F_o^2 - F_c^2)^2$, where $w = \{[\sigma(F_o)]^2 + (0.0781P)^2\}^{-1}$ and $P = (F_o^2 + 2F_c^2)/3$. Hydrogen atoms attached to boron were placed in idealized positions with B-H = 1.15 Å; the boranyl groups were allowed to rotate about their respective axis to find the best least-squares positions. The displacement parameters for the boranyl hydrogens were set equal to 1.2 times U_{eq} for the attached boron. The largest peak in the final Fourier difference map (0.23 eÅ^{-3}) was located 0.51 Å from H13.

Mo[$H_3BN(C_4H_8)BH_3$]$_2$, 2: The monoclinic lattice and systematic absences $0k0$ ($k \neq 2n$) and $h0l$ ($l \neq 2n$) were uniquely consistent with the space group $P2_1/c$, which was confirmed by the success of the subsequent refinement. The quantity minimized by the least-squares program was $\Sigma w(F_o^2 - F_c^2)^2$, where $w = \{[\sigma(F_o)]^2 + (0.257P)^2\}^{-1}$ and $P = (F_o^2 + 2F_c^2)/3$. Hydrogen atoms attached to carbon were located in the difference maps, and their positions were refined with independent isotropic displacement parameters. The chemically equivalent B–H distances within the BH_3 units were constrained to be equal within an esd of 0.01 Å. An isotropic extinction parameter was refined to a final value of x = 2.65(15) × 10^{-5} where F_c is multiplied by the factor $k[1 + F_c^2 x\lambda^3/\sin 2\theta]^{-1/4}$ with k being the overall scale factor. The largest peak in the final Fourier difference map (0.30 eÅ^{-3}) was located 1.12 Å from H22.

Er[$H_3BN(C_4H_8)BH_3$]$_3$(thf), 3: The systematic absences hkl ($h + k \neq 2n$) and $h0l$ ($l \neq 2n$) were consistent with the space groups Cc and $C2/c$. The non-centrosymmetric space group Cc was chosen, and this choice was confirmed by successful refinement of the proposed model. The quantity minimized by the least-squares program was $\Sigma w(F_o^2 - F_c^2)^2$, where $w = \{[\sigma(F_o)]^2 + (0.0335P)^2\}^{-1}$ and $P = (F_o^2 + 2F_c^2)/3$. The C-O and C-C bond distances

of the tetrahydrofuran molecule were fixed at 1.48 ± 0.005 and 1.52 ± 0.005Å, respectively . Hydrogen atoms attached to boron were placed in idealized positions with B-H = 1.15 Å; the boranyl groups were allowed to rotate about their respective axis to find the best least-squares positions. The displacement parameters for the boranyl hydrogens were set equal to 1.2 times U_{eq} for the attached boron. The largest peak in the final Fourier difference map (1.52 eÅ^{-3}) was located 0.97 Å from Er1.

$Mg(H_3BNEtHBH_3)_2$, 4: The triclinic lattice and the average values of the normalized structure factors suggested the space group $P\bar{1}$, which was confirmed by the success of the subsequent refinement. The quantity minimized by the least-squares program was $\Sigma w(F_O^2 - F_C^2)^2$, where $w = \{[\sigma(F_o)]^2 + (0.0599P)^2\}^{-1}$ and $P = (F_o^2 + 2F_c^2)/3$. The chemically equivalent B–H distances within the BH_3 units were constrained to be equal within an esd of 0.01 Å. An isotropic extinction parameter was refined to a final value of x = 2.7(4) × 10^{-5} where F_c is multiplied by the factor $k[1 + F_c^2 x\lambda^3/\sin 2\theta]^{-1/4}$ with k being the overall scale factor. Successful convergence was indicated by the maximum shift/error of 0.001 for the last cycle. The largest peak in the final Fourier difference map (0.27 eÅ^{-3}) was located 1.05 Å from H7A.

$Er(H_3BNH_2BH_3)Cl_2(thf)_3 \cdot thf$, 5. The monoclinic lattice and systematic absences $0k0$ ($k \neq 2n$) and $h0l$ ($h + l \neq 2n$) were uniquely consistent with the space group $P2_1/n$, which was confirmed by the success of the subsequent refinement. The quantity minimized by the least-squares program was $\Sigma w(F_O^2 - F_C^2)^2$, where $w = \{[\sigma(F_o)]^2 + (0.0112P)^2 + 2.0347P\}^{-1}$ and $P = (F_o^2 + 2F_c^2)/3$. The chemically equivalent N-H distances were constrained to be equal within 0.01 Å. The largest peak in the final Fourier difference map (0.96 eÅ^{-3}) was located 0.99 Å from Er1.

References

1. *Chemical Vapour Deposition: Precursors, Processes and Applications.* Jones, A. C.; Hitchman, M. L., Eds.; RSC Publishing: Cambridge, 2009.

2. George, S. M. *Chem. Rev.* **2010,** *110*, 111-131.

3. Yanguas-Gil, A.; Yang, Y.; Kumar, N.; Abelson, J. R. *J. Vac. Sci. Technol., A* **2009,** *27*, 1235-1243.

4. Putkonen, M.; Niinisto, L. *Top. Organomet. Chem.* **2005,** *9*, 125-145.

5. Leskela, M.; Ritala, M. *Angew. Chem., Int. Ed.* **2003,** *42*, 5548-5554.

6. Crowell, J. E. *J. Vac. Sci. Technol., A* **2003,** *21*, S88-S95.

7. Hampden-Smith, M. J.; Kodas, T. T. *Chem. Vap. Deposition* **1995,** *1*, 8-23.

8. McElwee-White, L. *Dalton Trans.* **2006**, 5327-5333.

9. Hubert-Pfalzgraf, L. G. *Inorg. Chem. Commun.* **2003,** *6*, 102-120.

10. Hubert-Pfalzgraf, L. G. *J. Mater. Chem.* **2004,** *14*, 3113-3123.

11. Hubert-Pfalzgraf, L. G.; Guillon, H. *Appl. Organomet. Chem.* **1998,** *12*, 221-236.

12. Jones, A. C. *J. Mater. Chem.* **2002,** *12*, 2576-2590.

13. Herrmann, W. A.; Anwander, R.; Munck, F. C.; Scherer, W. *Chem. Ber.* **1993,** *126*, 331-337.

14. Gordon, R. G. *Proc. - Electrochem. Soc.* **2000,** *2000-13*, 248-259.

15. Taylor, C. J.; Gilmer, D. C.; Colombo, D. G.; Wilk, G. D.; Campbell, S. A.; Roberts, J.; Gladfelter, W. L. *J. Am. Chem. Soc.* **1999,** *121*, 5220-5229.

16. Keller, P. C. *J. Chem. Soc. D* **1969**, 1465.

17. Keller, P. C. *Inorg. Chem.* **1971,** *10*, 2256-2259.

18. Nöth, H.; Thomas, S. *Eur. J. Inorg. Chem.* **1999**, 1373-1379.

19. Kim, D. Y. Part 1. Synthesis of metal hydroborates as potential chemical vapor deposition. Part 2. Chemical vapor deposition of titanium-doped magnesium diboraide thin films. Ph.D. Thesis, University of Illinois at Urbana-Champaign, 2007.

20. Kumar, N.; Yanguas-Gil, A.; Daly, S. R.; Girolami, G. S.; Abelson, J. R. *Appl. Phys. Lett.* **2009,** *95*, 144107/144101-144107/144103.

21. Daly, S. R.; Kim, D. Y.; Yang, Y.; Abelson, J. R.; Girolami, G. S. *J. Am. Chem. Soc.* **2010,** *132*, 2106-2107.

22. Eaton, G. R.; Lipscomb, W. N. *N.M.R. Studies of Boron Hydrides and Related Compounds*. Benjamin: New York, 1969.

23. Kim, D. Y.; Beddie, C. L.; Pérez, L. M.; Hall, M. B.; Girolami, G. S., manuscript in preparation.

24. Girolami, G. S.; Kim, D. Y.; Abelson, J. R.; Kumar, N.; Yang, Y.; Daly, S. U.S. Pat. Appl. 59728, April 9, 2008.

25. Bondi, A. *J. Phys. Chem.* **1964,** *68*, 441-451.

26. Lindgren, J.; Olovsson, I. *Acta Crystallogr., Sect. B* **1968,** *24*, 554-558.

27. Dilworth, J. R.; Richards, R. L. *Inorg. Synth.* **1990,** *28*, 33-43.

28. Brumaghim, J. L.; Priepot, J. G.; Girolami, G. S. *Organometallics* **1999,** *18*, 2139-2144.

29. Sheldrick, G. M. *TWINABS*, 2008.

CHAPTER 9. $Pr(H_3BNMe_2BH_3)_3$ and $Pr(thd)_3$ as Volatile Carriers for Actinium-225. The Deposition of Actinium-Doped Praseodymium Boride Thin Films

Introduction

Brachytherapy, also known as endocurietherapy, is a form of radiation treatment that involves implantation of a radioactive material into the body to treat malignant conditions such as cancer.[1] The key advantage of brachytherapy is that the radiation generated is localized, thus saving the rest of the body from the debilitating effects of full body irradiation. Such therapy is currently used to treat a wide-variety of cancers, the most common being cancers of the prostate, cervix, uterus, lung, and selected cancers of the head and neck (e.g., the thyroid and skull).[1, 2]

There are two types of brachytherapy treatments: short-term brachytherapy and permanent brachytherapy. As the name implies, short-term brachytherapy utilizes an implant for a limited duration before it is removed from the body. The method is effective for controlling the dose of radiation delivered and is required for emitters that have long half-lives. Permanent brachytherapy is commonly used for emitters that have short half-lives and that quickly decay to background radiation levels. The depleted material is left in the body permanently once the treatment is complete. For instance, the "seeds" commonly used to treat prostate cancer, which are small capsules of ^{125}I ($t_{½}$ = 59 days) or ^{103}Pd ($t_{½}$ = 17 days), are left in the body permanently.[3]

The radionuclides currently used for brachytherapy can be β, γ, or X-ray emitters, but recent studies have suggested that α-emitters may be the most effective for treating malignancies.[4-6] This benefit derives from the fact that α particles have a much higher linear energy transfer (LET) than β particles (60 – 230 keV/μm vs 0.1 – 1 keV/μm) and they have

short path lengths in tissue (50 – 90 μm corresponding to ~2-10 cell diameters), making them ideal for localized treatments without compromising healthy tissue around the treatment sites.[4] The α-particles also exhibit higher cell toxicity compared to β and γ-emitters, which is attributed to the increased probability of DNA double-strand breaks due to the high LET of the relatively large helium ion.[4]

The majority of targeted alpha therapy research, including clinical studies, has been dedicated to radioimmunotherapy, which utilizes monoclonal antibodies tagged with alpha-emitters, such as ^{213}Bi and ^{211}At, and more recently ^{225}Ac.[6, 7] Actinium-225 has been identified as an optimal candidate for radioimmunotherapy treatments because it has short half-life (~ 10 days), and each ^{225}Ac nuclei yields up to four α particles as it decays through the neptunium (4n + 1) decay series (Scheme 9.1). The ability of ^{225}Ac to produce multiple equivalents of α-particles has led to its description as an "alpha-particle nanogenerator".[7] These attributes make ^{225}Ac more potent than ^{211}At and ^{213}Bi because the latter have shorter half-lives and produce fewer alpha particles. The increased efficacy of ^{225}Ac conjugates in animal studies has been noted.[6-9]

Due to the short range of alpha particles in tissue, alpha emitters were expected to be ineffective in the brachytherapeutic treatment of solid tumors.[10] However, a new class of brachytherapy methods known as diffusing alpha-emitter radiation therapy (DART) has shown that this need not be the case. For instance, small wires containing 7 – 42 kBq (0.2 – 1.1 μCi) of ^{224}Ra have been used to inhibit and destroy tumors 6-7 mm in size in nude mice;[11, 12] the method is even more potent when used in combination with other cancer therapies.[13]

There have been no reports of using ^{225}Ac as an emitter for brachytherapy treatments, and in part this situation reflects the limited availability of this isotope, which is recovered as

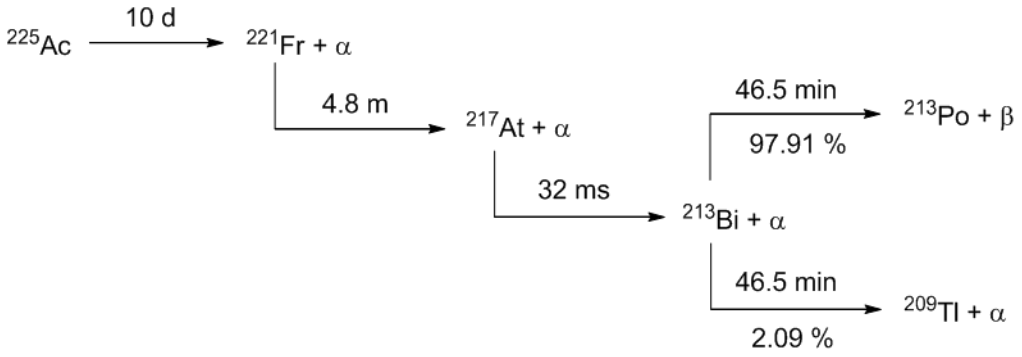

Scheme 9.1. Radioactive decay chain for ^{225}Ac, which is part of the neptunium (4n + 1) decay series.

a decay product from ^{229}Th ($t_{½}$ = 7340 years).[7, 14, 15] However, this problem can be circumvented by using a macroscopic carrier. For brachytherapy applications, the ^{225}Ac and its carrier must be formed into very thin coatings, so that the α-particles are not absorbed by the matrix and prevented from escaping to irradiate the surrounding environment.

An attractive method to produce thinly-dispersed materials suitable for use in brachytherapy is thin film deposition. Of the techniques available to deposit thin films, chemical vapor deposition (CVD) is the most promising because it can provide thin, uniform growth with good adhesion. However, two requirements must be met: (1) the CVD precursor must serve as a carrier for actinium (i.e., the actinium sublimes with the carrier) and (2) the deposited material must be resistant to chemical etching under physiological conditions. The use of volatile carriers for actinium has been previously reported: Cp_3Pr (Cp = cyclopentadienyl) has been used as a carrier for small amounts of ^{228}Ac (and also ^{147}Pm) in sublimation processes.[16] These studies were the first to provide evidence of the existence of Cp_3Ac and Cp_3Pm.[17] The results suggest that other lanthanide thin film precursors may also be able to serve as volatile carriers for actinium radionuclides.

The second requirement, chemical inertness of the radioactive implant, is relevant to all targeted radioimmunotherapy methods. Of concern here is to prevent movement of actinium and the decay daughters out of the implant, with consequent bioaccumulation of radioactivity in other areas of the body.[18-25] Most studies of lanthanide CVD precursors have been dedicated to the deposition of lanthanide oxide films, which may be unsuitable for brachytherapy owing to their susceptibility to hydrolysis in aqueous environments such as those found *in vivo*.[26] However, refractory materials, such as metal borides, would be well-suited for this application owing to their chemical inertness.[27]

Lanthanide complexes of the *N*,*N*-dimethylaminodiboranate anion (DMADB), such as $Pr(H_3BNMe_2BH_3)_3$, are highly volatile and have proven to be useful precursors for the deposition of lanthanide oxide films by CVD.[28] Although to date they have not been evaluated for the deposition of lanthanide boride films, we shown that transition metal and magnesium DMADB complexes are effective precursors for the deposition of metal diborides. We now describe efforts to use $Pr(H_3BNMe_2BH_3)_3$ and $Pr(thd)_3$, where thd = 2,2,6,6-tetramethylheptane-3,5-dionate, as volatile carriers for ^{225}Ac, and the deposition of actinium-doped praseodymium boride films from actinium-doped $Pr(H_3BNMe_2BH_3)_3$.

Results and Discussion

Synthesis of actinium-doped praseodymium compounds. The ideal carrier for a radionuclide is a compound of an element that has an identical radius and coordination chemistry. Actinium forms compounds only in its +3 oxidation state, and the radius of this species (1.12 Å) is the largest of all trivalent ions in the entire periodic table.[29] The lanthanides have the advantage that they readily form complexes in the +3 oxidation state, and their coordination chemistry is essentially identical to that of actinium, but even the largest Ln^{3+} ions – those of lanthanum (1.03 Å), cerium (1.01 Å), and praseodymium (0.99 Å) – are smaller than actinium.[29] Nevertheless, the radius mismatch is small enough that lanthanide compounds, particularly those of the earlier (i.e., larger) lanthanides, can serve as carriers for Ac, as has been shown in several studies.[16]

We decided to investigate two different classes of lanthanide complexes as carriers: compounds of the *N*,*N*-dimethylaminodiboranate (DMADB) anion, and compounds of the 2,2,6,6-tetramethylheptanedionate (thd) ion. We have shown elsewhere that lanthanide DMDAB complexes are highly volatile: they sublime at temperatures as low as 65 °C in

vacuum, are suitable for use as chemical vapor deposition (CVD) and atomic layer deposition (ALD) precursors to thin films. Volatile lanthanide complexes of thd were first reported over 35 years ago.[30] These air stable compounds can be prepared in yields of up to 92 % and were among the first lanthanide complexes to be evaluated as thin film precursors;[31] even after years of study, $Ln(thd)_3$ continue to be investigated for the deposition of thin films such as praseodymium oxide.[32] $Ln(thd)_3$ complexes are moderately volatile, subliming at 216 – 290 °C at atmospheric pressure; the volatility increases across the series from La to Lu as is typically observed. Direct comparisons of the volatility of $Ln(thd)_3$ to $Ln(H_3BNMe_2BH_3)_3$ complexes under similar conditions using thermogravimetric analysis reveals that $Ln(H_3BNMe_2BH_3)_3$ are more volatile (Chapter 4).

Although lanthanum and cerium have radii that most closely match that of actinium, DMADB complexes of these two lanthanides cannot be synthesized directly from their corresponding chlorides in thf (Chapter 4).[28] In contrast, $Pr(H_3BNMe_2BH_3)_3$ can be obtained directly from $PrCl_3$. As a result, this compound and the thd complex $Pr(thd)_3$ were selected as carriers in the present study.

Samples of ^{225}Ac were received as an aqueous solution. We used this solution to prepare actinium-doped $PrCl_3$, which was the starting material for the preparations of the volatile carriers. Solutions of $PrCl_3 \cdot 6H_2O$ in aqueous HCl were spiked with 2 - 4 μCi of ^{225}Ac solution. The mixture was evaporated and converted to anhydrous $PrCl_3$ by means of the ammonium chloride method.[33, 34] This approach ensures that the radionuclide was distributed homogeneously in the carrier.

Treatment of the ^{225}Ac doped $PrCl_3$ with three equivalents of Na(thd) produced $Pr(thd)_3$, which could be isolated by sublimation at 180 °C at 10^{-2} Torr. The recovery of

^{225}Ac in the green sublimate was 44.2 %; this value was determined by comparing the activity of the product with an equimolar amount of the doped $PrCl_3$ starting material,

Treatment of the ^{225}Ac doped $PrCl_3$ with three equiv of $Na(H_3BNMe_2BH_3)$ in tetrahydrofuran at room temperature, followed by removal of the solvent and crystallization of the resulting solid from diethyl ether, afforded $Pr(H_3BNMe_2BH_3)_3(thf)$, as previously described (Chapter 4). However, no activity was detected in the isolated crystals or in the mother liquor from which the crystals grew.[35] We conclude either that $AcCl_3$ does not react with $Na(H_3BNMe_2BH_3)$ or that it reacts but does not form an ether-soluble product. Similar behavior has been noted in the chemistry of La and Ce, whose atomic radii are most similar to that of Ac. Specifically, neither $LaCl_3$ nor $CeCl_3$ react with $Na(H_3BNMe_2BH_3)$ to give $M(H_3BNMe_2BH_3)_3(thf)$ products.

We were able to obtain evidence that the first explanation – that $AcCl_3$ is unreactive toward $Na(H_3BNMe_2BH_3)$ – is the correct one. We heated the $^{225}Ac/PrCl_3$ sample in refluxing tetrahydrofuran, which resulted in formation of the thf solvate $^{225}Ac/PrCl_3(thf)_3$. Treatment of this material with $Na(H_3BNMe_2BH_3)$ in diethyl ether, followed by extraction and crystallization from pentane, produced green crystals of ^{225}Ac-doped $Pr(H_3BNMe_2BH_3)_3(thf)$. This material was highly active: the net recovery of ^{225}Ac was 37.4 %, which is very similar to the 34 % recovery reported for ^{228}Ac using Cp_3Pr as a carrier.[16] The ^{225}Ac-doped $Pr(H_3BNMe_2BH_3)_3(thf)$ was then sublimed at 115 °C at 10^{-2} Torr to afford the corresponding base-free $Pr(H_3BNMe_2BH_3)_3$, as previously described (Chapter 4).

Owing to regulatory restrictions that govern the handling of samples containing ^{225}Ac, spectroscopic and microanalytical data for ^{225}Ac-doped $Pr(H_3BNMe_2BH_3)_3(thf)$ and $Pr(thd)_3$ could not be obtained. However, these compounds exhibit the properties and physical characteristics expected of the target compounds (solubility, sublimation temperatures, and

rapid hydrolysis of $Pr(H_3BNMe_2BH_3)_3(thf)$ and $Pr(H_3BNMe_2BH_3)_3$ in water and acid solutions). The results suggest that the actinium complexes $Ac(H_3BNMe_2BH_3)_3(thf)$, $Ac(H_3BNMe_2BH_3)_3$, and $Ac(thd)_3$ are generated under the reaction conditions used, and that these species both co-crystallize and co-sublime with their respective praseodymium analogs.

Deposition of ^{225}Ac-doped PrB_x films from doped $Pr(H_3BNMe_2BH_3)_3$ by CVD. The deposition of ^{225}Ac-doped films was conducted using a hot wall CVD reactor, as shown in Figure 9.1. The hot-wall reactor consisted of a Schlenk tube whose bottom served as the precursor reservoir. The tube was equipped with four indentations 3-5 cm from the bottom of the tube that served as a shelf to support the substrate above the precursor reservoir. Heating tape was wrapped around the middle of the tube to heat the substrate, and the precursor reservoir was heated using a sand bath to sublime the material through the hot zone. The vacuum was supplied by connecting the apparatus to a vacuum manifold with gum-rubber tubing. The advantage of this low-tech CVD apparatus, and the motivation for its use, is the depositions of radioactive material can be conducted in an approved fume hood designated for such work, and it avoids the regulatory and decontamination issues that would arise if a more sophisticated CVD reactor were used.

Initial control experiments were conducted with undoped $Pr(H_3BNMe_2BH_3)_3$; these experiments served to test the CVD apparatus and the deposition characteristics of this precursor on glass and on silicon. The substrates were heated to 300 °C and 30 - 45 mg of $Pr(H_3BNMe_2BH_3)_3$ was sublimed through the hot zone at 10^{-2} Torr. The resulting shiny, metallic thin films were characterized by SEM and XPS, which revealed that the morphology and compositions of the films were similar on the two substrates. SEM micrographs suggested that the films were amorphous, which was confirmed by the lack of diffraction peaks in the X-ray diffractograms (Figure 9.2). The film thickness, determined by SEM of

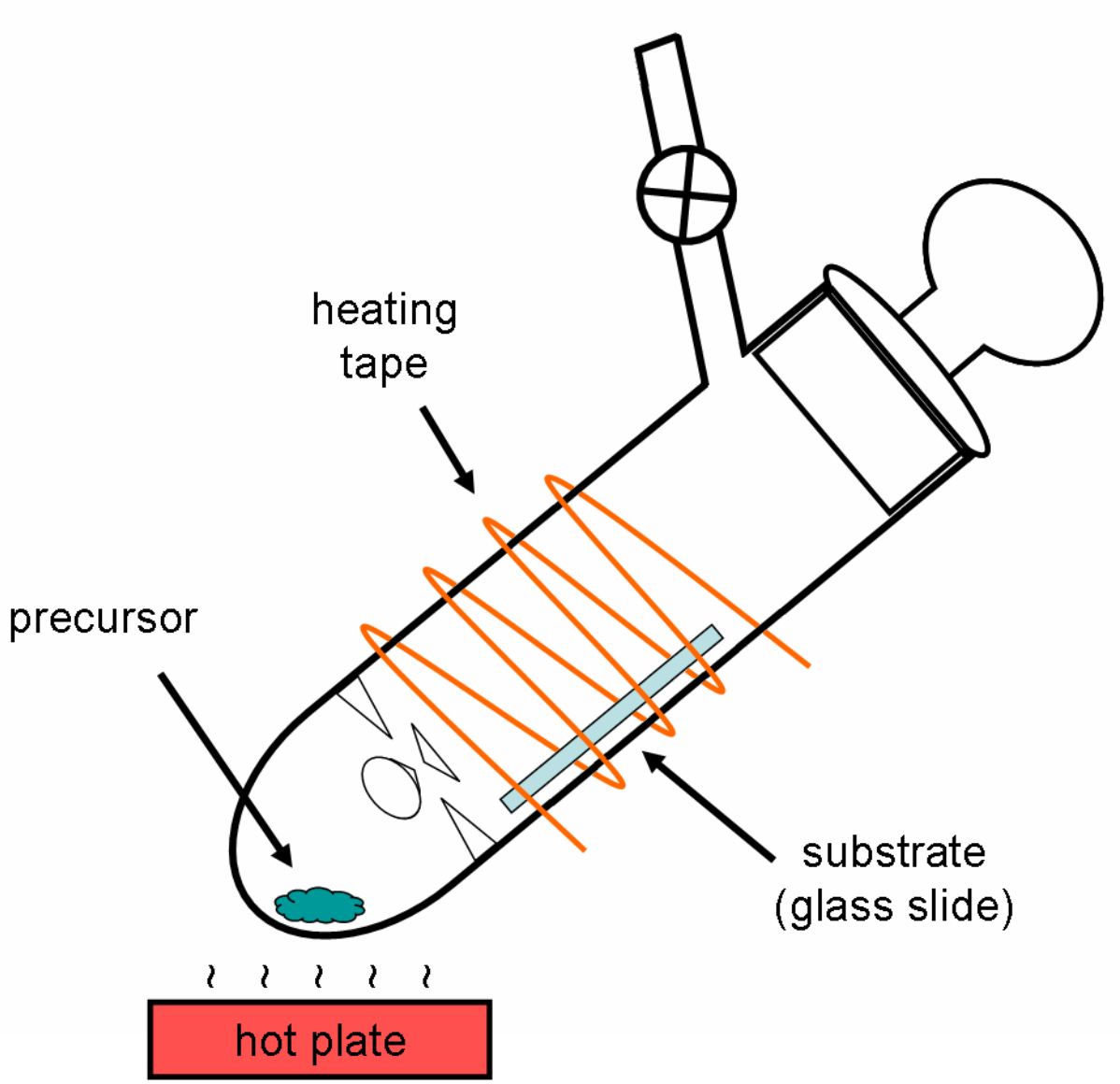

Figure 9.1. Schematic diagram of the hot-wall CVD reactor used for the deposition of actinium-doped films.

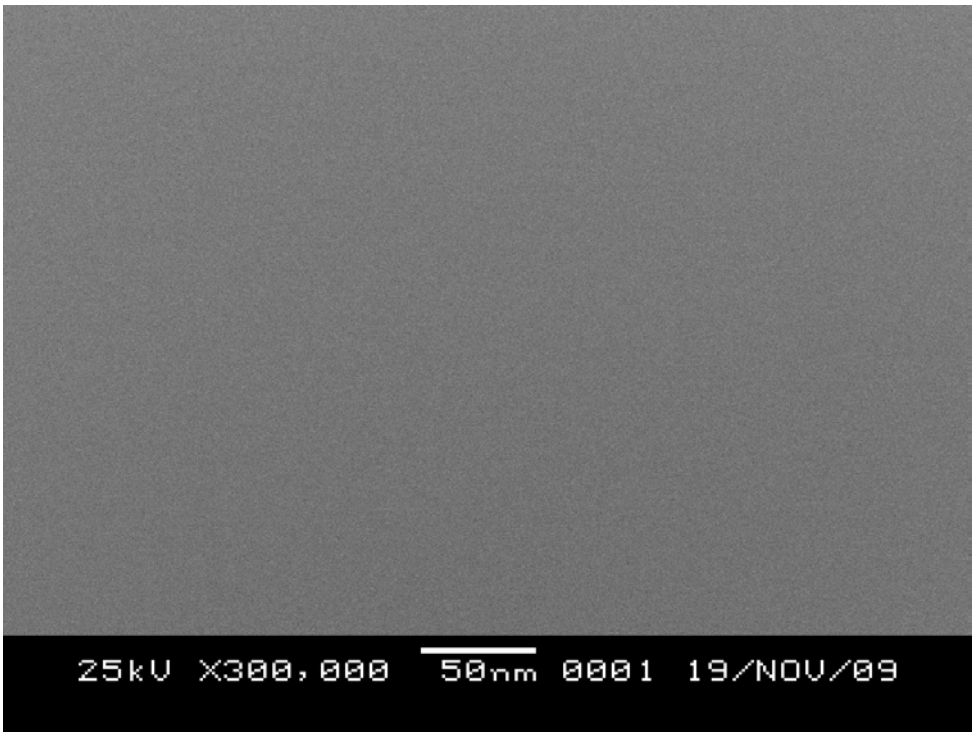

Figure 9.2. SEM micrograph of amorphous PrB_x film grown on silicon at 300 °C from $Pr(H_3BNMe_2BH_3)_3$. Imaged obtained by Brian J. Bellott.

fracture cross-sections, was ca. 550 nm. The XPS spectrum showed two peaks 955 and 934 eV corresponding to the praseodymium $3d_{3/2}$ and $3d_{5/2}$ ionizations, respectively (Figure 9.3), and a peak at 188.1 eV corresponding to the boron 1s ionization.[36] The boron 1s binding energy falls directly in the middle of the range expected for borides, which is 187.2 – 189.2 eV (Figure 9.4). For comparison, elemental boron ranges from 189.1 – 190.0 eV and B_2O_3 ranges from 192.2 – 193.5 eV.[36] The ratio of Pr to B for the films according to XPS is 1:5, which is not a known boride phase. The two most common praseodymium boride phases known are PrB_6 and PrB_4,[37] and the XPS data may indicate that the amorphous film is a mixture of these two components.

The films do not hydrolyze in air or water. They are slowly etched when immersed 12 M HCl but boride phases remain even after several days of this treatment. However, concentrated nitric acid is more effective, digesting the film in a matter of hours.

By following the protocol devised in the control experiments, we carried out depositions from ^{225}Ac-doped $Pr(H_3BNMe_2BH_3)_3$. The resulting film had the same characteristics as the undoped films and the presence of ^{225}Ac was confirmed using a Geiger counter. The film was analyzed by alpha spectrometry, which revealed the diagnostic alpha energy distributions for ^{225}Ac and its decay daughters ^{221}Fr and ^{217}At (Figure 9.5). The peaks are well resolved with only a small amount of tailing due to self-absorption effects, indicating that the films are thin and uniform.[38] The film emits only ca. 0.42 Bq (11 pCi) of α-particles but the activity can easily be increased by dosing the carrier with higher concentrations of ^{225}Ac.

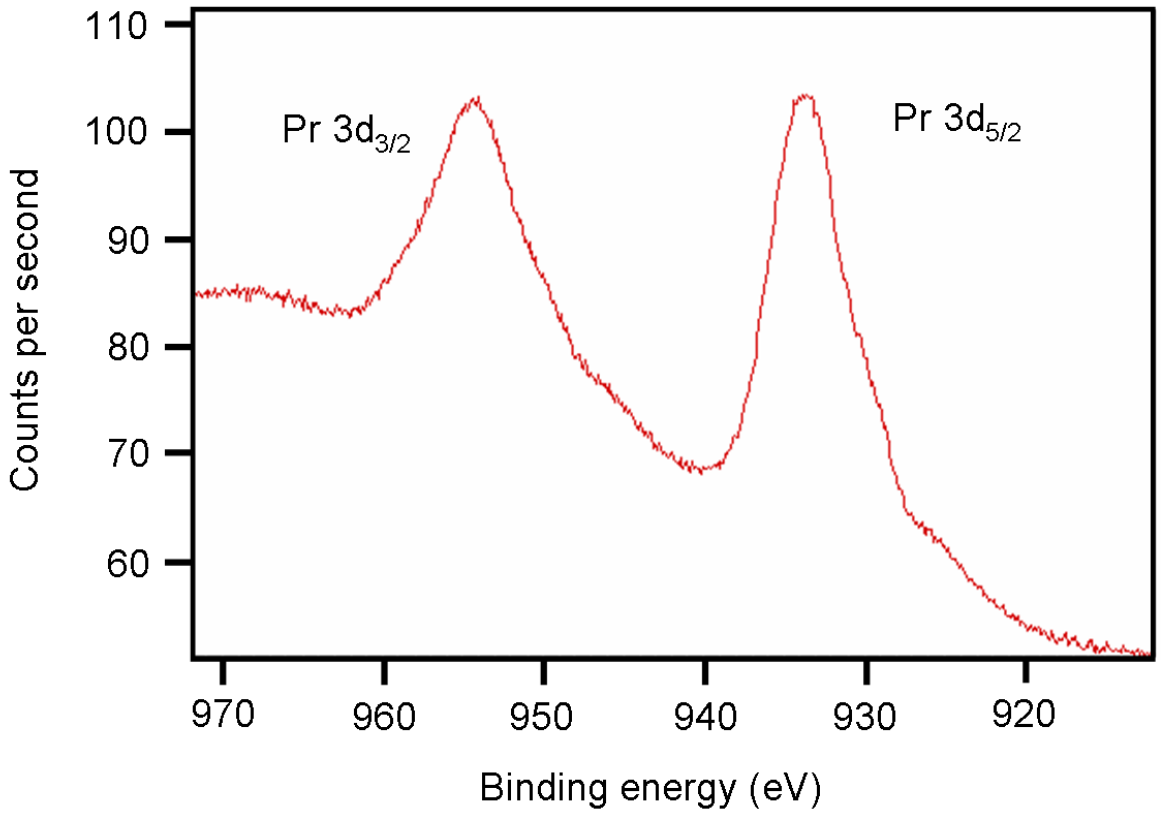

Figure 9.3. Diagnostic praseodymium region of the XPS spectrum of amorphous PrB_x film grown on glass at 300 °C from $Pr(H_3BNMe_2BH_3)_3$. Data collected by Brian J. Bellott.

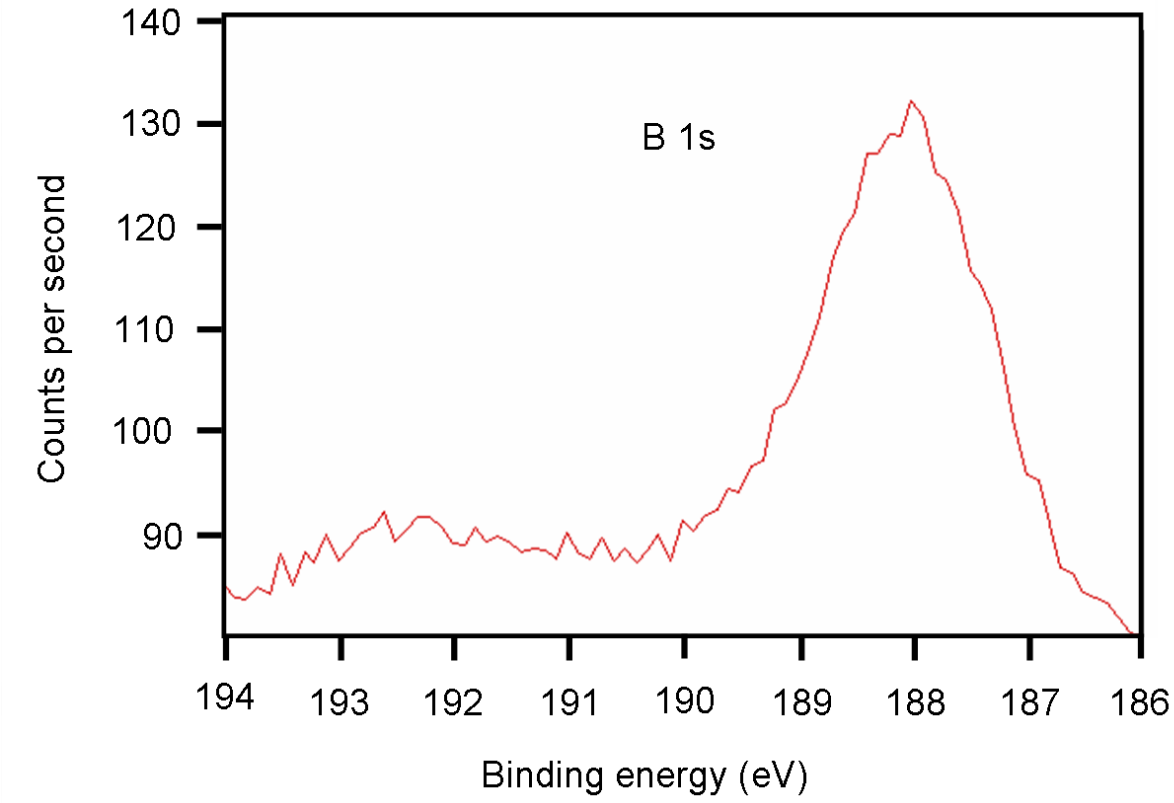

Figure 9.4. Diagnostic boron region of the XPS spectrum of amorphous PrB_x film grown on glass at 300 °C from $Pr(H_3BNMe_2BH_3)_3$. Data collected by Brian J. Bellott.

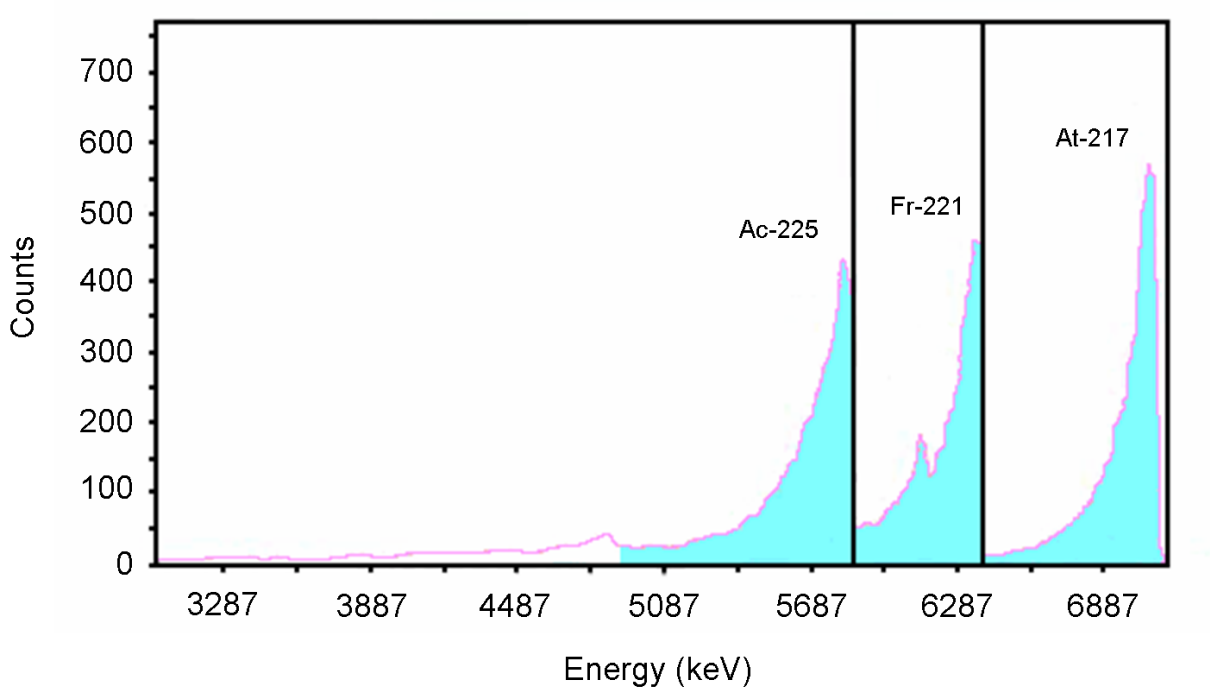

Figure 9.5. Alpha spectrum of the ^{225}Ac-doped PrB_x film grown on glass at 300 °C from ^{225}Ac-doped $Pr(H_3BNMe_2BH_3)_3$. The lines and shading represents integration endpoints for each radionuclide. Data collected by Dr. Daniel R. McCalister at the PG Research Foundation.

Concluding remarks

The deposition of ^{225}Ac-doped PrB_x films demonstrates that volatile lanthanide precursors can be used as carriers for actinium in CVD processes. The co-crystallization and co-sublimation of ^{225}Ac with the praseodymium carriers suggest that actinium forms compounds of stoichiometry $Ac(H_3BNMe_2BH_3)_3(thf)$, $Ac(H_3BNMe_2BH_3)_3$, and $Ac(thd)_3$, and that the first is soluble in pentane and the latter two are volatile.

The ^{225}Ac-doped PrB_x films deposited by using $Pr(H_3BNMe_2BH_3)_3$ as a carrier provide the first "proof-of-concept" that deposited ^{225}Ac-doped films are potentially useful for brachytherapy. The films are thin enough that the alpha particles can escape to irradiate surrounding tissue, as determined by the relatively high resolution of the alpha energy spectrum. The refractory boride films are chemically inert and are etched only under highly acidic conditions, which would not be encountered *in vivo*. The films also reveal another distinct advantage: the substrate can serve as shielding to protect healthy tissue around a malignant site. The presence of the decay daughters in the films also suggests that the film matrix helps prevent the loss of radionuclides into the surrounding environment, which would be a significant advantage over other radioimmunotherapy treatments.[19-22] The results suggest that ^{225}Ac-doped PrB_x can be used in implant devices for diffusing alpha-emitter radiation therapy (DART).

Experimental

All operations were carried out in vacuum or under argon using standard Schlenk techniques, unless stated otherwise. All glassware was dried in an oven at 150 °C, assembled hot, and allowed to cool under vacuum before use. Tetrahydrofuran, diethyl ether, and pentane were distilled under nitrogen from sodium/benzophenone and degassed with argon

immediately before use. NH_4Cl (Aldrich), $PrCl_3 \cdot 6H_2O$ (Aldrich), $DyCl_3 \cdot 6H_2O$ (Aldrich), and 12 M HCl (Fisher) were used as received. The reagents $Na(H_3BNMe_2BH_3)$ and Na(thd) were prepared by the literature routes.[39, 40] Samples of ^{225}Ac were obtained from PG Research Foundation as 0.5 M HCl solutions containing 1.5 – 8.0 μCi of ^{225}Ac (corresponding to 1 x 10^{-13} to 6 x 10^{-13} moles). Glass microscope slides (Fisherbrand) and Si(100) (University Wafer) were rinsed with deionized water, degreased with organic solvents, heated to 150 °C, and cooled under vacuum before use.

SEM, XPS, and XRD data were collected by Brian J. Bellott. Scanning electron micrographs were obtained on a JEOL JSM-6060LV instrument. X-ray photoelectron spectra were recorded on a Physical Electronics PHI 5400 system with a 15 kV, 300 W Mg Kα radiation source (1253.6 eV). The film crystallinity was analyzed on a Rigaku Laue/Buerger. powder X-ray diffractometer. Initial activity measurements were made using a Geiger counter to confirm the presence of ^{225}Ac. All quantitative alpha and gamma radiation measurements were performed by Dr. Daniel R. McCalister at PG Research Foundation (Darien, IL). The $^{225}Ac(^{221}Fr)$ contents of doped $PrCl_3$, $Pr(H_3BNMe_2BH_3)_3(thf)$, and $Pr(thd)_3$ samples were measured in 7 mL borosilicate glass vials using a model E5003 Packard Cobra Autogamma counter. The ^{225}Ac contents of the thin films were measured by an alpha spectrometer with surface barrier detectors.[38]

▪ CAUTION: Actinium-225 is an alpha emitter with a half-life of 10 days. Actinium containing materials should be handled in an approved fume hood with proper safety equipment and radiation monitoring instruments, as required by local regulations.

Representative synthesis of anhydrous ^{225}Ac-doped $PrCl_3$. The anhydrous chlorides were prepared in essentially quantitative yield, as previously described.[34] To a 250 mL beaker equipped with a stirring bar was added deionized water (31 mL) followed by 12

M HCl (23 mL). To the stirred solution was added $PrCl_3 \cdot 6H_2O$ (4.27 g, 12.0 mmol) and NH_4Cl (10.8 g, 0.202 mol), followed by the aqueous ^{225}Ac solution (0.5 mL, 4 μCi). The liquid was evaporated to dryness on a hot plate and the light green residue was carefully loaded into a Schlenk sublimation vessel and heated in a tube furnace under dynamic vacuum, as previously described.[34] A similar method was used to prepare ^{225}Ac-doped $DyCl_3$.

^{225}Ac-doped Pr($H_3BNMe_2BH_3$)$_3$(thf). To ^{225}Ac-doped $PrCl_3$ (0.32 g, 1.3 mmol) was added tetrahydrofuran (20 mL), and the mixture was refluxed for 20 h. The solution was evaporated to dryness under vacuum, and diethyl ether (15 mL) was added to the dried residue. At 0 °C, a solution of sodium *N*,*N*-dimethylaminodiboranate (0.37 g, 3.9 mmol) in diethyl ether (15 mL) was added to the mixture. The light green suspension was stirred at 0 °C for 15 min and then was warmed to room temperature. The resulting mixture was stirred for 15 h and evaporated to dryness under vacuum to afford a sticky, light green solid. The solid was extracted with pentane (50 mL), the extract was filtered, and the filtrate was concentrated to ca. 12 mL and cooled to -20 ˚C to afford large, green crystals. Yield: 0.31 g (56 %). The recovery of ^{225}Ac relative to the starting material was 37.4 %.

^{225}Ac-doped Pr($H_3BNMe_2BH_3$)$_3$. Sublimation of ^{225}Ac-doped Pr($H_3BNMe_2BH_3$)$_3$-(thf) (0.30 g, 0.70 mmol) at 115 °C at 10^{-2} Torr overnight yielded a green sublimate of ^{225}Ac-doped Pr($H_3BNMe_2BH_3$)$_3$. Yield: 0.22 g (88 %).

^{225}Ac-doped Pr(thd)$_3$. To a suspension of ^{225}Ac-doped $PrCl_3$ (0.32 g, 1.3 mmol) in tetrahydrofuran (15 mL) at 0 °C was added a solution of sodium *N*,*N*-dimethylaminodiboranate (0.44 g, 4.6 mmol) in tetrahydrofuran (15 mL). The reaction mixture was stirred at 0 °C for 15 min and then was warmed to room temperature and stirred for 15 h. The mixture was evaporated to dryness under vacuum to afford a light green solid.

The flask was equipped with a water cooled cold finger and the residue was sublimed at 180 °C and 10^{-2} Torr. Most of the material sublimed onto the walls of the flask but a small amount of light green sublimate was collected from the cold finger. Yield: 67.2 mg (7.5 %). The recovery of ^{225}Ac relative to the starting material was 44.2 %.

Deposition of PrB_x films by CVD. Films were deposited in the apparatus depicted in Figure 9.1 at a base pressure of 10^{-2} Torr. Sample charges of 30 - 45 mg of $Pr(H_3BNMe_2BH_3)_3$ were sublimed through the hot zone from a reservoir kept at 115 °C. The reactor wall and substrate were maintained at 300 °C throughout the deposition process. The substrate was either a glass microscope slide or a portion of a Si(100) wafer. A shiny film, metallic in appearance, deposited on the walls of the apparatus and on the substrate. The film thickness (550 nm) and microstructure were determined by SEM. No diffraction peaks appeared in the X-ray diffractogram.

References

1. Buono, S.; Burgio, N.; Hamoudeh, M.; Fessi, H.; Hiltbrand, E.; Maciocco, L.; Mehier-Humbert, S. *Anti-Cancer Agents Med. Chem.* **2007,** *7*, 411-424.

2. Nag, S.; Owen, J. B.; Farnan, N.; Pajak, T. F.; Martinez, A.; Porter, A.; Blasko, J.; Harrison, L. B. *Int. J. Radiat. Oncol. Biol. Phys.* **1995,** *31*, 103-107.

3. Moule Russell, N.; Hoskin Peter, J. *Surg. Oncol.* **2009,** *18*, 255-267.

4. Brechbiel, M. W. *Dalton Trans.* **2007**, 4918-4928.

5. Sgouros, G. *Adv. Drug Delivery Rev.* **2008,** *60*, 1402-1406.

6. Miederer, M.; Scheinberg, D. A.; McDevitt, M. R. *Adv. Drug Delivery Rev.* **2008,** *60*, 1371-1382.

7. McDevitt, M. R.; Ma, D.; Lai, L. T.; Simon, J.; Borchardt, P.; Frank, R. K.; Wu, K.; Pellegrini, V.; Curcio, M. J.; Miederer, M.; Bander, N. H.; Scheinberg, D. A. *Science* **2001,** *294*, 1537-1540.

8. Borchardt, P. E.; Yuan, R. R.; Miederer, M.; McDevitt, M. R.; Scheinberg, D. A. *Cancer Res.* **2003,** *63*, 5084-5090.

9. Song, H.; Hobbs, R. F.; Vajravelu, R.; Huso, D. L.; Esaias, C.; Apostolidis, C.; Morgenstern, A.; Sgouros, G. *Cancer Res.* **2009,** *69*, 8941-8948.

10. Kairemo, K. J. *Acta Oncol* **1996,** *35*, 343-355.

11. Cooks, T.; Arazi, L.; Schmidt, M.; Marshak, G.; Kelson, I.; Keisari, Y. *Int. J. Cancer* **2008,** *122*, 1657-1664.

12. Cooks, T.; Schmidt, M.; Bittan, H.; Lazarov, E.; Arazi, L.; Kelson, I.; Keisari, Y. *Int. J. Radiat. Oncol., Biol., Phys.* **2009,** *74*, 966-973.

13. Cooks, T.; Arazi, L.; Efrati, M.; Schmidt, M.; Marshak, G.; Kelson, I.; Keisari, Y. *Cancer* **2009,** *115*, 1791-1801.

14. Boll, R. A.; Malkemus, D.; Mirzadeh, S. *Appl. Radiat. Isot.* **2005,** *62*, 667-679.

15. Horwitz, E. P.; McAlister, D. R.; Thakkar, A. H. *Solvent Extr. Ion Exch.* **2008,** *26*, 12-24.

16. Kopunec, R.; Macasek, F.; Mikulaj, V.; Drienovsky, P. *Radiochem. Radioanal. Lett.* **1969,** *1*, 117-122.

17. Laubereau, P. G.; Burns, J. H. *Inorg. Chem.* **1970,** *9*, 1091-1095.

18. Deal, K. A.; Davis, I. A.; Mirzadeh, S.; Kennel, S. J.; Brechbiel, M. W. *J. Med. Chem.* **1999,** *42*, 2988-2992.

19. Davis, I. A.; Glowienka, K. A.; Boll, R. A.; Deal, K. A.; Brechbiel, M. W.; Stabin, M.; Bochsler, P. N.; Mirzadeh, S.; Kennel, S. J. *Nucl. Med. Biol.* **1999,** *26*, 581-589.

20. Kennel, S. J.; Chappell, L. L.; Dadachova, K.; Brechbiel, M. W.; Lankford, T. K.; Davis, I. A.; Stabin, M.; Mirzadeh, S. *Cancer Biother. Radiopharm.* **2000,** *15*, 235-244.

21. Chappell, L. L.; Deal, K. A.; Dadachova, E.; Brechbiel, M. W. *Bioconjugate Chem.* **2000,** *11*, 510-519.

22. Kennel, S. J.; Brechbiel, M. W.; Milenic, D. E.; Schlom, J.; Mirzadeh, S. *Cancer Biother. Radiopharm.* **2002,** *17*, 219-231.

23. Sofou, S.; Thomas, J. L.; Lin, H.-y.; McDevitt, M. R.; Scheinberg, D. A.; Sgouros, G. *J. Nucl. Med.* **2004,** *45*, 253-260.

24. Henriksen, G.; Schoultz, B. W.; Michaelsen, T. E.; Bruland, O. S.; Larsen, R. H. *Nucl. Med. Biol.* **2004,** *31*, 441-449.

25. Sofou, S.; Kappel, B. J.; Jaggi, J. S.; McDevitt, M. R.; Scheinberg, D. A.; Sgouros, G. *Bioconjugate Chem.* **2007,** *18*, 2061-2067.

26. Li, X. L.; Tsoutsou, D.; Scarel, G.; Wiemer, C.; Capelli, S. C.; Volkos, S. N.; Lamagna, L.; Fanciulli, M. *J. Vac. Sci. Technol., A* **2009,** *27*, L1-L7.

27. Castaing, J.; Costa, P. Properties and Uses of Diborides. In *Boron and Refractory Borides*, Matkovich, V. I., Ed. Springer: Berlin, 1977; pp 406-407.

28. Daly, S. R.; Kim, D. Y.; Yang, Y.; Abelson, J. R.; Girolami, G. S. *J. Am. Chem. Soc.* **2010,** *132*, 2106-2107.

29. Shannon, R. D. *Acta Crystallogr., Sect. A* **1976,** *A32*, 751-767.

30. Eisentraut, K. J.; Sievers, R. E. *J. Am. Chem. Soc.* **1965,** *87*, 5254-5256.

31. Tiitta, M.; Niinisto, L. *Chem. Vap. Deposition* **1997,** *3*, 167-182.

32. Lo Nigro, R.; Malandrino, G.; Toro, R. G.; Fragala, I. L. *Top. Appl. Phys.* **2007,** *106*, 33-51.

33. Meyer, G. *Inorg. Synth.* **1989,** *25*, 146-150.

34. Edleman, N. L.; Wang, A.; Belot, J. A.; Metz, A. W.; Babcock, J. R.; Kawaoka, A. M.; Ni, J.; Metz, M. V.; Flaschenriem, C. J.; Stern, C. L.; Liable-Sands, L. M.; Rheingold, A. L.; Markworth, P. R.; Chang, R. P. H.; Chudzik, M. P.; Kannewurf, C. R.; Marks, T. J. *Inorg. Chem.* **2002,** *41*, 5005-5023.

35. Similar results were obtained when $^{225}AcCl_3/DyCl_3$ was prepared and used to prepare $Dy(H_3BNMe_2BH_3)_3(thf)$.

36. Moulder, J. F.; Stickle, W. F.; Sobol, P. E.; Bomben, K. D. *Handbook of X-ray Photoelectron Spectroscopy*. Perkin-Elmer Corp: Eden Prairie, MN, 1992.

37. Spear, K. E. Rare Earth-Boron Phase Equilibria. In *Boron and Refractory Borides*, Matkovich, V. I., Ed. Springer-Verlag: Berlin, 1977; pp 439-456.

38. Glover, K. M. *Int. J. Appl. Radiat. Isot.* **1984,** *35*, 239-250.

39. Nöth, H.; Thomas, S. *Eur. J. Inorg. Chem.* **1999**, 1373-1379.

40. Shin, H. K.; Chi, K. M.; Farkas, J.; Hampden-Smith, M. J.; Kodas, T. T.; Duesler, E. N. *Inorg. Chem.* **1992,** *31*, 424-431.

APPENDIX A. Instructions to Generate Protein Database (PDB) Files from X-Ray Data Using SHELXTL

Protein database (PDB) files provide atomic coordinates of molecules from crystallographic data, and these files are often used to provide the initial structures of molecules being studied by computational methods. Before you begin, it is advisable to make a copy of the entire file you would like to use to generate this type of PDB files and work with it somewhere away from your solved data (on your desktop, for instance). This will help to keep the dummy files that you will be generating away from your solved data, which will help to prevent an accidental mix-up at a later date. It is also advisable to delete all files except for the generated PDB files once you are finished.

1. Open SHELXTL.

2. Open absfile.hkl containing the chemical species of interest.

3. Run XP.

4. Select all atoms and equivalent sites to be included in the PDB file using the GROW and/or PACK commands.
    a. If using the GROW command, FMOL after all the desired atoms have been selected to add the atoms to the atom list.
    b. To generate equivalent sites in the unit cell, use the MATR 1, 2, or 3 commands followed by PBOX to change the cell dimensions. Use the PACK

command to view the cell contents and select SGEN/FMOL once you are satisfied with the number of atoms/molecules included in the cell.

5. Once you have returned to the XP prompt, type “FILE dummyfile”, where dummyfile is an arbitrarily assigned filename of your choice. Write this name down for future reference. This will generate a dummy INS file.

6. XP will then ask “Enter name of file from which instructions (including HKLF but not atoms) should be copied [dummyfile.res]:” Enter absfile.res, where absfile is the file you opened in step 2 and hit enter to cycle through the new atom list.

7. Exit XP.

8. Make a copy of absfile.hkl and rename this file dummyfile.hkl, where dummyfile is the name of the file you made in step 5.

9. At the SHELXTL window, click project and drag to New. Select the hkl file you made in step 8 and click ok.

10. Click on edit and drag to edit.ins to edit the INS file you made in step 5.

11. Remove all SYMM cards by adding REM before all SYMM. (REM SYMM)

12. Change LATT N to LATT –N.

13. Remove ACTA card by adding REM before ACTA. (REM ACTA)

14. Change L.S. N to L.S. 0.

15. Add WPDB -2 anywhere between the UNIT and WGHT cards.

16. Save changes and close INS file.

17. Run XL.

18. A PDB file should now be generated in the folder containing the original hkl from step 2.

19. Sometimes this process causes some of the atom numbers to change, which can result in an error message when trying to run XL. Make sure that the atom labels correspond to the restraints being used in the INS file. If they do not, manually change the atom labels of the first molecule in the INS file back to the labels used in the original file and try XL again.

20. Check the PDB file for errors in a PDB viewer, such as RasMol.

AUTHOR'S BIOGRAPHY

Scott R. Daly was born on October 16, 1980 in Joliet, Illinois. He moved with his family to rural north central Florida in 1985, where he attended school. During that time he was active in sports, such as football and baseball, raised farm animals, rode horses through the swamp, and wrestled the occasional snake or alligator. Scott became interested in science at a young age: at six, his father gave him a copy of Reader's Digest Science Reader, which influenced him greatly. In middle school, he competed in science fairs, ascending all the way to state in the 8th grade and placing sixth for his investigations on algae and protozoa. During that time, he became interested in herpetology, and collected a wide variety of snakes and lizards.

Scott graduated from high school at the age of 17 and immediately enlisted in the United States Army as a M1 Abrams tank crewman. He completed the 16-week armor training school at Fort Knox, Kentucky, graduated first in his class, and received the distinguished General George S. Patton, Jr. award for his efforts. He was then stationed in the First Cavalry Division at Ft. Hood, Texas. He rapidly rose through the ranks and secured a position as a squad leader in 18 months, earning battalion soldier of the month honors along the way. In August of 2000, he was deployed with his platoon to Missoula, Montana to fight wildfires that were devastating the northwestern United States. Upon his return, he was invited to participate in the challenging Cavalry "spur ride", which he completed, becoming one of the youngest members inducted into the Order of the Spur. Scott was honorably discharged from active duty on August 20, 2001 at the age of 20.

Scott returned to the Chicago suburbs after the military and immediately enrolled at Joliet Junior College, where he attended as a pre-pharmacy candidate with little direction until 2004, when he decided to quit his job at Mack and pursue a degree in chemistry. He transferred to North Central College in Naperville, Illinois to complete his B.S. and to be close to the love of his life, Carin. He did undergraduate research with Phil Horwitz optimizing the chromatographic extraction of group 12 metals and actinides from soil and water matrices. He graduated from North Central College summa cum laude in June of 2006.

Scott enrolled at the University of Illinois at Urbana-Champaign in August of 2006 and joined the research group of Professor Gregory S. Girolami to study the chemistry of aminodiboranates. He graduated in May of 2010 and accepted a postdoctoral position at Los Alamos National Laboratory with Stosh Kozimor to study metal-ligand interactions by X-ray absorption spectroscopy.